CONTRACT AA550-CT7-29

STUDIES

29133

SOUTH ATLANTIC OCS PHYSICAL OCEANOGRAPHY

FINAL PROGRESS REPORT
(First Year)

Volume II: Technical Report

July 6, 1979

Prepared for
BUREAU OF LAND MANAGEMENT
Washington, D.C.

SCIENCE APPLICATIONS, INC.
4900 Water's Edge Drive, Suite 255
Raleigh, North Carolina 27606

This report has been reviewed by the Bureau of Land Management and approved for publication. Approval does not signify that the contents necessarily reflect the views and policies of the Bureau, nor does mention of trade names or commercial products constitute endorsement or recommendation for use.

SOUTH ATLANTIC OCS
PHYSICAL OCEANOGRAPHY

Final Report to the Bureau of Land Management U.S. Department of the Interior

Contract Number: AA550-CT7-29

Paul Debrule, Project Manager

TABLE OF CONTENTS

TABLE OF CONTENTS (Continued)

TABLE OF CONTENTS (Continued)

TABLE OF CONTENTS (Continued)

TABLE OF CONTENTS (Continued)

TABLE OF CONTENTS (Continued)

TABLE OF CONTENTS (Continued)

TABLE OF CONTENTS (Continued)

LIST OF TABLES

LIST OF TABLES (Continued)

LIST OF FIGURES

LIST OF FIGURES (Continued)

LIST OF FIGURES (Continued)

LIST OF FIGURES (Continued)

LIST OF FIGURES (Continued)

LIST OF FIGURES (Continued)

LIST OF FIGURES (Continued)

LIST OF FIGURES (Continued)

I. INTRODUCTION

This Draft Final Report presents a summary of all field activities and analyses of physical oceanographic and meteorological data collected on the Outer Continental Shelf (OCS) from Cape Fear, North Carolina to Cape Canaveral, Florida during the period of September 1977 through November 1978. The study, managed by Dr. P. Debrule, was conducted by Science Applications, Inc. (SAI), and a team of scientists from various universities and institutes for the Bureau of Land Management (BLM) under Contract Number AA550-CT7-29.

The present volume should be regarded as a progress report rather than a final document, as it covers only the efforts undertaken in the first year of a three-year data acquisition and synthesis program designed to provide sufficient understanding of the currents, circulation, and mixing processes in the Georgia Embayment/South Atlantic Bight (SAB) to assess the effects of OCS oil and gas activities on the biological environment, as well as on recreational and commercial fishing. The field data collection performed during the first year was considerably enhanced through close coordination with the Principal Investigators (P.I.'s) participating in a complementary program sponsored by the Department of Energy (DOE) in the same region. However, the data base currently available is still limited, and only tentative conclusions can be drawn at this stage. Serious gaps still exist in the information required for a more complete understanding of the physical mechanisms governing circulation and mixing in the area of interest, although it can reasonably be expected that most of these gaps will be bridged at the conclusion of the fourth year data acquisition program. In addition, some data sets required in support of the interpretation of the field measurements were not as readily available as anticipated and, in some cases, are still missing to date (for instance, some sea level data in support of circulation study). As a result, the P.I.'s involved in the characterization of shelf circulation could not, at this stage, rely on sufficient data to depict a complete picture of surface and subsurface current patterns in the Georgia Embayment. Therefore, the present report should only be viewed as a description of trends or events present in the data which appear to be related to identified forcing mechanisms over the shelf.

The present document is the second of four volumes composing the Final Progress Report. It contains the technical information inferred from the data collected throughout the first year's study. Volume I consists of an Executive Summary, presenting in concise form the findings of the P.I.'s. Volume III contains the Data Products generated in the areas of subsurface currents (short-term and long-term current meter moorings), hydrography, and wave-sea state analysis. Original surface wind maps prepared at six-hour intervals from September 1977 to November 30, 1977, and daily from December 1,

1977 to November 30, 1978, as well as LANDSAT satellite imagery used in the study of the temporal and spatial distribution of turbidity in the coastal zone are submitted in Volume IV.

1.1 STUDY OBJECTIVES

In order to provide the information required for the prediction, assessment, and management of impacts resulting from the exploration and development of offshore oil and gas resources on the human, marine, and coastal environments of the OCS and nearshore area, BLM has initiated a program of environmental studies focused towards the needs of the decision maker. As part of this program, the South Atlantic OCS Physical Oceanography Study has been designed to provide a description and understanding of circulation and mixing processes in the Georgia Embayment OCS and upper slope region, as well as the nature and relative importance of the forcing mechanisms which are responsible for them. At the completion of the field data acquisition program, scheduled to extend over a three- to four-year period, it can be anticipated that the physical processes involved in the transport and dispersion of surface, suspended or dissolved pollutants in the region will be sufficiently known to be parameterized in models predicting the probability of the paths along which contaminants resulting from offshore oil/gas activities may reach biologically sensitive areas (for instance, productive hard bottom areas), or the nearshore regions of the Georgia Embayment and Carolina Capes.

In a first step to meet this goal, physical oceanographic and meteorological data collected prior to 1977 were identified, displayed, analyzed, and interpreted in a project conducted by Environmental Research and Technology, Inc. (ERT) and a consortium of consultants (P. Kirshen, 1978). Concurrently, the present study was initiated in May 1977. Its first year consisted of a limited field data acquisition program comprised of the following elements:

a. Study of the transport of surface and near-surface borne materials across and/or along the turbid-clear water interface of the Georgia Embayment during both wet and dry seasons, as a first step towards the assessment of the ability of this feature to act as a natural barrier to the migration of pollutants towards shore or estuaries of the Embayment (Dr. E. Waddell, SAI, Principal Investigator).

b. Analysis of current and temperature time series obtained near the shelf edge to monitor the effects of Gulf Stream intrusions. Current meters were to be emplaced in support of hydrography conducted by the Benchmark Contractor, and integrated in a box array deployed under the auspices of DOE to provide optimum cross-shelf resolution (Dr. T. Lee, University of Miami, Principal Investigator).

c. Establishment of a long-term current meter station to determine the mean flow and the extent of perturbations at near-surface, mid-water, and near-bottom depths, due to meteorological forcing and Gulf Stream pulsing action.

d. Monitoring of seasonal characteristics of shelf water masses and of short-term variations in shelf edge water masses (i.e., fluctuations of the position of the western edge of the Gulf Stream) using Very High Resolution Radiometer (VHRR) satellite imagery.

e. Correlation of surface wind and wave field data on the South Atlantic OCS with coastal conditions, National Weather Service predictions, and information derived from satellite imagery in support of the interpretation of subsurface current measurements.

Added later to this program was the collection of hydrographic data, initially conducted by Texas Instruments, after early termination of the Benchmark Program in the Georgia Embayment. These measurements were performed in order to interpret Gulf Stream interactions with shelf water masses, to aid in determining shelf water residence times, and to infer shelf circulation patterns.

Data gaps were identified by the ERT study and recommendations regarding additional field measurements needed as inputs to the BLM decision making process were incorporated in the design of the second year's study. The tasks enumerated above indicate that the emphasis of the first year program was placed on the acquisition of subsurface current time series, and identification of forcing mechanisms responsible for the observed circulation. Among these mechanisms, the Gulf Stream interactions with the shelf waters, in the form of meanders, eddies, and/or intrusions and the response of the shelf to meteorological front passages were--or will be--investigated by merging current meter records with hydrographic measurements and thermal remote sensing imagery, and surface wind time series in the mooring areas, respectively. Somewhat uncoupled with the main thrust of the program was the study of the coastal front which, however, would prove extremely valuable, should leases be considered in the shallower waters of the coastal region. The interrelationship between the various tasks of the first year's program has, in turn, dictated the organization of the present report, described in the following section.

1.2 REPORT ORGANIZATION

As indicated earlier, the present document is the second of a four volume report. It summarizes the first year's activities, describes the methodology or techniques used in the accomplishment of the tasks mentioned in Section 1.1, and presents tentative conclusions reached

by the P.I.'s, as well as some of the data products generated in the course of their work. All data products are presented in Volume III, with the exception of some of the surface wind maps over the area of interest, prepared by Dr. J. Fernandez-Partagas on the 6-hourly or daily basis and the LANDSAT imagery used in the historical seasonal characterization of the coastal fronts along the Georgia Embayment, which are submitted in a single original volume (Volume IV). In addition, photographic mosaics documenting the first deployment of surface tracers near the turbid-clear water interface have been presented in a previous Trip Report and will not be reproduced here.

In an attempt to present the technical information obtained throughout the first year in a concise, yet comprehensive form, only those data products which are used to illustrate a methodology or support a conclusion are reproduced in this volume. Frequent references, however, will be made to Volumes III and IV, which provide the reader with the complete data sets from which tentative conclusions reported in this report were inferred.

A table summarizing the data collection during the first year's study is shown in the next section (1.3). The program's organizational structure is briefly presented in Section II (Program Management), together with a description of the SAI Data Management System and an outline of the Quality Assurance program implemented by SAI, with a maximum of cooperation from Nova University (P. Bedard) and Aero-Marine Surveys, Inc. (T. Flynn).

A review of existing literature pertaining to the physical oceanographic and meteorological information available for the Georgia Embayment OCS region is presented in Section III. Field work related to the characterization of the motion of tracers and dye simulating water borne pollutants in the vicinity of the turbid-clear water interface is described in Section IV, together with tentative conclusions regarding frontal dynamics and transport along or across the interface. Section V deals with current circulation in the South Atlantic OCS region. Grouped in this section are the subsurface current measurements, hydrographic sampling, surface wind time series at the location of the current meter moorings, and Gulf Stream monitoring by remote sensing techniques, as all these studies complement one another and contribute to depicting the current patterns observed in the region.

The methodologies followed in the establishment of correlations between surface winds obtained from the streamline-isotach method used by Dr. J. Fernandez-Partagas and surface winds obtained from other sources (satellite-derived winds, coastal observations, National Weather Service (NWS) predictions, etc.), and of relationships between wind and wave/sea state are presented in Section VI, together with a summary of the findings made by the respective

P.I.'s. Finally, the tasks to be accomplished in the second year's program and recommendations for a third year effort are outlined in Section VII.

1.3 SUMMARY OF DATA COLLECTED DURING THE FIRST YEAR'S STUDY

The data acquired during the first year's study are presented in Table I-1. Data actually collected in the field by SAI and its subcontractors consist of current meter measurements (two short-term moorings deployed from September 1, 1977 through November 2, 1977; and a long-term mooring monitoring current velocities and temperatures at three depths from November 4, 1977 through November 15, 1978, hydrographic data (four seasonal cruises in 1978, in addition to similar data collected by Texas Instruments in 1977) and surface currents and hydrographic sampling in the vicinity of the turbid-clear water interface (August 7 through 14, 1977 and April 30 through May 11, 1978). All cruises were very successful, and the data collected proved to be of excellent quality, with only minor data losses associated with current meter electronic failures. Details on the data return are provided in Sections 5.3.1.5, and 5.3.2.4. All data collected have been analyzed, with the exception of records provided by moorings 91 and 92. Wave and sea state data subsequent to September 30, 1978 are still unavailable. It is anticipated that these data will be incorporated in the Final Progress Report, scheduled for completion by June 15, 1979, or in separate technical addenda as soon as they become available.

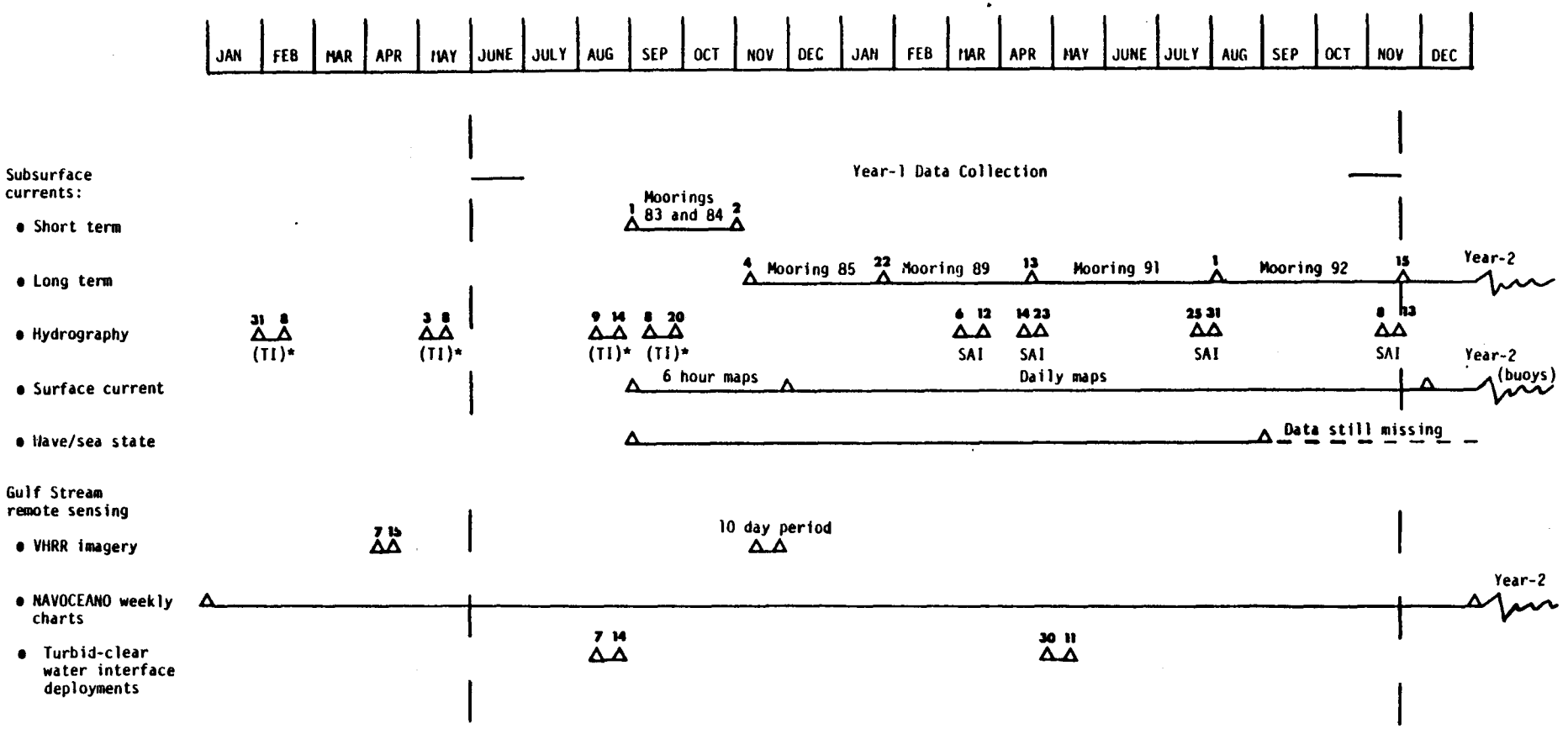

Table I-1. Summary of data collected during the first year's study.

II. PROGRAM MANAGEMENT

To conduct the study outlined in the previous section, SAI has assembled a team of eminent physical oceanographers with past experience in the Georgia Embayment. This team was structured on a functional basis as shown in Figure 2-1. The management organization can be divided into two subgroups: the program staff, all composed of SAI personnel, and the research staff, consisting of scientists from SAI and from various universities: University of Miami (UM), North Carolina State University (NCSU), and Nova University (NU). Logistics support was provided by SAI, the University of Miami (responsible for the scheduling and outfitting of the R/V ISELIN), Nova University (in charge of the checkout, assembly, and deployment of the current meter moorings), Aero-Marine Surveys, Inc. (AMS) (supplying fully equipped aircraft, boats, and personnel required for the two deployments of tracers in the vicinity of the turbid-clear water), University of Delaware (providing surface drogues and radio direction finders used in the second surface currents study as well as field personnel, including the services of Dr. R. Garvine in an advisory capacity), and Skidaway Institute of Oceanography (SKIO) (supplying the instrumentation for the SAI seasonal hydrographic sampling). The role played by SAI and its subcontractors is detailed in the following section.

2.1 PROGRAM PARTICIPANTS AND THEIR RESPONSIBILITIES

SAI has been primarily responsible for the technical and financial Program Management, Data Management (including development of an effective retrieval and variable sorting system), implementation and improvement of Quality Assurance plans, logistics coordination, as well as some technical tasks described below. As a result, the Program Management team consisted of the Program Manager (Dr. P. Debrule) assisted by a Data Manager (Dr. P. Hamilton), a Quality Assurance Manager (Mr. E. Bain), a Contracts Representative (Mr. T. Trevino assisted by Ms. S. Feldman), and an Administrator (Ms. E. Bivins). Interaction between this Program Management staff and the various P.I's composing the Research Team, and overall technical guidance was provided directly by the Program Manager. The Research Team, in turn, was formed of the following scientists, hereafter listed by major task undertaken during the first year's study.

2.1.1 Surface Currents (turbid-clear water study): Dr. E. Waddell (SAI).

Dr. Waddell was responsible for the design, planning and implementation of two deployments of surface tracers in the vicinity of the turbid-clear water interface (in the dry and wet seasons), data reduction, analysis and interpretation, focused on the determination of movement of water borne material relative to a migrating coastal front, and the examination of the dynamics of the exchange processes

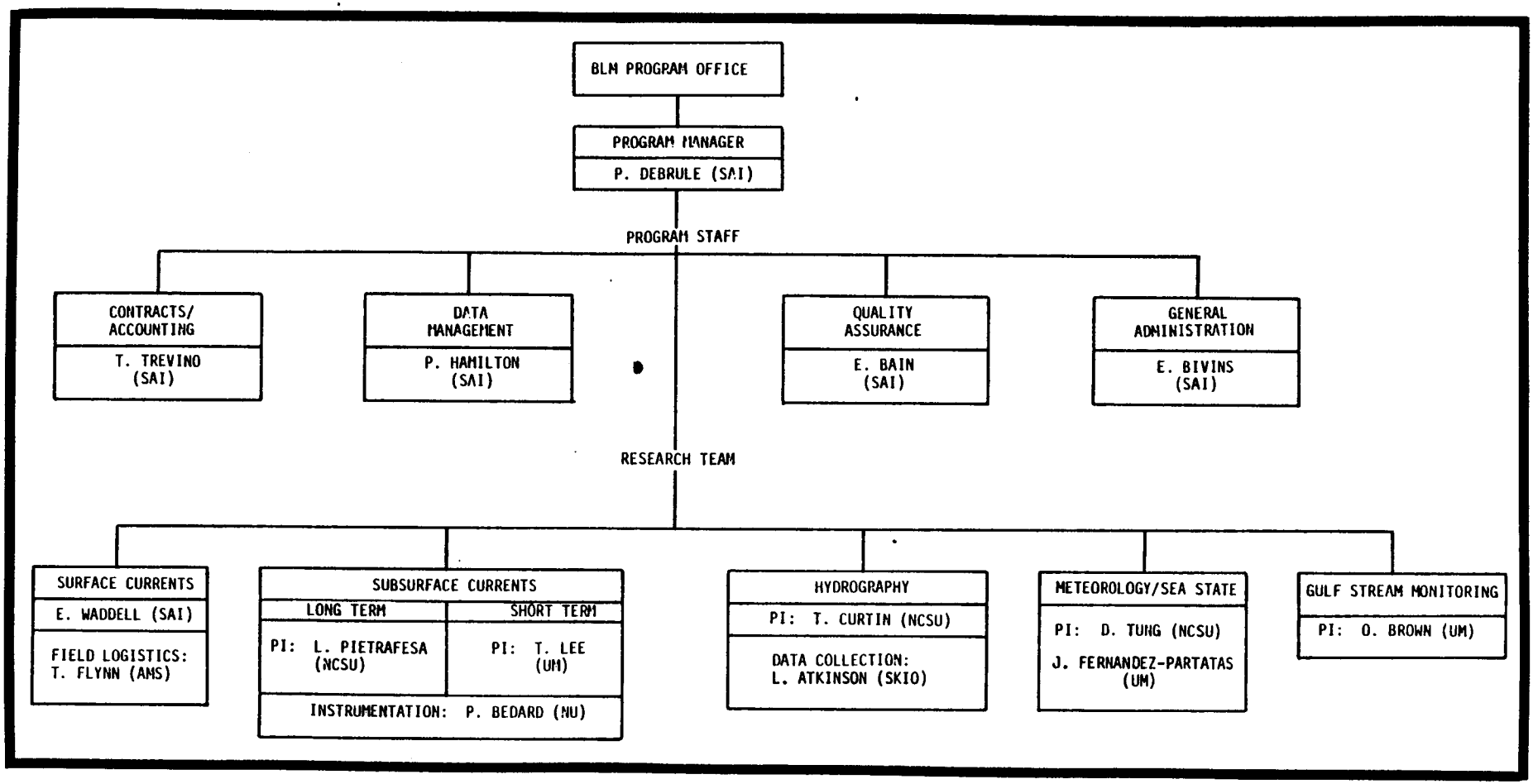

Figure 2-1. Program organization structure.

between the turbid estuarine and ambient shelf waters. Actual field work was performed in conjunction with personnel from the University of Delaware (including Dr. R. Garvine for the first deployment) and Aero-Marine Surveys, Inc., the latter firm also providing the aircraft, surface vessels, and instrumentation required for the aerial monitoring of the surface tracers. Examination of the temporal variations and spatial persistence of the turbid-clear water interface over the seasons and consecutive years was initiated by G. Davis (UD and later, AMS), using LANDSAT imagery, and completed by Dr. E. Waddell.

2.1.2 Subsurface Currents: Dr. T. Lee (UM) and Dr. L. Pietrafesa (NCSU).

Dr. Lee, acting as Chief Scientist on all current meter deployment/ retrieval cruises, was responsible for the design and launching of all moorings (together with P. Bedard [NU]), reduction of the Aanderaa current meter data mounted on one of the short-term moorings, and for analysis and interpretation of current and temperature data provided by the Vector Averaging Current Meters (VACM's) and Aanderaa supported by the two short-term moorings deployed off Savannah, Georgia (Ga) from September 1 through November 2, 1977. It was also Dr. Lee's responsibility to schedule and outfit the R/V ISELIN, operated by the University of Miami. Finally, T. Lee was in charge of the monitoring of surface temperature and salinity along the cruise tracks, using a thermosalinograph. Actual mooring design, checkout and assembly of all moorings (nos. 83, 84, 85, 89, 91, and 92), as well as the conversion of the (Vector-Averaging Current Meters) VACM data into a 9-track compatible tape were performed by Mr. P. Bedard, according to quality assurance procedures described in a manual prepared by Nova University. Dr. Pietrafesa provided inputs to the design of the long-term moorings and was responsible for the analysis and interpretation of the long-term VACM current and temperature records, collected from November 4, 1977 through November 15, 1978 off Charleston, South Carolina (SC).

2.1.3 Hydrography: Mr. T. Curtin (NCSU) and Dr. L. Atkinson (Skidaway).

Mr. T. Curtin was responsible for the analysis and interpretation of hydrographic data collected on a seasonal basis, first by Texas Instruments (T.I.), the Benchmark Contractor, and subsequently by SAI in 1978. Close interaction existed between T. Curtin and Dr. L. Atkinson (Skidaway), who participated in some of the T.I. cruises and designed, together with other P.I.'s, the sampling plan for 1978. Starting in March 1978, hydrographic measurements were performed under the direction of Mr. J. Singer (Skidaway), acting as Chief Scientist for the hydrocast leg of the cruises.

2.1.4 Monitoring of Gulf Stream Location and Surficial Thermal Structure by Remote Sensing Techniques: Dr. O. Brown (UM).

Dr. O. Brown was responsible for a study aimed at assessing the potential of satellite remote sensing as a tool to characterize with high accuracy the surface temperature distribution in the Georgia Embayment, and for the generation of seasonal mean and extrema charts for the Gulf Stream/Shelf Water interface. He was assisted in this task by Dr. R. Evans (UM).

2.1.5 Wind and Wave/Sea State Analysis: Dr. D. Tung (NCSU) and Dr. J. Fernandez-Partagas (UM).

Dr. D. Tung was in charge of the analysis of wave/sea state data collected by ships of opportunity for the period of September 1977 through November 1978, and for correlations of wave heights, period, and direction with surface wind fields generated by Dr. J. Fernandez-Partagas. The latter investigator also prepared surface wind time series at the approximate location of the current meter moorings, assessed the quality of wind reports from ship cruises, compared surface wind maps derived by the streamline-isotach method with satellite-derived winds, historical data, offshore diagnostic winds based on coastal reports, and NWS offshore wind forecasts.

2.2 DATA MANAGEMENT

The large quantity and diversity of the data collected throughout the first year of the South Atlantic OCS Physical Oceanography Program required that a sophisticated Data Management System be implemented by SAI. In its present form, this system fulfills five major functions:

- Data cataloguing. All data received are filed in a general computerized catalogue. Each entry provides all information necessary to completely describe the associated data file.

- Data validation and editing. Unedited data received on magnetic tapes are read and edited in a format compatible with the National Oceanographic Data Center (NODC) requirements. Data are examined for quality and consistency through standard plots (i.e. temperature-salinity plots for hydrographic data, display of time series for current meter records). If some of the data points appear of dubious quality, the data supplier is contacted and, if necessary, is required to provide a new tape of corrected data. A working tape of the validated and edited data is then created, copies transmitted to NODC and the Principal Investigators, and the original tape stored as back up.

- Data storage. All edited and validated data are stored at a central location (SAI - La Jolla, California, Computing Center), either on tape or disk, according to a file organization suitable for easy retrieval and subsequent use.

- Data retrieval. The file structure has been organized in such a way that data sets or subsets can be accessed through a single computer program, and retrieved in a form readily available for subsequent analysis or for use as inputs to predictive models of pollutant transport/ circulation. Any variable of a data set or subset can be treated as a sorting parameter. As an example, it is possible to search for and identify all hydrographic data taken during a particular time interval within a range of geographic coordinates, in water exceeding a selected depth.

- Data display. The above cataloguing data system is coupled with a graphics package which allows the display of cross-sections of any hydrographic variable (salinity, temperature, sigma-t, nutrients, dissolved oxygen and chlorophyll) along any transect of any SAI/Skidaway cruise, as well as the distribution of these parameters over the area of interest at selected depths. Similar display of time series of current meter and meteorological data is currently under development.

The present Data Management System has been developed through successive adaptations of an existing data management package originally created for the BLM Southern California Bight Program.

In addition to maintaining and improving the Data Management System, the Data Manager (Dr. P. Hamilton), assisted by J. Karpen, was also responsible for the submission to NODC of First Level Inventories of data and samples collected (Report of observations/samples collected on oceanographic programs, or "ROSCOP" forms), as well as appropriate "Data Documentation Forms" (DDF).

2.3 ENGINEERING QUALITY ASSURANCE PROGRAM

In order to optimize the quality of the data collected in the field throughout the program, an Engineering Quality Assurance (Q. A.) Program was implemented by SAI, under the direction of E. Bain, in three areas: pre- and post-deployment checkout of current meter mooring components, equipment and instrumentation used for the surface current study and hydrographic data collection. To that effect, a Q. A. Manual entitled "Current Meter Mooring Testing procedures", and dated October 1977 was prepared by Nova University. Likewise, a "Q. A. Plan for Surface Current Study" was prepared jointly by SAI and Aero-Marine Surveys, prior to the second

deployment (April 1978) and Q. A. Procedures followed by the Skidaway Institute of Oceanogrpahy were thoroughly discussed prior to the first sampling cruise (early March, 1978).

Q. A. procedures followed in the checkout of the current meter, acoustic release and other mooring components were documented in "Checkout Sheets" provided as part of the Q. A. Manual. These completed forms were reviewed by SAI Quality Assurance personnel to ensure that the recorded information was complete and accurate. Compliance with the provisions of the Q. A. Manual was further evaluated through a series of audits of the Nova University Physical Oceanographic Laboratory. As a result of these audits, Nova University personnel agreed to slightly modify and update the checkout sheets by defining ranges of acceptable tolerances for each measurement performed during the current meter pre-deployment checkout. Should actual data not be in conformance with the specified values, the Nova project supervisor (P. Bedard) was requested to provide technical justification, initial and date all noted hand-written non-compliance which, in his opinion, had no impact on the performance of the instrument. In the course of the audits, SAI also recommended that logging procedures providing traceability to failed sub-assemblies for the VACM's program control boards be reviewed.

Close adherence to Q. A. procedures resulted in a very good data return. Details on the quality of the current meter data collected during the first year's program are provided in Section 5.3.1.5 of the present volume.

The equipment, instrumentation and procedures used in the deployment of surface tracers in the vicinity of the turbid-clear water interface and their aerial monitoring was field-tested in a series of experiments and Q. A. checkouts conducted in Groton, Connecticut, by Aero-Marine Surveys, under the direction of the P. M. and P. I. All systems had to perform according to specifications prior to being transported to the experimental site (Hilton Head Island). These procedures greatly alleviated the potential risk of failures which could jeopardize the success of the marine and aerial operations.

Finally, compliance with the Q. A. procedures followed by Skidaway in the hydrographic sampling was witnessed by an SAI observer on-board all cruises conducted under the BLM/SAI program.

2.4 DELIVERABLES

A large number of reports were prepared by SAI and submitted to BLM in accordance with the contract requirements. They consisted of:

- Field trip reports, describing the field operations related to the deployment/retrieval of current meter moorings, collection of hydrographic data or marine/aerial operations

associated with the surface current study. Also included in these reports are a definition of the cruise/flight objectives, a description of the methodology and procedures used to accomplish these goals, a summary log, excerpts of the bridge log containing meteorological and wave/sea state observations, stations sheets and other information related to the field work accomplished during the cruises or pertaining to the turbid-clear water interface studies. Also submitted as Volume II of a Field Trip Report was a printout of the hydrographic data collected by SAI/ Skidaway, edited in an NODC-compatible format.

- Surface Current Reports, presenting a summary of the field activities related to the deployment and monitoring of tracers and hydrographic measurements in the vicinity of the turbid-clear water interface, the methodology followed in the data reduction and analysis, the data products and a discussion of the Lagrangian velocity field and mixing processes along/across the interface.

- Engineering Quality Assurance Reports, documenting the checkout procedures followed in the preparation of the current meter moorings prior to deployment and the condition of the instruments and other mooring components upon recovery, and assessing the quality of the data return. Similar reports were also submitted following completion of the surface current experiments.

- First Level Inventory Reports, reporting on an NODC "ROSCOP" form an inventory of all data and samples collected during each cruise or other field work.

- Data Documentation Forms (DDF), supplied to BLM and NODC in support of the processed and validated data collected in the field and transmitted to the Environmental Data Information Service (EDIS).

- Data Format Report, describing a system for cataloging the original data which facilitates rapid withdrawal, use and return of data. It is compatible with NODC formatting.

- Quarterly Progress Reports, which describes all work performed by the Principal Investigators during the preceding quarter, including the data collected, analysis underway or completed, data products and tentative conclusions.

- Quarterly Summary Reports, which summarize all activities performed by SAI and its subcontractors during the previous quarter, including program management, progress in data

management, quality assurance program, interactions with other programs, assessment of the performance to date vs. scheduled contract performance, a summary of all cruises completed, of all analyses underway or completed to date, a summarization of significant findings and any tentative conclusions drawn from the quarterly data.

All these reports are available for consultation by potential users at SAI, Raleigh, N. C. or the BLM office, New Orleans, Louisiana.

The schedule of delivery of the above reports is summarized in Table 2-1.

2.5 COORDINATION WITH OTHER PROGRAMS

A conscious effort has been made to coordinate the activities of the present BLM program with those of studies performed in the same general area of interest under the auspices of BLM or other funding agencies, in order to optimize the amount of information collected in the South Atlantic OCS. The major programs which were run in parallel with at least a portion of the BLM Georgia Embayment Physical Oceanography program are listed hereafter:

- DOE (ex-ERDA) physical, chemical and biological oceanography study, initiated in 1976 and currently on-going.

- BLM Benchmark Program (Texas Instrument), which consisted of seasonal hydrographic, chemical and biological sampling in the Georgia Embayment from February through November, 1977.

- BLM/U.S. Geological Surveys (USGS) sediment transport, bottom and subbottom profiling program, initiated in July 1977 and currently on-going.

- BLM literature survey, performed in 1977-1978 by ERT and consisting of an analysis of physical oceanographic and meteorological information on the continental shelf and Blake Plateau from Cape Hatteras to Cape Canaveral.

- BLM hard bottom study, performed by Continental Shelf Associates, Inc. and initiated in the later part of 1978 and currently underway.

- BLM sponsored National Aeronautics and Space Administration (NASA)-Wallops Island study of sea-surface transport and wave climatology inferred from satellite imagery and theoretical consideration, started in late 1978 and presently ongoing.

Table 2-1. Schedule of deliverables submitted to BLM during first year study.

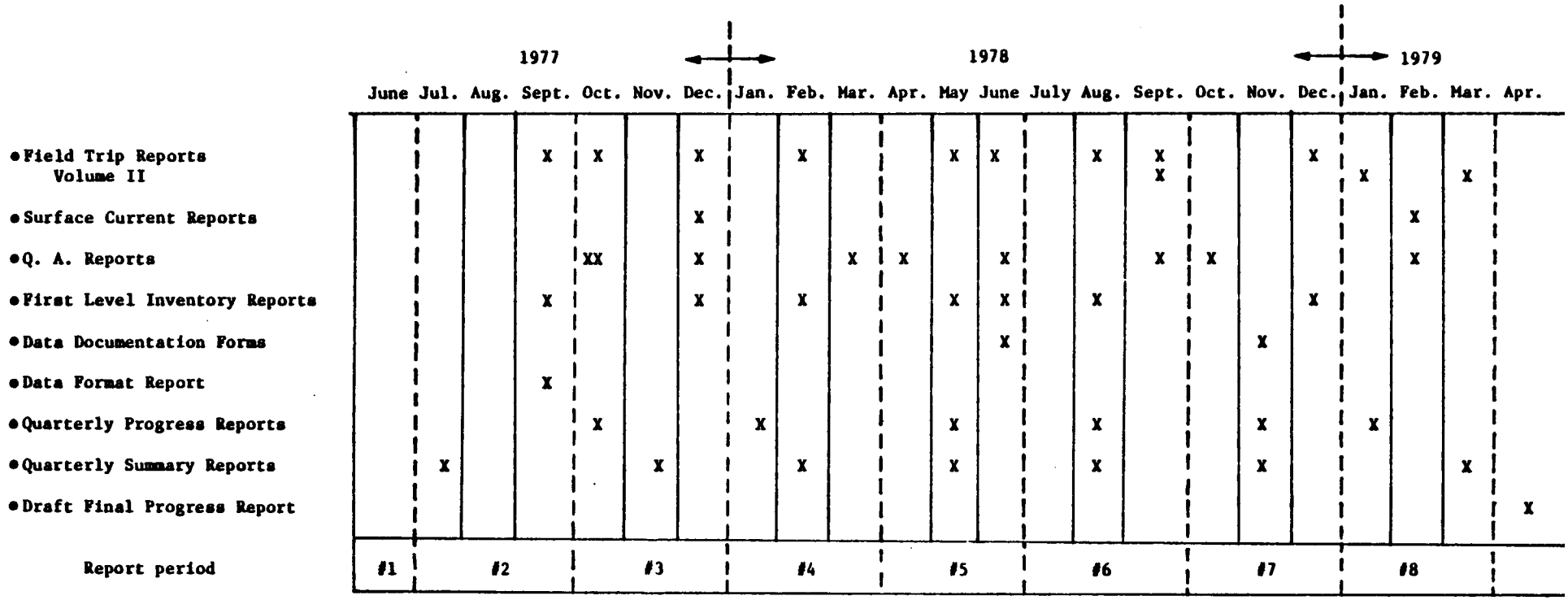

- BLM Cultural Resources Study, performed by SAI and initiated in October 1978 and currently underway.

- BLM-funded assessment of the state-of-the-art in modeling techniques of shelf circulation, managed by Jaycor, Inc.

- BLM-funded National Data Buoy Office (NDBO) program (deployment and operation of three offshore meteorological buoys in the Georgia Embayment).

Of the studies listed above, the most important one in terms of its impact on the design and implementation of the present program is the DOE project. The BLM and DOE programs are complementary, the BLM effort being more and more concentrated in long-term measurements in the northern section of the area of interest, and in seasonal variability, while the DOE project focusses on the southern region and is basically event-oriented. Close cooperation has existed from the very onset of this program between SAI and the principal investigators on the DOE program in the Georgia Embayment (current meter measurements: Dr. Lee, U. M.; hydrography: Dr. Atkinson, Skidaway; frontal study: Dr. Blanton, Skidaway). As a result, the BLM second year effort has been designed to complement the work sponsored by DOE and any overlap between the two projects has been eliminated. Furthermore, cruises are--and will continue to be--shared between the two agencies.

Coordination between SAI and the various P.M.'s and P. I.'s of the programs listed above was ensured through informal meetings and/or phone conversations, through presentations given at Quarterly Meetings organized by Texas Instruments in 1977 and SAI in 1978, and at Manager's Meetings sponsored by BLM in 1977 and early 1978.

Finally, a large volume of data required in support of the present program was provided by other agencies, namely:

- coastal meteorological data, from the National Weather Service (NWS)

- offshore meteorological forecasts, from NWS

- surface wind and sea stale observations from the National Hurricane Center, Miami

- sea level information from the National Ocean Survey (NOS), National Oceanic and Atmospheric Administration (NOAA)

- satellite imagery from National Environmental Satellite Service (NESS)

- analysis of thermal satellite imagery from U.S. Navy (NAVOCEANO)
- quarterly airborn radiation thermometer (ART) flight maps from U.S. Coast Guard.
- LANDSAT satellite data (Band-5) from Earth Resources Observation Systems (EROS), USGS, Sioux Falls, South Dakota
- river discharge data for the Georgia Embayment from USGS, Southeast Regional Water Resources Divison (Atlanta, Ga)
- Savannah Tower wind, currents information, through SKIO

Assistance provided by these agencies in making the above data available to the program is gratefully acknowledged.

III. REVIEW OF EXISTING LITERATURE

A synthesis and analysis of physical oceanographic and meteorological data collected before 1977 on the Continental Shelf and the Blake Plateau from Cape Hatteras to Cape Canaveral was conducted in 1977-1978 by ERT and a consortium of consultants for BLM. The study objectives of this project were to:

- identify and assemble recent oceanographic and meteorological data not available from NODC or National Climatic Center (NCC) for the South Atlantic region;
- organize the data on tapes in formats that are compatible with NODC/NCC and transmit them to NODC/NCC;
- update a previously prepared National Science Foundation (NSF) bibliography for the region;
- use recent and previously catalogued data to describe, display, analyze and interpret oceanographic and meteorological phenomena in the region; and
- make recommendations for future sampling and buoy sites, and programs based on the preceding analyses and a review of raw data and worked samples.

21 data sets that were not available from NODC were identified. They all consisted of physical oceanographic data (11 sets of hydrography, 10 sets of current meter data). 13 of these sets were edited, formatted and submitted to NODC. The South Atlantic OCS portion of the "Bibliography for Physical Dynamics of Continental Margins and Related Topics" (Witte, et al. 1976) was also updated.

A review of the work performed by a number of investigators is presented hereafter, together with an overall tentative picture of current circulation in the South Atlantic Bight, which has emerged from the combination of the first data sets obtained under the auspices of DOE and BLM with the findings of the previous and other current investigations regarding the influence of the Gulf Stream, meteorological forcing and/or water level changes on the continental shelf circulation.

3.1 BUMPUS (1973) CIRCULATION STUDY IN THE SOUTH ATLANTIC BIGHT

Bumpus (1973) reported on the circulation of the shelf from several thousand surface and bottom drifters. The surface drift is northward from Georgia to Cape Hatteras, January through March, though a weak southerly drift appears nearshore off the coast of the Carolinas in February and becomes more discernible in March due to the dynamics

associated with the development of low salinity and low temperature in Virginia coastal waters south of Cape Hatteras to Cape Lookout. In April, the weaker inshore current broadens seaward, though the extent and persistence of any of the flows is speculative in the spring. While July surface flow is northeasterly off North Carolina, a southerly set appears on the Georgian shelf. The Georgian condition extends to the Carolinas in August and September, though northerly reversals are not unusual along the Carolina Capes. In the fall, the southerly flow boundary migrates south to Georgia, and northerly flow begins to dominate along the Carolinas.

Bottom drifter recoveries indicate southerly and shoreward nearshore flow near the Carolina Capes and northerly set from mid-shelf seaward. Recoveries on the Georgian shelf are too sparse to indicate trends. Bumpus suggests that the Gulf Stream intrusions are reflected in the shoreward drifts from Georgia to Cape Hatteras, and that wind driven modification of the circulation exists on the Carolina shelf and to a lesser degree on the Georgia shelf.

3.2 STUDIES OF GULF STREAM INFLUENCE ON THE SOUTH ATLANTIC BIGHT SHELF CIRCULATION

The influence of the western boundary current, the Gulf Stream, which persists generally along the seaward edge of the continental margin between Capes Hatteras and Canaveral, upon the continental shelf between these end points is considerable in terms of physical, chemical and biological aspects of the oceanography of the region. This Gulf Stream influence has been the object of several investigations hereafter summarized by Dr. L. Pietrafesa.

A "Multiple Ship Survey" of 1950, reported on by Fuglister and Worthington (1951), was the first large scale, multi-vessel study of Gulf Stream fluctuations. The name "meanders" was introduced for the slow undulations observed in the location and structure of the Gulf Stream downstream of Cape Hatteras.

Several studies have provided evidence of eddying, entrainment, and intrusion of Gulf Stream and shelf waters. Von Arx, Bumpus, and Richardson (1955) found northeasterly oriented filaments of Gulf Stream water along the shelf break with dimensions of ten to one hundred km. These "shingles" could be mapped by the filaments in the thermal, velocity, and water type properties of the surface; the subsurface isothermal slopes, or patterns, remained unknown at that time.

During a 28-day study in May and June, 1958, Webster (1961a) made 120 consecutive crossings of the Gulf Stream axis off Onslow Bay, North Carolina. Measurements of surface velocity and salinity were performed, and bathythermograph temperatures were taken half-hourly to a depth of 200 m. Webster found that the axis of the current

meandered laterally, with a peak displacement of about 10 km. He found a strong correlation between the axis offshore distance and the alongshore surface atmospheric pressure gradient, when the latter was lagged about four days. The alongshore pressure gradient was presumed to be representative of the offshore geostrophic wind component over Onslow Bay. This implies that the Gulf Stream may affect offshore geostrophic winds. Correlation with the pressure gradient perpendicular to the current axis was not found. The dominant period of the axis meanders was about seven days; Webster estimated the alongstream meander scale to be about 100 km. Webster thus noted a strong apparent correlation with the onshore-offshore wind component, but he estimated the wind effect to be one or two orders of magnitude too weak to be the source of energy for the meanders. Three regions of local mechanical energy transfer between eddies and the mean motion can be noted. Webster (1961b) thus demonstrated that fluctuations on the 1-day to 1-week time scale were locally deriving mechanical energy from shear of the mean current on the surface at the shelf break. In the cyclonic shear zone, both the eddies and the mean flow were losing mechanical energy. On the anticyclonic side, the eddies were driving the mean flow. On the cross-stream average from Miami to Onslow Bay, he found a net flux to the mean Gulf Stream which could rapidly double the average surface speed of the Florida Current (i.e. the portion of the Gulf Stream confined by the Bahama Banks and the east coast of Florida). Such an acceleration is not observed; work of opposite sign is done by the pressure gradients near the surface. Sturges (1974) has made estimates of the mean downstream pressure gradient from coastal sea levels along the South Atlantic Bight and the Florida Straits; and he has found it to be large enough to provide the energy flux, at least at the shelf break, to balance the work done on the eddies. Following Webster's analysis, Oort (1964), using the thermal flux data corresponding to Webster's momentum flux data, found a counter-gradient heat flux in the surface layer which would sharpen the surface front. He also raised the question of a lower layer source for heat flux and intense potential energy release. Blanton (1971) combined a few short current meter records at the shelf break with hydrographic sections and interpreted the results two-dimensionally. He found near-bottom intrusions of Gulf Stream water, which had been suggested by Bumpus (1954), followed by vertical mixing with shelf waters and subsequent offshore flow of near-surface shelf water, which would give a counter-gradient heat flux near the surface. Schmitz and Niiler (1969) analyzed a new data set, i.e., dropsonde data, in an analogous fashion. They concluded that there existed negligible net transfer of kinetic energy between the eddies and the mean motion in the surface layer on the cross-stream average; instead, an internal redistribution of kinetic energy was occurring, as described above. Schmitz (1969) concluded that the interior of the Florida Current off Miami was essentially in inertial balance; Niiler (1975) found that the inertial balance is slowly eroded along the shelf break, and there is a vorticity flux into the Gulf Stream from the shelf.

Hansen (1970) traced the position of the Gulf Stream thermal front off North Carolina for twelve consecutive months in 1965 and 1966. He summarized the observed meanders as wave patterns of 200 to 400 km wave-length moving eastward with speeds of about 10 cm.s^{-1}.

Several theoretical accounts have been attempted for the meandering, eddying motion of the Florida Current/continental shelf system. Niiler and Mysak (1971) considered subinertial waves in a barotropic Gulf Stream with horizontal shear and variable cross-stream bottom topography; i.e., a model with potential vorticity gradients commensurate with the magnitude and form of the depth-integrated Florida Current was examined. They concluded that long waves could propagate north and south on the sheared current and that short waves could propagate northward and were unstable. The most unstable waves had a period of about 10 days and wave lengths of 150 km in the vicinity of the Blake Plateau (South Atlantic Bight). Orlanski (1969) considered a model with two "active" layers and bottom topography and found baroclinic instabilities to be possible for a parametric range observed in the South Atlantic Bight. The most unstable waves had a period of about 10 days and wave lengths of about 220 km. Orlanski also noted the need for observations through the water column to determine the various energy exchanges. Orlanski and Cox (1973) carried out analogous calculations for a continuously stratified system, with similar results. Additionally, finite-amplitude effects reduced the growth rate; maximum amplitudes were reached in about one week.

Richardson, Schmitz, and Niiler (1969) show mean velocity sections for the Florida Current, two of which are located off the South Atlantic Bight. The mean Florida Current extends over the relatively shallow shelf break (50 to 100 m deep); the bulk of the Florida Current lies over a deep shelf (800 m deep). Surface velocities up to 100 cm.s^{-1} occur over the shelf break. From one-third to half of the total volume transport occurs in the upper 200 m of the water column; thus, the outer shelf spans much of the Florida Current. Schmitz and Richardson (1968) found that the transport fluctuations were approximately one-third of the mean transport, 75% of the transport fluctuations were tidal, and no more than 10% occurred at periods greater than one day. Niiler and Richardson (1973) made a more precise estimate of the seasonal variation, finding a prominent maximum in summer (June). They concluded that the seasonal variations accounted for 45% of the transport variance.

De Szoeke (1975) found a bottom slope-induced hybrid instability which arises from an interaction between a topographically trapped baroclinic wave and a "thermal" baroclinic Rossby wave. De Szoeke states that the hybrid instability is not "fundamental in nature," but rather serves to redistribute the energy from the classical baroclinic energy source (cf. Pedlosky, 1964). De Szoeke's appli-

cation of the hybrid mechanism to the Florida Current neglected the importance of horizontal velocity shear to the overall vorticity dynamics.

Saltzman and Tang (1975) used an analytical model to demonstrate how second-order, nongeostrophic effects can modify a two-layer baroclinic wave system that grows exponentially from a small perturbation in a uniform zonal ocean current. Many of the asymmetric features characteristic of meandering ocean currents are shown to develop, including fronts and cutoff cyclonic cold pools to the south and anticyclonic warm pools to the north of the axis of the mean current. The implication is that all of these features can be viewed as being the simultaneous consequence of baroclinic instability of a broader, more uniform current that might tend to be forced externally by the wind stress thermohaline processes.

The Very-High-Resolution Radiometer on the NOAA-2 satellite has recently obtained imagery in the visible channel over a major portion of the coastal waters off the eastern seaboard of the United States. Strong and DeRycke (1973) indicated an abrupt change in surface roughness at the shoreward edge of the Gulf Stream Current from Florida to Cape Hatteras that could result from the opposition of waves propagating against the flow of the Gulf Stream. Herein, DeRycke, Rao (1973) pointed out an apparent relationship between the occurrence of eddies along the western side of the Gulf Stream and strong westerly winds.

Satellite images (Legeckis, 1975; Stumpf and Rao, 1975) suggest that the eddies evolve from growing instabilities (Florida Current meander), which may initially be wind induced. They manifest themselves as warm, southward-oriented, tongue-like extrusions of Florida Current water onto the shelf, similar to the shingle structure observed by Von Arx, Bumpus and Richardson (1955). In the Florida Straits they are confined by the narrow shelf coastal boundary and observed diameters range from 10 to 30 km. Eddy vertical extent is approximately 200 m. Lee (1975) concludes that spin-off eddies are a dominant mechanism for shelf water mass exchange off southeast Florida and estimates the shelf residence time as 1 week due to eddy water renewal. Singer, et al. (1977) and Blanton and Pietrafesa (1978) have essentially concluded that the similar flushing mechanism is at work throughout the whole of the South Atlantic Bight. Satellite imagery show that eddy-like excursions are a consistent feature along the shelf break of the SAB and appear to grow to much larger proportions.

Near the shelf break (50 to 75 m isobaths) Gulf Stream frontal instability processes, such as wave-like meanders and spin-off eddies become a significant contributor to current variability and water mass exchange (Lee, 1975; Lee and Mayer, 1977: Pietrafesa, 1979). The Gulf Stream surface front may meander about 10 to 25 km in the

east-west direction with a wave length of 100 to 200 km. These meanders are known to grow at times into the tongue-like disturbances. The cyclonic circulation in the eddies transports shelf water offshore in the southern region of the vorticity, which provides a mechanism for rapid water exchange. It is thus appreciated that eddy-like events displace large volumes of shelf water with onshore flows of Gulf Stream waters at the surface and bottom and offshore shelf water displacement and subsequent entrainment into the slope waters.

Flushing frequency is thought to tie directly to the frequency with which meanders and eddy events occur. Conventional wisdom is that meanders and eddy events occur at frequencies between 0.1 and 0.2 cycles per day, figures which embrace the pioneering study by Webster (1961a), as well as studies of sea level by Mysak and Hamon (1969), and present current studies. It should be pointed out that studies have yet to unambiguously link onshore/offshore flow cycles on the North Carolina Shelf with meanders or accelerations of the Gulf Stream. From the Lee and Pietrafesa DOE data sets, it is obvious that large amplitude current fluctuations with periods ranging from several days to several weeks are common features on the continental shelfs off both Georgia and North Carolina. These current meter data (Pietrafesa, et al., 1978b, 1978c) indicate that cycles in onshore/offshore flow often precede local wind events occurring more or less simultaneously at Cape Hatteras and Wilmington, North Carolina (separation-distance about 120 km). Perturbations in the Gulf Stream represent a mechanism which could be causing those flow cycles in mid-shelf that seem poorly correlated with local winds.

Blanton and Pietrafesa (1978) considered data covering 42 days collected during 1975 by Pietrafesa (1978b). Over this period, eight cycles of onshore/offshore flow occurred, about one cycle each 5 days. Hydrographic data obtained at the time the moorings were set showed Onslow Bay to be highly stratified in the vertical with a well mixed surface layer of about 27.5°C and salinities less than 35.5°/oo over a well mixed bottom layer whose temperature ranged from 25.5°C less than 20 km offshore to less than 22.5°C near the shelf break. Salinities were everywhere greater than 36°/oo in the lower layer. The bottom meters were within this bottom layer. Temperature and salinity (Atkinson, et al., 1976) confirm that the onshore/offshore flow cycles in this bottom layer transported water of Gulf Stream origin. If these events occur on the order of 5 days then approximately 2 months are required to flush a Carolina Cape.

This flushing rate of 2 months can be compared with other calculations for the shelf south of Cape Hatteras. Atkinson, Blanton and Haines (1977) calculated an overall flushing rate of 2.7 months based on the freshwater distribution and input to the Georgia Bight area. In that paper, it was shown that this rate was remarkedly constant from season to season, and a Gulf Stream entrainment model was

proposed to account for the rate at which freshwater could be removed from the Continental Shelf. Using typical freshwater filament dimensions and salinities observed by satellite and hydrographic cruises and assuming that the stream entrains one of these filaments each five days, it is speculated that about 2 to 3 months are required to remove the freshwater observed on the Continental Shelf in the South Atlantic Bight.

A significant feature within the surface thermal (VHRR) satellite imagery being collected and processed by NOAA/NESS is the quasi-permanent northward to eastward to northward large scale meander of the relatively warm Gulf Stream water away from the coast between Savannah, Ga. to Charleston, S.C. to Cape Fear, N.C. This feature has become known as the "Charleston Bump" and seems to be evident, in varying degrees, during all of the seasons. It is this persistence of the feature, which is both surface and subsurface in nature, which led Pietrafesa, Atkinson and Blanton (1978) to speculate that the feature was topographically induced, since topographic variations occur within the isobaths along the continental slope and are suggestive of a topographically generated wave or series of waves, called Topographic Rossby Waves which "stand" downstream of the "Bump" to Cape Hatteras.

Rooney, Janowitz and Pietrafesa (1978) have computed the characteristics of a downstream standing Topographic Rossby Wave (TRW) generated by a bump sitting on a continental slope below a barotropic jet on a B-plane. The basic questions addressed were: could the topographic feature known as the Charleston bump induce a "lee-wave" or downstream standing TRW? If so, do these waves, which would vary as the mean current varies, bear a relationship to the quasi-permanent meander in the Gulf Stream offshore of South Carolina? If so, is the surface thermal imagery, as well as the subsurface hydrography downstream of the "Bump" a resultant feature of these TRW's? If so, then are the eddy events observed in the VHRR imagery, hydrographic and moored current, temperature and conductivity sensors a resultant of TRW's presenting a mechanism wherein the baroclinic jet (i.e. the Gulf Stream) undergoes an instability which grows in time and space, becomes unstable and spins off an eddy? The mean current upstream of the bump fluctuates in time and space and as a result, even this simple barotropic model results in a superposition of standing lee waves, which differ in wave characteristics from one another as a function of temporal fluctuations in the mean current. Pietrafesa, Atkinson and Blanton showed, observationally, that the Gulf Stream Front was deflected to the east, offshore, a distance of 60-110 km approximately 70% of the time over a two year period and Rooney, Janowitz and Pietrafesa proved that a barotropic jet flowing along the continental margin of the SAB would be deflected 100 km offshore by an idealized bump sitting atop a continental slope, and furthermore that a TRW of wavelength 150 km would be generated downstream of the bump.

Since the quasi-permanent offshore deflection of the Gulf Stream Front occurs directly offshore of the BLM Long Term mooring site, this location becomes anomalous in the sense that the Gulf Stream is farther offshore at this latitude than at any other location between Capes Canaveral and Hatteras. The implications of this fact remain unknown at this stage.

3.3 STUDIES OF SHELF RESPONSE TO METEOROLOGICAL FORCING AND SEA LEVEL-COASTAL METEOROLOGY RELATIONSHIP

Another line of investigation has pursued the influence of meteorologic forcing, albeit in a less systematic manner. In the summer season, winds with northward (alongshore) components are common and often persistent. Green (1944) and Taylor and Steward (1959) reported evidence for summer coastal up-welling off northeast North Carolina. Bumpus (1973) then inferred that wind-driven up-welling probably occurred throughout the South Atlantic Bight in the summer season. Wunsch, et al. (1969) examined many years of sea level and meteorological data from the Florida Straits region and found no evidence for significant, systematic meteorological influence on the Florida Current.

In contrast, Mysak and Hamon (1969) found strong evidence of a nonbarometric response of sea level from the North Carolina coast, especially at periods of 3 to 10 days. The phase relationships were consistent with southward propagation of barotropic continental shelf waves with seasonal modulation of the phase speed due to seasonal variations of the Florida Current. They also noted a broad peak in the sea level spectrum centered on a period of about 15 days. The work of Mooers and Brooks (1976) shows energetic periods on time scales of two days to two weeks in internal (temperature) and external (sea level) fields of the Florida Straits. These are highly coherent with the local wind stress.

Recently, the relationships between sea-level and atmospheric variability have been of considerable interest (Pietrafesa, et al., 1978a, Brooks, 1978, Chao and Pietrafesa, 1979). The literature cited suggests that variations in atmospheric pressure, wind speed and direction, currents and subinertial phenomena, such as shelf waves, can significantly affect the coastal sea level signature. Sea level response to variations in coastal meteorological pressure fields can be expressed in terms of a factor which is frequency dependent. It can be best appreciated as the relationship between the input to a filter and the subsequent convolved output. Generally, a one cm depression (rise) in sea level per one mb increase (decrease) in barometric pressure is observed.

While the evidence for the existence of continental shelf waves in the area of interest has been at times inferred from the cross-statistical analyses of tidal and meteorological data, there have

been few actual current meter observations made at sufficiently extensive alongshore stations to corroborate the passage of these phenomena. The ongoing DOE and BLM current meter studies between Cape Lookout and Savannah by Dr. T. N. Lee (of the University of Miami) and Dr. L. J. Pietrafesa (of North Carolina State University) could confirm or refute the Mysak and Hamon (1969) contention of their existence.

The work of Pietrafesa, et al. (1978a) provides some further insights into the relationship between sea level and coastal meteorology at Charleston. Hourly values of sea level height for 1974 were obtained from the NOS, NOAA, Rockville, Maryland, for stations at Beaufort (BFT), Frying Pan Shoals (FPS) and Wilmington (WIL), North Carolina, and at Charleston (CHS), South Carolina. Three-hourly values of surface wind speed, wind direction, and atmospheric pressure for 1974 were obtained from the National Climatic Center, NOAA, Asheville, North Carolina for stations at Cape Hatteras, N. C., (HAT), Wilmington, N. C. (WIL), Charleston, S. C. (CHS) and Savannah, Ga. (SAV).

The sea level data were low-pass filtered using the Lanczos filter taper to attenuate the daily and semi-daily tides and inertial fluctuations (the inertial period at Charleston is 22.04_6 h). Attenuation at diurnal and higher frequencies is greater than 10^6 and 10^5 respectively. After filtering, the sea level data were resampled at 8- and 6-h intervals, for the two separate filtering intervals, respectively.

The radial distances between these stations are approximately: SAV-CHS/130 km; SAV-WIL/380 km; SAV-BFT/480 km; SAV-HAT/620 km; CHS-WIL/240 km; CHS-BFT/340 km; CHS-HAT/480 km; WIL-BFT/100 km; WIL-HAT/240 km; and BFT-HAT/140 km.

Three-hourly wind stress vector components in a right-handed rotated coordinate system, such that the alongshore component is 55.6° East of North, were computed from the raw wind speed and direction data, with the positive vector sense in the direction toward which the wind blows. The stress components were computed using a quadratic drag law with the drag coefficient $C_D = 1.5 \times 10^{-3}$ (Pond, 1975). The wind stress components and atmospheric pressure time series were low-pass filtered, using the same Lanczos filter. The atmospheric data were then subsampled at 9-h intervals and linearly interpolated to 8- and 6-h intervals to be commensurate with the respective sea level data. According to Pietrafesa, et al. (1978a), the filtered atmospheric pressure time series indicates that the SAV, CHS, WIL, and HAT stations are well correlated over most of the large and even small amplitude variations which is indicative of the high degree of horizontal coherence over length scales of the pressure field much greater than the SAV-HAT radial separation distance which is 620 km. The large horizontal coherence distance presumably reflects the

synoptic meteorological scales associated with mid-latitude atmospheric disturbances, especially during the fall, winter, spring periods. The alongshore wind stress components also show essential correlation over the SAV-HAT separation distance, but variations in intensity and structure between stations are more apparent than in the pressure time series. Vector representations, or stacks of stick diagrams of the wind stress during passage of cold front events indicate the clockwise rotation usually associated with the passage of such an event over the station(s). Here it is noted that HAT typically shows the largest stress magnitudes. Alongshore winds tend to dominate both in magnitude and duration relative to the cross-shelf components. Wind stress reversals, noted at all of the meteorological stations, occurred on time scales of several days to several weeks, which is the typical periods of forcing within the atmospheric stress continuum.

Kinetic Energy Density (KED) spectra of alongshelf and transshelf wind components at CHS (Pietrafesa, et al. 1978c) indicate that within the temporal period 2-14 days, the energy density rises approximately as the frequency to the minus three halves power, which is consistent with the findings of Oort and Taylor (1969) and Cragg and Sturges (1974) for other coastal regions and is attributed to the passages of cyclones and anticyclones. The KED curve flattens out at periods in excess of 14 days. Within the temporal ranges of interest of the BLM continental shelf study, (from the order of several days to a month), alongshore winds show a remarkably high degree of visual correlation, save for occasional several day departures, in the various station time series. One can observe similarly good visual correlation between transself wind components between station pairs over the whole of the radial separation distance with occasional departures, in the same figure series as above. Over the entire frequency range of 0.5-0.05 cpd, alongshore winds are more energetic than cross-shelf winds. There was a decrease in coherency between station pairs at a rate of 0.1 per 150 km increase in distance. Pietrafesa, et al. (1978a) thus concluded that winds recorded at any one of the coastal stations could, at least qualitatively, be representative of the wind fields at any of the other stations, with appropriate reservation. The adequacy of representation is an event-, season- or location-sensitive variable, but for events within the frequency band 0.3 to 0.05 cpd the contention is not without evidential basis. What is suggested herein is that the divergence of the alongshore wind stress may not be large, and furthermore that possibly the curl of the cross-shore wind stress may not be large but the data indicates little of a definitive nature about the curl of $\tau^{(y)}$ or the divergence of $\tau^{(x)}$ and moreover nothing about the offshore wind field structure, which is the actual mechanical forcing function.

In the Pietrafesa, et al. report, 40-h low-passed atmospheric pressure analyzed from the meteorological stations indicated a high degree of coherence with daily pressures rarely differing by more

than several millibars between stations. The phase shifts are nearly zero at all frequencies save for shifts of the order of 0-20 degrees over radial distances the order of 100-650 kms with the southerly meteorological stations typically leading the more northerly stations for the entire separate series lengths of years 1974 and 1975. It certainly appears, herein, from the cross-correlations between station pairs that the pressure spectrum at any individual station is reasonably representative of that at any other with minor adjustments in phase as a function of the pairing and the frequency. Coherence squared (C^2) is typically in excess of 0.9 over station radial separation distances the order of 200 km and drops off from 0.95 to 0.5 at distances in excess of 400 km in the 0.1-0.5 cpd band.

Among factors which significantly affect sea level, particular note in the Pietrafesa report was made to the variations in atmospheric pressure, atmospheric winds, oceanic currents and long-shelf wave phenomena. The response of the level of the sea surface to varying atmospheric pressure is more correctly expressed in terms of a frequency dependent barometric factor, i.e., a transfer function for the pressure and sea level system. Herein, the sea level data was "adjusted" (as well as left "unadjusted") for the so-called "Barometric effect." For frequencies below 1 cpd, the sea surface responds to changes in atmospheric pressure in a reasonably regular, nearly instantaneous fashion. The adjustment suggested over nearly the entire frequency range of interest in this study (Mysak and Hamon, 1969) for sea level fluctuations due to varying barometric pressure is about 1.0 $cm.mb^{-1}$, i.e., a one millibar increase (decrease) in pressure depresses (elevates) the sea surface approximately 1 centimeter.

Remarkably high C^2 results between sea level and alongshore winds, especially at frequencies below 0.35 cpd, over the 1974 and 1975 yearly series, as well as the 4 month series blocks, April-July and Sept.-Dec., 1974, considered in the report. The cross-coast wind vs. sea level comparisons, at co-incident or nearby sites, indicate more selective coherence bands. Some of the potential hazards which were noted in the Pietrafesa report were that the Wilmington tide gage is located 27 miles from the mouth of the Cape Fear River Estuary, a tidally influenced coastal plain estuary which undoubtedly has a sea level response signature very different from that of an open, coastal station. Consequently, any intercomparisons of sea level at WIL and any other station, save for one at the mouth or between, in the Cape Fear River Estuary, as was done by Brooks (1978) to confirm the existence and southerly propagation of continental shelf waves, must be done so with appropriate reservation.

Recently, Chao and Pietrafesa (1979) reviewed the shelf wave literature and have determined that the phenomena are probably not existent on the coast of the Carolinas, or if these waves do exist, they are of minor importance. These authors considered subtidal sea

level fluctuations of four tide-gage stations along the Carolina Capes coast (Beaufort, Wilmington, Cape Fear and Charleston) and their relations to atmospheric forcing. Their analyses of cross spectra of barometrically adjusted sea level between station pairs negate earlier concepts of southward propagating shelf wave. The cross spectra of alongshore wind stress versus adjusted sea level fluctuations indicate that there is a retardation of set up/down of 6 to 12 h at the Cape Fear coastal station (Wilmington). Therefore, these authors found that earlier findings (Mysak and Hamon, 1969; Brooks, 1978) of southward phase propagation in Onslow Bay were most likely the consequence of the retardation of set up/down at the Cape Fear, rather than of a continental shelf wave. Further detailed analysis shows that both the direct frictional set up/down and Ekman set up/down were present at Carolina coastal stations, while the former was more significant near the Cape Fear due to the excursion of shoals there and provided the right mechanism for the retardation of set up/down as observed. This paper also points out that, in cases where the amplitude of set up at the coast is comparable to sea level variation due to shelf waves, inferences of wave-length and phase speed etc. based on the use of the cross phase between two time series could be misleading.

3.4 CLIMATOLOGY

The atmospheric climate overlying the South Atlantic Bight is determined by both polar and tropical marine air masses, resulting in a "temperate rainy" climate with mild winters, long hot summers, and adequate moisture in all season, according to Koppen (see Pettersen, 1969). The north-south surface temperature gradient over the eastern U.S. reaches a seasonal maximum in late winter of approximately 1.5°C per degree latitude, which is about four times the summer gradient. The polar front, the actual zone of maximum temperature contrast which separates the colder continental air from the warmer, more moist tropical air, both intensifies and shifts southward in the winter to near Cape Hatteras, resulting in a region of intense cyclogenesis stretching along the eastern U.S. seaboard from Florida towards northern Europe. Most of the intense extratropical lows develop over the southeast U.S. but show their greatest growth as the storms move offshore over the warmer ocean, especially in the neighborhood of the Gulf Stream. The mean speed of these synoptic-scale cyclones is 5-7 $m.s^{-1}$ (10-15 kts), with less than 20% of the storms moving at speeds greater than 12.5 $m.s^{-1}$ (25 kts) (NOAA, 1970).

These wintertime extratropical cyclones (and to a lesser extent the accompanying anticyclones) can affect the coastal oceanic circulation in a number of direct and indirect ways. The surface pressure and wind stress patterns for a mature low can be coherent over 600 kms, can persist for 3 to 4 days, and can directly drive a large-scale coastal current. Intense lows are frequently accompanied by trailing outbreaks of very cold polar air, causing sharp cold fronts which

move southeastward over the southeastern states; and they can bring freezing weather and strong winds as far south as Florida. Smaller scale waves can develop along the polar front near the southeastern coast which exhibit highly variable stress and precipitation patterns on the subsynoptic (10-100 km) scale (Bosart, Vando, and Helsdon, 1972; Bosart, 1973). Bosart and Cussen (1973) have found surface pressure fluctuations of 4-5 mb amplitude along the coast and have attributed these perturbations to generation of atmospheric gravity wave created during frontogenesis (frontogenesis being a process by which atmospheric fronts or discontinuities are produced). Perhaps the most intense atmospheric pressure and surface wind stress patterns are associated with the large-scale tropical storms and hurricanes which develop primarily in August-October and occasionally migrate along the Southeast coast, visiting the Carolinian coast with a frequency of about one severe storm every two years (U.S. Navy, 1970). The meteorological forcing on the Carolina Shelf is thus dominated in winter by transient extratropical storms with considerable variability in strength, structure, and persistence of the important meteorological fields. The predominant winds are northwesterly to northeasterly, with some 30% of the observed speeds reported to NOAA (1970) exceeding 8 $m.s^{-1}$ (16 kts).

The summer meteorological regime along the Carolina coast is controlled by a strong weakening of the polar front and an intensification of the Azores-Bermuda high. The region of most intense cyclogenesis has shifted north of Cape Hatteras and while some active frontogenesis and cyclogenesis continues over the Southeast U.S. shelf, the atmospheric variability there is decreased in summer. The predominant winds are lighter and southerly to southwesterly. Some 60% of the NOAA-collected surface observations (NOAA, 1970) indicate wind speeds of less than 5 $m.s^{-1}$ (10 kts), while 15% indicate wind speeds greater than 8 $m.s^{-1}$ (16 kts). The standard deviation of the surface pressure shows both a strong seasonal fluctuation and a steady decrease with decreasing latitude south of Cape Hatteras (U.S. Navy, 1970). The standard deviation of the surface pressure at Charleston, S.C., is about one-half its mean winter value of 7 mb. Ward (1925) and his more recent co-workers suggest that a transition from a northern cyclonic-controlled climate to a more Gulf-like climate with higher temperatures and less dramatic weather occurs along the Southeast shelf near the latitude of Charleston.

The recent work of Saunders (1977) suggest that there is a great deal of offshore as well as alongshore structure to the mean wind fields which gives rise to the need for meteorological buoys which would allow for an assessment of the curl and divergence of the wind field as well as a mass and heat air/sea interaction evaluation. Saunders also points out an offshore wind stress maximum which occurs during early fall; he finds no apparent reason for this but it seems likely

that the air-sea temperature gradients may be largest during this time of the year, thereby increasing the drag coefficient and subsequently the relative stress field.

On localized scales, an appreciable diurnal sea/land breeze, as well as an apparent semi-diurnal harmonic thereof, are in evidence along the North Carolina coast (Pietrafesa, et al., 1978a) and may be evident at Charleston as well.

3.5 TENTATIVE DESCRIPTION OF CURRENT CIRCULATION IN THE SOUTH ATLANTIC BIGHT

A systematic effort was initiated by DOE in 1976 to gain a better understanding of the shelf circulation in the South Atlantic Bight, through intensive current meter, hydrographic, surface winds, water level and other physical, chemical and biological measurements. This study was complemented, shortly thereafter, by the present BLM program. Analysis of the data collected in the early stage of these projects, combined with the findings of the investigators referenced above has resulted in a tentative picture of current circulation in the SAB, presented hereafter.

The SAB can be divided into two shelf regimes: the Georgia Embayment, with a relatively wide and shallow shelf stretching uniformly from Cape Canaveral to Cape Romain; and the Carolina Capes, characterized by cuspate-shaped embayments decreasing in width from Cape Romain to Cape Hatteras. Shelf circulation results from the complex interaction of tidal, density, wind and offshore current (Gulf Stream) forcing. Response of the shelf waters to forcing can vary on time scales ranging from an hour to a year and can also vary with location on the shelf.

Fresh water enters the Georgia Embayment through a number of rivers along the western boundary. This runoff reaches a peak in late spring or early summer producing a near-shore band of low salinity water that tends to follow the 10-m bottom contour. The presence of the low salinity water makes the waters of the inner shelf less dense than the outer shelf. This density difference in turn tends to stratify the shelf vertically with less dense water moving offshore in the surface layer and heavier (saltier and colder) subsurface Gulf Stream waters moving onshore across the shelf near the bottom. Thus, during the summer, the vertically stratified shelf waters tend to drive the mean shelf current toward the south parallel to the bottom contour. Accompanying the development of summer stratification is an upwelling of nutrient-rich subsurface Gulf Stream water onto the shelf to serve as a food source for coastal marine life. Vertical stratification of the Carolina Capes shelf water is also a summer characteristic. However, because of the lack of river discharge, the stratification develops from atmospheric heating of the shallow near-shore waters, which warms the inner shelf relative to the outer

shelf, making them less dense and eventually stratifying the shelf. A summer mean flow to the south can also develop but it is probably not as strong as in the Georgia Embayment, because of the lesser amount of fresh water within the inner shelf.

During the winter, the combination of increased wind stirring during the passage of cold fronts and cyclones and the decrease in atmospheric temperatures tends to mix vertically the waters of both shelf regimes, producing colder water near-shore, which warms with nearness to the Gulf Stream and is nearly isothermal in the vertical. River runoff is at a minimum during this time in the Georgia Embayment so the cooling effect tends to make the near-shore waters more dense than the outer shelf waters, which in turn drives a weak mean current toward the north, following the bottom contours. A similar process occurs in the Carolina Capes shelf water; however, it is complicated by the transient occurrence of low salinity Virginia coastal water, which is driven around Cape Hatteras in the near-shore region during times of strong N to NE winds in winter storms. These low salinity waters can freshen the inner shelf, thus combatting the cooling effect on increasing inner shelf water density. In addition, subsurface intrusions of colder (more dense) Gulf Stream water can occur along the shelf bottom, which, combined with the presence of low salinity water in the inner shelf, can produce a two-cell vertical circulation with onshore flow near the surface and bottom, and offshore flow in the interior.

Despite many differences in the two shelf regimes, the fluctuating current field was found to be remarkably similar. By far, the greatest current variations occurred with time scales ranging from tidal to two weeks. Current oscillations in the outer shelf (near the shelf break or continental shelf edge) generally tended to be primarily produced by Gulf Stream disturbances, such as horizontal east-west meanders and eddies. Tide- and wind-induced current deviations were of lesser importance here. However, as the distance from the shelf break increased and the water depths decreased, the Gulf Stream influences diminished and tide- and wind-generated current variations began to dominate. From about mid-shelf to the near-shore waters, tide- and wind-generated currents tended to produce most of the current variations; tides were more influential on transshelf motions, and winds created most of the along-shelf fluctuations. These findings create a favorable situation for applying predictive modeling to mid-to-inter-shelf regions.

Tidal forcing in both shelf regions is caused primarily by the semi-diurnal lunar astronomical tide. The resulting tidal currents have a period of 12.4 h and have slightly larger speeds in the onshore-offshore direction (10 to 15 $cm.s^{-1}$. Also, since the shelf is wider in the Georgia Embayment, tidal currents will be slightly greater (approximately 10 to 15 $cm.s^{-1}$). This effect is also seen in

the tidal range of sea level, where along the coast of Georgia, the tidal range is about 1.8 to 2.4 m (6 to 8 ft) and along North Carolina, 1 to 1.2 m (3 to 4 ft).

Wind forcing of shelf water is most active during the winter months of November through March with the passage of cold fronts and cyclones. These events occur on time scales of two days to two weeks, which are also the time scales of the largest subtidal (occuring on time scales longer than 24 h) current and coastal sea-level fluctuations. Cold fronts tend to move southeasterly across the shelf producing a clockwise rotation and intensification of the winds at a given point on the shelf. A similar variation is normally observed in the shelf currents at the mid-to-inner-shelf locations. The effect is more pronounced in the along-shelf direction, since current fluctuations with periods longer than the tidal periods tend to be mainly in the along-shelf direction in shallow water. Also, since the weather systems have spatial dimensions of hundreds to thousands of kilometres (km), the wind forcing can act over large sections of the shelf nearly simultaneously, so that the shelf waters tend to move as a unit. This effect is also seen in coastal sea-level data. Winds to the south can generate an onshore surface current, rise of sea level at the coast, offshore near-bottom flow and a southward current in the shelf water interior. Winds to the north produce the opposite effect; offshore surface current, sea level decline at the coast, onshore bottom flow and northward currents in the shelf's interior. Along the outer shelf (near the shelf break) northward winds can produce an onshore near-bottom intrusion of subsurface, nutrient-rich, cool Gulf Stream water. These waters can mix with the shelf waters in the euphotic zone to serve as a basic food source for biological food chains. Wind effects appear to be similar in both the Carolina Capes and Georgia Embayment. However, in the Capes region, the curvature of the bottom contours may act to steer upwelled waters along the contours, causing freshly upwelled waters to enter the Onslow Bay in the southeast section and leave in the northeast. Also, wind systems such as winter lows tend to travel northward along or trailing a cold front. These systems break out in the coastal waters in the area of Georgia or North Florida and begin to intensify as they travel north, at times becoming major cyclones off the northeastern states. Thus their effect on shelf waters of the northern SAB may be greater than in the south.

Wind events may also generate horizontal east-west meanders of the western edge of the Gulf Stream. The western boundary of the Gulf Stream is identified by large increases in northward current speed and temperature as the Gulf Stream edge is crossed from the west. This feature is known as the "Gulf Stream Front." Satellite-derived pictures of sea-surface temperature show the east-west meander of the front. They also reveal that the meanders are not stationary, but tend to travel along the front toward the north and grow in size, eventually evolving into spin-off eddies.

The formation of Gulf Stream meanders and the eventual evolution into eddies takes place in a random fashion every two days to two weeks all along the shelf break from Florida to Cape Hatteras and at any time of year. The total life cycle involves the formation of a meander, which grows into an eddy that eventually elongates to a point where it breaks up or becomes stranded over the outer shelf. The whole process takes place in less than one month. This process is a vital part of the interaction of the larger Gulf Stream current system with its surrounding waters and takes place all along the Gulf Stream Front. The Gulf Stream front does not appear to have a steady state or configuration. Instead it appears to be always on the verge of being unstable; a slight kick or perturbation can initiate a meander. Thus, these disturbances can have many causes, such as the passage of a cold front, a pronounced feature in the bottom topography or the bending of the current through the Florida Straits.

In the Georgia Embayment, meanders and eddies influence the outer one-fourth to one-third of the shelf. They are inhibited from the inner shelf by the broad, shallow shelf bottom. The Gulf Stream Front is observed to meander approximately 10 to 25 km in the east-west. The eddies appear as elongated features that extrude out of the Gulf Stream over the shelf and toward the south. They have dimensions of tens to hundreds of kilometres; the along-shelf distance is two to four times greater than the cross-shelf. The vertical extent of the eddies has been observed as deep as 250 m.

In the Carolina Capes region, meanders and eddies having much greater dimensions occur, probably because of a bottom feature that protrudes eastward into the Gulf Stream off Charleston at a depth of 300 to 400 m. This feature, known as the "Charleston Bump," acts to steer the Gulf Stream around the bump toward the east, thus creating a very large meander. Once generated, the meander continues to oscillate and grow as it converges toward Cape Hatteras, forming large elongated extrusions of Gulf Stream water flowing south over the shelf (eddies). The extrusion can have lengths of several hundred km. The east-west scale of the meanders here is approximately 50 to 100 km. Since the meanders and eddies are larger in this region and the shelf width decreases toward Cape Hatteras, the influence of Gulf Stream-derived disturbances on shelf processes should increase as they approach Cape Hatteras.

Although meanders and eddies may affect a larger fraction of the Carolinas shelf, the influence of these disturbances on shelf processes is similar for both regions. An eastward meander of the Gulf Stream Front can produce a decrease in current speed and temperature in the outer shelf and an onshore intrusion of cool, nutrient-rich, subsurface Gulf Stream water. A portion of these upwelled waters will mix with the shelf waters, thus serving as a

means of water exchange that flushes the shelf and helps regulate the residence time. The upwelled waters also provide a food source for later biological uptake. An onshore meander has the opposite effect.

The occurrence of Gulf Stream spin-off eddies has even more dramatic effects. Eddies appear in the surface waters as warm tongue-like extrusions of Gulf Stream water flowing south over the shelf and eventually converging back into the stream. These events rotate counterclockwise. Their formation involves the capture of shelf water in the upper layer, which aids in flushing the shelf and reducing the residence time. In addition, the counterclockwise circulation produces an upwelling of cool, nutrient-rich, deeper Gulf Stream water into a central cold-core of the eddy. The upwelled waters also extend onto the shelf in a near-bottom layer. This pumping action provides an additional source of nutrients for biological processes on the shelf.

The time required to flush the shelf waters of the SAB by Gulf Stream-derived disturbances is approximately two to three months.

3.6 REFERENCES

Atkinson, L. P., J. J. Singer and L. J. Pietrafesa. 1976. Onslow Bay intrusion study. Hydrographic observations during current meter servicing cruises in August, October and December 1975 (OBIS I, III, and IV). Georgia Marine Science Center Technical Report 76-4.

Atkinson, L. P., J. O. Blanton, and E. Haines. 1977. Shelf flushing rates based on the distribution of salinity and freshwater in the Georgia Bight. Coastal and Estuarine Marine Science. (in press).

Blanton, J. O. 1971. Exchange of Gulf Stream Water with North Carolina Shelf Water in Onslow Bay during Stratified Conditions. Deep Sea Res., 18, 167-178.

Blanton, J. O. and L. J. Pietrafesa. 1978. Flushing of the Continental Shelf South of Cape Hatteras by the Gulf Stream. (in press).

Bosart, L. 1973. Detailed analysis of precipitation patterns associated with meso-scale features accompanying United States east coast cyclogenesis. Mon. Wea. Rev. 101 (1), 1-12.

Bosart, L., C. Vando and J. Helsdon. 1972. Coastal frontogenesis. J. of Appl. Meteor. 11 (8), 1236-1258.

Bosart, L. and J. Cussen. 1973. Gravity wave phenomena accompanying east coast cyclogenesis. Mon. Wea. Rev., 101 (5), 446-454.

Brooks, D. A. 1978. Sea level fluctuations off the Carolina Coasts and their relation to atmospheric forcing. Center for Marine and Coastal Studies, North Carolina State University, Technical Report 77-6.

Bumpus, D. F. 1954. The circulation over the Continental Shelf south of Cape Hatteras. Trans. Amer. Geophys. Un. 36 (4), 601-611.

Bumpus, D. F. 1973. A description at the circulation on the continental shelf of the east coast of the United States. Progress in Oceanography, Vol. 6, New York, Pergamon, 111-156.

Chao, S. Y. and L. J. Pietrafesa. 1979. The subtidal response of sea level to atmospheric forcing in the Carolina Capes. Submitted to Journal of Geophysical Research.

Cragg, J. and W. Sturges. 1974. Wind induced currents and sea surface slopes in the eastern Gulf of Mexico. Florida State University Technical Report. June.

DeRycke, R. J. and P. K. Rao. 1973. Eddies along a Gulf stream boundary from a very high resolution radiometer. J. Phys. Oceanogr., 3, 490-492.

Deszoeke, R. 1975. Some effects of bottom topography in baroclinic stability. J. Mar. Res., 33 (1), 93-122.

Fuglister, F. C. and L. V. Worthington. 1951. Some results of a multiple ship survey of the Gulf Stream. Tellus 3, 1-14.

Green, C. K. 1944. Summer upwelling - northeast coast of Florida. Science, 100 (1607), 546-547.

Hansen, D. V. 1970. Gulf Stream meanders between Cape Hatteras and the Grand Banks. Deep Sea Res. 17, 495-511.

Kirshen, P. H. 1978. Summary of analysis of physical oceanographic and meteorological information on the Continental Shelf and Blake Plateau from Cape Hatteras to Cape Canaveral. Final report to the Bureau of Land Management by Environmental Research and Technology, Inc. 4 Vols. Contract #AA550-CT7-16.

Lee, T. N. 1975. Proposal to Energy Research and Development Administration. (Personal Communication)

Lee, T. N. and D. A. Mayer. 1977. Low frequency current variability and spin-off eddies along the shelf off southeast Florida. J. Mar. Res., 35 (1), 193-220.

Lee, T. N. and D. A. Brooks. 1979. Initial observations of current, temperature and coastal sea level response to atmospheric and Gulf Stream forcing on the Georgia shelf. (Submitted to Geophys. Res. Letters).

Legeckis, R. 1975. Applications of synchronous meteorological satellite data to the study of time-dependent sea surface temperature changes along the boundary of the Gulf Stream. Geophys. Res. Letters, 2, 435-438.

Mooers, C. N. K. 1973. A technique for the cross-spectrum analysis of pairs of complex-valued time series, with emphasis on properties of polarized components and rotational invariants. Deep Sea Res., 20 (12), 1129-1142.

Mooers, C. N. K. and D. A. Brooks. 1976. Fluctuations in the Florida Current, Summer 1970. Deep Sea Res. (in press).

Mysak, L. A. and B. V. Hamon. 1969. Low Frequency sea level behavior and continental shelf waves. J. Geophys. Res., 74, 1397-1405.

Niiler, P. P. 1975. Variability in Western Boundary currents. Numerical Models of Ocean Circulation, National Academy of Sciences, Washington, D.C., p. 216-236.

Niiler, P. P. and L. A. Mysak. 1971. Barotrophic waves along the eastern continental shelf. Geophys. Fluid Dyn. 2, 273-288.

Niiler, P. P. and W. S. Richardson. 1973. Seasonal variability of the Florida Current. J. Mar. Res. 31 (3), 144-167.

NOAA. 1970. Environmental conditions within specific geographical regions: offshore east and west coasts of the United States and in the Gulf of Mexico. Final Report, NODC, Environmental Data Service, NOAA, Washington, D.C.

Oort, A. H. 1964. Computations of the eddy heat and density transports across the Gulf Stream. Tellus, 16, 55-63.

Oort, A. H. and A. Taylor. 1969. On the kinetic energy spectrum near the ground. Mon. Wea. Rev., 97, 623-636.

Orlanski, I. 1969. The influence of bottom topography on the stability of jets in a baroclinic fluid. J. Atm. Sci., 26, 1216-1232.

Orlanski, I. and M. D. Cox. 1973. Baroclinic instability in ocean currents. Geophys. Fluid Dyn., 4, 297-332.

Pedlosky, J. 1964. The stability of currents in the atmosphere and the ocean. Part I. J. Atm. Sci., 21, 201-219.

Pettersen, S. 1969. Introduction to Meteorology 3rd edition. McGraw-Hill, New York, 333 pp.

Pietrafesa, L. J. 1979. Progress report for Department of Energy on Contract #EY-76-S-09-0902 entitled Continental shelf processes affecting the oceanography on the South Atlantic Bight.

Pietrafesa, L. J., J. O. Banton and L. P. Atkinson. 1978. Evidence for deflection of the Gulf Stream at the Charleston rise. Gulf Stream, U.S. Dept. of Commerce, NOAA, IV. (9) p. 3-7.

Pietrafesa, L. J., R. D'Amato, C. Gabriel and R. J. Sawyer, Jr. 1978a. Continental margin atmospheric climatology and sea level 1974-75. Dept. Marine Sciences and Engineering, North Carolina State University, Report No. 78-2.

Pietrafesa, L. J., D. A. Brooks, R. D'Amato, L. P. Atkinson. 1978b. Onslow Bay physical/dynamical experiments; summer-fall, 1975. University of North Carolina, Sea Grant College Program Publication, UNC-SG-77-07.

Pietrafesa, L. J, R. D'Amato, C. Gabriel, R. J. Sawyer, Jr., D. A. Brooks, P. Blankinship and R. H. Weisberg. 1978c. Onslow Bay physical/dynamical experiments, summer 1976, data report. Department for Marine Science and Engineering, North Carolina State University, Report No. 78-5.

Pond, S. 1975. The exchanges of momentum, heat and moisture at the ocean-atmosphere interface. Numerical Models of Ocean Circulation, National Academy of Science, Washington, D.C., p. 26-38.

Richardson, W. S., W. J. Schmitz, Jr. and P. P. Niiler. 1969. The velocity structure of the Florida Current from the Straits of Florida to Cape Fear. Deep Sea Res., 16 (Supplement), 225-231.

Rooney, D. M., G. S. Janowitz and L. J. Pietrafesa. 1978. A simple model of deflection of the Gulf Stream by the Charleston rise. Gulf Stream, U.S. Dept. of Commerce, NOAA, IV (11), p. 3-7.

Saltzman, B. and C. Tang. 1975. Formation of meanders, fronts and cutoff thermal pools in a baroclinic ocean current. J. Phys. Oceanogr., 5, 86-92.

Saunders, P. M. 1977. Wind stress on the ocean over the eastern continental shelf of North America. J. Phys. Oceanogr., 7, 555-566.

Schmitz, W. J., Jr. 1969. On the dynamics of the Florida Current. J. Mar. Res., 27, (1), 121-150.

Schmitz, W. J. and W. S. Richardson. 1968. On the transport of the Florida Current. Deep Sea Res., 15, 679-693.

Schmitz, W. J., Jr. and P. P. Niiler. 1969. A note on the kinetic energy exchange between fluctuations and mean flow in the surface layer of the Florida Current. Tellus 21, 814-819.

Singer, J. J., L. P. Atkinson, W. S. Chandler, and P. G. O'Malley. 1977. Hydrographic observations in Onslow Bay, North Carolina, July-August 1976 (OBIS V), Data Graphics, Georgia Marine Science Center Technical Report 77-6.

Strong, A. E. and R. J. DeRycke. 1973. Ocean current monitoring employing a new satellite sensing technique. Science, 182 (4111), 432-484.

Stumpf, H. G. and P. K. Rao. 1975. Evolution of Gulf Stream eddies as seen in satellite infrared imagery. J. Phys. Oceanogr., 5, 388-393.

Sturges, W. 1974. Sea level slope along Continental boundaries. J. Geophys. Res., 79 (6), 825-830.

Taylor, C. B. and H. B. Steward, Jr. 1959. Summer upwelling along the east coast of Florida. J. Geophys. Res., 64 (1), 33-40.

U.S. Navy. 1970. Summary of synoptic meteorological observations (SSMO) for North American coastal marine areas. Naval Weather Service Environmental Detachment, Fed. Bldg., Asheville, N.C.

Von Arx, W. S., D. Bumpus and W. S. Richardson. 1955. On the fine structure of the Gulf Stream front. Deep Sea Res., 3, 46-65.

Ward, R. 1925. The Climates of the United States. Ginn, Boston, 338 pp.

Webster, F. 1961a. The effects of meanders on the kinetic energy balance of the Gulf Stream. Tellus, 13, 392-401.

Webster, F. 1961b. A description of Gulf Stream Meanders off Onslow Bay. Deep Sea Res., 8, 130-143.

Wunsch, C., D. V. Hansen and B. D. Zetler. 1969. Fluctuations of the Florida Current inferred from sea level records. Deep Sea Res., Suppl. to Vol. 16, 447-470.

IV. TURBID-CLEAR WATER INTERFACE STUDY

4.1. INTRODUCTION

4.1.1 Program Objectives

A study was made of surface currents in the vicinity of the turbid/clear-water interface (TCWI) in order to characterize the surface transport across and along this coastal front during both dry and wet seasons. Two deployments were specifically designed to investigate the tidal and runoff influence on the temporal and spatial variability of the interface, and to determine whether the interface exists as a continuous feature running parallel to the shoreline or as a succession of river plumes which may possibly merge under certain tidal and river runoff conditions. In addition, this study was aimed at documenting water mass dynamics in the vicinity of the interface and, in particular, at determining whether the interface is a region of local convergence. These goals were accomplished by deploying Lagrangian drifters, aluminum chips, and dyes in the vicinity of the front and monitoring their motion by aerial photography. Hydrographic casts were performed in order to help characterize vertical mixing processes between estuarine and shelf water masses.

In addition, LANDSAT imagery was examined to define temporal and spatial persistence of the TCWI in the South Atlantic Bight. This effort involved identifying coastal fronts and correlating their pattern and distribution with governing environmental factors such as tides, rainfall-controlled river flow, season, and winds.

The imagery of the Tybee Island-Hilton Head Island region, which was collected over a three-year period, was studied in detail to help define locally persistent patterns of plume growth and frontal migration, both crucial pieces of information in selecting a specific study area and establishing suitable experimental procedures.

The long-term objective of this study is to assess the importance of such interfaces in regulating transport of pollutants, since convergence zones have been known to capture and hold oil slicks and pollutants concentrated in surface films, and to transport some of this material down into the water column. The extent to which the turbid-clear water interface may act as a natural barrier to the motion of pollutants towards the coast, could be most important for the decision making process regarding the management of the coastal zone and its resources.

4.1.2 Experimental Design

Since salinity is usually the controlling parameter in governing density in the coastal zone, the relative magnitude of the freshwater contribution to a discharge plume should influence the density

difference between estuarine and shelf waters. Because the magnitude of this density difference helps govern the intensity of frontal dynamics (Garvine, 1974), it was decided to conduct investigations of the TCWI during both dry and wet seasons when the fresh water contribution should be lower and higher than average, respectively.

An effort was made in both deployments to correlate activities to the tidal cycle. From past observations of the TCWI, previous studies (e.g., Garvine, 1974), and an examination of selected LANDSAT images, it was apparent that tides had an important influence on the location, extent, and intensity of this coastal feature. These observations also indicated that the region offshore from the Savannah River and Hilton Head Island had persistent and active coastal fronts.

Periodic aerial color photography was used to document the fixed-frame displacement of fronts through the study area, and the motion of tracers in this fixed frame and relative to the moving front. Geographic locations and absolute movement of both the frontal features and drifters were determined by using a pattern of floating, fixed markers deployed at known locations which appear in each picture. By releasing both surficial and dispersed tracers in the vicinity of the TCWI, it was possible to estimate how generically different pollutants would respond to the circulation and exchange processes associated with these fronts. Detailed hydrographic measurements were also made to define vertical frontal structure, and to help identify the magnitude and nature of mixing between shelf and estuarine waters.

Field activities associated with the two deployments are described in Section 4.2. Procedures followed in the reduction and analysis of the data collected are presented in Section 4.3, followed by a discussion of the results in Section 4.4. Finally, the methodology used in the analysis of the LANDSAT imagery in support of the study of the TWCI is described in Section 4.5, together with a discussion of the findings regarding the spatial and temporal persistence of this coastal feature. Conclusions drawn from the experimental studies are summarized in Section 4.6.

4.2 FIELD ACTIVITIES

Two separate but similar deployments were conducted in August, 1977 and May, 1978. The first one which was performed over a much larger area (Figure 4-1) than the second one and involved no hydrographic measurements, provided an excellent process overview and much of the information necessary to optimize operations during the second experiment. The only substantative differences between the two field efforts were in the detailed methodology used for documentation of front and tracer migration and in the collection of conductivity-temperature-depth (CTD) profiles during the second experiment.

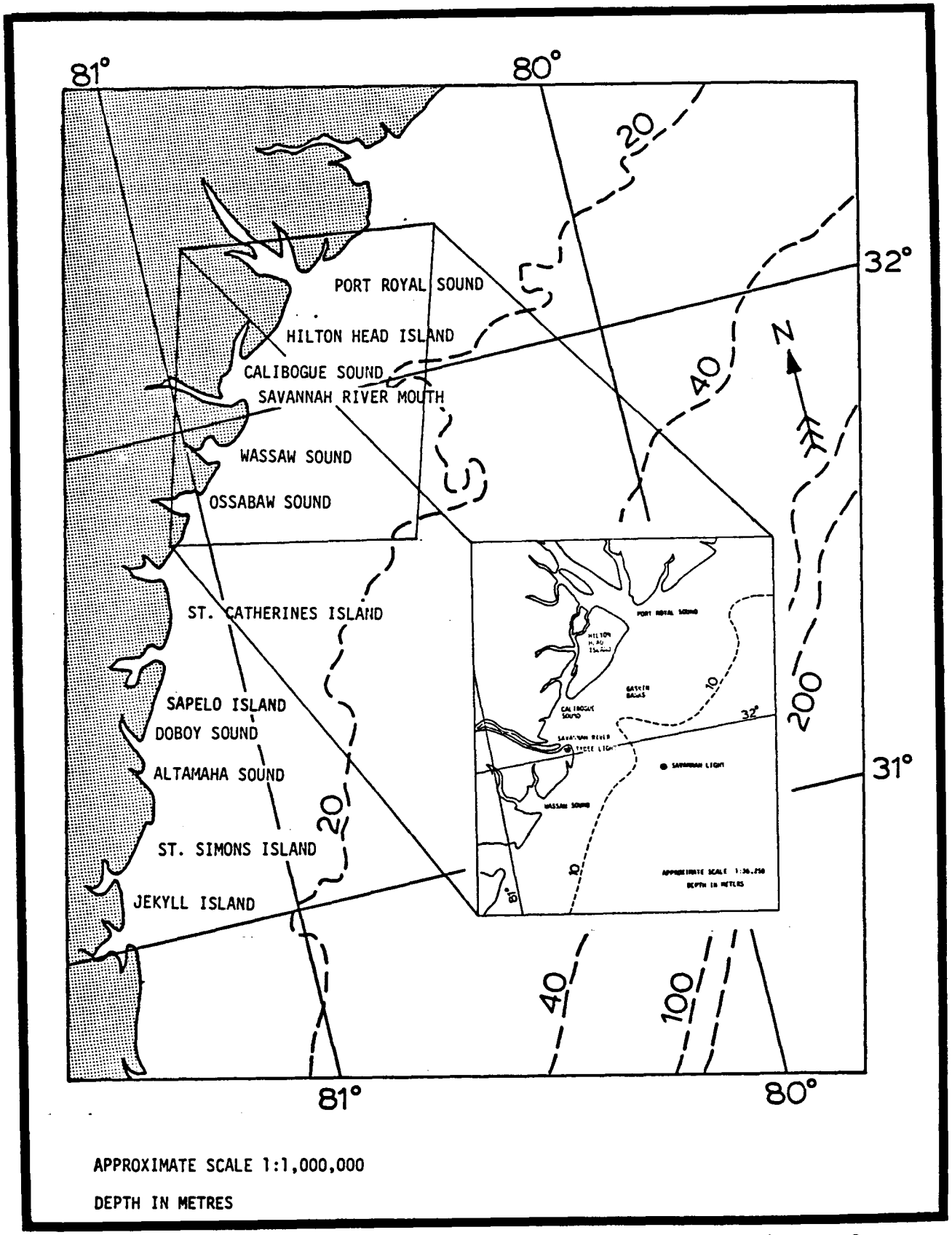

Figure 4-1. Regional map of Georgia-South Carolina coast with inset of general study area.

In the first deployment, a large format aerial camera was used which allowed resolution from greater elevation than the 70 mm system utilized in the second field experiment. This change to a smaller format was made to allow more operational flexibility and better data reduction and integration procedures. Hydrographic casts were added to the suite of measurements because of the importance of subsurface mixing to pollutant exchange and transfer processes in the vicinity of a coastal density front.

4.2.1 Study Area and Transects Location

The region offshore from Hilton Head Island and the mouth of the Savannah River was selected for study after a preliminary examination of LANDSAT imagery and evaluation of logistics requirements. Imagery showed that frontal-like features consistently occurred in this area. These observations were supported by a preliminary overflight during which a relatively continuous color front was observed. The region also has a convenient airport, boat moorings, and housing. The proximity of an adequate mooring facility to the anticipated study area was a requirement, in order to begin daylight operations as early as possible.

4.2.1.1 August 1977 Deployment

Based on the distribution of well developed portions of the interface, as determined from reconnaissance flights on August 7, 8, and 9, the original plan of transects perpendicular to the interface positioned at 5 km intervals along the interface was slightly modified: five transects would still be approximately perpendicular to the local interface; however, they would be concentrated in areas where the front was found to be well developed. Three transects, four to five kilometres apart, would be grouped in the northern region of the Savannah River mouth near Gaskin Bank, and two in the area southeast of Tybee Island (Figure 4-2). The two groups would be separated by approximately 16-20 km. These fronts appeared to be strongly influenced by tidal conditions and could migrate extremely rapidly (over 28 $cm.s^{-1}$ or 1 $km.h^{-1}$). Fortunately, spatial variability of the front over the tidal cycle appeared somewhat predictable. The position of the front during the reconnaissance flights dictated actual location and length of transects, as well as the number of reference markers required for adequate ground control on each line.

4.2.1.2 May 1978 Deployment

Experience from the August 1977 deployment showed that data products could be improved by concentrating photographic coverage on a smaller area. During the first field experiment (August) the large distances between the northern and southern groups of transects made coordina-

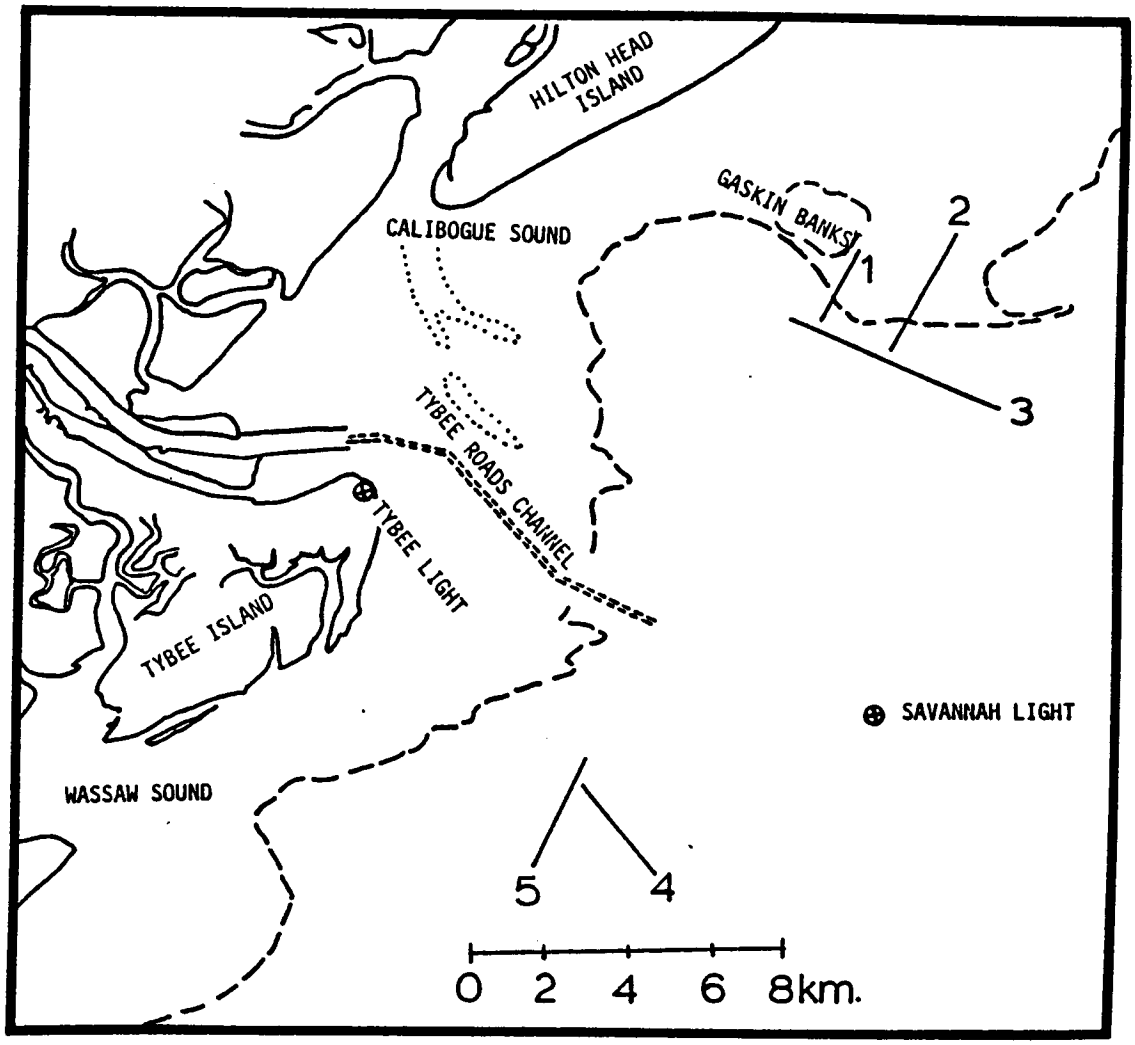

Figure 4-2. August, 1977 study with the five (5) deployment transects indicated.

tion of surface operations difficult and at times resulted in aerial photographs being taken at intervals too large for adequate documentation of the rapidly moving fronts and tracers.

In the second deployment, fixed markers were deployed in the area south of Gaskin Banks according to a pattern shown in Figure 4-3a. The exact location of this marker array was determined only after reconnaissance flights on April 30 and May 1, 3, and 5, 1978. As a result of losses due to vandalism after the May 7 deployment, remaining markers were regrouped for a second operation on May 10, 1978, as shown in Figure 4-3b. Also indicated on these figures are the locations at which hydrographic profiles were made.

4.2.2 Equipment

4.2.2.1 Boats and Aircraft

Two aircraft were used during both deployments. The larger one, a Cessna 337 Skymaster, contained the photographic equipment during both experiments. During the May deployment, a radiometer was also carried by this plane. A small single engined plane (a Cessna 150 or 172) was used as a mobile control center. Flying slowly at low altitude (often less than 300 m) the controller was able to monitor activities of and guide the various operational units (boats and planes). From this vantage point, he could see the location and extent of the front and could direct surface units to the most advantageous position for dye release and sampling. Throughout the operation, the larger plane proceeded with photographic coverage. Both aircraft were equipped with extensive communications systems.

During each experiment, three boats were used. Two 6-7.6 m (20-25 ft) outboards provided the speed and mobility required to respond quickly to directions from the mission controller. Each smaller boat was equipped with a magnetic compass and radio equipment for FM and CB communications. A third larger vessel was also used. During the August deployment, a 9 m shrimp boat carried the Mini-Ranger Receiver and extensive communications equipment. During the May deployment, this boat was replaced by a new small craft carrying a CTD unit and related recording equipment, winch and communications gear. It was also equipped with LORAN-C, a Mini-Ranger positioning system and a Raytheon echo-sounder (fathometer).

4.2.2.2 Photography

In the August 1977 deployment, a WILD RC-5 (22.7 cm x 22.7 cm format) aerial photographic camera was used to document the motions of the fronts and tracers. At the flight altitude, 1830 m, and lens angle used, photographs had a nominal scale of 1:12,000 and each covered a 7.5 km^2 area. A total of 259 images were taken.

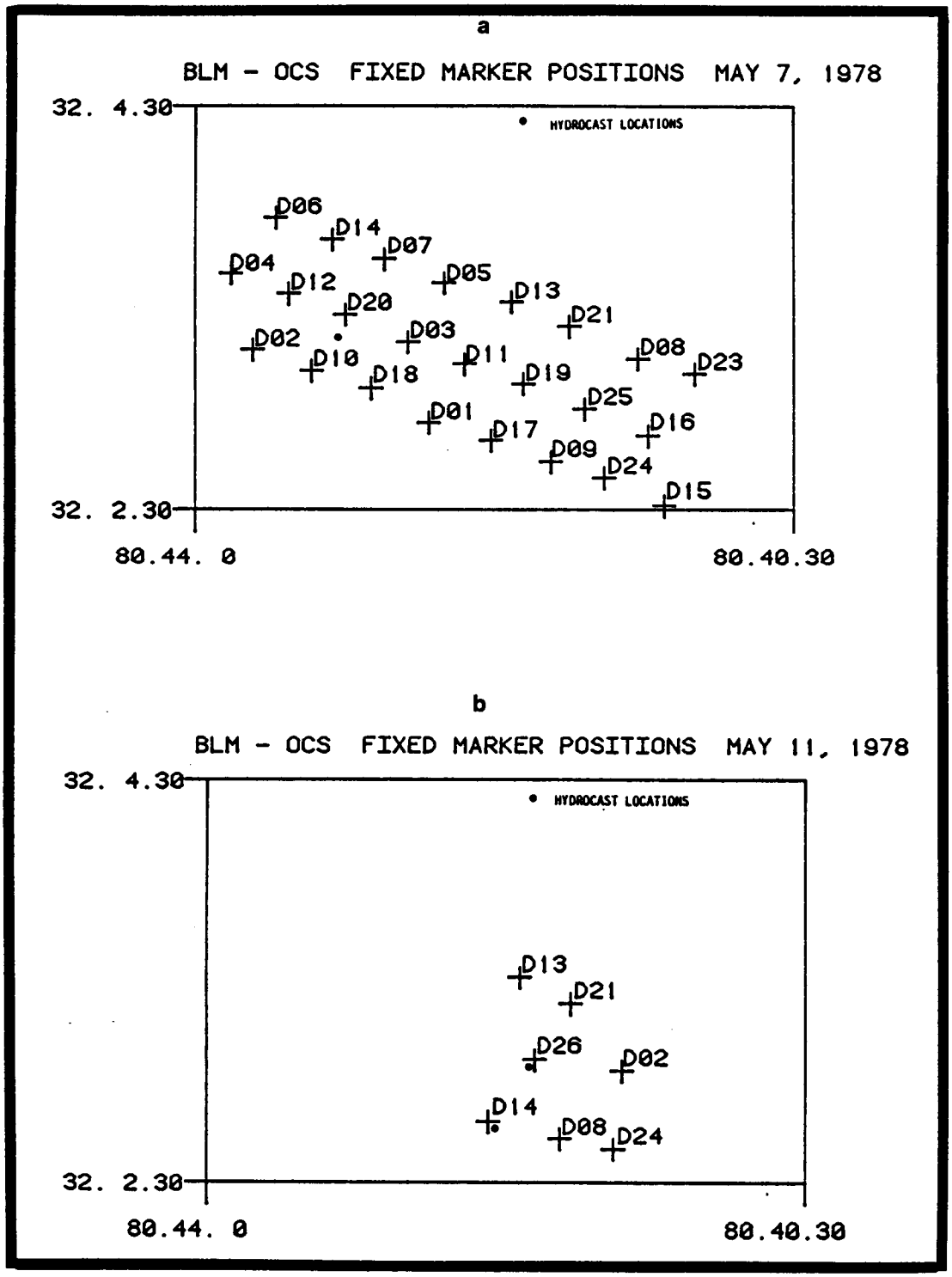

Figure 4-3a and b. Fixed marker deployment and hydrostation location, on May 7 and May 11, 1978, respectively.

In May 1978, the larger aircraft was equipped with two Hasselblad Mk-10 intermediate format (70 mm) cameras which were loaded with positive and negative film and provided simultaneous coverage of the water surface.

4.2.2.3 Reference Markers

Distinctive flat color coded fixed markers, designed to be easily identifiable from the air, were carefully positioned in the study area using the larger boat guided by the Mini-Ranger and LORAN-C. Deployment spacing was designed to be compatible with the aerial photography plan so that, at the flight altitude and camera format used, at least two markers would appear in each photo of the area. The deployment pattern was selected to optimize observation of frontal and tracer movement. Each of the 30 markers was coded with a color design and its geographic position recorded at placement.

4.2.2.4 Positioning Systems

Two positioning systems were used in the field. The larger aircraft had onboard LORAN-C as did the larger boat during the May 1978 experiment. In each deployment, the larger boat was equipped with a Motorola Mini-Ranger receiver installed on board which, in conjunction with two transceivers positioned at surveyed shore sites, provided very accurate positioning within the study area.

4.2.2.5 Dyes and Tracers

Two dyes, Rhodamine B and Fluorescein, used to simulate surface water transport of dissolved and suspended pollutants, and a tracer, Aluminum powder, simulating motion of a slick were dispensed during the experiments. All were easily seen from the air and photographed well in large concentrations. Rhodamine was systematically placed on the inshore or riverine side of the front, while fluorescein was deployed on the offshore or oceanic side of the front. All transects had dye dispensed on both sides of and in the immediate vicinity of the convergence. During the first deployment, sheets of paper were also released. This experience suggested that paper was supplying data redundant with the aluminum.

During the August experiment, each tracer was deployed separately from prepackaged containers. It was determined to be more effective to combine dye and aluminum in a single package so they could be deployed simultaneously.

4.2.2.6 Communications Equipment

Because continuous communications were essential to successful field operations, several networks were used. In August 1977, the two aircraft and larger boat had AM radios while each smaller boat and

the smaller plane were equipped with CB radios. These systems were substantially supplemented during the second deployment by providing each plane and the large boat with AM and FM radios, and each smaller boat and Radio Direction Finder (RDF) Shore Station with FM and CB radios. These extensive and in some cases redundant communication systems proved most adequate for exchanges between the various units participating in the field operations.

4.2.2.7 Radio-Equipped Drogues and RDF (May 1978 only)

Drogues equipped with radio transmitters and a dye release mechanism were deployed in the study area during a period of flood tide. The devices were tracked from the air during daylight and were positioned using the shore based RDF system until they moved inside the estuary.

4.2.2.8 Hydrography (May 1978 only)

On May 7, hydrographic measurements were made at one station from morning until late evening (Figure 4-2). Three well defined fronts moved to the northeast past the measurement station during ebbing tide. Also, plumes associated with these fronts were moved onshore past the station during part of the following flood tide. A Neil Brown Mark III CTD unit was used to document the hydrographic profiles. Hydrocasts were repeated on May 10, 1978.

4.2.3 Daily Activities

4.2.3.1 First Deployment, August 10 and 11, 1977

Two fluorescent dyes, Rhodamine B, and Fluorescein, used to simulate transport of dissolved and fine suspended pollutants, and Aluminum powder and sheets of mimeograph paper simulating surface pollutants were released according to the following pattern (Figure 4-2).

Transect 1	paper and dye
Transect 2	aluminum
Transect 3	paper and dye
Transect 4	aluminum
Transect 5	paper and aluminum

As mentioned previously, dyes were deployed so that rhodamine was placed on the inshore or riverine side of the front, and fluorescein on the offshore or oceanic side, in the immediate vicinity of the front.

For seeding, single injection quantities of dye and aluminum were packaged in paper bags prior to the day of use. Such a scheme was necessary because of the inherent difficulty of handling all powder dyes and aluminum chips.

It soon became apparent that because of the migration and dynamics of the front, transects would have to be continuously reseeded in order to provide sufficient tracers for determination of the Lagrangian velocity field. This reseeding operation required quick response and great mobility between transects, which was ideally provided by a light plane. Fortunately, it had been established during practice runs near New London, Connecticut that dyes and some of the tracers could successfully be deployed from an aircraft, and it had been decided that the Cessna 150 would carry a supply of dye and aluminum powder bag, weighted with stones, to supplement, if required, the dye and tracer injections done by the surface craft.

The two small boats dispensed dyes and tracers on the northern transects (numbers 1, 2, and 3), while the larger boat was taking care of the southern transects (numbers 4 and 5), the small plane supplementing the seeding as needed. Around 2:10 P.M., on August 10, the first day of operations, most of the boats were running short of dye and drifter supplies, since continuous reseeding of transects was not originally anticipated. Moreover, the interface was losing its definition and was likely to move out of the ground-controlled area while the plane was on the ground for refueling and film loading. In view of these facts, it was decided to end the first day deployment around 2:15 P.M. The last photographs were taken at 3:30 P.M.

On the second day, all boats started the seeding of the transects around 11:00 A.M. Atmospheric conditions (low ceiling), prevented an earlier deployment. The operation scheme established on August 10, 1977 was repeated. The final reseeding operation was completed at 3:00 P.M., while the aerial monitoring continued until 4:15 P.M. Because of its mobility, the light plane was invaluable in reseeding those regions of the front which were most dynamic. This was particularly true of the southern transects where the plane could often reseed transect 4 with aluminum powder.

Because of perspective from 1,830 m, personnel in the photographic plane could often anticipate transects which would need to be reseeded. This information was transmitted to the light plane, which then coordinated the reseeding operation.

Every effort was made to adhere to the original flight plan; however, modifications were at times necessary to accommodate rapidly changing conditions on and configuration of the front. Because of the relatively large distance between the northern and southern groups of transects and the rapid frontal movement, it was often more appropriate for the aircraft to monitor only that portion of the study area subjected to rapid changes, rather than to fly back and forth between northern and southern transects. Fortunately, periods of rapid change in the north and south did not often coincide. When frontal velocities decreased, a circular or rotational flight plan

was resumed in which northern and southern regions were photographed sequentially. These conditions were common at or near local low (ebbing) slack water.

4.2.3.2 Second Deployment, May 7 and 10, 1978

Field operations were begun on April 30, 1978 and continued through May 11. The first seven days of the field operation were spent preparing equipment and making reconnaissance flights. Poor weather conditions including low visibility and high seas precluded proceeding with the experiment on the timetable originally established. The time spent waiting for clear weather was put to effective use, however, since preliminary testing uncovered minor equipment malfunctions which were repaired during the interim. The marker buoys used for photoanalysis were deployed on May 6. With all equipment operational and weather permitting, plans were made to proceed with the experiment on May 7, 1978.

A detailed study of the frontal structure was begun on the morning of May 7. Atmospheric and sea conditions were excellent, with obvious frontal features active along the coast and within the array of fixed marker buoys. Unfortunately, a leak was discovered in the wing gas tank of the larger airplane, which required immediate repair. The monitoring operation was begun without the photo and radiometry coverage, using the small boats to place dye with direction from the Cessna-172. The front was easily identified from the air by the foam streak formed in the convergence zone or by the strongly contrasting adjacent water colors. In all, three fronts passed through the observation area during the day. The larger vessel remained at anchor taking CTD casts while the smaller vessels, directed from above, placed dye.

A front with a foam line moved into the study area from the southwest at approximately 10:45. Its orientation was nearly parallel to the fixed marker transects. Strong lateral shear occurred across the front with currents outside (seaward) directed toward the SE (125^{o}) and inside toward the W (270^{o}). Waves and eddies along the interface suggested the presence of a strong velocity shear. This was later photographed by the large aircraft.

Three drogues containing radio beacons were placed in the water at fixed markers in the middle of each transect. They were tracked from the shore based RDF stations.

At approximately 1400 a front defined by a color change moved into the study area. This lobate plume coalesced with the foam front south of Gaskin Bank. A third plume, darker than the second, moved into the area about an hour later.

Dyes were placed across each front and their general movement recorded. During advancing stages, the dyes behaved as expected for a migrating front with absolute or relative convergent flows. The distance between dyes and front continually decreased while a lateral movement of large magnitude was also taking place. Tracers placed outside of the plume were subducted down the shallow density interface along the front.

Aluminum powder and dye released simultaneously indicated that the dye moved with the near surface currents while the aluminum followed a pattern which indicated significant wind effects. Several times the aluminum powder was blown across the front.

The movement of the front was strongly influenced by tidal stage. During ebbing tide, migration was seaward. Within half an hour of low slack water at Savannah River Entrance (4-6 km SW of the study area), the positions became approximately stationary. During the flood, all fronts migrated toward the estuaries. Initial indications were that convergence was small or absent during the latter phase. Aerial observations suggested that each plume was advected as a unit during the early part of the flood.

The Skymaster was back in operation by 1530, and systematic aerial monitoring of the motion of the tracers and dye with respect to the front was performed until 1800. Since the surface currents in the vicinity of the turbid/clear-water interface could not be documented during a full tidal cycle, it was decided that the deployment would continue the following morning. Unfortunately, the weather deteriorated to the point that surface and air operations were impossible for the next two days.

Another intensive study of the fronts was begun on May 10. All surface and air units remained operational throughout the day, allowing CTD, dye, photo, and radiometry studies to be performed in the study area. The latter had to be reduced in size, because of the suspicious disappearance--most likely related to sport fishing activities--of a large number of markers deployed on May 6. A radio equipped buoy was also released with the intention of tracking it for 24 hours. The evening flood carried the marker toward the estuary mouth where it grounded on a bar at about 2100. On the next day, a bathymetric survey of the region extending from Gaskin Banks to the mouth of the Savannah River was conducted, the position of the reference markers verified using the Mini-Ranger system, and all material and equipment finally secured.

4.3 DATA ANALYSIS

4.3.1 Photographic Analysis

Different procedures were used to extract data from the two separate field operations. The large format photography used in the first deployment was amenable to making overlays which were integrated into

composite mappings of tracer and frontal location at a given time. This approach allowed for extensive coverage of the large study area. Each intermediate format photograph used in the second deployment provided detailed information about a more limited area, but an increase in number of photographs could provide coverage similar to that in the first deployment. Overlays were not an appropriate technique of data compilation with the smaller photographs. Consequently, position information and flight data for each photograph were digitized into a computer compatible format. Data compilation and integration was done by computer.

4.3.1.1 August 1977 Photo Reduction Procedure

The following steps were involved in constructing mosaic composites and maps of Lagrangian vectors.

(1) Air photos were indexed and catalogued.

(2) The center of each photo was plotted on a regional map of the study area.

(3) Sequences of photographs providing good overlap and coverage of the study areas were identified and selected.

(4) Overlays of each picture that was part of the selected sequence were made.

(5) Mosaics of these overlays were constructed.

(6) Composites of these graphic mosaics were constructed.

(7) From these composites, Lagrangian Vectors were constructed and plotted.

Step 1 allowed for cross referencing photographs between differing number systems, i.e., daily photograph number and the camera's internal numbering sequence. Dye patches and tracers were identified and codified. Careful attention was paid to the differentiation between patches produced during the initial seeding of the transects and those resulting from the reseeding operations. The tracer identification was, however, facilitated by making use of the aircraft log, which listed the times and locations of the successive reseeding operations, thus reducing the risks of potential confusion in the tracer cataloging.

Step 2 used LORAN-C coordinates to plot photograph centers. Knowing the size of the area covered by each aerial photograph, and the position of the center of each photo, sequences of photos were chosen which eliminated working on redundant information (Step 3). The selection was based on the criterion that each spatial sequence

provided extensive coverage of dyes and drifters and contained a minimum number of reference markers. An overlay of each photograph was constructed (Step 4) which included the location of the front, marker buoys, and dyes and tracers. These overlays were used to create mosaics of the sequences (Step 5). The knowledge of the positions of photograph centers and the locations of the reference markers greatly facilitated the construction of these graphic mosaics. Time sequences of these mosaics, or composites, were constructed (Step 6), from which Lagrangian vectors were drawn. Current magnitudes were determined using the time lapse between successive tracer positions.

4.3.1.2 May, 1978 Photo Reduction Procedure

Whenever a vertical photograph was taken, three cameras activated simultaneously. Two cameras, one containing color positive and the other color negative film, took simultaneous pictures of identical fields. This duplicity assured that a vertical would be taken even if one camera malfunctioned. Using both positives and negatives insured that all features would be easily distinguished on one or the other types of film. Additionally, for every vertical a special flight data panel was photographed, thus recording plane attitude, altitude, bearing, location (in LORAN-C coordinates), and time. A total of 499 vertical photos were taken on two days, May 7th, and May 10th.

Vertical photographs of the study area documented displacement of tracers and the locations of fronts. The exact geographic location of the moving tracers at any given time was determined from their location relative to a precise pattern of fixed markers deployed at specific predetermined locations. The marker deployment pattern attempted to maximize the number of markers occurring in each photograph.

By examining progressive locations of tracers, both circulation relative to fronts and the Lagrangian velocities can be computed. However, obtaining this information required the multistep data reduction process described below.

Each photo had to be uniquely identified to allow simple cross referencing between the three photo strips. This was accomplished by giving simultaneous photographs the same number with sequential photos receiving sequential numbers. Additionally, flight information was transcribed from the black and white photos.

Color positives were used as the information source since all markers, etc. were presented in a familiar color scheme. Each frame was examined, and all features (fixed markers, drifters, and dye patches) uniquely identified. This was a critical stage since

patches of dye had to retain the same identifier in sequential photo runs. Codes identifying a given feature completely defined its characteristics, i.e., rhodamine vs. fluorescein, etc.

Following the above, a first order data selection was made so redundant photographs would not be digitized. In some situations, successive photographs contained the same surface features, and photographs were selected for digitization only if they contained information not presented in a previously digitized picture.

Digitizing a selected frame resulted in the location of each uniquely coded surface feature being known in the frame-of-reference of that photograph. This coordinate system could be oriented geographically because the true ground location of the fixed markers was known.

Following digitization, all information (flight parameters and all digitized data) was placed on a computer compatible tape to allow rapid access and manipulation. A printout of this tape provided a detailed quality assurance check of data form and format.

Spatial relationships in photo images can be distorted if the film plane is not parallel to the ground plane. Additionally, variations in elevation produce different scales. Consequently, it was necessary to resection the location data taken from the photographs. After this procedure, corrected ground coordinates were known for all surface features.

Information for resectioning can be obtained two ways: (1) using flight parameters to make rotations and translations of relative positions due to deviations from straight and level flight, and (2) use known geographic locations in a photo to compute deviations in flight attitude and then make the corrections as in (1) above. Both approaches have been used. Results show that essentially straight and level flight was maintained almost all the time. However, a discrepancy was found in the compass reading recorded on the data panel. This was corrected in almost all frames since it required only two known locations in the picture.

Following resection, all ground positions were known in geographic coordinates. At this stage, data were stored in files structured on a frame number basis. For further analysis, it was necessary to restructure data files so successive positions and associated times of individual tracers would be listed sequentially. This required extensive sorting and reformatting.

The sorted data were accessed for use in programs which produced: (1) graphic presentation of sequential locations of individual or groups of tracers, and (2) maps of the Langrangian velocity vectors of individual or groups of tracers.

4.3.2 Hydrographic Data Reduction

The Neil Brown Instrument system used for CTD measurements is composed of two subsystems: (1) sensors and initial signal processing unit (i.e., the "fish"), and (2) deck unit for extensive signal processing. Output from the fish is a step incremental, frequency modulated signal in which deviation from the reference frequency constitutes the information. To insure availability of an accurate record, the analog signal from the fish was recorded on magnetic tape prior to being processed by the deck unit. This analog signal was reread and input to the deck unit immediately following recording so conditions at the sensor could be displayed in real time. At any future time, the recorded analog signal could again be input to the deck unit, and any of the three output forms including binary and analog signals could be regenerated.

After completion of the field work, the analog tape was processed through the deck unit, and a computer compatible nine track digital tape was created. Because of redundant observations on the digital tape, a sorting and selection procedure developed at SAI was used to create a working data set with one observation for each variable at each incremental depth.

Computer generated hydrographic data products were prepared to display:

1) simultaneous vertical profiles of measured and derived parameters. (Figure 4-4).

2) time sequential profiles, each offset by a constant amount. (Figure 4-5) One graph was made for each major parameter (salinity, temperature, and sigma-t).

3) isopycnals plots where each variable is presented as a function of depth and time (Figure 4-6).

Also, synthetic hydrographic cross sections were plotted by a multistep process which converted temporally sequential vertical hydrographic profiles at one point to an estimate of a corresponding spatial cross section through the front at one time. (Figure 4-7) One spatial section was created for each front passing the hydrostation. Steps taken in data conversion are:

1) Distance as a function of time between the front and the constant hydrostation were plotted based on data taken during field operations.

2) Based on the above curve, the distance from the front to the hydrostation was interpolated for each time corresponding to a hydrocast.

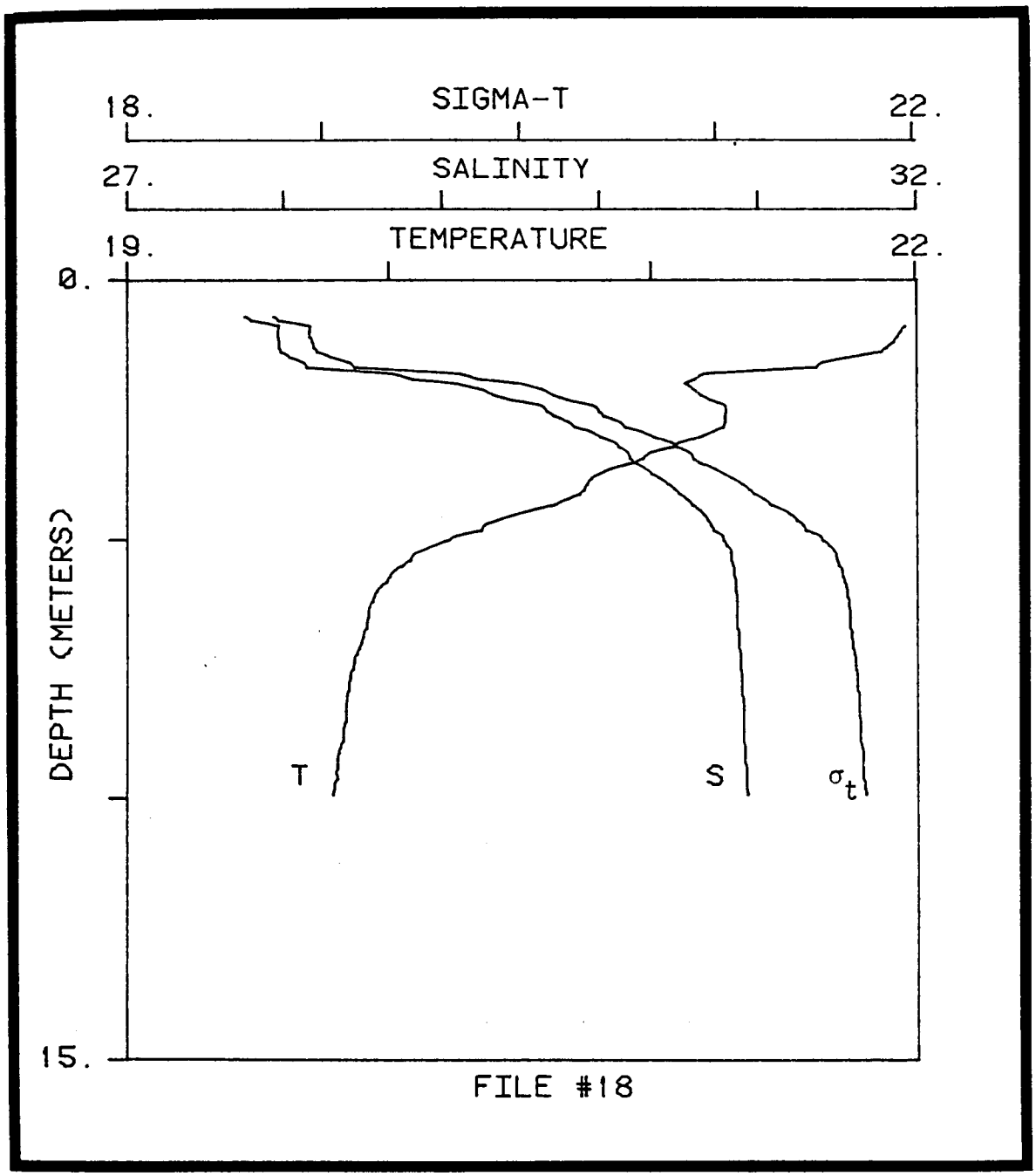

Figure 4-4. Simultaneous plots of temperature, salinity and sigma-t at 1505 hours on May 7, 1978. Profiles measured, under ebbing tide conditions, after three fronts had passed the measurement site.

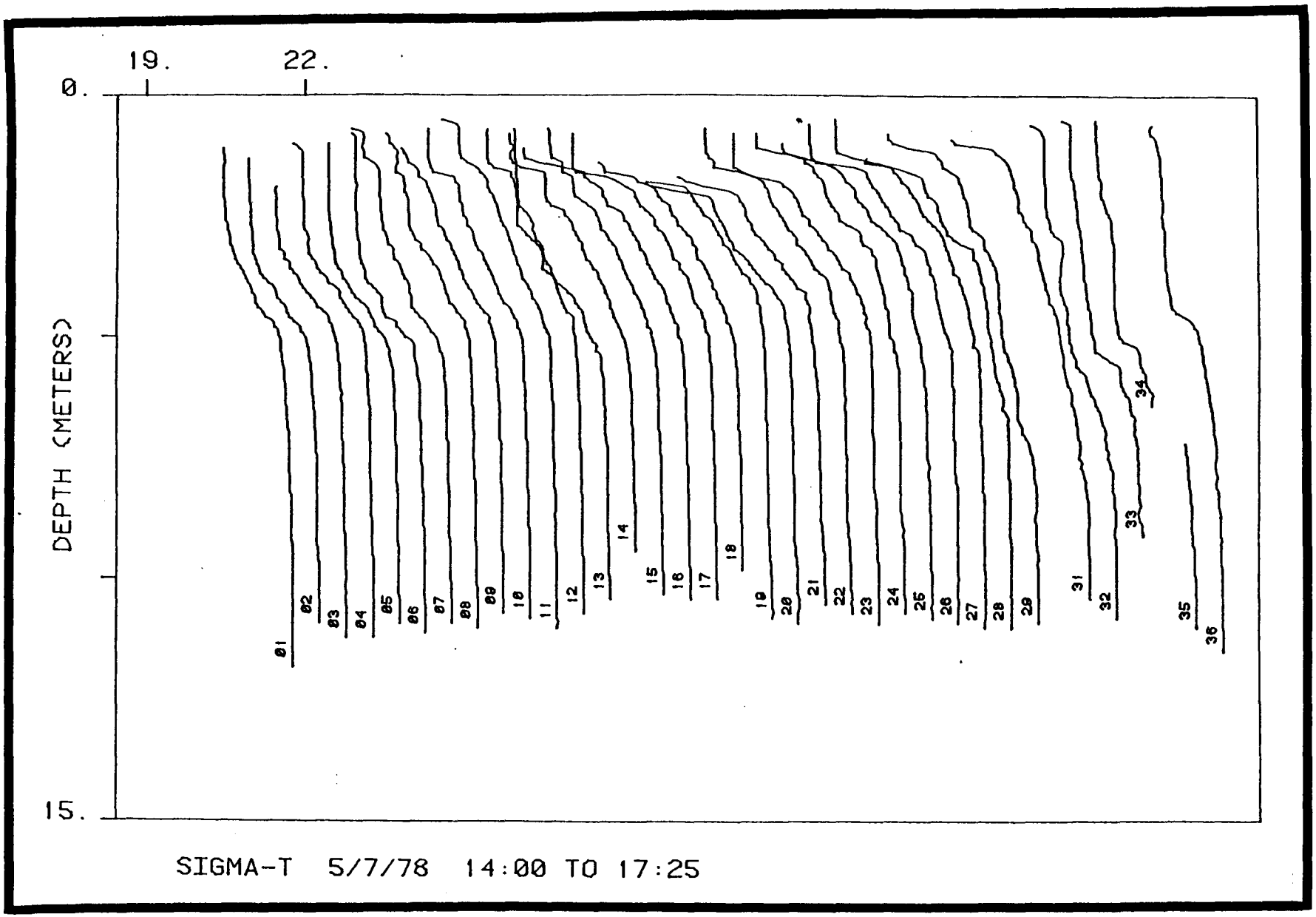

Figure 4-5. Offset plots of sigma-t between 1400 and 1725 hours, May 7, 1978. At profile 1, the first front had passed the measurement site more than an hour before. The second front passed after profile 6 and the third front passed after profile 12. The tide turned at approximately profile 21.

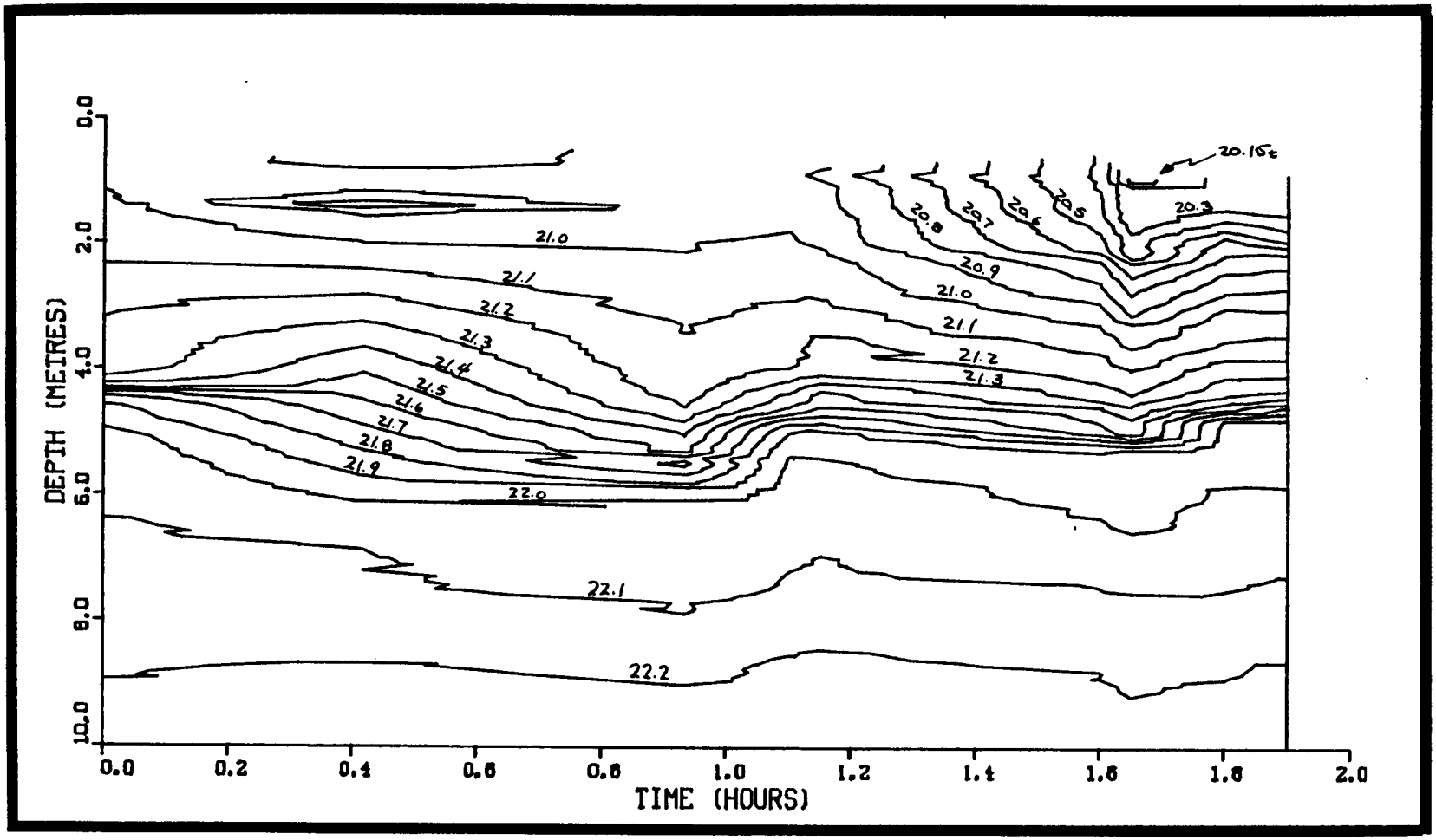

Figure 4-6. Isopycnals plot as a function of depth and time for hydrostation 2 on May 10, 1979.

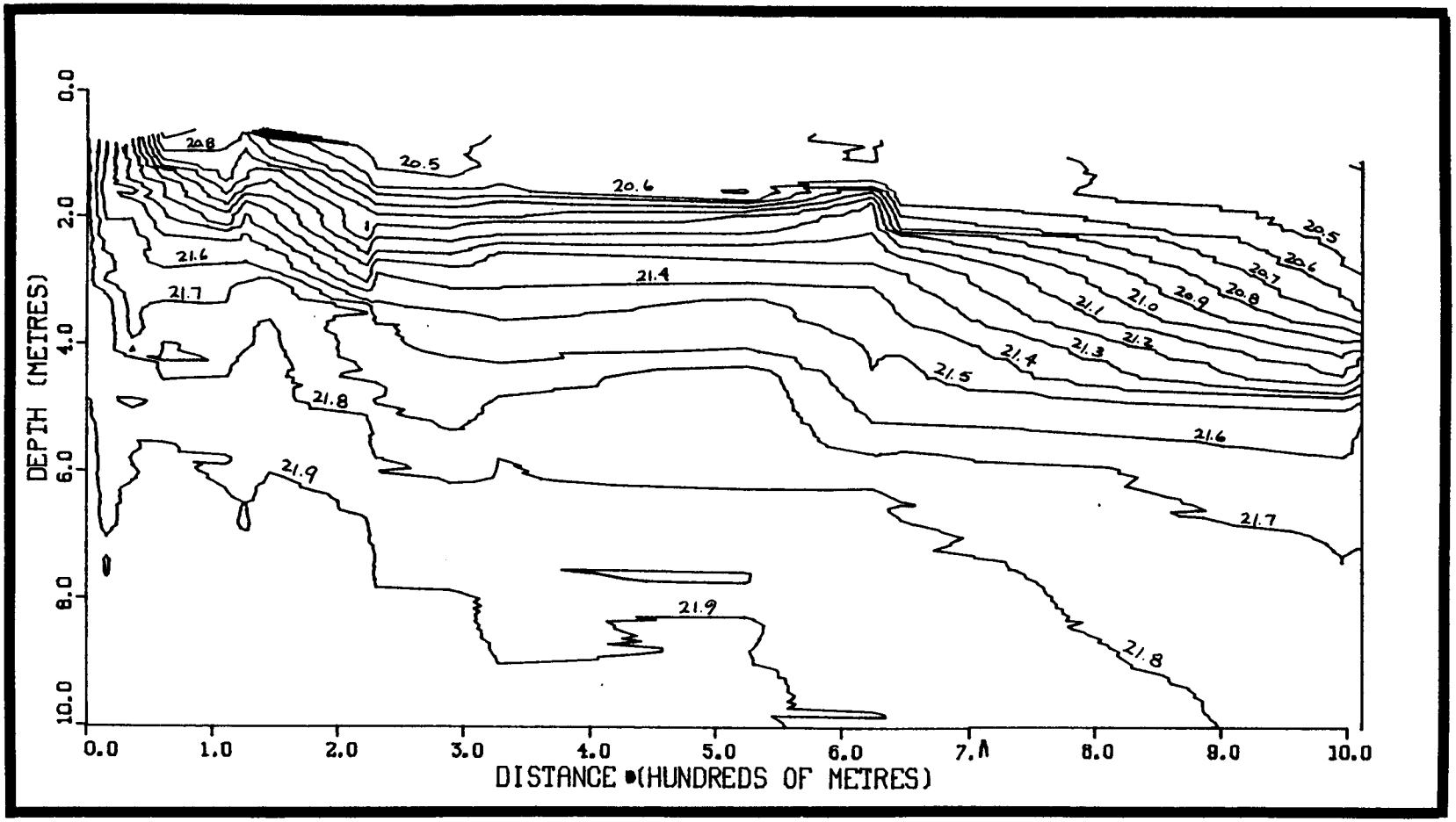

Figure 4-7. Isopycnals plot of synthetic density cross section for Front I on May 7, 1978.

3) The hydrographic parameters were then redefined as a function of depth and distance instead of depth and time. Since the velocity of the front was time dependent, this redefinition could either expand or compress portions of cross sections produced when parameters were plotted and contoured on the basis of depth and time.

4) A separate cross section plot was made for each parameter (temperature, salinity, and density) for each front.

Although the synthetic cross-sections are not the result of synoptic measurements, they have provided an informative presentation of the data. Also, if the plume morphology, as defined by its temperature and salinity, is described in a frame-of-reference having an origin at and moving with the front, and if plume hydrograph is time independent over the relatively short time period the measurements were made, then the synthetic cross sections are an accurate representation of the hydrographic field.

Creation of the cross-section for each front helped identify important consistencies and allowed identification of zones of mixing and of the water masses being mixed. This was particularly important with the embedded plumes where mixing occurred between the plume and previously mixed zones.

4.4 DISCUSSION OF RESULTS

4.4.1 Experimental Conditions

4.4.1.1 Tidal Regimes

Figure 4-8a depicts the tidal water level fluctuations and tidal currents at the Savannah River entrance, for the period of August 7 to 12, 1977, based on the 1977 Tidal Currents Table published by NOS. The tidal regimes corresponding to the two periods of aerial monitoring of the surface current tracers can be inferred from this figure.

In addition, currents at the Savannah Light are related to those at the Savannah River Entrance as indicated in Figure 4-8b, prepared from data obtained at the above source. A plot of these velocity vectors produces this tidal ellipse with the major axis oriented approximately in line with the Savannah River ship channel.

Likewise, tide heights and tidal currents for the Savannah River Entrance 15 to 25 km SSW of the study area for the period from 0600 hours, May 6, 1978 to 0600 hours, May 8, 1978 and 0600 hours, May 9, 1978 to 0600 hours May 11 are shown in Figures 4-9a and 4-9b respectively. Also indicated in the figure is the intensive study period. These tides as predicted in the NOS tables are mixed diurnal

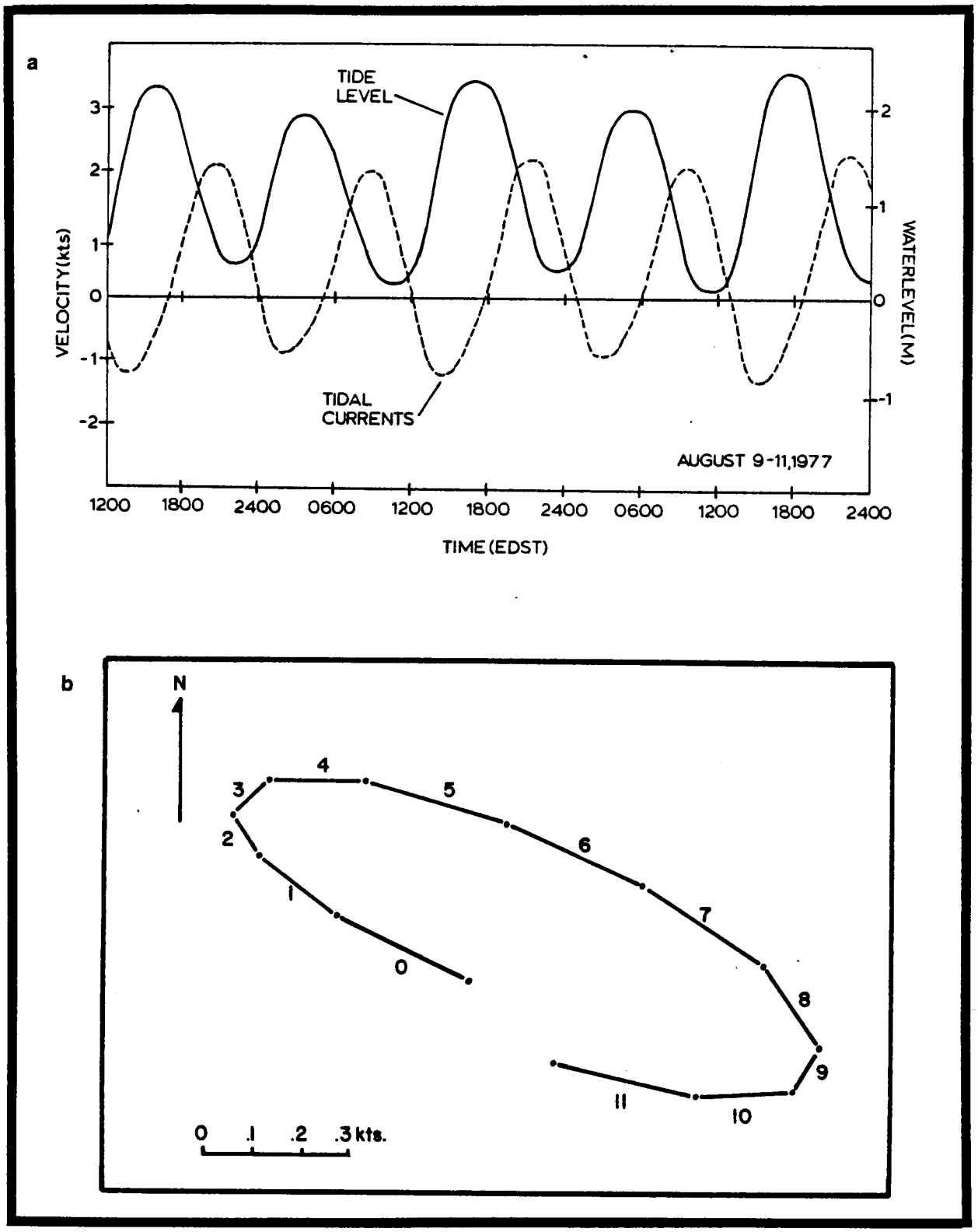

Figure 4-8a and b. (a) Tides of Savannah River Entrance, and (b) progressive vector diagrams of tidal currents at Savannah Light for August 9-11, 1977, from NOS TIDAL CURRENTS TABLES.

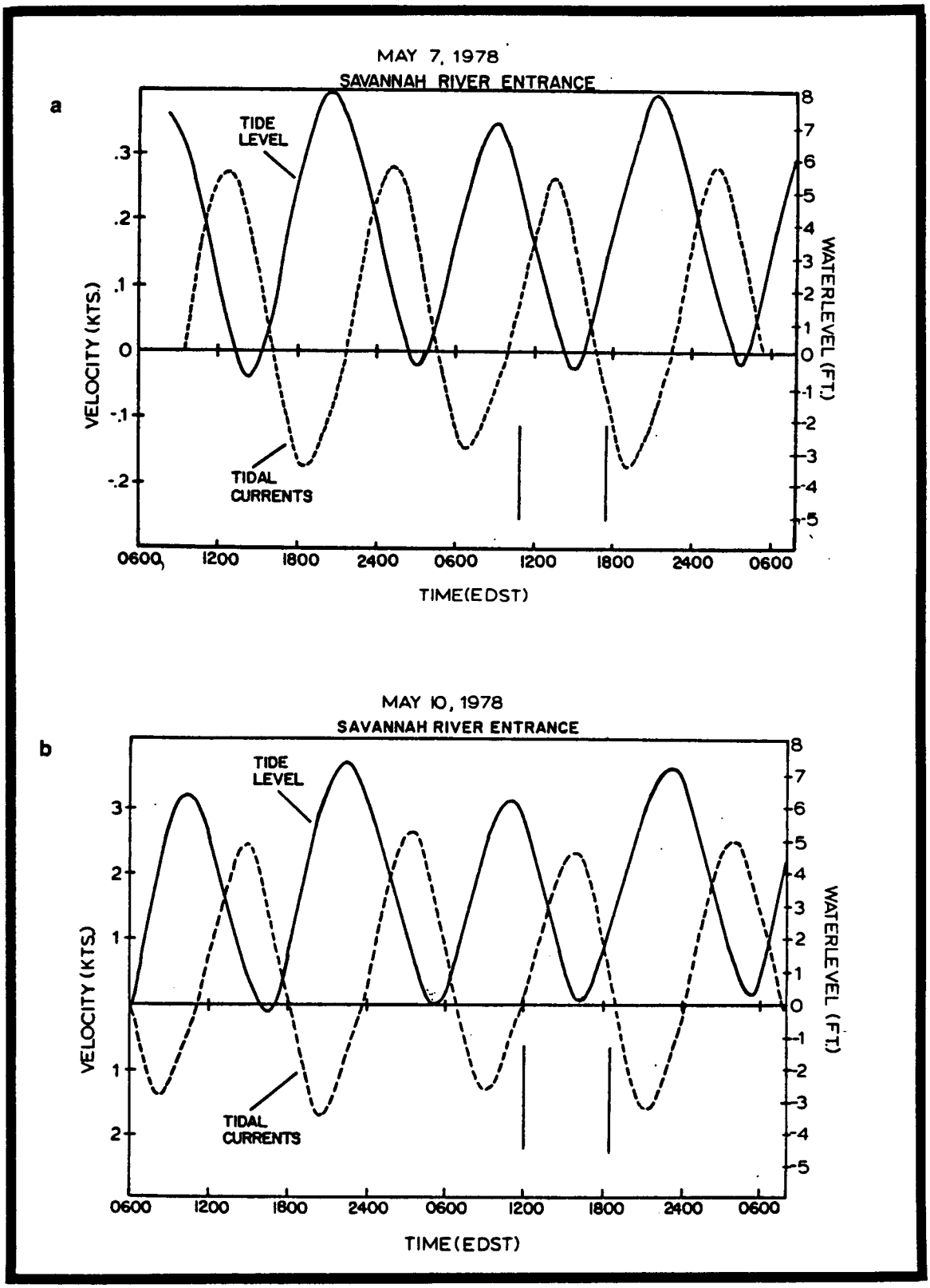

Figure 4-9a and b. Tide levels and tidal currents for Savannah River Entrance from (a) 0600, May 6 to 0600, May 8 and (b) 0600, May 9 to 0600, May 11.

and semidiurnal with water level and currents being out of phase by less than $\pi/2$ suggesting local tides are a mixture of standing and progressive waves.

On May 7, 1978, the semidiurnal cycle occurring during the intensive portion of the study had a range of 2.8 m and current range of approximately 2.2 $m \cdot s^{-1}$. Low water occurred at approximately 1500 and the slack ebb currents occurred at 1645. Within the study area, indications are that slack ebb occurred at approximately 1600. It was at this time that fronts and tracers began to move onshore.

On May 10, 1978, 1/4 of a semidiurnal cycle from slack ebb to past the succeeding max ebb was contained in the study period. It is expected from observations on May 7, that tides in the area would precede the Savannah River Entrance tidal characteristics by approximately one hour.

4.4.1.2 Run-off

A study area close to a river mouth was chosen so if detected, the effects of variable run-off could be examined. Program design called for wet and dry season deployments.

Since daily discharge of the Savannah River can vary considerably, it was necessary to select a general period during which there was a reasonable expectation of either high or low discharge. Using historical discharge data, August was selected as the low discharge (dry season) period while April-May was chosen as the high discharge (wet season) period.

On August 8 and 9, 1977, the daily mean discharge of the Savannah River at Clyo, Georgia was 260 $m^3 \cdot s^{-1}$ and 249 $m^3 \cdot s^{-1}$, respectively, which is approximately 60% of the mean daily discharge for the 1977 water year. On May 7 and 10, 1978, the discharge at Clyo was 320 $m^3 \cdot s^{-1}$ and 331 $m^3 \cdot s^{-1}$, respectively, which is about 23% greater than during the August deployment.

During the experiments, it was not possible to identify specific (orderly) effects due to run-off. However, during the dry season experiment, diurnal variability of discharge was small. In contrast, in May 1978, severe weather, which occurred just prior to the deployment, may have been responsible for what appeared, at times, to be chaotic frontal patterns.

4.4.1.3 Bathymetry - May, 1978

Bathymetry referenced to the local USC & GS datum is shown in Figure 4-10. Gaskin Bank is to the north and appears to have been an effective barrier to migration of a portion of the Calibogue Sound discharge plume. Inshore of Lines 2 and 3 is a depression, probably

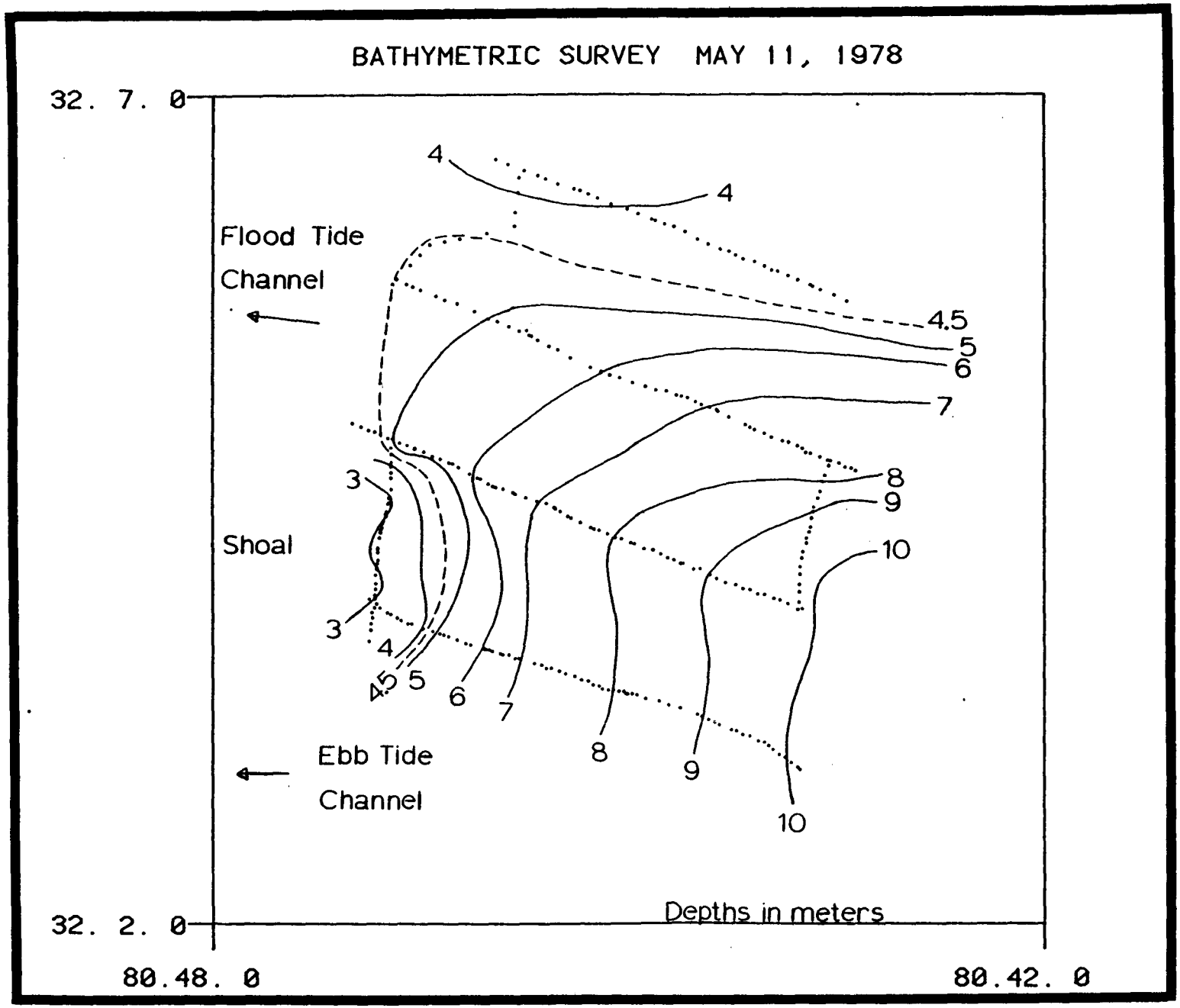

Figure 4-10. Contour plot of study area. Dots indicate digitized depth data. There are seven track lines. Starting in the north, Lines 1, 3, 5, and 7 are oriented NW-SE. Lines 2, 4, and 6 are oriented N-S.

associated with the flood tide system of feeder channels. During flooding tides, drogues released in the study area moved directly up this channel to the southern end of Hilton Head Island. The larger and deeper channel inshore of Line 7 is a major part of the ebb tide delta system. Strong ebbing currents were observed in this channel from near the bottom to the surface.

Details of bathymetry traces did not indicate existence of local bed forms which could be correlated with dominant local near bottom flows. (Sonu, et al., 1972).

4.4.2 Frontal Migration Patterns

Focus of this experimental study was placed on the turbid-clear water interface existing outside the Savannah River and Calibogue Sound estuaries in the coastal region of the Georgia Embayment. However, it is realized that this interface is but one portion of a continuous mixing process which begins well inside the estuary. Both the Savannah River and Calibogue Sound have tidally dominated discharge plumes which move outside the estuary during a portion of the ebbing and flooding tide. As a result of their orientation, respective mixing and discharge characteristics, these two plumes often coalesce soon after leaving their estuaries. Because of their different sources, the waters in the coalescing lobes have different densities and a front is formed along the contact. As a result, what was two plumes, each with an associated semi-circular front, becomes one plume with two lobes of differing density. Frontal migration patterns observed during the two deployments are described hereafter.

4.4.2.1 August 1977 Deployment

Front location number 1 in Figure 4-11a illustrates the plume shape soon after coalescing. With subsequent growth, the front associated with the Calibogue Sound is seen to expand northward and eastward while that associated with the Savannah River discharge expands eastward and southward.

In the north, the plume expands to Gaskin Bank where movement slows and stops. This consistent coincidence of Gaskin Bank and the northern boundary of the Calibogue Sound plume is a persistent pattern seen repeatedly throughout the study period, as illustrated in Figure 4-11b. While northward movement appears inhibited by Gaskin Bank, the eastern boundary continues to move rapidly seaward. An additional sequence of front motion (and tracer migration, described in Section 4.4.3) is shown in Figures 4-12a and b for times ranging from 1144 to 1240.

During low slack water and initial portions of the flooding tide, the northern boundary began to recede to the south, while on the eastern boundary moves to the east (Figure 4-12c, 1300 through 1430 EDT). During this phase, the front became visually less discernible.

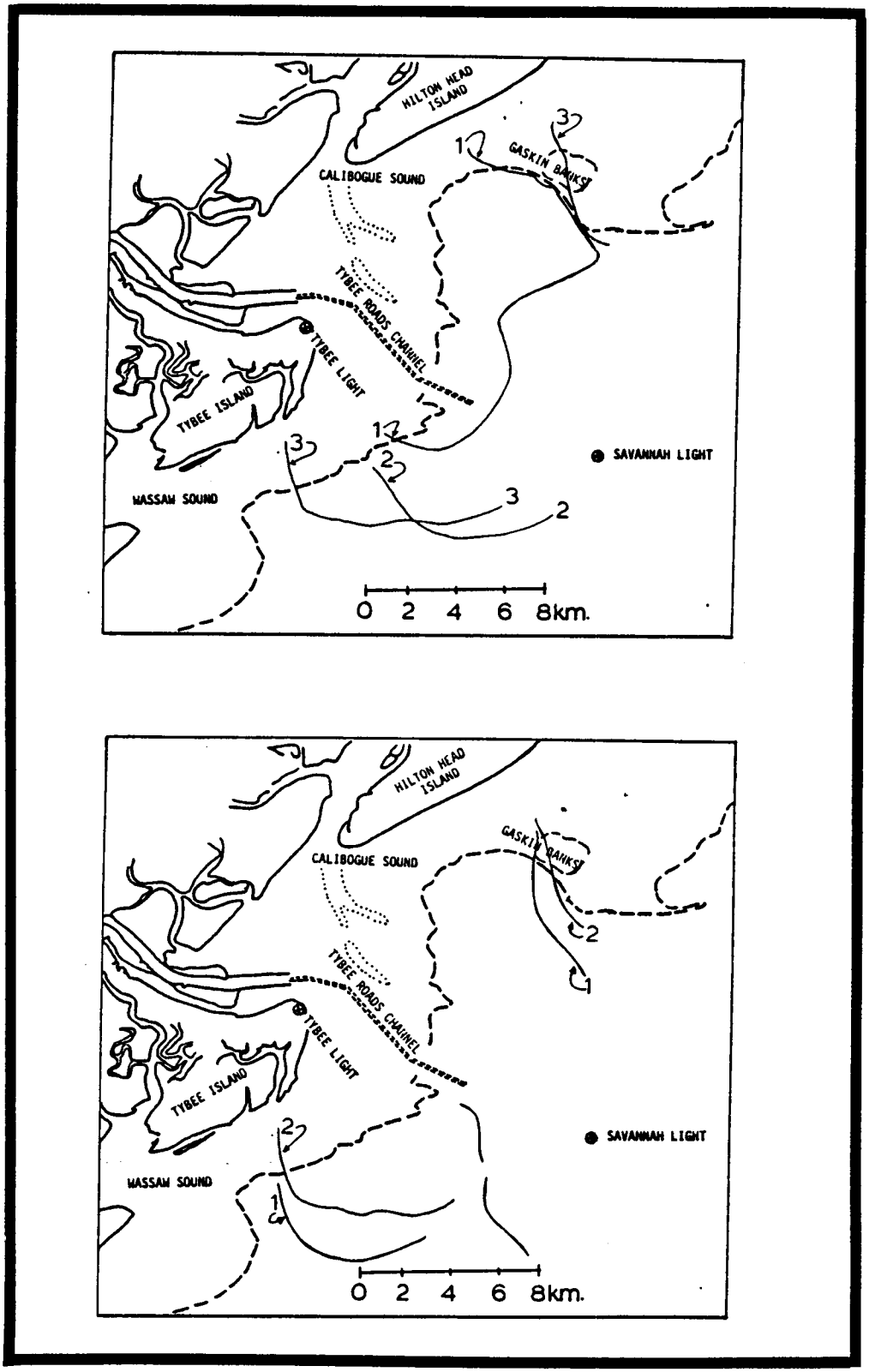

Figure 4-11a and b. (a) Frontal mappings (August 1977) and (b) Overlay of frontal location during similar tidal stages on 8/8/77 and 8/9/77. 1 = 8/8/77 at 1:30-2:00 PM; 2 = 8/9/77 at 2:30-3:00 PM.

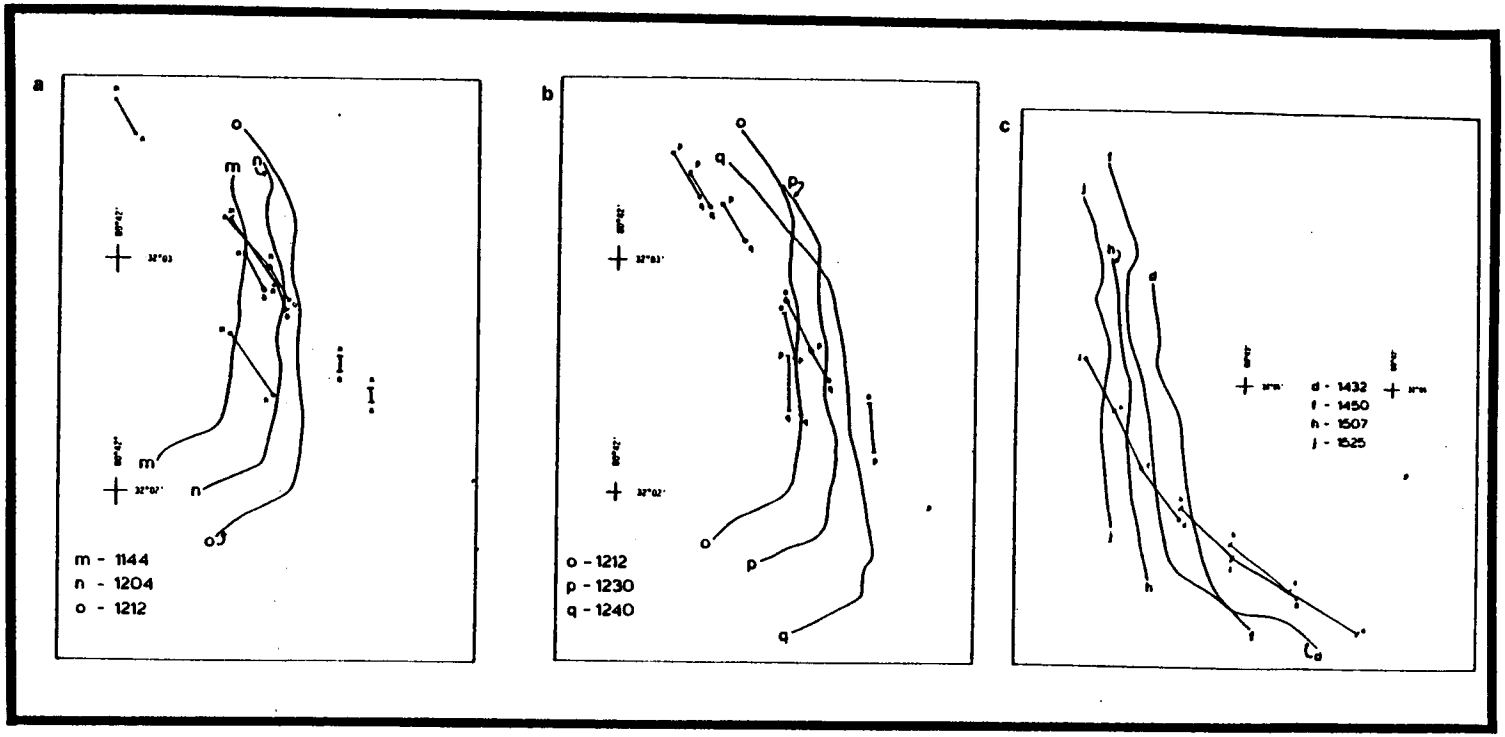

Figure 4-12a, b and c. August, 1977, northern transects. (a) Movement of front and tracers from 1144(m) till 1212(o). (b) Movement of front and tracers from 1212(o) till 1240(q). (c) Movement of front and tracers from 1432 (d) till 1525(j) during flooding tide.

In the northern study area, there appears to be a coincidence of front behavior and tidal currents, with initiation of frontal retreat coinciding with slack water between ebbing flooding tide. This is not unexpected, since a cessation of tidal outflow would eliminate the mass and momentum sources which can cause frontal expansion and associated convergence. Garvin (1974) indicates that local frontal convergence is heavily dependent upon free surface slope in the vicinity of the front which is closely related to tidal stage and flux.

In the southern study area, Figure 4-13 a, b shows the growth of the Savannah River discharge plume. This sequential growth extends southeastward at a very rapid rate (on the order of 1 kt) once the front is outside and south of the ship channel. This very rapid migration was seen and documented repeatedly during this study. Additionally, on August 10 and 11, this front had essentially identical maximum excursion points, which appeared to be quite close to the edge of the ebb tidal delta.

The above excursions of the front were followed by a counter-clockwise radiation of the western edge, categorized as lateral plume expansion. This lateral expansion generally coincided with cessation of seaward expansion. Following the above maximum south-east excursions, the front expanded in the region in the lee of Tybee Island (oriented NE-SW).

Garvine (1974) indicated that lateral expansion of the discharge plume is fundamental to explaining the variable rate of propagation of the front. As might be expected for given discharge and ambient water conditions, increased lateral expansion was associated with a decreased rate of seaward propagation of the front. For the Connecticut River, the particular sequence of plume expansion and growth appeared related to river discharge.

In this southern study area, a feature which appeared to be produced by the convergence of two fronts was seen and photographed. It is assumed that the southern of the two fronts was associated with a tidal plume from Wassaw Sound. Continued expansion of both plumes caused the two fronts to eventually merge at an angle. This situation is somewhat similar to an inverted occluding meteorological front, with the less dense plume remaining at the free surface, i.e., overriding. In this case, it appears that the Savannah River plume is the less dense, as would be expected for the time of year.

As indicated previously, in the central portion of the study area the front was consistently poorly defined. Even though there was an occasional foam line or line of discontinuous color, there was no identifiable feature which would suggest that it defined the leading edge of these plumes of less dense water. The reason for the absence

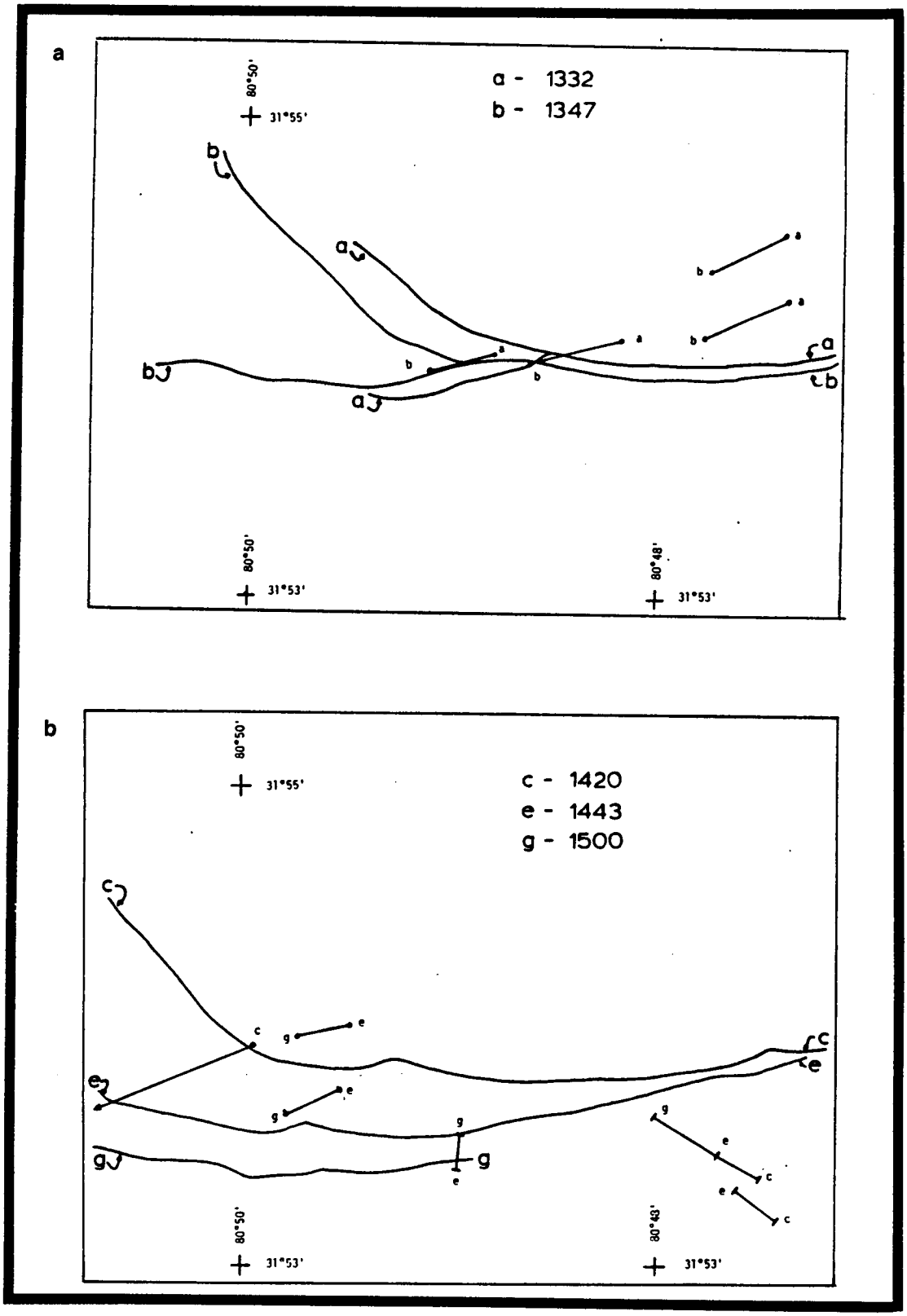

Figure 4-13a and b. August, 1977 southern transect area during ebbing tide. (a) Movement of front and tracers from 1332(a) till 1347(b). (b) Movement of front and tracers from 1420(c) till 1500(g).

of an identifiable feature is not apparent. It is possible that this is a region of increased shear which would encourage mixing which may extend throughout the rather thin surface layer. Garvin (1974) also found intermittent frontal definition in the Connecticut River plume.

4.4.2.2 May, 1978 Deployment

During the second deployment, fronts moved through the study area regularly, as can be seen from Figure 4-14. Although the orientation varied, their presence was rather consistent during some portion of the ebbing tide. Following the initial mapping on May 1, a period of severe weather occurred with strong onshore winds and some associated local heavy rainfall. The combination of wind effects in augmenting tidal flows and high local run-off significantly perturbed plumes from Calibogue Sound. During overflights on May 5, i.e., the day following the end of severe weather, discharge from Calibogue Sound appeared to be greater than usual and a well defined pattern of fronts was not readily apparent. Foam lines and color discontinuities were observed at various times and locations, but they were not distributed in the rather systematic pattern seen previously.

Fronts #1 and #2 (Figure 4-14) are most representative of conditions observed previously and of conditions seen several days following the episode of severe weather. Both of these fronts moved through the study area in an approximately SE direction. The northern plume edge was south of and approximately parallel to Gaskin Bank. By selecting a study area which was slightly inshore of these greater frontal excursions, the probability would be small that some front would not reach the study area before moving onshore with the flooding tide. This was an appropriate decision since multiple fronts moved through the study area during the deployment.

4.4.2.2.1 May 7, 1978 Deployment

On May 7, three distinct fronts moved into and in one case through the study area. Displacement, as a function of time, of each front relative to the fixed hydrostation is shown in Figure 4-15. Distance to the front was measured along a line passing through the hydrostation and approximately normal to the front. Because of the dynamics of frontal migration this normal line generally indicates the direction of most rapid frontal displacement.

The first front (associated with Plume I), and the only one having a foam line, moved past the profiling station at 1200 (EDST) with a velocity of 15 $cm.s^{-1}$ (.3 kt). After 1330, the foam line decelerated until 1430 when it became almost stationary. The shoreward migration of this front during the flooding tide could not be documented in detail because the observation plane had to return to the airport for fuel. The reason for the relatively stationary position from 1430 to

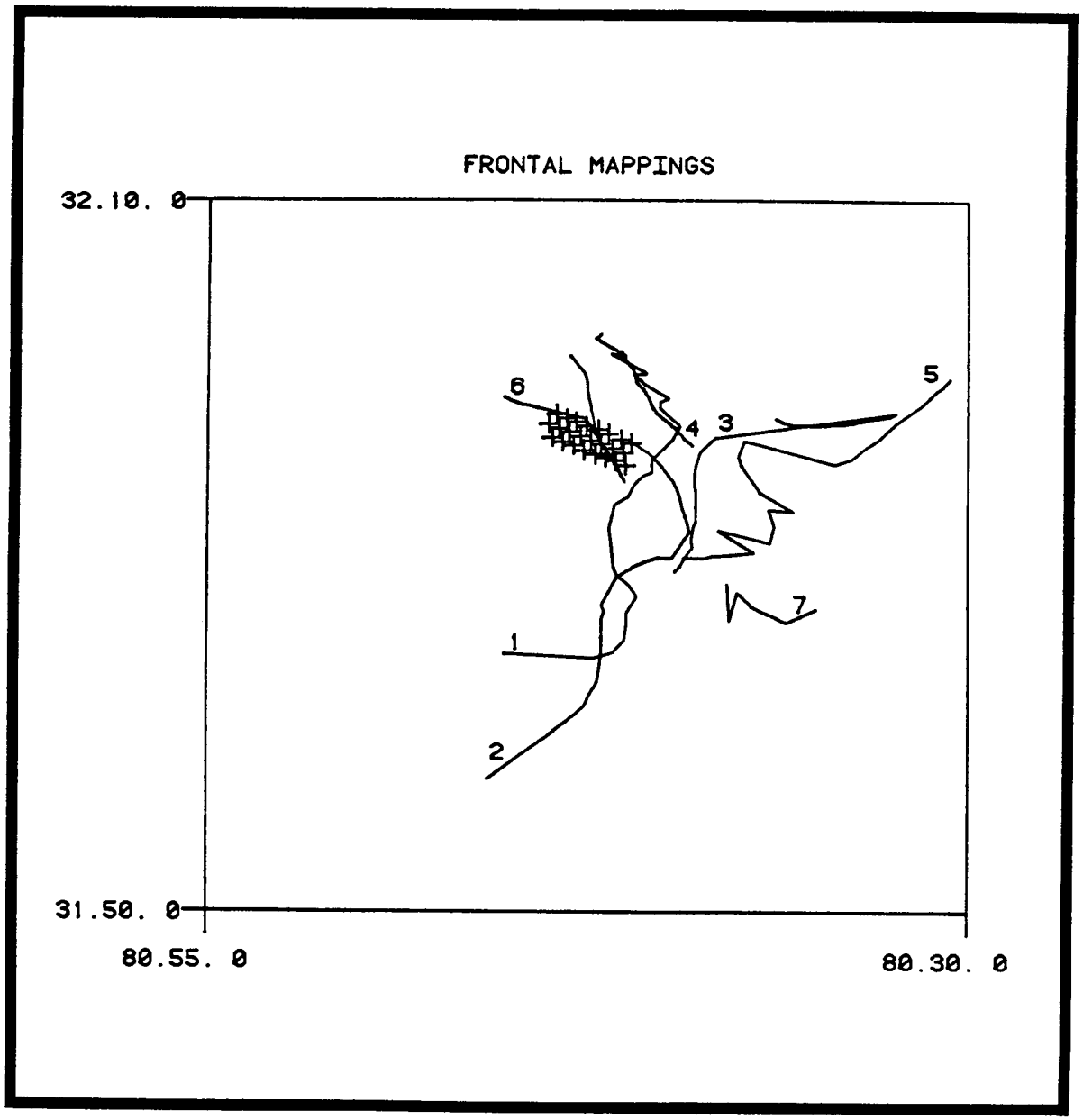

Figure 4-14. Frontal mappings taken on 5/1/78 (1) and 5/5/78 (2-6). The selected study area is indicated by the initial deployment sites of the fixed markers (x).

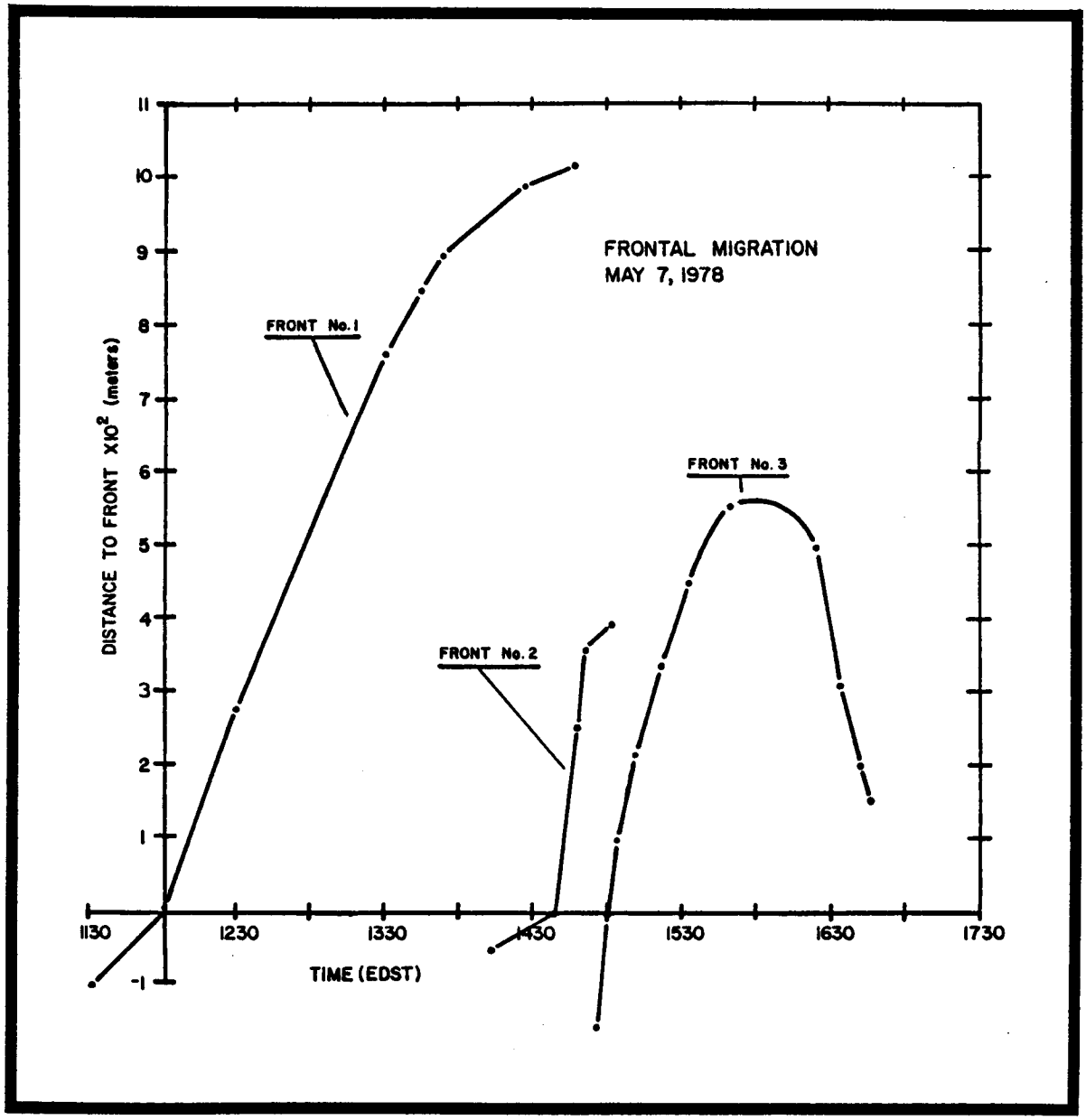

Figure 4-15. Frontal migrations from May 7, 1978 relative to the fixed hydrographic station. The horizontal axis shows time (EDST) and the vertical axis indicates distance from C,T,D, station to the front.

1600 is not known. It is possible that either Port Royal Sound discharge or the presence of Gaskin Banks could have influenced movement of the front.

The second front (associated with Plume II) moved past the measurement station at 1437 (EDST) and advanced rapidly an additional 300-400 m with a velocity of approximately 50 cm.s^{-1} (1 kt). However, the front decelerated rapidly and became quite difficult to identify. This identification had previously been made on the basis of a distinct color change.

Front #3 (associated with Plume III) moved by the hydrostation twice, once moving offshore during ebbing tide with a velocity of approximately 22 cm.s^{-1} (.43 kt) and once moving onshore during flooding tide with a velocity similar to that of the ebbing movement.

As shown in Figure 4-15, this front continually decelerated till approximately 1600 (EDST) when it reached maximum excursion. This front was also defined by a change in water color which was maintained throughout the migration off and onshore.

On the seaward excursions, all fronts had rapid motion followed by deceleration. However, slowing of fronts 1 and 2 and the slowing of front 3 resulted from different causes. The movement of front 3 was closely linked to the turning of the tides while the deceleration of the first two fronts occurred entirely during the ebbing phase.

4.4.2.2.2 May 10, 1978 Deployment

Because of the need to consolidate surface floats, the study area was confined, making it more difficult to assure that a front moved into or through the area during photo flights.

The area where floats were consolidated had had fronts move through on other occasions, however, on the 10th two fronts converged toward the markers from the north and south, but neither front reached the area until near the end of the day. Because of the time required to reposition fixed markers, frontal documentation did not begin until near the end of the flooding tide. Thus, much of the frontal movement was associated with ebbing tide which is a time of strong frontal growth and migration. Many fronts are advected by the ambient current field and there is reason to believe that one front which eventually moved into the monitoring area was due to the southern portion of the Port Royal Sound plume.

4.4.3 Tracer Migration and Lagrangian Velocity Vectors

4.4.3.1 Determination of Tracer Location on a Photograph

As discussed elsewhere, dyes spread laterally and vertically with time. Consequently, in photos taken during successive overflights, the shape and maximum color density of the dye patches evolved with

time. Obviously, some degree of judgment is involved with identifying "one point" as the location of the dye patch. Generally, the region of maximum color density was used as the representative point used to characterize the mean advective velocity of the dye patch. Spreading relative to this point is, in turn, related to diffusion and dispersion, if these processes are active.

Movement of dyes placed in ambient water (i.e., outside of a front) are dictated in part by currents which may be uncorrelated with flows associated with fronts. Thus, what appears to be convergence from the outside of a front may be produced by movement of the front toward the dye. Such movement can be readily identified if displacements are examined in a fixed frame as opposed to a frame-of-reference moving with the front.

4.4.3.2 Tracer Displacement

4.4.3.2.1 August, 1977 Deployment

Displacement of tracers was considerably different in the northern and southern study areas. Consequently, each area will be described separately and then integrated into a comprehensive picture. Reference is made to Figures 4-12a, b, c and 4-13 a, b, which show the tracer migration with respect to the moving front.

In the northern area, for the period of photographic coverage, movement of tracers within the discharge plume can be divided into three separate stages: Stage 1 is associated with ebb tide dominance, State 2 at approximately low slack water when longshore coastal currents dominate, and Stage 3, associated with the combined influence of a flooding tide and longshore coastal currents.

During Stage 1 (Figure 4-12a), tracers within the plume moved eastward in the direction of frontal advance and parallel to the stationary northern frontal boundary. In close proximity to the eastern front, there was a tendency for tracers to be displaced slightly southward by local southerly longshore current. Tracers in the shelf waters also showed a general southerly displacement, with lower velocities over Gaskin Bank and higher ones in deeper water.

During Stage 2 (Figure 4-12b) and the transition to slack water, convergent currents within the tidal plume were small. However, tracers still exhibited considerable fixed frame displacement. This apparent contradiction resulted from the displacement of the entire plume to the south. Transition from Stage 1 to Stage 2 caused the tracers to describe a path showing continued deflection to the right (clockwise rotation).

During Stage 3 (Figure 4-12c), tracers imbedded in the plume appear to have been advected to the northwest at velocities larger than

observed in previous stages. The front became more difficult to identify and elongated patterns of dye suggested intense shear along the submerged density interface.

In the southern study area (Figure 4-13), tracers exhibited a consistent displacement pattern on both sides of the front. This pattern showed a dominant westward drift with a tendency for tracers within the plume to be displaced slightly southward, and tracers outside the plume to be displaced slightly northward. When evaluating this pattern, it is necessary to remember that tracers both north and south of the front were probably imbedded in a tidal plume.

Data from August 10 show general retreat and rotation of the front and an associated tracer convergence toward the front from the ocean side. On the plume side there are indications of slight divergence or no net displacement relative to the front.

To summarize, conditions documented on the northern study area tended to show a lack of strong frontal convergence in spite of large Lagrangian displacements of tracers.

In the southern area within the plume, virtually all tracers were displaced generally westward in conjunction with lateral plume expansion and associated westward and southwestern growth of the front. In most cases there was convergence toward the front although slowly, the tracer displacement component normal to nearest front being small. Tracers injected in shelf waters were consistently displaced to the northwest and therefore converged to the front at an angle.

Results of this experiment indicate that the surface tracers, i.e., aluminum powder and paper, did not move across the front. Whether the material arrived at the front from the plume side or ocean side, there was no known incident where the tracer crossed the interface. This is not the case for the dyes representing dispersed pollutants. In a few isolated cases, rhodamine was observed to reach the front from the plume side and be transported down the density interface. Likewise, it was found on several occasions that fluorescein arrived at the front from the ocean side and streamed down the interface.

4.4.3.2.2 May, 1978 Deployment

During ebbing tide, dyes released in the more turbid plume water fairly consistently moved to the front and were subducted back down along the density interface. Figure 4-16 gives a schematic illustration of the velocity field relative to a frame of reference moving with the front. At the surface, tracers will converge to the front only if their velocity exceeds the rate of advance of the front. Thus, in a fixed frame, surface tracer displacement could be

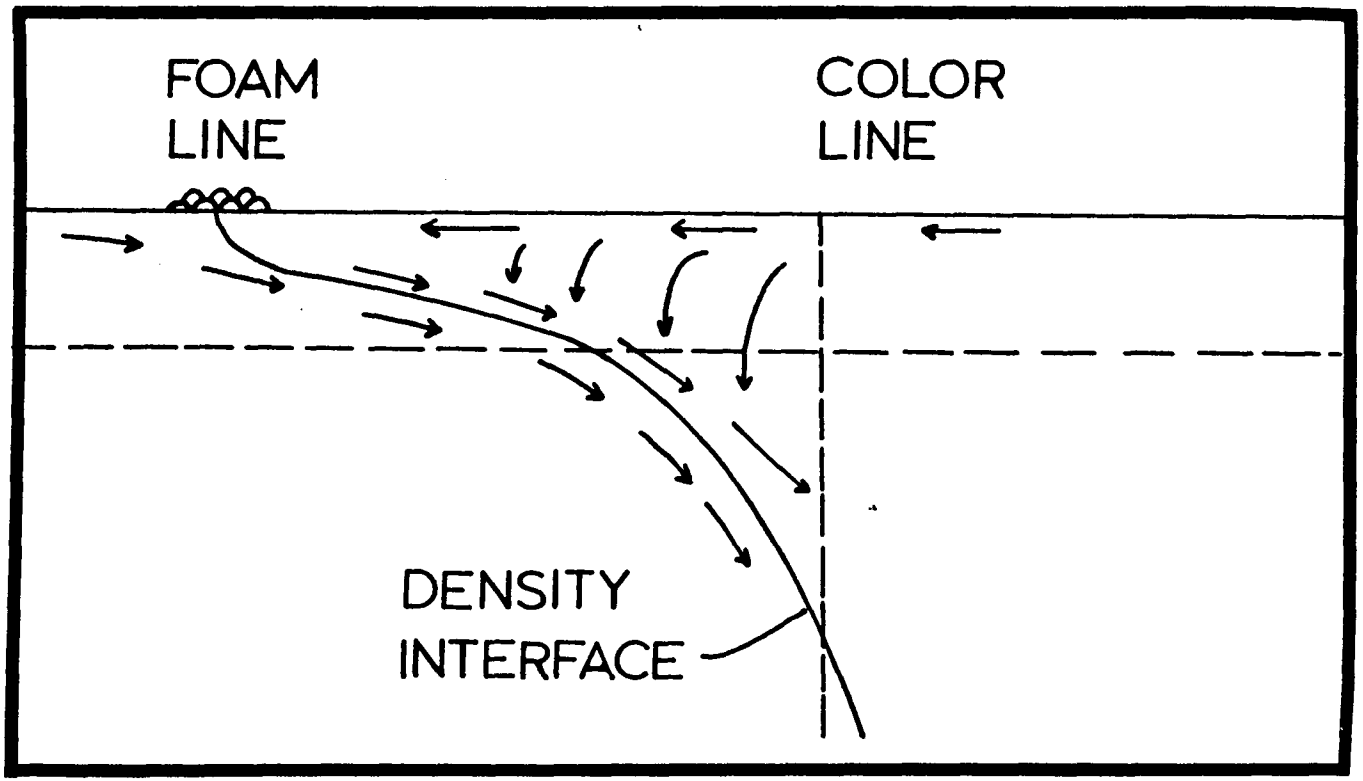

Figure 4-16. Schematic of frontal cross-section showing velocities relative to an origin moving with the front. Note convergent surface velocities and subduction along the density interface.

very large with rapid frontal migration (about 20 $cm.s^{-1}$ although velocities of 40-50 $cm.s^{-1}$ were observed outside the study area, in particular close to the mouth of the estuary). Thus, during ebbing tide, expected fixed frame tracer velocities should be greater than approximately 20 $cm.s^{-1}$.

May 7, 1978 Deployment

As indicated by the fixed markers, the deployment region was the western half of the larger study area shown in Figure 4-2. The mouth of Calibogue Sound was directly onshore of the three NW-SW oriented rows of fixed markers, therefore, movement parallel to rows of fixed markers was movement toward or away from Calibogue Sound.

Because of delays due to a gas leak in the camera plane, the first aerial photographs were taken at approximately 1600, about the time local tidal currents changed from ebb to flood. Consequently, photographically documented tracer migration was completely within the flooding tide.

All dyes, aluminum flakes, and drogues migrated toward Calibogue Sound supporting the assumption that the documented movement was completely within the flooding tide phase. The general pattern indicated an expected slight onshore acceleration from 1600 to 1700 with relatively constant velocities following 1700. Tracer migration velocities were generally between 20 and 40 $cm.s^{-1}$ with most being between 20 and 30 $cm.s^{-1}$.

A representative example of movement of tracers deployed seaward of a front is given by the migration pattern of R5D and AR5D in Figure 4-17a and b. These two tracers were initially injected inshore of a front which was not seen in the photographs as mentioned above. Therefore, relative to the digitized front, movement of these tracers reflect behavior of tracers deployed offshore of the plotted front. Both dye and aluminum particles converged toward the front as all were displaced toward Calibogue Sound. Velocity of both types of tracer differed little. The aluminum moved across and eventually well past the front. Dye also moved slightly past the front in the final observation. After crossing the front, the position of the dye in the water column is uncertain; however, if it was consistent with previous situations, it was being subducted down the interface.

Apparently, the general pattern of the dye movement is independent of tides, however, the forces driving the system may be considerably different during the ebbing and flooding tide. As developed in an integral model by Garvine (1975), frontal dynamics were driven by the density field and an associated sea surface slope and included shear along the density interface. During the flooding tide and the associated decreased local sea surface slope, it is possible that the local tidal flow created sufficient shear along the density interface to drive a similar two dimensional circulation pattern.

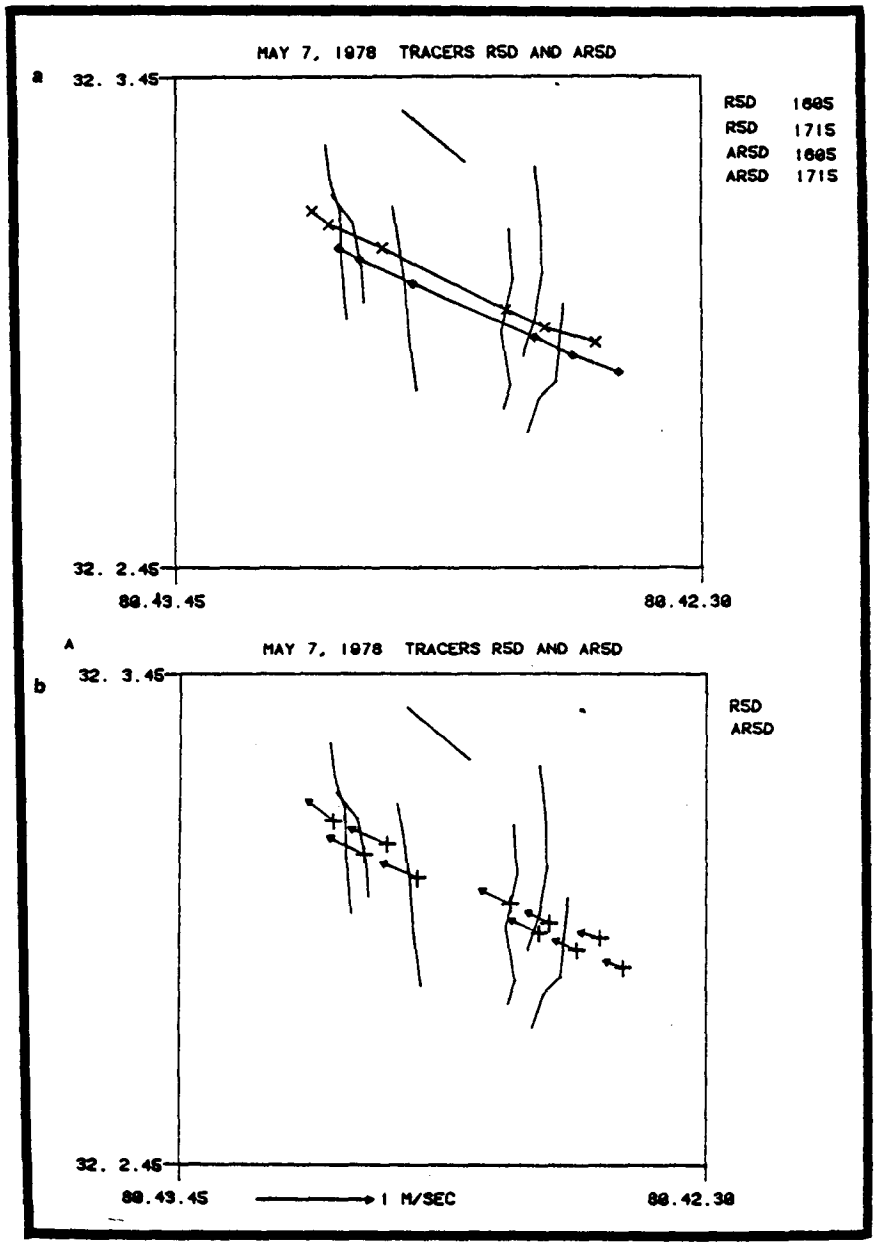

Figure 4-17a and b. (a) shows sequential displacement of dye patch R5D (◈) and associated aluminum AR5D (x). (b) shows Lagrangian vectors for displacement shown in (a). Vector magnitudes scaled by the unit vector (m/s) at the bottom. Front locations are shown for each determination of tracer position. The eastern or northern front was associated with the initial eastern or northern tracer position. The tracers and associated fronts moved sequentially westward or southward.

Behavior of the aluminum differed significantly from patterns seen in the first deployment (August 1977) when particles accumulated along the convergence zone. During that study, the pattern of accumulation was relatively independent of tide stage. During the present study, winds were consistently onshore and, as discussed in a following section, were sufficiently strong to create elongated streaks and possibly Langmuir circulations. The impact of winds was most evident when they were obviously retarding or enhancing aluminum migration relative to dye migration. During the ebbing tide, an excellent example occurred when tracers were moving directly into the wind due to currents, however, the aluminum was moving at about half the speed of dispersed dyes.

Figures 4-18a and b illustrate the behavior of dyes inshore of the front. The net direction of motion was onshore, however, relative to the front the dye moved toward the front and the aluminum particles moved away from the front. This is an excellent example of possible differential response of surficial and dispersed pollutants. These figures also show the somewhat divergent migration of tracers initially deployed in close proximity to one another.

Another example of divergent migration of dyes and aluminum and differing dye releases is shown in Figure 4-18c for R6A, AR6A, R6B, and AR6B.

The observed differential movement of the dyes was probably associated with intermediate scale diffusion while the divergence of dyes and associated aluminum resulted from both diffusion processes and the influence of wind drag on the aluminum.

These tracers were deployed normal to the front when the latter was in position A. During the documented interval, fronts moved onshore and to the south. The combination of frontal movement and surface velocities caused the tracers to tend to converge toward the side (northern) boundary of the plume. The convergent velocity was a small component of the total velocity with the dominant velocity component being parallel to front B.

May 10, 1978 Deployment

Migration of tracers was documented photographically from 1247 to 1832 on May 10, 1978. This interval includes a complete ebbing tide, the tide turning from ebb to flood at approximately 1830, with the preceeding high slack water occurring at approximately 1230. Front did not move into the limited study area until 1600 hours. Prior to this time, eight non-radio bearing drogues were released and their motion tracked. Photographic monitoring of these drogues provided much of the information regarding the general circulation pattern.

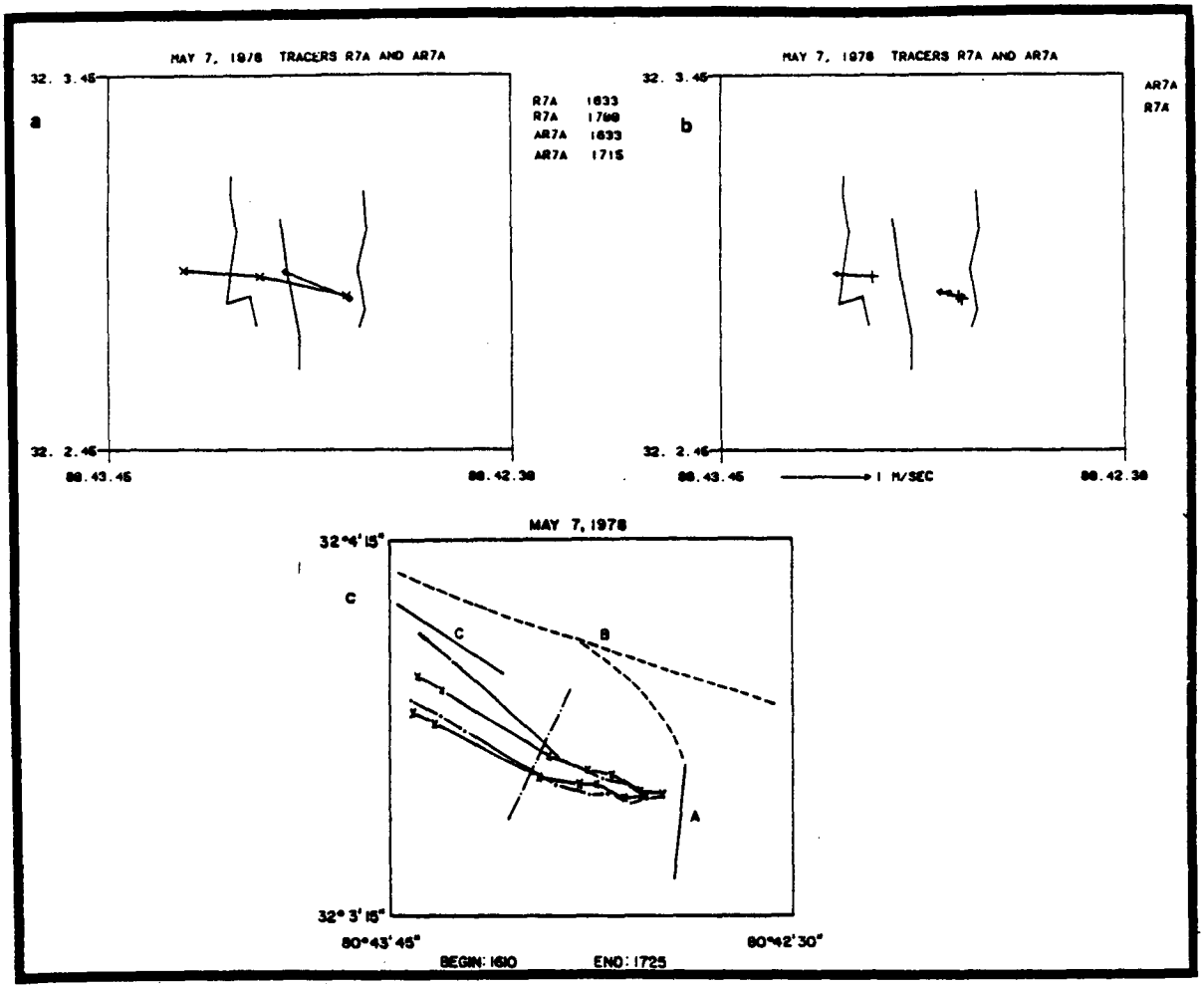

Figure 4-18a, b and c. (a) shows sequential displacement of dye R7A (◈) and associated aluminum AR7A (x). (b) shows Lagrangian vectors for displacement shown in (a). Vector magnitudes scaled by unit vector (m/s) at bottom. Front locations are shown for each determination of tracer position. The eastern or northern front was associated with the initial eastern or northern tracer position. The tracers and associated fronts moved sequentially westward or southward. (c) Sequential migration of R6A(-·-), R6B(-·-), AR6A(x), and AR6B(x). Tracer identifiers ending in 6A were initially deployed closer to the front. Segment A was the location of the front about which these tracers were deployed closer to the front. Segment A was the location of the front about which these tracers were deployed. Dashed line B(---) shows the larger pattern of fronts existing at 1610. Segment C is the location of the northern boundary of the front at 1725, i.e. B had moved SW to position C. The line crossing all the trajectories is referred to in the text.

The general fixed frame pattern of tracer migration is illustrated in Figure 4-19, which combines the displacement path of radio drogues 645 and 662, from 1237 to 1330 and 1433 to 1603, respectively, and dye patch F2C from 1618 to 1832. The combination of trajectories provides an approximation of a total single displacement during the indicated period.

Similarities between the above tracer trajectories and the Eulerian progressive vector diagram for tidal currents at the Savannah Light are strong with a coincidence of key events such as high and low slack water. Such a comparison may be somewhat justified because the actual Lagrangian displacements all occurred in the same general area (.37 km^2). Due to the similarity of these trajectories, it is probable that dominant tracer motion was tidally induced. This should hold for plume and tracer motion.

During the ebbing tide, there were numerous incidences of convergence and subduction. Only representative examples will be discussed here. Behavior of dyes released inside the plume are illustrated in Figures 4-20a and b, for R5A, AR5A, R5B, and AR5B from 1707 to 1806. Both dye patches (R5A and R5B) converged to the front as did the associated aluminum tracers AR5A and AR5B. In each case, the aluminum moved further to the south than did the dye. During this period, the front moved .7 km to the SW, i.e. had a SW directed velocity of 19 $cm.s^{-1}$. Relative to the front, the tracers had a velocity of approximately 1.4 $cm.s^{-1}$ or a fixed frame velocity of 20.5 $cm.s^{-1}$ to the SW. Thus, the convergent velocity was only 7% of the combined tidal and frontal velocity and, considering the magnitude of tidal currents at the Savannah Light close to low slack water, about 10% of the plume driven frontal velocity.

Convergence toward the front from outside the plume is illustrated in Figure 4-21a and b for F5E and AF5E. In approximately 40 min, the front moved to the SW 30% faster than the dye and aluminum. The aluminum and dye have divergent paths. After being deployed initially at the same location, they were 100 m^{-1} apart after 40 min, i.e. had a divergent relative velocity of 4 $cm.s^{-1}$.

4.4.3.3 Behavior of Dyes and Tracers Along/Across the Interface

Since all dyes were injected from a stationary or very slow moving boat, initial dye patches were vertically and laterally concentrated. Also, since dye and aluminum were contained in the same packet, both types of tracer were deployed at the same location. Any subsequent position differences resulted from differential response due to the type of material (surficial or dispersed) or from the relative influence of active processes (e.g. wind drag on aluminum).

Following deployment, some dyes were dispersed vertically, laterally, and longitudinally. Dyes placed at the surface and away from the front began to spread almost immediately due to wave related mixing.

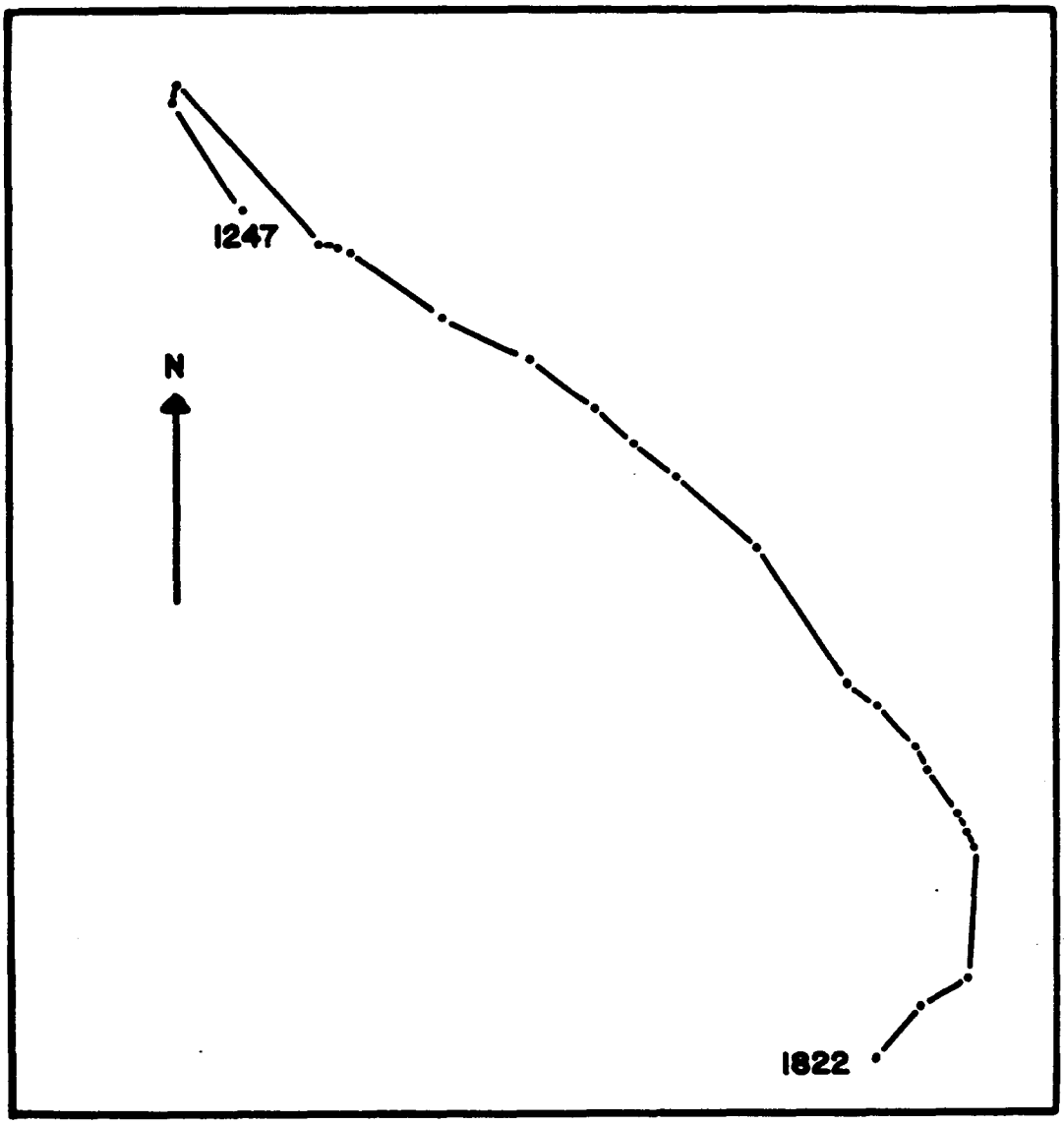

Figure 4-19. Composite of tracer migrations of May 10, 1247 to 1822. Displacement of three separate tracers for three separate intervals were positioned end to end to approximate displacement of a tracer during the entire period.

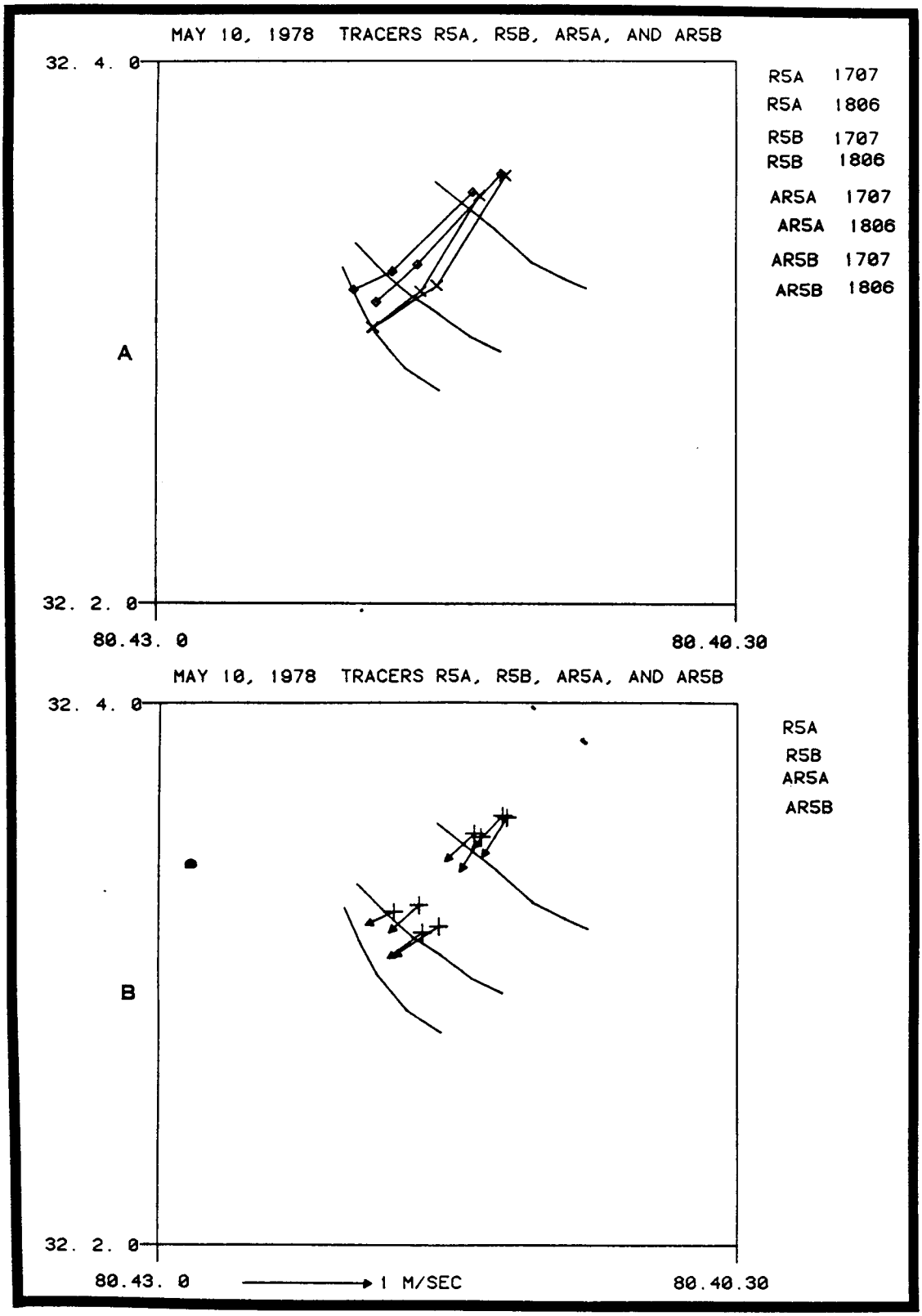

Figure 4-20a and b. (a) Sequential displacement of dyes R5A and R5B (◇) and associated aluminum AR5A and AR5B(x). (b) Lagrangian vectors for R5A and AR5A above. Vector magnitudes scaled by unit vector (m/s) at bottom. Frontal locations are shown for each determination of tracer position. The eastern or northern front was associated with initial eastern or nothern tracer position. The tracers and associated fronts moved sequentially westward or southward.

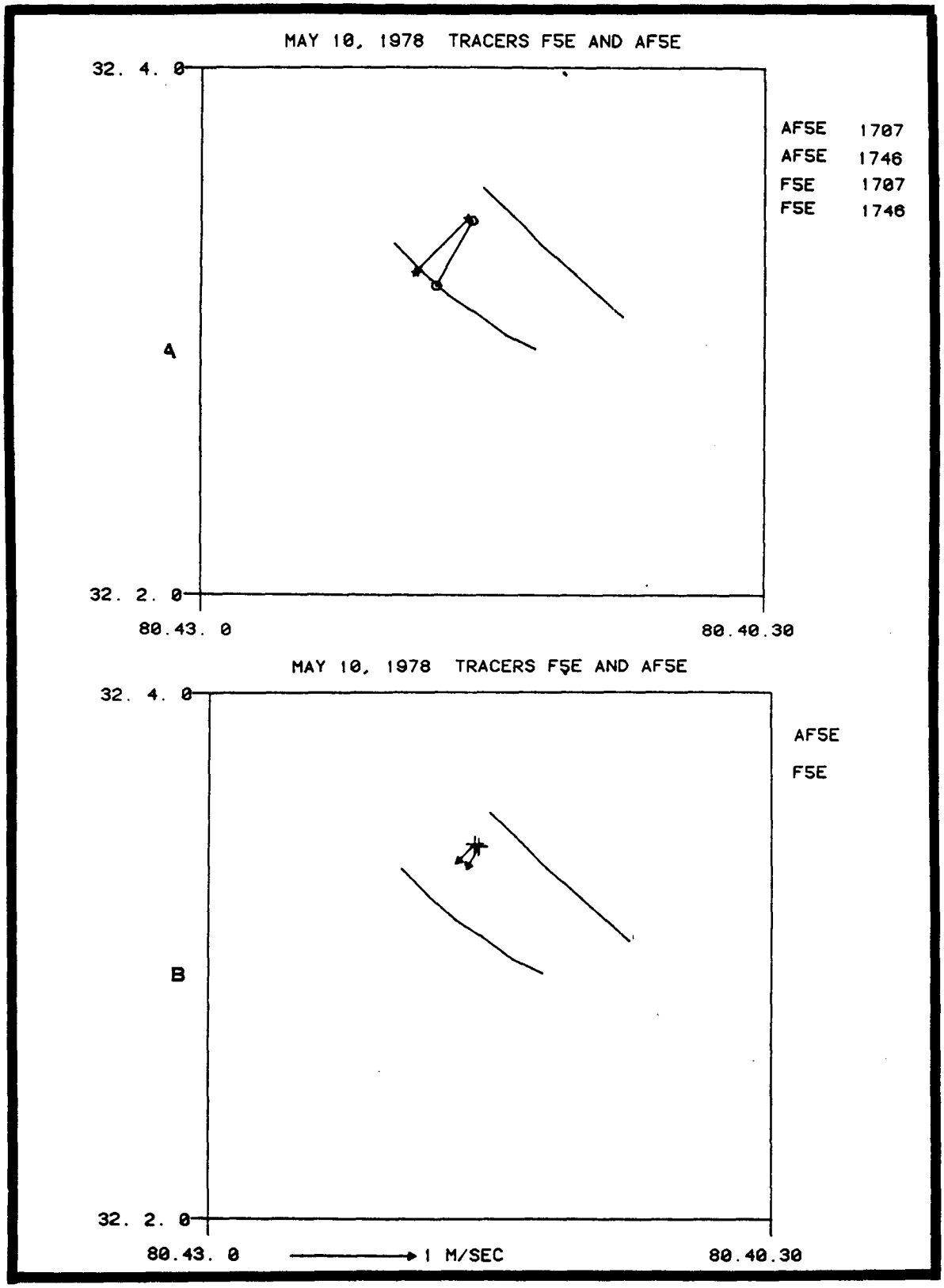

Figure 4-21a and b. (a) shows sequential displacement of dyes F5E (*) and associated aluminum AF7E (⌂). (b) shows Lagrangian vectors for displacement shown in (a). Vector magnitudes scaled by unit (m/s) at bottom. Frontal locations are shown for each determination of tracer position. The eastern or northern front was associated with initial eastern or northern tracer position. The tracers and associated fronts moved sequentially westward or southward.

In addition, some dye movement suggested the existence of lateral shears which could enhance any lateral displacement. The scale of such shear and of the associated diffusion could not be estimated.

In the vicinity of active fronts, three dimensional diffusion and dispersion interacted primarily because of the local flow field and mixing induced by shear, the most important one being vertical. Mass exchange resulting from vertical mixing produced by vertical shear can transport dyes toward the submerged density interface without actually reaching the surface front and being subducted down along the density interface. These somewhat diluted concentrations of dye can begin moving down the density interface before any substantial quantity of surface dye reaches the front. This is a continuous mixing process which becomes more apparent with proximity to the front where vertical shears can intensify. If the dye concentration is vertically integrated, which approximates viewing these dye concentrations from the air, the above process appears as longitudinal spreading.

Depending on conditions, e.g. oblique convergence to the front from both sides, etc., multiple scenarios can be developed, many of which have been observed. However, they all result in continued dilution of the initial concentrated dye patch into a rather diffuse stain. Note that the above process can result in more apparent lateral spreading for dyes released in plume water than for dyes injected offshore of the front.

For dyes deployed in the plume, the spreading sequence described above could occur even if there is little mixing between plume and ambient water. The pycnocline between water masses was often fairly strong and hydrographic data suggests that mixing across the pycnocline was strongly inhibited. However, within the plume water, i.e. above the main pycnocline, where density gradients were much weaker but visual observations suggested vertical velocity gradients existed, the described vertical mixing sequence seems to have occurred. Although direct velocity measurements were not made in this study, results from Garvine (1974) and Garvine and Monk (1974) support the existence of a strong shear zone across the local pycnocline and into the relatively undiluted plume.

In several instances, particularly near the time of slack water, longitudinal dispersion resulted from vertical mixing in the presence of a non-uniform, but quite possibly unidirectional, vertical velocity profile. If dye is distributed vertically by some mechanism, the different magnitude velocities occurring at various depths cause differential displacement (of the water and dyes) with time. If the mean velocity gradient is sufficiently strong to induce vertical mixing, then even if dye is initially deployed only at the surface, longitudinal spreading eventually results. The longitudinal spreading is due to dispersion, not diffusion, although vertical

diffusion may have been responsible for dyes being distributed through the water column. One rather obvious example of this occurred where local flows were parallel to a weak foam line.

As indicated previously, there were several instances when dyes and aluminum had considerably different trajectories due to wind shear. Sometimes, under strong wind conditions, both dye and aluminum were seen to move in the direction of the current, but the aluminum exhibited a more rapid or slower displacement than the dye, depending on whether the wind stress was in support of or in opposition to the currents, or if wind stress acted at any angle to the frontal driven currents, aluminum particles would have a component displacement transverse to the movement of the dyes. Both situations were observed at different times and locations.

4.4.4 Hydrography

4.4.4.1 Introduction

During this study the density field was dominated by salinity. There were no instances when temperature caused the shape of the density profile to differ substantially from the salinity profile and only few cases where stability as dictated by temperature would differ from stability as dictated by salinity, i.e. if salinity was stably stratified, then so was temperature.

In spite of the apparent minor role of heat in influencing the field of mass, temperature did provide an excellent tracer to help define vertical and horizontal mixing processes, as temperature profiles showed important features more succinctly than do the salinity or density profiles. Thus, the upper boundary of the relatively unmixed shelf water was often more apparent in temperature than in salinity profiles. Likewise, following turning of the tide, vertical mixing through this previously rather uniform layer was more discernible in the temperature profiles.

A feature which is identifiable only in the temperature data is the persistent inversion which occurred with the passage of Front #2 on May 7, 1978. These inversions apparently resulted because of overriding of and subduction along the density interface, in this case the pycnocline. Profiles show a very stable distribution of density which suppressed vertical mixing and which apparently allowed such a thermal feature to be maintained for over an hour and hundreds of metres behind the front. This conclusion was not apparent from an examination of salinity which indicated only the stable density field.

4.4.4.2 Cross Sections

Although cross sections of the density, temperature and salinity structures were produced for both deployment days (May 7 and May 10), only those related to the May 7 experiment will be discussed hereafter. A similar discussion of the May 10 results was submitted in a Surface Current Report, dated February 1979. Because salinity dominated the density field, a discussion of the density cross sections also applies to the salinity field.

4.4.4.2.1 Density Cross Sections

Although strong horizontal and vertical hydrographic gradients existed during this study, transitions between readily identifiable features did not generally occur as a discontinuity. However, for this discussion, appropriate isopycnals are used to define boundaries between regions.

As seen in Figure 4-7 shown in a previous section, the lower boundary of Plume I is defined by the 20.6 σ_t isopycnal. Spatial density gradients are weak above this surface which originates immediately behind the front and descends to 1.6 m approximately 200 m behind the front. This depth is maintained till 600 m where the 20.6 σ_t isopycnal descends to 3.5 m.

The upper boundary of the undiluted shelf water is defined by the 21.8 σ_t isopycnal which extends from the surface just seaward of the front to the bottom about 840 m behind the front. This isopycnal descends rapidly near the front, then gradually deepens until approximately 620 m where it descends relatively rapidly until intersecting the bottom. Between Plume I and the undiluted ambient water is the region of mixing between the two water types with the strongest density gradient generally falling in the upper portion of the layer. The strongest pycnocline occurs in this region in the vicinity of the front, with changes of .9 σ_t in approximately 30 cm normal to the isopycnals, or 60 cm in the vertical. Continued mixing causes a spreading of the density surfaces so that for positions more than 100 m behind the front, the pycnocline is spread over 1.5 to 2 m. From 240 m to 600 m, the pycnocline remains essentially unchanged. At 600 m a local intensification of the pycnocline is observed, after which the density gradient becomes less steep and descends with an associated expansion of relatively undiluted plume water.

Approximately 80 m, 240 m, and 630 m, behind the front, abrupt vertical displacements of isopycnals can be identified. It is interesting to note that the change generally occurs only in the pycnocline. As an example, the change at 240 m is not evident in upper density surfaces in the pycnocline nor was it well defined

below the pycnocline. This latter was also the case at 80 and 630 m. At first inspection these features have some of the morphology of an internal bore.

Plume III is delimited by the 19.1 σ_t isopycnal, Figure 4-22. Above this surface, horizontal density gradients are weak although well behind front 3, i.e. greater than 400 m, the 19.0 and 19.1 isopycnals converge to become part of the pycnocline. Below Plume III, definition of regions becomes complicated because they reflect mixing resulting from the first two plumes. Below the 21.6 σ_t isopycnal, the distribution of density, resulting from very weak mixing of shelf and Plume I waters, change little from a point 800 m behind Front 1, and in front of Front 2. The region between the 21.6 σ_t and 20.6 σ_t results from significant mixing between Plume I and ambient shelf water. The zone between the 20.6 σ_t and 20.0 σ_t isopycnals results from mixing of water from Plume II and water having characteristics dictated by prior mixing of Plume I and shelf water. Between 20.0 σ_t and 19.1 σ_t isopycnals, the hydrographic characteristics are produced, for the most part, by mixing of Plume II and Plume III water. Above the 19.1 σ_t surface is Plume III described above.

4.4.4.2.2 Temperature Cross Sections

The temperature cross section corresponding to the density section shown in Figure 4-7 is presented in Figure 4-23. As indicated above, temperatures show a very strong similarity with salinity, and hence density sections although it provides greater resolution in some cases because the total change in temperature results in more incremental ($\Delta T = .1^{o}C$) steps. The similarity is expected since hydrographic parameters result from characteristics of separate water masses or mixing between water masses -- the latter obviously involving mass exchange and hence associated moderation of respective characteristics.

The series of pycnocline undulations are readily visible in the temperature section and, in fact, are slightly better defined. A feature which is very well delineated is the fanning out of isotherms following the almost discontinuous temperature jump approximately 600 m behind the front. By approximately 900 m behind the front, the thermocline has become quite diffuse in comparison to previous conditions. This indicates that vertical mixing was taking place which resulted in a sequential expansion of the thermocline from a feature less than 1 m wide to more than 2 m. It should be noted also that the thermocline expanded downward only since the upper isotherm of the thermocline is seen to remain fairly level until it gradually descends between 900 and 1000 m. The isotherms at mid- depth, 5 m also remain at a constant level following the almost discontinuous undulation occurring at 600 m. Below the horizontal mid-depth isotherm, isotherms descend to the bottom.

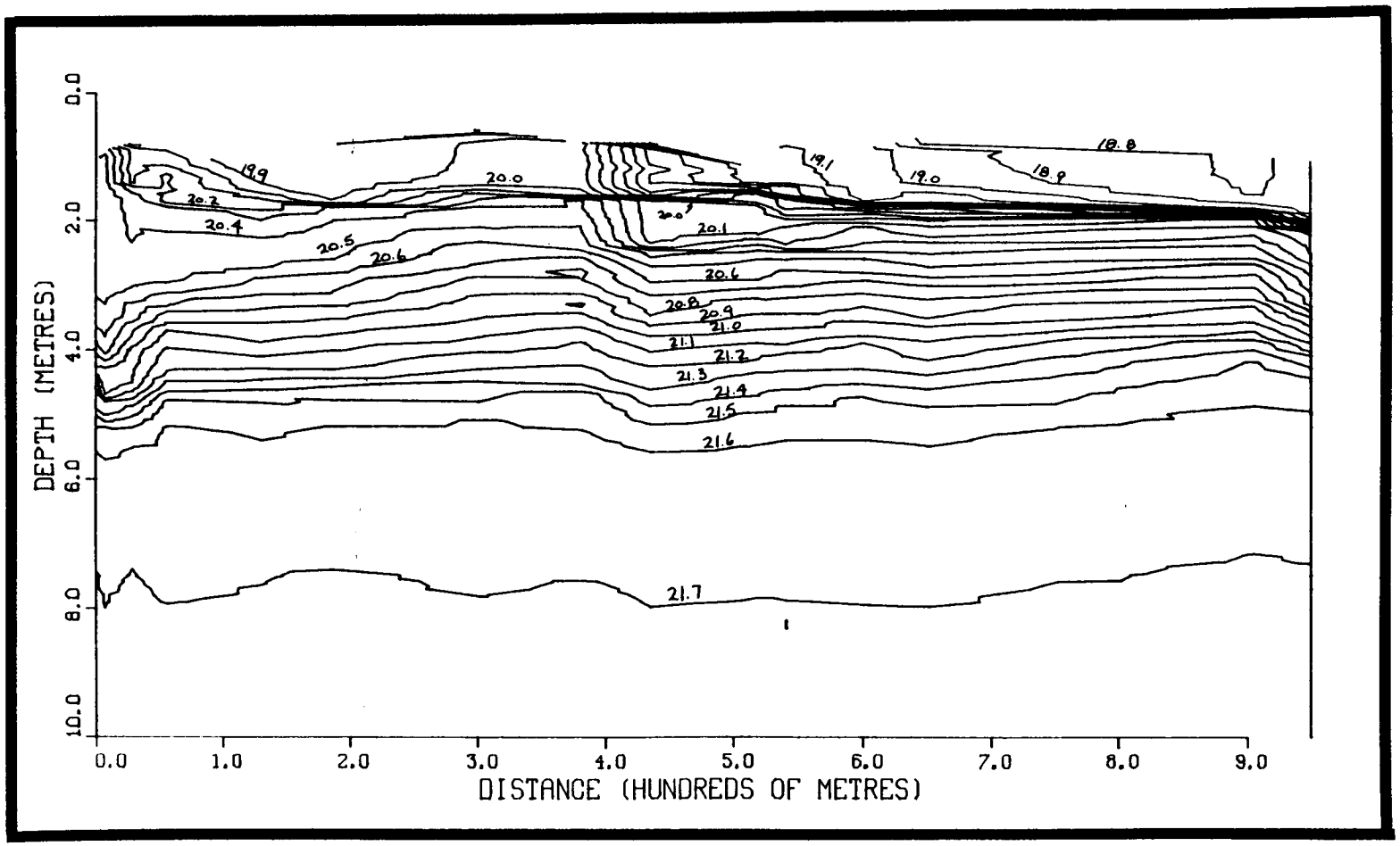

Figure 4-22. Contour plot of synthetic density cross section for Fronts II and III, May 7, 1978.

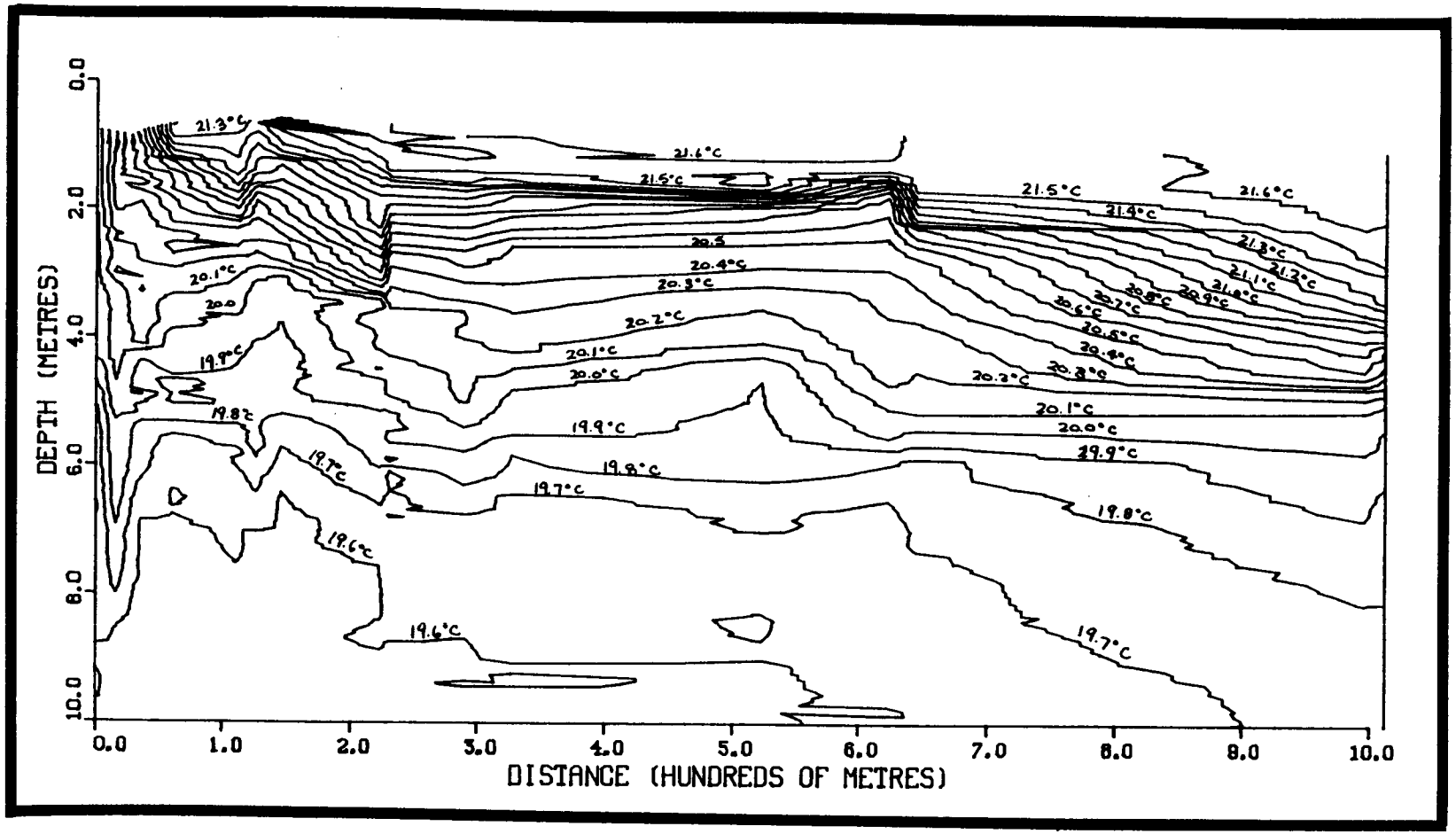

Figure 4-23. Temperature cross section corresponding to density section in Figure 4-7.

Temperature cross sections corresponding to the density structure presented in Figure 4-22 is shown in Figure 4-24. Below approximately 4 m, the stably stratified isotherms remain approximately level suggesting a lack of vertical mixing. Above 4 m, several very prominent features can be identified. A temperature inversion is found below and behind both Fronts 2 and 3. Prior to arrival of Front 2, the warmest identified temperature surface isotherm was the 21.6°C isotherm at about 2.2 m. Plume II appears to have overridden this water, forcing it down and underneath the warmer, fresher plume water. This results in a temperature inversion which persists well behind the plume front. A similar feature also occurs beneath and behind Front 3.

The precise dynamics which created such features is not immediately evident. Certainly, vertical mixing beneath the plume must be inhibited where density gradients are strong, otherwise the feature would not have persisted (see density cross sections). However, where the warmer water has intruded below the cooler water, the density gradients are much weaker than in the surrounding water, above and below. The salinity of the warm water intrusion was the same as the surface water prior to the arrival of the front. This arrangement occurred for the warm water intrusions under Plumes II and III. It is known that the fronts were advancing with convergent surface currents. However, subsurface currents are unknown and, therefore, it is not possible to determine exactly why the surface water was being subducted and remained relatively unmixed for an extended period of time.

Under the front associated with Plume III, there was a relatively large mass of unmixed surface water which eventually intruded below the plume and below part of the previously mixed ambient water. Without knowledge of the velocities, this situation seems to have been dictated by density field.

4.4.4.3 Discussion of Observed Frontal Structures

The Neil-Brown CTD unit provided measurements of the vertical hydrographic parameters with great accuracy and fine resolution. Consequently, detailed frontal features could be identified.

The plumes documented in this study were often similar in configuration to Connecticut River plumes documented in the series of studies reported in Garvine (1974a), Garvine and Monk (1974), Garvine (1974b), and Garvine (1975). Below the front the density interface descended rather rapidly with the slope being on the order of 1:80, to a depth of one to two metres depending on the plume. On reaching this level, the pycnocline maintained a rather constant depth for several hundred metres behind the front. When multiple fronts occurred, the depth to which the latter density interface descended was generally less. This probably resulted because of changes in the density field into which each successive plume was moving.

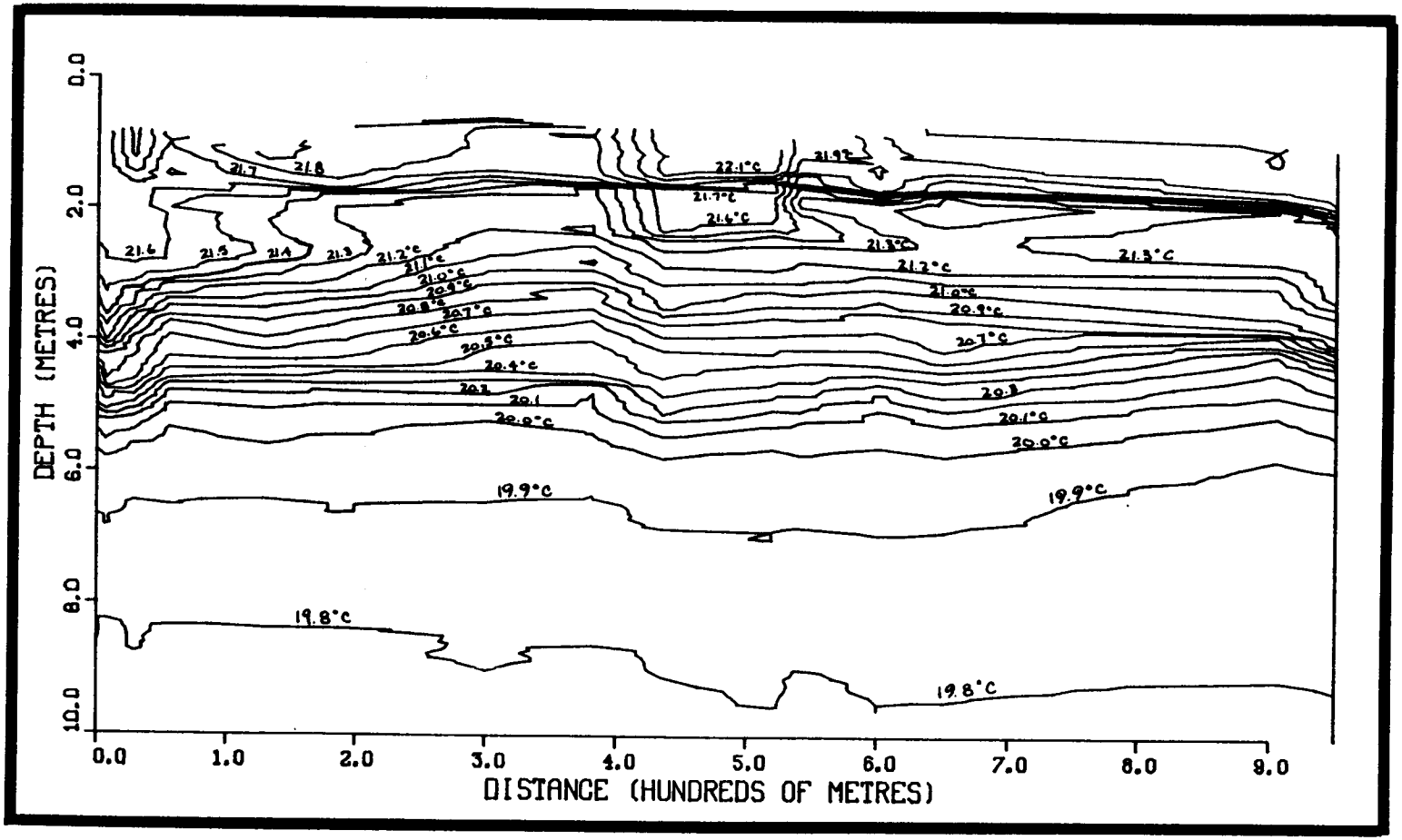

Figure 4-24. Temperature cross section corresponding to density section in Figure 4-22.

In a dynamic model, as generally defined by Garvine (1974), the plume interfacial depth is not statically determined, but is also dependent upon the local velocity field and shear acting along the interface. However, for a given ambient velocity field, as shown by Garvine (1974), the friction coefficient, hence the shear along the density interface, is directly related to the slope of the density interface, and the shear is inversely related to the strength of the pycnocline. Thus, all else being equal, increased density differences, and hence a stronger pycnocline are associated with a reduced friction coefficient, reduced shear, lower reduced vertical transport, and a shallower depth of the pycnocline.

Observed density differences were rather small when compared to those seen for the Connecticut River plume (Garvine 1974). However, the Calibogue Sound drains an estuary system which has relatively low freshwater contribution and is probably better mixed because of the higher degree of channelization within the estuary.

It is interesting to note that the depth of the pycnocline at Hilton Head was quite similar to that observed for the Connecticut River plume being discharged into Long Island Sound, in spite of the differences mentioned above. This suggests that either the depth of the pycnocline is rather insensitive to differing conditions or that local conditions at Hilton Head Island balanced in such a way as to mimic the vertical morphology of the Connecticut River plume.

The presence of ambient water being overrun or drawn down along or below the density surface separating ambient and plume water was previously identified and illustrated by Garvine and Monk (1974) for the Connecticut River plume discharging into Long Island Sound. Their measurements made relative to the moving front showed a somewhat unresolved mass of surface water below and slightly behind the front. They did not indicate that this water maintained its integrity well behind the front as found in some observations in the present study.

Following passage of and well behind Front 1 on May 7, where mixing had time to occur, the pycnocline tended to become slightly more diffuse, so that the zone of influence of plume water descends in the water column. In general this agrees with Garvine (1974) who indicated that if mixing across the pycnocline occurs, it is by downward entrainment of plume water.

Evidence for downward mixing of less saline water can be seen in vertical salinity profiles and cross sections. In virtually every case where the pycnocline changes elevation or becomes less intense, the isopycnals descend or fan progressively downward as opposed to fanning out upward and downward which would indicate downward transport of fresher water and upward transport of more saline water.

The vertical mixing within the plume implies no loss of less saline water; however, mixing across the pycnocline could result in gradual depletion of the available reservoir. Mass considerations dictate that only if mixing across the pycnocline is greater than the input of water behind the front, due to estuarine discharge, will eventual depletion occur. For a given discharge, the overall rate at which brackish water is extracted is dependent upon the intensity of the vertical mixing and the overall area of the plume. The likelihood of depletion tends to decrease if topography and other plumes act to confine the lateral growth and hence the overall area of the plume. Also, a very stable local mass distribution can inhibit vertical mixing and hence possible brackish water depletion. On the other hand, it is possible that local breakdown of the pycnocline may result in potential for further vertical mixing.

4.4.5 Mixing and Exchange Processes

4.4.5.1 Stability Criteria

Vertical density profiles show that conditions varied from essentially uniform prior to the arrival of a front when the mixed layer extends from surface to bottom, to intensely stratified two and three layered systems which would require intense shear to create mixing instabilities.

The relationship between stabilizing buoyancy effects and destabilizing shear forces is given by the gradient Richardson number, R_i, defined as

$$R_i = \frac{\frac{g}{\rho}\frac{\delta\rho}{\delta z}}{\left(\frac{\partial u}{\partial z}\right)^2}$$

where g = acceleration due to gravity, ρ = density, $\delta\rho$ = change in density including effects due to pressure, u = horizontal velocity, and z = vertical coordinate which is measured positively downward. If $R_i > 0$, i.e. if density increases with depth, then the density field has a stable configuration.

In a basically two layered system such as measured in the study area, this minimum value of R_i at which a disturbance is unstable is 0.25. Below this value, stability or instability can prevail, depending upon the ratio of wave length of the perturbation to the characteristic length scale. At $R_i = 0.25$, the wave length of an unstable perturbation is given by

$$\lambda = 7.5h$$

where λ is the wave length and h is the characteristic length scale. This may give some order of magnitude of the length scale of

disturbances existing along the pycnocline. For h 1.5 m, an estimate of the width of the strongest portion of the pycnocline, the wave length for which a disturbance would be unstable is 11.25 m.

Figure 4-25 shows specific ranges based on a value of 1.5 for h. For values of less than approximately 7.5 m, all disturbances are stable under the above assumed conditions.

For generation of unstable disturbances, velocity shear must coincide with the density gradients, otherwise, the disturbances will not amplify. For R_i = 0.25, and the observed density gradients, it would be necessary to have velocity gradients of 1 $m.s^{-1}$ per m during some of the more stable configurations, i.e. after passage of all three fronts on May 7. After passage of Front 1 on May 7, for R_i = 0.25 to exist on the pycnocline, a vertical velocity gradient of 45 $cm.s^{-1}$ per m would be necessary. Obviously, very strong shears were needed if disturbances were to become unstable.

4.4.5.2 Horizontal Mixing

Although vertical mixing processes dominate, several observations suggest that horizontal mixing may be taking place. In oblique photographs taken during both deployments, the front (i.e. foam line) assumes shapes which strongly suggest the presence of lateral shear and instability features.

During the May 7, deployment a series of features were seen along the first front to pass the hydrostation which ranged from sinusoidal, quite regular oscillations in the front to distorted and skewed features. When these features were observed, the front was migrating quite slowly and currents moved in opposite directions across the front. In such a situation undulations could easily develop, grow, become unstable, and cause mixing of differing density water masses.

4.5 ANALYSIS OF COASTAL TURBIDITY DISTRIBUTION FROM LANDSAT IMAGERY

4.5.1 Methodology

Each point on the earth's surface radiates and reflects a broad spectrum energy. By partitioning the reflected energy into discrete frequency (wavelength) bands and evaluating the absolute and relative energy content of each band, considerable information can be gained about the reflecting surface. This is the basic principle and function of the ERTS/LANDSAT multispectral imagery used in this study. By using the satellite imagery in the visual range of the reflected spectrum, it is possible to determine spatial changes in fixed specific color bands, and even estimate the color of the reflecting surface.

Estuarine water discharged onto the shelf is usually of a different density and often of a different color than the ambient water. This color change is often produced by turbidity differences resulting from variations in the concentration and character of the suspended particulates. Thus, if a front, a density feature, forms between

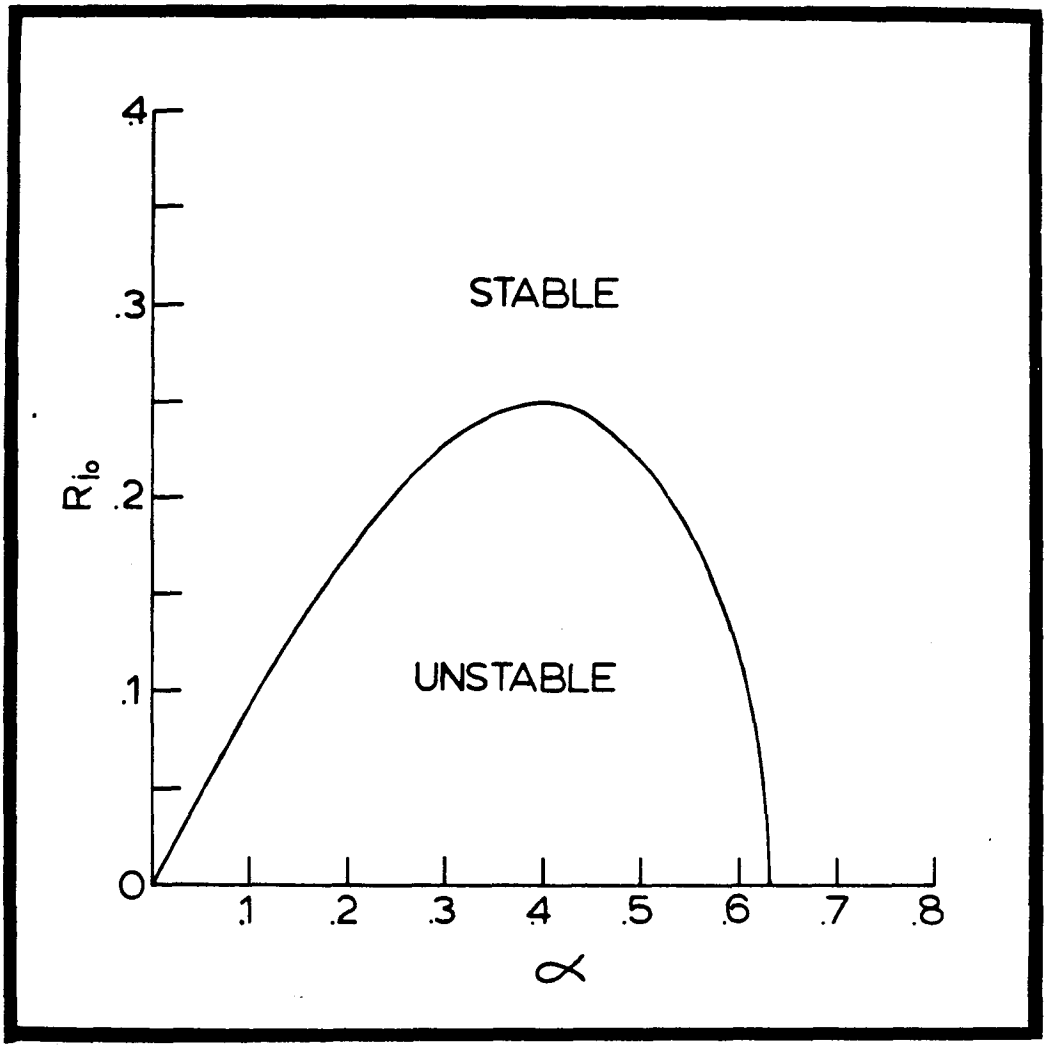

Figure 4-25. Plot of gradient Richardson number, R_{io}, as a function of α, which equals 1/2 kh, where k is the wave number and h a characteristic length. In the situation being examined, when R_{io} = 1/4, k ≈ 0.52 and h = 1.5 m (from Turner, 1973).

estuarine and shelf water, it may be indicated by a rather abrupt spatial color change which can be sensed in one or more of the discrete frequency bands being monitored in the LANDSAT imagery.

The LANDSAT satellite flies a polar orbit 920 km above the earth's surface, circling the earth every 103 min. The orbits are offset so that the coverage includes the entire globe at least every 18 days. A unique feature of this orbit is that it always views a point on the earth's surface at the same time of day. Each LANDSAT print covers a 185 km x 185 km section of the earth's surface. In this study the image prints were centered on WRS map coordinates 17-37.

Each black and white image contains a 15 step gray scale to help in evaluation and control of printing. Each print also contains all pertinent details about the image such as date, time, band number, etc.

A list of available imagery is given in Table 4-1 and includes a qualitative evaluation of the imagery in each band. Images with more than over 30% cloud cover were not used in this study.

4.5.2 Photo Analysis

The sequence of graphs in Figure 4-26a shows the effect of the atmosphere and water on incoming solar radiation. Figure 4-26b further illustrates what happens to this incoming solar radiation as it penetrates the water column. It must be noted that in the red band (LANDSAT BAND 5, .6-.7 μm) energy is attenuated (absorbed) very rapidly with depth, while in the green band (LANDSAT BAND 4, .5-.6 μm) energy is transmitted much more rapidly.

Turbidity of the estuarine discharge creates a yellow to brown near surface layer inside the front. Incident wide band radiation in the green-blue is both transmitted and absorbed, while red-yellow tends to be reflected from the turbid water surface. By contrast, in the less turbid shelf water, the red band radiation tends to be absorbed, not reflected.

In the shelf water, ambiguity may occur if shallow water and water clarity combine to permit some incident radiation to be reflected from the bottom. This is a particular problem in shoal areas where the bottom is sandy. Because such light must traverse the water column twice (once up, once down), this should be a concern only in the very shallow areas.

In order to minimize bias, identification of front-like features was completed prior to and separately from any detailed interpretation. However, as the identifications were made, experience was gained. Consequently, to assure uniformity, each image was examined at least twice. Only one photointerpreter was used to minimize any operator related differences.

Table 4-1. Monthly summary of LANDSAT Imagery of the study area.

Date	ID Number	% CC	Quality 4 5 6 7
01/11/73	1172-15324	10	G G G G
01/29/73	1190-15325	30	G G G G
01/23/74	1549-15233	20	P P G G
01/04/76	2347-15133	20	F F F F
01/13/76	5269-14522	10	G G G G
01/22/76	2365-15131	0	F G F F
01/23/76	2366-15183	0	G G G G
01/16/77	2725-15021	10	G G G G
*	*	*	*
02/16/73	1208-15331	10	G G G G
02/10/74	1567-15230	10	P G G G
02/11/74	1568-15284	0	P G G G
02/28/74	1585-15224	10	G P G P
02/15/75	2024-15215	30	G G G G
02/09/76	2383-15130	0	G G G G
02/10/76	2383-15181	0	G G G G
02/18/76	5305-14494	30	G G F G
02/19/76	5306-14552	0	G G G G
02/27/76	2401-15123	0	G F G G
02/21/77	2761-15005	10	G G F F
*	*	*	*
03/05/73	1225-15280	20	P G G G
03/24/73	1244-15332	10	G G G G
03/01/74	1586-15280	10	G G G G
03/18/74	1603-15222	0	G G G P
03/19/74	1604-15274	10	P P P P
03/05/75	2042-15214	30	G G G G
03/31/75	1981-15085	10	G G G G
03/08/76	5323-14482	30	G G G G
03/26/76	5342-14525	20	G G G G
03/29/77	2797-14591	10	F G G F
*	*	*	*
04/10/73	1261-15280	0	G G G G
04/29/73	1280-15332	0	P P G G
04/23/74	1639-15214	20	P P P P
04/18/75	1999-15084	0	F G G G
04/28/75	2096-15210	20	G G F F
04/03/76	2437-15112	0	G G G G
04/12/76	5359-14460	10	G G G G
04/13/76	5360-15615	10	G G G G
04/16/77	2815-14581	10	F F G G
*	*	*	*

Table 4-1. Monthly summary of LANDSAT Imagery of the study area (continued).

Date	ID Number	% CC	Quality 4 5 6 7
05/17/73	1298-15331	10	G P G G
05/11/74	1657-15211	20	G G G G
05/12/74	1658-15262	20	G G G G
05/06/75	5017-15065	0	G G G G
05/24/75	5035-15063	10	F F F G
05/25/75	5036-15114	0	G G G F
05/10/76	2474-15160	20	G G G G
05/19/76	5396-14491	0	G G G G
05/04/77	2833-14561	30	G G G G
05/10/77	5732-14133	0	P G G G
05/21/77	2851-14561	40	G G G G
*	*	*	*
06/03/73	1315-15274	0	G P G G
06/17/74	1694-15252	0	G G G G
06/03/75	2132-15210	10	F F G G
06/20/75	2149-15155	20	F F G G
06/06/76	5414-14480	10	G G G G
06/14/76	2509-15092	10	G G G G
06/18/77	2869-14552	10	G G G G
*	*	*	*
07/10/73	1352-15323	10	G G G G
07/27/73	1369-15270	20	G G G G
07/02/76	2527-15085	30	G G G G
07/11/76	5449-14395	10	G G G G
07/12/76	5450-14451	30	G G G F
07/20/76	2454-15082	30	G G G G
07/30/76	5468-14434	10	G G G G
07/03/77	5806-14084	40	- G F G
07/05/77	2905-14533	20	G G G G
07/21/77	5824-14062	10	- G G G
*	*	*	*
08/02/72	1010-15322	10	G G G G
08/20/72	1028-15322	30	P P G G
08/14/73	1387-15264	10	G G G G
08/15/73	1388-15320	10	G G G G
08/27/74	1765-15173	20	G G G G
08/14/75	2204-15201	10	F F G F
08/14/75	2204-15204	30	G G G G
08/22/75	5125-15060	0	F F F G
08/23/75	5126-15063	10	G G G G
08/07/76	2563-15075	30	G G G G
08/16/76	5485-14365	10	G G G G
08/25/76	2581-15072	30	G G G G
08/02/77	2923-14524	40	G G G G
08/07/77	5841-13585	10	- G F G
08/08/77	5842-14041	10	- G F G
08/08/77	5842-14044	20	- G G G
08/26/77	5860-14030	40	- F G G

Table 4-1. Monthly summary of LANDSAT Imagery of the study area (continued).

Date	ID Number	% CC	Quality 4 5 6 7
09/07/72	1046-15322	30	P G G G
09/24/72	1063-15272	30	G G G G
09/14/72	0783-15162	10	G G G G
09/19/75	2240-15202	40	G G G G
09/27/75	5161-14590	0	F F F G
09/22/75	5522-14391	0	G G G G
09/13/77	5878-14001	10	- F F G
09/25/77	5878-14493	20	G G G G
*	*	*	*
10/30/72	1099-15273	20	G G G G
10/07/73	1441-15253	30	G G G G
10/08/73	1442-15305	20	G G G G
10/25/73	1459-15250	20	P G G G
10/26/73	1460-15305	0	P G G G
10/03/74	1802-15215	10	G G G G
10/20/74	1819-15160	20	P G G G
10/21/74	1820-15212	0	G G G G
10/15/75	5179-14573	10	F F G F
10/29/75	2311-15135	20	F F F F
10/18/76	2635-15052	10	G G G F
10/20/77	5915 14022	0	- G G G
*	*	*	*
11/18/72	1118-15330	10	G G G G
11/12/73	1477-15250	0	G G P G
11/13/73	1478-15304	10	G G G P
11/30/73	1495-15245	0	P G G G
11/07/74	1837-15152	20	G G G P
11/25/74	1855-15144	30	G P G G
11/26/74	1856-15195	0	G P P P
11/02/75	5197-14565	30	F F F F
11/03/75	5198-15021	10	F F F F
11/20/75	5215-14555	10	F F F F
11/05/76	2653-15050	30	F F G F
11/23/76	2671-15042	10	G G G G
11/01/77	6014-14525	30	F G F G
11/07/77	5933-14002	10	- F F P
*	*	*	*
12/02/73	1496-15301	20	G G G G
12/14/74	1874-15191	10	G G G G
12/31/74	1891-15131	20	G G G F
12/29/76	2707-15025	10	G G G G
12/06/77	6049-14455	10	F F F P

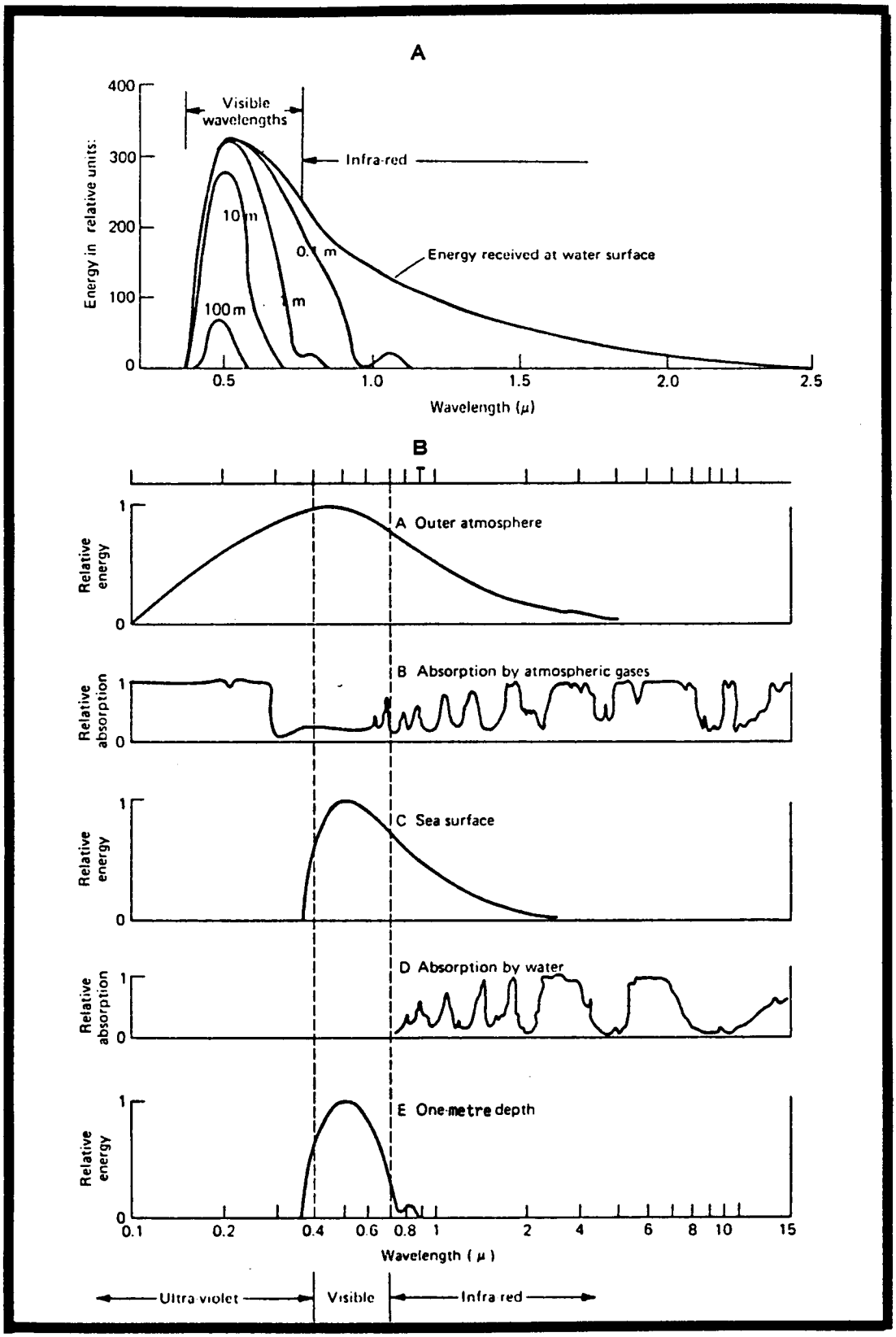

Figure 4-26a and b. (a) Effect of atmosphere and water on incoming solar radiation, and (b) curves of incident energy reaching various water depths in clear water vs. wavelength.

Prints of imagery were evaluated at two scales: a regional view with a scale of 1:1,000,000 (Figure 4-27), and a local view of the proposed TCWI study area at a scale of 1:36,250 (Figure 4-28). Continuous gray tone, black and white positive prints were used for analysis. In these, the whiter the color, the greater the incident of radiation in that band. Each print was examined for abrupt changes in color in the coastal zone. Each such feature was accentuated in ink.

4.5.3 Discussion of Results

4.5.3.1 Tidal Influence

Available imagery was subdivided on the basis of local semidiurnal tidal stage. This separation was made because of the important primary role tides can have on the extent and intensity of frontal development. Tides at Savannah River Entrance were used for this separation.

The tidal current cycle was divided into four quarters, each running from maximum to slack current or slack to maximum current (Figure 4-29). For this discussion, quarters will be number 1-4 beginning at high slack water. In this system, Quarter 2 is the second half of ebbing currents, etc. Of the 22 images used, 10 occurred during Quarter 2, 7 during Quarter 4, 3 during Quarter 1, and 2 in Quarter 3.

In terms of probability of identifying fronts, Quarter 2 is the most probable, Quarter 4 the least probable, and Quarters 1 and 3 could have fronts, if time and conditions were correct. It is expected that during Quarter 2, fronts should be well defined and may have maximum offshore extent. During Quarter 4, fronts may be either absent or close to shore; if present, they may exhibit a skewed orientation to the south. It is expected that during this quarter, if fronts are identified they will probably be discontinuous alongshore.

Because the pattern of tidal dominance can be modified by variations in local discharge, for each set of imagery any pertinent rainfall events have been noted (Table 4-2).

4.5.3.2 Well Developed Fronts

As will be shown, well developed frontal patterns were at times both continuous and discontinuous. For the data available, there is no method which allows a priori determination of when either of these two conditions would exist. Seldom was a front absolutely continuous, having no breaks, but often there were long continuous sections apparently separated by small breaks. These interruptions may have been more a function of the inability to discriminate a

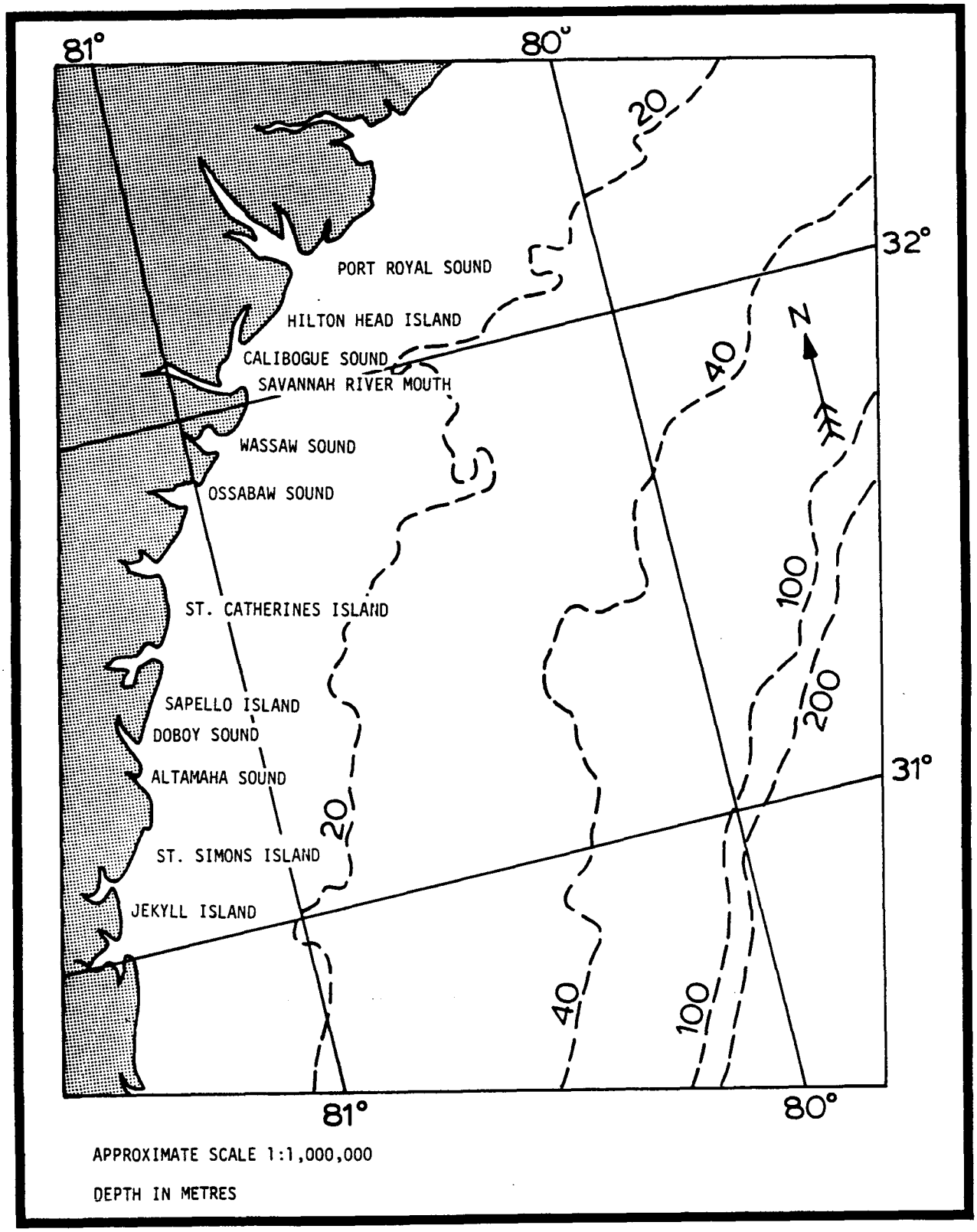

Figure 4-27. Map of the portion of coast covered in the imagery. The area of interest was off of Hilton Head Island, S.C., and the Savannah River (Georgia).

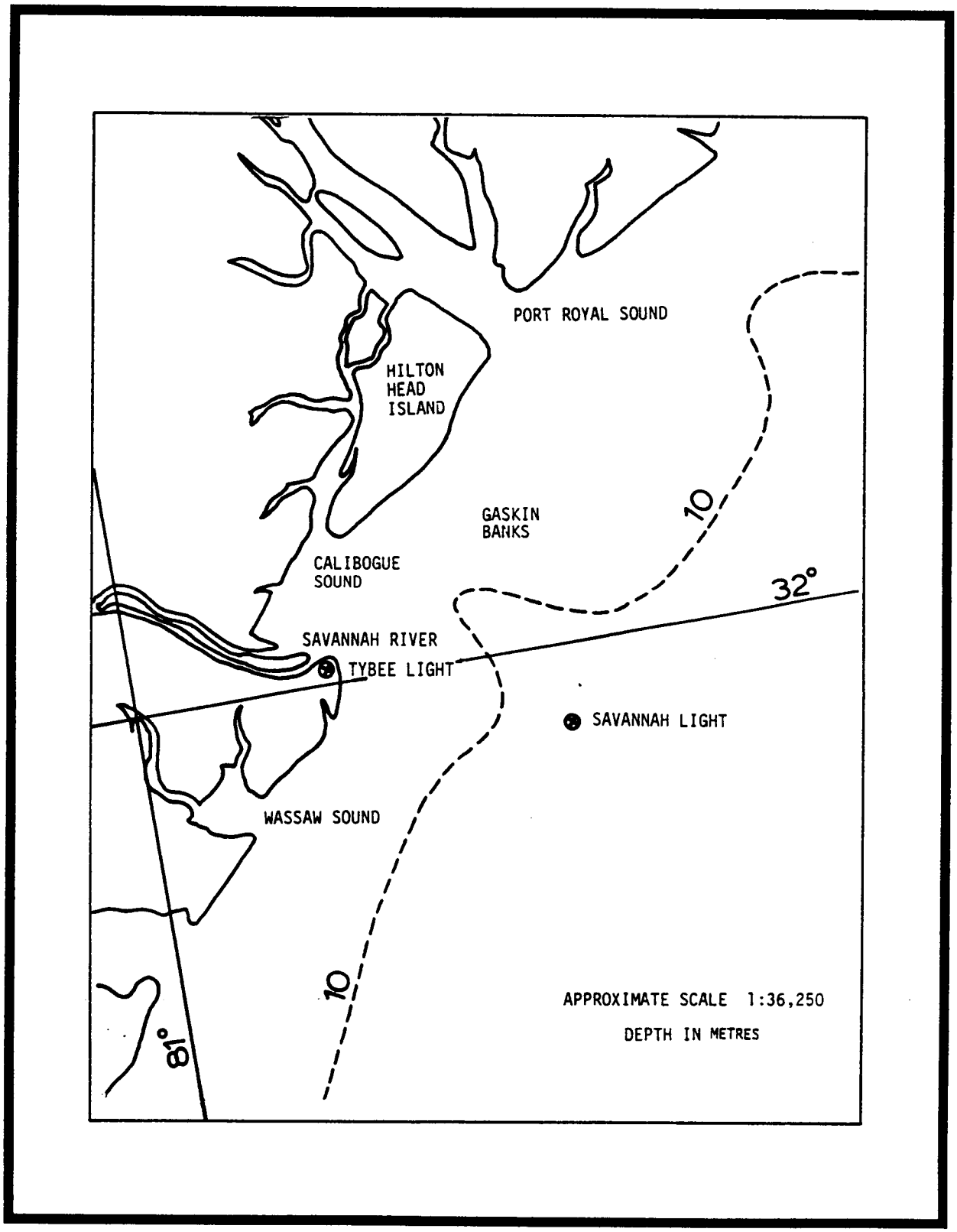

Figure 4-28. Map of the study area and vicinity, obtained from enlargement of LANDSAT imagery.

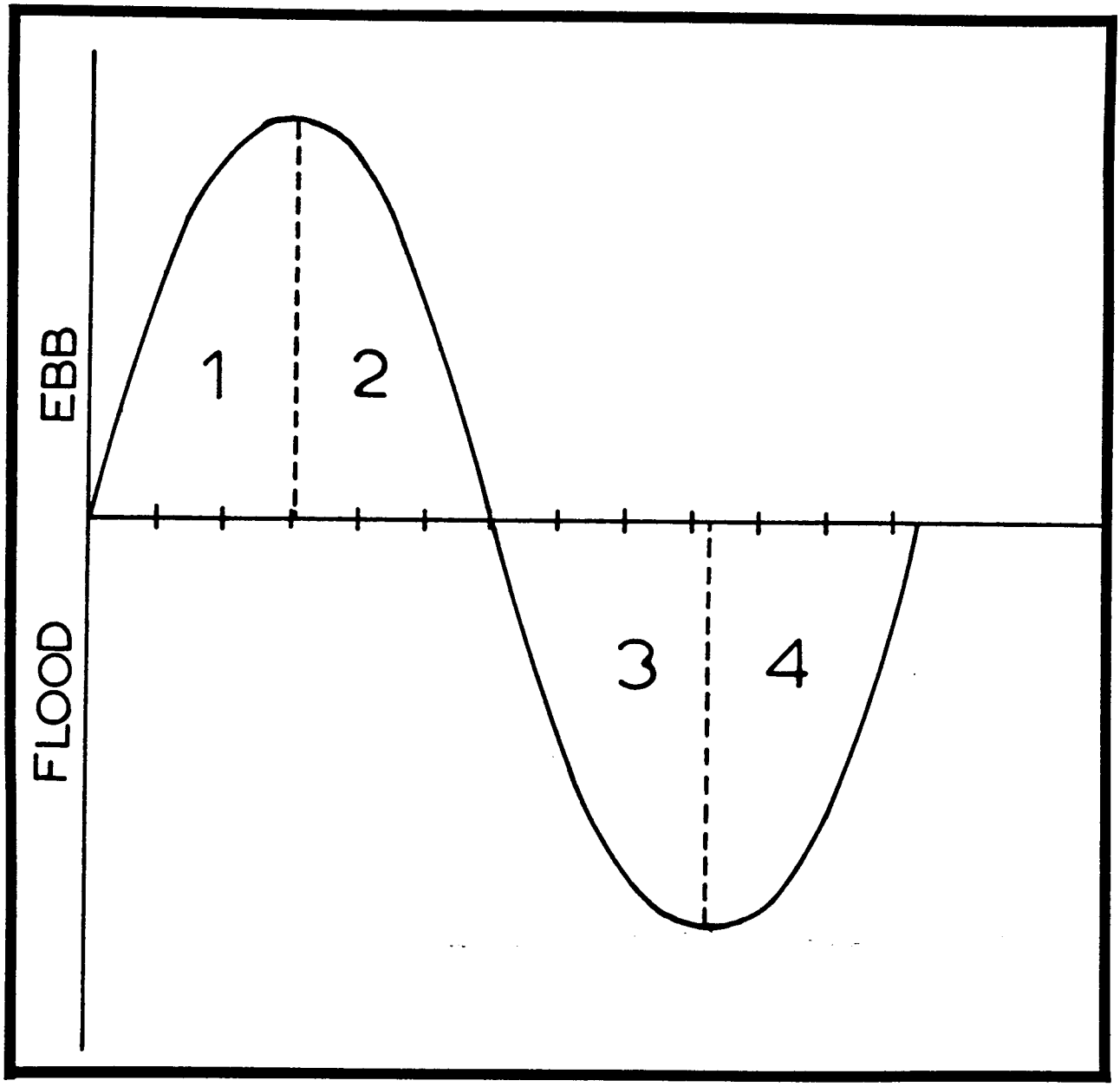

Figure 4-29. Subdivision of the semidiurnal tidal cycle into 4 quarters beginning with the first half of the ebbing tide.

Table 4-2. Listing of LANDSAT imagery used to evaluate the Turbid-Clear Water Interface. Pertinent tidal and rainfall data is included.

DATE	TIME	PHOTO ID. NO.	TIDAL STAGE	RAINFALL
01/13/76	0952	5269-14522-5	1/2 h after max ebb	
01/22/76	1013	2365-15131-5	1/2 h before max flood	
02/09/76	1013	2383-15130-5	slack ebb	
02/27/76	1012	2401-15123-5	1/2 h before slack ebb	12.7 cm rain, 4 days prior
12/29/76	1002	2707-15025-5	slack ebb	2.5 cm rain 2 days prior
01/16/77	1002	2725-15021-5	1/2 h after max ebb	2 cm rain 1 day prior
02/21/77	1000	2761-15005-5	2 h after max flood	
12/06/77	0945	6049-14455-5	1.5 h after max ebb	3.5 cm rain 4 days prior
04/03/76	1011	2437-15112-5	2 h after max flood	
03/29/77	0959	2797-14591-5	2.5 h after max ebb	
04/16/77	0958	2815-14581-5	1 h before max ebb	
08/03/75	1014	2203-15145-5	slack flood	
06.14/76	1009	2509-15092-5	.5 h before slack flood	
07/20/76	1008	2545-15082-5	slack ebb	2.5 cm rain 1 day prior
08/07/76	1007	2563-15075-5	max ebb	12.7 cm rain 3,4 Aug.
08/16/76	0936	5485-14365-5	1/2 h before max flood	
08/25/76	1007	2581-15072-5	2 h before max flood	4.8 cm rain 17-24 Aug.
06/09/77	0955	2869-14552-5	slack ebb	.9 cm rain 2 days prior
08/ /77	0904	5842-14041-5		
11/29/75	1013	2311-15135-5	1.5 h after max ebb	
11/23/76	1004	2671-1504204	slack flood	
09/25/77	0949	2977-14493-5	1 hr before max ebb	

frontal feature in the imagery than the absence of a front. The alongshore continuity resulted from the coalescing or merging of adjacent plumes. For merging to occur, lateral spreading and discharge has to have been rather large. If discharge was not sufficient to cause coalescence, then the second condition above, i.e., many discontinuous fronts, would be expected. Thus, the alongshore continuity of the front at some time during the tidal cycle was largely a function of the magnitude of estuarine discharge, itself dependent upon a variety of environmental factors (such as local rainfall, river control, etc.).

4.5.3.2.1 Regional Patterns

Three examples of a well developed TCWI are given in Figures 4-30, 4-31, and 4-32, obtained in 1/16/77, 12/6/77 and 2/27/76 under conditions summarized in Table 4-2. They represent conditions .5, 1.5, and 2.5 h after maximum ebb currents. In Figure 4-30, the TCWI was alongshore persistent, although occasionally interrupted. The major fragments were generally 12 to 20 km in length. The only large interruption in alongshore extent occurred offshore of Port Royal Sound. This semi-continuous front was positioned about 12 km offshore and closely paralleled the shoreline. The Savannah River discharge appeared to retain a very lobate, plume-like shape.

Figure 4-31 is an example of a slightly better developed front corresponding to a later tidal stage (1.5 h after maximum ebb) on 12/6/77. In this example, the front was continuous alongshore. At the 1:1,000,000 scale, there appear to be no interruptions. Again the alongshore continuous TCWI was 10 to 12 km from the coast. Figure 4-32 represents condition 2.5 h after maximum ebb ($\sim$.5 h before low slack water). The front was not as well developed as that shown in Figure 4-31, but this could be due to environmental factors decreasing either discharge or resolution of the front. The latter is an important consideration, since there can be considerable variability in the turbidity of discharge plumes.

4.5.3.2.2 Fronts in Proposed Study Area

These images in Figures 4-30, 4-31 and 4-32 from Quarter 2 also illustrate details of frontal movement in the field study area offshore of Hilton Head Island. In Figure 4-30, on 1/16/77, the Savannah River plume is directly offshore of the northern end of Tybee Island. The side boundaries become rather difficult to identify in this image. In the offshore region between Tybee and Hilton Head Island, no fronts could be identified. In this region, it is possible that the Calibogue Sound plume was less dynamic, further inshore, and thus harder to discriminate. Fronts offshore of Hilton Head Island were probably associated with the Port Royal Sound plume. The front, perpendicular to the coast and south of Gaskin

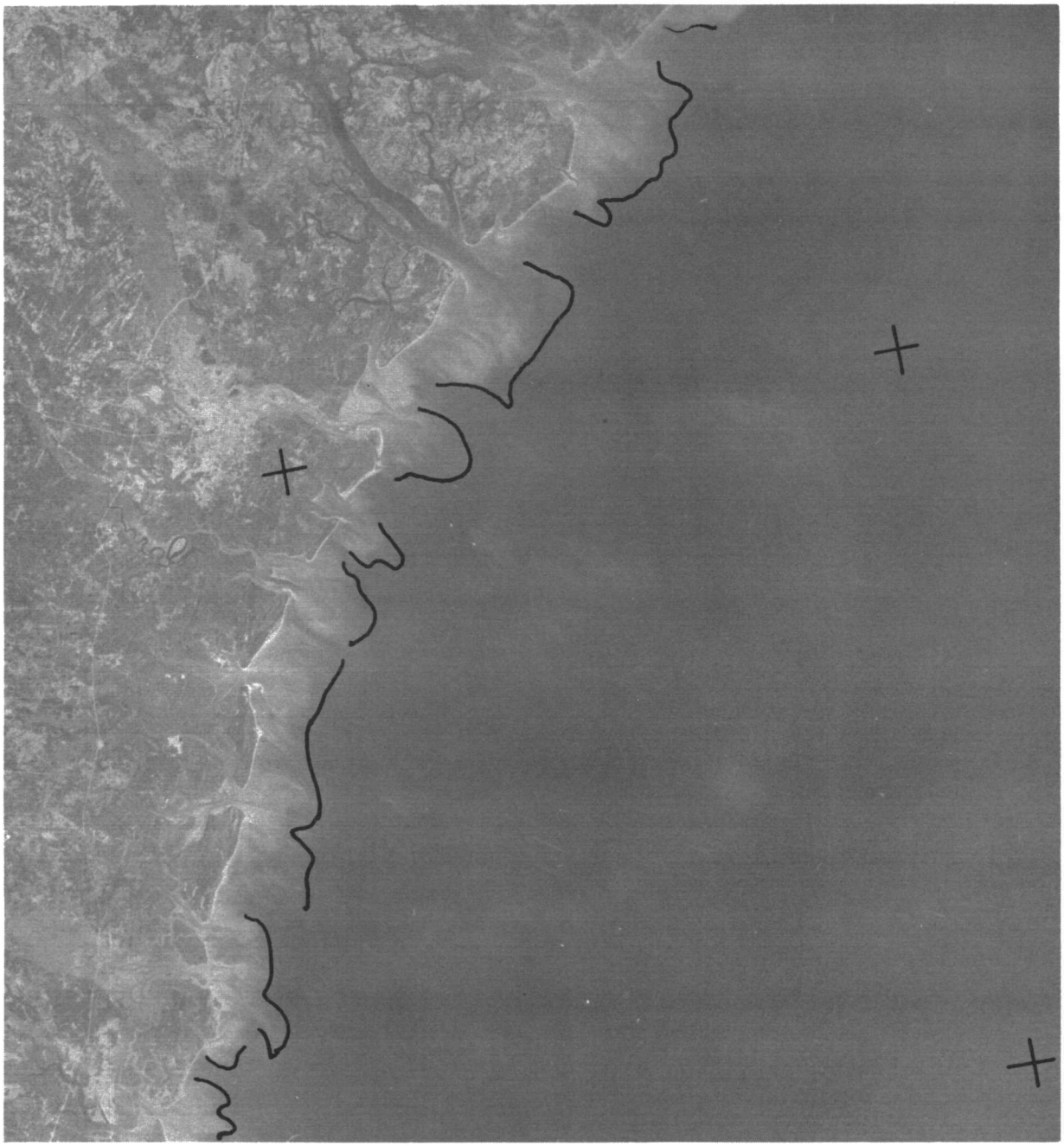

Figure 4-30.

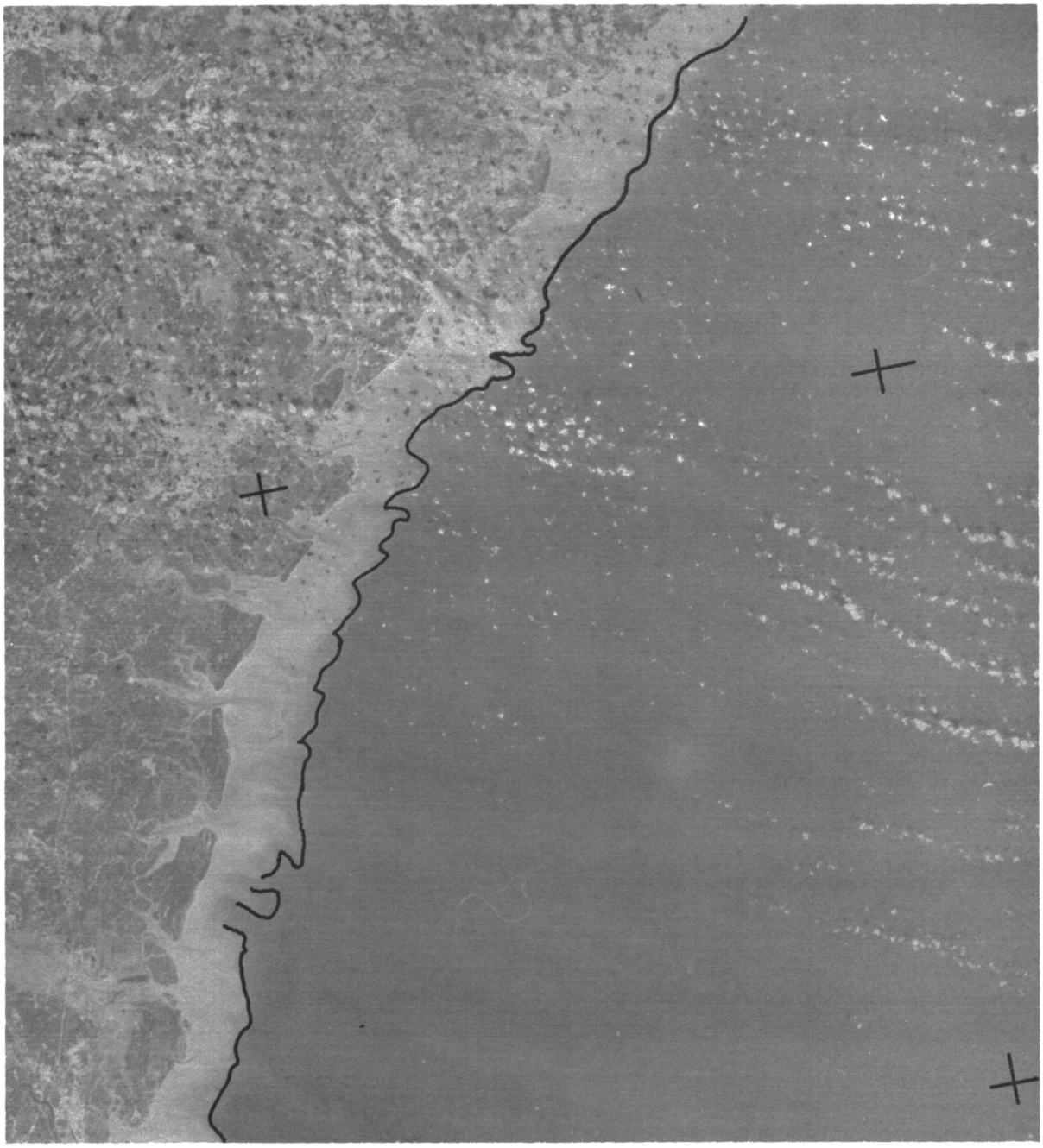

Figure 4-31.

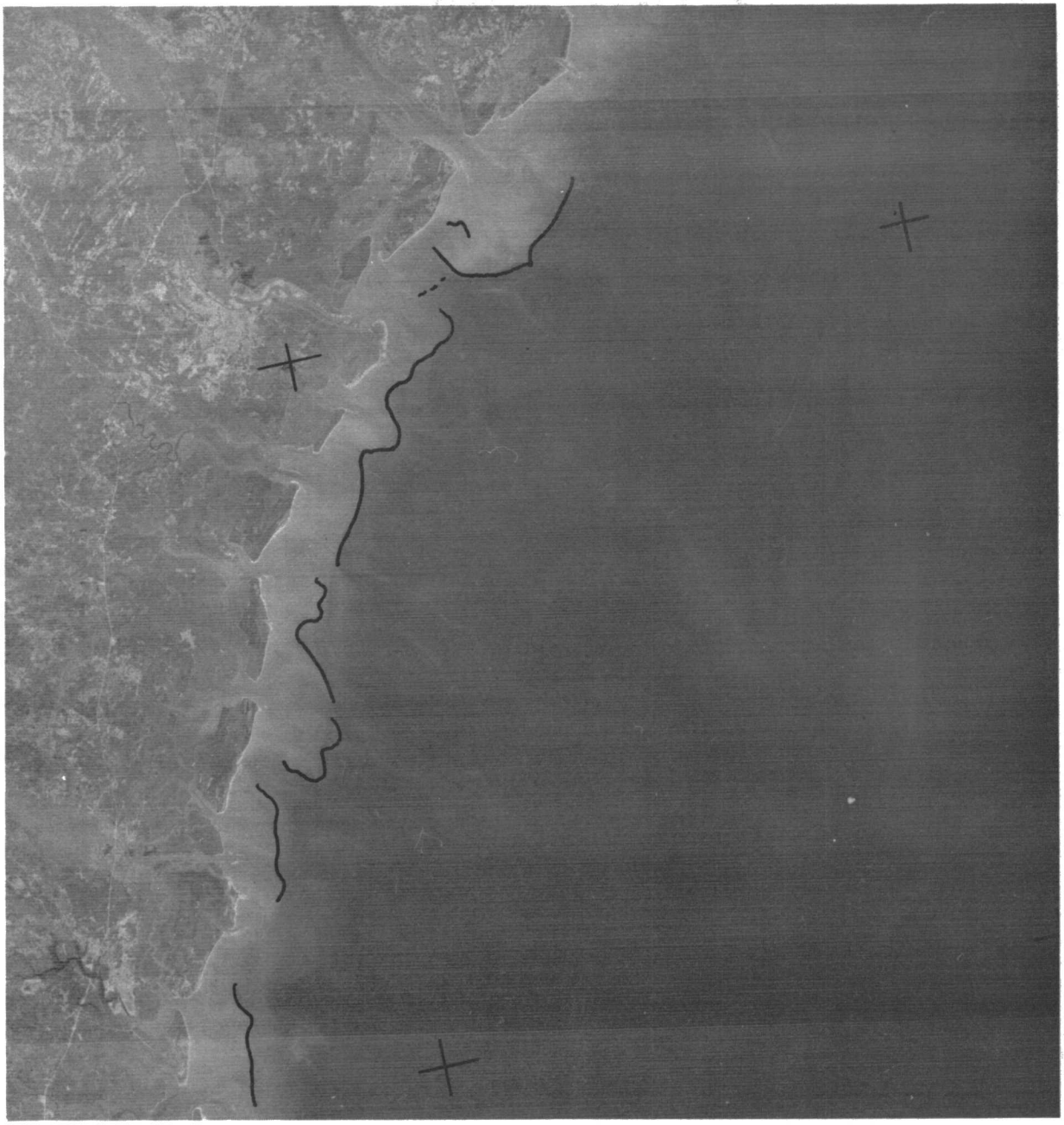

Figure 4-32.

Bank, has been observed at that location many times. The Calibogue Sound plume often creates a complex pattern of fronts due to interaction with the Port Royal and Savannah River plumes.

Figure 4-31, for conditions 1.5 h after maximum ebb, shows continued growth of plumes coming from sounds adjacent to the study area. There is a coalescing of discharges. The Savannah River and Port Royal Sound plumes are similar to that seen in Figure 4-32; however, the Calibogue Sound plume is growing seaward between the two more dynamic features.

At about low slack water ($\sim$.5 h) the offshore boundary of the TCWI parallels the coast and is almost continuous alongshore. As shown here, fronts may migrate almost due east through the field study area, a pattern seen on May 7, 1978, the time of the second TCWI field deployment.

It is important to note that the Calibogue Sound plume was constantly more poorly defined than the Savannah River and Port Royal Sound plumes. This is not unexpected because each had a greater component of fresh (riverine) water which created a more intense front and quite possibly a more turbid plume. This pattern has been observed visually on several occasions.

There was often a fairly strong similarity in the offshore shape of the continuous or well developed fronts and the local isobaths. The 10 m isobath often looped onshore between Tybee and Hilton Head Islands. Inshore of this feature is where the fronts were often absent or poorly defined, and it is in this area that the front had its least offshore displacement. This pattern was observed in much of the imagery containing extensive and continuous fronts.

4.5.3.3 Poorly Developed Fronts

Although it is not possible to make an absolute generalization, the presence of fronts are least expected during the second half of a flooding tide (Quarter 4). Experience suggests, and imagery supports the assumption, that by this portion of the tidal cycle, fronts have been broken down by the local tidal currents, have moved back into the estuaries, or have been moved laterally by coastal and tidal currents. In some estuaries, the net discharge may have been large enough to inhibit movement of the front back into the estuary. These can be displaced laterally. Regardless of the cause, it is during this tidal stage when fronts may be locally absent and widely separated alongshore.

4.5.3.3.1 Regional Patterns

In the presentations for 2/21/77 (Figure 4-33), 1/22/76 (Figure 4-34), and 4/3/76 (Figure 4-35), the expectation of irregular and poorly developed fronts is supported. All these examples were taken

Figure 4-33.

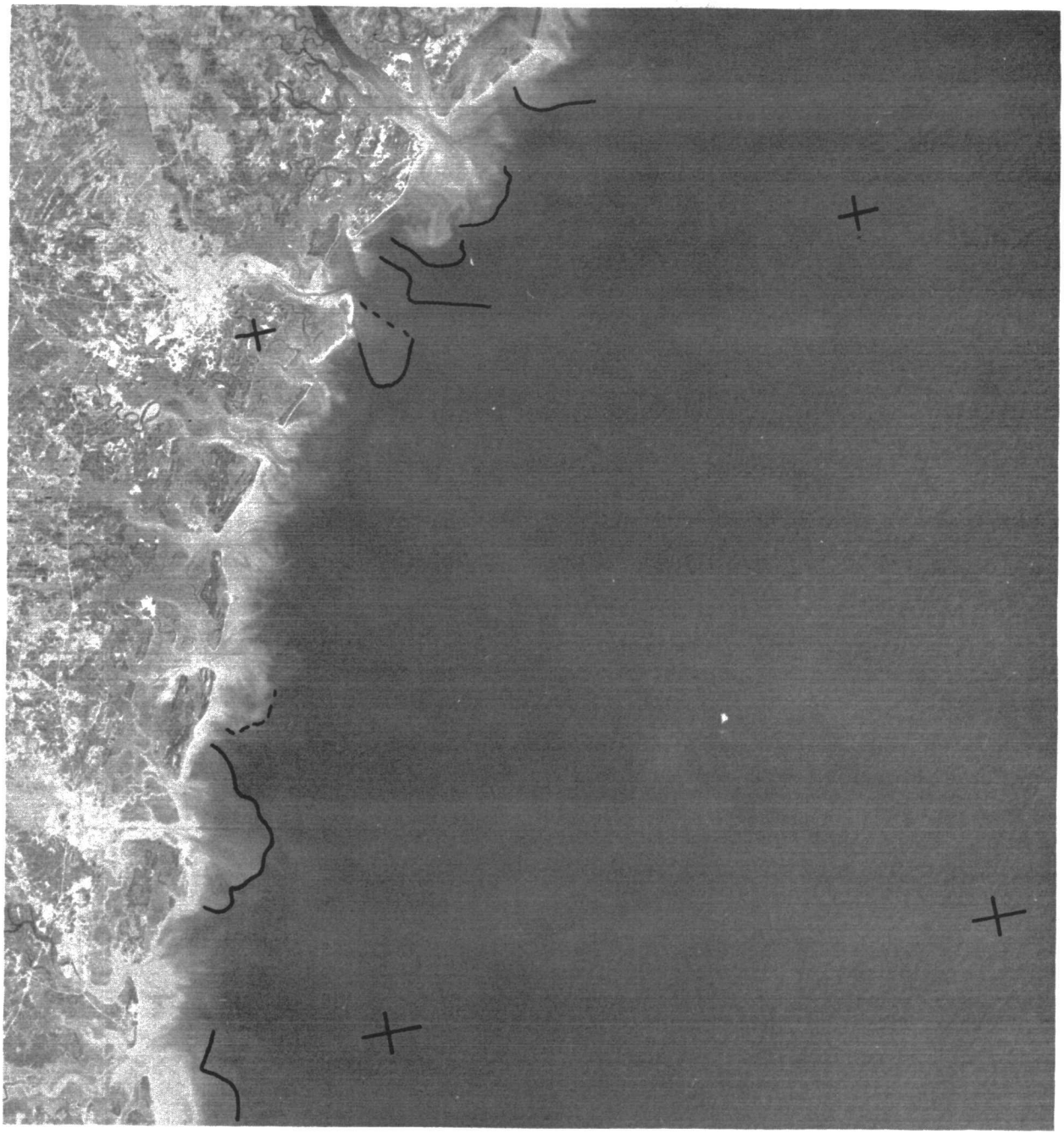

Figure 4-34.

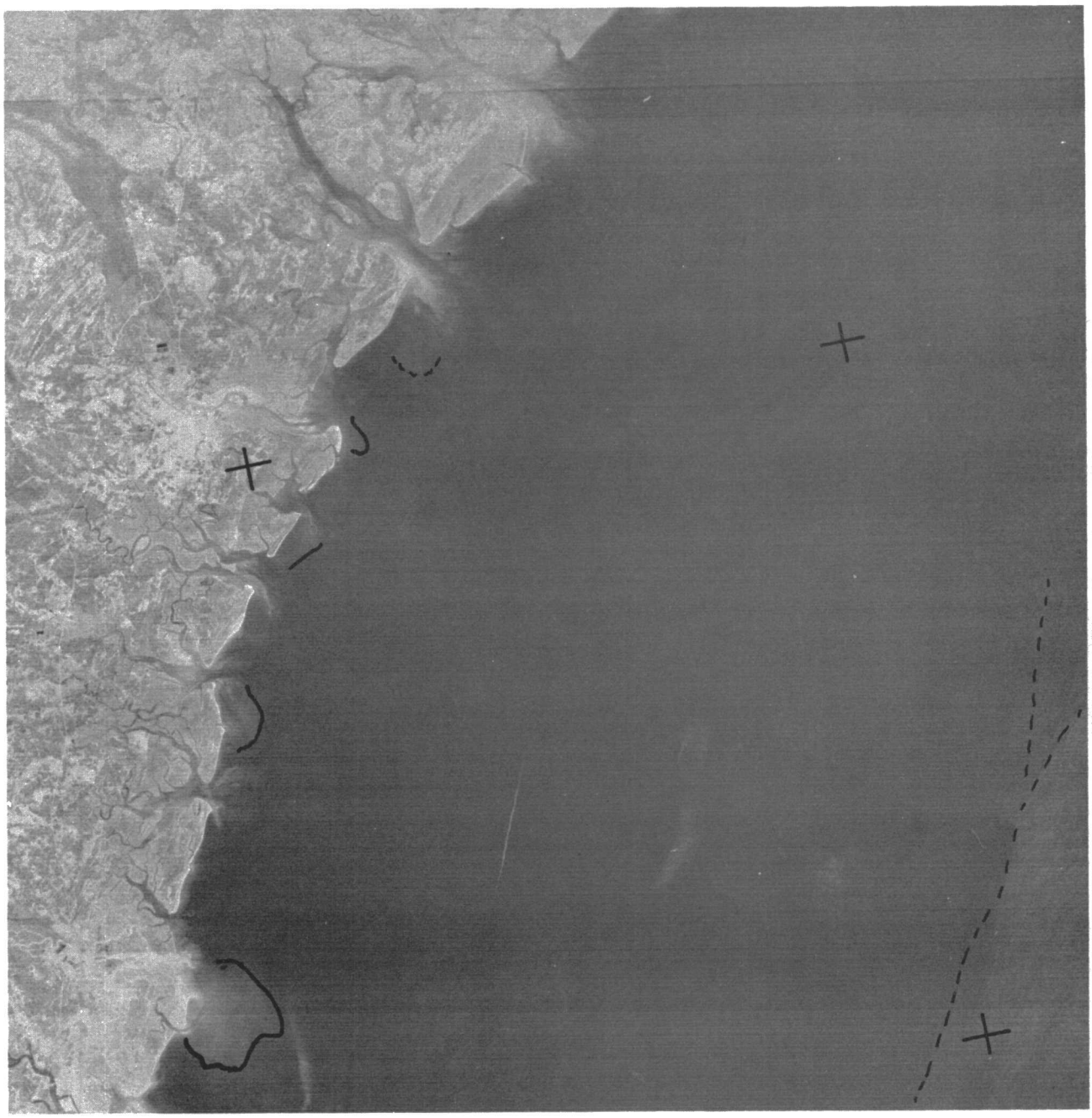

Figure 4-35.

in the interval from maximum flooding currents to high slack water. On 2/21/77, only four fragmentary fronts are visible: off Port Royal Sound, Calibogue Sound, Doboy and Altamaha Sound, and St. Andrews Sound. These frontal fragments were irregularly spaced along the coast. Many of the estuaries had no visible plume. This imagery was made two hours after maximum flood -- or about an hour before the beginning of ebbing currents -- and should represent some of the poorest frontal development both in intensity and in alongshore extent. Images from 4/3/76 represent a similar tide stage and again show poorly developed and fragmentary fronts. Only one plume in the south seems to have retained its defining front.

Imagery from 1/22/76 shows conditions only .5 h after maximum flood. Fronts are expected to be fragmentary to some extent, but to have a greater alongshore persistence and to better define plumes. Several plumes retained their appearance, in particular off Doboy and Altamaha Sounds and the southern boundary of the Savannah River plume just southeast of Tybee Island. Also there are a series of fronts perpendicular to the coast off Hilton Head Island. This pattern has been observed several times and is probably associated with the Calibogue Sound and Port Royal Sound plumes being displaced to the south.

4.5.3.3.2 Fronts in Proposed Study Area

In both examples representing conditions an hour before high slack water (Figures 4-33 and 4-34), a front existed close to and just east of the northern end of Tybee Island. On 2/21/77, a weak line in the vicinity of Gaskin Bank may be a front, or could be bottom reflection. At times the Port Royal Sound plume moves southward over these shoals, and it is possible it has become stranded and remained relatively undisturbed.

On 1/22/76, a half hour after maximum flood, several rather well defined fronts are still visible. The Savannah River plume extends to the south past the southern end of Tybee Island. The northern boundary of this plume is poorly defined and thus not indicated. However, patterns of shading do suggest the plume was being pinched off at the northern end of Tybee Island. Fronts off the southern end of Hilton Head Island are very weak but do follow a pattern seen on several occasions.

4.5.4 Summary

In spite of possible contamination by bottom reflected light, the imagery tends to support the idea that tidally dominated estuarine discharge can at times create a continuous alongshore turbid front. This front is created by coalescing of individual plumes emanating from many small and large estuaries which discharge onto the shelf on this section of South Atlantic Bight.

Because of tidal dominance, presence of the front is variable on a short time scale. It is often fragmentary and does not appear as a continuous, permanent frontal feature. However, if presence is weighted according to tidal stage, the series of fronts appears to have been rather persistent.

4.6 SUMMARY AND CONCLUSIONS

This study was developed to examine the following basic processes: (1) surface currents in the vicinity of the TCWI, i.e. a coastal front, (2) behavior of pollutants in the vicinity of these fronts, (3) mixing across the front and associated density interface, and (4) what appear to be the controlling variables in frontal dynamics and pollutant migration. Results pertinent to each topic will be summarized.

1) Qualitatively, surface currents within, i.e. shoreward of, the front tend to converge to the front. In a fixed frame of reference, the surface currents can be rather large, however, relative to an origin moving with the front, the observed convergent velocities were generally small compared with the frontal migration velocity. During this study, differing tide stages affected the magnitude of the convergent velocity but not the sign. During flooding and ebbing tides, tracers released seaward of the front generally tended to converge to the front.

2) Dispersed (i.e. neutrally buoyant) pollutants released shoreward of the front tended to spread laterally and vertically. This nonadvective motion was more intense near the front where vertical velocity gradients were probably more severe. An oblique approach to the front caused more intense and rapid spreading of dyes. Until reaching the front, dyes released seaward of the front showed less lateral spreading than those dispensed inshore.

Surface pollutant simulators were influenced by both currents and winds. Their movement was a weighted vector sum of the two shears. If sufficiently strong, the wind shear caused the aluminum particles to move contrary to local surface currents, especially if currents were weak such as when the tide was turning. At times, dyes and aluminum moved on divergent paths because of the larger influence of wind stress on the aluminum.

3) Within discharge plumes and in the vicinity of the front, vertical mixing was rather common and not unexpected considering the relatively weak density gradient above the pycnocline. By contrast, the pycnocline appeared to be a relatively stable feature which inhibited exchange between plume and ambient water masses. Some examples of mixing across the pycnocline supported the assumption of Garvine (1974) that the vertical flux was most often a downward

movement of fresher water. Multiple fronts tended to intensify the pycnocline thus further inhibiting vertical exchange between water masses.

What was believed to be horizontal mixing in the vicinity of the front was observed in the presence of very strong lateral shear. Such mixing in conjunction with vertical mixing close to the front caused surface density gradients to be less than discontinuous. In the vicinity of a foam line or color change, the surface density change occurred over a horizontal distance of approximately 50 m and was not abrupt and coincident with the visual front.

4) Growth of plumes and associated frontal migrations can occur whenever less dense water empties into an ambient water mass. However, in the situation examined in this study, tides significantly influenced local processes and the rate of discharge of estuarine water from Calibogue Sound. Because of the coincidence of plume dynamics and local tidal conditions, it was readily apparent that tide was a primary factor in plume behavior. Intensity of convergence, degree of vertical and lateral spreading, and intensity of density gradients changed with the tides.

The information regarding hydrography provided more detailed information than previously available. The photographic coverage provided both fixed frame velocities and velocities relative to the front which had not been fully documented previously. However, because subsurface velocities were not measured, quantitative evaluation of pollutant behavior along the density interface could not be made. Such information would greatly enhance the understanding of mixing between plume and ambient water, and, thus, an understanding of what governs frontal pollutant exchange processes.

4.7 REFERENCES

Collins, C. A., C. N. K. Mooers, M. R. Stevenson, R. L. Smith, and J. G. Pattollo, (1968), Direct current measurements in the frontal zone of a coastal upwelling region, Journal of Oceanographic Society of Japan, Vol. 24, pp. 31-42.

Dyer, K., 1973, Estuaries: A Physical Introduction, John Wiley and Sons, New York, p. 140.

Garvine, R. W., 1974, Dynamics of Small Scale Oceanic Fronts, Journal of Physical Oceanography, Vol. 4, No. 4, pp. 557-569.

Garvine, R. W., 1974, Physical Features of the Connecticut River Outflow During High Discharge, JGR, Vol. 79, No. 6, pp. 831-846.

Garvine, R. W., and J. D. Monk, 1974, Frontal Structure of a River Plume, JGR, Vol. 79, No. 15, pp. 2251-2259.

Garvine, R. W., 1975, The Distribution of Salinity and Temperature in the Connecticut River Estuary, Journal of Geophysical Research (JGR), Vol. 80, No. 9, pp. 1176-1183.

Garvine, R. W., 1979, An Integral Hydrodynamic Model of Upper Ocean Frontal Dynamics, Part 1, Development and Analysis, and, Part II, Physical Characteristics and Comparison with Observations, JPO, Vol. 9, pp. 1-36.

Harris, W. P., G. C. Tewinkel, and C. A. Whitten, 1963, Analytic Aerotriangulation, US Coast and Geodetic Survey, Technical Bulletin No. 21.

Ingram, R. G., 1978, Internal wave observations off Isle Verte, Journal of Marine Research, Vol. 36, No. 4, pp. 715-724.

Keller, M. and G. C. Tewinkel, 1966, Space Resection in Photogrammetry, US Coast and Geodetic Survey Technical Bulletin No. 32.

Officer, C. B., 1976, Physical Oceanography of Estuaries (and Associated Coastal Waters), John Wiley and Sons, New York, p. 1-465.

Turner, J. S., 1973, Buoyancy Effects in Fluids, Cambridge University Press, Cambridge, p. 367.

Wright, L. D., and J. M. Coleman, 1971, Effluent expansion and interfacial mixing in the presence of a saltwedge, Mississippi River Delta, JGR, Vol. 76, pp. 8649-8661.

Wright, L. O., C. J. Sonu, and W. V. Keilhorn, 1972, Water Mass Stratification and Bedform Characteristics in East Pass, Detin, Florida, Marine Geology, Vol. 12, pp. 43-58.

V. CIRCULATION IN SOUTH ATLANTIC OCS REGION

5.1 INTRODUCTION

Presented in this section are the studies of subsurface currents (performed by Dr. T. Lee and Dr. L. Pietrafesa), hydrographic sampling (T. Curtin), Gulf Stream monitoring by remote sensing techniques (Dr. O. Brown) as well as surface wind time series at the location of the long-term current meter moorings, derived from the study performed by Dr. J. Fernandez-Partagas (presented in Section VI). These tasks have been regrouped as they complement one another and all contribute to depicting the current patterns observed in the region.

The objectives of each individual study are presented in Section 5.2. The next section (5.3) deals with the procedures followed for the acquisition of field data (subsurface current measurements and hydrographic sampling) as well as data sets obtained from other sources (thermal satellite imagery, meteorological observations, sea level data). Section 5.4 describes the methodology used in the analysis of current meter and hydrographic data. Data Products are presented in Section 5.5, followed by a discussion of the findings resulting from the short-term and long-term current studies, hydrographic analysis and Gulf Stream monitoring by remote sensing techniques. Finally, conclusions are summarized in Section 5.7.

5.2 STUDY OBJECTIVES

5.2.1 Current Meter Measurements

Two current meter moorings were deployed off the Georgia coast in order to investigate the short-term horizontal and vertical variability of the current and temperature structures in a region of high oil and gas interest, and in particular, the effects of wind forcing and the Gulf Stream related events--such as intrusions, eddy formation and meandering--on the shelf circulation. These current meters were emplaced in the vicinity of a hydrographic transect of the BLM Benchmark program, and integrated in a box array deployed under the auspices of DOE to provide optimum cross-shelf resolution of current patterns in the Georgia Embayment. This information, in turn, will contribute to estimating residence times of shelf waters and can also be used in the development of realistic models for the prediction of dispersal, dilution, flushing and final distribution of the pollutants which may be introduced in the marine environment as a result of OCS related oil and gas activities. The long-term mooring station was established to determine the mean flow and extent of perturbations at near-surface, mid-water and near-bottom depths in another area of oil and gas interest, and to relate the observed

current spectral energy distribution and its variability to meteorological and coastal sea level forcing as well as the Gulf Stream pulsing action.

5.2.2 Hydrographic Measurements

The collection and analysis of hydrographic data is critical to the characterization of the circulation over the South Atlantic region. Such data are necessary to derive the density field, a dynamically important variable and one which is not directly measurable with the required precision. They may also serve as velocity field tracers, providing an indication of flow patterns as well as possible mixing and dissipation regions. Finally, these data reflect water properties that can actively affect rates and interactions within the various biological chemical systems.

A variety of flow patterns in the region associated with particularly energetic processes during some observation periods have been previously identified through hydrographic casts. These processes include: for the on-offshelf flow, bottom intrusions and shelf break cascading; for the alongshelf flow, exchange between discrete circulation cells; for the Gulf Stream, meandering spin-off eddies and detached filaments; for the resultant flow, Continental Shelf and other wave motions. Furthermore, growth rates, feeding activity, and saturation levels are but a few of the parameters that are functions of the hydrographic variables.

5.2.3 Gulf Stream Monitoring from Thermal Satellite Imagery

The Gulf Stream behavior can be efficiently monitored on a synoptic basis by remote sensing techniques, using sea surface temperature as a tracer in the examination of its interactions with the shelf waters. Such information, in turn, is essential for sound interpretation of the hydrographic data collected along cross shelf transects on a seasonal basis (BLM program) or centered around Gulf Stream events such as intrusions and (or) formation and decay of eddies (DOE program), as well as for the analysis of current meter records obtained at the location of the short-term and long-term moorings.

The objective of the remote sensing program undertaken by Dr. O. Brown were three-fold: first, the study was intended to assess the potential of infrared satellite mapping techniques for the determination of the variability of the Gulf Stream/Shelf water front on time scales ranging from daily to seasonal. Next, the effort was aimed at assessing the representativeness of the hydrographic cruise data in characterizing seasonal variability of the shelf and shelf edge waters. Finally, a purpose of the remote sensing study was to generate seasonal means and extrema frontal location maps from satellite observations.

5.2.4 Surface Wind Field Determination

The availability or generation of sequential maps of surface winds over the region of the current meter moorings is essential for the characterization of the shelf waters response to the passage of meteorological fronts, and, therefore, for the interpretation of the subsurface current measurements. To that effect, maps of surface wind streamlines and isotachs were prepared by Dr. J. Fernandez-Partagas for the duration of the mooring deployments, first on a 6-hourly basis for the first three months, and daily thereafter, in support of the short-term and long-term current meter data analysis, respectively. The study was also intended to address the feasibility of using coastal wind data from shore meteorological stations, satellite-derived winds and the National Weather Service (NWS) predictions to characterize offshore wind conditions.

Finally, correlations of surface wind and wave field data were developed in support of the interpretation of subsurface current measurements, and as a possible tool for the statistical prediction of wave climatology based on offshore wind observations.

Only those data products used in the analysis of subsurface and hydrographic measurements are described in the present Section V. The methodology followed in the performance of this study as well as the findings and conclusions are presented in Section VI: "Meteorology/Sea State Analysis."

5.3 DATA ACQUISITION

5.3.1 Current Meter Measurements

Two sets of current meter moorings, hereafter denoted "short-term moorings" and "long-term moorings" were deployed in the Georgia Embayment during the first year's study. The "short-term" moorings consisted of two strings deployed off the coast of Georgia on September 1, 1977, on the 37 m (mooring #83) and 45 m (mooring #84) isobaths, at the locations shown in Figure 5-1, ($30^{o}55.24'N$, $80^{o}16.84'W$ and $30^{o}51.5'N$, $80^{o}06.2'W$ respectively), and recovered on November 2, 1977. They contained VACM current/temperature/pressure sensors located 17 m below the surface and 3 m above the bottom. In addition, the deeper mooring was equipped with an Aanderaa current/temperature/pressure recorder positioned 1 m below the upper VACM. The timing of the current meter measurements was established to overlap the BLM benchmark time series cruises.

Subsequently, a long-term mooring was deployed off Charleston, S.C. on November 4, 1977, near $32^{o}38'N$ and $78^{o}42'W$, at a nominal depth of 45 m. This mooring, also shown in Figure 5-1, was rotated on a three-

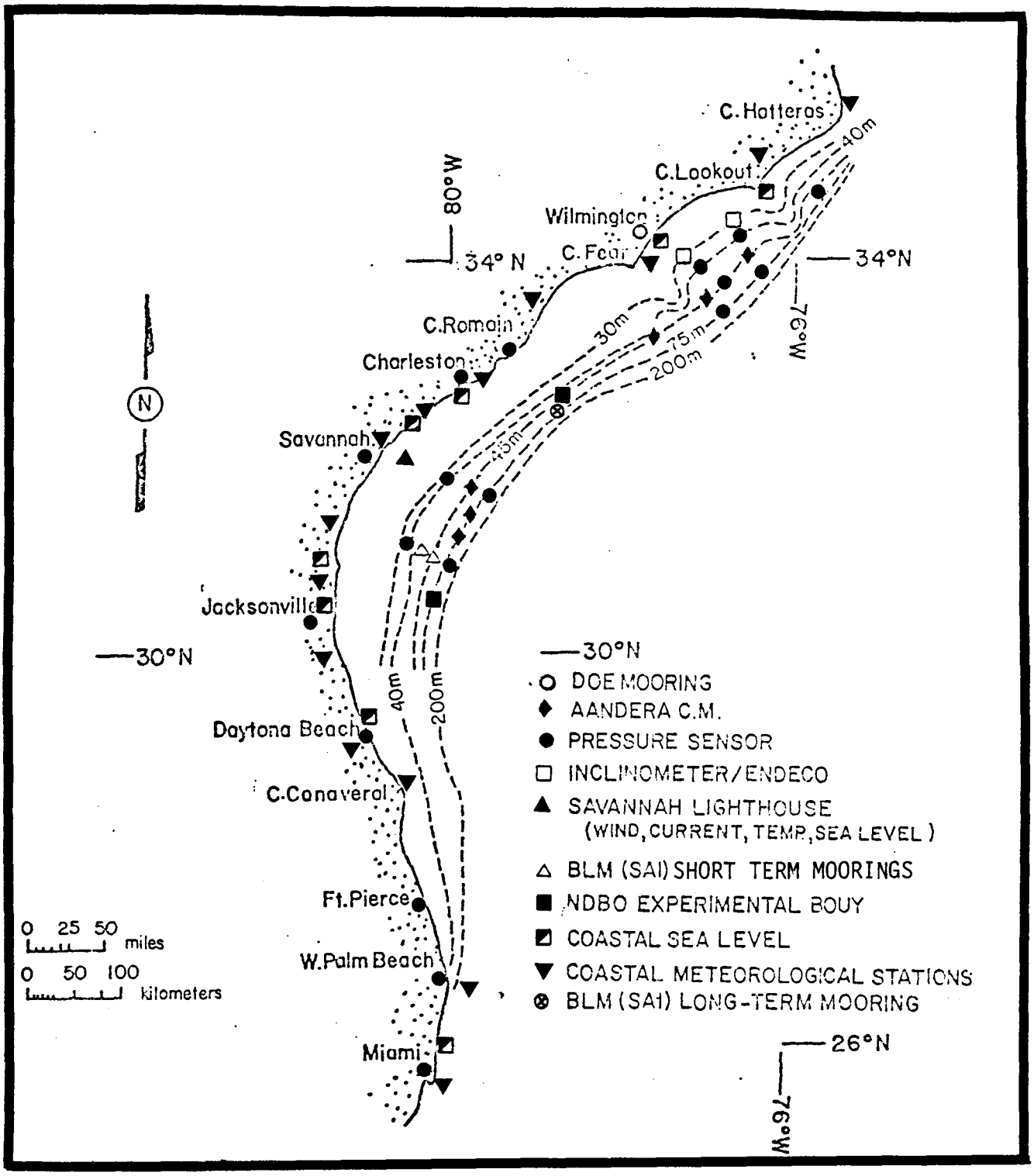

Figure 5-1. Instrumentation in South Atlantic Bight, 1977-1978.

month basis to provide a year-long time series of currents and temperatures at depths of 10, 17 and 42 m. The objectives of these subsurface current studies were briefly stated in Section 5.2.1.

5.3.1.1 Current Meter Mooring Location

5.3.1.1.1 Short Term Current Meter Moorings

As indicated above the two short-term current meter moorings were positioned at depths of 37 and 45 m and locations characterized by $30^{o}55.24'N$, $80^{o}16.84'W$ and $30^{o}51.5'N$, $80^{o}06.2'W$ respectively. Several factors were considered in the selection of these mooring sites. First, as part of a program funded by DOE, two moorings were to be deployed from June 30 to November 1, 1977 at depths of 30 and 75 m, as part of a box array shown in Figure 5-1. It was, therefore, desirable to optimize the cross-shelf resolution of currents and exchange by deploying the two BLM moorings at approximately equal spacing between the 30 and 75 m isobaths. Furthermore, the moorings were to be positioned near the center of the area of highest oil and gas interest, and near a transect of the BLM Benchmark program, in order to support the interpretation of the summer hydrographic sampling. Finally, in order to facilitate the analysis of longshore coherence, it was preferable to deploy the BLM strings on the same isobaths as the DOE moorings, both in the Georgia Embayment and the Caroline Cape regions. The selected locations fulfilled all these criteria.

Furthermore, in order to simplify the integration of the DOE and BLM data, it was decided that the upper FACM of the two short term moorings would be emplaced at the same depth (17 m) as that of the upper Aanderaa meters equipping the DOE strings. This depth, in turn, had been chosen by the DOE principal investigators in order to get as close to the surface as possible (within the surface mixed layer), while minimizing wave induced motions. In order to monitor bottom currents and temperature the lower meters were positioned 3 m above the bottom, i.e., as close to the sea floor as allowed by the height of AMF acoustic releases equipping the moorings. This depth was judged quite acceptable for it was within the boundary layer and close enough to the bottom to record subsurface intrusion events.

5.3.1.1.2 Long Term Current Meter Mooring

The long term current meter mooring was maintained in the northern Georgia Embayment for a year at a mean water depth of 45 m and a location of $32^{o}38'N$, $78^{o}42'W$, chosen as being near the center of an area of oil and/or gas interest. It should be pointed out, however, that this site is somewhat unusual for the Georgia Embayment: in this region, the Gulf Stream seemingly departs from the continental margin/slope and veers to the right, at about 32^{o} N latitude, in a quasi-permanent feature referred to as the "Charleston Bump" by the

local oceanographers (Atkinson, Pietrafesa, Lee, Janowitz, etc.) who have become aware of the persistence of this feature in the remote sensing data. The Florida Current appears to return to the continental shelf at approximately 33° to 34° N latitude. This feature may be topographic in origin. A blow up of the bathymetry near the mooring location, shown in Figure 5-2, reveals a distinct veering of the isobaths from their 45° east of north alongshore trend to approximately due east and back to the 45° NE norm. The mooring location is a pocket in terms of local topography. This anomaly could result in a local steering of the circulation.

Previous investigations in the region have indicated that the current and density fields of the shelf water exhibit a vertical structure. Therefore, it was deemed desirable to use three current/temperature sensors (VACM's) stacked in a vertical array, in order to sample the temporal characteristics of the stratification. The lowest sensor was placed 3 m above the bottom to allow room for the acoustic release mechanism but was still sufficiently close to record near bottom intrusions. The uppermost sensor was placed at a depth of 10 m below the surface in order to be within the surface mixed layer and allow comparison between these near-surface currents and measurements made with surface drogues, as well as data provided by near surface DOE current meters placed in other locations on the shelf. The third sensor was placed at midwater depth in order to thoroughly sample the water column.

5.3.1.2 Current Meter Mooring Design

The criteria used in the design of the current meter moorings deployed during the first year study, an outline of the analytical calculations performed to establish their most suitable configuration, an assessment of the validity of the assumptions made in the design computations, regarding the probable current profiles prevailing at the mooring locations, and descriptions of the instrumentation, flotation and other mooring components are provided in the following sections.

5.3.1.2.1 Design Criteria and Computations of Mooring Configurations

The following criteria were used for the design of the current meter moorings:

- They were designed such that the angle of inclination of each current meter does not exceed 15° from the vertical, in order to insure the quality of the currents data.

- All instruments were shackled to sufficient flotation to raise the instrument and associated hardware in the event of a mooring failure in the worst location.

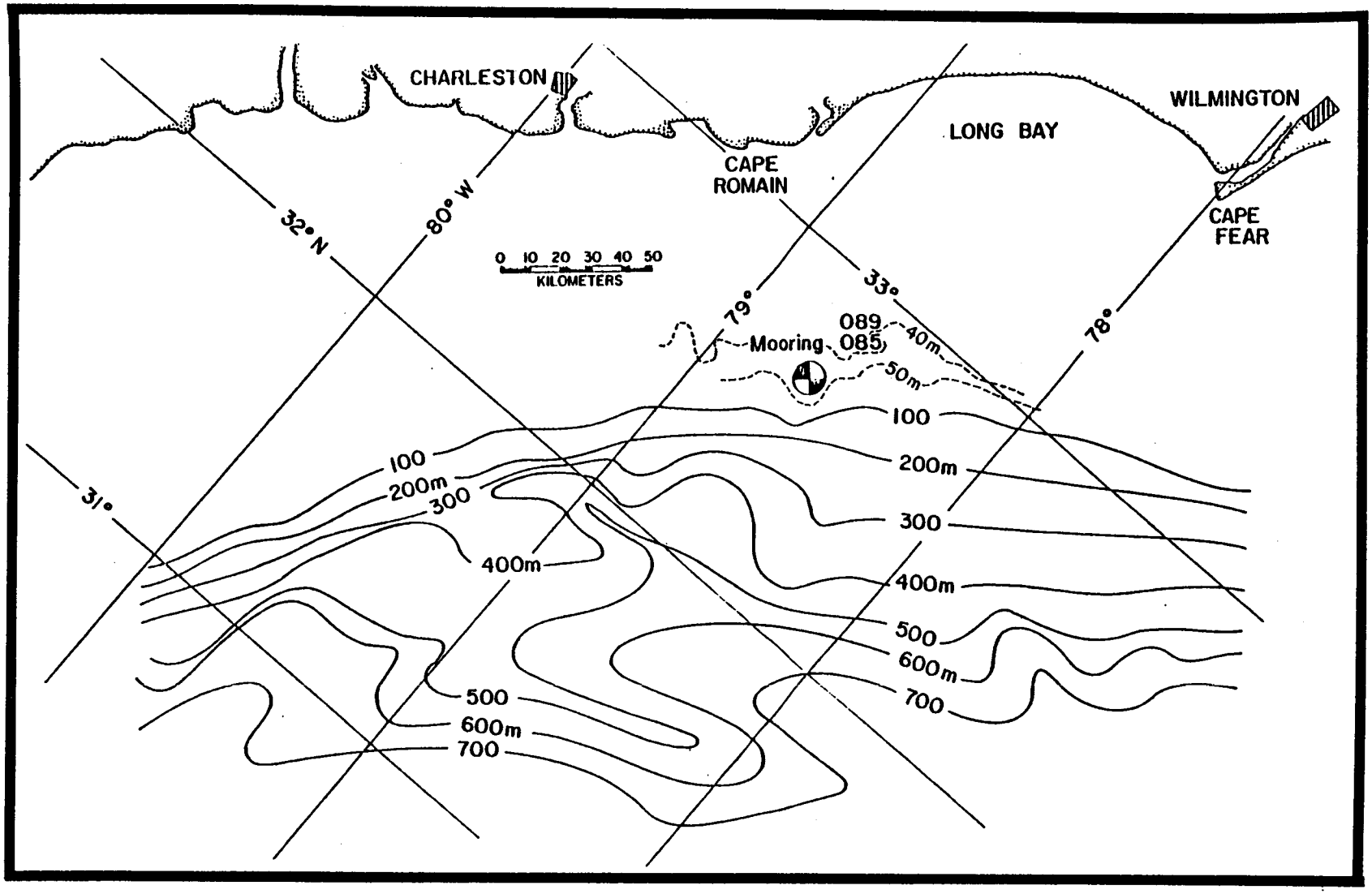

Figure 5-2. Topography in the vicinity of the BLM long-term mooring.

- Insofar as possible, galvanized steel was used in the mooring components. Where this was not possible, dissimilar materials were isolated from one another.

- Two acoustically actuated release devices were used to detach the anchor from the rest of the mooring system in order to recover the instruments. They were configured in a parallel arrangement, so that release could be affected if only one of the releases functioned.

The final mooring design also took into consideration cost trade-offs, component availability, drag minimization, corrosion, and deck handling ease.

The static configuration of the moorings was determined using a program originally developed by Woods Hole Oceanographic Institute (WHOI), (Moller, 1976), which calculates the deflection of the current meter array when submitted to a given current profile, the tensile load and reserve buoyancy at the elevation of every mooring element. The vertical current distributions shown in Table 5-1, were provided by the principal investigators based on their previous work in the region, and input to the program as representative of extreme conditions likely to prevail at the mooring sites.

Profile A was used to check that the computer has adjusted the wire lengths properly and that the instruments have been positioned at the desired depths.

These computations revealed that when submitted to profile B, the inclination of the upper current meters of the short term moorings could exceed 15^{o} for the mooring configuration described in Section 5.3.1.2.2. However, it was felt that the length of time for which a particular instrument would be exposed to a tilt larger than that value would be short, and that modifying the flotation and anchor weight to increase the mooring stiffness would be an unnecessary expense.

Likewise, for the most extreme currents (profile E), the analytical model predicted that the tilt of the upper VACM of the long-term mooring in the configuration shown in Section 5.3.1.2.2 may exceed the design criterion of 15^{o} and reach a value of 17.1^{o}. However, it was felt that any further attempts to fine-tune the mooring design would be futile. Subsequent evaluations with additional flotation in support of the upper meter (43 cm glass floats in addition to a 71 cm diameter steel sphere) showed only little improvement to the tilt angle, while jeopardizing the stability of the upper float. Therefore, the decision was made to adopt the mooring configurations presented in the upcoming section.

Table 5-1. Current profiles used as inputs to the design of short-term and long-term current meter moorings.

Depth (m)	Current Speed ($cm.s^{-1}$)				
	Reference	Short-term moorings		Long-term moorings	
	Profile A	Profile B	Profile C	Profile D	Profile E
0	0	90	70	80	90
		L	L		
		I	I		
10	0	N	N	80	90
		E	E		
		A	A		
		R	R	L	L
				I	I
37 or 40	0	40	45	N	N
				E	E
				A	A
				R	R
42	0			40	60
45	0			40	60

5.3.1.2.2 Mooring Configurations

Short Term Moorings

The two short term moorings are sketched in Figure 5-3. The first one (mooring #083), designed for a nominal depth of 35 m, supports two AMF VACM's, the upper current/temperature/pressure sensor being located 17 m below the surface, and the lower VACM (current/temperature sensor) 3 m above the bottom. The second mooring (#084), deployed on the 45 m isobath, consists of one upper VACM (recording current, temperature, and pressure) located 17 m below the surface, one Aanderaa current/temperature/pressure recorder positioned 1 m below the upper VACM and one lower VACM 3 m above the bottom. The Aanderaa meter, provided by the University of Miami, has been added to the deeper mooring, not only to facilitate the integration of the ERDA data with the set of data collected during the BLM program, but also to compare the dynamic response of the VACM and Aanderaa in the Georgia Embayment environment.

Both moorings are basically similar. The primary flotation on each mooring is provided by welded steel spheres, 71 cm (28") in diameter, and each providing 134 kg (296 lbs) of flotation. Where necessary, additional flotation is provided by 43 cm (17") glass spheres, each providing 23.5 kg (52 lbs) of buoyancy when bolted to a 0.95 cm (3/8") galvanized chain. The uppermost element on each mooring consists of a float molded of a composite of syntactic foam and 5 cm (2") diameter resin spheres. This float is surrounded by a steel framework that serves as a lifting bale during recovery operations and provides support for the radio beacon transmitter and Xenon flasher. The mooring is separated from its anchor at the end of the deployment period by making use of two acoustic release mechanisms arranged in a parallel configuration. The arrangement is such that anchor release is effected upon actuation of either release.

Long Term Moorings

The long-term moorings first deployed on November 4, 1977 and rotated thereafter on a 3-month basis are sketched in Figure 5-4. Designed for a nominal depth of 45 m, they support three AMF Vector-Averaging Current Meters (VACM), the upper current/temperature/pressure sensor being located 10 m below the surface, the second VACM (current/temperature) at mid-depth (22.5 m) and the lower one (current/temperature) 3 m above the bottom. The design of the upper portion of the mooring differs slightly from that used in the short-term moorings. On the latter arrays, the uppermost float extended nearly 7 m above the sensor level of the upper current meters. Due to the requirement that the upper VACM of the long-term mooring be located higher in the water column (10 m against 17 m for the short-term moorings), it was decided to modify a 71 cm (28") steel sphere by the addition of instrument wells that would house the radio and flashing

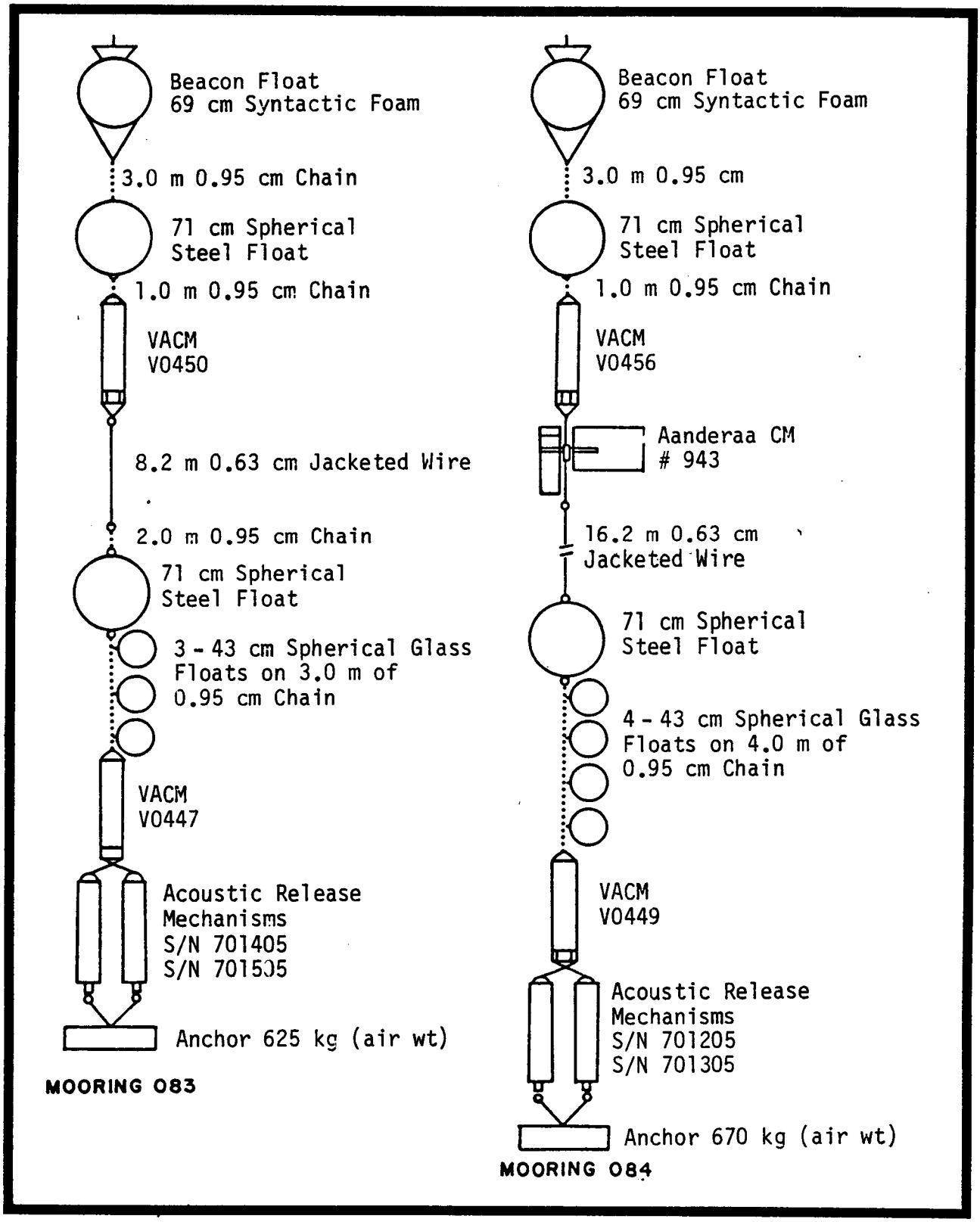

Figure 5-3. Short-term mooring configurations.

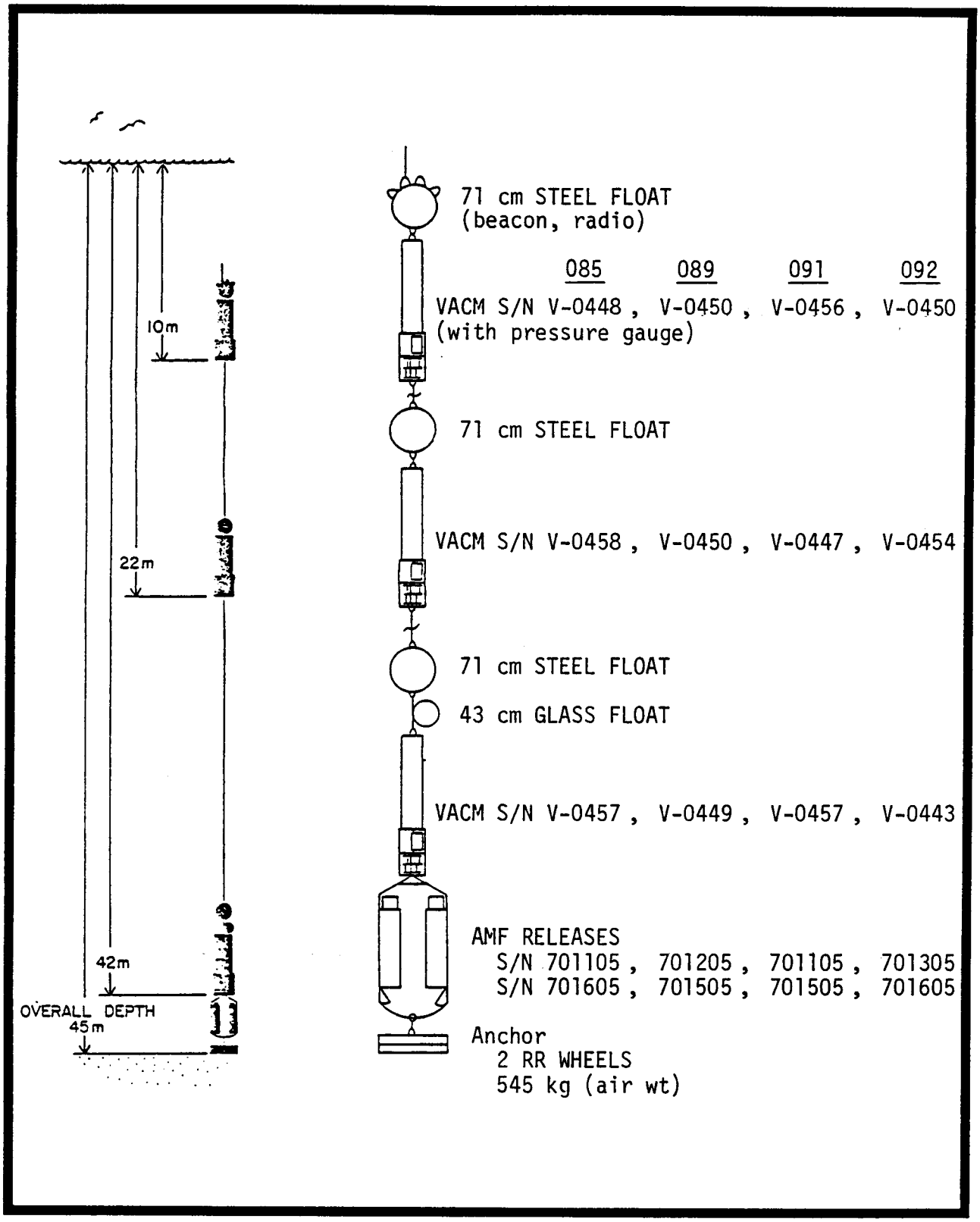

Figure 5-4. Long-term mooring configurations.

light beacons required for recovery operations. Use of this float resulted in the uppermost float extending only 3 m above the sensor level of the upper current meter.

As for the short-term current meter moorings, the long-term array is separated from its anchor at the end of the deployment period by making use of two acoustic release mechanisms arranged in a parallel configuration.

5.3.1.2.3 Description of Mooring Components

Current Meters

With the exception of one Aanderaa current meter mounted on the short term mooring #084, all current meters were VACM's, Model 610-C, manufactured by AMF Inc., Alexandria, VA. Both instruments, shown schematically in Figure 5-5, record current speed and direction as well as temperature. Current speed is sensed by a Savonius rotor, a device which has accumulated a long history of calibration and performance data. Each revolution of the rotor represents a fixed displacement of water past the instrument (36 cm per revolution in the case of the VACM). By coupling the number of revolutions of the rotor (i.e., the distance water has traveled past the instrument) with a time count, the current speed can be readily computed. Temperature is sensed by a thermistor.

The Aanderaa and VACM record current direction in a different way. The Aanderaa has a large vane that orients the current meter with the direction of the flow. With this current meter, current direction is obtained by measuring the orientation of the current meter (and therefore the flow direction) using a magnetic compass. In the VACM, no vane is employed to orient the current meter with the flow, the housing being free to assume any orientation. It is therefore necessary to measure both the orientation of the current meter, using a magnetic compass (θ_c, Figure 5-6) and the orientation of the flow with respect to the current meter, provided by the direction vane (θ_v, Figure 5-6). Combining these two readings yields the current direction θ_m as illustrated in Figure 5-6.

The data gathering process in the VACM starts upon receipt of a pulse from the rotor sensing circuit (8 pulses are generated for each rotor revolution). A unit vector is generated with a length equal to the distance constant of the rotor and a direction equal to the direction from which the current is coming. This unit vector is first resolved into east and north components. These components are summed over an averaging period (normally 15 minutes), at which time they are recorded on a digital cassette recorder. This vector averaging technique is employed in order to minimize data storage requirements while retaining a high sampling rate. Thus, with an averaging period

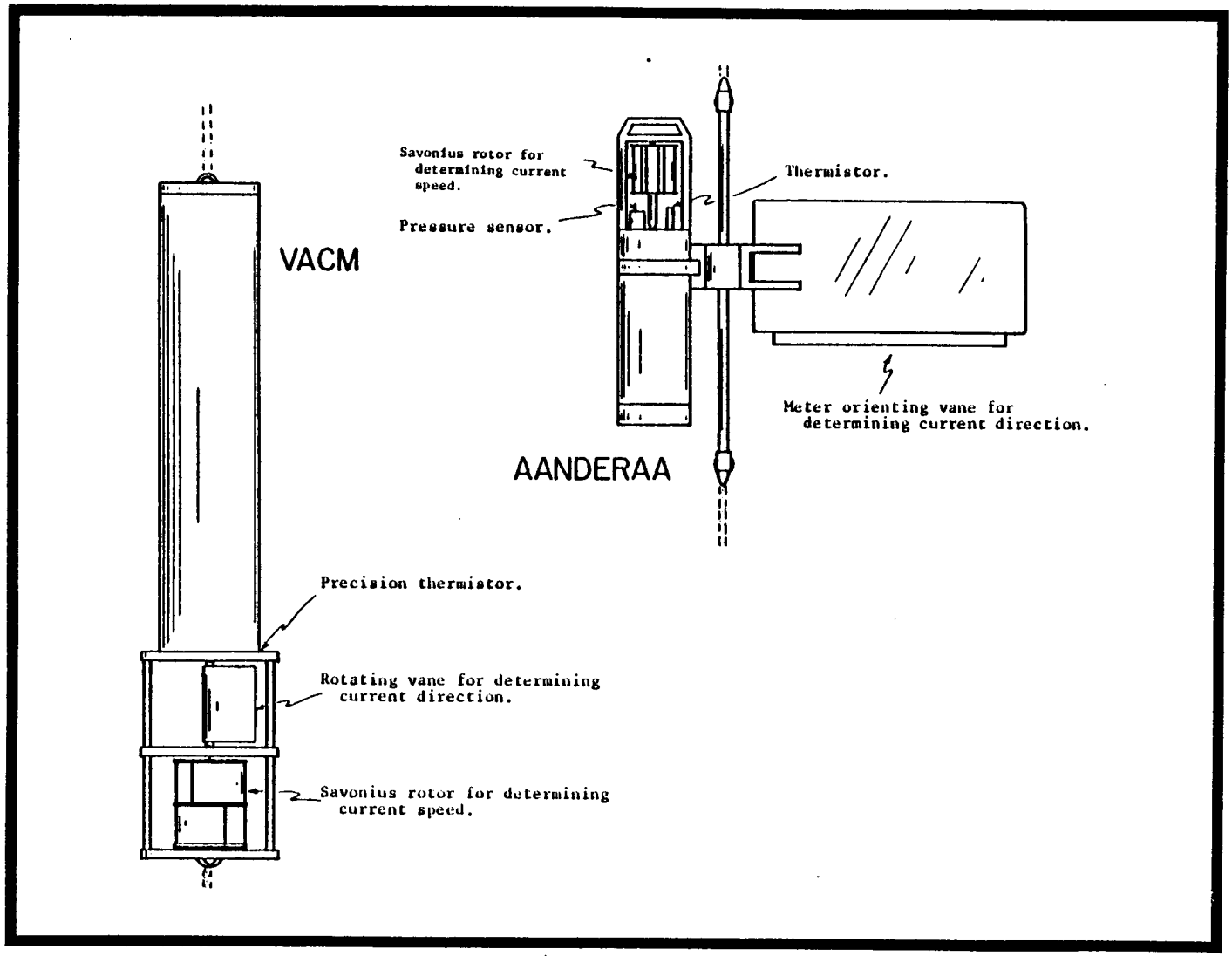

Figure 5-5. Schematics of Aanderaa and VACM current meters.

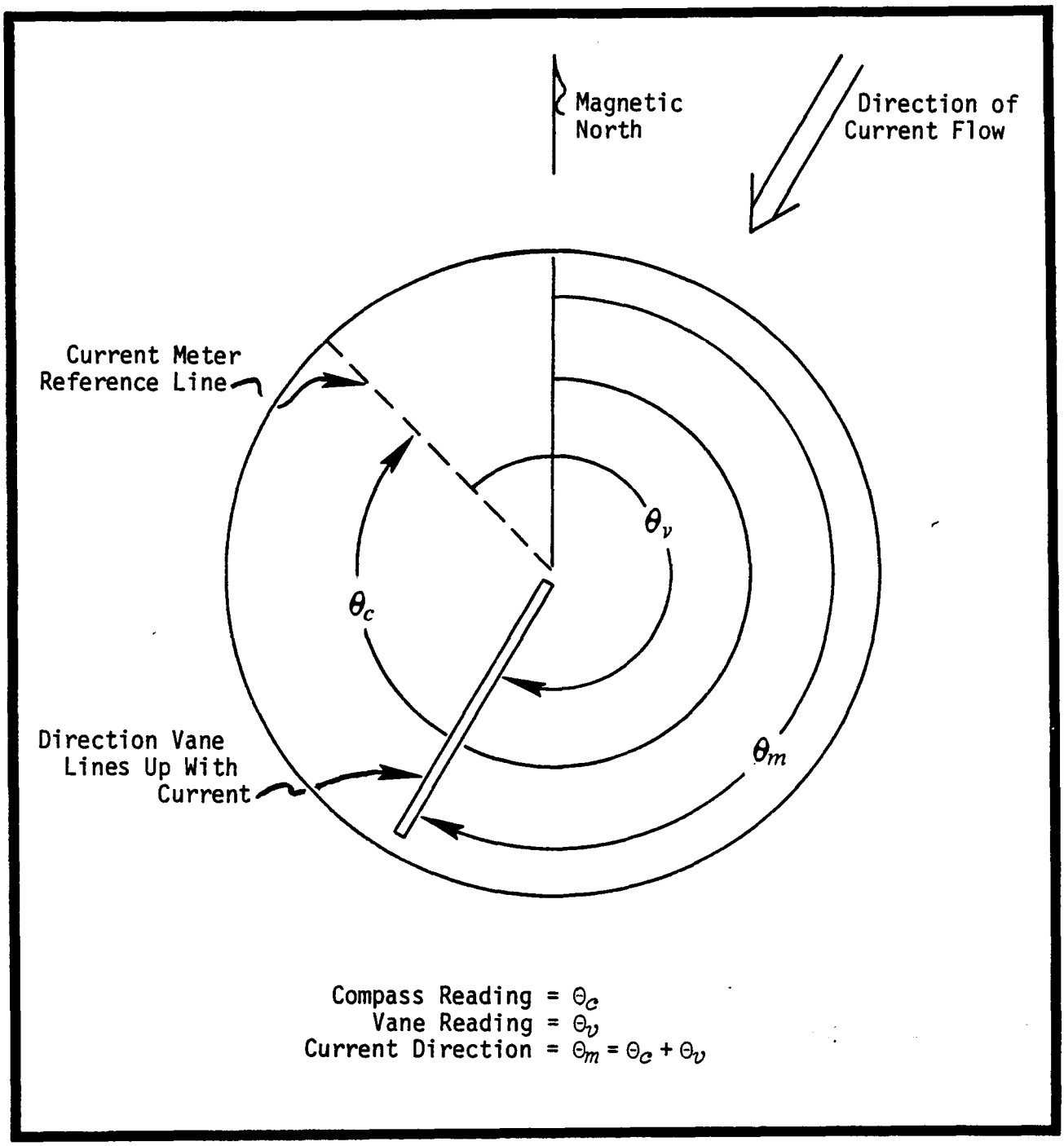

Figure 5-6. Schematics of determination of current direction with a VACM.

of 15 minutes, a current of 50 cm.s^{-1} initiates 10,000 separate calculations. Without the averaging technique, this would require recording 10,000 compass readings and 10,000 vane readings each interval, quickly exhausting storage capacity.

Each rotor pulse initiates the following compute sequence:

Power up computer circuit
Read compass
Store compass
Read vane follower
Add vane reading to stored compass reading (Result is magnetic direction, θ_m)
Look up sin θ_m
Add sin θ_m to contents of east counter
Look up cos θ_m
Add cos θ_m to contents of north counter
Increment rotor counter by 1
Power down computer to wait for next rotor pulse

The sums contained in the east and north current component counters, along with the sum of the rotor counts, a vane reading, a compass reading, an elapsed time count and a temperature count are recorded on a 4-track digital cassette recorder. The single vane follower and compass readings are recorded to aid in analysis of instrument performance and can also be used to compute current direction directly. The time clock in the VACM performs two functions: it controls the interval (normally 15 minutes) at which the data is recorded, and also provides an elapsed time word which is recorded as part of the data. Temperature is measured by a thermistor (mounted in the bottom of the current meter) which controls the output frequency of a precision voltage to frequency converter. The output of this converter is summed over the averaging period and the resulting count written as part of the data word.

At a 15 minute sampling interval, the VACM is capable of storing data for over a year. However, operation in the coastal environment is usually restricted to approximately three to four months due to biological activity.

Release Mechanisms

The release mechanisms used to separate the mooring from its anchor at the end of the deployment period were the Model 322 Recoverable Acoustic Transponder manufactured by AMF, Inc., Alexandria, VA. These instruments were used side-by-side in a parallel arrangement which allows the mooring to be released from the anchor by either unit. In addition to the release function which is performed by firing a small explosive squib, these units are equipped to perform the following functions:

- Reply Pinger - Upon receipt of the appropriate command, the unit transmits acoustic pulses for a period of 90 seconds.

- Tilt Switch - A tilt switch was incorporated to give an indication of the attitude of the mechanisms. If the release exceeds 45^{o} from the vertical, then the pulse rate from the reply pinger is doubled. This feature will determine whether or not a mooring failure has occurred.

- Transponder - This enables the recovering vessel to obtain an accurate slant range to the release mechanism, both before and after the release has been activated. Confirmation of release is obtained by the underwater unit transmitting a double pulse in return to the interrogating pulse. After the release has been activated and release confirmation received, the ranging information is used to locate the surfaced mooring.

Flotation and Anchor

Each instrument was shackled directly to a flotation element large enough to support the instrument and any associated mooring components down to the next flotation element. This ensured that, should the mooring fail at any point, all elements below the break would still be recoverable. The primary float (upper one) was a steel sphere, 71 cm in diameter providing 134 kg of positive buoyancy. This float was preferred because of its low cost to buoyancy ratio. On the basis of tests done at the University of Miami Rosenstiel School of Marine and Atmospheric Science (RSMAS), the net drag on this sphere in a velocity of 60 $cm.s^{-1}$ was determined to be less than 9 kg. In order to protect the steel from corrosion, two 9.45 kg, zinc anodes were attached. As required, additional 46 cm (17 inch) glass sphere in a protective plastic "hard hat" providing 22 kg of buoyancy each were positioned immediately above the lower current meter. No flotation was placed between the lower current meter and the release in order to be able to locate this meter as close to the bottom as possible (3 m).

The weight of the anchor was designed in such a way that the mooring would drag before the mooring wire is subjected to a strain near its elastic limit.

Mooring Wire Hardware

The wire used to connect mooring elements together was .635 cm (1/4") 3 x 19 plastic jacketed wire from Macwhyte Wire Rope Company. The 3-strand rope was selected for its relatively torque-free construction. Macwhyte's process of plastic jacketing ensures complete coverage of each strand, thereby reducing the chance of a corrosion-related

failure, should the jacket be damaged. The wire was terminated by means of oversized swage terminals applied at Nova's current meter facility. The fittings used were .95 cm (3/8") blank fittings that are specially drilled for the 6 mm (1/4") wire, and were selected to give a large bearing surface between the fitting and the shackle. The wire-fitting joint was protected by means of a molded polyurethane boot that is slid down over the fitting after it had been swaged to the wire. This boot extended 15 cm down over the cable jacket and also served to prevent cable strumming from causing fatigue in the wire where it enters the fitting.

Mooring elements were connected by means of 1.25 cm (1/2") galvanized safety pin anchor shackles. The nut of the shackle was secured by means of a stainless steel cotter pin. This type shackle is much easier to use than screw-pin shackles as it does not require the use of seizing wire. Shackles were used in pairs, with a galvanized pear link between them. This pear link was used on launch and recovery for temporarily stopping off the mooring. One half inch galvanized chain was used between the release mechanism and the anchor and between instruments and flotations elements when deemed advisable for ease of handling in launch or recovery.

Potential Fouling Problems

Equipment deployed in the ocean for long periods of time is subject to fouling by marine growth. This condition leads to inaccurate and spurious data and may eventually cause failure of the instrument. Current meter moving parts are particularly vulnerable because of close tolerances required for minimum velocity thresholds.

5.3.1.2.4 Mooring Design Evaluation

During the first year of the study the current speeds were in excess of the standard profile velocity of 80 $cm.s^{-1}$ at the upper meter and 40 $cm.s^{-1}$ at the lower meter, for one 33 h period. This occurred during the second long-term mooring deployment. It looked as though the current meter tilt exceeded the design criterion of 15^{o} from the vertical for 33 records (8 h 15 min.) out of the entire record length. No such excess of the standard velocity profile occurred during the first 3 month deployment.

Although it would be possible to redesign the mooring to eliminate this minor contamination, it is felt that the theoretical gain in data quality which could be obtained by stiffening the mooring would not justify the additional expense related to the procurement of larger ORE spherical floats, at least until the above data are confirmed in a longer record.

5.3.1.3 Current Meter Mooring Checkout Procedures and Quality Assurance

As mentioned in Section 2.3, a quality assurance (Q.A) program was implemented by SAI to optimize the quality of the data return. An Engineering Quality Assurance Manual, dated October 1977 was prepared by Nova University. It describes the testing procedures of the VACM's and other mooring components prior to deployment. A similar Q.A. Manual, listing the various steps involved in the checkout of Aanderaa meters, is also followed by the University of Miami. An outline of these procedures is presented hereafter.

5.3.1.3.1 VACM Checkout Procedures

It was the responsibility of Nova University to perform the checkout and maintenance of the VACM's prior to and between deployments. In what follows, the procedures followed in the preparation of these instruments are briefly described.

Instrument Preparation

Current meters are first given a thorough visual inspection to check for any damaged or missing components. The serial numbers of the individual components (circuit cards, speed sensor, compass, vane follower, etc.) are recorded and the compass and vane follower set aside for individual tests. The rotor and direction vane cage is disassembled and the manufacturers bearings are replaced. (The original equipment bearings have proven to be unreliable and are replaced with a bearing designed at Woods Hole Oceanographic Institution). The cage is reassembled and rotor and vane bearings adjusted.

The compass and vane followers are placed on a rotating test fixture to check for bearing friction and balance. The compass and vane follower must be linear within $\pm$ 1 bit under conditions of the horizontal field being reduced to 60 m-gauss in the case of the compass and in the case of the vane follower, the sensor is separated from its drive magnet by 10 cm instead of the normal 2.5 cm. The compass is then checked for balance of a tilt of 25^{o}, with a specification of $\pm$2 bits.

The electronic tests are then commenced, using a power supply set to give an output voltage representative of the end-of-life voltage to be expected from a battery pack. The three diodes in series with the power supply are checked for continuity. The output voltages from the various current meter power supplies are measured and adjusted if necessary.

The measurement of current drains is one of the two most important in the entire checkout procedure. Any deviation from specifications is investigated and the source of excessive current drain located and

replaced. Not all components causing excessive current drain have logical faults, but would cause premature failure by draining the battery. Both total quiescent current and individual circuit board currents are measured and logged.

Dynamic currents are measured with the rotor turning and tape recorder running. The currents driving the LED's in the compass and vane follower and the currents out of the direction-sensing phototransistors are measured. The voltage level on the phototransistors is checked for zero level. Any offset of the zero level causes a photo transistor to turn on, yielding a false direction.

The next series of tests are performed in a cold room, set to $5^{o}C$, to duplicate actual operating temperatures. The tape recorder drive signals are checked for frequency and adjusted if necessary. The main time clock is also adjusted, if necessary. It should be noted that a period of operation of up to 24 months may be necessary before a clock will always be within the spec of $\pm.5 \times 10^{-5}$ at the end of a deployment.

After a check of vector computer operation and quiescent current, a test tape is made over a period of 36 to 48 hours. The rotor is turned by a fan during this test and the record rate is stepped up to 1 record every 56 s to give a readable number of records. The test tape is then put on Nova's Sea-Data Cassette Reader, and strip chart records of the contents of the East, North, Rotor, Time and Temperature counters are made.

Reading of this test tape and quiescent current being within specification are the two most important tests in the VACM checkout.

Final test covers the procedures performed immediately prior to sealing the pressure housing. These include a last measurement of quiescent current, confirmation of vector computation, speed sensor operation, and compass and vane operation.

The current meter is then loaded with a fresh cassette which has been bulk erased and the tape recorder advanced several steps. The current meter (up to 6 at a time) has its time clock reset to zero, and the time of reset recorded.

After the final test, the electronics chassis is inserted into the pressure housing and the attachment bolts are torqued to the manufacturer's specification. To ensure a dry atmosphere for the current meter electronics to operate in, the housing is purged with freon. The housing is pressurized to 700 $gr.c,^{-2}$ and $vented_{-2}$ four times. The housing is then pressurized to 140 to 280 $gr.cm^{-2}$ and sealed.

VACM Rotor Calibration

Calibration of the VACM Savonius rotors was not performed in a tow rank, a free surface water tunnel or circulating flume. Instead, use was made of calibration curves prepared for representative rotors, but not individual sensors. This is consistent with practice followed by Woods Hole, NOAA and other agencies or institutes.

Thermistor Calibration

Thermistors were calibrated for the Nova Current Meter Facility at Woods Hole in accordance with the procedures detailed in WHOI Tech. Report 76-94, "Accuracy of Temperature Measurements with the VACM".

Thermistors are calibrated in a precision temperature bath designed specifically for VACM thermistors. The voltage applied to the thermistor during calibration is equal to the operating voltage when installed in the current meter.

The report referenced above, gives the sum of systematic errors as $0.0014^{o}C$ (this is the bath and measuring system error).

Overall temperature accuracy is $\pm.01^{o}C.$, with a drift rate of less than $.005^{o}C$ per year. (It takes up to two years to determine the drift rate of the thermistors, after several pre- and post-deployment calibrations.)

5.3.1.3.2 Aanderaa Current Meter Checkout Procedures

Instrument Preparation

The Aanderaa Current meter mounted on the short term mooring #84 was checked out and calibrated according to the University of Miami current meter maintenance program. The latter provides for the complete disassembly, cleaning, testing, rebuilding and calibration of each instrument prior to use to improve reliability and accuracy. A detailed description of this program can be found in Lee and Shutts, 1978. Electronic and mechanical components are tested separately to note their response and to detect and correct minor malfunctions. Each sensor is individually cleaned and rewired according to the desired measuring parameters, then bench-tested before any major calibration procedure begins. The completed assembly is retested and calibrated.

A history is kept in each instrument's log book of all maintenance procedures, sensor responses, part replacements, physical condition of the circuit boards, end plates and pressure case, as well as calibration data. Mooring locations, dates of deployment and recovery are also documented.

Aanderaa Current Meter Calibration

Temperature. A 100 gallon salt water bath fitted with a 20,000 BTU refrigeration unit, heaters, rotor stirrers and thermometers is used to calibrate current meters before and after their deployment. The bath temperature is measured by immersing chemical thermometers, accurate to 0.01°C, and a Hewlett Packard 2801A Quartz Thermometer, which is resolvable to 0.001°C, 12.5 cm below the water's surface in the center of the tank. A temperature comparison between the outer edges and the center of the bath reveals no relative change when the water is stirred. Nine instruments can be simultaneously calibrated. The water temperature may be adjusted to the sensor's upper or lower limit; however, since it is faster to heat than to cool, the temperature is started at the lower limit. Each instrument is entirely immersed in the bath and allowed to equilibrate, then it is triggered approximately every 2°C, after allowing the bath to equalize for five minutes at each step. The instruments are manually triggered through an electrical terminal on the top of their end plates. Depending upon the thermistor's range, approximately twelve points are recorded. If the sensor is not linear, appropriate adjustments are made and the instrument is recalibrated. An example of a temperature calibration plot is shown in Figure 5-7.

Pressure. Aanderaa pressure sensors are calibrated in five and ten meter steps, depending upon the range of the sensor used. Linearity is determined by employing an Ametak dead weight pressure tester. Accuracy of this tester is $\pm$ 0.03% of pressure reading. Data is certified traceable to the National Bureau of Standards. An example of a pressure calibration is shown in Figure 5-7.

Direction. The compass is calibrated before and after each instrument deployment in order to determine the offset and slope of each compass and potentiometer-follower. The compass calibration facility consists of an all-aluminum platform with holding mounts for four instruments. The platform rotates 360° in the horizontal plane. Indexing holes are spaced every 10° around the circumference of the platform and a master hole, at the same radius, is located in the stationary platform base. At the present, platform rotation and instrument triggering is accomplished by hand. A typical compass calibration is shown in Figure 5-7.

Speed. Without a towing tank it is very difficult to adequately calibrate the current speed sensor; however, linearity can be checked. Before each use the mechanical or electrical rotor counter (gear box) is removed from the current meter, cleaned, and inspected. The gear box is then coupled to a magnetic stirrer and the output voltage is tested for linearity and maximum speed. The gear box is reinstalled in the current meter and the Savonious type rotor is revolved at increasing speeds in order that data from the speed channel, in Aanderaa bits, can be recorded on a calibration log for linearity checks.

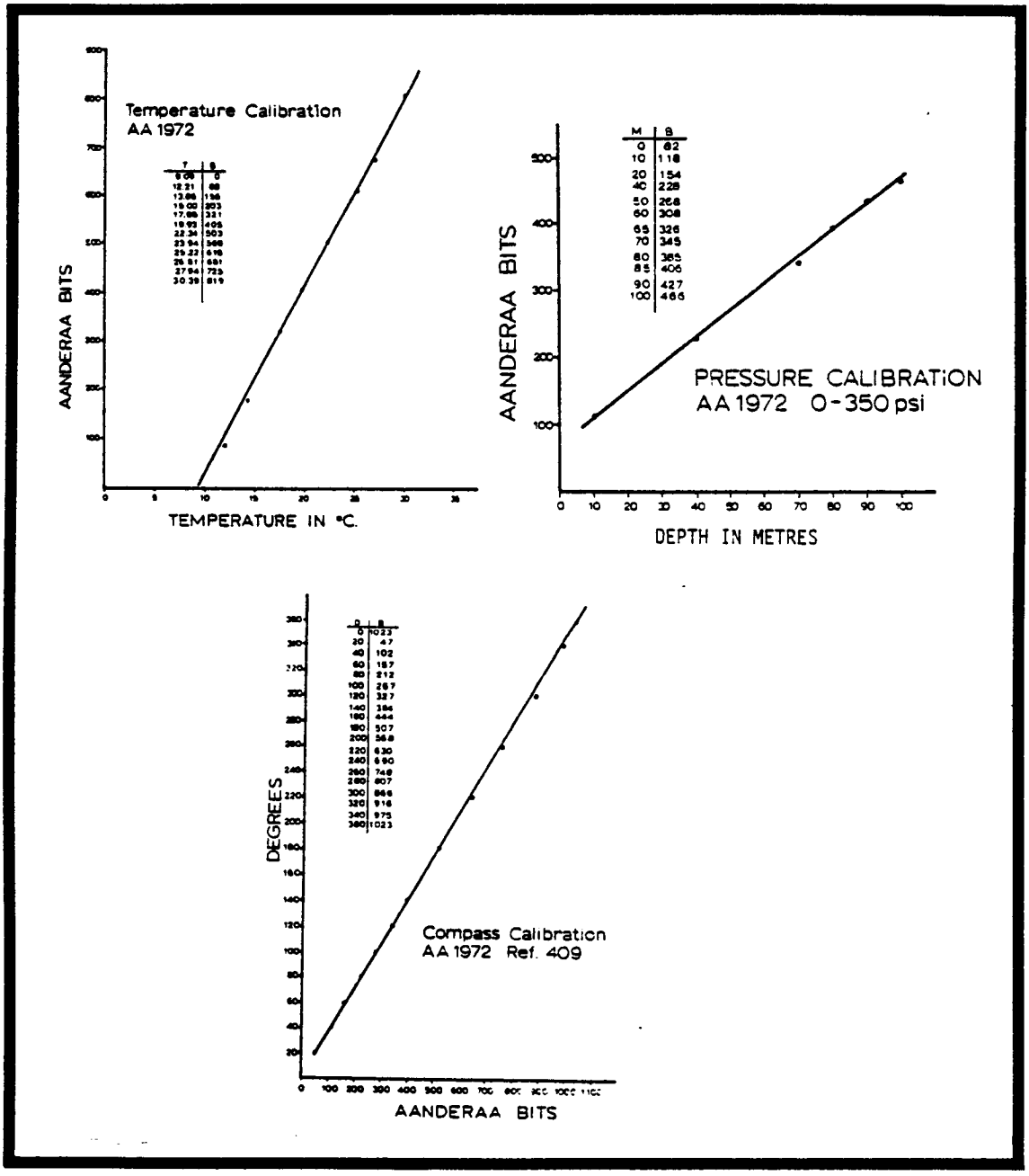

Figure 5-7. Typical temperature, pressure and compass calibration of an Aanderaa current meter.

Encoder and Recording System. Calibration data from all channels are collected on 1/4" magnetic tape and read on a PDP-11 computer. This data is analyzed for sensor failure as well as discrepancies indicating operating malfunctions. This data is then logged for each instrument before deployment. Additional calibration data is utilized as stated in the National Oceanographic Instrumentation Center's "Instrument Fact Sheet, IFS-75002, Model RCM-4 and RCM-5 Aanderaa Recording Current Meter."

5.3.1.3.3 Release Mechanisms

Of prime importance to the success of the subsurface current measurement program is the operation of the acoustic release mechanisms. The maintenance procedures currently in use at the Nova Current Meter Facility rely heavily on those developed at WHOI. The release mechanism is divided into two main sections: the command receiver and the transponder section.

After a release is received, the first step is to connect the two receiver batteries and to power up the release for 24 to 36 h. After that period, the battery voltages are read and recorded, as well as the standby current drains. The command receiver is then checked for the proper response to test signals using an AMF Model 210 Release Mechanism Test Set. If necessary, the circuits are adjusted for the proper timing values at this time. The same tests are repeated for all three receiver commands. Each release is capable of responding to three commands: Release, Timed Pinger/Transponder Enable, and Transponder Disable.

The transponder section, upon receipt of an interrogation pulse, transmits a return pulse with a known turn-around time. The timing and pulse relationship of this circuit are checked and adjusted, if necessary.

The timed pinger, transponder enable/disable circuit, and firing circuit are checked for proper operation.

All the above tests are repeated at a temperature of $5^{o}C$, to determine proper operation under low temperatures. Prior to sealing the electronics chassis in its pressure housing, the transducer is connected and a signal from the test set is acoustically coupled to the release mechanism to give a final end-to-end check of all functions. After assembly into its housing, the release mechanism is purged with freon to ensure a dry operating environment for the electronics. All new release mechanisms are fired at least once prior to deployment on a mooring.

When the release is returned from the field, the first step is to thoroughly clean and re-arm the squib firing assembly. After that has been done, the electronic tests are performed as above.

5.3.1.4 Field Operations

Presented in this section is a summary of the schedule of the short- and long-term current meter mooring deployment and retrieval cruises, as well as the methodology followed for these marine operations.

5.3.1.4.1 Schedule of Mooring Deployment/Retrieval

The two short-term moorings (#83 and 84) were deployed on September 1, 1977, using the R/V ADVANCE II, operated by the Cape Fear Institute. They were retrieved on November 2, 1977, by the R/V ISELIN, operated by the University of Miami. On the same cruise, the long-term mooring, #85 was deployed on November 4, 1977. All subsequent long-term mooring rotation cruises were accomplished using the R/V ISELIN: mooring #85 was retrieved on January 22, 1978 and replaced by a similar mooring #89. The latter was in turn rotated on April 13 and replaced by mooring #91, itself retrieved on August 1 and substituted by mooring #92. The latter was finally retrieved on November 15, 1978. Table 5-2 shows, for each mooring, the record duration, deployment location (latitude-longitude, Loran-C and Loran-A coordinates), water and current meter depths, type of current meter deployed, their serial number and notation used in the upcoming sections.

5.3.1.4.2 Procedures for Mooring Deployment

As indicated previously, the complete current meter checkout was accomplished at the Nova University laboratories. There, the instruments were turned on and sealed prior to being transported to the port from which the mooring cruise was scheduled to depart. No failures attributable to shipping the operating meters have been reported and this procedure has become standard. All functions of the acoustic release mechanisms, with the exception of firing the explosive squib were checked on board ship prior to deployment.

The components of the mooring system were labeled prior to being placed on board the ship as to their individual place along a mooring string. They were completely assembled on deck and terminations were checked prior to deployment. Upon reaching the vicinity of the mooring site, using in most cases Loran-C for navigation, a bathymetric search was conducted in order to find the correct depth for deployment. This operation was necessary as the wire had already been cut and terminated on shore. Once the proper depth located and a match of Loran-C coordinates found, the ship would position itself in such a manner as to steam across the mooring and against the sea.

The details of setting the mooring depend upon the moving configuration, prevailing weather and the deck equipment of the ship used for the current meter operation.

Table 5-2. Short- and long-term mooring information.

Mooring #	Record duration From	Record duration To	Location Lat./Long	Location Loran C	Location Loran A	Water Depth, (m)	Instr. Depth, (m)	Instr. Type	Instr. Serial #	Meter Notation
083	1732 hrs 1 Sept.'77	0720 hrs 2 Nov.'77	30°55.24'N 80°16.84'N	56078.25 71142.65	N/A	37	17	VACM	V-0450	83T
							34	VACM	V-0447	83B
084	2009 hrs 1 Sept.'77	0912 hrs 2 Nov.'77	30°51.5'N 80°06.2'W	56072.30 71205.75	N/A	45	17	VACM	V-0456	84T
							18	Aanderaa	g43	84T
							42	VACM	V-0449	84B
085	0912 hrs 4 Nov.'77	2110 hrs 22 Jan.'78	32°34'N 78°39'W	15198.2 71746.5	4805 3638	45	10	VACM	V-0448	8501
							22	VACM	V-0458	8502
							42	VACM	V-0457	8503
089	2215 hrs 22 Jan.'78	1345 hrs 13 Apr.'78	32°34'N 78°39'N	15194.3 71745.4	4800.5 3633.4	47	12	VACM	V-0450	8901
							24	VACM	V-0454	8902
							44	VACM	V-0449	8903
091	1639 hrs 13 Apr.'78	1 Aug.'78	32°34.0'N 78°38.5'W	15199.6 71747.3	4804 3635	46	11	VACM	V-0456	9101
							23	VACM	V-0447	9102
							43	VACM	V-0457	9103
092	1932 hrs 1 Aug.'78	1321 hrs 15 Nov.'78	32°34.0'N 78°38.4'W	15200.3 71748.2	N/A	46	11	VACM	V-0450	9201
							23	VACM	V-0454	9202
							43	VACM	V-0449	9203

When using the R/V ADVANCE II for deployment of the short-term mooring, the launch operation was conducted from the port side of the ship's fantail, alongside a surface float marking the mooring site, and using the slight wind drift to stream the upper mooring elements off the windward side of the vessel.

The first step in the deployment was to lift the anchor (composed of two railroad wheels) over the rail by means of the boom, where it was secured against the side of the ship until ready for release. The upper portion of the mooring was then lifted from the bottom of the beacon float and the two upper floats and VACM dropped into the water.

The remainder of the flotation and instrumentation (entire assembly of bottom floats, current meter, and release mechanisms) were then lifted from a point at the top of the lower 71 cm spherical float until they cleared the rail. The release mechanisms, once lifted clear of the rail, were shackled to the still-hanging anchor. The top of the float, once lowered to the rail, was shackled to the chain leading to the upper portion of the mooring. With the upper portion of the mooring streamed astern, the lower section was released from the top of the lower float. The anchor lashings were cleared and the entire assembly quickly lowered into the water.

This free fall procedure is considered the safest mode of deployment for it involves a minimum handling time of anchors. If a problem develops on the upper mooring assembly then it can be brought aboard with ease. This also reduces the time of maximum mooring load so that the duration of peak transient loads due to wave and ship motions are reduced. Anchor-last deployment streams the mooring away from the ship which lessens the danger of mooring fouling with the ship. It also provides greater ship maneuverability which helps in station keeping and allows final adjustments in the mooring location to be made if necessary. Nova University, University of Miami and NCSU principal investigators have found through experience that the mooring is not damaged on impact after a free fall. The buoyancy of the components and subsurface flotation is sufficient to hold the mooring upright during free fall. In deployments conducted by Nova, scientific considerations dictated that a precision pressure gauge be mounted directly on the anchor, with the release mechanisms 1 m or less above. In all instances, there was no indication that the release mechanism impacted on the pressure gauge, the anchor or the bottom. The impact of the mooring on contact with the bottom is actually the same on an anchor last or anchor first deployment due to the fact that terminal velocity is reached within about 10 m after release.

The ship was left drifting, and the transponder interrogated until the range was approximately 500 m. The command to disable (turn off) the transponder function was then sent. Proper receipt of this

command is indicated when the transponder no longer responds to an interrogate pulse. The transponders were always left in the off state, so that the battery supply would not be depleted by the transponder replying to noise pulses.

Deployment of the first and second long-term moorings was accomplished from the starboard quarter of the R/V ISELIN. The anchor (composed of two railroad wheels) was first lowered over the side, under the starboard gallows frame of the vessel. Mooring components were then added in a bottom-to-top sequence (release mechanisms, bottom current meter, bottom float) and were tied off at the top of the bottom float. The anchor and release mechanisms served as a damper that prevented the instruments from moving too violently. The top float and current meter were then placed in the water over the starboard quarter by means of an articulated hydraulic crane located aft of the gallows frame. The ship was dead in the water with the wind on the starboard side so she would drift away from the mooring. The middle float and current meter were then picked up, lowered over the side of the ship, and the mooring wire coming from the upper current meter was attached to the middle float. The wire from the bottom of the middle current meter was then attached to the top of the bottom float, which had previously been tied off. After a few minutes of drifting to ensure that the mooring was properly stretched out and no entanglement would occur, the mooring was released from a point at the top of the lower float.

Finally, the third and fourth long-term moorings were launched down the stern ramp of the R/V ISELIN. Use was made of the ship's deck crane, which is preferred over lifting the mooring to the top of the "A" frame by means of the trawl winch wire.

5.3.1.4.3 Procedures for Mooring Retrieval

Typically, in a mooring retrieval operation, the ship was brought in the immediate vicinity of the mooring using Loran C navigation. The acoustic ranging system was then immersed, to determine range to the mooring. Once the distance between the mooring and the ship was 1 km or less, release mechanisms were actuated. The entire scientific party was on deck to act as spotters. After breaking the surface, the mooring was located either by sight or with a Radio Direction Finder depending on nearness to the ship and sea conditions. If necessary, an acoustic range measurement was made to determine if the mooring flotation should be visible from the ship's upper deck. Once located, the ship was converging on the mooring, keeping the latter on the lee side under the auxiliary control station.

The subsurface float was then grabbed with a Renfroe hook working from the starboard "A" frame in conjunction with a hydraulic winch. This hook was attached to the end of a line wound on the winch. A static length of chain, approximately 4 m long, had been attached to

the top of the "A" frame, with a stainless steel snap hook attached to the free end. Once the surface marker hooked, the ship was positioned so that the mooring was trailing behind the ship. The actual recovery operation could then begin.

The subsurface buoy was lifted up with the winch and drawn on board by the "A" frame. The load was then transferred from the winch wire to the chain and snap hook. The section on deck was dismantled and stored. The winch line was reattached below the snap hook and drawn in until the winch had taken up the load. The snap hook was removed and wire was taken up until the next instrument package was landed on the deck. This procedure was repeated until the whole mooring was on board.

A post-recovery inspection was made of each mooring, noting the condition of instruments, biofouling, corrosion, and any unusual signs of stress. Photographs were taken of the vane and rotor assemblies of each current meter upon recovery, to give a qualitative assessment of the amount of biological fouling present on the sensors.

Retrieval operations were greatly facilitated by equipping the upper float of the mooring with a radio beacon and xenon flasher. Indeed, when the current meter array has risen to the surface, it presents a very low profile, making it necessary to use locating aids if fairly far away from the ship.

The radio beacons are tracked by means of an automatic direction finder which gives the mooring recovery team an unambiguous indication of the relative bearing of the array from the recovery vessel. Manufactured by Ocean Applied Research, they operate in the VHF (150 MH_Z) band, selected in view of the excessive amount of interference experienced in operating relatively near shore with beacons which operate in citizens band (27 MHZ). They are equipped with pressure switches to turn the units off when submerged.

The xenon flasher is used in the event the array has not been located before nightfall. It is manufactured by Ocean Applied Research, Inc. and operates at a 1/2 s rate. This rate was selected after field use determined that the standard period of 2 s caused the buoy to frequently be hidden behind the waves.

5.3.1.5 Assessment of Data Return

The data recorded during the "short-term" current meter measurements are of excellent quality; however, the upper VACM on mooring #84 completely failed, as a result of an electrical malfunction. Fortunately this failure did not result in a loss of data from that location for an Aanderaa current meter was positioned only one meter below and worked perfectly. An assessment of the data quality and the percentage of data return for each instrument broken down by parameter is given in Table 5-3.

Table 5-3 . Data return assessment - short term current meters.

Mooring #	Current Meter	Instrument Type	Parameter	# Data Points	Sample Interval (min)	% Data Return	Quality Assessment
83	T	VACM	Speed	3054	15	52	Excellent
			Dir.	3054	15	52	Excellent
			Temp.	3054	15	52	Excellent
			Pressure	3054	15	52	Excellent
83	B	VACM	Speed	1249	15	21	Excellent
			Dir.	1249	15	21	Excellent
			Temp.	1249	15	21	Excellent
84	T	VACM	Speed	0	15	0	No Data
			Dir.	0	15	0	No Data
			Temp.	0	15	0	No Data
			Pressure	0	15	0	No Data
84	T	Aanderaa	Speed	4436	20	100	Excellent
			Dir.	4436	20	100	Excellent
			Temp.	4436	20	100	Excellent
			Pressure	4436	20	0	Recorder Malfunction
84	B	VACM	Speed	5906	15	100	Excellent
			Dir.	5906	15	100	Excellent
			Temp.	5906	15	100	Excellent

The total data return from all parameters is only 48% due to the failure of the upper VACM on mooring #84. This figure, however, is misleading, as if this instrument is discarded as not having resulted in a data loss at that location and depth, then the total data return for the four current meter locations is 62%. Furthermore, if pressure is also neglected, then the total data return from the more important speed, direction and temperature parameters is a respectable 73%. The overall quality of the data is excellent for all parameters. The time series are extremely clean with very few errors. The total number of errors identified by spiking ranged from about 3 to 40 for each parameter time series or a total only 0.2 to 0.6% of the records.

The data return provided by the long term current meter moorings proved to be excellent. Table 5-4 shows the number of data points (or percentage) obtained for each variable and instrument. The total data return for all variables monitored was 88%. The only malfunctions occurred with the top and mid meter of the first long term mooring (#8501 and #8502), and the mid meter of the third mooring (#9102). VACM's 8501 and 8502 both experienced a failure in the counter-shift registers that count and store the East and North counts. The top meter failed at 1715 hrs., 7 December, 1977 and the mid meter experienced a malfunction on 20 October, 1977, i.e., prior to being deployed. Results of this failure is that full vector velocity information (speed and direction obtained from averaged East and North counts) is available only through the time of register failure. After that time, only rotor count and compass and vane readings are available. The record then obtained is similar to that from an Aanderaa current meter with the rotor count being summed over the averaging period, and a single direction sample being taken at the end of that period. More noise is expected in this type of data when obtained from a VACM (compared to an Aanderaa) due to the small size (9 cm x 17 cm) of the VACM direction vane.

The vibrating wire pressure sensor installed on 8501 to monitor vertical mooring motions failed to operate. The unit stopped vibrating when the unit was deployed, and started operating again immediately upon recovery. The vibrating wire ('Vibrotron') sensors used have traditionally had problems in maintaining oscillation under conditions of varying temperature and pressure.

The mid current meter of the third long term mooring failed to give any velocity information (speed or direction) although a temperature record was obtained. It is likely that the cause of this failure is in the Program Control circuit board, the location of past malfunctions.

It should be pointed out that the u and v components of current meter 8502 could be derived from the scalar speed and compass/vane follower

Table 5-4. Data return from long-term current meter moorings.

Mooring	Meter	Form	Start time GMT	End time GMT	Δt (hrs)	Temp	UCMP	VCMP	VSPD	UVDIR	SSPD	CVDIR	PRESS	% Data Return
085	8501	Raw	0930 hrs. 4 Nov.'77	1730 hrs. 22 Jan.'78	.25	7619	3197**	3197**	3197**	3197**	7619	7619	0	58%
	8502	Raw	0930 hrs. 4 Nov.'77	1730 hrs. 22 Jan.'78	.25	7628*	0**	0**	0**	0**	7628**	7628**	---	43%
	8503	Raw	0930 hrs. 4 Nov.'77	1730 hrs. 22 Jan.'78	.25	7628**	7628**	7628**	7628**	7628**	7628**	7628**	---	100%
	8501 8503	3 HRLP	1730 hrs. 4 Nov.'77	0930 hrs. 22 Jan.'78	1.0	1889	1889	1889	----	----	----	----	---	---
	8501-8503	40 HRLP	1730 hrs. 8 Nov.'77	0930 hrs. 18 Jan.'78	6.0	283	283	283	----	----	----	----	---	---
089	8901	Raw	2215 hrs. 22 Jan.'78	1345 hrs. 13 Apr.'78	.25	7743	7743	7743	7743	7743	7743	7743	7743	100%
	8902	Raw	2215 hrs. 22 Jan.'78	1345 hrs. 13 Apr.'78	.25	7743	7743	7743	7743	7743	7743	7743	---	100%
	8903	Raw	2215 hrs. 22 Jan.'78	1345 hrs. 13 Apr.'78	.00625	30958***	30968***	30968***	30968***	30968***	30968***	30968***	---	100%
	8901-8903	3 HRLP	0615 hrs. 23 Jan.'78	0515 hrs. 13 Apr.'78	1.0	1920	1920	1920	1920	1920	1920	1920	---	---
	8901-8903	40 HRLP	0615 hrs. 27 Jan.'78	0015 hrs. 9 Apr.'78	6.0	288	288	288	288	288	288	288	---	---
091	9101	Raw			.25	100%	100%	100%	100%	100%	100%	100%	100%	100%
	9102	Raw	1639 hrs. 13 Apr.'78	1 Aug.'78	.00625	100%	0%	0%	0%	0%	0%	100%	---	29%
	9103	Raw			.25	100%	100%	100%	100%	100%	100%	100%	---	100%
092	9201	Raw			.25	100%	100%	100%	100%	100%	100%	100%	100%	100%
	9202	Raw	1932 hrs. 1 Aug.'78	1321 hrs. 15 Nov.'78	.25	100%	100%	100%	100%	100%	100%	100%	---	100%
	9203	Raw			.00625	100%	100%	100%	100%	100%	100%	100%	---	100%

*These data files were chopped to 7619 points to match meter 8501.
plotting of these parameters

**The FIESTA files for the analyses and plotting of these parameters (see Volume III, Section 2.2) were expanded to 7619 points using derived points from SSPD and CVDIR.
(Note: Expanded VSPD & UVDIR were not plotted since they are the same as SSPD and CVDIR).

***This raw data had Δt = .00625. Data was averaged to Δt = .25 hrs. and all filtered data used this averaged data.

Temp = Temperature in ^{o}C
UCMP = current speed in cm/s on the east-west axis; a positive value is east, a negative value is west.
VCMP = current speed in cm/s on the north-south axis; a positive value is north, a negative values is south.
VSPD = current speed in cm/s derived from vector addition of the u and v speed components, i.e., $(u^2 + v^2)^{\frac{1}{2}}$.
UVDIR = direction in degree from magnetic north derived from the u and v speeds ($o = \tan^{-1} u/v$).
SSPD = scalon speed, or current speed in cm/s derived from the ratio count only, without reference to direction.
DVDIR = direction in degrees from magnetic north derived from the single reading

readings, despite the electronic failures this meter experienced. Therefore, if one excludes these malfunctions, as not having actually contributed to a loss of data, the data return is an impressive 92%.

Here again, the time series were extremely clean, with very few errors.

5.3.2 Hydrographic Measurements

From February 1977 through November 1978, eight seasonal hydrographic cruises were conducted in the South Atlantic OCS region. Measurements performed in 1977 were part of the BLM-Texas Instruments Benchmark Program, combining chemical and biological sampling with physical observations. Following cancellation of this program, and starting early March 1978, hydrographic data collection was accomplished by Skidaway Institute of Oceanography, under the direction of SAI. The sampling plan designed by Texas Instruments (TI) was substantially revised, in order to improve vertical and horizontal resolution of the density field and of nutrients, dissolved oxygen and chlorophyll-a concentrations. Procedures followed by TI for the data collection and reduction were summarized in the Benchmark Contractor's report and will not be repeated here. Presented in this section is a description of the types of measurements made, the sampling plan implemented by SAI/Skidway and the rationale behind its development, the instrumentation used and actual field operations. Finally, quality of the data return is assessed.

5.3.2.1 Sampling Plan

5.3.2.1.1 Variables Sampled

A conductivity-temperature-depth (CTD) cast was made at each sampling station. Each CTD lowering included calibration samples taken near the surface and near bottom. Expendable temperature probes (XBT) and salinity samples were shot if water depths exceeded the equipment limitations or if required due to CTD failure or poor weather conditions. A rosette Multi-Bottle array of Niskin bottles, attached to the CTD was used to obtain water samples, usually collected during the upcast, at depths selected based on the characteristics of the water column observed during the downcast. These samples were analyzed for nutrients (nitrate, reactive inorganic phosphate, and reactive silicate), dissolved oxygen, salinity, and chlorophyll-a. Thermosalinograph measurements were made continuously while working in the sampling area and steaming between stations. These latter data provided continuous temperature and salinity information of the near surface water.

Additional routine activities included monitoring of ship position using LORAN-C, depth measurement by precision depth recorder (PDR) accurate to at least 1000 m, and hourly meteorological and sea state/swell observations, throughout the duration of the cruise.

5.3.2.1.2 Location and Spacing of Hydrographic Stations

Hydrographic measurements were usually conducted along six onshore/offshore sections approximately 100 km (55 NM) apart between New Smyrna Beach, Florida and Cape Fear, North Carolina. The approximate location of these transects, labeled A to F, is presented in Figure 5-8. Along these sections, stations 20 km (10.9 NM) apart were occupied, starting at approximately the 10 m (5.5 fms) isobath. However, in order to better define shelf water/Gulf Stream interaction, the spacing was decreased to 10 km (5.4 miles) for three stations beginning near the 50 m (27 fms) isobath and going offshore. Station spacing then reverted to 20 km (10.8 miles) until the Gulf Stream core was reached (20^{o}C isotherm at 100 m depth) or up to a water depth of 400 m (217 fms), whichever come first. The one exception to this criterion was on Section E, where the outer limit was defined by the western edge of the Gulf Stream, identified from thermosalinograph measurements, and/or from remote sensing imagery. It was felt that measurements of hydrographic properties out to the western edge of the Gulf Stream near the "Charleston Bump", where the stream is known to frequently develop a large meander to the east, were required to aid in the interpretation of the current meter data from the BLM long-term mooring off Charleston and the understanding of the dynamics of the region (including part of the Blake Plateau).

The spacing between transects has been selected on the basis of three somewhat conflicting criteria. First, the DOE study is focused on the monitoring of Gulf Stream intrusions and shelf break upwellings, rather than on systematic hydrographic measurements along transects in the region south of Savannah. As a result, SAI and its P.I.'s had to conceive a sampling plan which would cover the entire area of Cape Fear to Cape Canaveral. Next, the cruise track had to be designed to provide maximum resolution for modeling techniques. Yet, ship time had to be maintained within reasonable limits, not only because of budgetary constraints and potential problems of ship and manpower availability, but also because of a need for synopticity of the measurements as well. Finally, the spacing had to be consistent with alongshelf coherence calculated from current meter records previously obtained in the region by T. Lee, or observed in previous hydrographic data by L. Atkinson. Based on the examination of the latter data it was concluded that a spacing of 100 km between transects would be adequate to describe the alongshore shelf variability, and, therefore, that six transects would be required, off the coasts of Cape Fear, Cape Romain, Savannah, Brunswick, St. Augustine, and New Smyrna Beach, respectively (transects F, E, D, C, B, and A in Figure 5-8). Sections F, E, and D approximately coincide with Benchmark sections, run the previous year by Texas Instruments. The time required to cover a total of 1050 nautical miles between Miami, FL and Charleston, SC and perform the hydrographic measurements was esti-

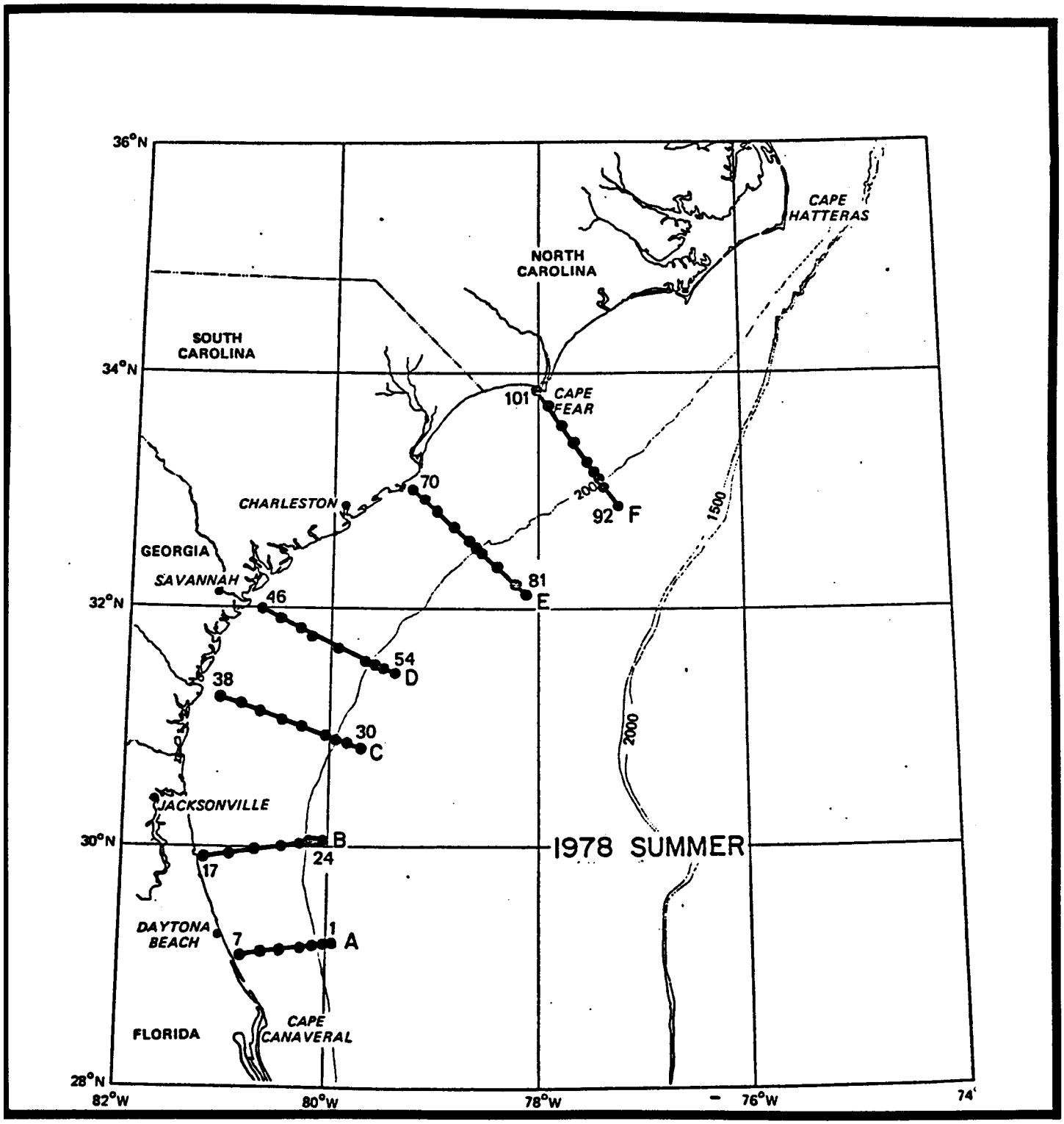

Figure 5-8. Typical transect location for SAI/Skidaway hydrographic sampling.

mated as being approximately 8 days. This number of days appeared acceptable from the viewpoints of ship and manpower availability, and synopticity of the sampling.

According to this design, approximately 50 CTD stations along the above six transects were occupied during the seasonal cruises. The number of stations varied slightly from cruise to cruise, depending upon the actual location of the Gulf Stream, as well as the conditions prevailing on the shelf during the sampling period. Departures from this general design were planned for the winter and spring 1978 cruises, in order to better complement, or accommodate the work performed under the auspices of DOE. Thus a total of 72 stations located along 8 transects were sampled early March 1978 to characterize the winter conditions, while 41 hydrocasts were performed along 5 cross-shelf sections in the spring of 1978.

Table 5-5 summarizes the samples collected during the 1978 hydrographic cruises.

5.3.2.2 Instrumentation and Quality Assurance

5.3.2.2.1 CTD Measurements and Water Column Sampling

The temperature-salinity structure was determined with a Plessey 9400 CTD and HP 9825A computing controller data acquisition system, designed for onboard real time processing and providing redundant data display and storage, thus assuring that no data loss would result from the malfunctioning of the primary data acquisition system.

An XBT system was used as backup for the CTD and also for cases when the water column is expected to be well mixed. XBT traces were digitized by a Hewlett-Packard (HP) digitizer and merged into the data set.

The CTD system utilized for the SAI/Skidaway cruises was composed of four major components:

- the underwater unit, consisting of the depth, conductivity, and temperature sensors and a mixer that powers the sensors and multiplexes the signals. Multiplexing involves the simultaneous transmission of two or more signals (in this case conductivity, temperature and depth frequencies) over the same wire.

The sensors output AC signals of frequencies proportional to the parameter being sensed. The specifications are as follows:

Temperature	2127-4193 hz	-2 to 35°C
Conductivity	4995-7901 hz	0 to 60 mmhos.cm^{-1}
Depth	9712-11288 hz	0 to 600 m

1978 Cruise	Vessel Used	# transects	# stations	CTD casts	XBT casts	Dissolved oxygen samples	Nutrient samples	Chlorophyll-a samples (pairs)	Salinity calibration samples
Winter	R/V PIERCE	8	72	42	33	159	159	159	91
Spring	R/V ISELIN	5	41	41	--	123	123	113	36
Summer	R/V ISELIN	6	52	52	--	161	161	153	88
Fall	R/V ISELIN	6	50	50	4	157	157	138	85

Table 5-5. Samples collected during the 1978 hydrographic cruises.

The three AC signals are multiplexed through the conductor wire to the deck unit. Thus only one conductor is required by the CTD for input power and an output multiplexed signal. To guard against reverse voltage being applied to the CTD sensors, a reverse biased diode was installed on the power input line to the mixer. The Skidaway system is dismantled and reassembled so many times that such protection is good insurance.

The pressure vessels housing the sensors protect the sensors to 600 m. Flooding of the vessels, even at shallow depths, which had been a problem in the past, did not occur during the sampling. Wet pins in the connectors were routinely investigated and dried out when necessary. Care was exercised when handling the O-rings and connectors. Silicon grease was used to seal the connections, but sparingly to avoid insulating the electrical connecting parts.

Spare C, T, and D sensors, connectors, Scotchcast electrical splicing kits, and wire harnesses were available on board the research vessel, so that any malfunctioning part could be replaced. Thus sampling could go on while repairs are made.

- the winch, conductor wire, and Rosette Multi-Bottle Array fitted with a variety of Niskin sampling bottles.

Most oceanographic ships, including the R/V ISELIN were equipped with conductor winches. However, the wire and/or slip rings can often be in disrepair. For this reason, a portable winch was always brought on board as a backup.

The winch provided by Skidaway (Plessey Model 7400) has 250 m of 4 conductor wire. It is run on 110 AC and at a constant speed of 15 $m.min^{-1}$. It can handle a maximum load of 200 pounds (91 kg), which is a minimum acceptable capability.

The Rosette Multi-Bottle Array, manufactured by General Oceanics as are the Niskin bottles mounted on it, was used for sample collection. The rosette was installed on a frame within which the CTD sensor system was mounted. Reference to the "fish" includes the CTD sensors and rosette as one unit. The sensors were beneath the rosette so that they would not be in the wake of the rosette as it is lowered through the water column. Conversely, during the upcast they were in the wake of the rosette, which can result in data regradation. The Niskin bottles were triggered serially on command from the deck unit.

Use of a multi-conductor oceanographic cable allowed separate rosette and CTD operation. A branching sea cable connected the different slip rings wires to the rosette deck unit and The Digital Data Logger (DDL).

The rosette needs continual maintenance if it is to perform reliably. After every cast, the cam/trip mechanism was washed with fresh water and sprayed with a penetrating lubricant such as CRC.

A Helle pinger was mounted on the frame of the fish to aid in recovery if the fish were to be severed from the conductor wire. A marker buoy, chain, and anchor were also kept handy.

- the Plessey Model 8400 Digital Data Logger (DDL) which provides power to the CTD fish, receives and demultiplexes the CTD signal and determines the frequencies for depth, conductivity and temperature for output to recording devices.

The system was substantially modified to make control of the system more convenient. For instance, a push-button switch to turn the power to the fish on and off, and a voltmeter and ammeter were installed in the front panel of the DDL to readily indicate the power status of the CTD and rosette. Likewise, the 741 operational amplifier was replaced by a high grade ultra linear operational amplifier in the DDL.

Spare parts included depth, conductivity and temperature counting and digitizing boards, which are essentially interchangeable.

The digital signal output from the DDL could be recorded on a Kennedy Model 1600 incremental magnetic tape recorder, in case the primary data acquisition system became inoperative.

The digital-to-analog converter in the DDL outputs an analog voltage proportional to the input range which drives an HP-XYY' Recorder (Model 7046A). The DDL folds the signals proportional to 0 to 10 volts full scale.

- the data processing system that records and processes the data in a variety of ways.

The primary data acquisition system used during the data collection was an HP 9825A Calculator and peripherals. This permits data acquisition to become more real time and less costly than after the fact magnetic tape processing. The HP recording devices are the tape cartridge and printer in the 9825A Calculator, the 9862A Plotter and the 9885M Flexible Disk.

5.3.2.2.2 Thermosalinograph Measurements

Near surface temperature and salinity were continuously recorded with a Bissett-Berman T-6000 thermosalinograph along the ship tracks of the hydrographic cruises. This data was used in conjunction with the hydrographic station and XBT data to produce maps of the surface

temperature and salinity distributions. The measurement technique involved continuous pumping of sea water from a depth of 3 m through a port in the hull of the research vessel. The water was flowing through a de-bubble chamber at a rate of approximately 20 $l.min^{-1}$ and then through a sensor chamber containing an inductive type conductivity toroid sensor and a thermistor. The electrical signals generated were converted to salinity and temperature and then continuously recorded on a 2-pen strip chart recorder. The recorder had a variable chart speed capable of 2.5 $cm.h^{-1}$, 15.25 $cm.h^{-1}$ and 30.5 $cm.h^{-1}$ speeds. Temperature and salinity had variable ranges capable of sensing a total range of salinity from 20 to 38 °/oo with an accuracy of ±0.15 °/oo and temperature from -2 to 36 °C with an accuracy of ± 0.1 °C.

5.3.2.3 Field Operations

5.3.2.3.1 Cruise Schedule

Hydrographic measurements were accomplished in 1977 by Texas Instruments, and the data delivered to SAI for analysis by T. Curtin (NCSU). Four seasonal sampling and a time series experiment (in the summer time) were conducted from January 31, to February 8, 1977; May 3 to 8, 1977; August 9 to 14, 1977 and the time series from September 8 to 20, 1977. No usable hydrographic data were obtained in the fall 1977.

The SAI/Skidaway cruises, fully merged with a complementary DOE effort were conducted from March 6 to 12, 1978, using the R/V PIERCE from Tracor Marine; from April 14 to 23, 1978 on board the R/V ISELIN, operated by the University of Miami; from July 25 to 31, 1978 and November 8 to 13, 1978, the latter cruises also performed with the R/V ISELIN.

5.3.2.3.2 Sampling Procedure

Prior to arriving on station, the CTD system, bottles, and thermometers were checked, the rosette cocked, and the station sheets initially filled in. On station, the on-deck depth and conductivity frequencies were logged for zero determination. The Plessey CTD and General Oceanics rosette supporting 1.7 liter Niskin bottles were than launched into the water and lowered to 1 to 3 m, depending on the sea state. The surface frequencies were logged, bottom depth was checked, and the cast started. All operations were timed and prompted by the HP9825. The normal heading was with the wind on the port quarter to keep the wire away from the ship. Since the stations only involved CTD casts, no special precautions were taken to avoid contamination other than sanitary sewerage.

During the downcast, conductivity and temperature were plotted versus depth on an analog HP-XYY', while temperature was displayed versus depth on an HP plotter. All data were logged on an HP data cassette.

The rosette/CTD was held at the bottom depth for four mintues while the reversing thermometers equilibrated. This was timed by the HP system, which also displayed the quality of the bottom data relative to the equilibration data. During this time, the sample depths for the upcast were selected. The upcast was identical to the downcast, except that the rosette was tripped at a selected depth.

The sample depths were selected on the basis of the following criteria:

- Depths less than 50 m
  Mixed - top and bottom
  Two layer - top, bottom of thermocline, bottom

- Depths greater than 50 m, less than 100 m
  0, 25, 50, 75, bottom

- Depths greater than 100 m
  0, 50, 100, 150, 200, 300, 400, etc.

Often, because of special situations, other depths were added or deleted to more sensibly sample the water column. It must be stressed that the South Atlantic Bight shelf waters represent some of the most variable and stratified conditions in the ocean. The variability combined with the dominant effects of the Gulf Stream make adherence to a specific sampling criterion difficult and often scientifically meaningless.

Once a cast was completed, the dissolved oxygen sample was drawn first, using normal precautions. The reagents were added, the ground glass stopper replaced, and the sample stored in a dark case. Nutrient samples were drawn into a 125 ml poly bottle after two rinses. They were then stored in a freezer until analysis in the laboratory. Likewise, salinity samples were drawn into a 125 ml glass bottle after two rinses, the caps were secured and the samples stored until analysis. Samples for Chlorophyll analysis were drawn immediately and analyzed in the Turner Designs fluorimeter. Occasionally samples were taken for in vitro analysis. Finally, the reversing thermometers were read after equilibration to ambient temperature.

On-board analysis of dissolved oxygen was performed strictly according to the method described by Strickland and Parsons. Samples were accumulated until a sufficient number were on hand to justify analysis. During this time, they were stored in the dark with the glass stoppers secured. Samples were also analyzed for chlorophyll content immediately after sampling by the in vivo analysis.

Surface temperature and salinities were also recorded along the cruise track, using a Bissett-Berman T-6000 thermosalinograph. These data, together with hydrographic station data, were analyzed to

construct surface maps of the temperature and salinity distributions. As indicated before, the instrument had been calibrated and installed by University of Miami personnel.

5.3.2.4 Assessment of Data Return

Collection of hydrographic data by SAI/Skidaway proved to be a total success. All instruments functioned perfectly, yielding data of excellent quality. All stations were occupied and sampled according to plan, with the exception of two deepest stations in the fall cruise. Likewise, very few CTD casts had to be substituted by XBT profiles because of weather conditions or malfunctions of the CTD system. Excellence of the data is evident in Section 5.4.2.6. dealing with calibration procedures and error analysis, as well as from the examination of the Temperature-Salinity (TS) and nitrate-phosphate plots used as an additional data validation procedure. The same statement cannot be made for the hydrographic sampling performed in 1977 by Texas Instruments. Malfunctions of the sensors resulted in a total loss of the fall 1977 data. Furthermore, some of their data (particularly dissolved oxygen) appeared to be of suspicious quality, when analysed by the Principal Investigator, T. Curtin (NCSU). All temperature and salinity data forwarded by Texas Instruments have been incorporated in the plots presented in Section 5.6.2.

5.3.3 Collection of Remote Sensing Imagery for Gulf Stream Western Edge Monitoring

As indicated in Section 5.2.3, the first objective of the remote sensing program undertaken by Dr. O. Brown was to assess the potential confidence levels and spatial resolution of infrared satellite mapping techniques for the determination of the variability of the western edge of the Gulf Stream on time scales ranging from daily to seasonal. To that effect, satellite imagery and data were obtained from NOAA/NESS for 10 days in April 1977 and a similar period in November 1977, i.e. 40 tapes and 40 images. Ground truth was provided by the ship track information for the April 1977 cruise in the Georgia embayment, conducted by Dr. T. Lee.

In order to assess the representativeness of the hydrographic cruise data in characterizing seasonal variability of the shelf and shelf edge waters, and generate maps of seasonal means and extrema for the Gulf Stream front, NAVOCEANO weekly charts from 29 December 1976 to present (i.e. more than 100 chart pairs) were collected. The data base was supplemented with U.S. Coast Guard quarterly ART flight maps, from Spring 1977 to present ($\sim$ 10 charts).

5.3.4 Surface Wind Data Collection

In order to assess the response of the shelf waters to meteorological forcing, it is essential that a temporal and spatial description of the surface wind field be obtained for the area of the moorings. This three-dimensional surface wind determination was achieved by analyzing wind reports collected operationally by the meteorological services. Observations reported within the area bounded by latitudes 25°N and 35°N, longitude 72°W and the U.S. Southeast coast were plotted on maps over a fifteen month period from September 1977 to November 1978 at time intervals of six hours for the first three months of this period and twenty four hours thereafter. When the time increment was six hours, maps were prepared for 0000, 0600, 1200 and 1800 GMT while daily maps were drawn for 1200 GMT. It should be noted that the area defined above extends much farther east than the Georgia Embayment. This area was chosen to facilitate the wind analysis in the region of interest.

The surface wind observations used in the description of the surface wind field consisted of reports from coastal and island stations, buoys, lighthouses and ships which are operationally received at the National Hurricane Center (NHC), Coral Gables, Florida. These reports are obtained directly from teletype messages or extracted from surface weather maps prepared by NHC. The reports were plotted on the aforementioned maps in accordance with a standard convention used in meteorology. In addition, some annotation concerning the wind direction and/or speed was written down beside most plotted reports. Once plotted on maps, the wind reports were analyzed by following straightforward streamline-isotach method. This wind analysis technique is independent of the dynamic balance of the atmospheric flow; the method just describes the instantaneous wind direction and speed over an area based solely on wind reports. Free-hand streamlines and isotachs were drawn to denote wind direction and speed, respectively. Streamlines were represented by arrowed, solid lines on the maps while isotachs at five-knot intervals were shown by dashed lines. Map-to-map space and time continuity for surface wind features were taken into account as streamlines and isotachs were drawn.

This data collection and analysis procedure resulted in the production of 729 maps for the period of September 1977 to November 1978, based on more than 18,000 surface wind reports.

In addition, monthly summary sheets of surface wind speed, wind direction, atmospheric pressure, temperature, etc. were obtained by NCSU from the National Climatic Center, NOAA, Asheville, N.C. for the coastal Charleston station located at 32°46'N, 79°56'W. An example of these sheets for the month of November 1977 is shown in Table 5-6. Magnetic tapes of the three-hourly data were also requested for the period October, 1977 to date but no magnetic tape data for the period

NATIONAL WEATHER SERVICE OFC
MUNICIPAL AIRPORT

MONTHLY SUMMARY

LATITUDE 32° 54 'N LONGITUDE, 80° 02 'W ELEVATION (GROUND) 40 FT. STANDARD TIME USED: EASTERN WBAN #13880

DATE	TEMPERATURE °F MAXIMUM	MINIMUM	AVERAGE	DEPARTURE FROM NORMAL	AVERAGE DEW POINT	DEGREE DAYS BASE 65° HEATING (SEASON BEGINS WITH JULY)	COOLING (SEASON BEGINS WITH JAN.)	WEATHER TYPES OR CODES OF OCCURRENCE	SNOW, ICE PELLETS OR ICE ON GROUND AT 07AM IN.	PRECIPITATION WATER EQUIVALENT IN	SNOW, ICE PELLETS IN.	AVG. STATION PRESS SURF IN. ELEV. 40 FEET M.S.L.	WIND RESULTANT DIR.	RESULTANT SPEED M.P.H.	AVERAGE SPEED M.P.H.	FASTEST MILE SPEED M.P.H.	FASTEST MILE DIRECTION	SUNSHINE MINUTES	SUNSHINE PERCENT OF POSSIBLE	SKY COVER TENTHS SUNRISE TO SUNSET	SKY COVER TENTHS MIDNIGHT TO MIDNIGHT	DATE
1	75	56	66	5	56	0	1		0	0	0	30.00	02	13.7	14.1	18	03	264	41	9	9	1
2	78	65	71	11	63	0	6		0	T	0	29.93	03	10.7	11.1	14	05	59	9	10	10	2
3	78	68	72	12	67	0	7	1	0	.03	0	29.93	05	8.2	8.3	12	05	9	1	10	10	3
4	82	67	75	15	68	0	10	1	0	T	0	29.86	08	7.4	8.9	14	12	301	47	8	8	4
5	83*	67	75*	15	69	0	10		0	.24	0	29.94	08	8.9	9.4	15	12	493	78	8	8	5
6	80	63	72	13	65	0	7	1	0	T	0	29.80	21	3.5	6.8	13	18	364	57	8	4	6
7	77	60	69	10	60	0	4		0	0	0	29.79	23	8.0	8.3	13	27	528	82	3	3	7
8	78	58	69	10	59	0	4	1 8	0	0	0	29.90	25	2.7	3.8	12	27	434	68	4	5	8
9	79	58	69	11	60	0	4	2 8	0	0	0	29.98	18	2.2	2.9	12	13	474	74	7	8	9
10	79	43	61	3	51	4	0	1	0	0	0	29.93	24	9.7	11.1	21	26	417	66	8	5	10
11	61	38	49	-9	27	16	0		0	0	0	30.12	28	7.1	7.6	15	30	616	96	1	0	11
12	60	31	46	-11	24	19	0		0	0	0	30.17	31	7.7	9.1	15	30	633	100	0	0	12
13	52	30	41*	-16	20	24	0		0	0	0	30.35	01	7.8	7.9	20	02	632	100	0	0	13
14	60	27	44	-13	28	21	0		0	0	0	30.32	14	.7	2.9	9	17	589	93	3	2	14
15	70	34	52	-4	41	13	0	1 8	0	0	0	30.21	19	2.6	3.5	10	19	563	90	5	5	15
16	75	49	62	6	56	3	0		0	0	0	30.06	18	5.6	6.3	15	17	388	62	9	9	16
17	81	61	71	15	61	0	6		0	0	0	29.91	22	8.8	9.5	18	25	461	74	5	5	17
18	68	43	56	1	39	9	0		0	0	0	30.10	30	3.1	7.1	13	02	572	92	3	4	18
19	67	40	54	-1	37	11	0		0	0	0	30.24	05	5.2	6.2	12	06	308	49	9	6	19
20	73	48	61	6	50	4	0		0	T	0	30.30	08	7.9	9.4	15	09	574	92	3	6	20
21	77	58	68	13	58	0	3		0	0	0	30.27	08	6.8	7.3	15	11	513	83	7	8	21
22	77	56	67	13	61	0	2	8	0	.36	0	30.15	08	4.9	5.9	14	11	216	35	10	9	22
23	73	63	68	14	64	0	3	1 8	0	.03	0	30.03	10	3.2	4.0	8	07	51	8	10	9	23
24	70	60	65	11	61	0	0	2	0	.08	0	29.96	07	2.6	4.6	9	03	25	4	10	10	24
25	70	56	63	9	61	2	0	1	0	.19	0	29.74	21	2.4	7.8	21	29	98	16	8	8	25
26	56	30	43	-10	27	22	0		0	0	0	29.82	28	12.8	13.4	23	28	614	100	0	0	26
27	58	27*	43	-10	33	22	0		0	0	0	30.15	15	4.6	6.2	14	14	564	92	2	2	27
28	77	43	60	7	51	5	0	8	0	0	0	30.21	22	3.9	5.9	14	21	515	84	5	4	28
29	80	52	66	14	58	0	1		0	T	0	30.27	09	6.1	7.8	16	14	465	76	9	9	29
30	72	63	68	18	65	0	3	1 8	0	.85	0	30.00	09	4.5	7.9	17	22	106	17	10	10	30
	SUM 2164	SUM 1512				TOTAL 175	TOTAL 71			TOTAL 1.76	TOTAL 0	30.05	FOR THE MONTH 051	.8	7.5	23	28	TOTAL 11846	% FOR POSSIBLE MONTH 63	SUM 182	SUM 175	
	AVG. 72.1	AVG. 52.4	AVG. 61.3	DEP. 5.0	AVG. 51	DEP. -96	DEP. 51	PRECIPITATION .01 INCH	7	-0.37						DATE	26		10966	63	AVG. 6.1	AVG. 5.8	
						SEASON TO DATE		SNOW, ICE PELLETS														
	NUMBER OF DAYS					TOTAL	TOTAL	1.0 INCH	0	GREATEST IN 24 HOURS AND DATES			GREATEST DEPTH ON GROUND OF SNOW, ICE PELLETS OR ICE AND DATE									
	MAXIMUM TEMP.		MINIMUM TEMP.			287	2583	THUNDERSTORMS	0	PRECIPITATION		SNOW, ICE PELLETS										
	≥ 90°	≤ 32°	≤ 32°	≤ 0°		DEP.	DEP.	HEAVY FOG	2	.95	30	0										
	0	2	5	0		-58	535	CLEAR 9	PARTLY CLOUDY 7	CLOUDY 14												

* EXTREME FOR THE MONTH - LAST OCCURRENCE IF MORE THAN ONE.
T TRACE AMOUNT
- ALSO ON AN EARLIER DATE, OR DATES.
HEAVY FOG - VISIBILITY 1/4 MILE OR LESS.
FIGURES FOR WIND DIRECTIONS ARE TENS OF DEGREES CLOCKWISE FROM TRUE NORTH. 00 = CALM. DATA IN COLS. 6 AND 12-15 ARE BASED ON 7 OR MORE OBSERVATIONS PER DAY AT 3-HOUR INTERVALS. FASTEST MILE WIND SPEEDS ARE FASTEST OBSERVED ONE-MINUTE VALUES WHEN DIRECTIONS ARE IN TENS OF DEGREES. THE / WITH THE DIRECTION INDICATES PEAK GUST SPEED.
ANY ERRORS DETECTED WILL BE CORRECTED AND CHANGES IN SUMMARY DATA WILL BE ANNOTATED IN THE ANNUAL SUMMARY

SUMMARY BY HOURS

HOUR (LOCAL TIME)	SKY COVER TENTHS	AVERAGES STATION PRESSURE IN.	TEMPERATURE AIR °F	TEMPERATURE WET BULB °F	TEMPERATURE DEW PT. °F	RELATIVE HUMIDITY %	WIND SPEED M.P.H.	RESULTANT WIND DIRECTION	RESULTANT WIND SPEED M.P.H.
01	5	30.05	56	53	51	84	5.4	01	2.1
04	6	30.04	54	52	50	86	5.7	35	2.5
07	7	30.07	54	52	50	88	5.8	01	2.3
10	6	30.09	64	58	52	68	9.8	04	2.4
13	6	30.04	70	60	52	55	10.8	17	2.1
16	6	30.02	69	60	52	57	10.8	19	1.9
19	6	30.04	61	57	53	78	6.4	12	1.9
22	5	30.06	58	55	52	82	5.5	06	1.3

HOURLY PRECIPITATION (WATER EQUIVALENT IN INCHES)

DAY	A. M. HOUR ENDING AT 1	2	3	4	5	6	7	8	9	10	11	12	P. M. HOUR ENDING AT 1	2	3	4	5	6	7	8	9	10	11	12	DAY
1																									1
2		T	T			T	T														T	T	T		2
3														T	.01	.02	T								3
4				T																					4
5					T	.04	.02											T	T	.02			.05	.11	5
6	T																								6
7																									7
8																									8
9																									9
10																									10
11																									11
12																									12
13																									13
14																									14
15																									15
16																									16
17																									17
18																									18
19																									19
20																							T		20
21																									21
22																					T	.22	.06	.08	22
23	.01				T	.01		T	T	.01	T	T												T	23
24	T			.01	.01					T									T	T	T	.01	.03		24
25	.03	.01	.04	.06	T	T			T	T											.05	T			25
26																									26
27																									27
28																									28
29					T																				29
30	T	T	.11	.14	.04	.03	.01	.06	.31				.10	T	T				T	T	.05				30

SUBSCRIPTION PRICE: $2.55 PER YEAR, FOREIGN MAILING $1.85 EXTRA. SINGLE COPY: 20 CENTS FOR MONTHLY ISSUE, 20 CENTS FOR ANNUAL SUMMARY. OTHER DATA IN RECORDS ON FILE CAN BE FURNISHED AT COST VIA MICROFILM, MICROFICHE, OR PAPER COPIES OF ORIGINAL RECORDS. MAKE CHECKS PAYABLE TO DEPARTMENT OF COMMERCE, NOAA. SEND PAYMENTS, ORDERS, AND INQUIRIES TO NATIONAL CLIMATIC CENTER, FEDERAL BUILDING, ASHEVILLE, NORTH CAROLINA 28801.

I CERTIFY THAT THIS IS AN OFFICIAL PUBLICATION OF THE NATIONAL OCEANIC AND ATMOSPHERIC ADMINISTRATION, AND IS COMPILED FROM RECORDS ON FILE AT THE NATIONAL CLIMATIC CENTER, ASHEVILLE, NORTH CAROLINA 28801.

noaa NATIONAL OCEANIC AND ATMOSPHERIC ADMINISTRATION / ENVIRONMENTAL DATA SERVICE

Daniel B. Mitchell
DIRECTOR, NATIONAL CLIMATIC CENTER

USCOMM--NOAA--ASHEVILLE 12/19/77 425

Table 5-6 OBSERVATIONS AT 3-HOUR INTERVALS

HOUR	Sky Cover (tenths)	Ceiling (hundreds of ft.)	Visibility: Statute miles	Visibility: Tenths of mile	Weather	Temperature: Air °F	Temperature: Wet Bulb °F	Temperature: Dew Pt. °F	Rel. Hum. %	Wind: Dir	Wind: Speed knots
DAY 01											
01	0	UNL	10			56	54	52	87	36	14
04	8	18	10			57	54	52	83	36	14
07	7	250	10			56	54	52	87	02	12
10	8	100	15			66	61	57	73	03	16
13	8	28	15			74	65	60	62	02	13
16	10	33	15			73	65	60	64	03	10
19	10	28	10			69	63	60	73	04	6
22	10	17	10			66	61	58	76	03	13
DAY 02											
01	10	10	10			65	62	60	84	03	11
04	10	8	8			65	63	62	90	02	10
07	10	8	8			65	63	62	90	03	9
10	10	10	8			68	65	63	81	05	12
13	9	15	12			74	68	65	74	02	10
16	10	20	10			73	68	65	76	36	10
19	10	28	10			71	67	64	78	02	7
22	10	5	6		L	68	66	65	90	03	8
DAY 03											
01	10	5	7			69	67	66	90	03	10
04	10	4	5		F	68	68	67	93	05	9
07	10	7	7			69	67	66	90	04	7
10	10	8	8			72	69	67	84	06	8
13	10	13	10			76	71	68	76	04	7
16	10	4	1	8	RF	72	70	69	90	06	6
19	10	6	7			71	69	68	90	05	6
22	10	1	1	8	F	70	68	68	93	05	8
DAY 04											
01	10	1	0	8	F	68	68	67	93	05	4
04	10	17	3		F	68	68	67	93	02	4
07	8	55	4		F	68	68	67	93	06	8
10	9	35	6		F	74	71	70	87	09	8
13	9	80	10			80	73	68	68	12	11
16	8	120	15			78	71	67	68	12	12
19	7	80	15			74	70	68	82	06	8
22	3	UNL	15			70	68	67	90	08	8
DAY 05											
01	4	UNL	10			68	67	66	90	05	4
04	7	33	8			68	68	67	93	06	8
07	10	35	10			68	68	67	93	05	5
10	9	130	15			78	73	70	74	08	9
13	4	UNL	15			83	73	68	61	10	11
16	7	28	15			78	72	68	68	09	10
19	10	7	5		RW	74	72	71	90	08	11
22	10	6	8			73	72	71	93	09	7
DAY 06											
01	8	15	5		F	73	72	71	93	08	4
04	6	33	9		F	70	68	68	87	25	5
07	3	UNL	7			66	65	65	87	22	4
10	10	70	10			71	68	67	87	34	2
13	3	UNL	10			78	68	62	56	22	5
16	3	UNL	15			77	68	64	64	18	11
19	1	UNL	15			68	63	62	87	21	7
22	0	UNL	15			63	62	61	93	15	4
DAY 07											
01	3	UNL	8			63	62	62	97	20	5
04	0	UNL	8			64	63	62	93	22	6
07	3	UNL	7			62	61	60	93	24	7
10	0	UNL	10			68	63	60	73	24	9
13	2	UNL	15			77	65	57	50	24	10
16	6	45	15			73	63	57	57	24	8
19	0	UNL	12			65	63	61	87	20	7
22	0	UNL	12			62	61	60	93	21	6
DAY 08											
01	0	UNL	7			61	60	59	93	00	0
04	10	70	10			58	57	56	93	00	0
07	8	55	5		F	62	61	60	93	00	0
10	0	UNL	8		M	71	65	62	73	20	4
13	4	UNL	8		M	78	68	58	52	27	10
16	3	UNL	8		M	77	65	58	52	28	7
19	7	UNL	8			66	63	61	84	18	2
22	7	UNL	7			63	61	60	90	15	2
DAY 09											
01	8	UNL	1		F	60	59	58	97	00	0
04	8	1	0	1	F	58	57	57	96	00	0
07	10	0	0	1	F	58	57	57	96	00	0
10	4	UNL	5		F	66	65	63	84	00	0
13	9	250	7			77	67	61	58	24	6
16	7	UNL	6		M	76	67	62	62	15	9
19	7	UNL	7			66	63	62	87	15	3
22	9	UNL	7			63	62	61	93	18	2
DAY 10											
01	4	UNL	5		F	61	60	60	97	20	3
04	3	UNL	5		F	60	58	58	97	22	4
07	10	50	5		F	69	64	64	87	20	5
10	10	17	8			74	69	66	76	22	13
13	9	33	15			77	67	61	58	22	15
16	2	UNL	25			87	72	58	35	26	18
19	4	UNL	20			54	44	33	43	28	10
22	0	UNL	20			48	38	27	44	28	9
DAY 11											
01	0	UNL	15			42	35	25	51	27	7
04	0	UNL	15			38	34	28	80	27	7
07	1	UNL	20			38	32	28	87	26	8
10	0	UNL	20			51	41	28	41	31	8
13	0	UNL	25			58	45	28	28	30	8
16	1	UNL	25			60	45	24	25	28	12
19	0	UNL	20			48	40	28	44	26	4
22	0	UNL	20			38	36	32	79	23	3
DAY 12											
01	0	UNL	20			40	35	28	57	25	6
04	0	UNL	20			37	32	24	56	30	7
07	0	UNL	20			32	30	28	78	30	5
10	0	UNL	20			52	41	28	37	32	7
13	0	UNL	20			58	44	25	25	29	11
16	0	UNL	20			58	43	21	23	31	11
19	0	UNL	20			44	37	27	51	34	6
22	0	UNL	20			44	34	18	32	01	10
DAY 13											
01	0	UNL	20			37	30	18	46	01	5
04	0	UNL	20			34	28	20	57	02	5
07	0	UNL	20			34	28	20	57	01	6
10	0	UNL	20			44	34	17	34	02	14
13	0	UNL	20			48	37	18	29	02	13
16	0	UNL	20			50	38	17	27	36	10
19	0	UNL	20			35	31	24	84	00	0
22	0	UNL	20			34	31	28	73	00	0
DAY 14											
01	0	UNL	20			31	28	25	78	00	0
04	0	UNL	20			28	27	24	85	32	3
07	0	UNL	20			32	30	28	78	00	0
10	0	UNL	20			48	38	28	38	08	6
13	0	UNL	20			57	43	22	26	21	6
16	0	UNL	20			58	46	32	37	14	5
19	0	UNL	20			49	42	38	77	00	0
22	0	UNL	15			41	38	38	82	00	0
DAY 15											
01	0	UNL	15			37	36	34	89	00	0
04	0	UNL	15			36	35	33	89	00	0
07	1	UNL	5		F	35	34	32	88	00	0
10	0	UNL	3		RW	58	53	47	65	04	3
13	9	UNL	10			67	54	42	40	20	7
16	10	UNL	10			67	56	46	47	18	8
19	10	UNL	10			53	50	47	80	18	5
22	10	250	10			54	51	48	83	00	0
DAY 16											
01	10	250	10			50	48	47	89	00	0
04	10	250	10			51	50	48	93	00	0
07	10	250	10			52	51	50	93	12	4
10	9	UNL	10			71	64	58	68	22	8
13	9	120	10			71	64	60	68	18	9
16	10	250	10			71	64	60	68	17	11
19	10	250	10			65	62	60	84	17	7
22	10	34	7			64	62	60	87	21	5
DAY 17											
01	10	85	7			63	61	60	90	18	6
04	10	35	7			62	60	59	90	20	7
07	10	18	7			65	62	60	84	23	8
10	9	UNL	12			71	65	61	71	23	12
13	4	UNL	15			80	68	62	54	21	7
16	4	UNL	15			77	67	61	58	25	12
19	0	UNL	10			64	62	60	87	20	6
22	7	UNL	10			66	63	61	84	24	7
DAY 18											
01	7	UNL	15			63	57	53	70	27	8
04	10	250	15			57	52	47	69	30	8
07	7	UNL	15			48	46	42	77	34	7
10	1	UNL	15			62	48	33	34	02	11
13	2	UNL	15			65	48	30	27	19	6
16	2	UNL	15			68	50	31	27	26	6
19	5	UNL	10			54	47	40	59	13	3
22	4	UNL	10			45	42	38	80	00	0
DAY 19											
01	3	UNL	10			43	41	39	88	02	3
04	3	UNL	10			41	40	38	88	00	0
07	10	250	10			43	42	41	93	31	4
10	10	230	10			57	47	38	46	04	8
13	9	120	15			63	48	30	29	06	10
16	9	130	15			66	52	37	34	09	7
19	9	90	15			58	48	39	48	05	8
22	1	UNL	15			51	45	39	84	04	5
DAY 20											
01	1	UNL	15			48	44	38	89	05	7
04	3	UNL	10			53	47	41	84	05	8
07	10	250	10			53	48	46	77	04	8
10	10	230	10			64	57	52	65	13	9
13	9	120	15			72	62	56	57	09	13
16	9	130	15			71	63	57	61	10	11
19	9	90	15			61	58	56	84	09	5
22	10	UNL	10			55	54	53	93	02	4
DAY 21											
01	10	40	10			58	58	57	93	08	4
04	10	40	7			60	58	56	93	05	3
07	8	UNL	7			58	58	57	93	05	4
10	7	UNL	8			73	64	58	58	08	10
13	9	30	10			75	64	57	54	09	8
16	5	UNL	10			73	64	58	59	12	8
19	5	UNL	10			68	62	58	68	06	7
22	8	55	10			65	61	58	78	08	7
DAY 22											
01	4	UNL	10			61	58	58	90	03	3
04	8	35	10			57	56	56	96	01	4
07	8	35	7			58	58	57	93	03	3
10	9	110	7			71	66	63	76	05	4
13	10	130	10			74	68	64	71	09	9
16	10	130	10			79	67	63	66	11	8
19	10	120	10			68	65	64	87	10	10
22	10	4	4		R	67	64	63	93	00	0
DAY 23											
01	10	45	7			68	65	64	93	08	5
04	10	3	3		FR	65	64	64	97	09	4
07	10	1	0	8	F	65	64	64	97	09	4
10	9	110	1	8	RF	66	65	64	93	10	5
13	10	10	5		H	70	67	65	64	12	5
16	10	250	7			71	67	64	78	16	5
19	6	UNL	8			66	65	64	93	00	0
22	10	4	1		F	64	63	62	93	00	0
DAY 24											
01	10	2	1	8	F	64	63	63	97	09	5
04	10	1	0	8	LF	62	62	62	100	08	5
07	10	1	0	4	F	60	60	60	100	01	4
10	10	3	0	12	F	61	60	60	97	09	3
13	10	12	7			69	64	61	76	15	3
16	10	12	7			68	64	62	81	30	5
19	10	80	5		F	65	63	61	87	10	4
22	10	2	2		RF	63	62	61	93	06	3
DAY 25											
01	10	2	2		RF	63	62	61	93	04	4
04	10	2	2		RF	63	62	61	93	06	5
07	10	2	1	8	F	62	61	61	97	04	6
10	10	4	1		F	62	61	60	93	08	3
13	10	10	4		F	66	63	62	87	21	7
16	3	UNL	10			70	65	62	77	23	10
19	10	3	7			64	63	62	93	20	12
22	6	70	7			58	56	55	90	26	7
DAY 26											
01	0	UNL	15			54	50	47	77	27	14
04	0	UNL	20			48	43	37	63	27	10
07	0	UNL	20			45	41	36	71	26	8
10	0	UNL	20			46	38	22	40	28	20
13	0	UNL	20			47	38	23	38	29	19
16	0	UNL	20			48	35	18	30	29	18
19	0	UNL	20			35	28	17	48	33	7
22	0	UNL	20			34	28	20	57	00	0
DAY 27											
01	0	UNL	20			30	27	22	72	00	0
04	1	UNL	20			28	27	23	82	02	4
07	2	UNL	15			31	28	24	75	05	4
10	1	UNL	15			46	37	25	46	11	5
13	1	UNL	15			55	46	37	51	16	12
16	1	UNL	15			50	51	44	58	17	8
19	6	38	15			50	47	45	85	17	4
22	2	UNL	15			48	46	44	86	17	5
DAY 28											
01	0	UNL	15			47	46	45	93	00	0
04	2	UNL	10			44	43	42	93	36	3
07	7	UNL	5		M	48	46	44	93	00	0
10	3	UNL	10			66	60	56	70	25	10
13	7	250	15			75	64	56	52	22	12
16	5	UNL	15			75	64	57	54	20	10
19	6	UNL	15			62	58	56	81	18	3
22	0	UNL	10			57	55	54	90	08	3
DAY 29											
01	3	UNL	10			54	53	52	93	36	3
04	3	50	8			54	53	52	93	02	3
07	7	60	7			61	58	56	90	06	3
10	8	65	10			72	66	62	71	09	8
13	10	UNL	10			79	67	58	50	14	14
16	10	250	10			75	65	58	58	10	10
19	10	70	10			68	64	61	76	06	5
22	10	55	10			66	64	61	78	08	8
DAY 30											
01	10	30	7		R	67	64	62	84	04	7
04	10	3	3		R	63	62	62	97	02	5
07	10	2	2		RF	64	63	62	93	04	8
10	10	3	4		FH	67	66	65	93	06	8
13	10	4	2	8	RFH	68	67	66	93	15	5
16	10	5	5		FH	70	68	67	90	11	5
19	10	8	7			68	68	67	93	13	7
22	10	5	8			72	71	70	93	19	8

STATION: CHARLESTON S C

YEAR & MONTH: 77 11

NOTES

CEILING

UNL indicates unlimited

WEATHER

- T TORNADO
- T THUNDERSTORM
- G SQUALL
- R RAIN
- RW RAIN SHOWERS
- ZR FREEZING RAIN
- L DRIZZLE
- ZL FREEZING DRIZZLE
- S SNOW
- SP SNOW PELLETS
- IC ICE CRYSTALS
- SW SNOW SHOWERS
- SG SNOW GRAINS
- IP ICE PELLETS
- H HAIL
- F FOG
- IF ICE FOG
- GF GROUND FOG
- BD BLOWING DUST
- BN BLOWING SAND
- BS BLOWING SNOW
- BY BLOWING SPRAY
- K SMOKE
- H HAZE
- D DUST

WIND

DIRECTIONS ARE THOSE FROM WHICH THE WIND BLOWS. INDICATED IN TENS OF DEGREES FROM TRUE NORTH: I.E., 09 FOR EAST, 18 FOR SOUTH, 27 FOR WEST. ENTRY OF 00 IN THE DIRECTION COLUMN INDICATES CALM.

SPEED IS EXPRESSED IN KNOTS; MULTIPLY BY 1.15 TO CONVERT TO MILES PER HOUR.

subsequent to December 31, 1977 has been received at NCSU. Thus, the Principal Investigator had to rely on monthly summary sheets of the 3-hourly data to obtain a representative picture of the atmospheric variability. Meteorological data being collected from NDBO buoys east of Charleston has also been requested but has not yet been received either, although only a very short overlap will exist between the period of the long-term mooring deployment and the wind time series provided by the buoy.

5.3.5 Sea Level Data Collection

Charleston sea level tapes have been ordered from NOAA/NOS in Rockville, Maryland, but to date, only data through 1977 has been received. Fortunately, the relationships between sea level and atmospheric variability at the Charleston site ($32^{o}46'N$, $79^{o}56'W$) have been of considerable recent interest (Pietrafesa, et al., 1978a; Brocks, 1978; Chao and Pietrafesa, 1979), as evidenced in Section 3.3, and, in the absence of actual sea level data for 1978, the experience of the Principal Investigator proved most helpful in the interpretation of the current meter records.

5.4 DATA REDUCTION PROCEDURES

5.4.1 Current Meter Data Analysis

5.4.1.1 Transcription of VACM Current Meters Data Tapes

VACM data cassettes retrieved upon mooring recovery were transcribed into computer compatible tapes by Nova University. Some difficulties were experienced in this process, resulting in unanticipated delays, particularly for the third and fourth long-term current meter data, only available for analysis by the P.I. in February and April 1979, respectively.

The transcription of the VACM data tapes into a computer compatible format is briefly described hereafter.

Data are stored serially in the current meter shift registers as follows:

East count	24 bits
North count	24 bits
Rotor count	24 bits
Compass reading	8 bits
Vane reading	8 bits

Time count 16 bits

Temperature count 24 bits

The data are transferred to the cassette in four-bit characters, forming 32 data characters. The cassette data are then transcribed to a 9-track computer compatible tape, using a Sea Data Model 12 Cassette Reader. During the transcription process the data are evaluated for proper track signal level, compass and vane follower operation, rotor operation, east and north calculation, clock operation, and temperature circuit operation. Examples of the types of problems that are typically detected in this process are failure in the computation with the VACM (no east or north count), rotor bearing failure, and failure of the clock counter to increment properly.

The processing of the data occurs in three steps: Sort, Edit, and Convert.

- Sort

Each data record ("logical record") is broken into its component parameters and a file of all records is created.

- Edit

Each record is searched for obviously faulty values (extremely high currents, temperatures greater than $30^{o}C$ or less than $0^{o}C$) and for proper incrementing of the clock. Records are added or deleted as necessary to make the clock count conform to the actual elapsed time.

- Convert

The counts are not directly readable in speed, direction, time, or temperature. The clock is an elapsed time clock, so the clock value must be added to the clock reset time to obtain actual time. The East, North, and Rotor counts are converted to East and North speeds by the following algorithms:

$$\text{East Speed} = \frac{2E-R}{R}\left(\frac{aR}{8T} + b\right) \text{ cm.s}^{-1}$$

$$\text{North Speed} = \frac{2N-R}{R}\left(\frac{aR}{8T} + b\right) \text{ cm.s}^{-1}$$

where

E = value contained in East counter

N = value contained in North counter

R = value contained in Rotor counter

T = averaging period in seconds

a, b are the rotor calibration constants selected as follows according to the value of $\frac{R}{8T}$

for $\frac{R}{8T} > .915$, a = 32.6 cm, b = 5.2 cm

for $\frac{R}{8T} < .915$, a = 36.1 cm, b = 2.0 cm

$$\overline{\theta_m} = \tan^{-1} \frac{\text{East speed}}{\text{North speed}}$$ (See Figure 5-9)

The temperature count is first converted to an equivalent thermistor resistance. This resistance is then converted to temperature by the following algorithm:

$$\frac{1}{T_{abs}} = A + B \ln R + C (\ln R)^3$$

where T_{abs} = absolute temperature

and A, B, C are calibration constants unique to each thermistor.

Derivation of the above algorithms is considered to be beyond the scope of this report. Readers interested in pursuing these further shall consult the following reports:

"Vector Averaging Current Meter Speed Calibration and Recording Technique" by J. R. McCullough. Woods Hole Oceanographic Institution Technical Report 75-44, Sept. 1975 UNPUBLISHED MANUSCRIPT.

"Accuracy of Temperature Measurements With the VACM" by R. E. Payne, A. L. Bradshaw, J. P. Dean, and K. Schleicher. Woods Hole Oceanographic Institution Technical Report 76-94, October 1976. UNPUBLISHED MANUSCRIPT.

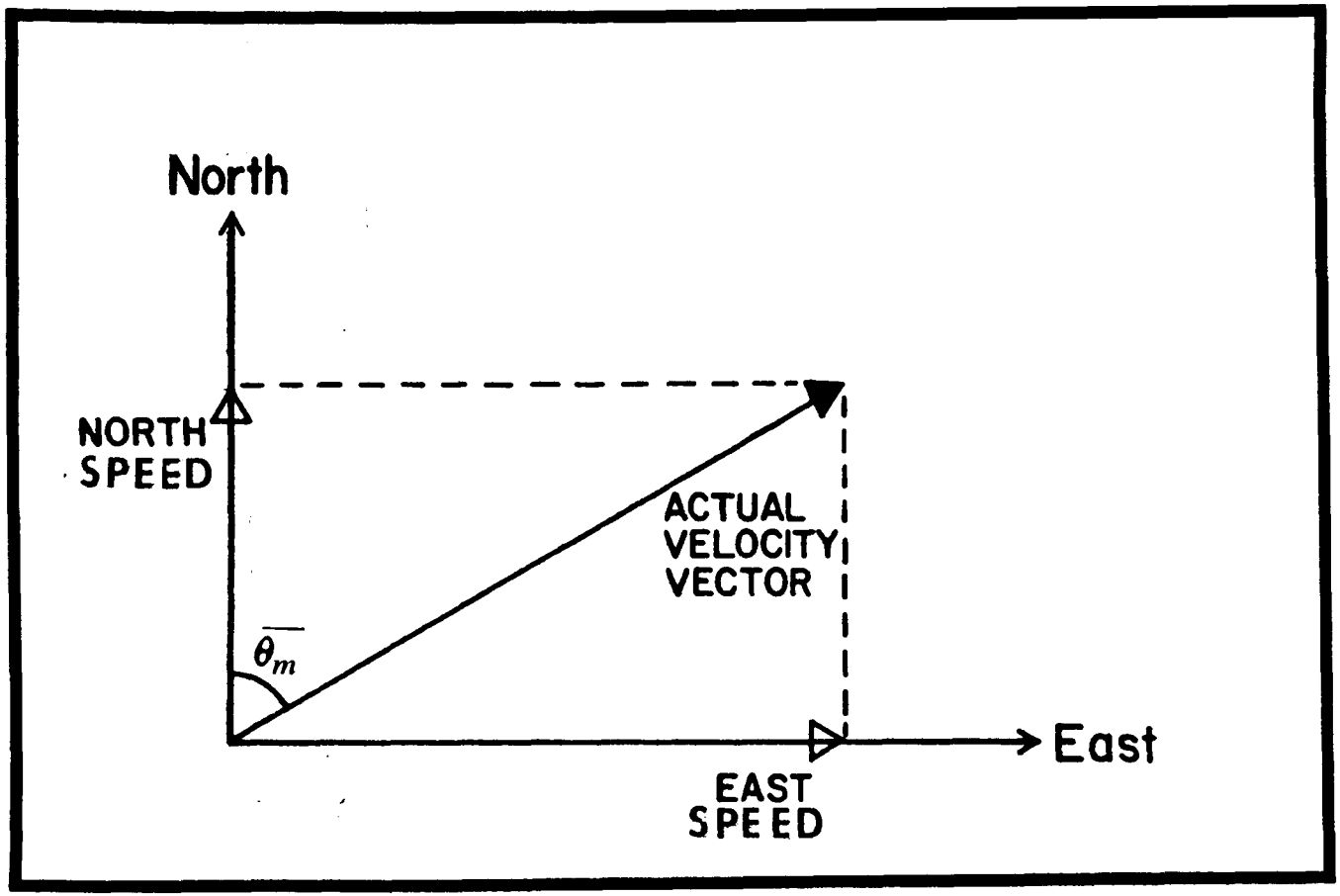

Figure 5-9. Resolution of current velocity vector north and east components.

5.4.1.2 Transcription of Aanderaa Data Tapes

Transcription of Aanderaa tapes was performed at the Rosenstiel School of Marine and Atmospheric Science, division of meteorology and physical oceanography (RSMAS/MPO), utilizing an integrated hardware/software system based on a Digital Equipment Corp. PDP-11/55 computer. The hardware consists of a standard audio Revox tape deck, a specialized decoder interface, and the PDP-11/55. Functions of the decoder interface include digital signal integration and determination of hardware detectable bit errors. Data and status indicators are communicated to the PDP-11/55 where software checks are made to establish encoder stability and completeness of data. Data frames and status indicators are assembled into blocks containing 16 records and recorded on 9-track tape.

Aanderaa recorders employ a saturated recording technique where ones and zeroes are distinguished by pulse width. Frame format consists of a single bit sync word followed by six 10-bit data words; the first word is a reference and serves both as an indicator of encoder stability and instrument identification. The decoder interface accepts an analog pulse train from the audio recorder and performs digital integration using a timer to count the width of each pulse. As the pulse train is decoded, it is assembled into data words. An additional timing circuit is used to determine valid intervals over which bits are distinguishable as belonging to a single word. To become a valid output, a data word must contain exactly 10 bits which must occur within a specific interval. Communication with the computer includes a 2-level interrupt and a 16-bit data word composed from 10 bits of Aanderaa data, a 4-bit indicator specifying the number of bits in the Aanderaa word, and 2 tape transport status bits.

The purpose of the two interrupts is to directly indicate whether a fully decoded data word contains 10 unambiguous bits (good word), or contains less than 10 bits due either to missing bits or noise bits.

All interval timers provide for a 30^{o} timing variation in order to accept data tapes from several generations of Aanderaa current meters. This is necessary due to differences in clock timing and recording density between generations. This is also needed to deskew the data for slight encoding timing variations introduced by the current meter. Automatic gain control circuitry featuring fast attack, slow recovery is included to compensate for signal amplitude changes encountered during the decoding process.

Data are transmitted from the decoder interface to a PDP-11/55 parallel interface where quality control checks are made prior to insertion of the data into the output record. These checks include tests for frame sync (6 data words per record with a stable instrument identification word), presence of noise bits and existence of good data. If partial words are detected, i.e., less than 10 bits,

an indicator of erroneous data is placed into the output record and the interpreted count of bad bits is examined to determine if a series of partial words constitute one or more Aanderaa words. This step is necessary to maintain sync lock since the Aanderaa recorder does not encode time on the instrument tape and, therefore, time can only be inferred from frame count. Furthermore, by indicating the presence of invalid data in the output record, the task of editing the data is considerably simplified. A complete output record includes the 6 data words, frame sync indicator, count of the number of valid and invalid data words, and frame number. These additional status indicators provide a mechanism to identify which data words are lost if a frame contains less than 6 entries. Any detected errors are reported to the operator at time of decoding to allow possible manual intervention.

The integrated hardware/software approach yields excellent results provided data tapes are not inadvertently exposed to high thermal or magnetic stress, quality recording tape is used, and the Aanderaa batteries are not depleted. Recent experience has shown a range of approximately 2 to 20 hardware detectable errors on an 8,000 plus record tape.

Several decoded systems have been used at the University of Miami to transcribe Aanderaa data tapes over the past years. The interface described above is the only system which yields consistent decodings of the same data tape over a number of repeated transcriptions. Thus, it is believed that random digitization errors introduced in the transcription stage are minimal to nonexistent and, therefore, do not contribute significantly to the overall error bounds of the measuring system.

5.4.1.3 Data Analysis Procedures

As indicated previously, preliminary data reduction of VACM and Aanderaa tapes were performed at Nova University and the University of Miami, respectively. As each VACM data cassette was read, the record was checked for hardware errors and missing samples. Averaged speed and direction components were generated by vector addition of the east and north rotor counters and all components were converted to CGS units. Magnetic variation was also applied at this time. Finally, the data were put on 9-track magnetic tape and sent to the Principal Investigators. Tapes received by Dr. T. Lee were transferred to the University of Miami Data Management System (DMS) for subsequent processing. Data received by Dr. L. Pietrafesa were sent to the Triangle Universities Computation Center (TUCC) at the Research Triangle Park, N.C. for storage and convenient access. A preliminary analysis of the tape was made to verify both the quality of the tape surface and the number of data files present. Each data file was copied to online disk and a printed listing produced. A single editing pass was made to detect missing samples which have

been flagged by Nova University. These samples were replaced either by deriving east or north speeds from corresponding speed and direction values, or through linear interpolation where all components were missing from a given sample. The files were adjusted to a common length and start time and stored in FESTSA (Fast and Easy Time Series Analysis) format for further processing.

Although, as implied above, the short- and long-term current meter data were analyzed by two different P.I.'s relying on software packages available at their own university, the methodology followed by Drs. Lee and Pietrafesa to prepare the standard data products is almost identical. Data analysis procedures are summarized hereafter.

5.4.1.3.1 Current Meter Data Filtering

After the VACM and Aanderaa data have been transcribed, calibrated, converted to cgs units and edited, they are then smoothed with a 3-hour low-pass (3-HLP) Lanczos filter to reduce noise due to surface gravity waves and other high-frequency contamination. Filter response characteristics are given in Table 5-7 and plot of the energy response is shown in Figure 5-10. The 3-HLP filter results in a data loss of 8 hours on either end of the original time series and effectively removes fluctuations with periods less than 3 hours. The original data are decimated to produce 3-HLP time series with hourly sample intervals. A 40-HLP Lanczos filter is then applied to the 3-HLP data to suppress tidal variations. The filter response characteristics and energy response are given in Table 5-8 and Figure 5-11, respectively. The 40-HLP filter results in a data loss of 4 days on each end of the time series. An hourly 3-40 HBP bandpass series is created by subtraction, and the data are further decimated to produce 40-HLP time series with 6-hourly sample intervals. This filter removes fluctuations with periods less than 40-hour.

The purpose of filtering of time series is to suppress oscillations in a particular frequency range. Thus, low-pass filters are used to suppress the amplitude of frequency fluctuations higher than the cut-off frequency of the filter, while keeping the amplitude of low frequency fluctuations relatively unaffected. Thus, filtering allows isolation of a particular frequency range while eliminating fluctuations outside that range. In the present analysis the 3-HLP surpresses oscillations having periods less than 3 hours without affecting tidal (12.4 hour) and longer period fluctuations. The 40-HLP suppresses all variance having a period lower than 40 hours, thus eliminating all significant tidal influence.

An example of unfiltered current meter data, 3-HLP and 40-HLP filtered data is given in Figure 5-12a, b, and c. In Figure 5-12a, the high frequency fluctuations are obvious, and the presence of lower frequency variance is suggested by visually averaging the data.

Table 5- 7 . Lanczos filter response characteristics for 3-HLP filter.

Low Pass Filter 1/4 power response	-	3 Hour (period)
Half width	-	25 points
Taper	-	Lanczos

Frequency (CPD)	Period (Hour)	Response (Power)
2	12	0.994
4	6	0.988
6	4	1.011
8	3	0.250
10	2.4	10^{-4}
12	2	10^{-5}
14	1.71	10^{-7}

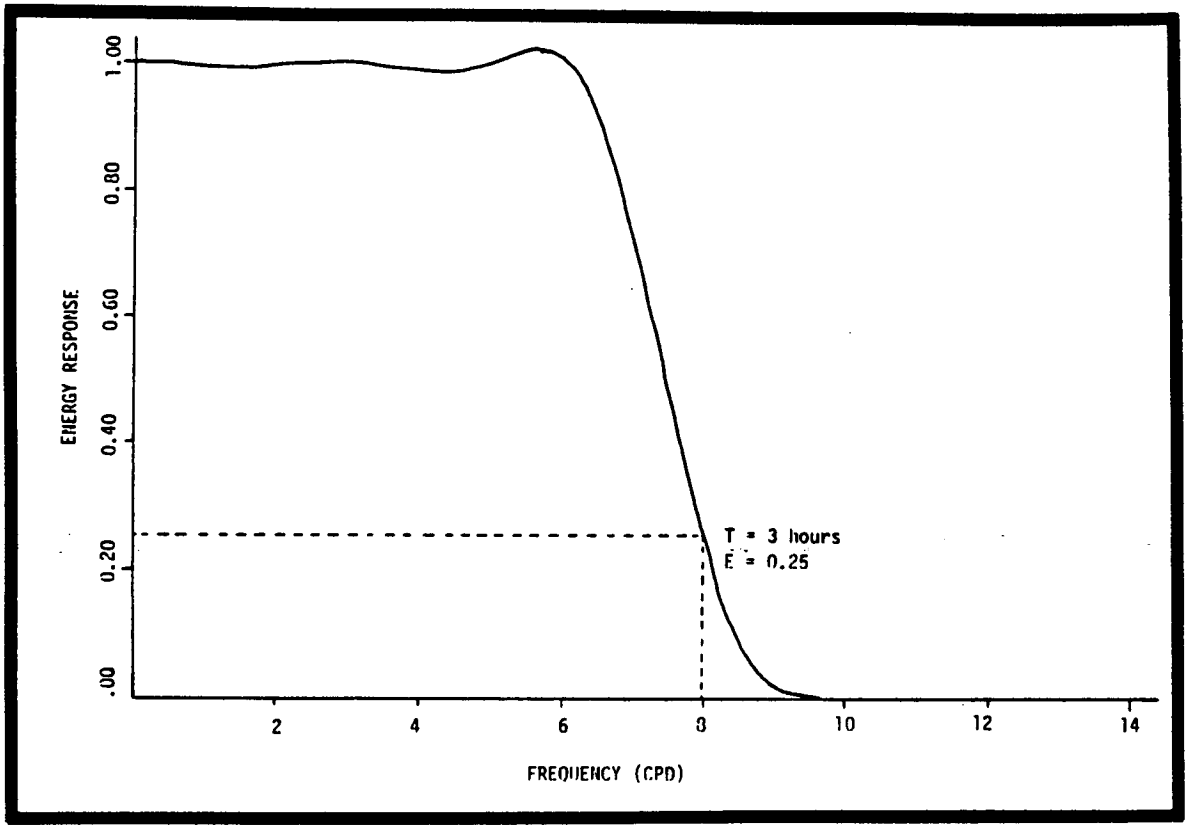

Figure 5-10 . Plot of the energy response for 3-HLP Lanczos filter.

Table 5- 8 . Lanczos filter response characteristics for 40-HLP filter.

1/4 Power Response - 40 Hour (period)

Half width - 97 point

Taper - Lanczos

Frequency (CPD)	Period (Day)	Response (Power)
0.1	10	1.006
0.2	5	1.003
0.3	3.33	0.996
0.4	2.50	1.024
0.5	2.00	0.805
0.6	1.67 (40 h)	0.250
0.7	1.43	10^{-2}
0.8	1.25	10^{-4}
0.9	1.11	10^{-5}
1.0	1.00	10^{-7}
1.5	0.67	10^{-7}
2.0	0.50	10^{-7}

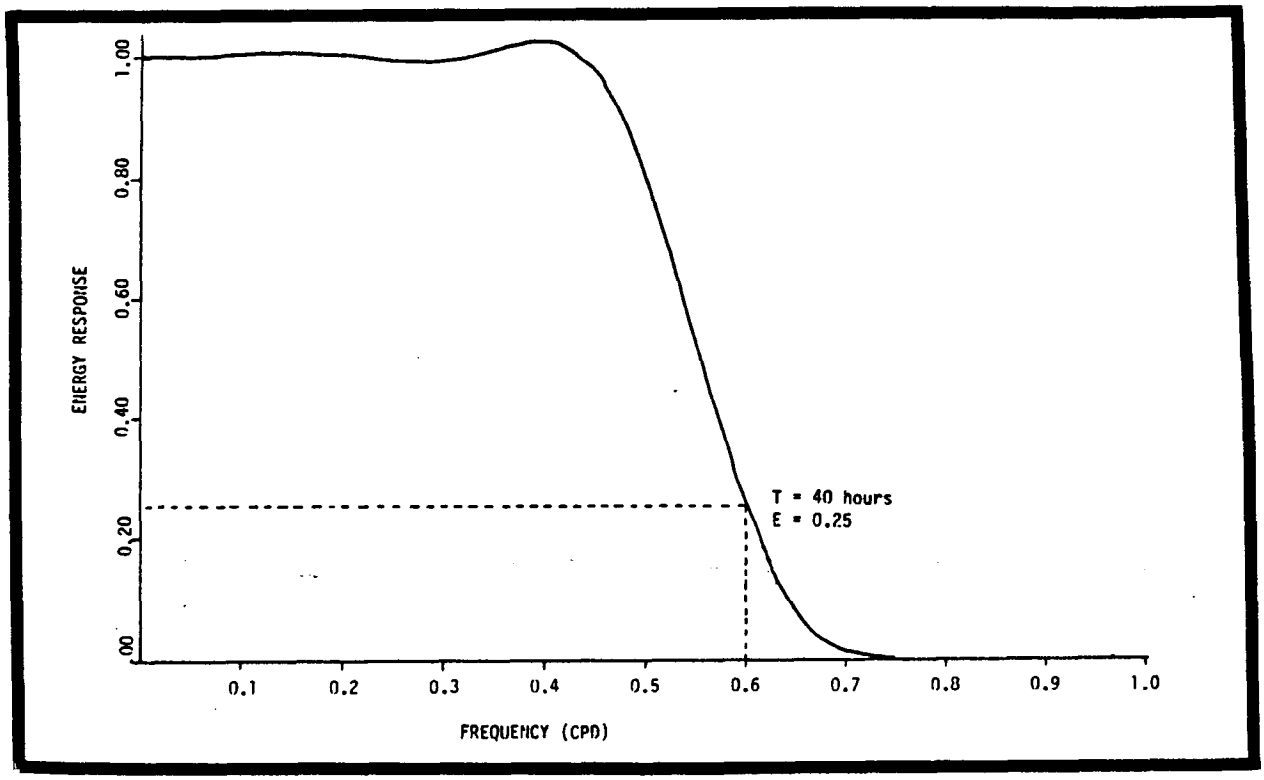

Figure 5- 11 . Plot of the energy response for 40-HLP Lanczos filter.

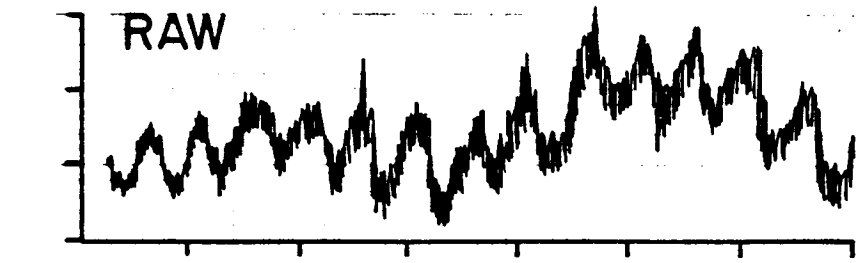

a Raw data as taken off the current meter.

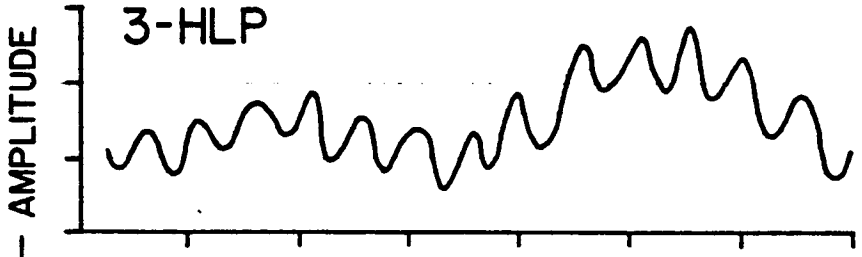

b 3-HLP Raw data is filtered so that all signals with a period less than 3 hours, such as high frequency noise contamination, are filtered out. Beneficial for viewing tidal effects on currents.

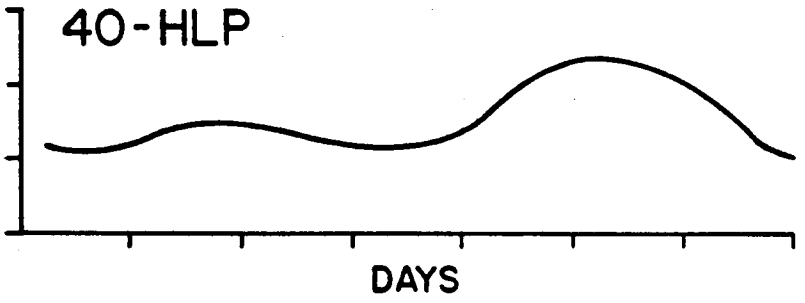

c 40-HLP 3-HLP data is filtered so that all signals with a period less than 40 hours, such as tides, are filtered out. Beneficial for viewing non-tidal effects on currents, i.e. winds, Gulf Stream, etc....

Figure 5-12. Example of (a) unfiltered data, and application of (b) 3-HLP filtering and (c) 40-HLP filtering.

The 3-HLP filtered data surpresses the highest frequency fluctuations in time series (Figure 5-12b) allowing tidal fluctuations, superposed to lower frequency fluctuations, to be readily discerned. After 40-HLP filtering (Figure 5-12c) tidal fluctuations are eliminated and the low frequency variance contained in the current meter data becomes readily obvious.

5.4.1.3.2 Coordinate Rotation

Up to now in the processing of the current meter records, geographic axes have been used, i.e., u is the eastward component and v is the northward component. These axes are not very useful in coastal oceanography because the motion of the water column has a tendency to follow the local isobath. However, the direction of the local isobath at the current meter mooring is sometimes difficult to determine in a precise manner. The solution adopted here is to use principal axis, which may be defined as those axes along which the two orthogonal components of the velocity fluctuations are uncorrelated in time. The advantage of rotating the axes such that the cross-shelf component u' and the alongshore component v' are uncorrelated, is that u' and v' can be treated as separate unrelated time series. This simplifies the interpretation when these time series are correlated with time series from other current meters and wind stations. It turns out that the principal axes usually align reasonably closely to the direction of the local isobaths.

The calculation of the angle of rotation of the principal axes from the geographic axis requires that the variance and covariance be calculated for the original u and v components. These variances are calculated for the filtered time series. The angle of rotation is determined and applied to the original unfiltered time series. The rotated unfiltered pair of time series are then filtered by the appropriate low pass filter to produce the cross-shelf component and the alongshore component, u' and v' respectively. We note also that, of all the orthogonal axis that could have been chosen, the principal axes maximize the variance in one component (in this case v') and minimize the variance in the other component (u').

In this manner for the short-term moorings, the principal axes were found to be approximately 30^{o} to the right of the cartesian coordinates at each current meter, which agrees with the alignment of the local isobaths or "natural coordinates" (Huyer, et al., 1975) within 5%. Using this criterion, the 3- and 40-HLP current component time series from each current meter were rotated by -30^{o} to form the "basic" cross-shelf (u+ offshore; 120^{o}T) and along-shelf (v+ to the northeast; 30^{o}T) time series.

5.4.1.3.3 Statistics

First order statistics of the u, v, T time series from each current meter were computed for the original and "basic" 3- and 40-HLP rotated data. In the case of the short-term moorings, statistics were also calculated for the Partagas winds (6-hourly wind estimates made for the center of the DOE box array by Jose Partagas) and DOE moorings A and B, which were located along the same transect as the "short-term" moorings at the 30 and 75 m isobaths, respectively, for the 4-month period July-October 1977. These statistics include the number of data points (N), average over the time series (Mean), standard deviation (S.D.), variance (Var), minimum (Min), and maximum (Max).

5.4.1.3.4 Spectra

Spectra, co-spectra, cross-spectra, phase and coherence squared of the basic 3- and 40-HLP u, v, T time series were computed using standard University of Miami FESTSA (Fast and East Time Series Analysis) programs (Jacobsen, 1974), also available at NCSU. These computations are shown in Volume III.

Spectral analysis is used as a tool to examine the variance of a time series. This variance is partitioned according to frequency (the inverse of the period). In the case of velocity time series, the spectral density at a given frequency is directly proportional to the total observed kinetic energy of the fluctuating component of velocity corresponding to that frequency. Similarly, spectral analysis of a time series of coastal water level would resolve the relative magnitude and frequency of the water level component fluctuations. Thus water level spectra would have local spectral peaks at the frequencies of the major tidal constituents, e.g., at a period of 12.4 hours. Such a spectrum is shown in Figure 5-13a. If the water level record contained a significant number of fluctuations with a 2-day period, as could occur due to wind forcing, then the spectrum would also contain an energy peak at the 0.5 cycle per day frequency, as shown schematically in Figure 5-13b.

When comparing two time series, it is possible to characterize the degree of correlation between the two records through cross-spectral analysis. The cross-spectrum divides the covariance of the time series as a function of frequency. The same information is contained in the coherence squared, which is the normalized cross-spectrum, (i.e., always less than or equal to one). Thus, two identical time series will have coherence squared of one at all frequencies.

The cross-spectrum is a complex number, thus having real and imaginary components. The magnitudes of these components are the coincident ("co") and quadrature spectra ("quad") respectively. By

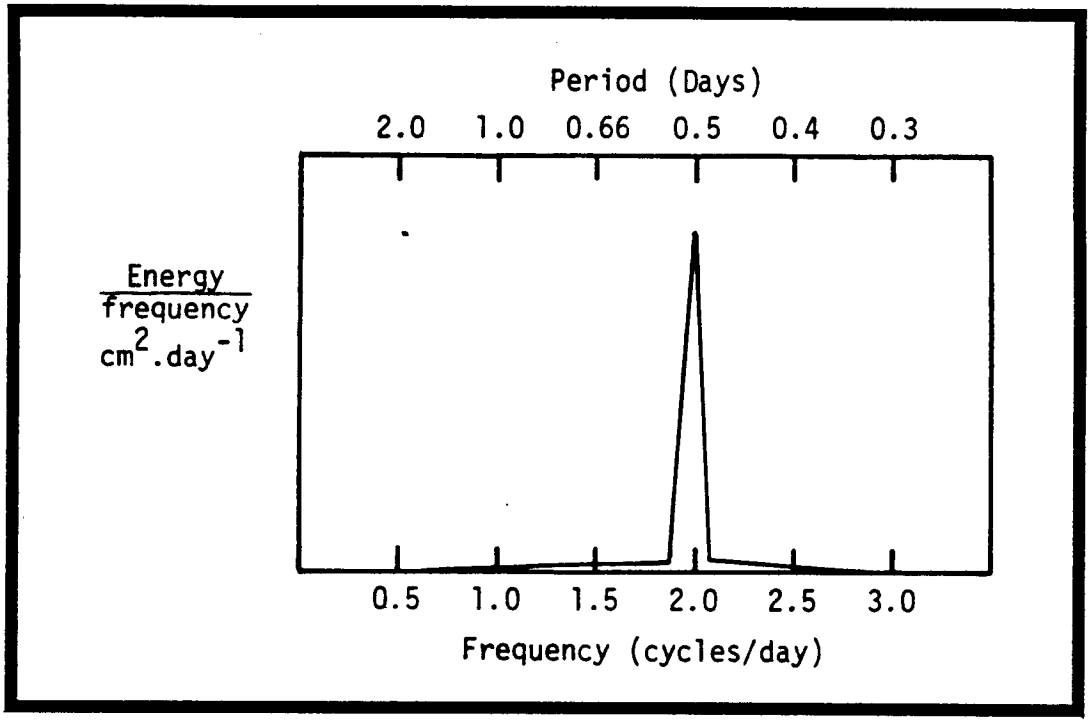

Figure 5-13a. Schematic spectrum of coastal sea level.

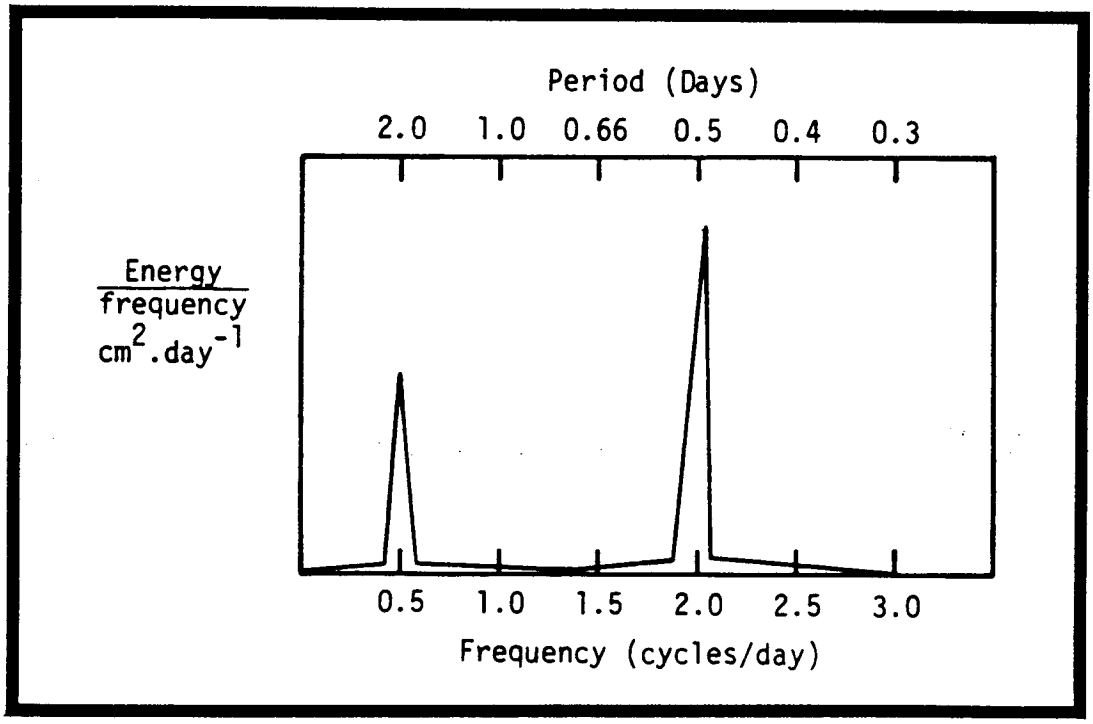

Figure 5-13b. Schematic spectrum of coastal sea level with both tidal and wind forcing.

comparing the relative magnitude of these components of cross spectra, phase lag between the original two time series can be estimated as a function of the frequency of the oscillation.

If the two time series being examined are u' and v', the fluctuating components of transshelf and alongshore velocities, then the covariance (cross-spectrum) is a measure of the horizontal flux of momentum. Similarly, if the two time series are u' and t', (fluctuating components of velocity and temperature, respectively) the cross-spectrum is a measure of the transshelf flux of heat.

5.4.2 Hydrographic Data Analysis

Procedures used by Skidaway in the data reduction of the CTD hydrocasts and analysis of nutrients, dissolved oxygen and chlorophyll-a samples described hereafter.

5.4.2.1 CTD Data Processing

5.4.2.1.1 Post-cruise Data Reduction

After a cruise, the magnetic tape of the data collected is sent to the University of Georgia computer center and stored at the tape library. The tape is then processed at Skidaway which has access to interactive time-sharing of the University's Control Data Corporation Cyber 70 through a telephone link.

The processing of tape data has been adapted from that described by Scarlet (1975). Table 5-9 shows the basic data flow, which, however, may need to be modified for special situations that arise for each new data set, or adapted to the amount of data processing already performed on-board in real time while a cast is in progress. CTDRUN copies the tape data to a prescribed computer file. MAGREAD converts binary coded data to decimal frequencies and CTDUNIT converts frequencies to engineering units. LAGFILT treats the data for the temperature sensor lag and coarse filters the data for noise. Then, BROENK calculates uncorrected salinity and sigma-t values. At this stage, salinity and temperature offset corrections are made from the primary calibration data. Then flow is resumed by repeating BROENK with the added correction factors, DLATCH deletes lines with repeated depths due to ship roll and CTDAVE presents the data in average one-meter increments. NODCFO converts the data to NODC format and NUTMERG merges additional data, i.e., nutrients, weather, latitude, longitude, etc for submission to the NODC. CEMLIST calculates specific volume anomally, oxygen saturation and apparent oxygen utilization (from the International Oceanographic Tables, 1966), the distance between successive stations, and reads all other data and formats all data for presentation in a technical report. This final product is stored on magnetic tape and all data, i.e., CTD, XBT, chemical, etc., made available to NODC in a format compatible with their requirements.

Table 5-9. CTD Data Flow: Shipboard acquisition to NODC submission.

Data Source/Disposition	Program	Data File
Digital Data Logger to Tape	CTDRUN (Copies tape data to a computer file)	KEYWORD
	MAGREAD (Converts binary coded data to decimal)	BIRANG
	CTDUNIT (Converts decimal units to engineering units)	LAG
	LAGFILT (Temperature lag and coarse filter)	CAL
Primary Calibration from Bottle Casts	BROENK (Calculates salinity and sigma-t)	LATCH
	DLATCH (Removed decreasing and repeated depths)	CTDATA
	CTDAVE (One meter averaged data)	AVE
	NODCFO (Converts to NODC format)	NODC + HEAD
	NUTMERG (Merged NODC data with headers and chemical data)	FINAL
Submission to NODC		(9-track magnetic tape)
	CHEMLIST (Calculates specific volume anamally, oxygen utilization, etc.0	TECHNICAL REPORT

Several steps of the basic data flow outlined above are essential to ensure that the total error resulting from the accuracy of the sensors and the data reduction procedures be minimized.

Offsets and Course Filter

A depth offset, determined by the frequency for depth while the fish is not in the water is applied in program CTDUNIT. No offset, however, is made for conductivity though it, like depth, has been observed to drift slightly with age. This drift is compensated for later in the final salinity offset as measured against actual water samples. Offsets for temperature are also addressed. The temperature sensor used by Skidaway has shown no signs of drift with age, when compared with protected reversing thermometer readings. The sensor and thermometers agree within the range of accuracy for the two ($\pm$ 0.02°C), so usually no offset is necessary.

LAGFILT then course filters slipring, winch and other electronic noise. The windows are $\pm$5m, $\pm$0.8 mmhos/cm, and $\pm$0.5°C.

Temperature Lag

The temperature sensor response time is slower than that of the depth (D) and conductivity (C) sensors. Therefore, the actual temperature (T) at the time D and C are sampled must be calculated from the "indicated" T. From Scarlet, 1975:

$$T_{R(n)} = T_{I(n)} + \left(\frac{T_o \, (T_{I(n+1)} - T_{I(n-1)})}{2\sigma} \right)$$

where: T_R is the real temperature, T_I is the indicated temperature, T_o is the sensor time constant, σ is the sampling rate, and n is the CTD scan number. This correction works for both downcasts and upcasts. However, the quality of the downcast data is generally considered better than that of upcasts, as during the upcast, the CTD is in the wake of the rosette, causing turbulent disturbance of the water being sampled. Consequently, upcast data are reported only when downcast data have been lost or not recoverable.

The Plessey temperature sensor time constant is reported to be 0.35 s. The depth and conductivity sensors each have a reported 0.1 s time constant so that temperature lags behind depth and conductivity. The Digital-to-analog Converter in the DDL updates a CTD scan at the rate determined by the systems slowest count time base, which for this system is the temperature time base of 0.229235 s.

Depth Latch and Averaging.

The normal descent rate of .25 $m.s^{-1}$ and scan rate of .229 s should provide 17 $scans.m^{-1}$. The number of $scans.m^{-1}$ varies because the motion of the fish reflects ship roll. Repeated depths are removed by the DLATCH program. The average number of scans (remaining) through 1 m intervals is 10, $\pm$ 7. Scans of data 0.5 m above and below each 1 m are averaged for depths less than 100 m and data 2.5 m above and below each 5 m are averaged for depths greater than 100 m.

Salinity

Salinity is calculated from CTD scans using shortened equations adapted from those of Bradshaw and Schleicher (1965) and Cox et al. (1967) (Broenkow, 1977) and shown in Table 5-10). The effects of pressure and temperature on the conductivity sensor require an uncorrected, then corrected salinity calculation according to the steps indicated in the same table.

5.4.2.1.2 On-board Data Processing

An on-board data acquisition and processing system based on a Hewlett-Packard (HP) 9825 desk top computer has been in the process of development by Skidaway.

A single Hewlett-Packard (HP) tape cartridge, structured with two parallel tracks, contains programs for the CTD acquisition on one track and has space for data storage for as many as 30 stations on the other. Loading and running the master program instructs the operator how to initiate a CTD cast. Special function keys are defined by this program that enable interactive control of data acquisition modes, i.e., downcast, upcast, equilibration routines. All subsequent programs prompt the operator on procedures and ask for the necessary variable entries, i.e., offsets, file numbers.

Data acquired by the Hewlett-Packard is treated according to the same data reduction procedure as the one described in the previous section, but in real time. This includes conversion of frequencies to engineering units, following definitions of offsets and corrections for temperature lag. For purposes of CTD calibrations, the CTD fish is lowered to within 3 m of the bottom, where the fish descent is stopped and equilibration routine begins. Depth, temperature and salinities are displayed and printed during the four minutes required for the reversing thermometers to equilibrate. These printed values of T and S are then used to calibrate the instrument against the reversing thermometers and salinity bottles samples taken at that depth.

The preliminary downcast data is then averaged to meter values and recorded permanently on the HP tape cartridge. Data collection during upcasts is taken in the same way. If calibration is to be

Table 5-10. Flow using Broenkow's salinity equations and calculations flow.

$$R_Z = 1 + .01(1.551 - 0.0453T + 59 \times 10^{-5}T^2) + \tfrac{1}{4}(35-S)(.043 - .0017T + 23 \times 10^{-6}T^2))(1.037 \times 10^{-3}Z - 32 \times 10^{-9}Z^2)$$

$$A_T = (676547 + 20131.5T + 99.89T^2 - .1943T^3 - .00672T^4)\ 10^{-6}$$

$$R_T = \frac{C(S,T,Z)}{R_Z A_T 42.896}$$

$$\Delta_{15} = R_T(R_T-1)(T-15)(96.7 - 72R_T + 37.3R_T^2 - (.63 + 21R_T^2)\ (T - 15))10^{-5}$$

$$R_{15} = R_T + \Delta_{15}$$

$$S^o/oo = .08996 + 28.2972R_{15} + 12.80832R_{15}^2 - 10.67869R_{15}^3 + 5.98624R_{15}^4 - 1.32311R_{15}^5$$

where: Z = depth (meters)

T = temperature (^oC)

C = measured conductivity (μmhos/cm)

R = conductivity ratio

S = salinity ($^o/oo$)

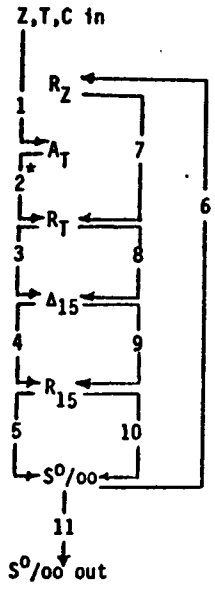

*without the R_Z term

R_Z = pressure effect on conductivity

Δ_T = temperature effect

R_T = R(S,t,p) conductivity ratio

Δ_{15} = t_{15} correction (International Oceanographic Tables, 1966)

R_{15} = R(S,15°C,0)

done at depths other than the deepest sample depth, a mid-depth equilibration routine is used to print D, T and S while a rosette bottle is being tripped. The mid-depth equilibration can also be used at any time the CTD fish is stopped, so that excessive data are not recorded. At the end of the upcast the preliminary data is averaged to meter values and recorded on a permanent file.

Further data workup is done aboard ship. Salinity (preferably from downcast data) is plotted versus depth. Until calibration data becomes available, plots are made using uncorrected salinity values.

5.4.2.2 Thermosalinograph Measurements

Selected isotherms and isohalines are plotted on the cruise track near the exact position recorded by assuming a constant ship speed and direction between stations. The ship's crew are careful to maintain these conditions so that the assumptions are good to the accuracy of the automatic steering. The resulting maps display contours of temperature every $1^{o}C$ and salinity every $1^{o}/oo$ up to $36^{o}/oo$, then every $0.2^{o}/oo$. The contours are hand drawn connecting known locations of temperature and salinity values along the ship track without any of the usual interpolation between hydrographic stations. Thus, this technique shows the actual temperature and salinity distributions along the ship tracks, giving realistic frontal (gradient) information.

5.4.2.3 Nutrients Analysis

The analyses of dissolved silicate (reactive), phosphorus (reactive) and nitrate are based on minor modifications of the Strickland and Parsons methods (1972).

5.4.2.4 Dissolved Oxygen Analysis

Dissolved oxygen concentrations are determined using the exact method of Strickland and Parsons (1972).

5.4.2.5 Chlorophyll-a Analysis

Chlorophyll-a was measured using the *in vitro* flurometric method modified from Strickland and Parsons (1972). This method is based on the use of the Turner fluorometer as suggested by Yentsch and Menzel (1963) and subsequently investigated by Holm-Hansen et al. (1965). This method has the convenience of speed and the requirement of much smaller sample volumes for a given sensitivity. Only Chlorophyll-a is determined.

5.4.2.6 Calibration Procedures and Error Analysis

High accuracy of the data derived from the CTD sensors, XBT's and bottle casts is critical to the correct interpretation of oceanographic processes. To insure the highest quality data, an extensive calibration scheme of salinity, temperature and depth recorded by the instrument against bottle casts has been implemented by Skidaway.

5.4.2.6.1 CTD Calibrations

Three salinity offsets, i.e. constant, depth dependent and time dependent salinity offsets were determined by examining the differences between salinity values obtained from bottle sample analysis and the CTD readings, and plots of these discrepancies versus depth and time, respectively. Likewise, a mean difference and standard deviation between CTD and reversing thermometer readings was obtained for each seasonal sampling, and a systematic correction applied to the data if deemed necessary. Finally, a depth offset was determined by comparing the CTD depth sensor readings with the length of wire out under conditions of zero wire angle.

A summary of the various calibrations offsets determined for each seasonal cruise is presented in Table 5-11, which also shows the results of an intercomparison of salinity between Skidaway and NCSU (summer cruise) and U. Miami (fall cruise). These intercomparisons served as a check on the salinometer analysis of water samples used to calibrate the CTD. Excellent agreement was found between the Institute and NCSU for the summer cruise. The results of the intercomparison with the University of Miami were not as good as anticipated. An explanation for the discrepancy, however, appears to exist in the variability of the Miami readings as opposed to the Skidaway readings. For such shallow waters (<30 m) a mean salinity offset with a small standard deviation would be expected as obtained from the Skidaway samples (s.d. = 0.010). Since the Miami data do not meet these criteria (s.d. = 0.060), some instrumental or procedural problem is supected. Further, since a good intercomparison was made between NCSU and Skidaway Institute in July, the Skidaway methods and instrumentation are not thought to be suspect.

5.4.2.6.2. XBT calibrations

When XBT's were used in supplement or replacement to CTD casts, the system was calibrated against three coincidental CTD casts in the mixed layer near bottom and against surface buckets at these stations with well mixed surface layers. Both comparisons yielded a 0.2°C offset, for the shallow XBT system as well as the deep one (250 m and 450 m respectively).

Table 5-11 Hydrographic data calibration.

	Depth dependent Offset	Time dependent Offset	Constant Offset (°/oo)	Mean difference between CTD and Reversing Thermometer (°C	Depth Calibration Depth offset	Dissolved Oxygen f-factor	Dissolved Oxygen blank value (ml)
Winter cruise 78	None	None	+0.042±0.013	+0.014±0.012	None	1.00 to 1.02	0.01
Spring cruise 78	None	None	+0.124±0.012	+0.020±0.009	None	1.05 to 1.03	0.00
Summer cruise 78	$S = So^* + 0.083 - 1.57 \times 10^{-4} D^*$			+0.012±0.014	None	1.04 to 1.03	0.000
Fall cruise 78	$S = So^* + 0.100 - 1.28 \times 10^{-4} D^*$			+0.015±0.009	None	1.02 to 1.01	0.00

*So is the uncorrected salinity
*D is the depth

Bottle #	N.C. State Univ.	Skidaway Institute	Diff.
106	35.867	35.873	-.006
120	36.373	36.380	-.007
132	36.033	36.043	-0.010
169	35.784	35.770	+.014
181	35.630	35.627	+.003
	Mean		-.001
	Std. Dev.		.010

Salinometer salinity intercomparison with N.C. State University (Summer cruise)

Bottle #	Univ. of Miami	Bottle #	*Skidaway Institute	Diff.
186	36.123	187	36.006	.117
188	35.579	189	35.571	.008
190	35.175	191	35.127	.048
194	35.092	193	35.130	-.038
		Mean		.034
		Std. Dev.		.066

*Skidaway's readings were made after double rinses and the same conductivity ratio to within ±0.00005 was then obtained twice from the remaining sample water for a total of four fillings of the sample cell.

Salinometer salinity intercomparison with University of Miami. (Fall cruise).

5.4.2.6.3 Nutrient calibrations

Except for the winter cruise, the nutrient analysis was performed at Duke University Marine Laboratory under subcontract from Skidaway, using Standard Technicon autoanalyser techniques. A nitrate vs. phosphate plot was made as a means to validate the data and check them against historical standards. They showed a typical N:P ratio of 16:1 for deep waters.

5.4.2.6.4 Dissolved oxygen calibration

The thiosulfate was calibrated against standard biiodate during each run. The f-factor and blank value were determined for each cruise, and are given in Table 5-11.

5.4.2.6.5 Chlorophyll calibration

Chlorophyll concentration was determined by the Strickland and Parsons fluorometric *in vitro* method. Typically, 10 replicate samples for *in vivo* (using a Turner Design Fluorometer) and *in vitro* (extracted) chlorophyll concentrations were taken at stations representative of water found near-shore, mid-shelf, shelf break and Gulf Stream, respectively. At the remaining stations, only *in vivo* samples were taken. For these representative stations, a linear regression of *in vivo* to *in vitro* chlorophyll concentration was calculated, from which values for extracted chlorophyll were predicted for those stations where no extracted chlorophyll concentration corresponding to *in vivo* fluorometer reading was determined.

5.5 DATA PRODUCTS

5.5.1 Subsurface Current Measurements

A list of the data products provided by the short-term and long-term current meter studies is given in Tables 5-12 and 5-13, respectively. Presentation of these products is in Volume III.

It should be noted that, to date, only the first two long-term current meter data have been analyzed, because of unanticipated delays in the transcription of the VACM cassettes into computer-compatible tapes. The missing data will be submitted in a technical addendum as soon as these data sets become available.

5.5.2 Hydrographic Measurements

For each cruise performed on a seasonal basis in 1977 and 1978, horizontal fields of temperature, salinity, sigma-t, nutrients, dissolved oxygen and chlorophyll concentrations were plotted for selected

Table 5-12. Data products from "short-term" current meter measurements.

	Data Products	Location
1.	Printouts of data samples taken from averaged (60-minute values for 3-HLP Lanczos filtered time series) measurements of u, v, T, P.	Stored on magnetic tape at SAI and U. of Miami.
2.	Statistics from original and 3- and 40-HLP "basic" time series of u, v, T, P, to include: mean, maximum, minimum, S.D. and variance.	Tables 5-14, 5-15, 5-16
3.	Probability distributions (histograms) of all current meter variables from both the 3- and 40-HLP series and Partagas wind.	Figures 2.1-1 to 2.1-9. Volume III, Section 2.1
4.	Time series plots of temperature, available pressure and horizontal current and wind components resolved along and across isobaths, for the 60-minute values from the 3-HLP data and for 6-hourly data from 40-HLP time series (tidal and higher frequencies removed).	Volume III, Section 2.1 Figures 2.1-10 to 2.1-22
5.	Stack plots of 1-hourly current velocities (3-HLP) as a function of time (stick-plot of vector plots).	Volume III, Section 2.1 Figure 2.1-23.
6.	Stack plots of current meter velocities as a function of time with tidal and higher frequencies removed (stick-plots of 6-hourly values from the 40-HLP series).	Volume III, Section 2.1 Figure 2.1-24.
7.	Progressive vector diagrams of the 3- and 40-HLP time series for each current meter over the recording period and Partagas wind.	Volume III, Section 2.1 Figures 2.1-25 to 2.1-32.
8.	Spectra, co-spectra, cross-spectra, phase and coherence squared of horizontal current components and temperature for the 3- and 40-HLP time series (u, v, T).	Volume III, Section 2.1 Figures 2.1-33 to 2.1-53.
9.	Stick plots of daily average velocities resulting from the application of a 5-day low-pass filter of the original data series.	Volume III, Section 2.1 Figure 2.1-54.
10.	Current stick-plots, T and P of one untreated 3-day period of original information (the 3-day period will be selected to include an introsuion event during the time series benchmark study, if one is clearly definable.	Volume III, Section 2.1 Figures 2.1-54 to 2.1-57.

Table 5-13. Data products from "long-term" current meter measurements.

	Data Products	Location
1.	Printouts of data samples from unfiltered measurements of u, v, T, P.	Stored on magnetic tape at Triangle Univ. Computation Center (TUCC) and printouts at NCSU.
2.	Statistics from unfiltered time series of u, v, T to include: minimum, maximum, mean and S.D. for both true north coordinate and principal axis systems.	Tables 2.2-2, 2.2-4, 2.2-7 and 2.2-8. Volume III, Section 2.2
3.	Statistics of 2-week mean velocities giving the discrete and cumulative means in true north coordinate and principal axis systems.	Tables 2.2-1, 2.2-2, 2.2-5 and 2.2-6. Volume III, Section 2.2
4.	Probability distributions (histograms) of current directions from 3HRLP series.	Figures 2.2-61 to 2.2-63 and 2.2-126 to 2.2-128. Volume III, Section 2.2
5.	Stacked time series of temperature, current speed and direction, and velocity components from unfiltered data in true north coordinates (excepting 8903-A).	Figures 2.2-1 to 2.2-6, 2.2-64 & 2.2-65. Volume III, Section 2.2
6.	Stacked time series of temperature and velocity components and vectors from 40HRLP data in principal axis (089 only) and true north coordinate systems.	Figures 2.2-7 to 2.2-9 and 2.2-73 to 2.2-79. Volume III, Section 2.2
7.	Stacked time series of temperature and velocity components from 3HRLP data (089 only) in true north coordinates.	Figures 2.2-67 to 2.2-72. Volume III, Section 2.2
8.	Stacked stick plots of current velocity from 40HRLP data in principal axis system.	Figures 2.2-11 and 2.2-80. Volume III, Section 2.2
9.	Progressive vector diagrams from unfiltered (089 only), 3HRLP (085 only) and 40HRLP (084 only) data in principal axis system.	Figures 2.2-12 to 2.2-17 and 2.2-82 to 2.2-84. Volume III, Section 2.2.
10.	Vector addition of 2-week mean velocities in true north coordinate system.	Figures 2.2-18 and 2.2-91. Volume III, Section 2.2.
11.	Spectra, co-spectra, cross-spectra, phase and coherence and quadspectra (089 only) current components and temperature from 40HRLP data.	Figures 2.2-19 to 2.2-60 and 2.2-92 to 2.2-125. Volume III, Section 2.2.
12.	Stacked time series of 40HRLP temperature from 089.	Figure 2.2-81. Volume III, Section 2.2.

depths. Likewise, vertical cross-sections of the above parameters along each cross shelf transect were prepared for each cruise. This voluminous set of data products is presented in Volume III, Section 3.2. A discussion of the main hydrographic features appearing in this data set is given in Section 5.6.2.

5.5.3 Gulf Stream Variability

Data Products resulting from the analysis, by remote sensing techniques, of the Gulf Stream temporal and spatial variability consist mainly of figures which have been inserted in the discussion of the findings presented in Section 5.6.3.

5.6 DISCUSSION OF THE RESULTS

Presented in this section is a discussion of the findings resulting from the interpretation of the subsurface current measurements and distribution of hydrographic variables over the shelf on a seasonal basis. Analysis of the remote sensing data and findings regarding the Gulf Stream variability are also discussed hereafter.

5.6.1 Current Meter Measurements

This section contains a discussion of Data Products listed in the previous section, presented by Dr. T. Lee (short-term moorings) and Dr. L. Pietrafesa (long-term moorings). It shall be recalled that although the collection of subsurface current and temperature data at the location of the long-term array has been successfully completed, only the first two sets of records, covering the period of November 4, 1977 to April 13, 1978 have currently been analyzed, because of delays incurred in the transcription of the VACM cassettes in a computer-compatible tape. Analysis and interpretation of the remaining two data sets will be ongoing between the dates of submission of the present draft report and of the final version (approximately June 15) and every effort will be made to incorporate them in the camera-ready report.

5.6.1.1 Short-term Current Meter Measurements

Data from the combined BLM (moorings 83 and 84) and DOE (moorings A and B) cross-shelf array are used with Partagas winds to discuss the current and temperature variability in the mid to outer regions of the Georgia Shelf during the "Summer 1977" (30 June - 1 November 1977). First order statistics of these data are presented in Tables 5-14 to 5-16 and the basic 3- and 40-HLP rotated time series are shown in Volume III (Figures 2.1-10 to 2.1-32).

Large amplitude current and temperature fluctuations occurred on time scales ranging from tidal to two weeks at all current measuring locations. Current fluctuations tended to have greater amplitudes in the

Table 5-14. First order statistics from original (non-rotated) time series - "short-term" current meter measurements Δt = 20 m for Aanderaa, u and v are cm/s, T is in ^{o}C.

Mooring #	Current Meter #	Instrument Depth (m)	Water Depth (m)	Parameter	# Data Points	Mean	Max.	Min.	+S.D.	Var.
83	T	17	40	u	3054	-2.9	54.0	-61.1	25.7	660
	T	17	40	v	3054	-5.6	49.4	-68.9	21.4	460
	T	17	40	T	3054	26.6	28.1	23.8	1.2	1.4
83	B	37	40	u	1249	-0.3	35.5	-40.0	18.0	324
	B	37	40	v	1249	2.5	37.6	-44.7	17.0	289
	B	37	40	T	1249	24.7	26.4	22.4	1.0	1.0
84	T	17	45	u	4436	3.7	90.3	-74.3	29.1	847
	T	17	45	v	4436	9.6	126.3	-80.4	33.4	1116
	T	17	45	T	4436	25.6	28.4	18.6	1.6	2.6
84	B	42	45	u	5906	-0.3	47.9	-66.2	20.3	412
	B	42	45	v	5906	6.4	64.4	-57.2	19.2	369
	B	42	45	T	5906	23.3	28.4	16.8	2.3	5.3
A	T	17	30	u	8549	1.2	55.1	-52.6	21.6	467.6
	T	17	30	v	8549	0.4	47.0	-56.4	16.2	262.7
	T	17	30	T	8549	25.7	27.7	21.6	1.2	1.5
A	B	27	30	u	1331	1.0	36.5	-32.7	13.6	185.1
	B	27	30	v	1331	3.8	39.1	-26.4	11.1	124.2
	B	27	30	T	8847	25.6	27.6	21.6	1.3	1.7
B	T	17	75	u	8038	21.7	124.7	-63.3	30.8	951.8
	T	17	75	v	8038	49.6	193.1	-74.0	54.6	2985.6
	T	17	75	T	8038	25.4	29.2	16.0	2.8	7.7
B	B	72	75	u	2349	6.3	41.7	-27.5	10.5	110.5
	B	72	75	v	2349	9.4	54.2	-27.5	13.5	181.4
	B	72	75	T	2349	19.0	27.4	9.9	3.9	15.5

Table 5-15. First order statistics of 3-HLP "basic" rotated time series from "short-term" current meter measurements, DOE moorings A and B and Partagas winds, Δt = 1 h for current meters and 6 h for wind, units are currents (cm/s), T (^{o}C) and wind (m/s).

Mooring #	Current Meter #	Instrument Depth (m)	Water Depth (m)	Parameter	# Data Points	Mean	Max.	Min.	+S.D.	Var.
83	T	17	40	u	752	0.4	61.2	-54.7	27.1	753.6
	T	17	40	v	752	-6.3	47.2	-62.0	19.6	385.6
	T	17	40	T	752	26.7	28.0	23.8	0.8	0.6
83	B	37	40	u	301	-1.4	46.3	-43.2	20.6	423.3
	B	37	40	v	301	2.3	29.5	-37.7	13.7	186.9
	B	37	40	T	301	24.7	26.4	22.4	1.0	1.1
84	T	17	45	u	1467	-1.6	70.0	-73.7	29.0	841.6
	T	17	45	v	1467	10.5	116.7	-81.7	33.3	1106.0
	T	17	45	T	1467	25.6	28.4	18.7	1.5	2.3
84	B	42	45	u	1465	-3.6	52.2	-63.5	21.6	466.5
	B	42	45	v	1465	5.6	63.5	-50.8	17.5	305.3
	B	42	45	T	1465	23.4	28.3	16.8	2.2	5.0
A	T	17	30	u	2838	0.8	58.5	-49.7	23.3	541.3
	T	17	30	v	2838	0.9	41.1	-45.5	13.3	176.6
	T	17	30	T	2838	25.8	27.7	21.6	1.2	1.5
A	B	27	30	u	432	-1.3	36.5	-40.5	15.9	251.8
	B	27	30	v	432	3.8	26.0	-16.3	7.3	52.7
	B	27	30	T	2937	25.6	27.6	21.6	1.3	1.7
B	T	17	75	u	2668	-6.0	63.8	-93.8	23.5	551.9
	T	17	75	v	2668	53.8	208.5	-77.3	58.1	3370.2
	T	17	75	T	2668	25.4	29.2	16.5	2.8	7.7
B	B	72	75	u	771	0.7	33.6	-22.3	9.5	91.0
	B	72	75	v	771	11.5	54.5	-26.6	13.6	186.1
	B	72	75	T	771	19.0	27.2	9.6	3.9	15.2
Partagas wind				u	607	-0.5	15.4	-10.1	4.4	19.1
Partagas wind				v	607	0.5	10.3	-16.4	4.8	23.0

Table 5-16. First order statistics from 40-HLP "basic" rotated time series from "short-term" current meter measurements, DOE moorings A and B and Partagas winds, Δt = 6 h, units are currents (cm/s), T (°C) and wind (m/s).

Mooring #	Current Meter #	Instrument Depth (m)	Water Depth (m)	Parameter	# Data Points	Mean	Max.	Min.	+S.D.	Var.
83	T	17	40	u	94	-0.2	16.3	-19.8	7.2	52.5
	T	17	40	v	94	-8.2	31.9	-39.4	15.9	252.3
	T	17	40	T	94	26.5	27.7	25.2	0.6	0.4
84	T	17	45	u	213	-1.9	32.2	-49.1	12.4	154.5
	T	17	45	v	213	12.5	87.2	-36.0	26.5	700.3
	T	17	45	T	213	25.6	28.5	21.6	1.4	2.0
84	B	42	45	u	213	-4.6	17.4	-43.2	11.3	127.3
	B	42	45	v	213	7.0	50.7	-15.3	14.5	209.7
	B	42	45	T	213	23.3	28.3	17.4	2.3	5.3
A	T	17	30	u	441	0.9	12.7	-8.6	3.2	10.3
	T	17	30	v	441	1.0	31.0	-26.2	9.8	96.4
	T	17	30	T	441	25.9	27.6	22.6	1.1	1.3
B	T	17	75	u	413	-6.3	28.7	-74.5	14.7	216.1
	T	17	75	v	413	53.4	181.8	-62.6	55.7	3106.1
	T	17	75	T	413	25.3	29.2	18.0	2.7	7.3
B	B	72	75	u	97	0.5	11.4	-6.8	3.9	15.7
	B	72	75	v	97	12.9	36.3	-20.3	13.1	172.1
	B	72	75	T	97	19.3	26.2	13.6	3.6	12.8
Partagas winds					575	-0.5	14.8	-919	4.1	17.2
Partagas winds					575	0.5	9.4	-13.8	4.6	20.8

upper layer, whereas temperature changes were greatest in the lower layer. Current and temperature fluctuations at the outer shelf locations (moorings 84 and B at the 45 m and 75 m isobaths, respectively) tended to have greater amplitudes than the mid-shelf locations (moorings A and 83 at the 30 and 40 m isobaths), presumably due to the close proximity of the Gulf Stream. The western edge of the Gulf Stream tends to follow the shelf break (75 m isobath) which is only 8.3 km from mooring 84. Therefore at the 45 m and 75 m sites a strong Gulf Stream influence is indicated. At the shelf break upper layer, along-shelf currents reached speeds of 208 $cm.s^{-1}$ toward the north. The mean flow (average over record length) was also toward the north at 54 $cm.s^{-1}$ with a 6 $cm.s^{-1}$ onshore component. The standard deviation of the subtidal flow was $\pm$ 56 $cm.s^{-1}$. Subtidal current fluctuations with amplitudes up to 100 $cm.s^{-1}$ occurred that are visually correlated with the lower layer. However, the lower layer current meter did not record over a sufficient length of time to obtain reliable statistics. At the 45 m isobath the mean flow had a northward along-shelf component of 12 $cm.s^{-1}$ and an onshore component of 2 $cm.s^{-1}$ in the upper layer. In the lower layer the mean flow was northward at 7 $cm.s^{-1}$ with a strong onshore component of 5 $cm.s^{-1}$. Subtidal standard deviations were several times the means and the fluctuations in both layers were strongly coupled visually. Mean flow at the 40 m isobath during September was to the south parallel to the isobaths at about 8 $cm.s^{-1}$. The lower current meter record length was too short for significant mean flow estimates. At mid-shelf (30 m isobath) the 4 month mean flow, averaged over July through October, was weak northerly at 1.0 $cm.s^{-1}$ with a 0.9 $cm.s^{-1}$ offshore component in the upper layer. However, a one month mean averaged over September would be southward similar to the 40 m mean flow. The bottom current meter record length was only 18 days so mean flow estimates are of questionable validity.

The temperature data from moorings 83 and 84 also indicate that the average flow was to the south during the measurements. The mean temperature was stratified both horizontally and vertically, with temperature decreasing in an offshore direction, indicating downward sloping isotherms toward the west and southerly geostrophic flow. Mean vertical stratification was 1.9°C over the 20 m separation at the 40 m isobath and 2.3°C over the 25 m distance between sensors at the 45 m isobath. Stratification varied near the shelf break from about 0 to 5°C between sensors. When current speeds increased, vertical and horizontal mixing will increase and may account for the well-mixed water column. Decreasing current speeds which can decrease mixing, plus upwelling cooler water along the bottom, increased vertical stratification. Also the semi-diurnal internal tide produced temperature fluctuations at the 17 m depth with amplitudes ranging from $\pm$ 2 to $\pm$ 5°C, which in turn resulted in large tidal variations in the stratification. This appeared to be strongest during stratified periods when the surface barotropic tide had the largest amplitudes (spring tide) (Figure 5-14). Temperature varia-

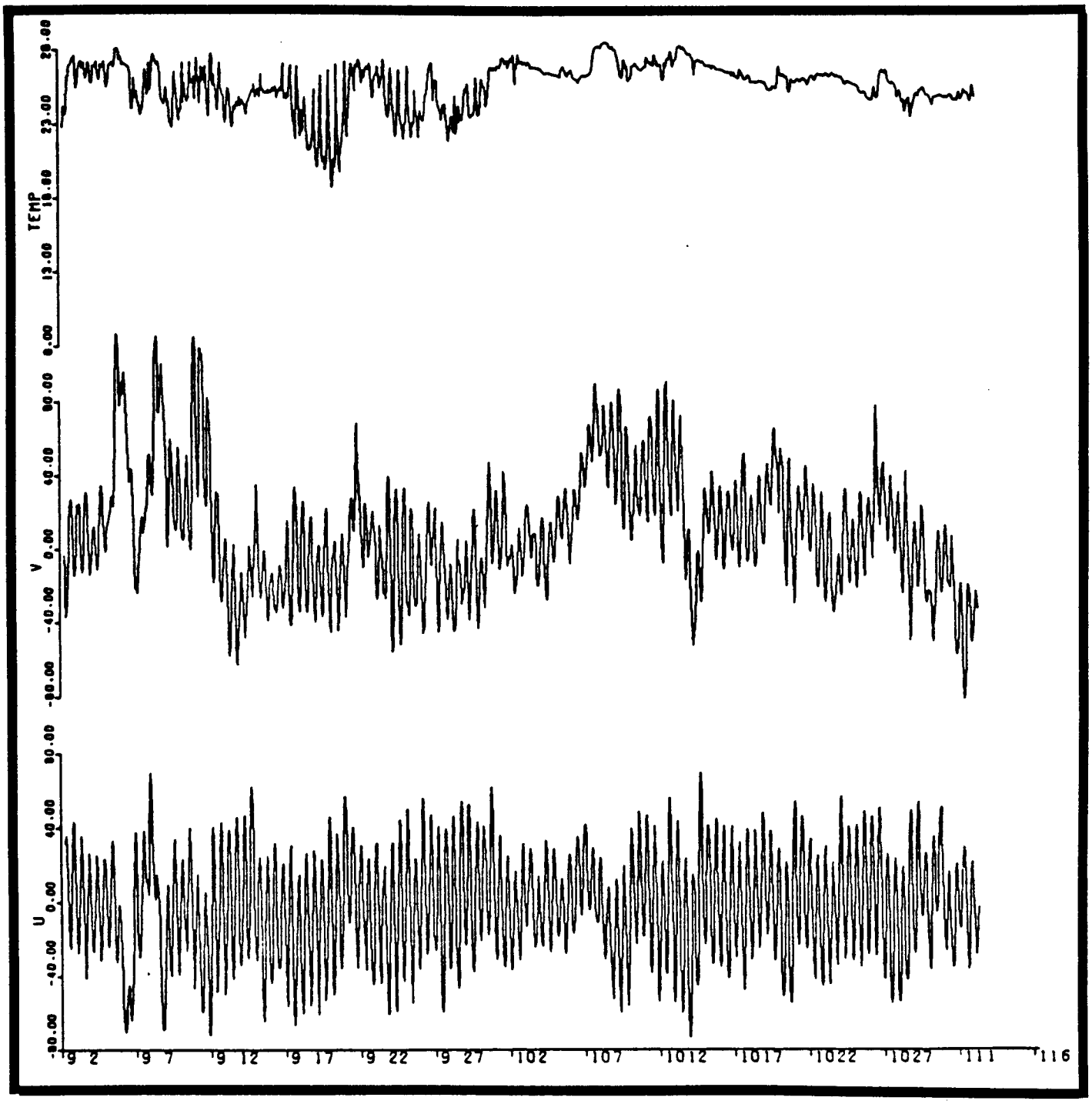

Figure 5-14. 3-HLP rotated velocity components u and v (cm/s) and temperature (^{o}C) from current meter 84 T, September and October 1977.

tions were larger near bottom than in the upper layer and increased in amplitude with nearness to the Gulf Stream. The largest variations occurred near the bottom at the shelf break with a standard deviation of about $\pm$ 4°C and a range of 17.6°C from 9.6°C minimum to 27.2°C maximum.

Temperature fluctuations were much smaller at the 40 m isobath than at the outer-shelf and showed little interstation visual correlation except at the semi-diurnal tidal period. The variation in stratification appeared to be opposite to that at 45 m. During strong northerly flow events at the outer shelf, stratification would be greatest at mid-shelf (9/6, 9/8 and 9/11, Figures 2.1-10 and 2.1-11, Volume III.

5.6.1.1.1 Tidal Fluctuations

The semi-diurnal barotropic surface tide appears to produce a large part of the current variability at all four locations (Figures 2.1-10 to 2.1-13, Volume III). The u-component has higher amplitudes than the v-component, similar to the winter findings. There is also a tendency for the upper layer to have larger tidal amplitudes ($\pm$ 30 to $\pm$ 40 cm.s^{-1}) than the lower layer ($\pm$ 20 to $\pm$ 30 cm.s^{-1}), Figure 5-14.

Spectra of 3-HLP current components from 84 T (Figure 5-15) indicate that at the 45 m isobath semi-diurnal fluctuations dominate the cross-shelf current variance; whereas in the along-shelf direction, the most energetic oscillations occurred with subtidal frequencies. The u and v spectra also verify that the cross-shelf M_2 tidal current was about a factor of 2 more energetic than the along-shelf M_2 tidal component, and that there was very little energy at the diurnal or inertial frequencies in either component. The M_2 tide in the SAB is nearly a pure Poincare wave (Redfield, 1958) which travels primarily in an onshore-offshore direction. Thus, the cross-shelf tidal component will have the greatest current amplitudes. Also maximum cross-shelf tidal currents should occur at about the mid-shelf location.

The percent of current variability due to fluctuations with periods less than 40 hours (predominantly tidal) and periods greater than 40 hours (low frequency fluctuations) were determined by taking the ratio of the 40-HLP to 3-HLP variances from Tables 5-15 and 5-16. These percentages are given in Table 5-17. In the upper layer at the shelf break (BT) about 90% of the along-shelf current variability and 60% of the cross-shelf was due to low frequency motions. Near the bottom approximately 80% of the along-shelf variance and 50% of the cross-shelf was due to low frequency events. There was a general decrease in the percent of low-frequency fluctuations and an increase in high-frequency in the onshore direction, i.e., as the distance from the Gulf Stream increased. At the 45 m isobath (84 T and 84 B) the percent variability due to low-frequency oscillations was about 60% in v and 30% in u in both layers. At the 40 m isobath (83 T) the

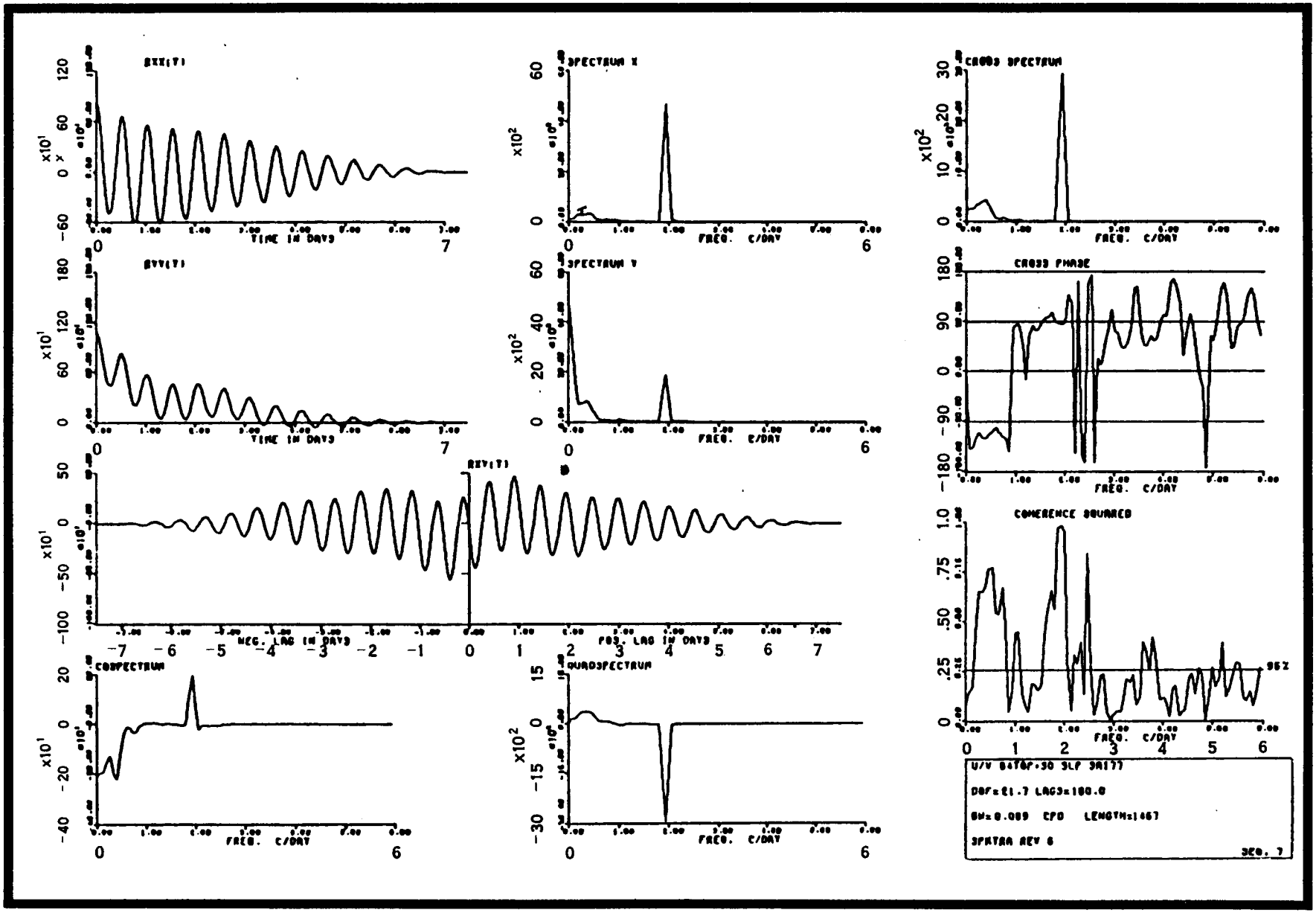

Figure 5-15. Cross-spectra of u vs. v from 3-HLP rotated time series of current meter 84-T.

Table 5-17. Percent of variance due to high-frequency (periods of <40 h, primarily tides) and low-frequency (periods >40 h) fluctuations.

Current Meter	Parameter	% Variance Due to High-Frequency Fluctuations	% Variance Due to Low-Frequency Fluctuations
AT	u	93	7
AT	v	70	30
AT	T	13	87
83 T	u	73	13
83 T	v	53	47
83 T	T	33	67
84 T	u	74	26
84 T	v	42	58
84 T	T	10	90
84 B	u	68	32
84 B	v	43	57
84 B	T	0	100
BT	u	39	61
BT	v	8	92
BT	T	5	95
BB	u	53	47
BB	v	20	80
BB	T	16	84

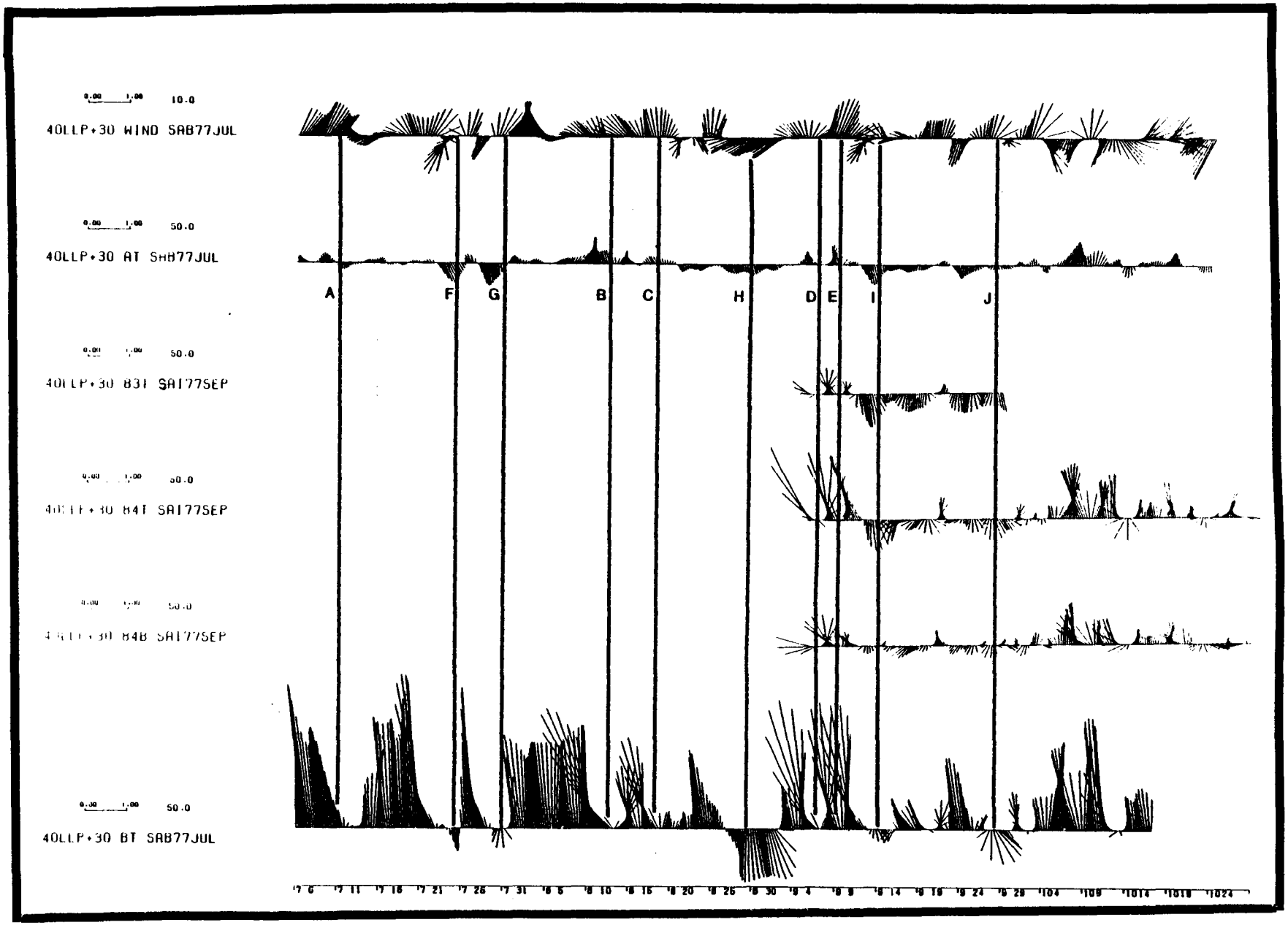

Figure 5-16. Time series of 6-hourly, rotated current and wind vectors from 40-HLP combined BLM and DOE "Summary 77" experiment. Current scale = 50 cm/s, wind scale = 10 m/s. Vertical lines are for event identification.

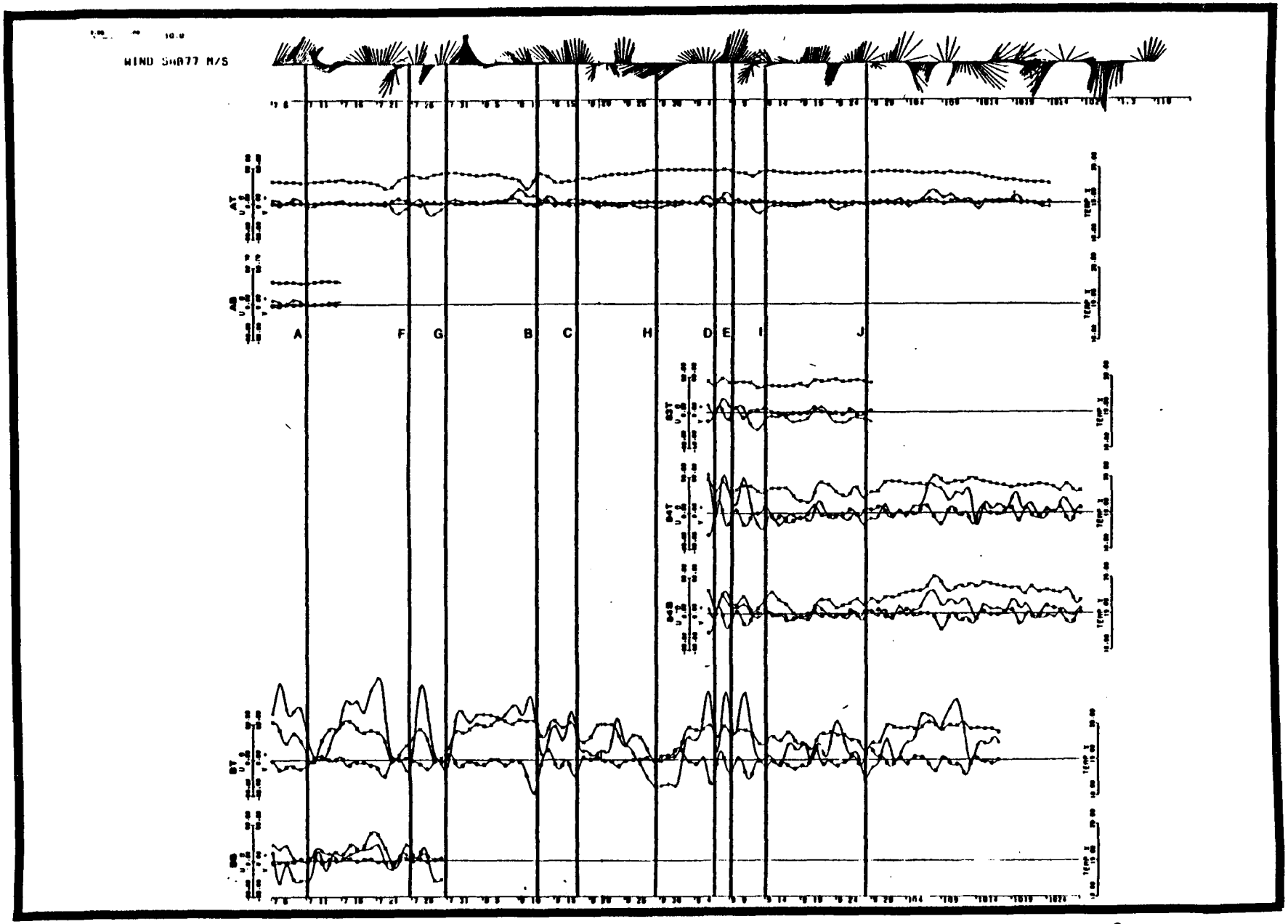

Figure 5-17. 40-HLP rotated velocity components u and v (cm/s), temperature (^{o}C) and 6-hourly vectors of Partagas winds (scale = 10 m/s) from combined BLM and DOE "Summer 77" experiment. Vertical lines are for event

contribution from low and high-frequency events was about equal in the along-shelf direction, but in the cross-shelf high frequency motions dominated (73%). At the 30 m isobath (AT) the M_2 tide was the major contributor to current variability, accounting for about 70% of the along-shelf variance and 70% of the cross-shelf. Temperature variations were primarily produced by low-frequency processes. The percent of temperature variance due to low-frequency events ranged from 67 to 100% over all current meter sites. Temperature spectra also revealed that there was very little energy at tidal and inertial frequencies (Figures 2.1-34, 2.1-37, 2.1-40 and 2.1-43, Volume III). The cross-shelf trend in variance percentages due to low and high frequency processes is very similar as found for the preceding winter (Lee, 1978). However, the percentage of low frequency variability near the shelf break was greater in the summer as was the percentage of tidal induced variance at mid-shelf locations.

5.6.1.1.2 Low-Frequency Fluctuations

Subtidal current, wind and temperature time series are displayed in Figures 5-16 and 5-17. Cross-spectra of the 40-HLP current components and temperature from moorings 83 and 84 were given in Figures 2.1-45 to 2.1-53, Volume III. Cross-spectra of 40-HLP time series from current meters AT and BT computed for the total 4 month "Summer 77" experiment are shown in Figures 5-18 to 5-23. Each cross-spectra figure displays 10 panels plus identification information in the lower righthand corner. The identification is as follows for the example u/v ATOP + 30 40LLP SAB77JUL: u is time series x of the panels and v is time series y; ATOP is current meter AT (mooring A); +30 means that the time series have been rotated 30^{o}, 40 LLP signifies a 40-h low pass filter; SAB77JUL means the area is the South Atlantic Bight and the instrument was deployed in July 1977; DOF is degrees of freedom; LAGS is number of lags; BW is bandwidth in cycles per day (CPD); length is the number of data points. The ten panels consist of: (1) autovariance function of series x (top left); (2) autovariance function of series y (below 1); (3) covariance function of series x and y, positive and negative lags (below 2); (4) autospectrum of energy density spectrum of series x (top middle); (5) autospectrum of series y (below 4); (6) co-spectrum (bottom left); (7) quadrature spectrum (bottom middle); (8) amplitude of cross-spectrum (top right); (9) phase of cross-spectrum (middle right); (10) coherence squared (bottom right). The 95% significance level for coherence squared is drawn as a solid line.

5.6.1.1.3 Time Domain.

Vector time series (Figure 5-16) reveal large amplitude, low-frequency current modulations which seem, at times, to be coherent in all current records and with the wind. Lee and Brooks, 1979, showed that during winter conditions the Georgia shelf could be divided in two flow regimes: the outer shelf where subtidal currents are

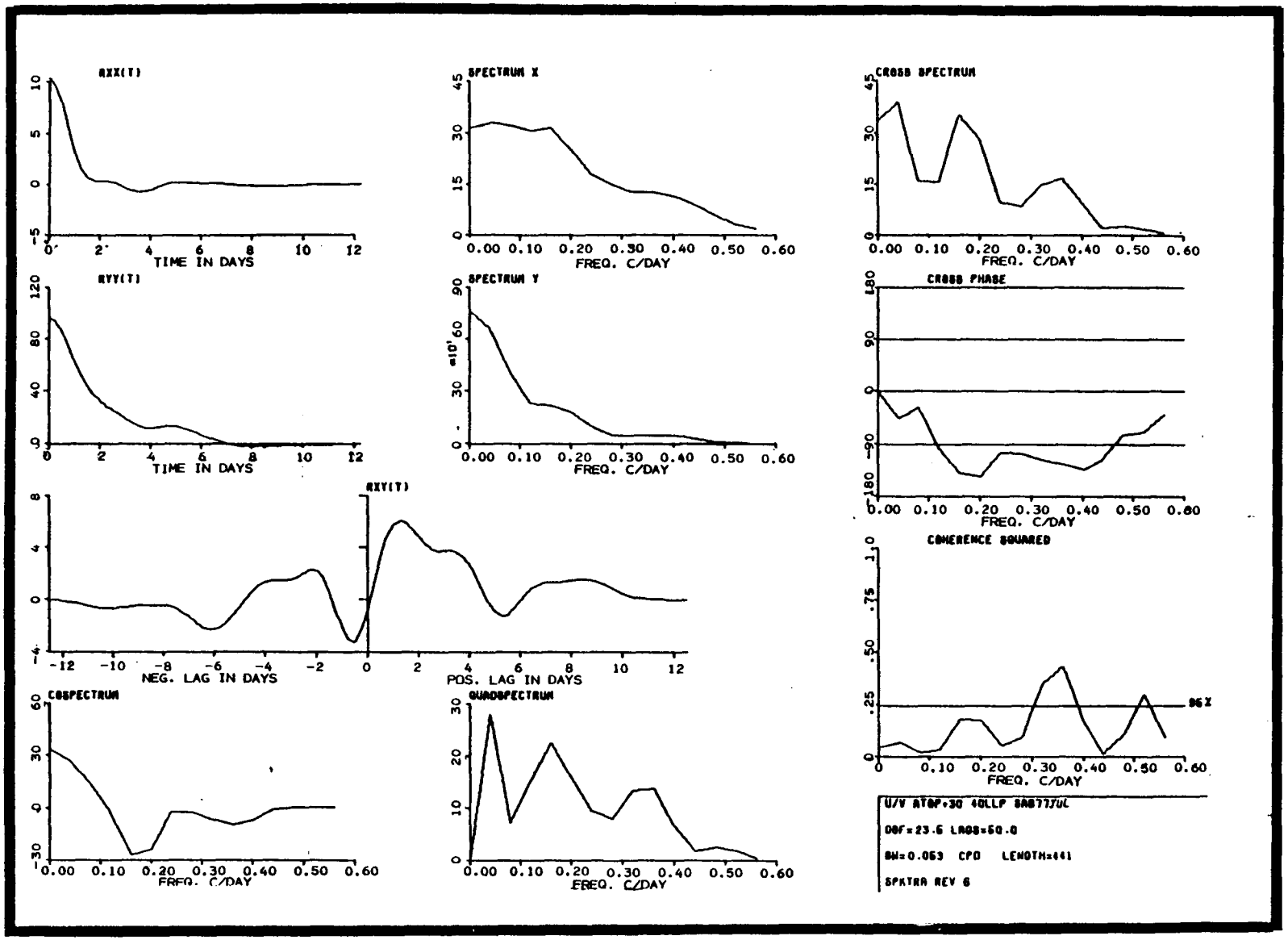

Figure 5-18. Cross spectra of u vs. v from 40-HLP rotated time series of current meter AT.

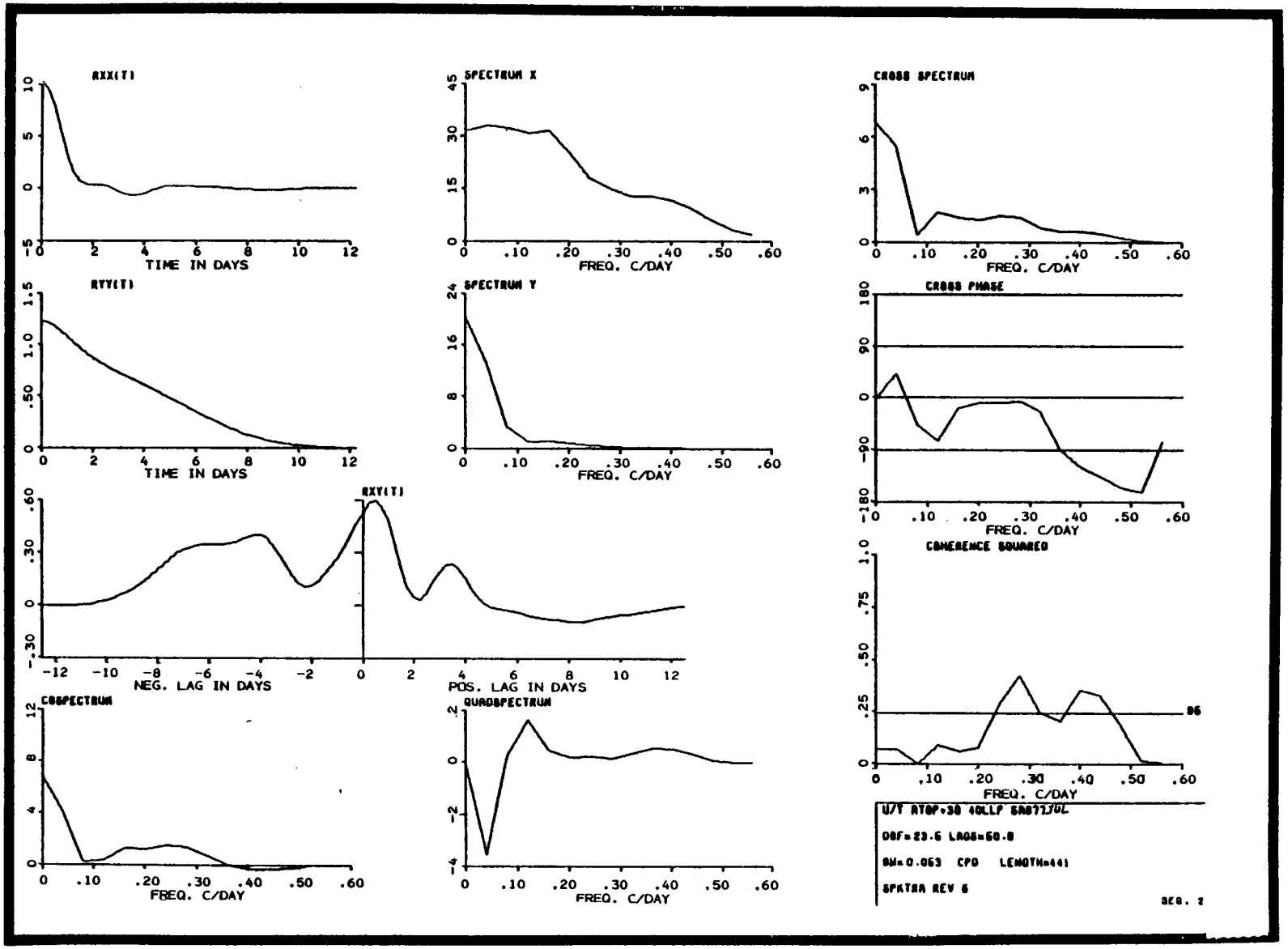

Figure 5-19. Cross spectra of u vs. T from 40-HLP rotated time series of current meter AT.

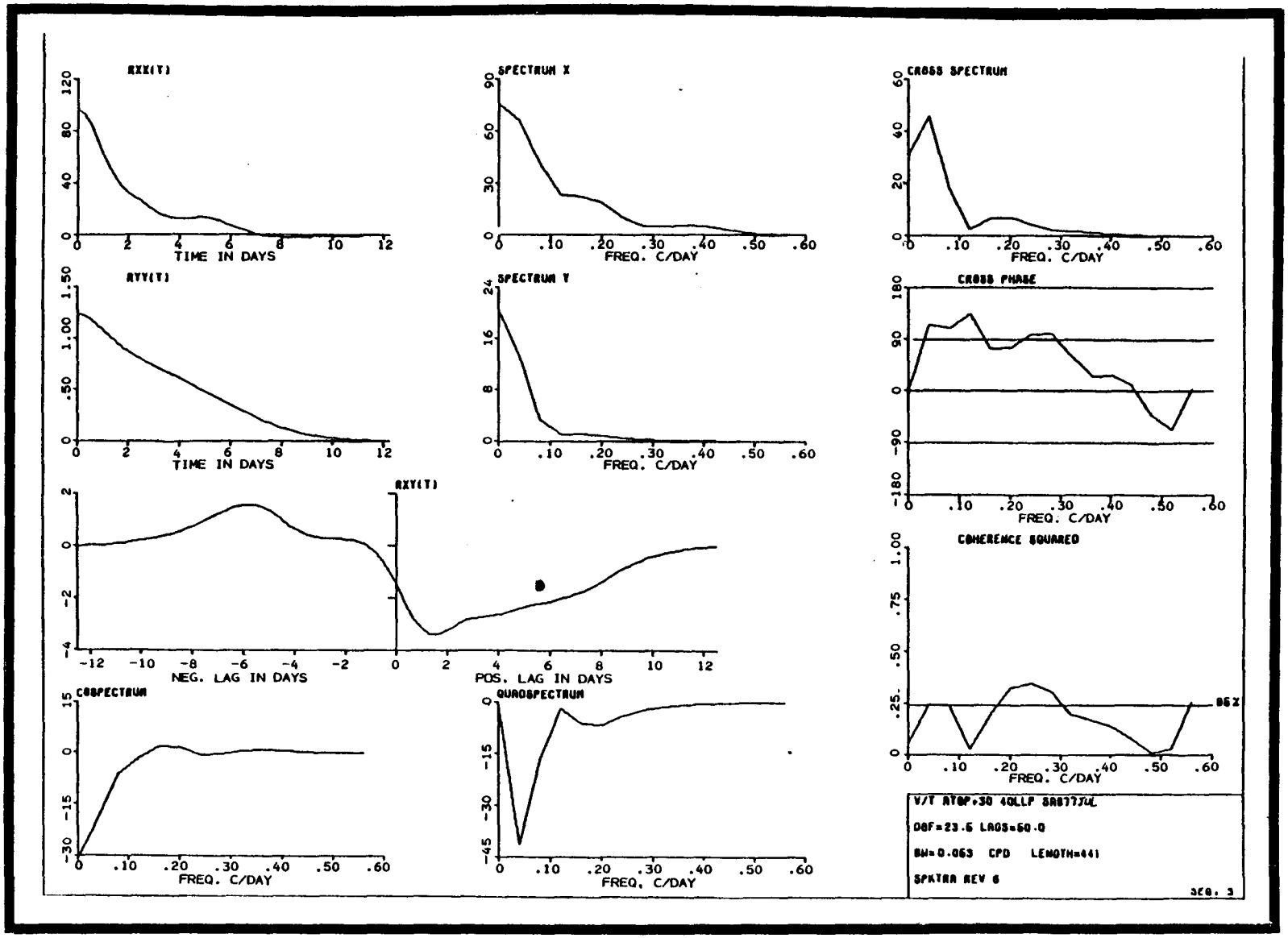

Figure 5-20. Cross spectra of v vs. T from 40-HLP rotated time series of current meter AT.

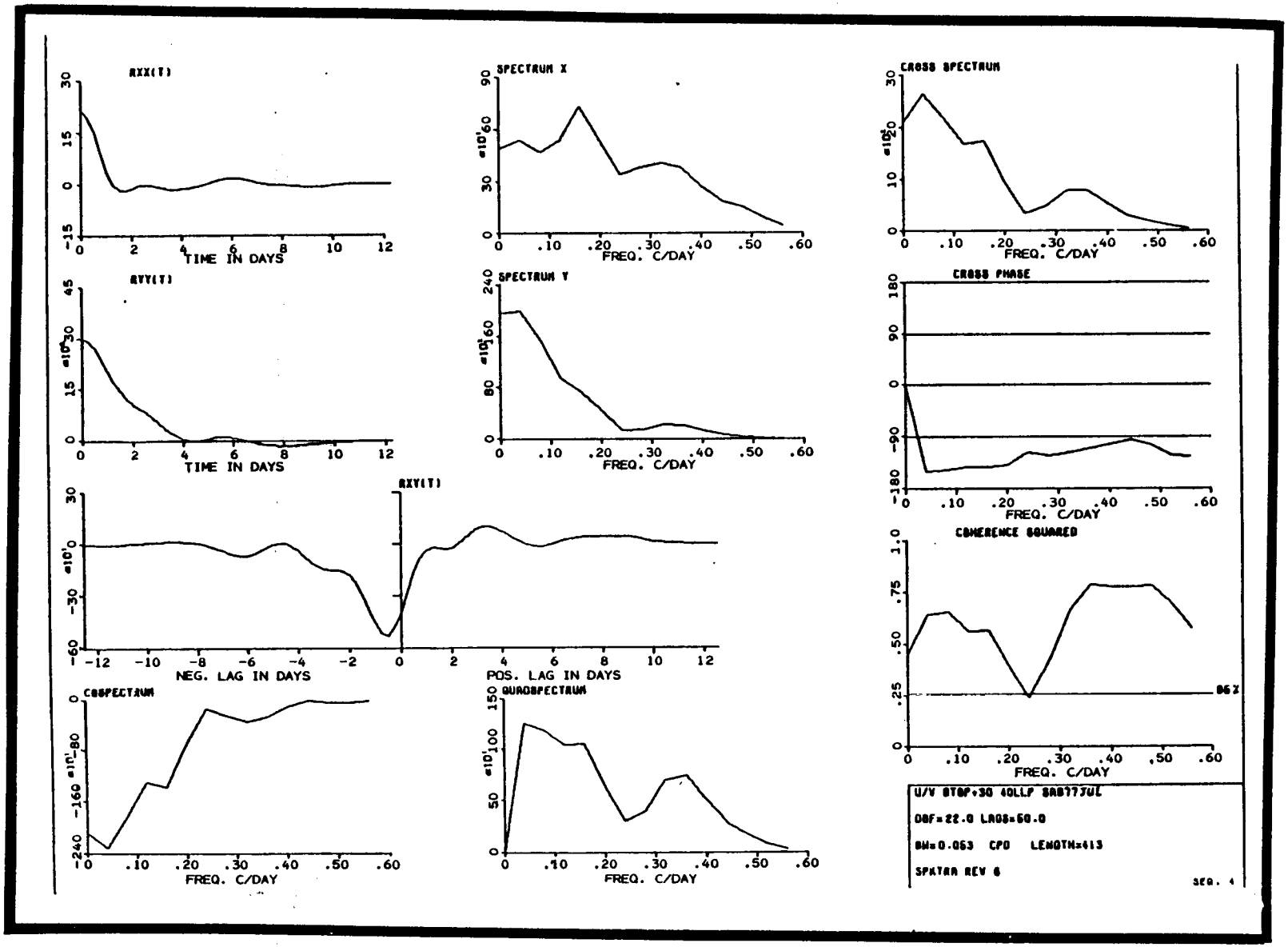

Figure 5-21. Cross spectra of u vs. v from 40-HLP rotated time series of current meter BT.

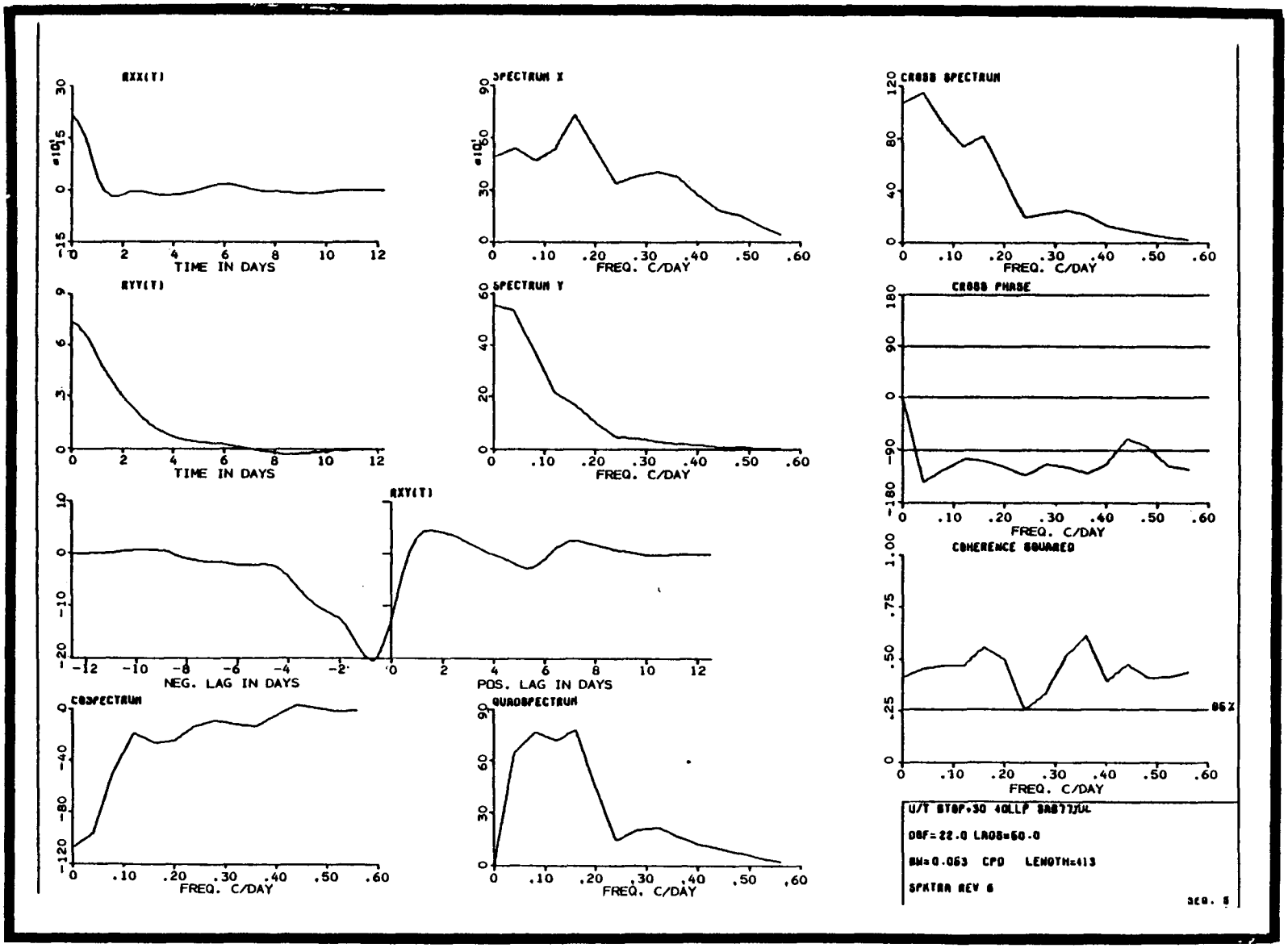

Figure 5-22. Cross spectra of u vs. T, from 40-HLP rotated time series of current meter BT.

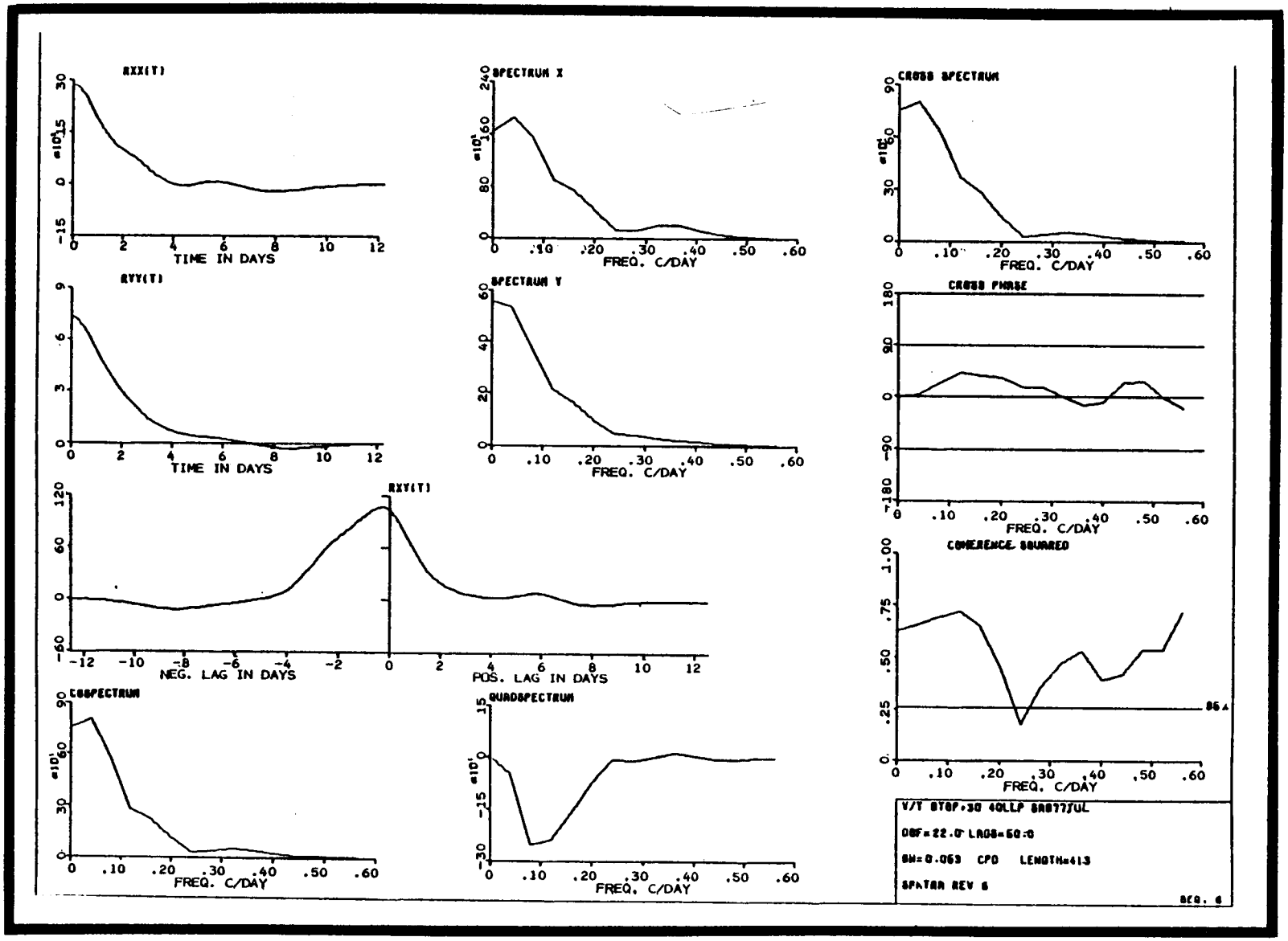

Figure 5-23. Cross spectra of v vs. T from 40-HLP rotated time series of current meter BT.

dominated by Gulf Stream meanders and cyclonic, cold-core spin-off eddies, and the mid- to inner-shelf where low-frequency flow is primarily wind-controlled. Mid-shelf currents in the summer (30 m isobath) appear to be visually well correlated with the wind, especially during July and August. The correlation still appears significant in September and October, but there are exceptions around September 19-20 and 25-30, October 6-9 and 11-14. Shelf break currents display strong northward flow events with speeds up to 170 $cm.s^{-1}$ typical of onshore Gulf Stream meanders (Lee, 1978) and flow reversals which were shown to be produced by the passage of cyclonic, spin-off eddies (Lee, et al., 1979). However, these shelf break current variations appear to be more strongly coupled to similar fluctuations at the other current meter locations than was the case during the winter (see event lines in Figure 5-16).

Bumpus (1973) concluded from drifter data that the mean flow should be toward the south during August and September in the SAB. The subtidal current measurements show that flow over the mid- to outer-Georgia shelf in the summer is strongly event dependent, and southward (northward) flow episodes usually coincide with southward (northward) wind events, as was the case during winter (Figure 5-16). The mean flow at mid-shelf averaged over the total July-October recording period was weak northerly at 1.0 $cm.s^{-1}$ with an offshore component of 0.9 $cm.s^{-1}$. However, prolonged periods of southward flow did occur during a 16-day period from August 20 to September 4 and a 20-day period from September 11 to 30, which appears to be similar to the findings by Bumpus. Winds were weak and variable over these periods, indicating that the persistent southward flow was probably not wind induced. Since the shelf is known to be both horizontally and vertically stratified in density during the summer, due to river run-off and atmospheric heating, the most likely cause of persistent southward flow is geostrophic adjustment to the density field. This will be addressed in more detail when the BLM hydrographic data are available.

5.6.1.1.4 Frequency Domain.

Energetic, broad-banded spectrum peaks at periods of 2.5 to 3 and 5 to 10 days occurred in the cross-shelf current component of all current meters. Along-shelf currents and temperature tend to have red spectra (i.e. spectra where the energy is increasing with decreasing frequencies, or increasing with increasing periods, without any significant energy peaks, i.e. with a nearly constant slope). Most of the energy in these spectra is associated with fluctuations occurring with periods longer than 5 days. The coherence between along-shelf and cross-shelf velocity components at the shelf break is high in the 2 to 3 and 5 to 20 day period bands with u leading in phase by about 90^{o}, which is indicative of progressive wave-like motion (Figure 5-21). The negative co-spectra of u'v' and u'T' in these period bands suggest that frictional

processes in the outer-shelf region tend to transfer momentum and heat from the Gulf Stream to the shelf similar to winter findings (Lee, 1978). At the 30 m isobath velocity components were significantly coherent near 2 and 3 day periods only with u leading v by about 90° in phase (Figure 5-18). This is different from the winter, when velocity components were also coherent at the 5 day period with near 0 phase.

Cross-shelf coherence and phase were computed for u, v and T 40-HLP series from all combinations of upper layer current meters over the 53 day period in September and October of the combined BLM and DOE array. In addition, the AT and BT combinations were recomputed over the 103 day period (July-October) of the total "Summer 77" experiment. For the longer records v was found to be significantly coherent over the 45 km separation between AT and BT in period bands of 3, 5 to 7 and 12 to 25 days with the mid-shelf station leading in the 3 and 12 to 25 day band and nearly 0 phase for the 5 to 7 day band. Surprisingly u and T were also coherent at periods of 2 to 3 days and 5 to 8 days for u, and 12 to 25 days for T with the mid-shelf location leading in all cases. During the previous winter cross-shelf currents were found to be uncorrelated for cross-shelf separation distances greater than 17 km and temperature was not coherent even at 17 km scales, suggesting that the effect of traveling disturbances along the shelf break may penetrate to mid-shelf during summer stratified conditions.

During the "short-term" combined array along-shelf current fluctuations were coherent between AT and BT at the 8 to 16 day period band only. Cross-shelf currents were coherent at periods of 2.5 days and temperature at 3.2 day periods. Again, fluctuations occurred first at the mid-shelf location for all 3 parameters. Interstation cross-shelf coherence generally increased as station separation distance decreased. Coherence of along-shelf currents was very high for all periods longer than 2 days between AT and 83 T (19 km separation), AT and 84 T (38 km) and 83 T and 84 T (19 km), with the shallower station leading in all cases. The coherence was still significant between stations BT and 84 T (8 km) and BT and 83 T (27 km) with near 0 phase, but a gap in coherence occurred over periods of about 4 to 6 days. Cross-shelf currents were significantly correlated over all of the above separation distances for the period band of 2 to 10 days with near 0 phase. Cross-shelf coherence and phase of temperature is more complicated than current for it varied more with frequency and separation distance. The coherence was high between BT and 84 T in the period bands of 2 to 2.5 and 4 to 16 days, but was significant between BT and 83 T and 84 T and 83 T at periods of 2 to 2.5 days only. Temperature was not coherent at any period greater than 2 days between 84 T and AT and was only slightly coherent at periods of 2 and 3.3 days between 83 T and AT.

The vertical coherence between upper and lower current meters on mooring 84 was high for u, v and T at all periods greater than 2 days with the bottom current meter leading in v and near 0 phase for u and T. The record lengths of the bottom current meters were too short at the other moorings for statistically meaningful cross-spectra computations.

5.6.1.1.5 Wind Influence

Visual inspection of the subtidal vector time series (Figure 5-16) indicates that there was a considerable amount of coherency between wind and mid-shelf currents. Cross-spectra of along-shelf wind and current from the upper current meters for the period of short-term measurements and the longer "Summer 77" period are shown in Figures 5-24 to 5-29. Cross-spectra of along-shelf wind and current from the mid-shelf location (AT and 83 T) show significant coherence over the period band of 3 to 10 days with the wind leading by less than one day (Figures 5-24 and 5-29). At the 40 m isobath (83 T) there was an additional coherent peak at about the 2-day period. Along-shelf currents at the outer-shelf locations (84 T and BT) did not show any significant coherence with the wind (Figures 5-26 and 5-27). Along-shelf currents at mid-shelf (AT) recorded over the longer period showed a similar high correlation with the wind as during the "short-term" measurements (Figure 5-28). Along-shelf currents at the shelf break (BT) also show a similar lack of coherence with along-shelf wind during the short and long computation periods (Figure 5-29).

A conceptual Ekman frictional equilibrium model was used to explain a large portion of the subtidal current and coastal sea level response to wind forcing on the Georgia shelf in the winter (Lee and Brooks, 1979). Wind stress is weaker during the summer but the current response still appears to be similar to the winter case. Therefore the following frictional equilibrium model, illustrated in Figure 5-30, may account for a significant part of mid- to inner-shelf current variability throughout the year. Future analyses using coastal sea level data should be able to determine this. Northward wind stress, which occurs with the advance of a cold front, produces a transient mass flux in the surface layer directed away from the shore, causing sea level to fall along the coast and establishing an onshore pressure gradient which is in approximate balance with the resulting northward geostrophic interior flow over the shelf. A similar response was observed in the winter in the Mid-Atlantic Bight by Beardsley and Butman, 1974, and Scott and Csanady, 1976. The time necessary to establish frictional equilibrium flow at the 30 m isobath is less than one inertial period, at which time the surface wind stress is nearly balanced by an opposing bottom stress and the cross-shelf slope is balanced by an alongshore barotropic flow.

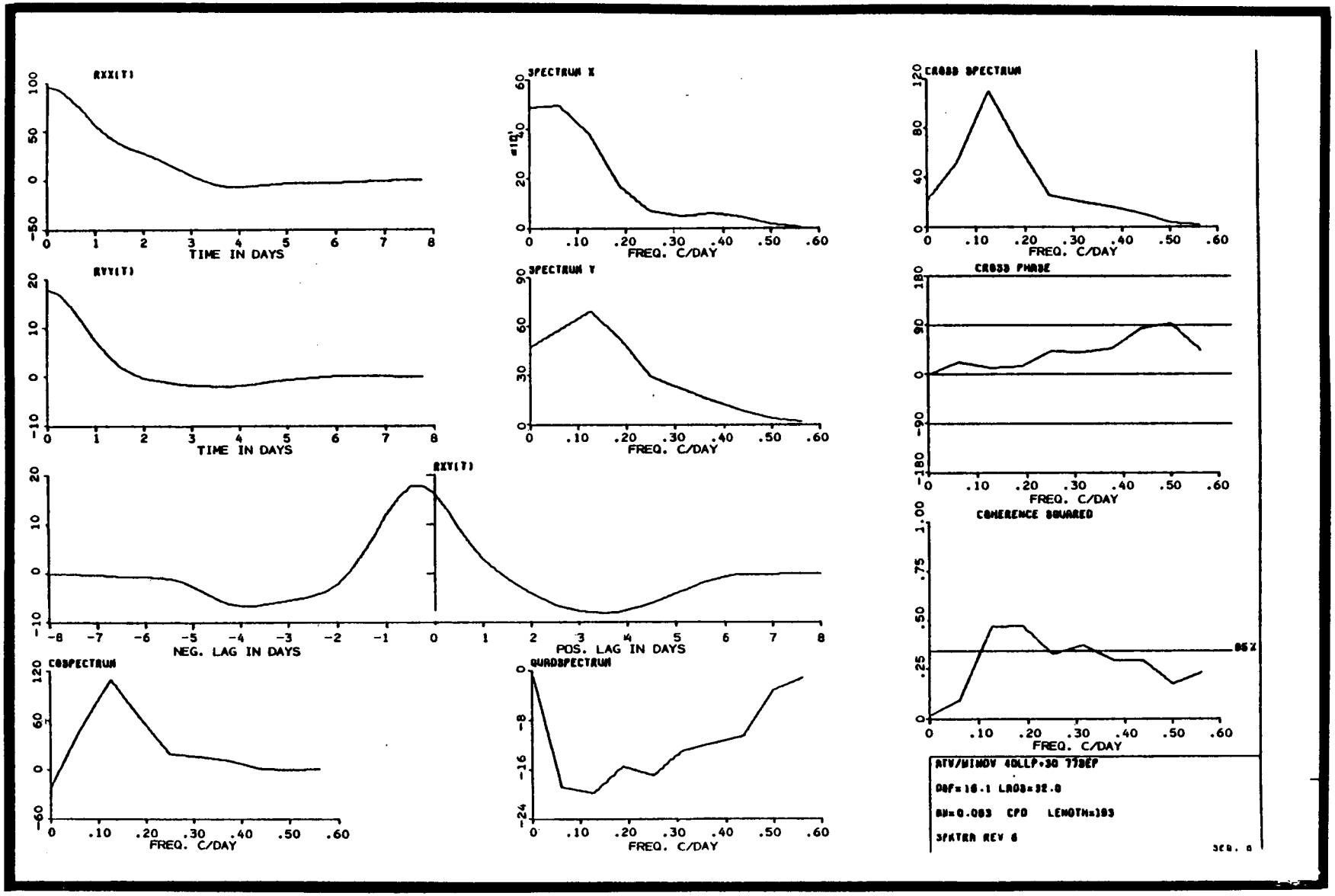

Figure 5-24. Cross spectra of 40-HLP v component rotated time series from current meter AT and Partagas winds over "short-term" measurements.

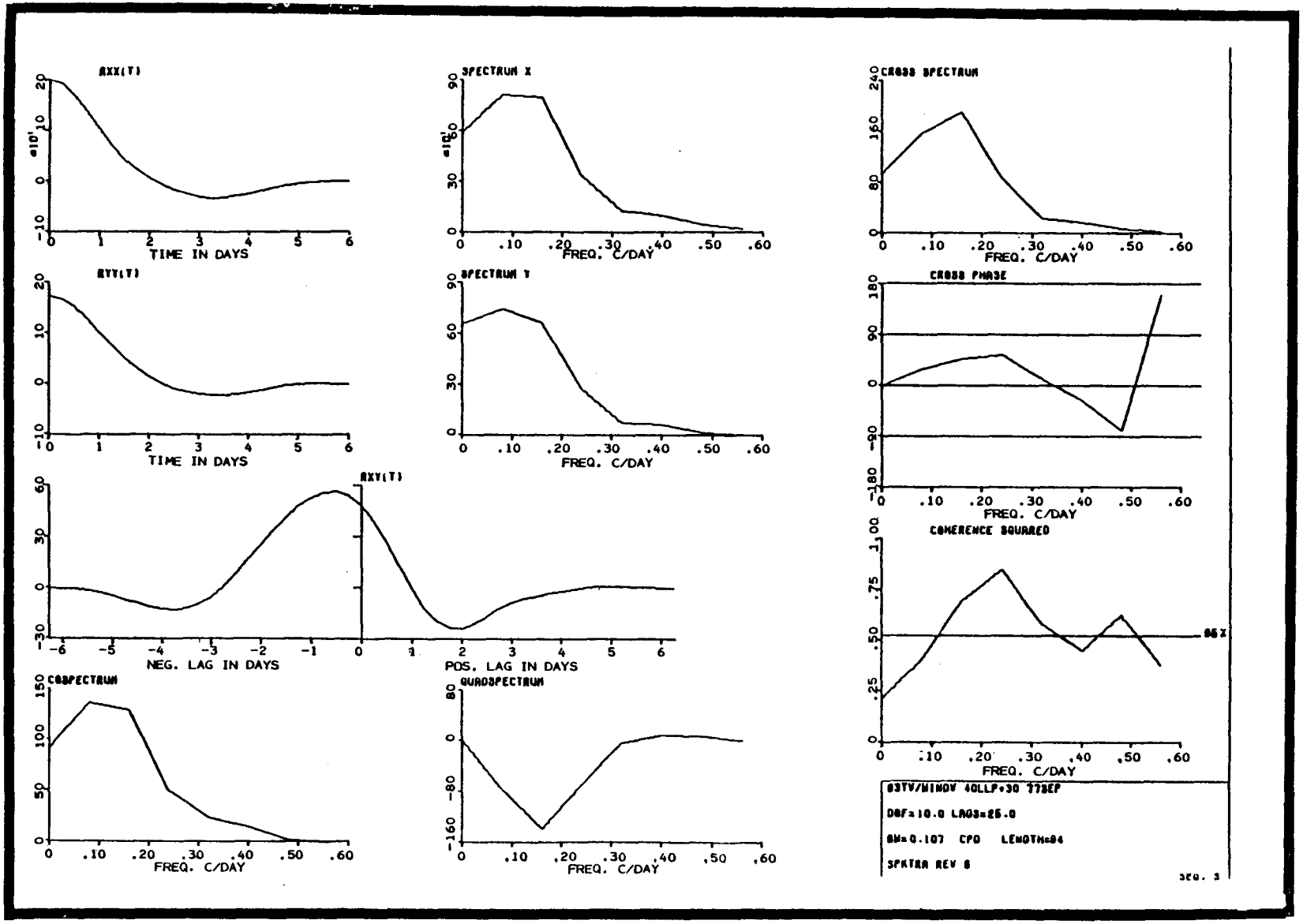

Figure 5-25. Cross spectra of 40-HLP v component rotated time series from current meter 83 T and Partagas winds over "short-term" measurements.

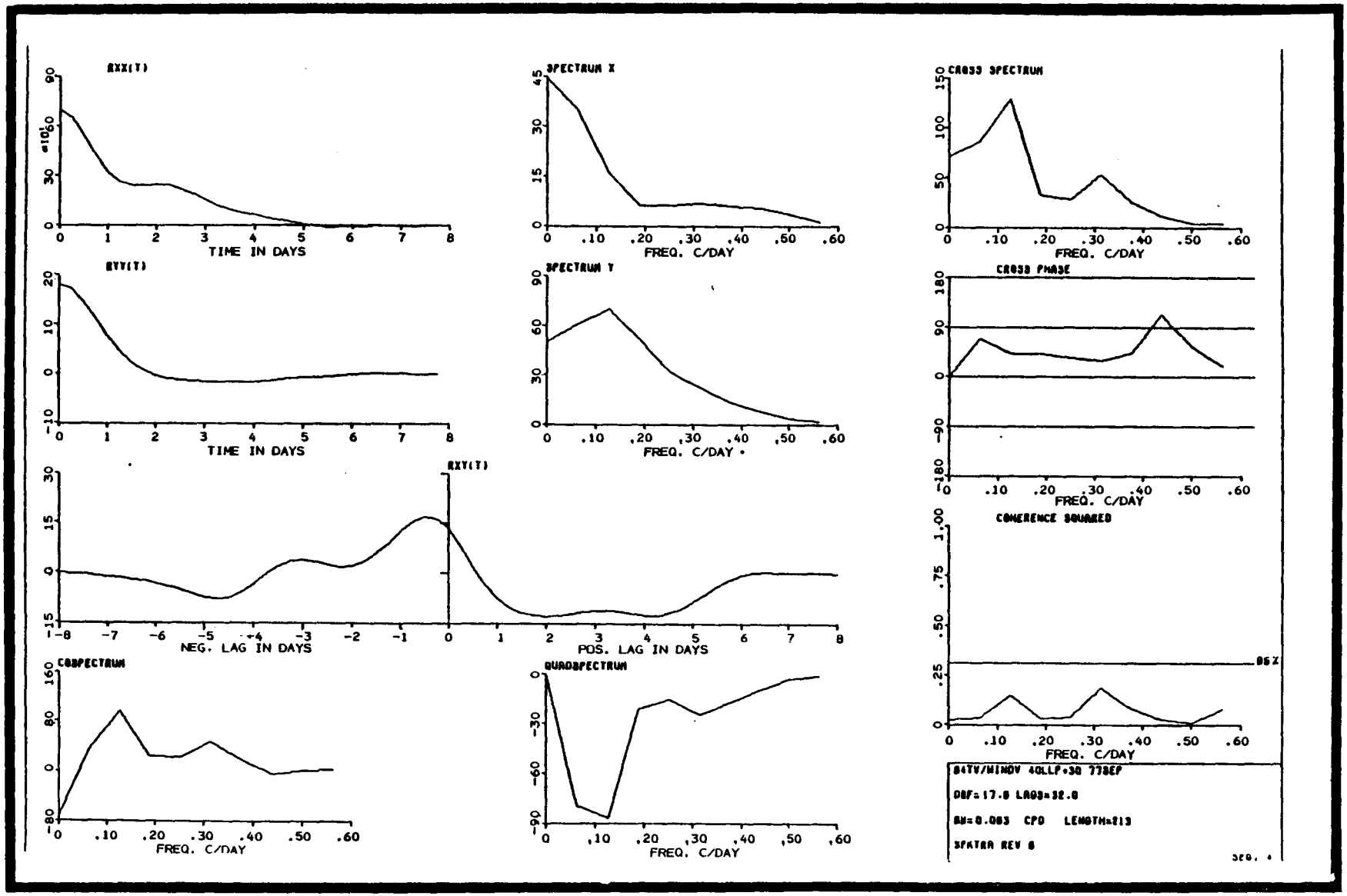

Figure 5-26. Cross spectra of 40-HLP v component rotated time series from current meter 84 T and Partagas winds over "short-term" measurements.

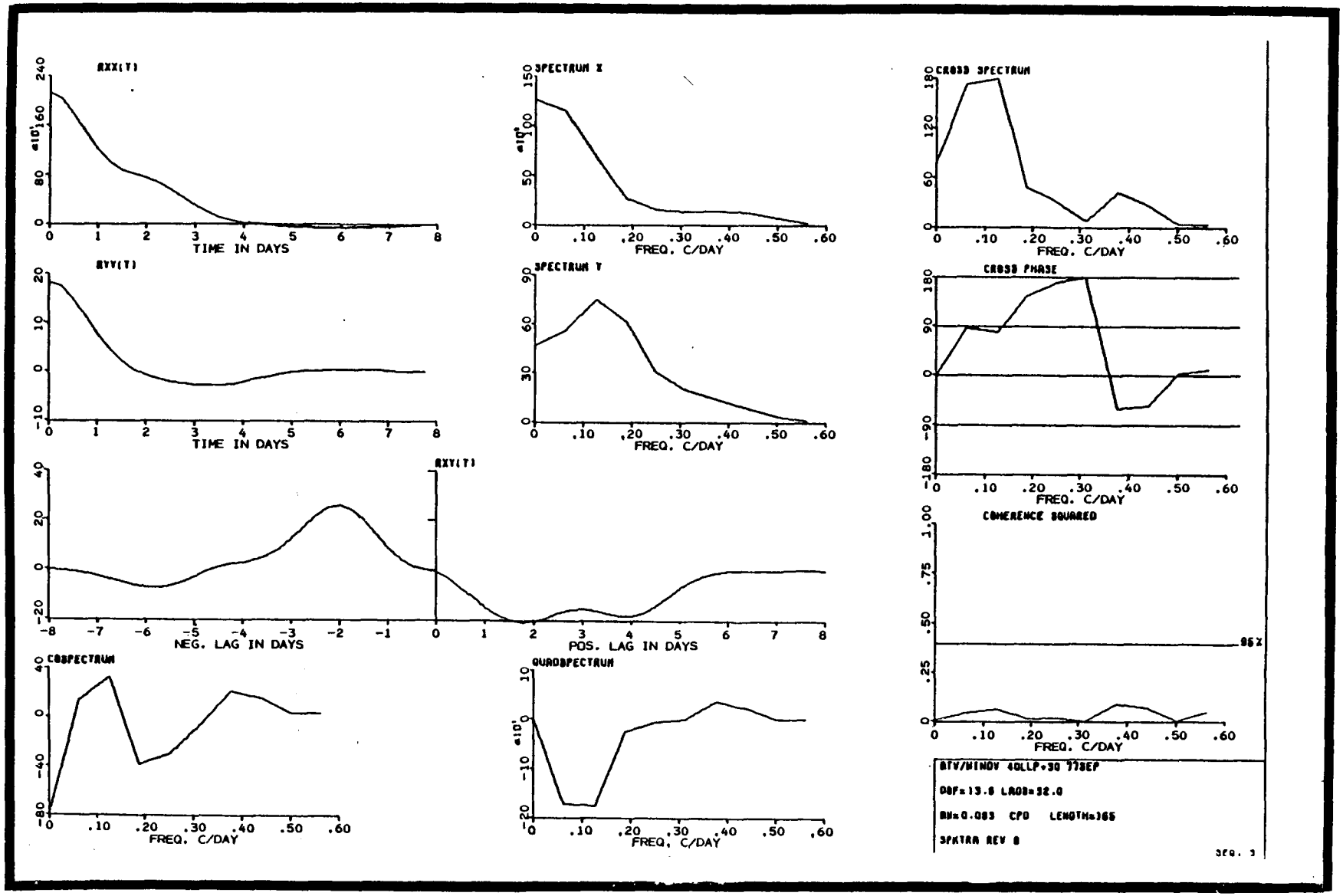

Figure 5-27. Cross spectra of 40-HLP v component rotated time series from current meter BT and Partagas winds over "short-term" measurements.

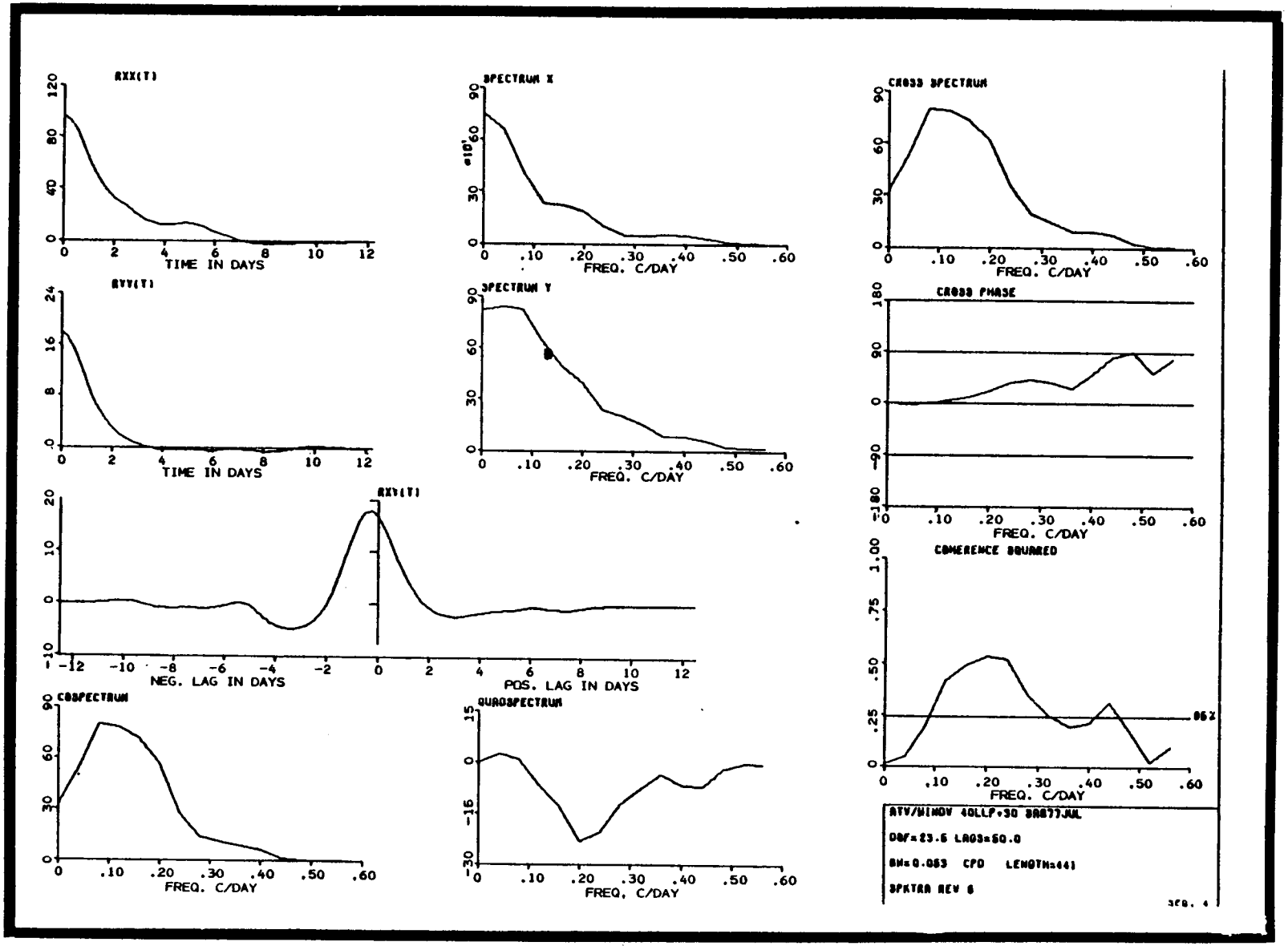

Figure 5-28. Cross spectra of 40-HLP v component rotated time series from current meter AT and Partagas winds over "Summer 77" experiment.

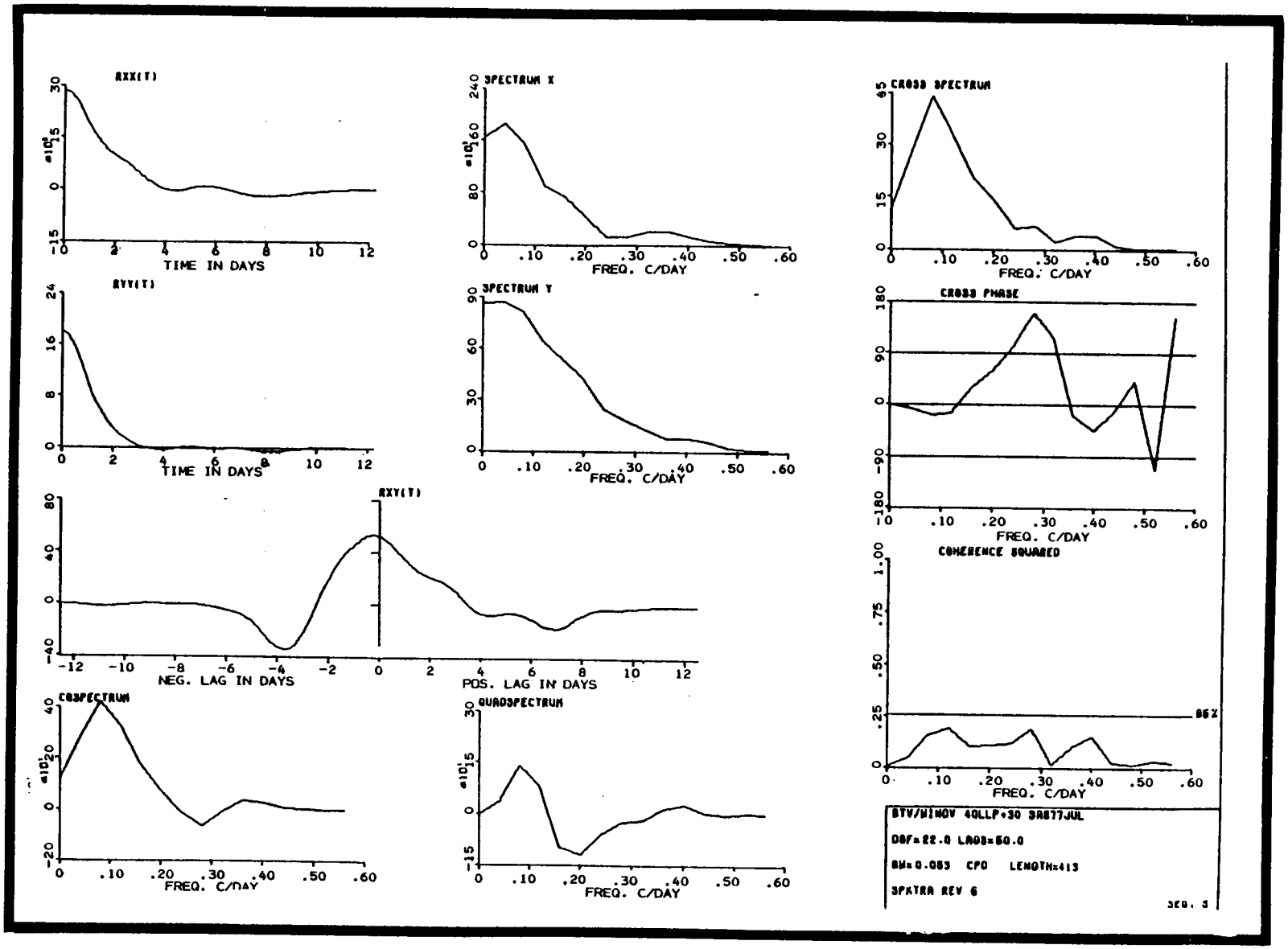

Figure 5-29. Cross spectra of 40-HLP v component rotated time series from current meter BT and Partagas winds over "Summer 77" experiment.

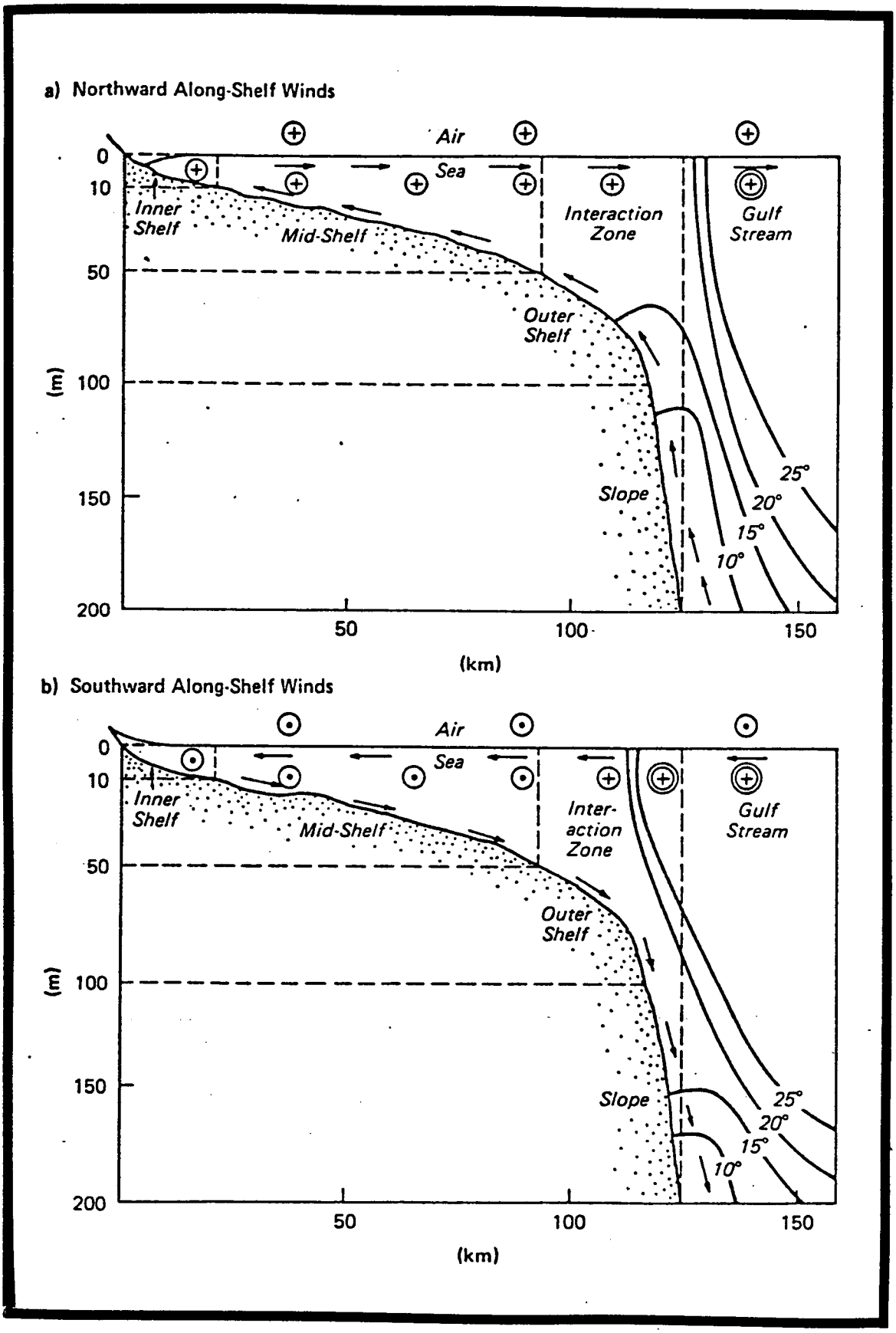

Figure 5-30. Schematic of shelf waters response to passage of a cold front in the Georgia Embayment.

Along the shelf break the offshore surface Ekman flux associated with northward winds may at times generate an eastward meander of the Gulf Stream cyclonic front and upwelling of cooler, deeper Gulf Stream waters along the slope. Since the Gulf Stream is displaced further offshore, a decrease in northward alongshore current speed occurs nearly simultaneously with the decrease in temperature brought about by upwelling. This is different than a pure wind-driven upwelling response, which in the absence of a Gulf Stream would generate a baroclinic alongshore jet near the shelf break and an increase in northward current speed.

Southward wind episodes produce the opposite response, i.e., onshore mass flux in the surface Ekman layer and offshore flux in the bottom layer, set-up of sea level along the coast, southward geostrophic flow in the shelf interior waters, an onshore Gulf Stream meander and associated downwelling, causing increased temperatures and northward current speeds along the shelf break.

5.6.1.1.6 Gulf Stream Influence

Winter studies of circulation on the Georgia shelf have shown that the large amplitude subtidal current and temperature fluctuations which occur in the outer-shelf region are primarily produced by Gulf Stream wave-like meanders and spin-off eddies (Lee, 1978; Lee and Brooks, 1979; Lee, et al., 1979). During summer conditions similar large amplitude modulations are observed in the outer-shelf subtidal data even though the intensity of wind events is considerably reduced (Figures 5-16 and 5-17). However, shelf break fluctuations in the summer were more strongly coupled to flow variations in the mid-shelf region. Numerous investigations have shown that the western edge of the Gulf Stream meanders laterally across the shelf break in the SAB as the Stream follows its path northward (Webster, 1961; Richardson, et al., 1969; Stefansson, et al., 1971; Atkinson, 1977). The cross-shelf horizontal scale of meanders is about 25 km in the region from Cape Canaveral to Charleston and approximately 100 km between Charleston and Cape Hatteras, due to amplification by the "Charleston Bump" (Legeckis, 1979). Shelf-edge Gulf Stream meanders are observed to propagate northward more slowly than the mean Gulf Stream speed and frequently evolve into elongated "shingle" structures (von Arx, et al., 1955; Legeckis, 1975), indicative of the formation of "spin-off eddies" (Lee, 1975; Stumpf and Rao, 1975; Lee and Mayer, 1977). Observations of Gulf Stream meanders reveal many of the characteristics predicted for both unstable barotropic waves (Niiler and Mysak, 1971) and unstable baroclinic waves (Orlanski, 1969), i.e., periods of about 10 days and wavelengths of 100-300 km. In the Florida Straits spin-off eddies have been shown to occur with similar time scales, resulting in a cyclonic rotation of current vectors and transient southward flow over the outer-shelf (Lee, 1975; Lee and Mayer, 1977). To fully explain summer shelf break variability requires a significant amount of supporting data, such as hydro-

graphy, satellite sea surface temperature, coastal winds and sea level, which are not at this time ready for data synthesis. Therefore, the following discussion will be limited to the current meter data at hand.

5.6.1.1.7 Gulf Stream Meanders.

The Gulf Stream meander signature in current and temperature records from the Georgia shelf break during winter conditions was observed to consist of nearly simultaneous decreasing (increasing) northward current speed and temperature for offshore (onshore) meanders (Lee, 1978). As the Gulf Stream surface front moves offshore, upwelling of cool, deeper Gulf Stream water occurs along the slope, as illustrated in Figure 5-31a. Since the Gulf Stream is further offshore a decrease in northerly along-shelf current occurs. Thus during an offshore meander both northerly current speeds and temperature will decrease near the shelf break throughout the water column. During an onshore meander the Gulf Stream cyclonic front moves closer to the shelf break, increasing the northerly current speeds there. Therefore, an onshore meander causes an increase in northward along-shelf currents and temperature of the water column in the vicinity of the shelf break, as represented schematically in Figure 5-31b. The meander may be either directly wind-forced as suggested by Webster, 1961, off Onslow Bay, or due to a southward propagating wave (shelf wave) that may have initially been wind generated (Brooks and Mooers, 1977). When the speed of the southward propagating shelf wave is less than the mean northward speed of the Gulf Stream, it becomes advected northward so that the observed direction is to the north in the upper layer near the shelf break. The signature in a current/temperature record from the shelf break would be the same for either process. Examples of the meander signature are shown in Figures 5-16 and 5-17 as events A-E. The simultaneous decrease of temperature and northward current speed in the outer shelf appears to occur following northward wind episodes for each meander event, suggesting that the offshore Ekman transport associated with northward winds may trigger Gulf Stream meanders, similar to winter findings (Lee, 1978).

5.6.1.1.8 Spin-off Eddies.

Due to the large horizontal and vertical shear of the Gulf Stream cyclonic front, wave-like disturbances become rapidly unstable and grow in time. Both barotropic (Niiler and Mysak, 1971) and baroclinic (Orlanski, 1969) instabilities are possible in the Florida Current. The fastest growing waves travel north with periods around 10 days and wavelengths of 150-220 km. Maximum amplitudes are reached in about one week. Some disturbances eventually grow into cyclonic "spin-off eddies" (Lee, 1975; Lee and Mayer, 1977; Lee, et al., 1979), which produce tongue-like southward extrusions of Gulf Stream water onto the shelf. Such a spin-off eddy is schematically

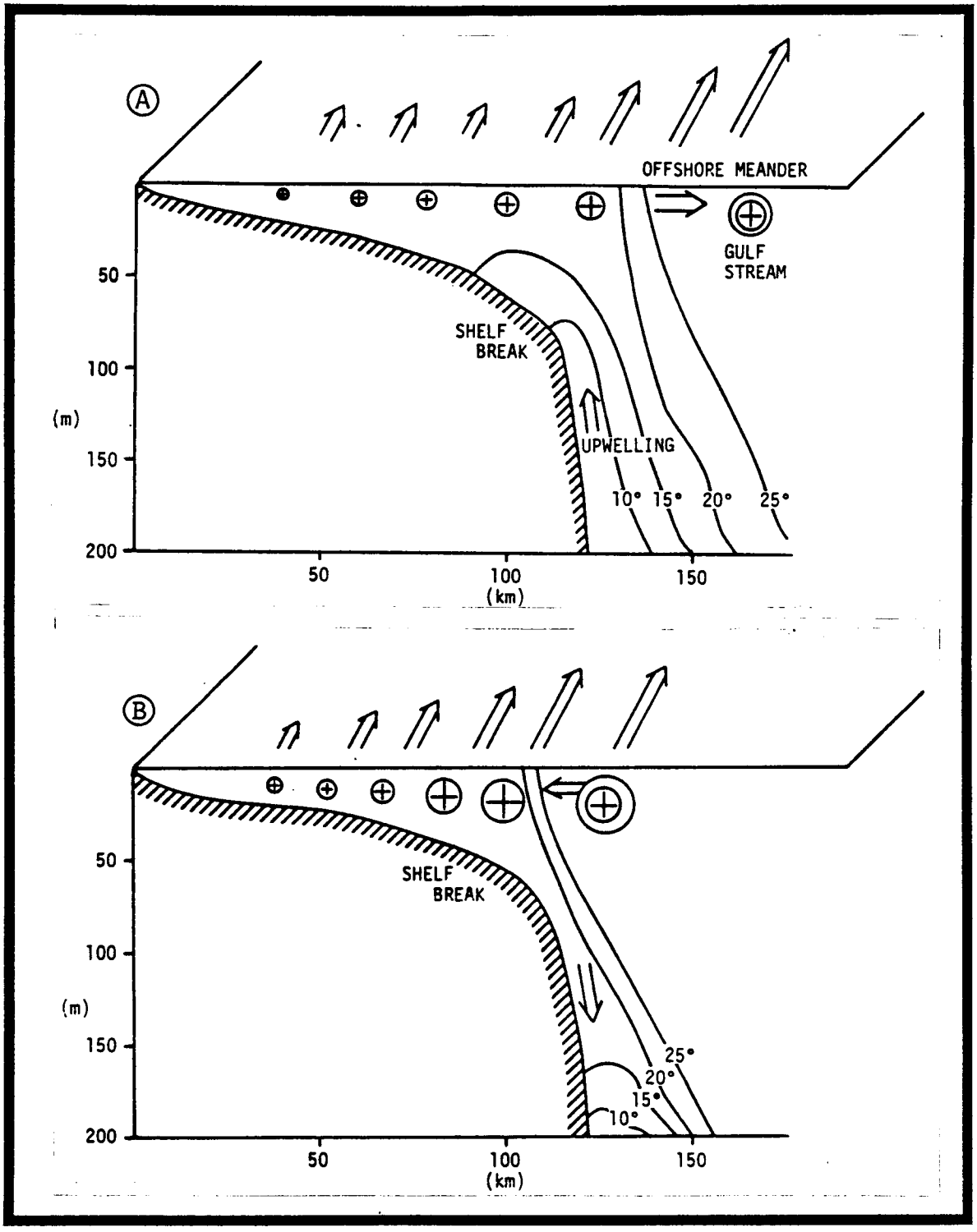

Figure 5-31. Schematic of offshore (Figure 5-31a) and onshore (Figure 5-31b) Gulf Stream meanders.

shown in Figure 5-31. Eddy evolution has been observed in satellite images by Legeckis, 1975, and Stumpf and Rao, 1975. The most recent observations of eddy development occurred in April 1977 which marked the first time an edge-eddy has been observed simultaneously with satellite, hydrography, chemistry and current meter observations (Lee, et al., 1979).

Eddies are advected to the north along the shelf break by the Gulf Stream. The signature of an eddy passage in a current/temperature record is a cyclonic rotation of current direction with u leading v by about 90^{o}. During times of maximum southward flow the temperature in the upper layer may increase if it is located in the warm Gulf Stream waters flowing southward over the shelf, and near bottom temperatures should decrease due to geostrophic induced upwelling in the eddies central cold core. The subtidal current and temperature data from the "Summer 77" experiment indicate that 6 eddies occurred during the 103-day low-frequency records or nearly 1 eddy every 2 weeks on the average. Examples of these eddies are shown by event lines F - J in Figures 5-15 and 5-16. In each case the cyclonic flow reversal in the outer shelf followed an anti-cyclonic wind reversal (northward to southward winds). The lag time was 1 day for events F, H and I, 2 days for event G and about 4 days for J. This suggests that eddy events may at times be wind generated if conditions are favorable. The exact nature of these conditions is not clearly understood, but it appears that northward flow at the shelf break begins to decrease by a northward wind stress generating an offshore meander of the Gulf Stream and if this is soon followed by southward winds of sufficient strength then the flow may reverse, a process which transforms a meander into an eddy. However, at present these ideas are pure speculation. Cyclonic flow reversals at the mid-shelf stations occurred 2 to 7 days prior to those at the outer shelf and appear to be a frictional equilibrium response to the southward wind events.

Eddy event I was chosen for more detailed investigation, for there was considerable supporting hydrographic data collected during this period by the BLM benchmark time series hydrographic cruises. The velocity and temperature variations associated with this event are shown in Figures 5-32, 5-33, 5-34. The event is observed as a cyclonic low-frequency flow reversal that is coherent at all recording locations. Strong semi-diurnal tidal currents are clearly shown superimposed upon the low-frequency reversal (Figure 5-32). The reversal appears to have occurred first at the 40 m isobath (83 T) towards the end of September 11. Subtidal current vectors indicate that southward currents in the event had a cross-shelf maximum at the 40 and 45 m isobaths of about 40 $cm.s^{-1}$ (Figure 5-33). The large decrease in near bottom temperature at the outer-shelf which accompanied the cyclonic flow reversal suggests that the event was a cyclonic, cold-core spin-off eddy (Figure 5-34). The near bottom temperature decrease was most likely produced by upwelling of cooler,

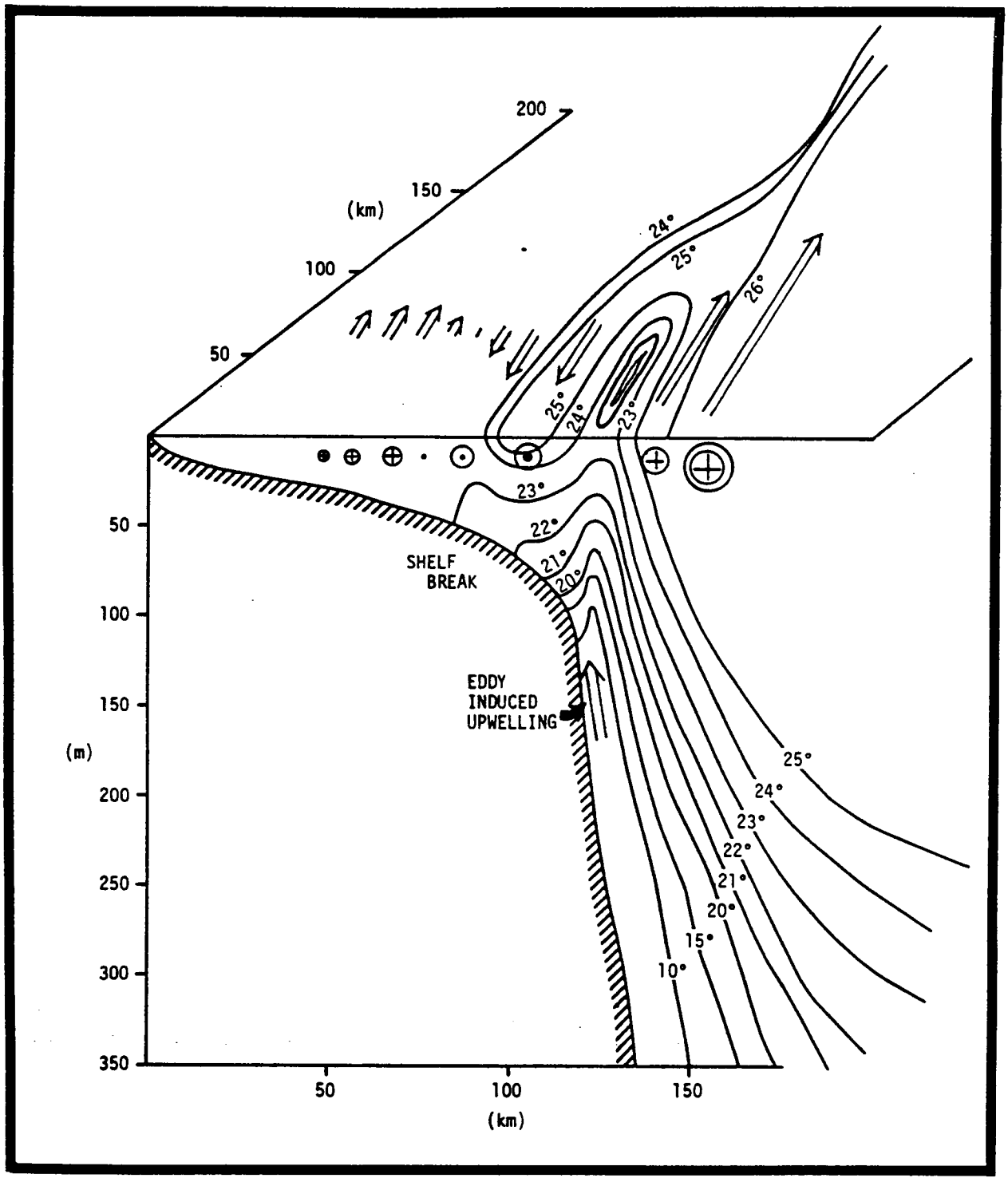

Figure 5-32. Schematic of Gulf Stream spin-off eddy.

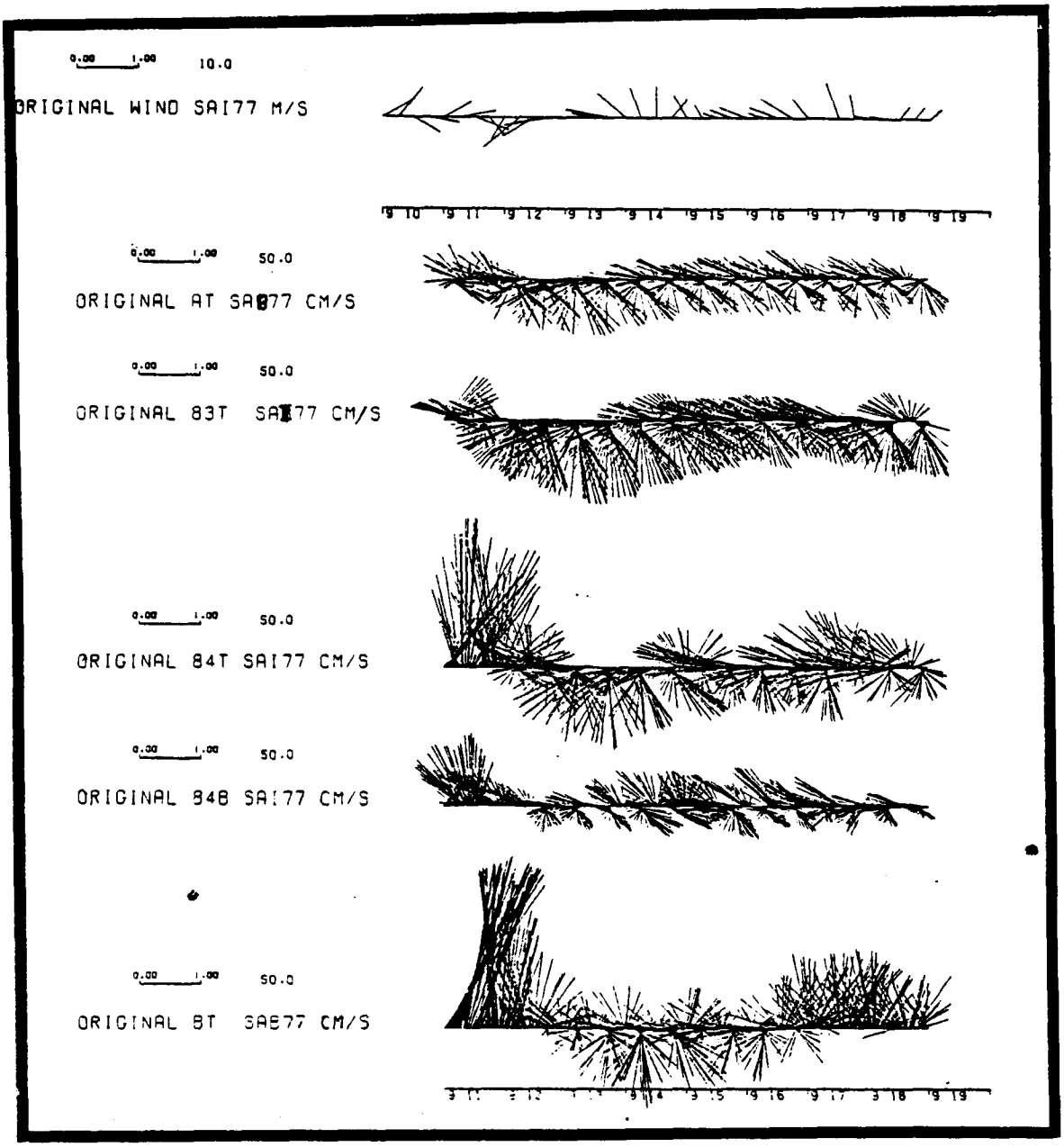

Figure 5-33. Time series of original (no rotation) current vectors from "short-term" measurements for 8-day period 11-18 September 1977. Current scale = 50 cm/s. Current meters AT and BT are from DOE array (30 and 75 m isobaths).

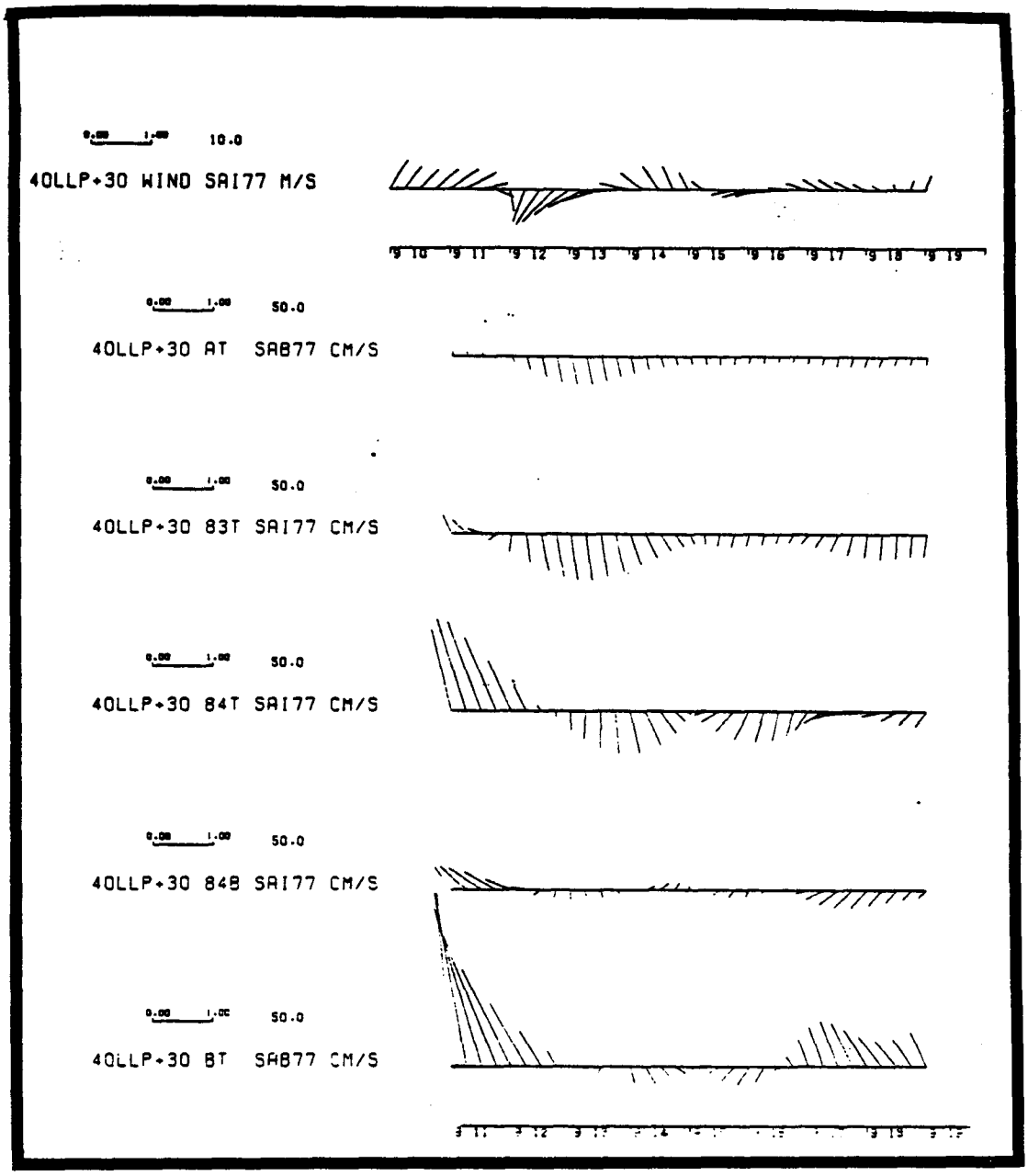

Figure 5-34. Time series of 6-hourly current vectors from 40-HLP rotated date of "short-term" measurements for period 11-18 September 1977. Current scale = 50 cm/s. Current meters AT and BT are from DOE array (30 and 75 m isobaths).

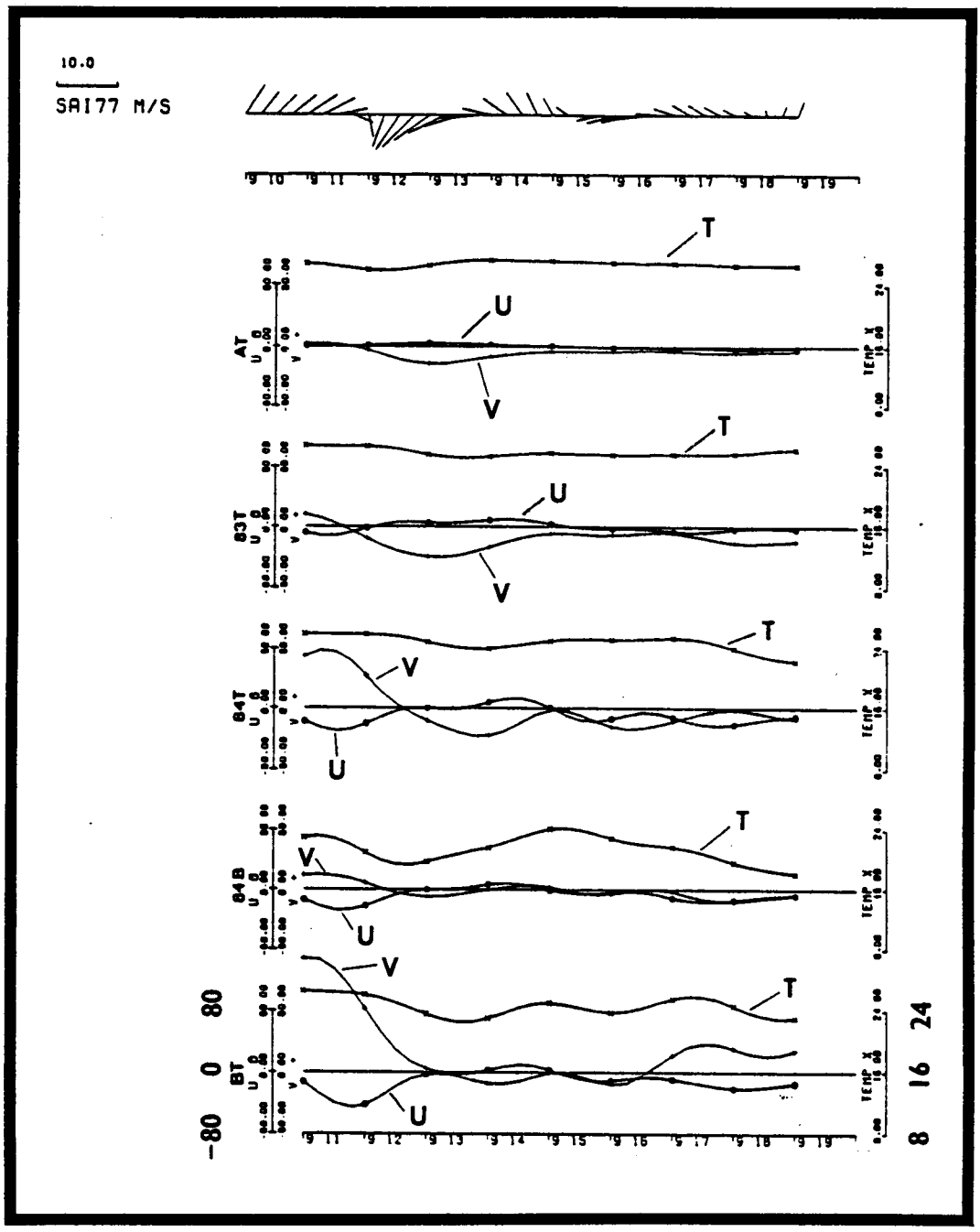

Figure 5-35. Time series of u and v velocity components and temperature T from 40-HLP rotated data of "short-term" measurements for period 11-18 September 1977. Current meters AT and BT are from DOE array (30 and 75 m isobaths). u = o-o-o, v = +-+-+, T = x-x-x.

deeper Gulf Stream water within the cold-core. There is some indication from the current vector and temperature distributions of AT and 84 T, which display 2 southward current maxima associated with 2 temperature minima (September 14 and 16), that 2 eddies may have occurred very close together. Southward flow continued at the shelf stations for about 12 days even though the flow at the shelf break had changed to the north on September 16 (Figure 5-15). The persistence of southward flow over the shelf suggests that a density driven, geostrophic flow may also be involved. Further explanations must wait for an intercomparison of the current meter and hydrographic data.

5.6.1.2 Long-Term Current Meter Measurements

Water motions on the continental shelf of the South Atlantic Bight are caused by numerous physical processes. Synoptic and seasonal scale motions occur in response to direct forcing by the weather (principally wind and atmospheric pressure) at synoptic scales and variations in thermohaline inputs (heat and salt) at seasonal scales. Synoptic variability occurs predominantly over the range of time scales spanning 2-14 days, the scales of the cyclonic and anticyclonic perturbations of the wind field. Other low frequency fluctuations occur in response to external forcing from the deep ocean, the Gulf Stream meanders, spin off eddies and Gulf Stream intrusions. Due to its sloping bottom the continental shelf region can support free modes of oscillation generally spanning similar time scales as the atmospheric forcing. The free modes are commonly referred to as quasi-geostrophic, topographic Rossby, or continental shelf waves. The combined low frequency oscillations observed at any position on the continental shelf, including the Charleston site, is expected to reflect a complex mixture of these aforementioned processes.

At higher frequencies, the astronomically forced semi-diurnal tides (i.e. rise and fall of sea level twice a day, due to the complex interactions of the earth-moon-sun system) propagating shoreward from the deep ocean are a dominant feature observed at the Charleston site. Between these semi-diurnal tides and the lower frequency weather continuum, three processes occur in varying degrees across the shelf: diurnal tides (i.e. rise and fall of sea level once a day), inertial oscillations (i.e. a perturbation which will seek a circular course due to a balance of the Coriolis and centripetal forces), and sea breeze (i.e. movement of air due to differential heating and cooling of land and water, onshore during the day and offshore at night at the coast). These all have time scales of roughly one day. Processes occurring at frequencies higher than the semi-diurnal tides include internal inertia-gravity waves (or subsurface waves under the influence of gravity and having periods of inertial oscillations), surface gravity waves (or large waves on the

water surface influenced by gravity), and finally edge waves (or surface gravity waves that are refracted and trapped in coastal waters).

As one looks at the unfiltered u, v and T data shown in Volume III, Figures 2.2-1 to 2.2-6, the most apparent features are an implication of semi-diurnal tidal components superimposed upon a low frequency background. While the u, v data from the second current meter mooring 089 is visually similar to that of 085, the first one, the T data is significantly different and therefore the two mooring periods (085 and 089) will be treated separately unless otherwise denoted.

Mean velocity components recorded by mooring 085 are presented in Tables 5-18 and 5-19 (in True North coordinates and Principal Axis, respectively), while net vectors are depicted in Figure 5-35; the u, v and T variables are expressed in discrete two week blocks as well as in a cumulative sense. The Principal axis rotation angles for each current meter on mooring 085 is shown in Figure 5-36 (67^{o}, 61^{o} and 44^{o} for top, middle and bottom meter, respectively, the solid arrows pointing in the direction of the principal axis for currents). The technique of principal axis rotation has been described in Section 5.4.1.3.2. During the November 1977 through January 1978 period, an alongshore mean to the southwest, compatible with the predominant wind direction, is suggested at all three levels (10 m, 22 m, and 42 m from the surface). A net cyclonic rotation of the velocity vectors from top to bottom is apparent over the entire record lengths. Reversals in the currents, i.e., departures of the 2 week means from the means of the entire record lengths occur more dramatically at the upper sensors with the middle sensor displaying less reversal magnitude than the top most element but more magnitude and rotation than the near bottom sensor. During this time of year, the horizontal offshore temperature gradient is relatively strong and the density gradient is substantially negative. Thermal wind inferences suggest that the alongshore velocity component will become either more positive or less negative from bottom to top in the water column. Clearly this is not the case, which suggest that the alongshore velocity component may have a close relationship with wintertime winds.

A look at the temperature data as well as an assessment of the local influence of the Gulf Stream will aid in this determination. Bumpus (1973) reports that the recovery rate of the drift bottles used in his study was poor in the long term mooring area during the winter months. He does suggest that there may be a northerly drift from Georgia to Cape Hatteras in January, but is somewhat inconclusive on this point in the Charleston area. Data collected by the long term mooring indicates that the net flow is southerly during the winter months November-January at this location. Raw, 3-hour low passed (3-HLP) and 40-hour low passed (40-HLP) current data indicate large amplitude fluctuations ranging from semi-diurnal tidal to fortnightly at all levels.

Table 5-18. Mean velocities (true north coordinates)

Meter	Meter Depth, m	Parameter cm/sec	Period Weeks 1 + 2	3 + 4	5 + 6	7 + 8	9 + 10	11 + 2.3 days	
			1-1344	1345-2688	2687-4032	4033-5376	5377-6720	6721-7619	File Points
8501	10	UCMP	5.2616	-21.7950	6.9408	-18.6054	13.4549	2.7156	Discrete Mean
			5.2616	-8.2667	-3.1976	-7.0495	-2.9486	-2.2803	Cumulative Mean
		VCMP	-1.8990	-10.7443	2.5992	-7.9030	7.7443	-0.9154	Discrete Mean
			-1.8990	-6.3216	-3.3480	-4.4868	-2.0405	-1.9078	Cumulative Mean
8502	22	UCMP	2.7587	-20.7846	5.7230	-18.1920	10.6852	-1.1941	Discrete Mean
			2.7587	-9.0129	-4.1009	-7.6237	-3.9619	-3.6353	Cumulative Mean
		VCMP	-4.5589	-14.2326	1.1957	-9.8654	6.4067	-2.8982	Discrete Mean
			-4.5589	-9.3957	-5.8652	-6.8653	-4.2109	-4.0560	Cumulative Mean
8503	42	UCMP	0.9910	-9.6938	1.3855	-11.3133	4.3625	-2.3539	Discrete Mean
			0.9910	-4.3514	-2.4391	-4.6576	-2.8536	-2.7946	Cumulative Mean
		VCMP	-4.3215	-15.5044	-1.1460	-13.6990	-0.3759	-5.0716	Discrete Mean
			-4.3215	-9.9130	-6.9907	-8.6677	-7.0094	-6.7807	Cumulative Mean

Table 5-19. Mean velocities (principal axis = R)

Meter	Meter Depth, m	R°	Parameter cm/sec	Period Weeks 1 + 2	3 + 4	5 + 6	7 + 8	9 + 10	11 + 2.3 days	
				1-1344	1345-2688	2689-4032	4032-5376	5377-6720	6721-7619	File Points
8501	10	67	UCMP	3.8036	1.3744	0.3197	0.0055	-1.8720	1.9037	Discrete Mean
				3.8036	2.5890	1.8326	1.3758	0.7262	0.8652	Cumulative Mean
			VCMP	4.1013	-24.2608	7.4046	-20.2145	15.4115	2.1421	Discrete Mean
				4.1013	-10.0798	-4.2517	-8.2424	-3.5116	-2.8445	Cumulative Mean
8502	22	61	UCMP	5.3243	2.3718	1.7292	-0.1908	-0.4235	1.9557	Discrete Mean
				5.3243	3.8480	3.1417	2.3086	1.7622	1.7850	Cumulative Mean
			VCMP	0.2027	-25.0789	5.5850	-20.6942	12.4518	-2.4493	Discrete Mean
				0.2027	-12.4381	-6.4304	-9.9964	-5.5067	-5.1460	Cumulative Mean
8503	42	44	UCMP	3.7146	3.7968	1.7928	1.3779	3.3992	1.8297	Discrete Mean
				3.7146	3.7557	3.1014	2.6705	2.8163	2.6999	Cumulative Mean
			VCMP	-2.4200	-17.8871	0.1381	-17.7135	2.7602	-5.2830	Discrete Mean
				-2.4200	-10.1536	-6.7230	-9.4706	-7.245	-6.8190	Cumulative Mean

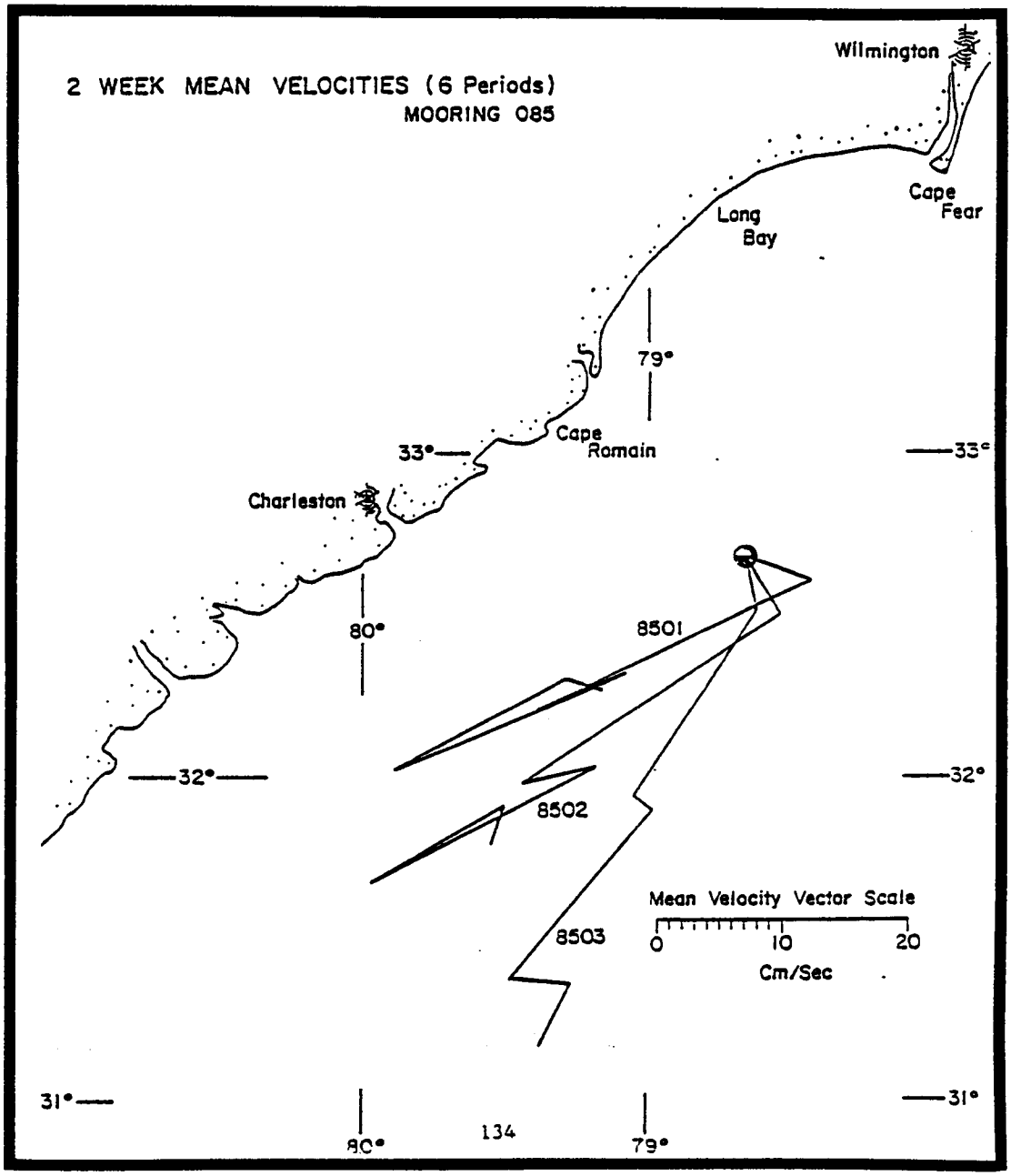

Figure 5-36. Vector addition of 2-week mean velocities for meters 8501, 8502, and 8503 in true north coordinate system (refer to Table 5-18).

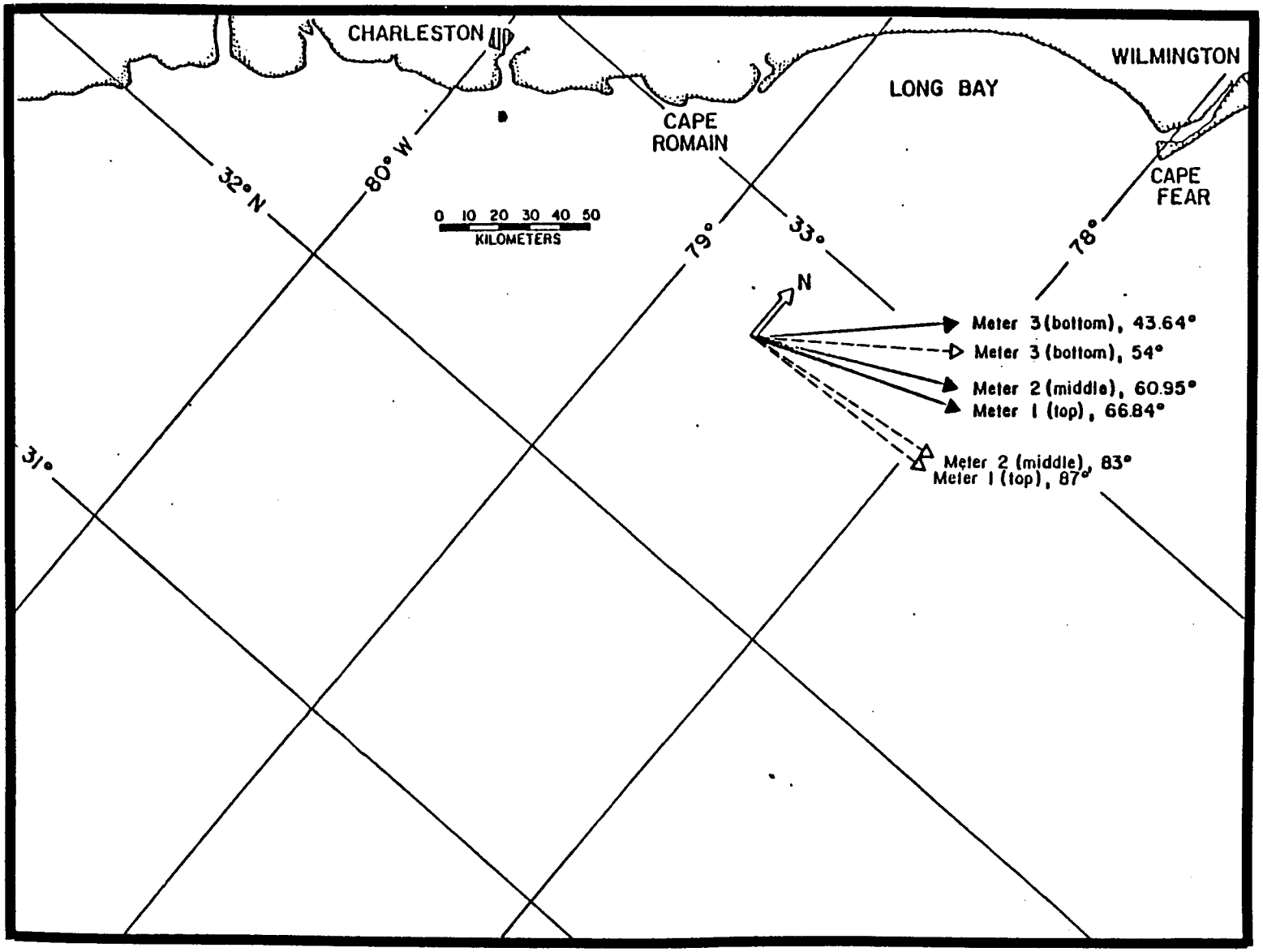

Figure 5-37. Principal axis rotation angles for each current meter on mooring 085.

From 40-HLP velocity vectors, best seen in the stack of stick plots (Figure 5-38), typical speeds were observed to be of the order of 30 to 50 $cm.s^{-1}$, with slight decrease in magnitude from top to bottom. Temperatures are nearly identical throughout the water column, their fluctuations are not important with a minor decrease in their magnitude from top to bottom. On November 27th, raw speeds of 90 $cm.s^{-1}$ were reached at the upper meter. There was some vertical shear in the southwesterly currents which appear to have been driven by a northwesterly 10-15 kt (5-7 m) wind.

The semi-diurnal current amplitude fluctuation evidently controls a large portion of the current variability. Redfield (1958) analyzed sea level records along the east coast and concluded that the principal lunar semi-diurnal tide on the continental shelf is a co-oscillation caused by the reflection of an incident oceanic wave by the coast. The portion of the oceanic wave transmitted onto the shelf reflects off the coast resulting in an increase in the tidal amplitude with distance from the continental slope. This type of reflected inertia gravity wave is called a Poincare wave. It has a maximum elevation slightly seaward of the coast and the associated water particle motions in the horizontal plane are elliptical, clockwise polarized, and oriented with the semi-major axis along the direction of propagation. The ratio of semi-minor to semi-major axis is theoretically predicted to be a pendulum day ($2\pi/f$) divided by the wave period (in this case 12.41 h). Thus the predicted axis ratio is 0.559 at the latitude of $32^{o}38'$. From the raw and/or 3-HLP data, it is clear that the amplitude of the tidal current decreases with depth. This effect may be attributed to bottom friction. A small phase shift (less than 1 h) also occurs between the upper and lower tidal current due to bottom friction. If one defines an effective pressure gradient as the resultant of the pressure gradient and tide generating forces, then the currents at any depth attain their maxima when the frictional forces are in balance with the effective pressure gradient. At this phase the effective pressure gradients will be decreasing so the currents will attain their maxima before the effective pressure gradients vanish. The frictional forces arise from the bottom. Assuming that those near the bottom are greater than those higher up, it follows that the bottom currents will reach their maxima earlier than the higher currents and consequently all phases of the bottom currents will occur earlier than corresponding phases of the higher currents.

The semi-diurnal tide is the only regular, deterministic process of any appreciable magnitude at the site of the CLTM.

The u, v, T 40-HRLP time series shown in Figures 5-39 to 5-41 display low frequency signatures which are consistently coherent throughout the entire 32 m of sampled water column. The alongshore velocity component and temperature time series overlay almost identically at

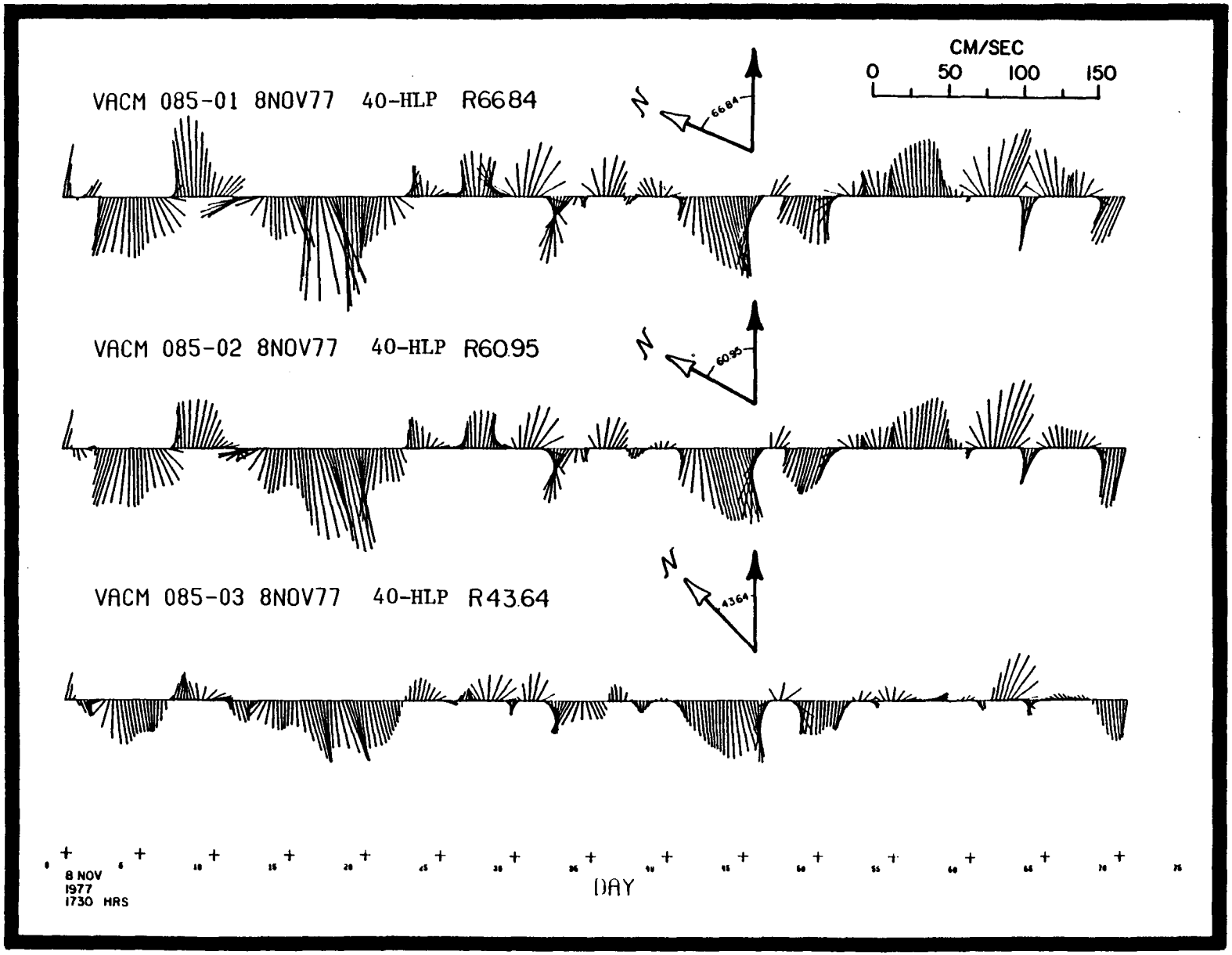

Figure 5-38. Comparison of 40-HLP current vectors from meters, 8501, 8502 and 8503.

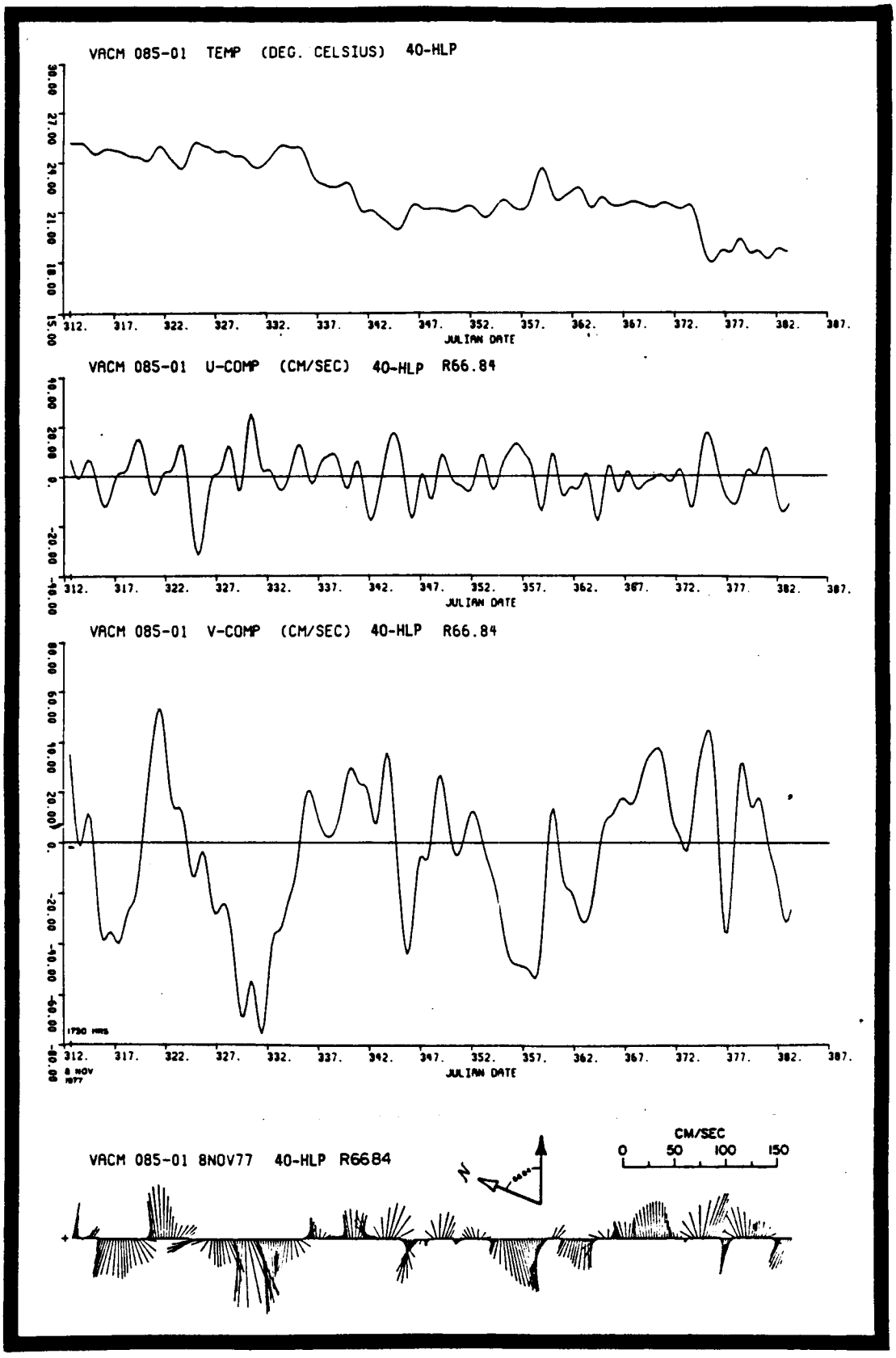

Figure 5-39. 40-HLP temperature, current velocity components and vectors from meter 8501.

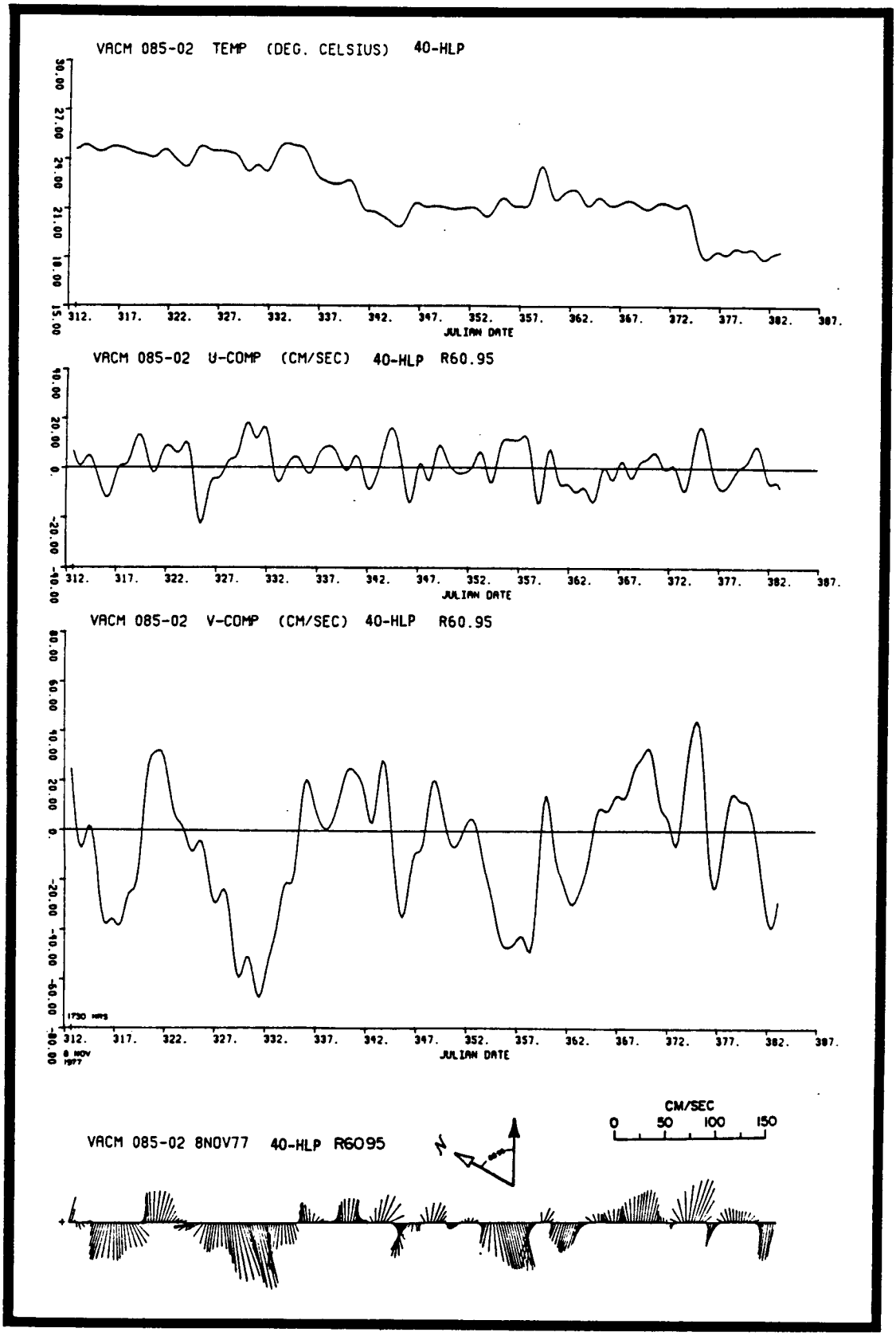

Figure 5-40. 40-HLP temperature, current velocity components and vectors from meter 8502.

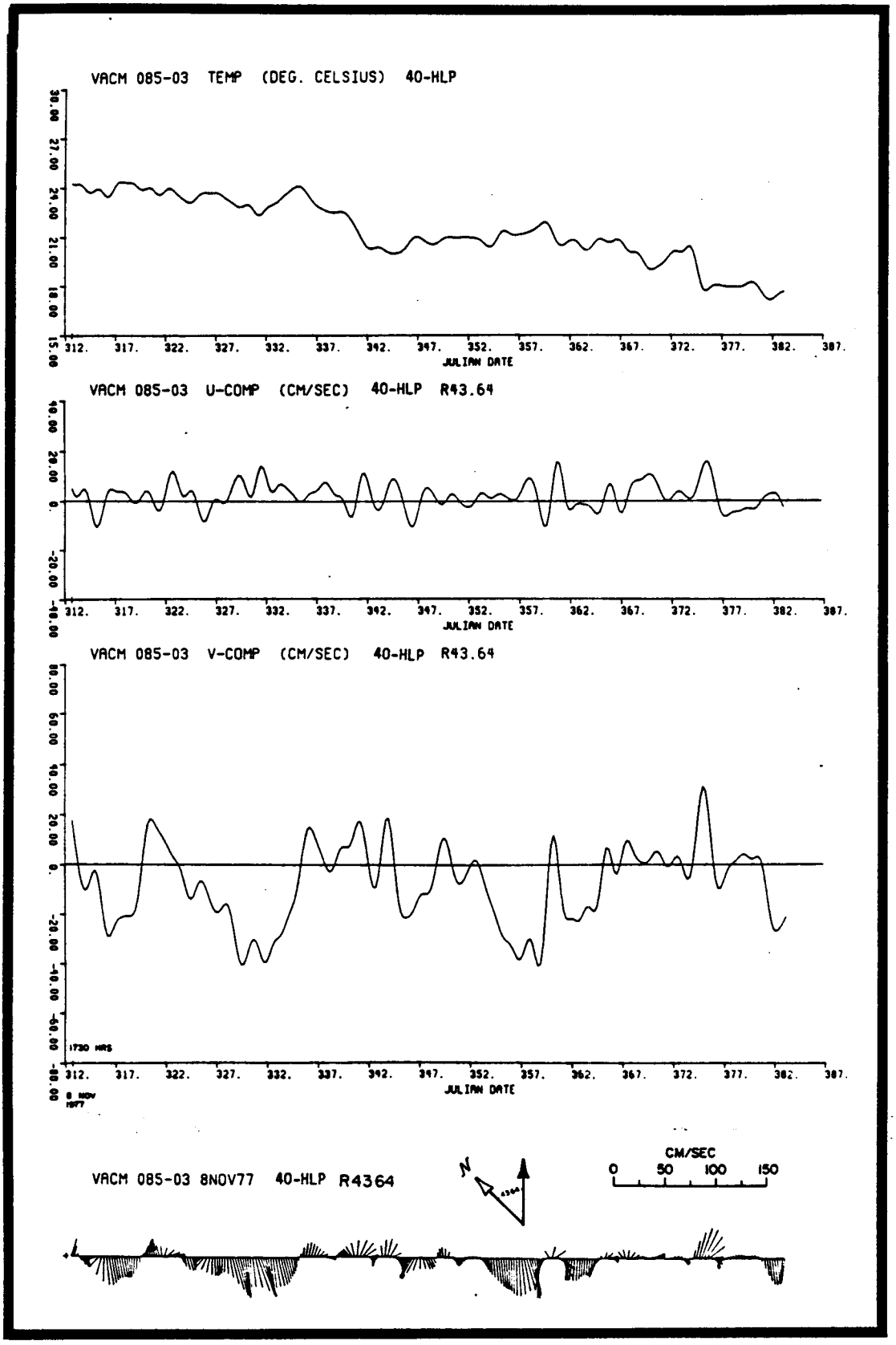

Figure 5-41. 40-HLP temperature, current velocity components and vectors from meter 8503.

all three levels while the cross-shelf current time series displays minimal departure from surprisingly strong coherence. It appears that the mooring site was in a region of minimal Gulf Stream influence during this time of year. The low frequency, i.e., subtidal, physical processes are dominated by the mechanical forcing of the wind. In fact, VHRR imagery collected during this three month period showed Gulf Stream spin-off eddies to be conspicuous by their absence. In fact, Charleston sea level data shows its seasonal minimum during this period (cf. Figure 5-41) which is entirely consistent with the seasonal cooling of the shelf. As the density of the shelf rises with decreasing temperatures, the net steric effect is a fall in sea level. Additionally, Iselin (1940) used hydrographic sections and tide gauge data to show that the Gulf Stream transport is at a minimum during the initial part of this time of year. Rooney, Janowitz and Pietrafesa (1978) have shown that a decrease in net transport of the Gulf Stream results in a larger deflection of the Gulf Stream Front offshore, at the site of the Charleston Bump ("rise"). The picture then is one of temperature and sea level falling on the shelf, Gulf Stream transport at a yearly low, and a deflection of the Gulf Stream farther offshore by the Charleston bump. The Gulf Stream thus is expected to have less effect on shelf waters off Charleston than at any other time of year in that region.

The time series picture of the currents then is one of a vertically homogeneous shelf with weak vertical shear and rotation of the horizontal currents. The dynamical balance suggested is one of a surface stress driven barotropic geostrophic flow, principally alongshore, with weak baroclinic geostrophic forcing in the alongshore and cross-shelf directions. Gulf Stream influence is of minimal importance with no evidence of either meandering processes or spin off eddies present. Inertial oscillations are evident. Subtidal currents are larger in the alongshore direction and decrease downward. There is a net flow to the southwest at all three levels with the maximum net displacement to the SW decreasing upward and tidal variability is a stable deterministic process which is described as a bottom frictionally modified Poincare wave.

The frequency domain shows well defined broad banded peaks at periods between 3 1/2 and 11 days and at 2 1/2 days in the cross-shelf direction. Cross spectrum u's, v's and T's between levels consistently show coherencies in excess of the 95% confidence level at periods larger than 2.5 days. Phase lags suggest upper water column variables leading lower like variables by the order of several hours. A look at the cospectra of u vs. T and v vs. T at the various levels (Figures 2.2-55 and 2.2-60, Volume III) in the frequency bands where the cross-spectra of these variables show high coherence squared values indicate that there is a low frequency, subtidal flux of hot water onto the shelf, in the cross-shelf direction, and a flux of heat to the southwest to south in the alongshore direction.

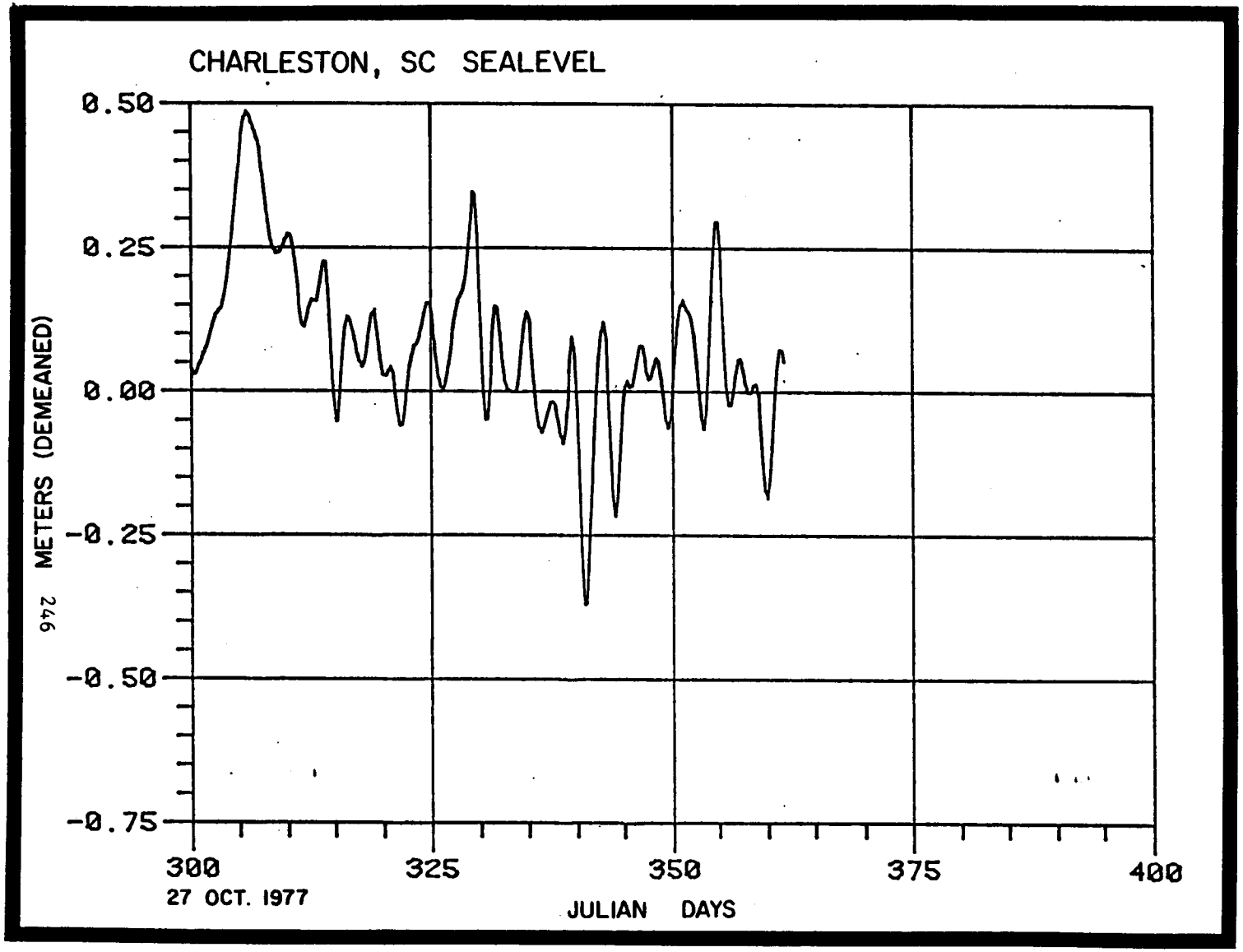

Figure 5-42. Sea level at Charleston, S.C. for 27 October, 1977 - 31 December, 1977.

Likewise, a low frequency, subtidal flux of cold water off of the shelf in the cross-shelf direction, and a flux of cold water to the northeast to north in the alongshore direction is also seen in the cross-spectra. Magnitudes of the cospectra consistently show larger fluxes of heat in the along-shelf direction than in the cross-shelf direction, as is suggested by the u, v, T time series (Figures 5-39 and 5-41). This frequency domain picture of the directional flux of heat is entirely consistent with the hydrographic conditions present on the continental margin during the winter period. The conditions are simply that the horizontal temperature gradients are positive in both the northeasterly and offshore directions; offshore (onshore) transport and southerly (northerly) transport necessarily involve movement of relatively colder (warmer) waters.

A wintertime cold front, advancing from the continent seaward will first exhibit alongshore winds generally from the northwest to northeast, and since the Charleston latitude is in the lower portion of the atmospheric vortex, the wind vectors at a point on the coast will subsequently rotate clockwise. Winds on the backside of the event are generally directed towards the southeast to southwest. The frequency and persistence of these types of atmospheric events, so common to late fall to mid winter, during the 085 and 089 mooring periods is not yet known since meteorological data tapes were not available. Nonetheless, based on the examination of 3-hourly meteorological summary sheets, one can speculate on the response characteristics of the currents to wind events such as the one described hereafter.

During days 9-15 of November, 1977, a cold front advanced off the coast of South Carolina. On days 9 to 10, winds were generally southwesterly. As the event developed, as viewed by a fixed coastal observer, the winds rotated clockwise; by day 12 they had become northwesterly and by day 13 the effective winds were northerly to north-northeasterly. The meteorological event was accompanied by an outbreak of cold air which saw a daily high of 78^{o}F on the 8th drop to a high of 50^{o}F on the 13th. The current regime on the 8th preceeding the onset of the net event was directed towards the northeast from top to bottom with approximately 20^{o} rotational shear of the horizontal current vector between topmost and bottom most instruments (cf. Figure 5-38). As the event struck and passed, sea level at Charleston fell about 27 cm, in concert with the winds from northwest to northeast and then rose 18 cm (cf. Figure 5-42) with the clockwise progression of the wind as it became northerly offshore. Currents at all levels also rotated clockwise then counterclockwise to become mainly alongshore to the southwest and partially onshore to the west at the top to being mainly alongshore to the southwest and partially offshore to the south at the bottom. It appears that the alongshore currents were barotropic geostrophic in nature while the upper and lower currents were quasi-conventional coastal downwelling in nature, "on" at the top and "off" at the bottom. The theoretical basis for

describing the observed response in the presence of horizontal stratification can be obtained from the results of Pietrafesa (1973). The work of Scott and Csanady (1976) could also be invoked to describe the downwelling favorable wind case discussed but their work does not compare favorably to observations for cases of upwelling favorable winds while Pietrafesa's model would fit either wind direction.

The temperature data (cf. Figures 5-39 to 5-41) indicate on overall drop of 7°C during the 72 day period analyzed. While several dramatic temperature fluctuations are evident in the 40-HLP time series, the major decrease in T with time occurred between 1-10 December following persistently southwesterly currents in concert with a net depression of sea level at the coast of about 35 cm and with winds that blew intermittently from the WNW to NE.

The 089 CLTM data sets display essentially the same characteristics, during the first part of the mooring period, as those described for 085. Tidal dynamics are certainly similar. Departures in the description begin to occur after 1 February when a 4°C rise and gradual fall in temperature occurred, superimposed on what appears to be the onset of a gradual increase in temperature throughout the entire water column associated with a rapid clockwise rotation of the three current vectors (cf. Figures 5-43 to 5-46). Satellite VHRR imagery does show that between the 25th of January and the 8th of February an enlarged meander was present offshore of the area and that discernable surface temperatures at the site of the mooring increased from 58°F to 71°F though no eddy appeared to be present. It may be that an enlarged meander or old eddy escaped detection by the satellite but was nonetheless evident in the moored meter data. Presumably also, a coastward meander of the Gulf Stream Front could have simply sloshed across the shelf and become mixed with resident waters.

From 12-19 February (cf. Figure 5-46) a very dramatic clockwise rotation of velocity vectors occurs at all three levels, contemporaneous with a 4°C rise in temperature. This event appears to have little relationship with the winds present at the time and is, in probable fact, an indication of a large spin-off eddy. Satellite VHRR imagery, supplied by NOAA/NESS (see Figure 5-47, courtesy of Dr. R. Legeckis) distinctly shows the mooring on the upper, northwestern side of a large warm filament. If the u, v, T signatures do characterize the passage of a Gulf Stream spin-off eddy then the scenario described hereafter is contrary to observations of SAB eddies reported upon in the available literature (Lee, 1975; Lee and Mayer, 1977; Duing, Mooers and Lee, 1977; Lee and Brooks, 1979). The eddy observed during this period not only resulted in a warming of the shelf waters, locally, but also rotated clockwise at a point contrary to the previous observations noted above. Recently, Pietrafesa and Janowitz (1979) discussed the possible signatures

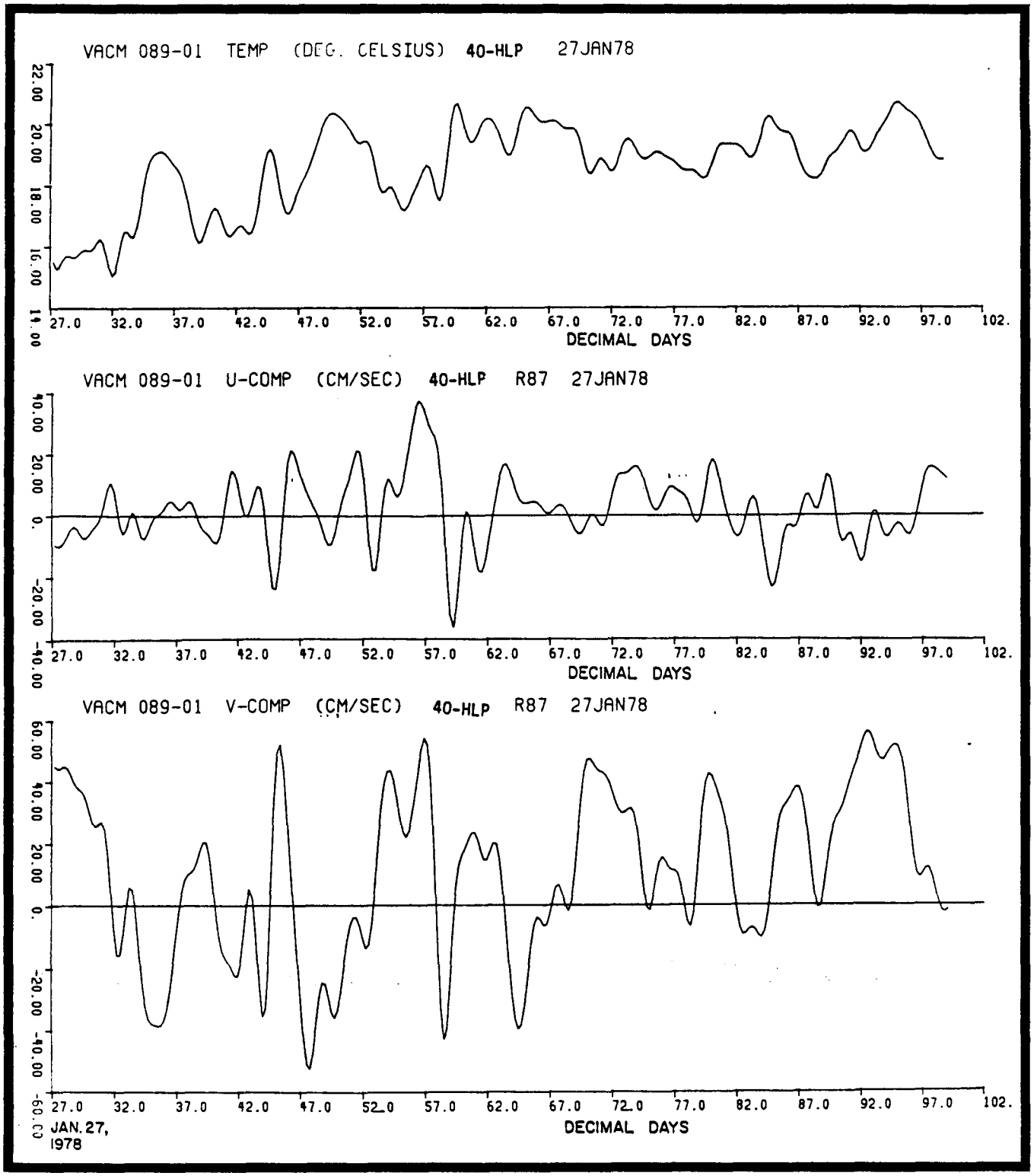

Figure 5-43. 40-HLP temperature and current velocity components from meter 8901.

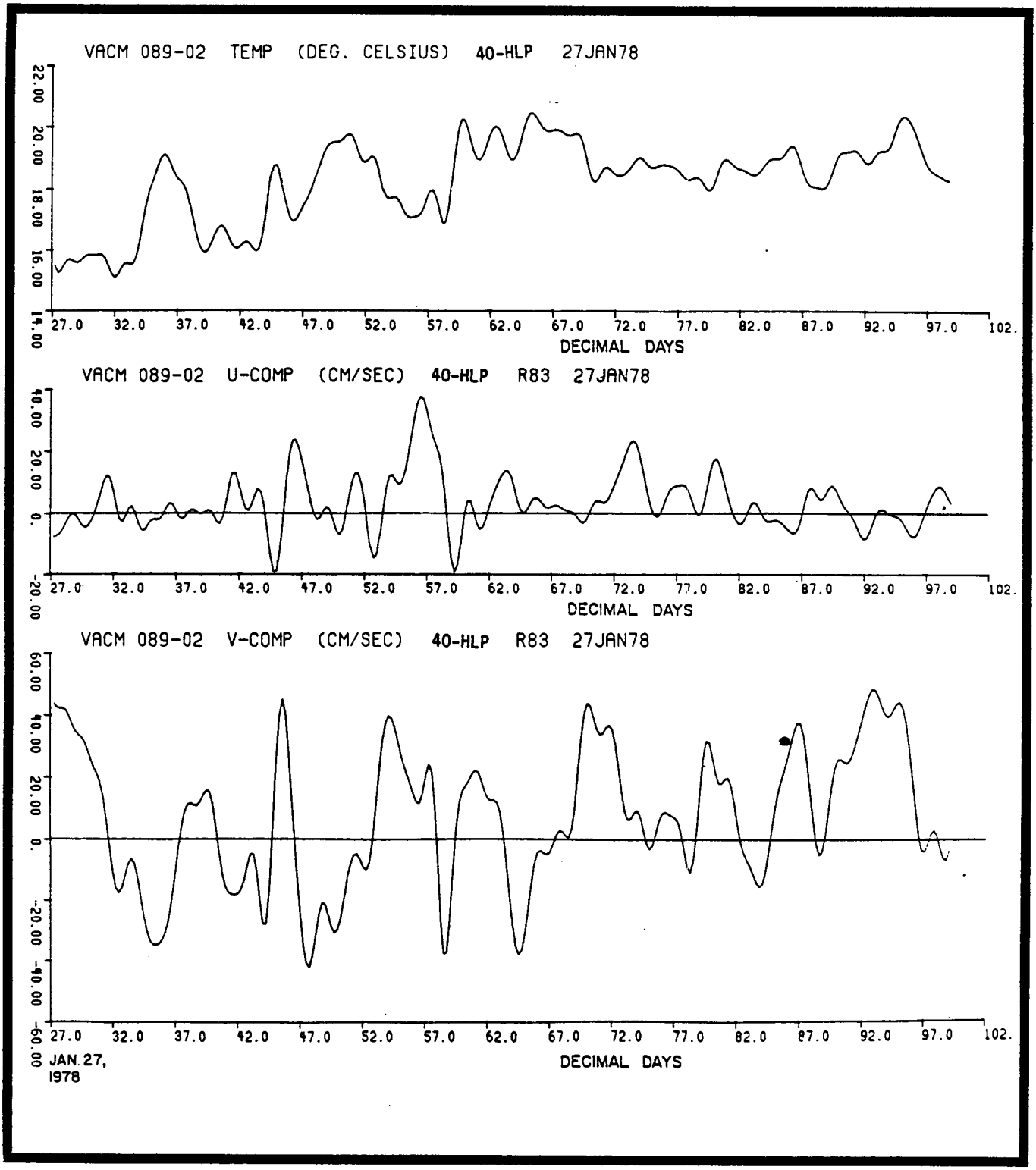

Figure 5-44. 40-HLP temperature and current velocity components from meter 8902.

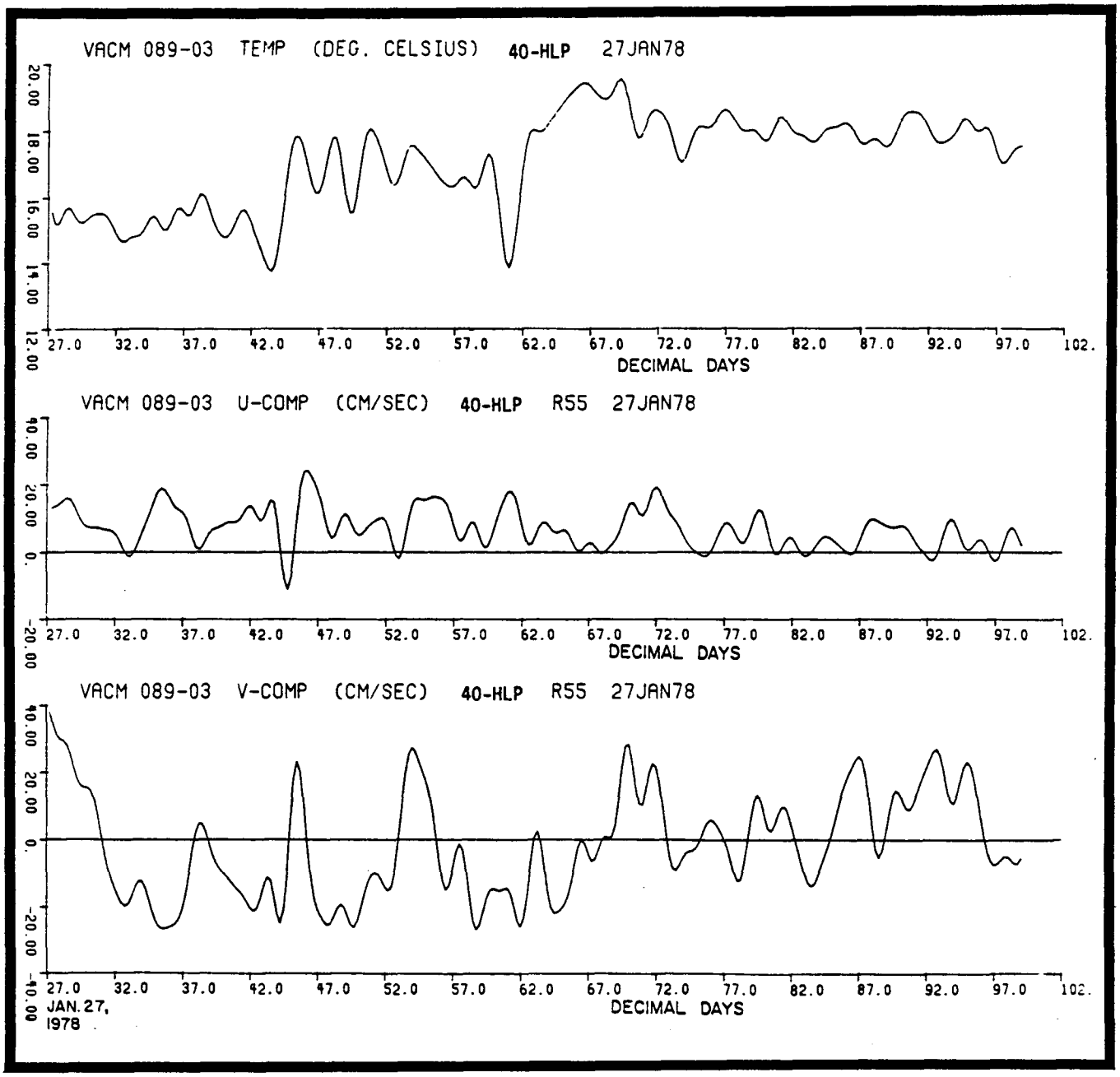

Figure 5-45. 40-HLP temperature and current meter velocity components from meter 8903.

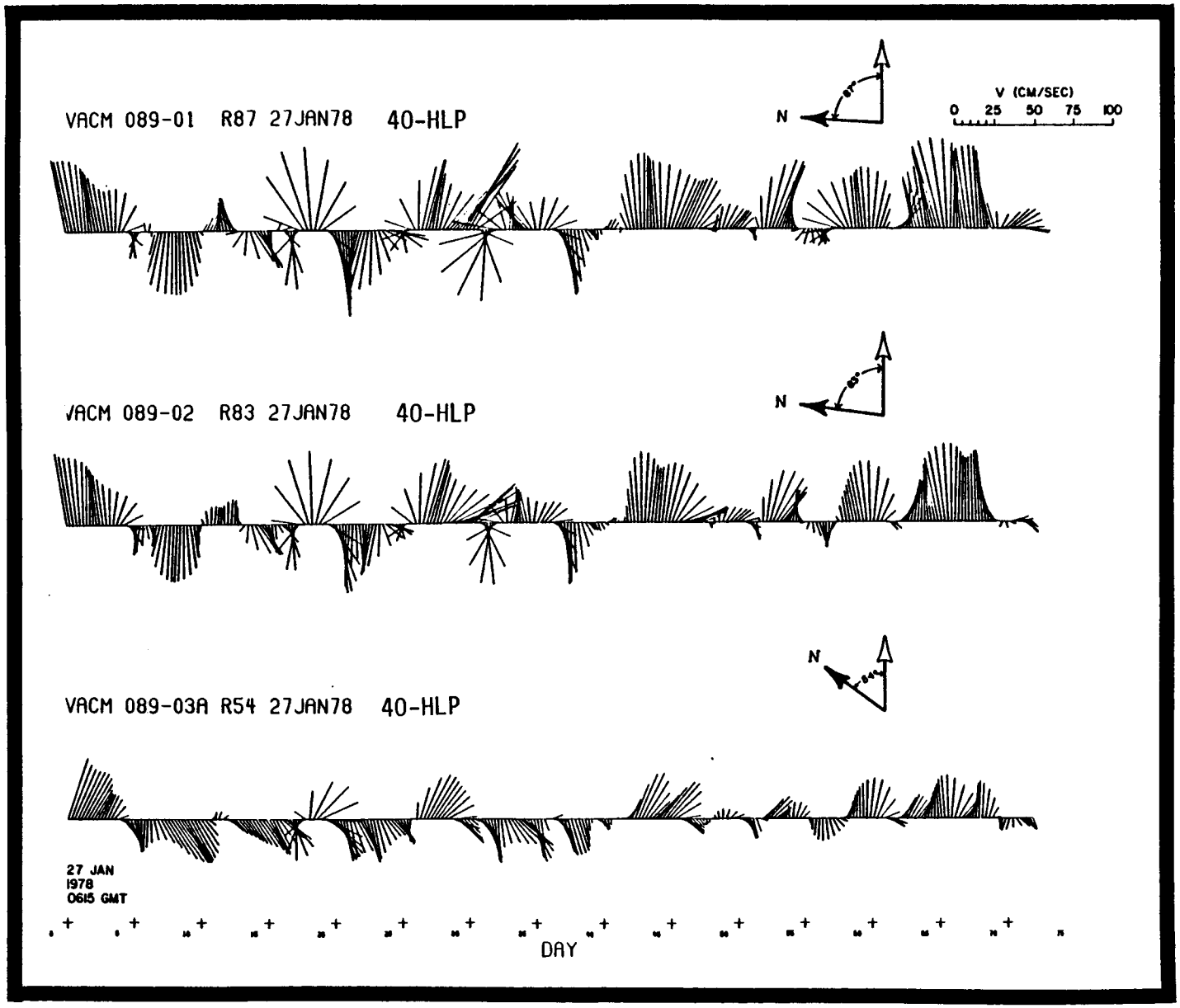

Figure 5-46. Comparison of 40-HLP current vectors from meters 8901, 8902 and 8903.

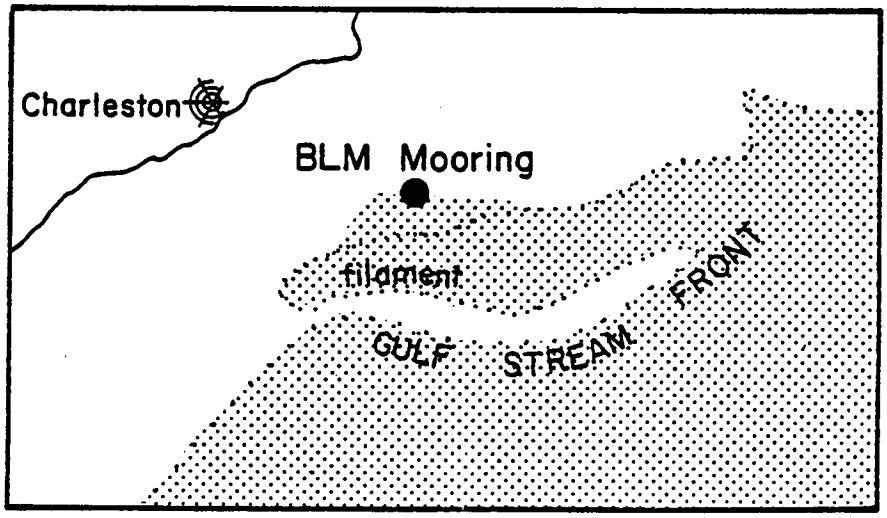

Figure 5-47. Gulf Stream eddy filament observed in Very High Resolution Radiometer satellite imagery at 13:38z on 12 February, 1978 (courtesy of Dr. R. Legeckis, NOAA/NESS).

which an eddy would have at different times of year to an observer fixed at a point in space and have determined that an Eulerian representation on the "upper" side (point A, Figure 5-48) of an eddy will always exhibit clockwise rotating currents in the eddy interior. It can be seen from Figure 5-47 that the long-term mooring was positioned as point A, Figure 5-48 on February 12, 1978. Examination of Figure 5-48 shows that at that point, the rotation of velocity vectors is predicted to be clockwise, and indeed, the current record (Figure 5-46) exhibits this clockwise rotation on February 12-19, 1978. Additionally, since water masses of Gulf Stream origin are generally warmer than shelf waters during the winter months, the passage of an eddy will appear as a sudden warming of the shelf at a point in space. Prior to the passage of this event, there was a $2^{o}C$ difference in T from the upper to lower sensors which is associated with the reestablishment of the seasonal, winter-spring, stratification of the shelf proper.

Another event similar to that described above occurred on 4 March (cf. Figures 5-45 to 5-46), simultaneous with satellite observations of the presence of an eddy at the mooring site. Once again the mooring was on the upper side of the filament as depicted in the satellite imagery. This event was conspicuous not only by its occurrence but also because it was immediately followed by a generally warming of the shelf which persists through the duration of the three time series of temperature. This leads to a speculation that the shelf experienced its spring transition in hydrography in response to a triggering mechanism: the passage of a Gulf Stream spin-off eddy.

The alongshore density gradient becomes strongly positive following the sudden warming of the Charleston shelf and the thermal wind relationship requires that the current become more positive (or less negative) as one moves upward in the water column. The 40-HLP current data appear to be following this balance subsequent to 13 March. Coastal meteorological data and coastal sea level data for 1978 and 1979 are still not available on magnetic tape, from either the National Climatic Center or the National Ocean Survey, respectively. The unavailability of these data has frustrated efforts in attempts to obtain a more complete understanding of the long-term mooring data.

Given the present unavailability of contemporaneous coastal meteorological and sea level data, data collected from several years past (1974-1977) at the Charleston coastal location has been reviewed and culled for relevant insights into the variabilities of atmospheric and sea level data, and relationships of the latter to the former. This analysis proved to be extremely useful. The close relationship between sea level signature and atmospheric forcing is encouraging for the parameterization of the processes governing circulation, since the response is dramatic and direct. There is, in fact, no

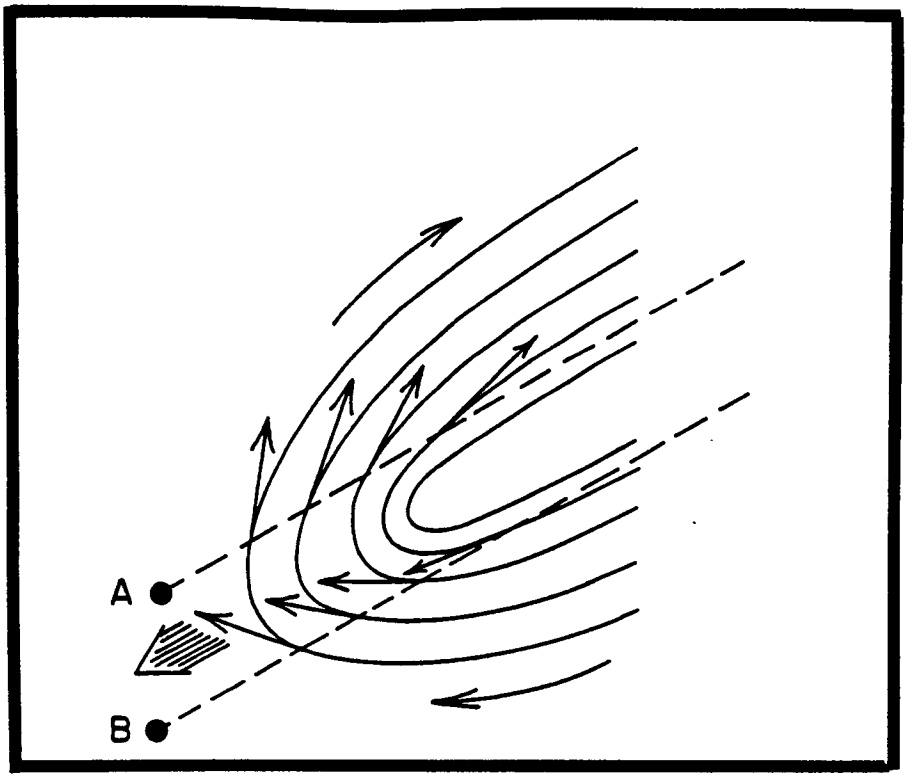

Figure 5-48a. Clockwise rotating eddy-filament (Event I) advecting towards points A and B.

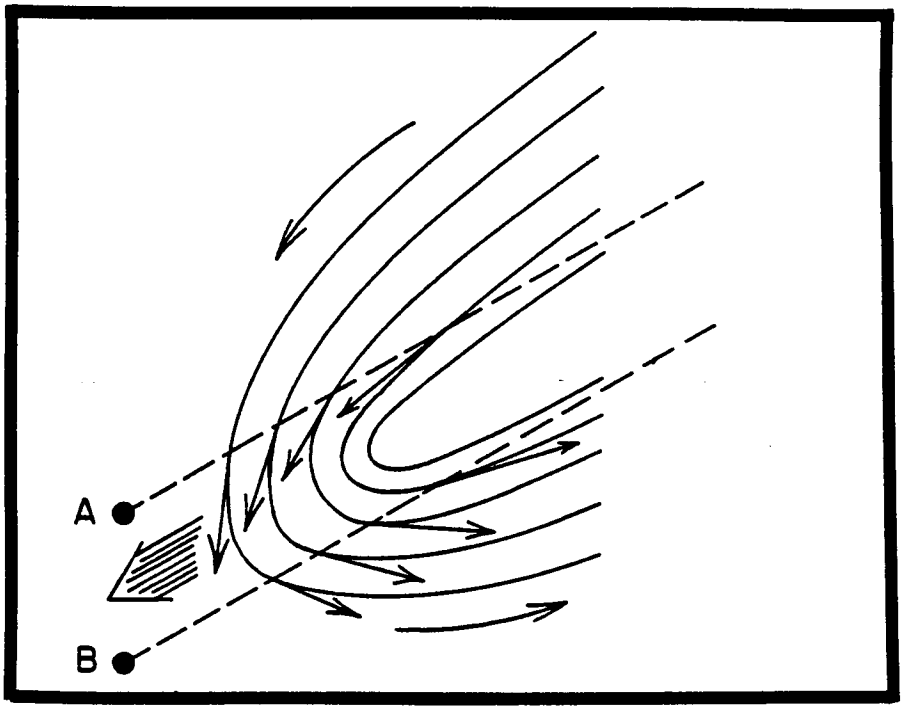

Figure 5-48b. Cyclonically rotating eddy-filament (Event II) advecting towards points A and B.

evidence of the propagation of continental shelf waves past the site, which is contrary to the implications of Mysak and Hamon (1969) and Brooks (1978). The recent work of Chao and Pietrafesa (1979) provided a complete rationale for the response of sea level to atmospheric forcing at Charleston without the invocation of continental shelf waves. These latter authors show definitively that the barometrically corrected, subtidal tide gauge signal, in the 2-10 day period band, is related to direct, set-up and set-down and can be easily explained in terms of conventional coastal Ekman theory. The steric response of sea level to the atmospheric cooling and heating of the water column is demonstrated; sea level falls (rises) as shelf temperatures drop (rise).

5.6.2 Hydrographic Measurements

Presented in this section is a discussion of the seasonal variability and events identified from the voluminous set of data products presented in Volume III, Section 3. The experimental design was evidently focusing on the seasonal variability of the water masses over the shelf. Such seasonal time scale was addressed primarily for two reasons.

First, the residual circulation on the continental shelf is a long-term integral of the net effects of many events occurring in the high frequency/wave-number portion of the spectrum. Natural limits for these integrals are seasonal, since the wind field, insolation and precipitation levels are strongly coupled to this time scale. Second, precise determination of the turbulent fluxes of various quantities, such as heat and salt, within a specific continental shelf region required accurate knowledge of the mean values over an appropriately long period. The seasonal means may contribute optimally to such calculations.

Water properties over the continental shelf and Blake Plateau within the South Atlantic Bight (SAB) region are principally determined by a number of identifiable component processes (Blanton 1971; Stefansson et al. 1971; Bumpus 1973; Atkinson 1977), each of which is most energetic during specific seasons. The Gulf Stream, flowing over the Blake Plateau and roughly paralleling the continental margin, meanders on time scales from several days to several weeks during all seasons, and in the process can mix warm, saline water with ambient shelf water (by overriding, interleaving or eddy entrainment). The same mechanism can also supply to the shelf (by bottom intrusions) cool, low salinity, high nutrient-laden water found on the inshore or cylonic side of the main subsurface Gulf Stream front. Subsurface intrusions are believed to be most energetic in late summer during periods of southerly winds. In spring and early summer, freshwater runoff may reduce temperature and salinity near the shore and enhance local stratification. In late winter and spring, during periods of northerly winds, Virginia water transport past Cape Hatteras may

markedly reduce temperature and salinity and accelerate low salinity water exchange. In winter, convection caused by surface cooling may lead to shelf waters cascading down the shelf and slope, thus reducing the available supply of nutrients in the photic zone.

The SAB regime, typical of most continental shelf environments, is characterized by a high level of variability in its hydrographic properties. The degree of variability combined with a data base of marginal statistical stability in space and time allow only cautious generalizations. As such, the following description of the component SAB hydrographic regime has been formulated (Curtin, 1979).

Four component water masses (in a broad sense) can be defined on the basis of temperature, salinity data and geographical location. Virginia Water (VW), Carolina Water (CW), Georgia Water (GW) and Gulf Stream Water (GSW) are shown on a temperature-salinity (T-S) diagram in Figure 5-49. VW, relatively cool and fresh, is formed north of Cape Hatteras as a mixture of runoff and slope water and is the source water on the northern boundary of the SAB shelf. GW, as fresh as VW but warmer, is formed near the shore in the Georgia embayment as a mixture of runoff and shelf water and is the source water on the southern boundary of the SAB shelf. CW, spanning VW and GW in temperature, but more saline than both, is formed over the shelf as a mixture of near-shore water and GSW. CW is the densest water formed on the shelf in the SAB, and the densest CW is formed in winter. During summer, VW and GW may have identical properties as defined by T-S vectors; however, CW always separates the two spatially.

The transitions between winter and spring, and summer and fall effect the largest amplitude shifts in water mass boundaries. The direction and phase of movement of the VW and GW boundaries suggest that the different prevailing seasonal wind fields (NE-NW in fall-winter; SW-SE in spring-summer) are directly forced. It is possible to describe the variation of the GSW front as an annual period modulation of a standing wave form associated with the topographic deflection of the Gulf Stream off South Carolina.

The observed configuration and phase is such that statistically the Gulf Stream appears farthest over the shelf in the Onslow Bay region during spring and summer and in the Georgia embayment region during fall and winter. In the Long Bay region, the GSW front remains relatively fixed in position off-shelf during all seasons. These seasonal trends most likely comprise a spectrum of shorter period and, in many cases, greater amplitude events or episodes. Most of these events seem to be forced by the wind, either locally or remotely, by such processes as Ekman layer divergences and convergences, topographically trapped wave generation and propagation, and lateral and vertical eddy and turbulence formation generated by instabilities. Episodic runoff and periods of intense insolation or cooling also contribute, but seemingly to a lesser extent.

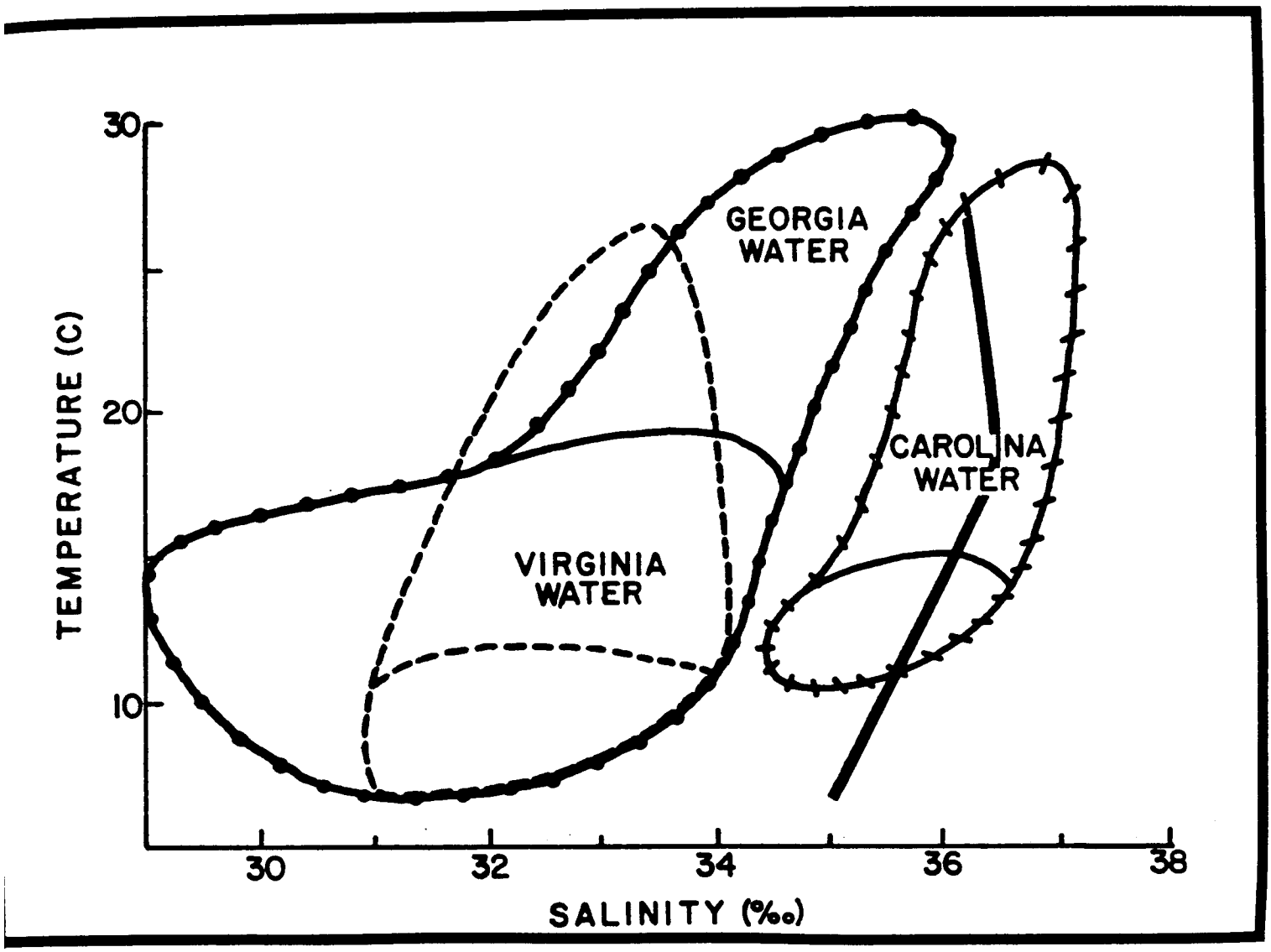

Figure 5-49. Locus of SAB component water masses: — — — Virginia Water; —●—●— Georgia Water; —/—/— Carolina Water; ——— Gulf Stream Water.

On the basis of the overall temperature/salinity structure observed (Figure 5-50), the SAB water masses appeared to be colder and less variable in 1978 over all seasons relative to 1977. The contrast in variability as well as the limiting variable ranges, however, may reflect the differences in sampling methods between the two years. For example, in 1977 the cruise durations exceeded those in 1978, and in 1977 not as many very near-shore stations were occupied as in 1978. Both of these factors contribute towards what appears to be annual variations in water properties, but may in fact be sampling bias. The relative importance of these effects cannot be ascertained from the existing data sets. Thus, within overall experimental error, similar seasonal water masses were observed over the SAB during both years, 1977 and 1978.

To differentiate the waters bounding the shelf, data from stations located shoreward of the 20 m isobath and from stations in the vicinity of the shelfbreak were culled and examined separately, Figures 5-51 and 5-52, respectively. For a given season nearshore, density variations were primarily a function of salinity. During all seasons, water of Gulf Stream origin (>36 $^{o}/_{oo}$) was observed, relatively unmixed, nearshore (e.g., winter, 1978). Density variations within such water were primarily a function of temperature. At the shelfbreak, a well defined water mass, Gulf Stream Water, occurred during all seasons. The characteristic GSW salinity maximum (36.6 $^{o}/_{oo}$) was associated with 20 to 21 ^{o}C (25.5 σ_t), during summer and fall. The nature of the scatter in the 1977 data, particularly spring and summer, is suggestive of systematic errors in sampling, although oceanic processes such as mixing near the shelfbreak cannot be ruled out as a contributing cause. The water over the shelf in the SAB from the shelfbreak shoreward to the 20 m isobath is primarily a mixture of GSW and the fresher waters found nearshore.

The overall average seasonal properties of SAB water may be summarized by a set of envelopes in (T,S) space, Figure 5-53. Each envelope defines a seasonal band or locus of T,S characteristic for SAB water during a specific season. Observed properties will be skewed toward the lower part of each band for anomalously cool seasons (atmospherically), and toward the upper part for warm seasons. Analogously, observed properties will be skewed toward the right within each band during anomalously dry seasons (low rainfall and runoff), and toward the left during wet seasons. Transition regions separate the seasonal bands and provide a continuous sweep in T,S space through the annual cycle. In the mixing of GSW with nearshore waters of various types, Figure 5-53 illustrates that such mixing occurring along constant density surfaces is most favored in winter. In summer, such mixing paths occur almost orthogonal to isopycnic surfaces. The winter minimum energy requirement together with a maximum in atmospheric energy input through storm activity results in efficient cross-shelf mixing during this season. The summary diagram together with

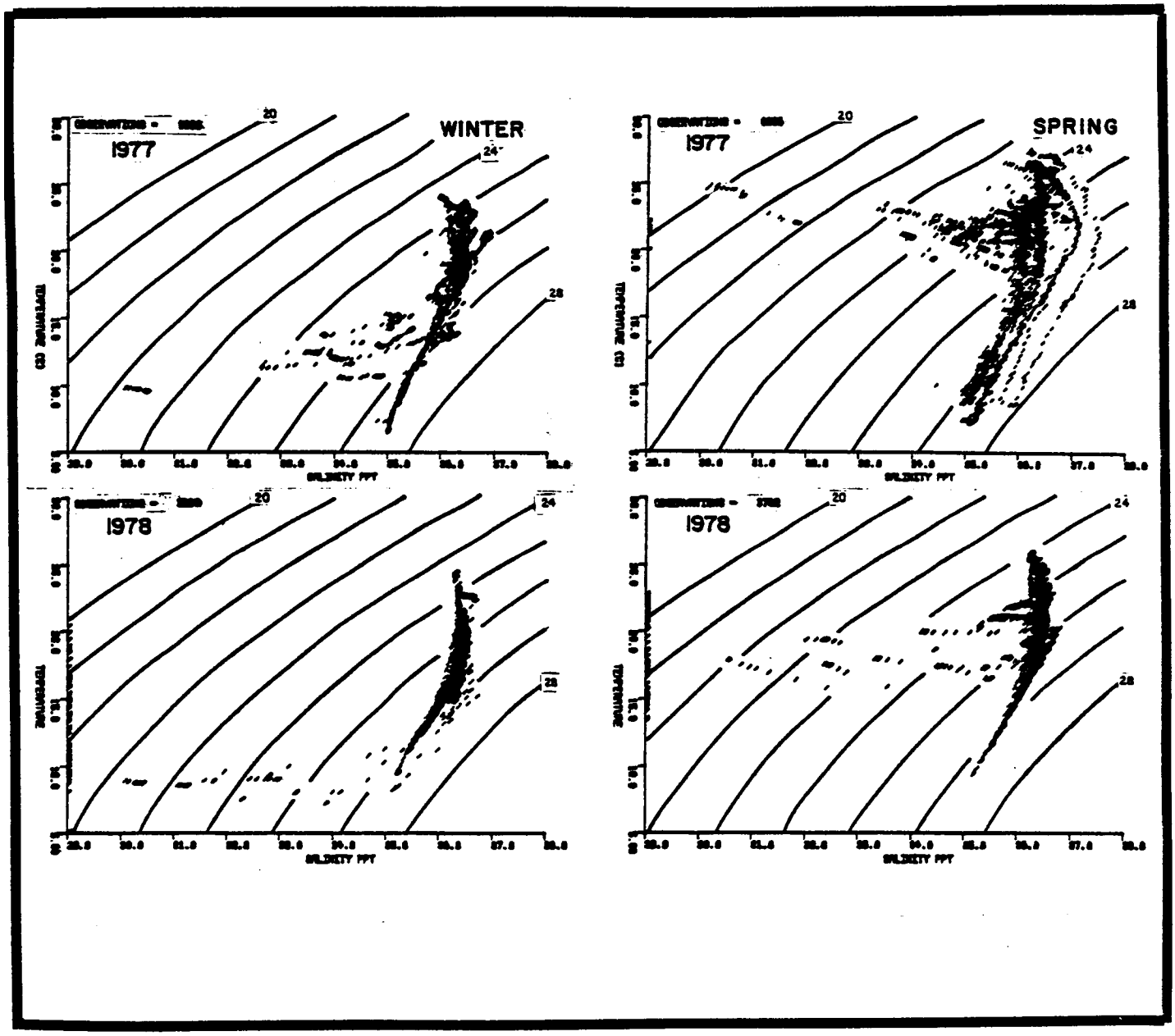

Figure 5-50. Overall SAB 1977/1978 temperature/salinity characteristics by season.

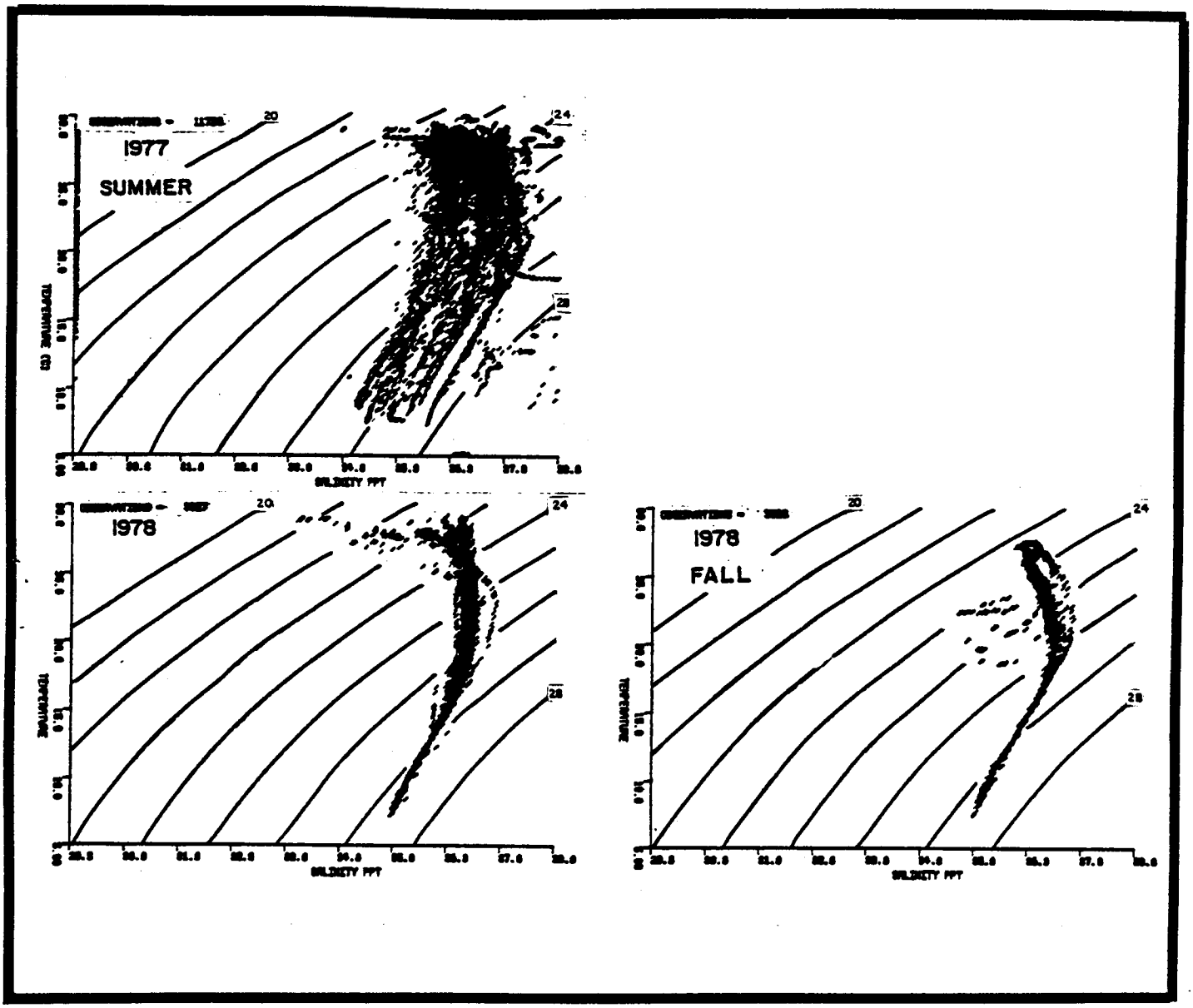

Figure 5-50. Overall SAB 1977/1978 temperature/salinity characteristics by season. (Continued).

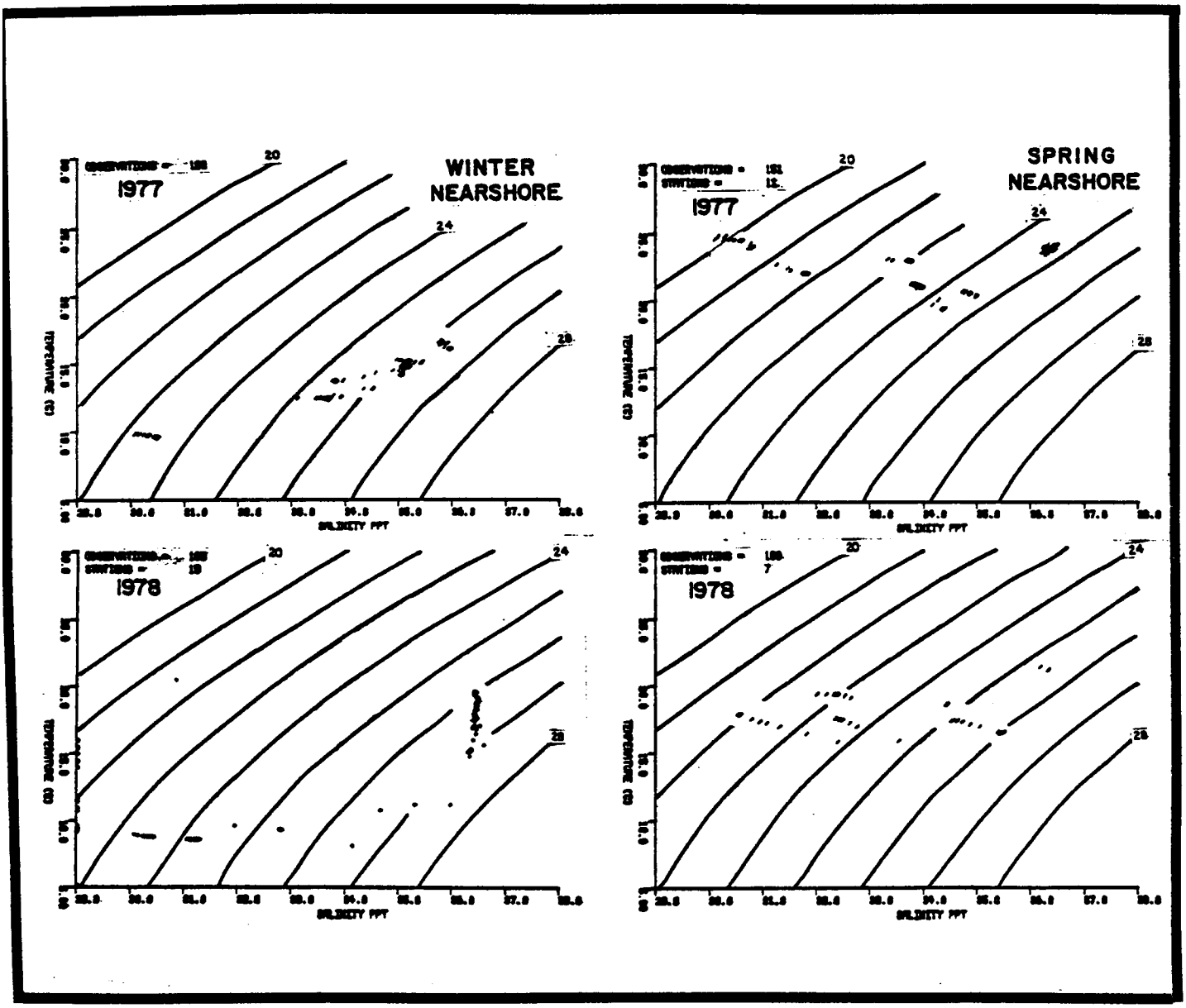

Figure 5-51. Nearshore SAB 1977/1978 temperature/salinity characteristics by season.

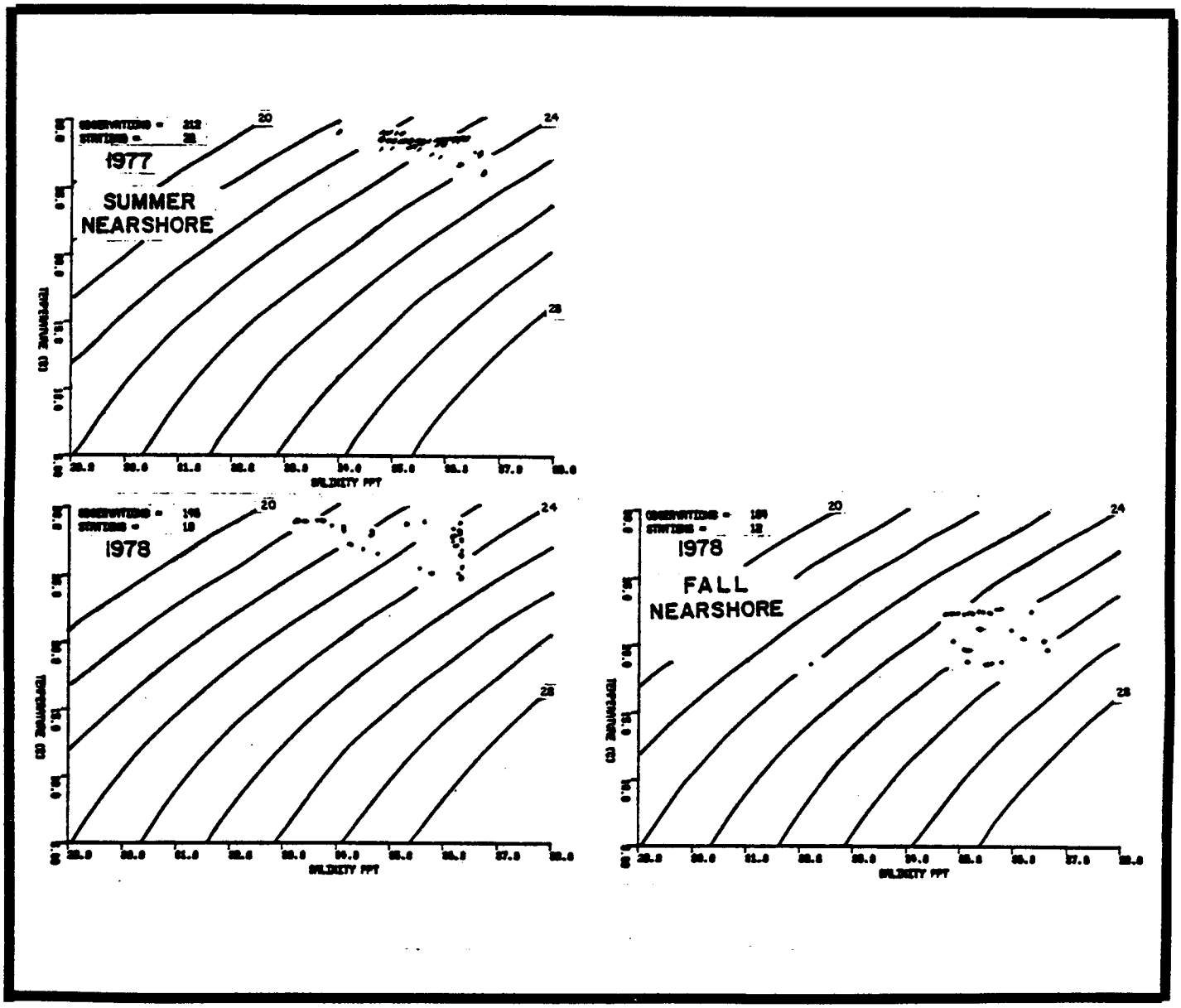

Figure 5-51. Nearshore SAB 1977/1978 temperature/salinity characteristics by season. (Continued).

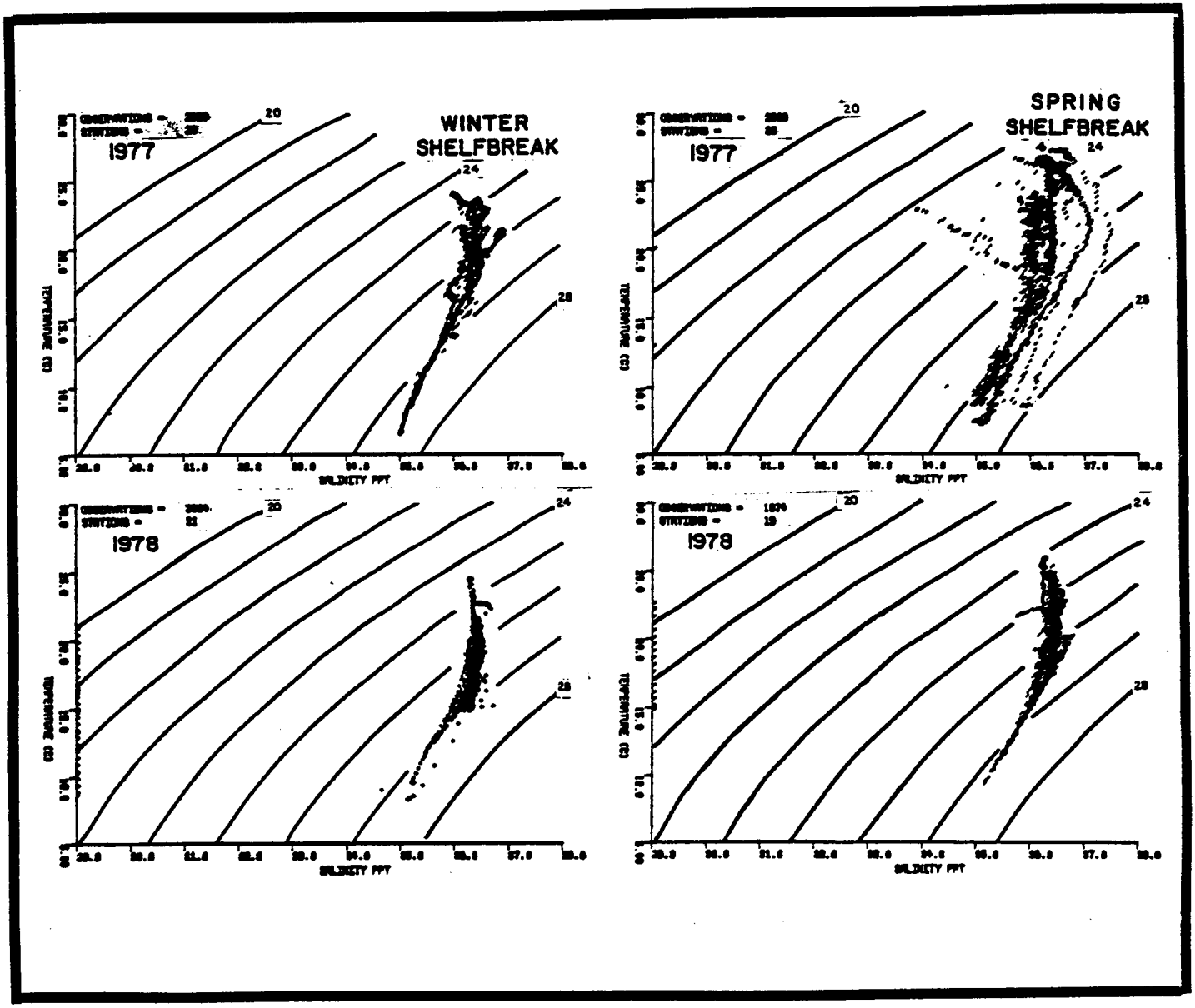

Figure 5-52. Shelfbreak SAB 1977/1978 temperature/salinity characteristics by season.

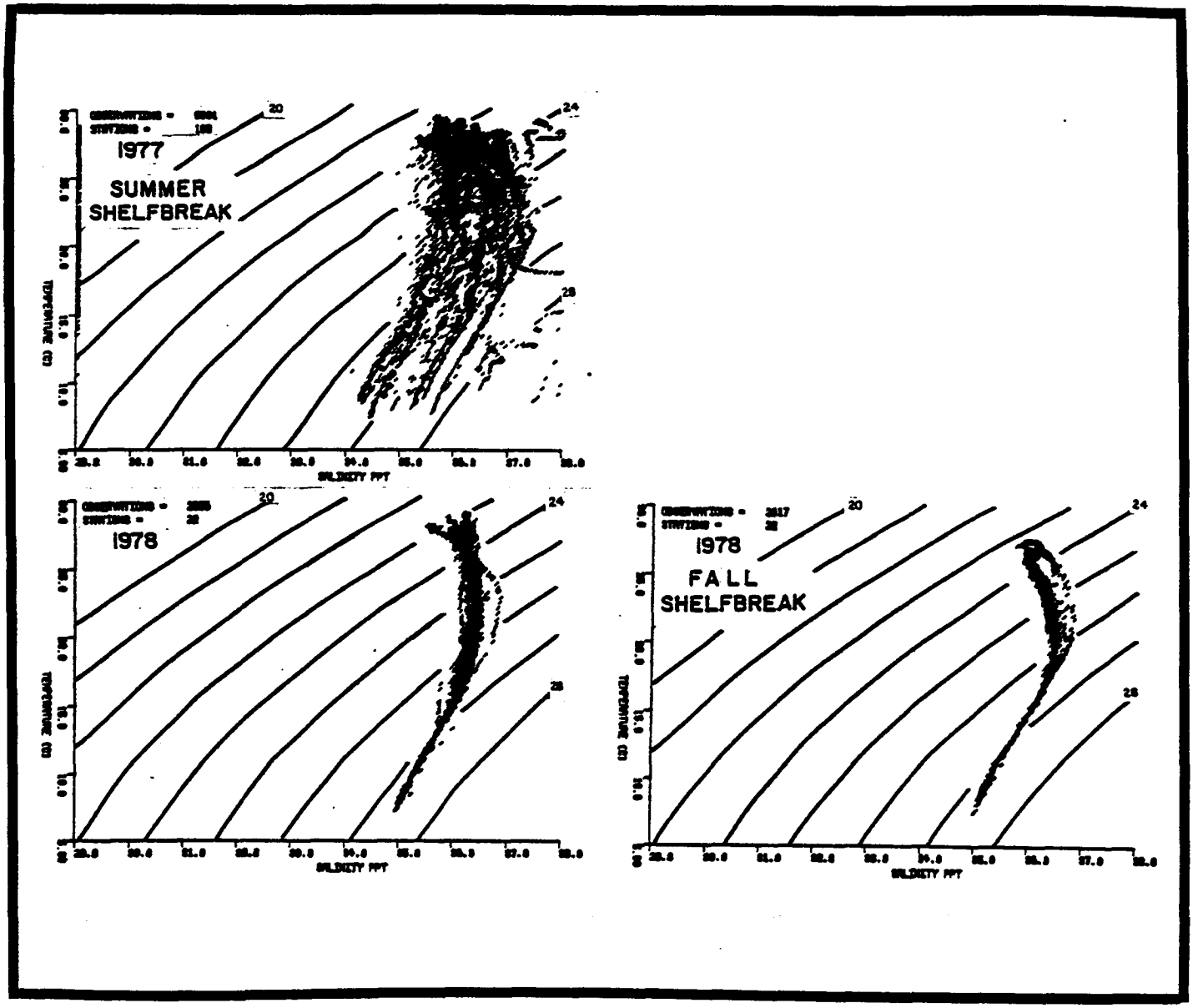

Figure 5-52. Shelfbreak SAB 1977/1978 temperature/salinity characteristics by season. (Continued).

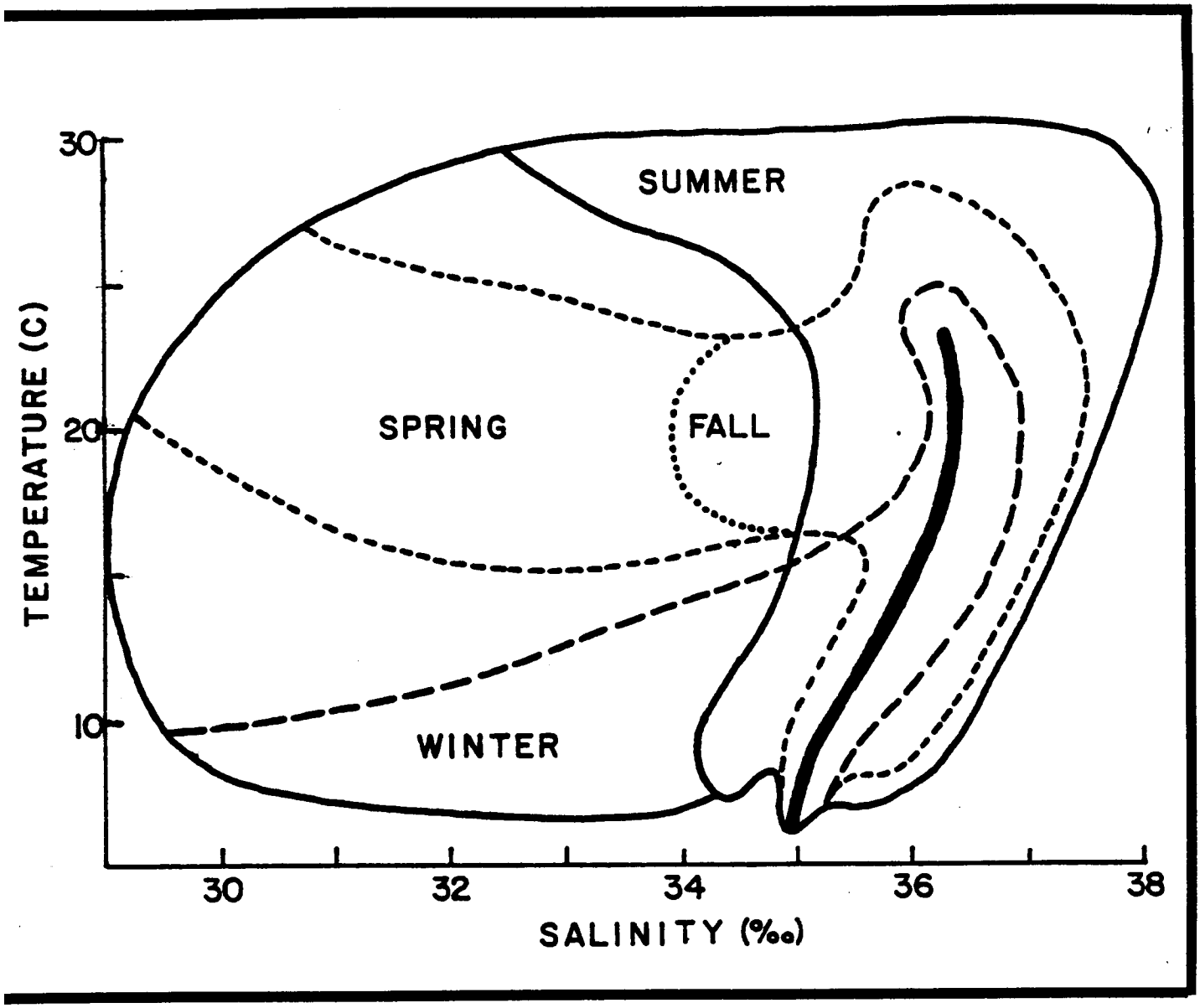

Figure 5-53. Schematic of overall, seasonal SAB water mass regime.

forecast seasonal atmospheric conditions allow an overall prediction of resultant SAB water properties. Alongshelf regional focus may be obtained through the added use of Figure 5-49.

The process of spin-off eddy formation and its influence on the shelf water was documented in the fall, 1978 survey data. The surface salinity field, Figure 5-54a, illustrates an elongated band of high salinity water detached from the Gulf Stream and located about mid-shelf. The subsurface fields, Figure 5-54b, show that the core of this eddy penetrated to the bottom and it extended across most of the shelf. The density field was consistent with cyclonic rotation if the motion was approximately geostrophic. The horizontal structure of the observed fields suggests that along-shelf advection may have been important in ultimately dissipating the detached water mass.

Runoff, usually most important during spring and early summer, is illustrated clearly in its effects in the spring, 1978 data. The surface salinity, Figure 5-55a, nearshore in the vicinity of Savannah was less than $31^{o}/oo$, with an almost linear gradient seaward to $35^{o}/oo$ at mid-shelf. The alongshore limits of the source region were clearly defined. Subsurface, Figure 5-55b, the relatively fresh water mass could be traced out to the shelf-break where in the upper layers it abutted Gulf Stream water forming a sharp surface front, and in the lower layers it over-rode the more saline shelf/slope water mass. Dynamical processes associated with the resultant sharp density front may be the dominant mechanism for mixing these two water masses.

The process of lateral entrainment along the Gulf Stream western front may be important at times in affecting hydrographic properties in the SAB. An example of the process occurred in the winter 1978 data set. The surface salinity field, Figure 5-56a, south of Savannah along the shelfbreak indicated penetration of high salinity water well onto the shelf. The subsurface transects, Figure 5-56b, showed a complex vertical structure in this region with several isolated anomalies. Indications of organized deformation scale eddy-type motion were absent and lateral mixing or vertical overturning seemed plausible. Presumably, this process is associated with Gulf Stream meandering as a result of long wave propagation, topographic influences, and/or dynamic instabilities.

The Gulf Stream intrusion process is one of the primary mechanisms for nutrient replenishment on the shelf (Atkinson, 1977). The summer, 1977 time series data off Jacksonville provide an example of a relatively limited cross-shelf intrusion. The surface fields, Figure 5-57a, showed a shoreward meander in the Stream over the shelf and then a deflection seaward again further north. The associated divergence drove upwelling at the shelfbreak, Figure 5-57b. Succes-

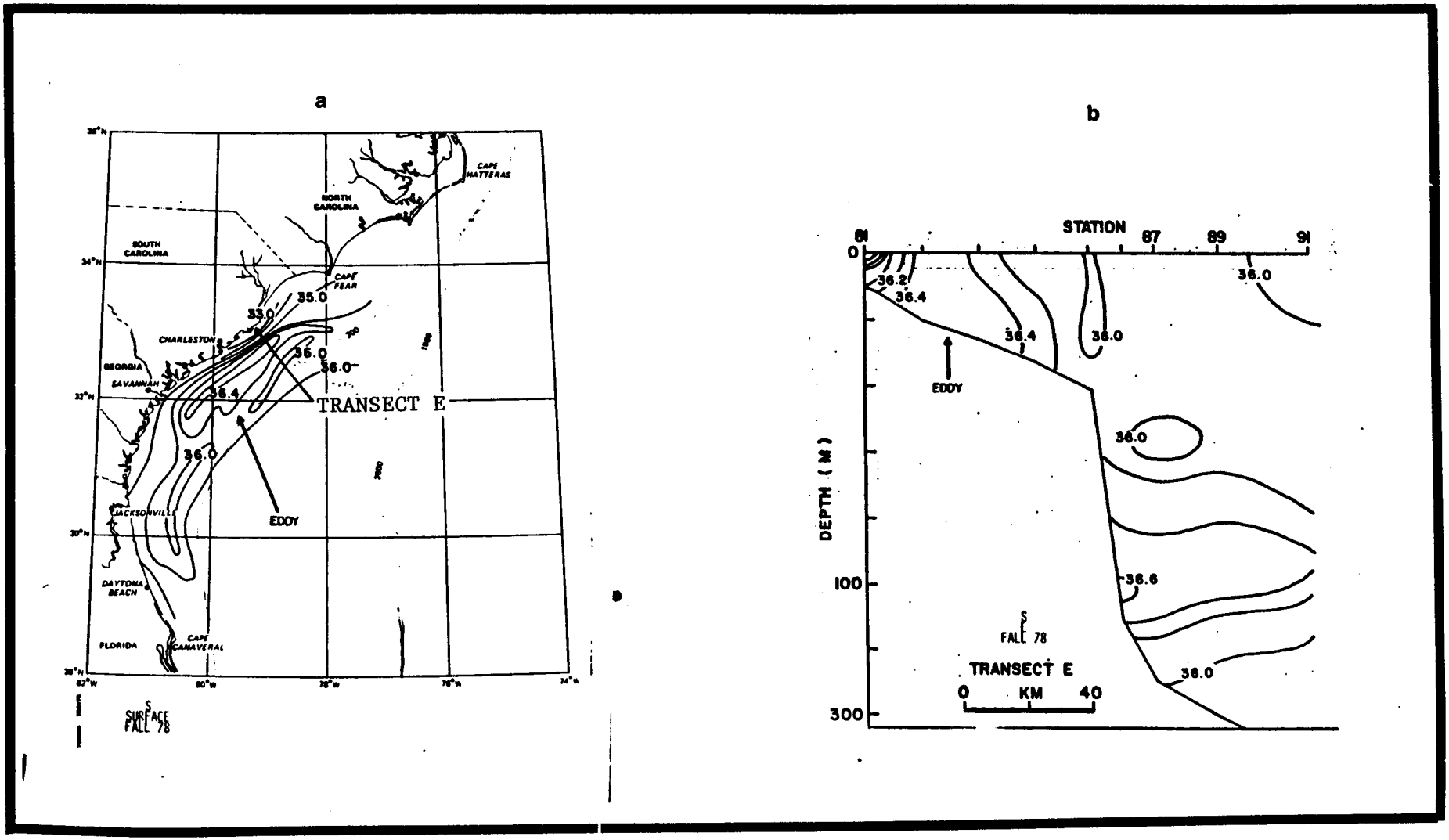

Figure 5-54. Examples of observed Gulf Stream eddy formation.

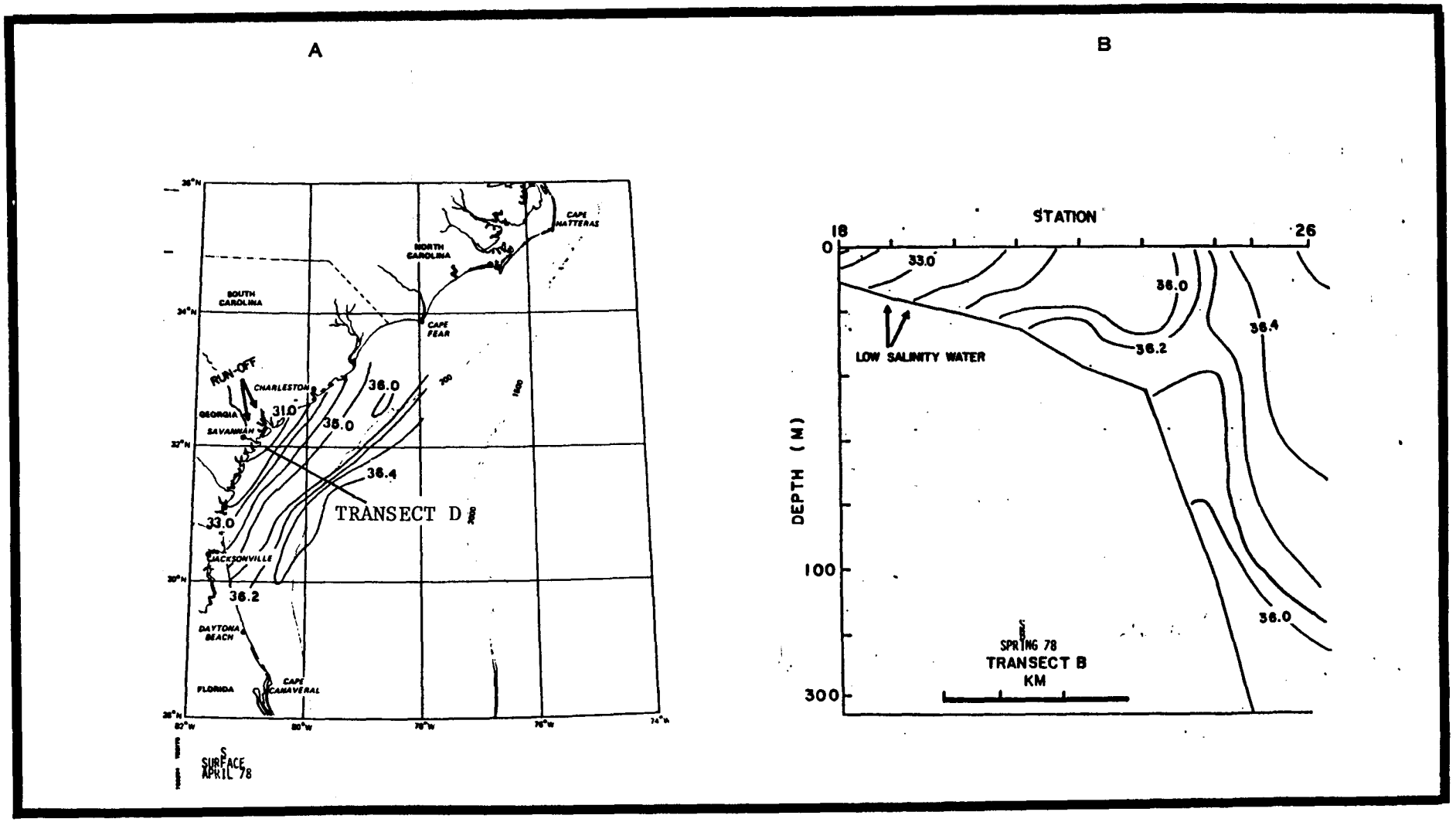

Figure 5-55. Examples of observed run-off.

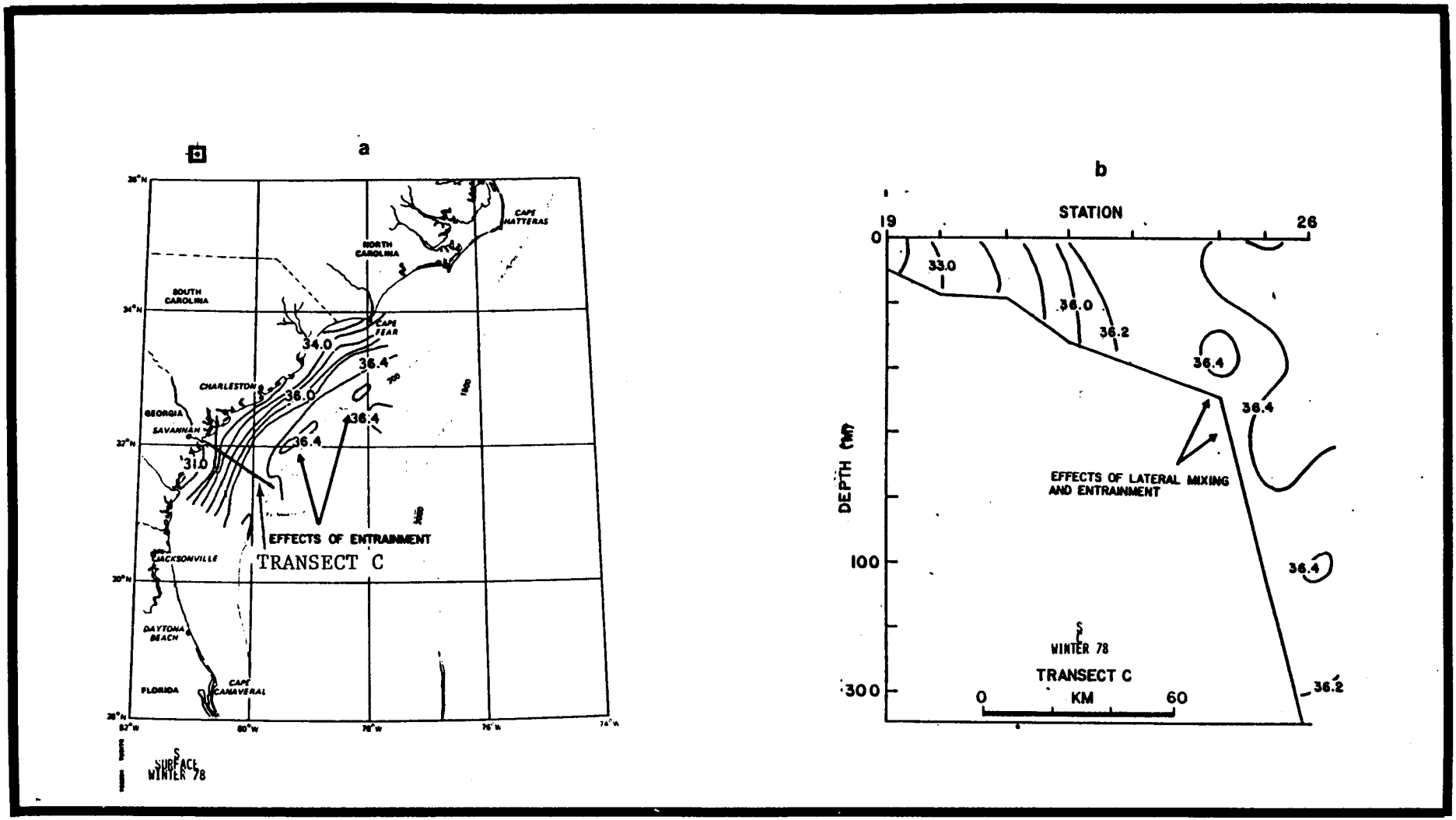

Figure 5-56. Examples of observed Gulf Stream lateral entrainment.

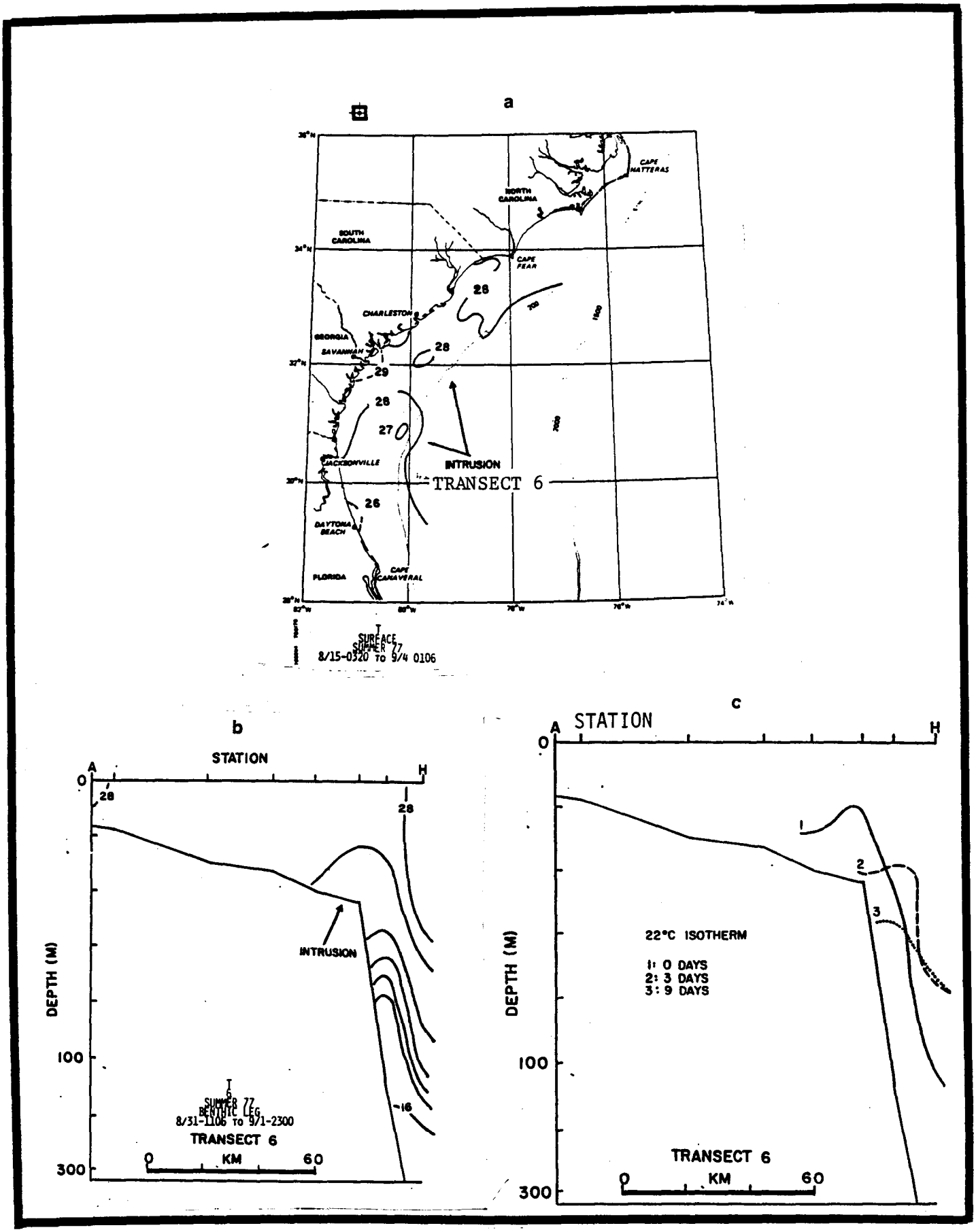

Figure 5-57. Example of observed Gulf Stream intrusion.

sive positions of a selected subsurface isotherm (22°C), Figure 5-57c, resulted in a 40 m vertical excursion in 9 days or about a 5 x 10^{-3} $cm.s^{-1}$ vertical velocity near the slope region.

In winter, cooling and wave stiring in shallow, nearshore waters result in a source of supply of relatively dense water inshore which subsequently may spread seaward across the shelf nearbottom and spill over the shelf edge down the slope. An example of this cascading process can be seen in the winter 1978 data. Nearbottom, laterally, Figure 5-58a, a source of dense water can be observed nearshore between Charleston and Savannah. Transects in this region, Figure 5-58b, showed the shelfbreak of almost 100 m. Neighboring transects (cf. Volume III, Section 3.2) showed a similar subsurface structure.

Virginia Water could not be positively identified in any of the hydrography in this report. This water mass can rarely be traced further south than Raleigh Bay which is north of the area over which present investigations were carried out.

5.6.3 Gulf Stream Variability from Remote Sensing Techniques

As indicated in Section 5.2.3, the purpose of this analysis was three-fold. The investigation was aimed at assessing the efficacy and confidence levels that can be placed in satellite derived frontal motion statistics. It was also addressing the question of representativeness of the ship survey data in determining seasonal variability. Finally, this effort was to provide seasonal mean and extrema charts for the Gulf Stream/Shelf Water interface on a seasonal basis. Techniques used in the analysis and conclusions resulting from this study are presented in the upcoming section.

5.6.3.1 Assessments of Satellite Infrared Mapping Techniques for Gulf Stream Monitoring

During this first year's activities, the feasibility of tracking fine to large scale variability in the Gulf Stream shelf water interface via satellite infrared remote sensing was demonstrated, and image navigation, mapping and enhancement techniques that permit direct intercomparison of satellite and ship data were successfully developed.

Figure 5-59 shows a navigated VHRR image for April 10, 1977. Continental outlines and state boundaries have been inserted into the image to permit unbiased assessment of the navigational transform. The light blue zig-zag line off the Georgia coast is the located ship track for the R/V ISELIN (April 10, 1977, to April 12, 1977) generated from the ship's position log. This particular track was chosen since it purposely heavily samples the slope water/Gulf Stream interface and was considered ideal for satellite vs. ship observations comparisons, as errors in satellite image navigation or

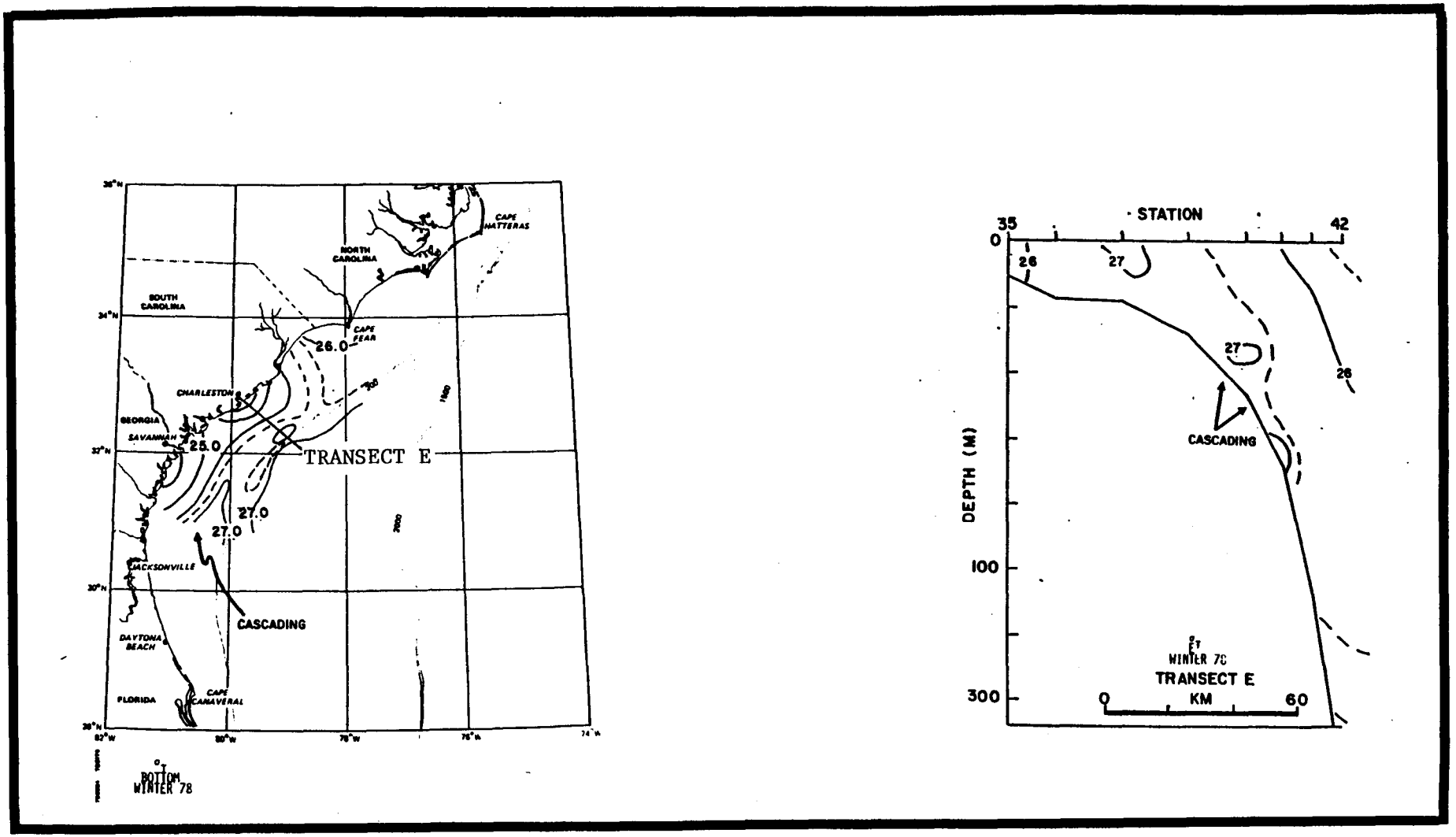

Figure 5-58. Examples of observed cross-shelf cascading.

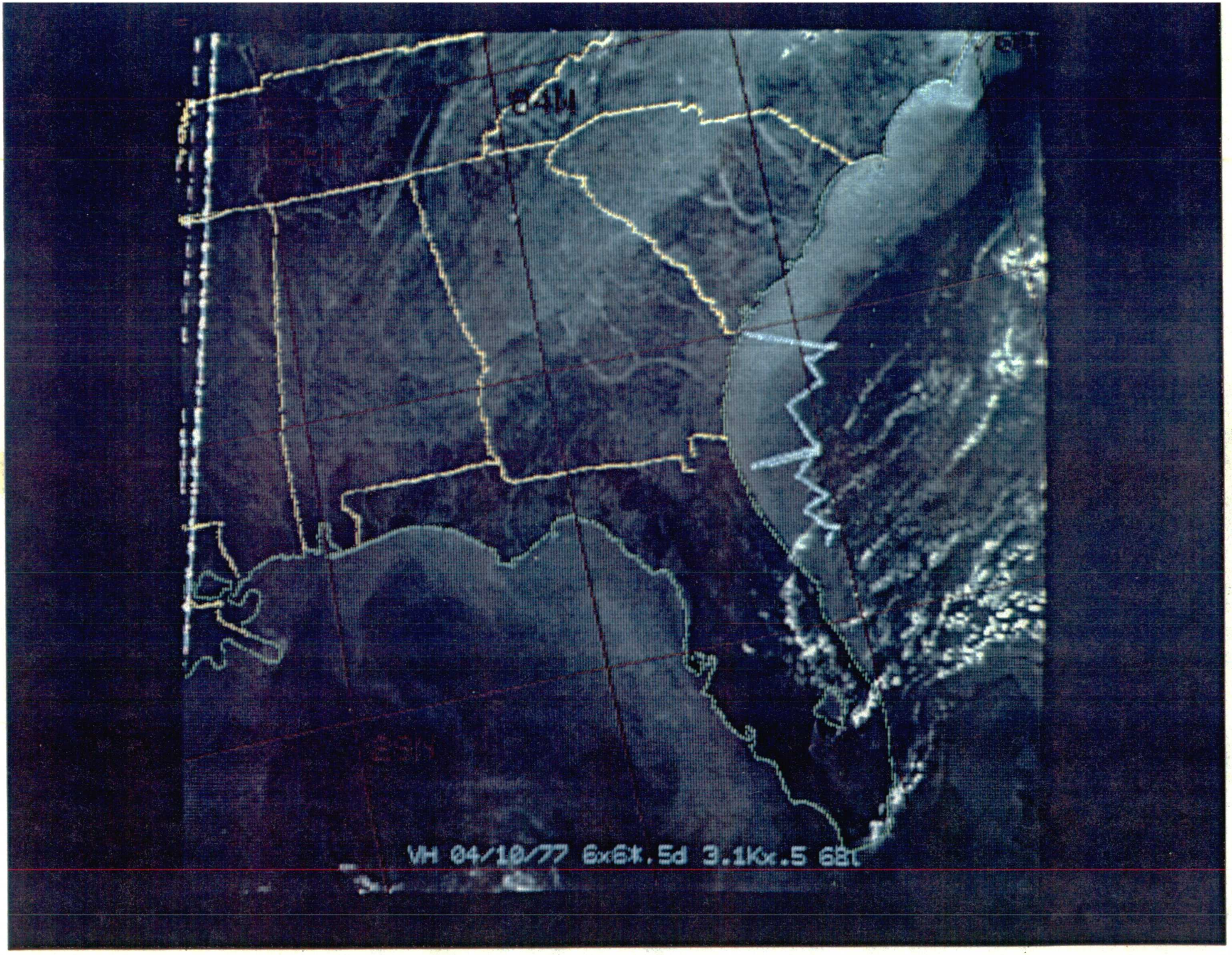
VH 04/10/77 6x6%.5d 3.1Kx.5 68%

temperature calibration would be readily apparent. Sea surface temperature were measured by Dr. T. Lee on board the vessel with a continuously recording thermosalinograph.

Figure 5-60 presents the surface temperature observations by ship and satellite as a function of distance along ship track. A mean bias has been removed from the satellite observations by comparison of a section of ship and satellite temperatures on the isothermal area near the Georgia coast. This calculated bias is $-1.62^{o}K$; the plotted data has been adjusted to the nearest digital level, i.e., by $-1.5^{o}K$. Correlation coefficient between the two series is 0.89 with the standard deviation of the difference, $1.1^{o}K$. Visual examination of the two series shows very good coherence in the frontal structure delineation by the satellite observations, as well as faithful reproduction of the lower spatial frequency variability.

Such an image can be rectified, e.g., Figure 5-61, by applying the navigation information to a mapping function. The resultant image has 512 x 512 ($.025^{o}$ x $.025^{o}$) pixels centered at $78.7^{o}W$, $32^{o}N$. As this image is formed from a radiometrically correct digital surface temperature field, it is readily converted to a conventional two-dimensional temperature contour map, Figure 5-62. The precise location of a given isotherm is now available for the analysis purposes. A time series of rectified images permits generation of variability on temporal scales determined by the sampling interval. A week of retrieved Gulf Stream-slope boundaries derived from contour maps are shown in Figure 5-63. Northward propagation and development of a spinoff eddy in the lower left hand corner of the retrieval rectangle is easily seen; propagation speeds of 30 $cm.s^{-1}$ are determined by successive differentiation of the eddy position. In the northern part of the area, a larger scale oscillation of the boundary with 80 km amplitude is observable.

It was concluded that satellite remote sensing can give highly accurate surface thermal maps in the Georgia Bight and that Gulf Stream variability of a time scale of one to three days can be synoptically monitored using this technique.

5.6.3.2 Seasonal Gulf Stream frontal variability and representativeness of hydrographic cruise data.

The U. S. Navy/NAVOCEANO weekly Gulf Stream frontal analysis based on satellite observations were used to prepare longer-term variability maps in order to assess the adequacy of the hydrographic data collected along cross-shelf transects in characterizing seasonal variability over the shelf and near the shelf break.

There were 5 BLM sponsored hydrographic cruises in the Georgia Bight during 1977. They occurred over the periods of February 1 to 8, May

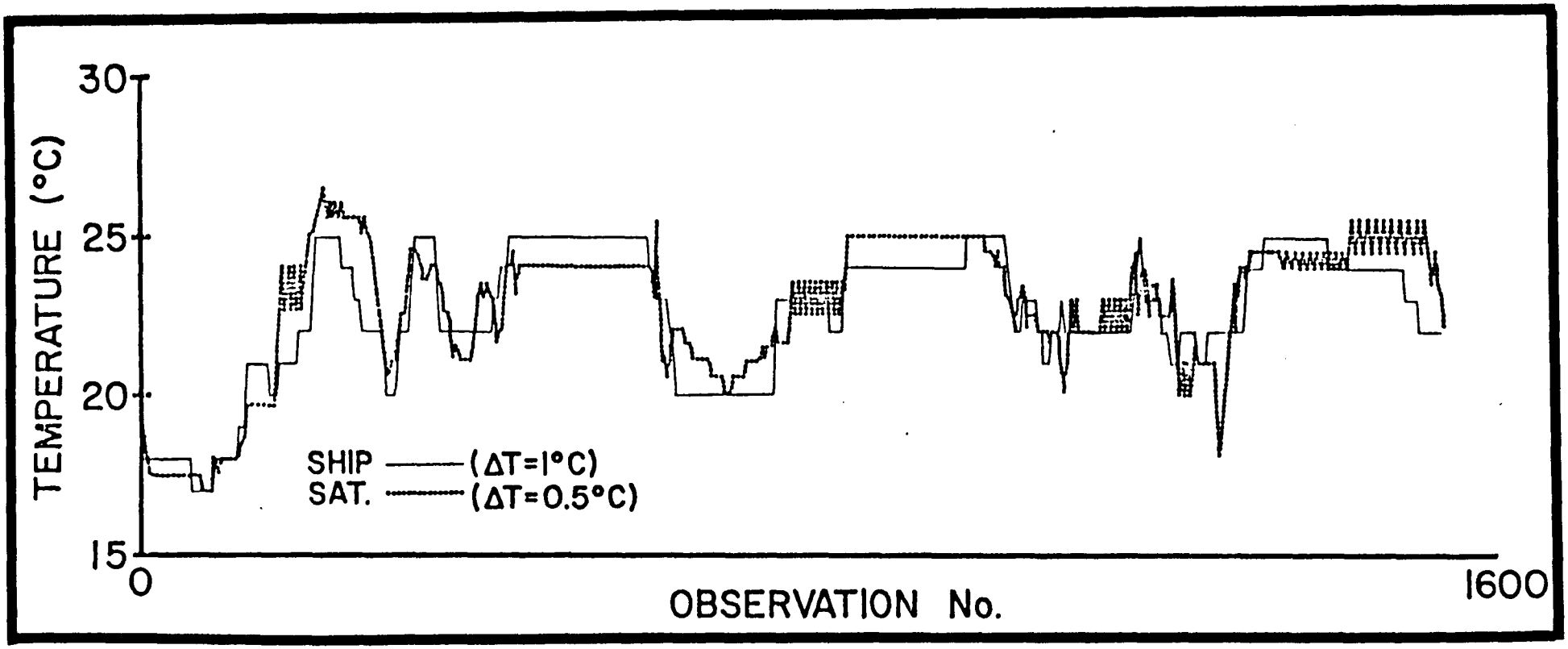

Figure 5-60. Intercomparisons of surface thermal observations aboard the R/V ISELIN with satellite infrared retrievals (04/10/77).

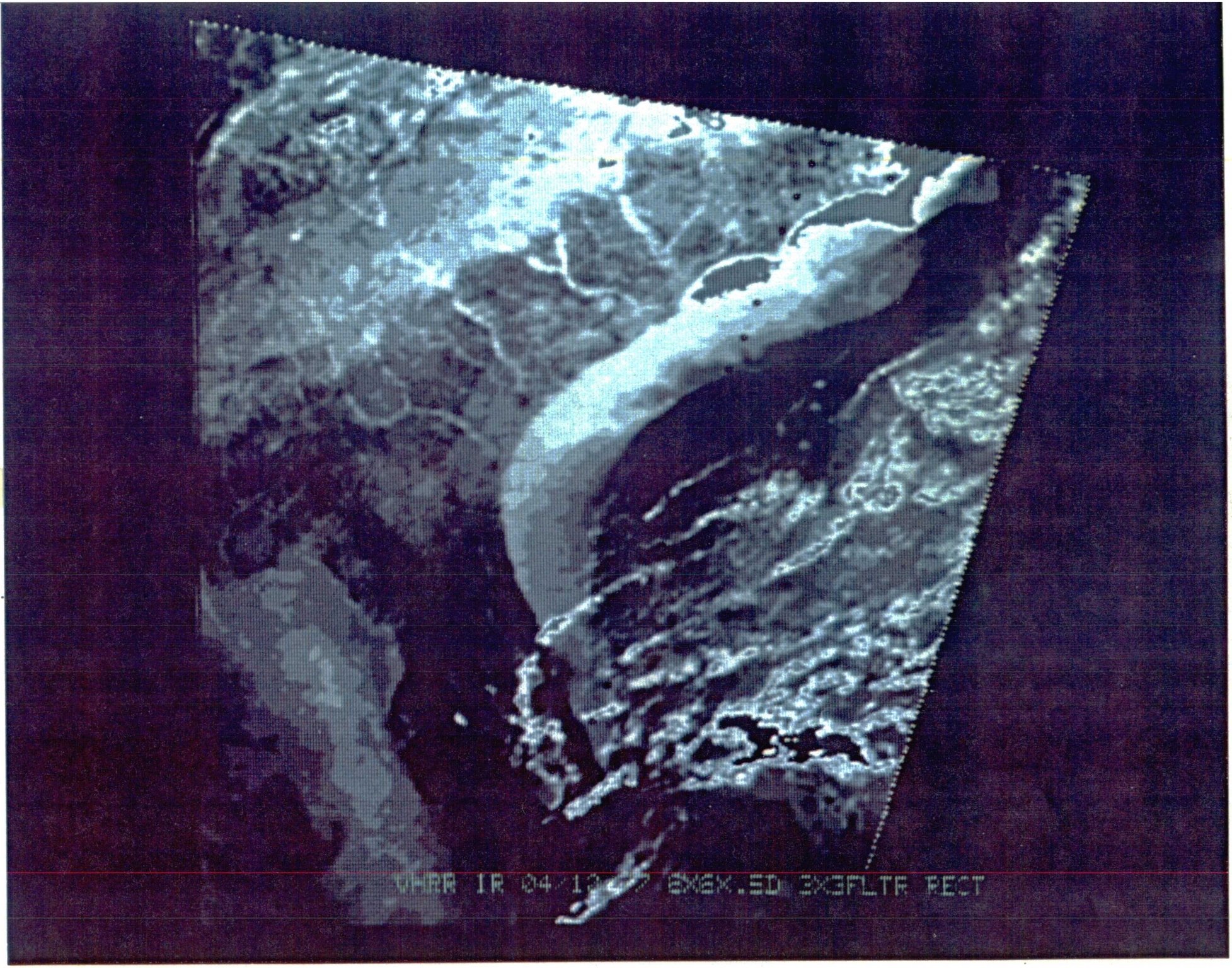
GHRR IR 04/12 0X6X.SD 3XGFLTR RECT

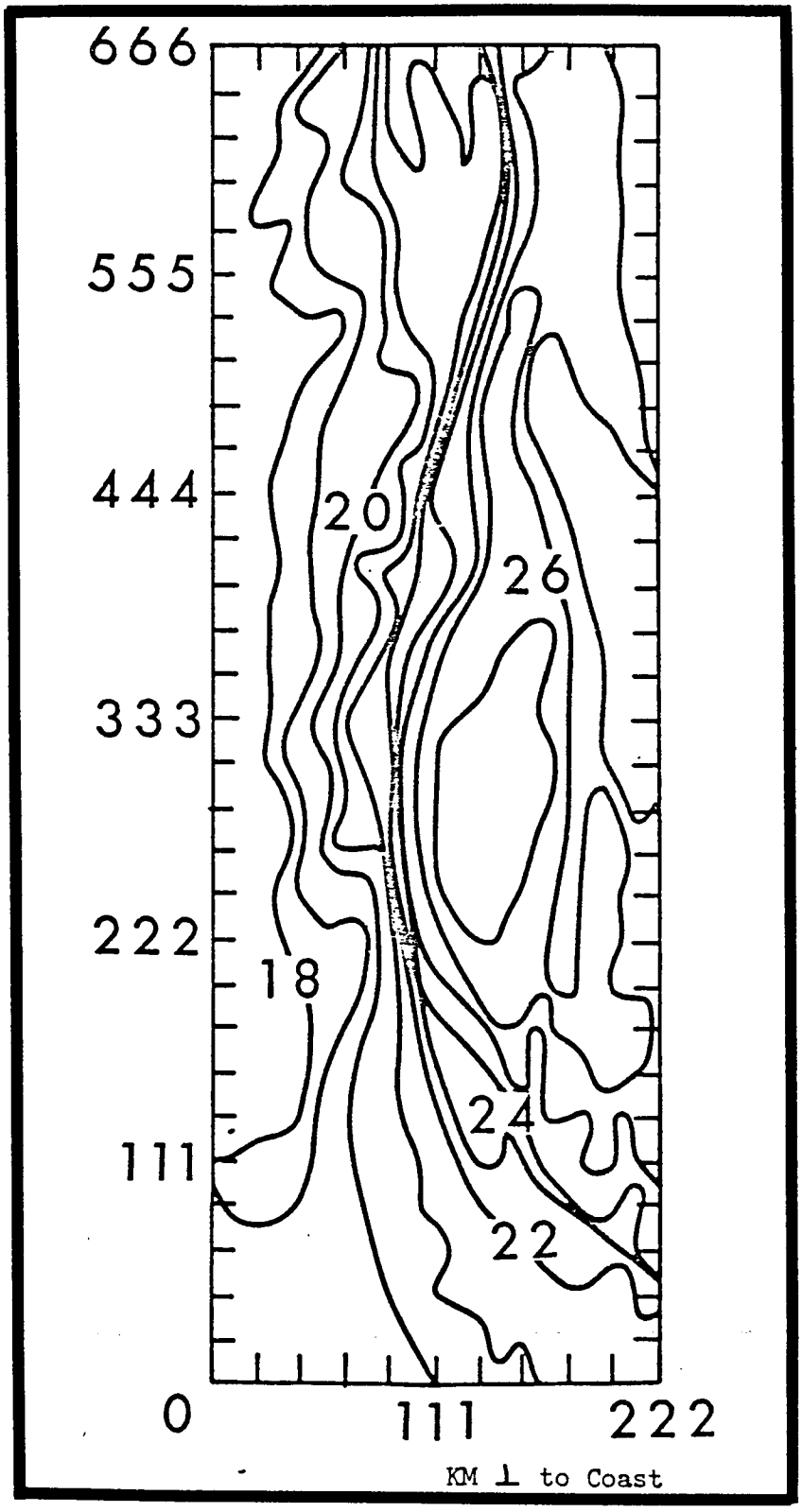

Figure 5-62. Contour map generated from satellite infrared observations in the Georgia Bight (04/10/77), centered at 78.7°W, 32°N.

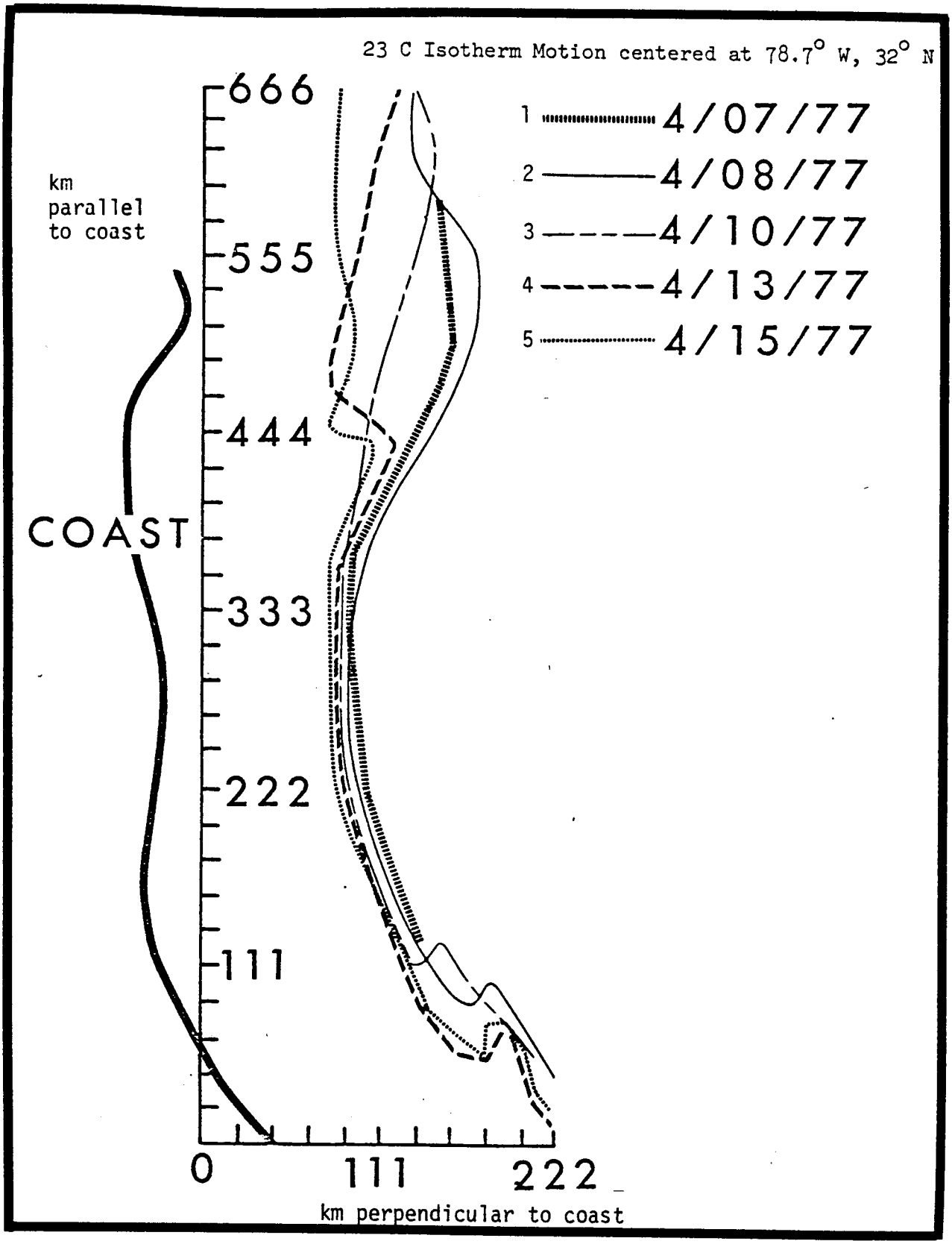

Figure 5-63. Variability of Gulf Stream/Slope Water interface position for week of 7 April 1977.

3 to 8, August 9 to 14, September 8 to 29 and November 10 to 29, 1977. They are hereafter referred to as Winter, Spring, Summer, Time-series, and Fall, respectively.

Charts were composed by overlaying successive weekly location data on a common reference map for the intervals noted to display:

a) Gulf Stream frontal location before and after a given cruise (Figures 5-64 to 5-68);

b) Gulf Stream frontal location on a strict seasonal basis (Figures 5-69 to 5-72);

c) Annual envelope of Gulf Stream frontal location (Figure 5-73);

d) Envelope inferred from cruise-time charts (Figure 5-74).

Comparison of Figures 5-73 and 5-74 shows that the Gulf Stream during the sampling was further offshore than the mean or extrema would suggest as its more ordinary location. Therefore, it would appear that the Benchmark cruises sampling was biased by these offshore Gulf Stream positions. The charts indicate that "the setting" of the various transects vis-a-vis the overall seasonal variation is good.

The extrema charts (Figures 5-69 - 5-72) show significant seasonal variation. Spring is the season of the year with the largest on-off shore frontal variability in the southern part of Georgia OCS. Summer manifests the largest variabilities in the northern section.

5.7 CONCLUSIONS

Based on the analysis of short-term current meter moorings records, current and temperature variability during the summer at the outer-shelf appears quite similar to winter conditions. Gulf Stream spawned events, such as wave-like meanders, instabilities and eddies continue to dominate the temporal behavior of the flow and temperature fields near the shelf break. Onshore-offshore meanders produce in phase, coherent fluctuations of velocity and temperature at periods of 2.5 to 3 and 5 to 10 days, similar to winter findings.

In the region of the box array deployed off Savannah, Georgia, the summer mean flow was toward the north at the shelf break, parallel to the local isobaths at 54 $cm.s^{-1}$ in the upper layer. At mid-shelf the summer mean flow was weak and northerly at 1.0 $cm.s^{-1}$ with an offshore component of 0.9 $cm.s^{-1}$. Prolonged southward flow episodes did occur in August and September for durations of 16 and 20 days that may have been partly wind generated and partly density driven.

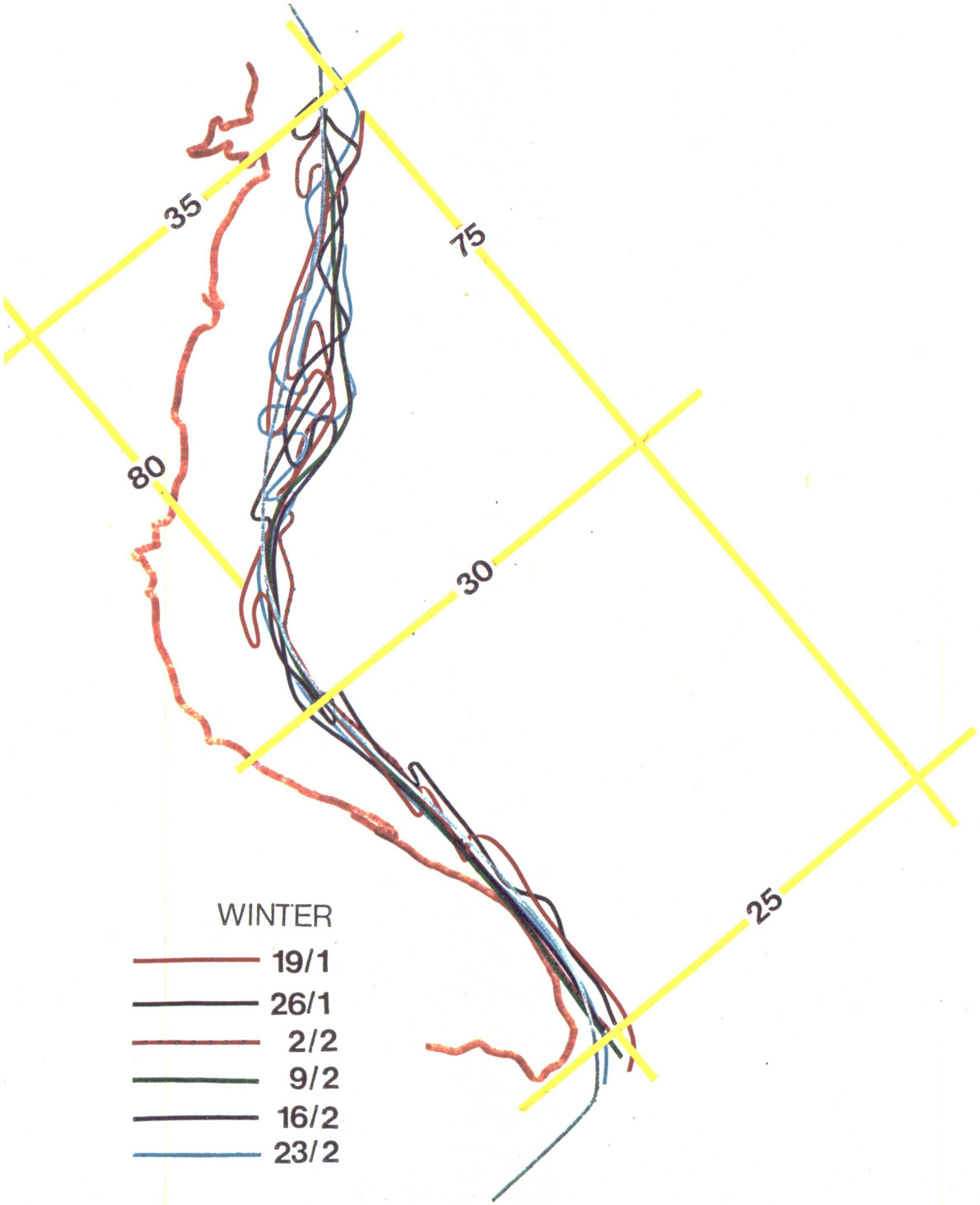

Figure 5-64. Gulf Stream front location for Winter cruise (week of cruise in red).

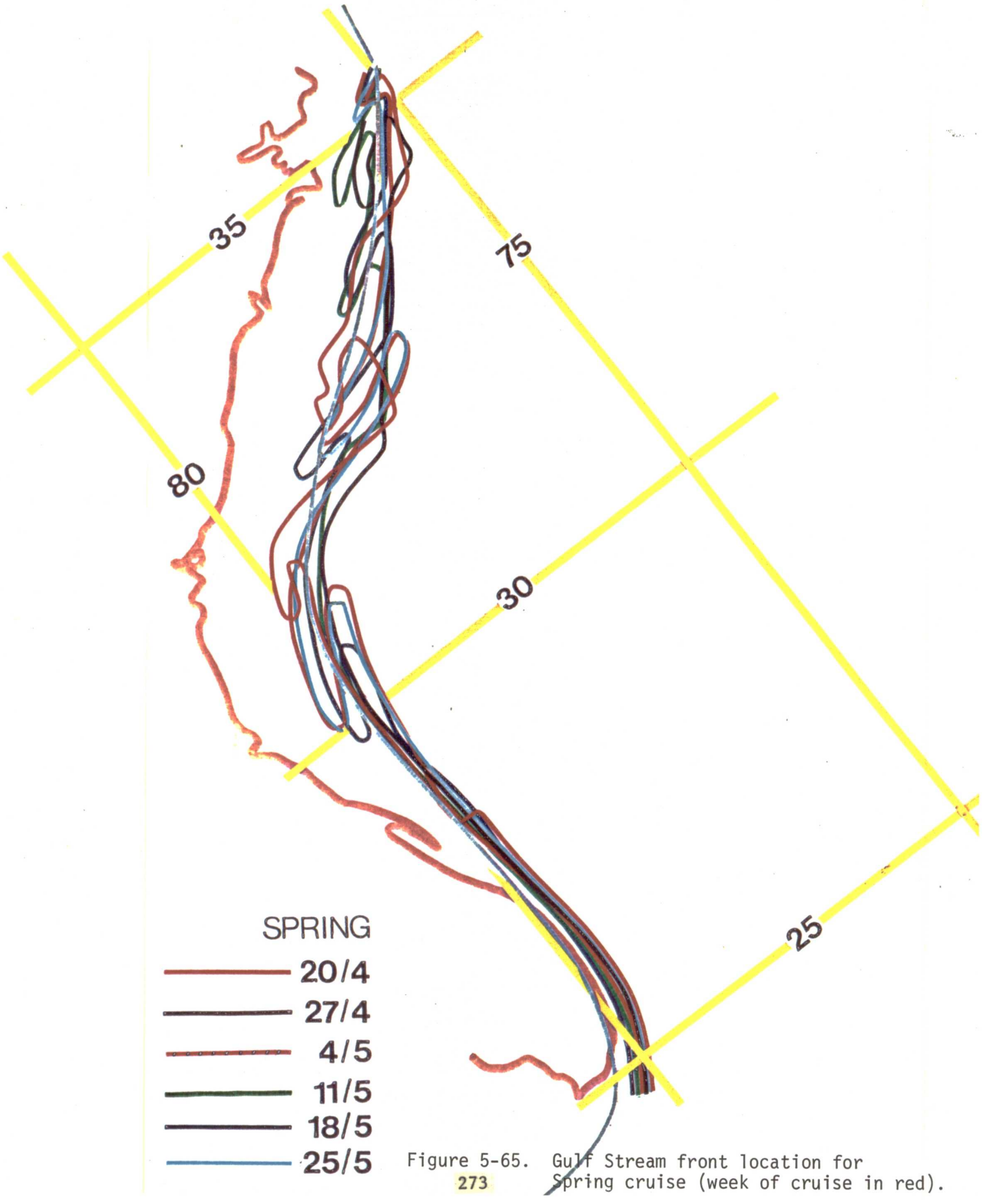

Figure 5-65. Gulf Stream front location for Spring cruise (week of cruise in red).

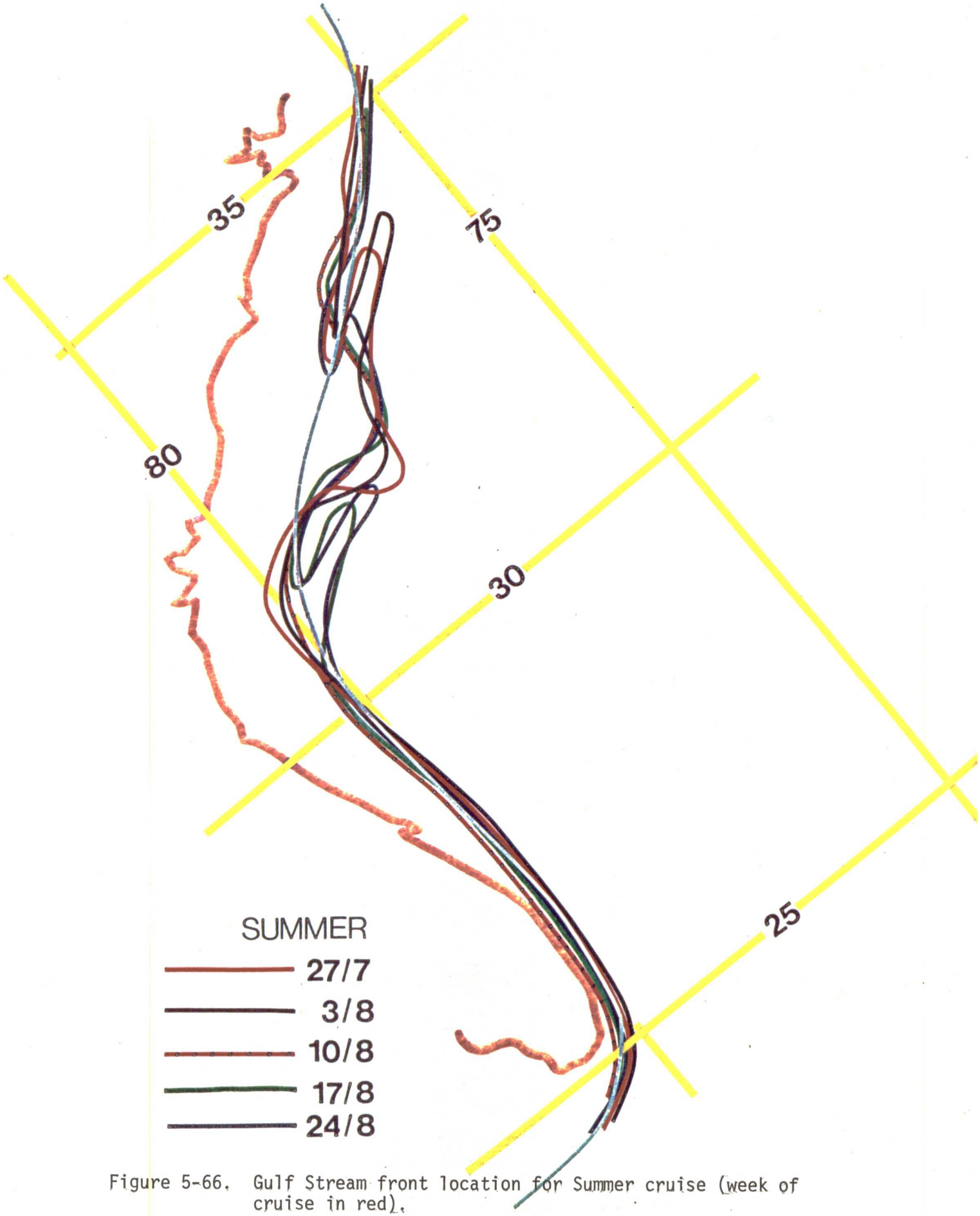

Figure 5-66. Gulf Stream front location for Summer cruise (week of cruise in red).

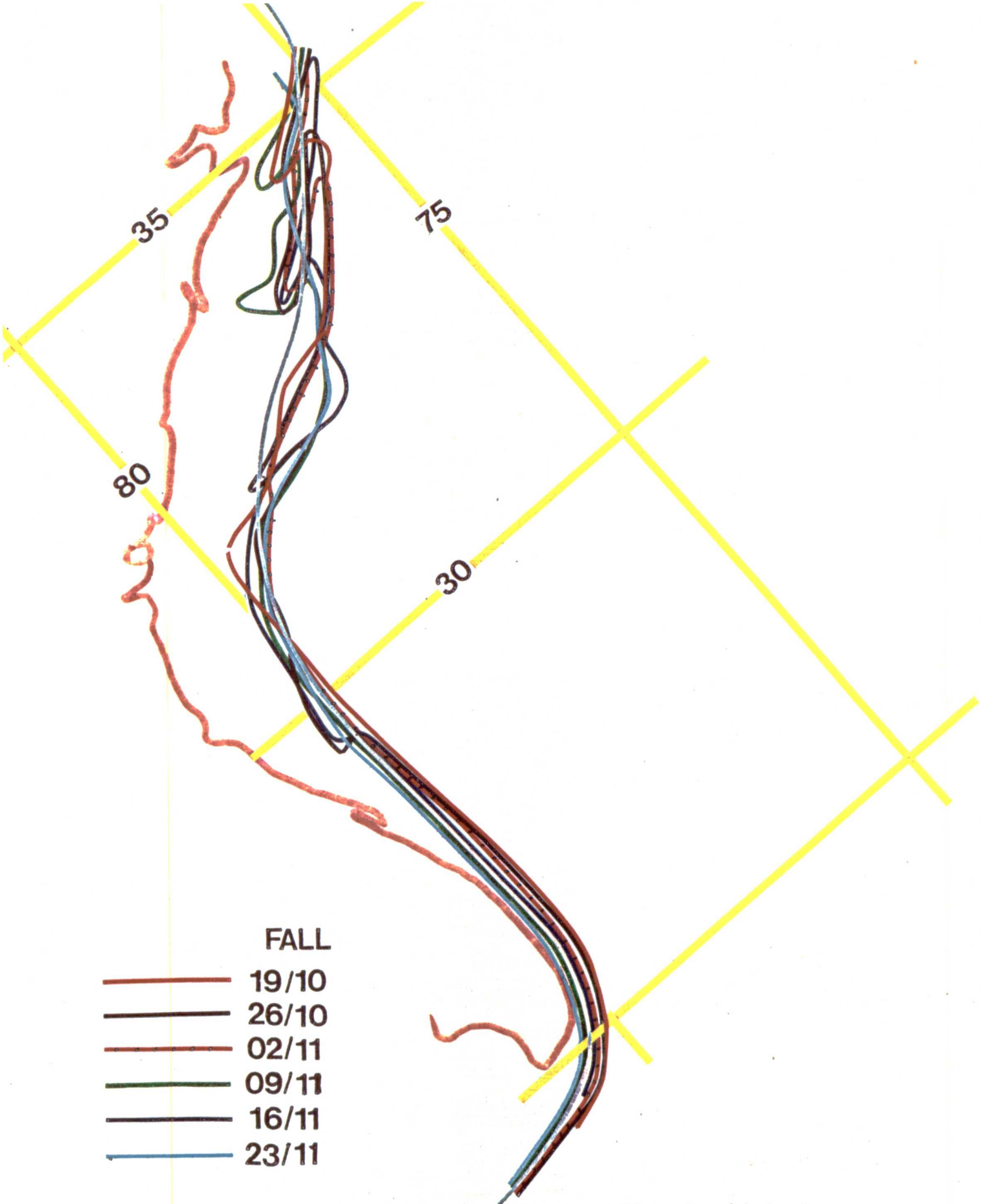

Figure 5-67. Gulf Stream front location for Fall cruise (week of cruise in red).

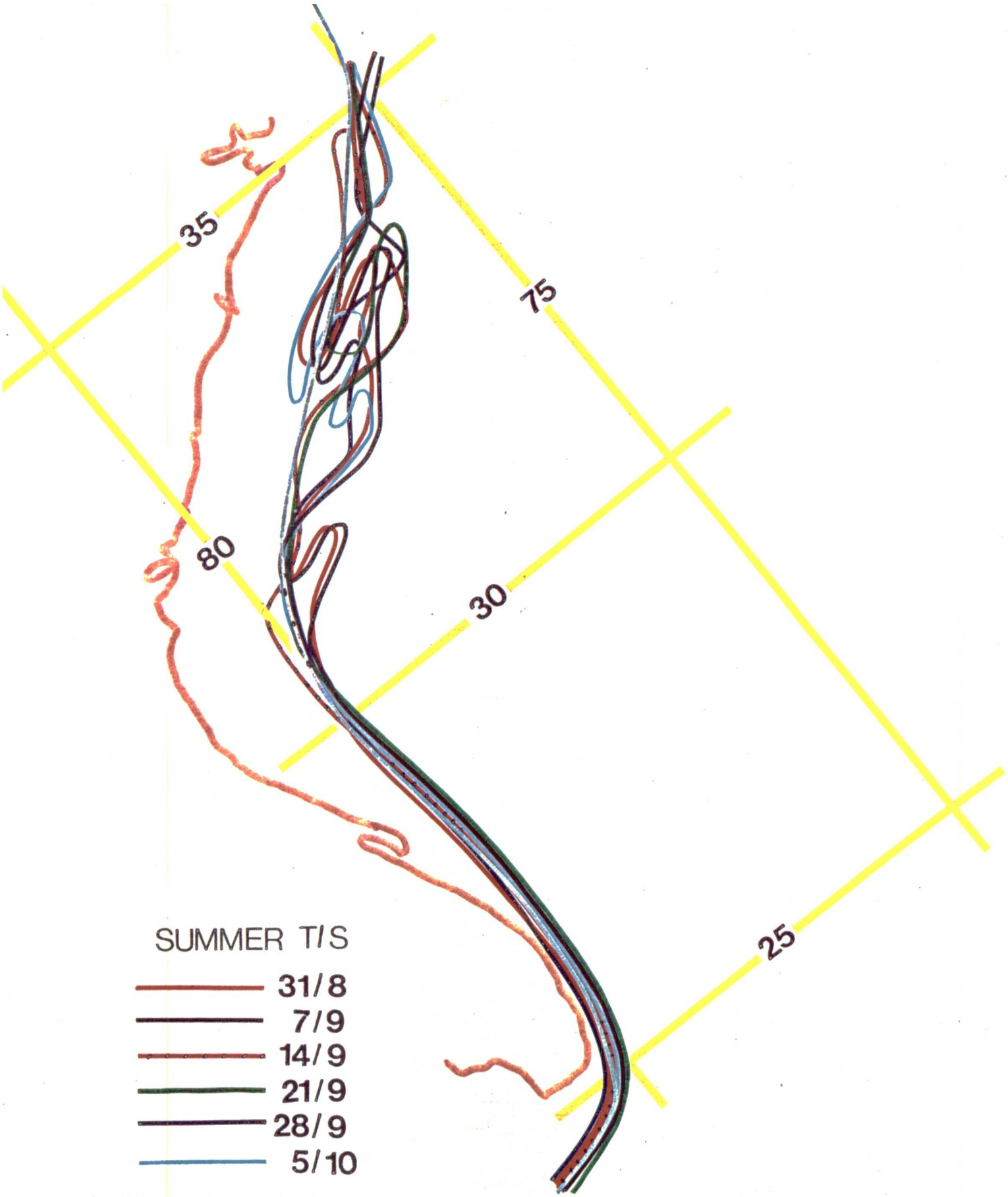

Figure 5-68. Gulf Stream front location for Summer Time Series.

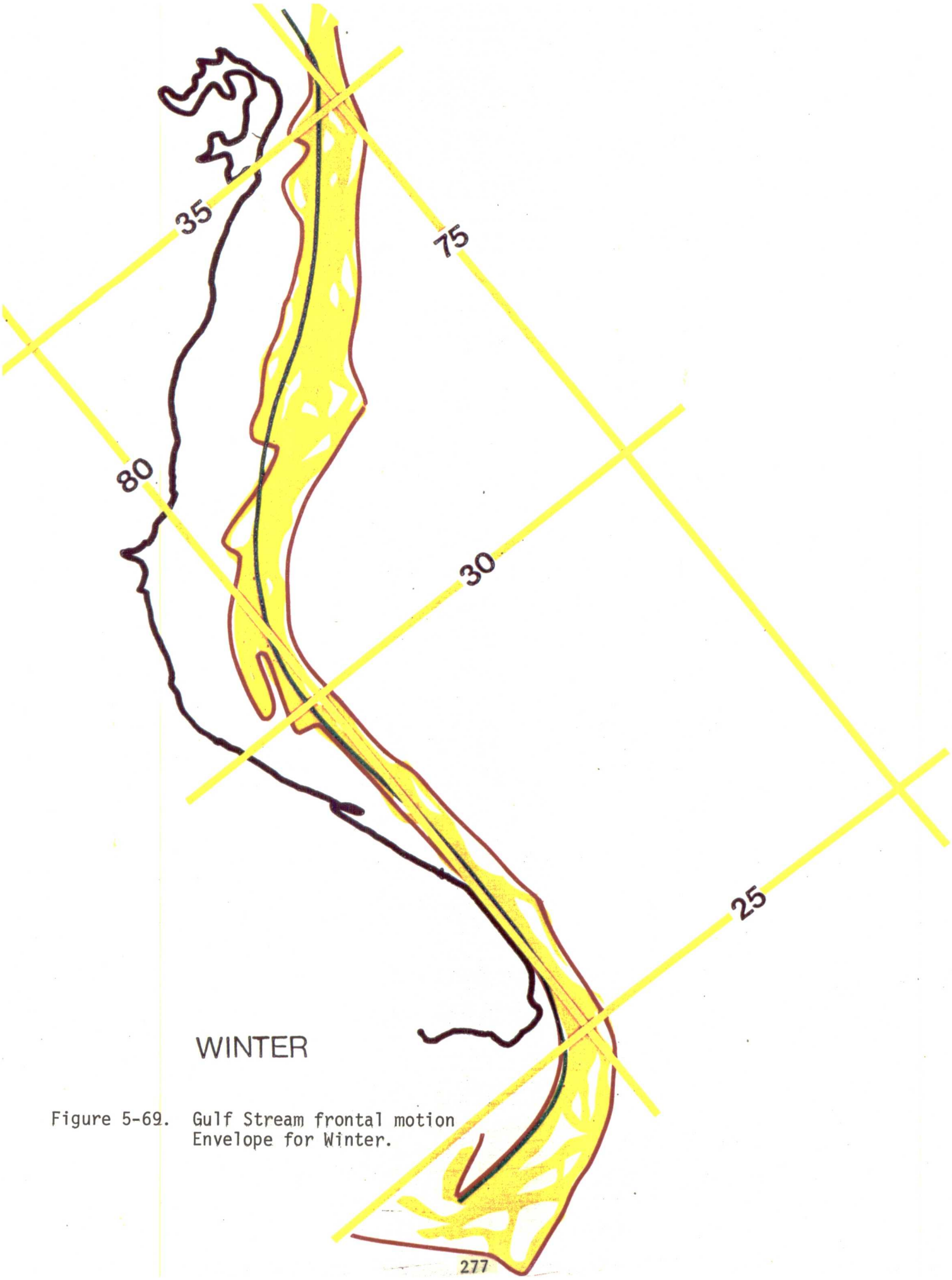

Figure 5-69. Gulf Stream frontal motion Envelope for Winter.

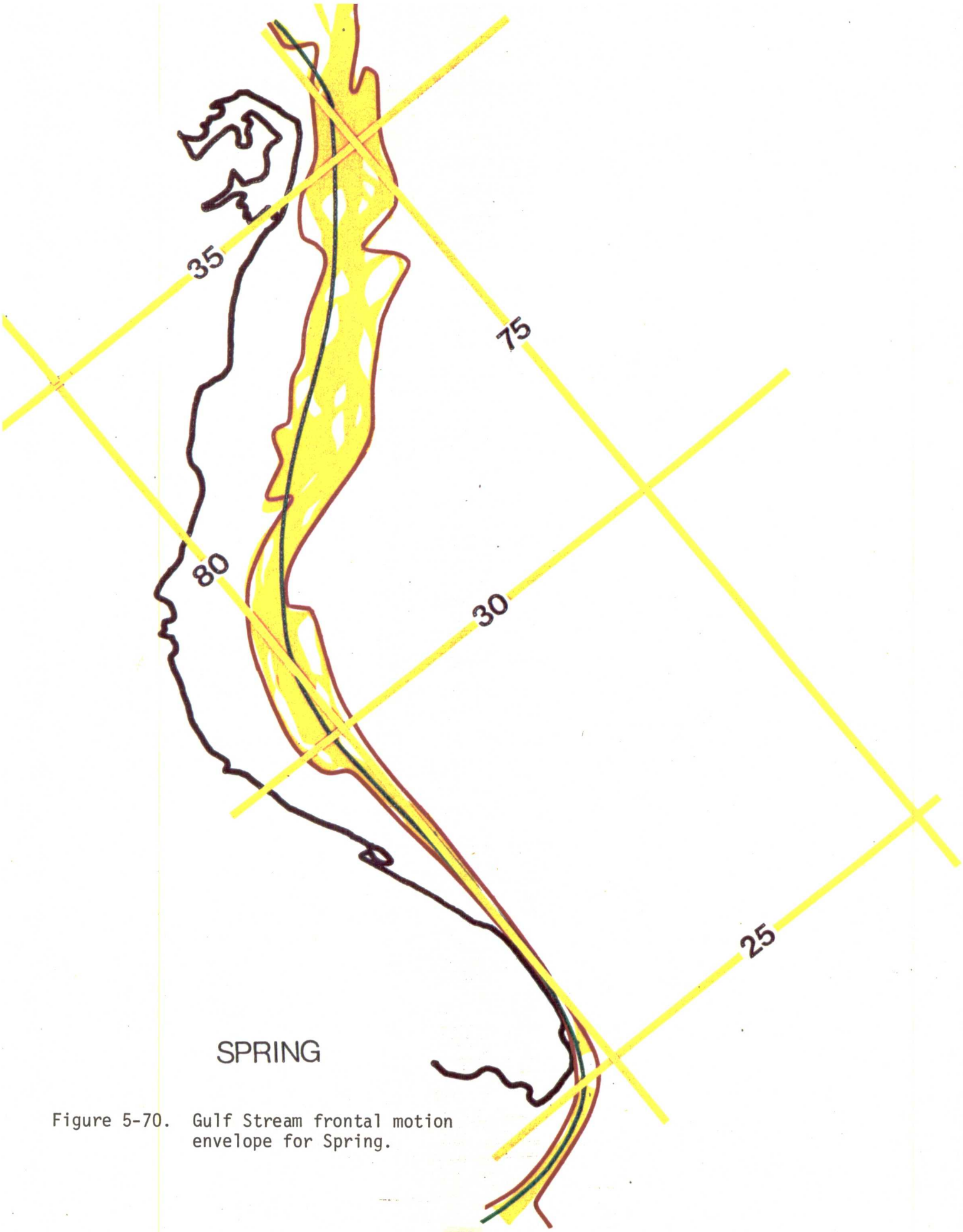

Figure 5-70. Gulf Stream frontal motion envelope for Spring.

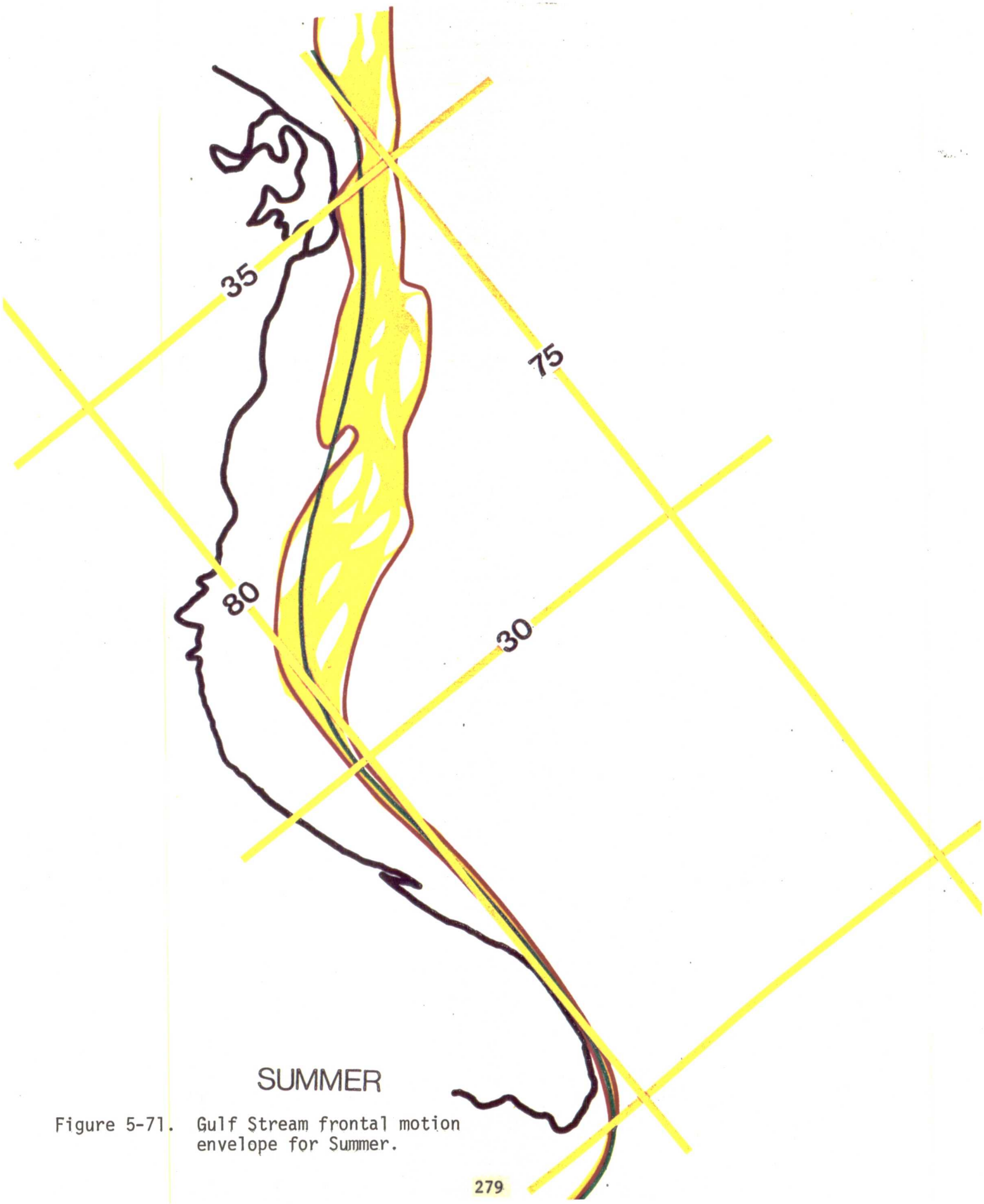

Figure 5-71. Gulf Stream frontal motion envelope for Summer.

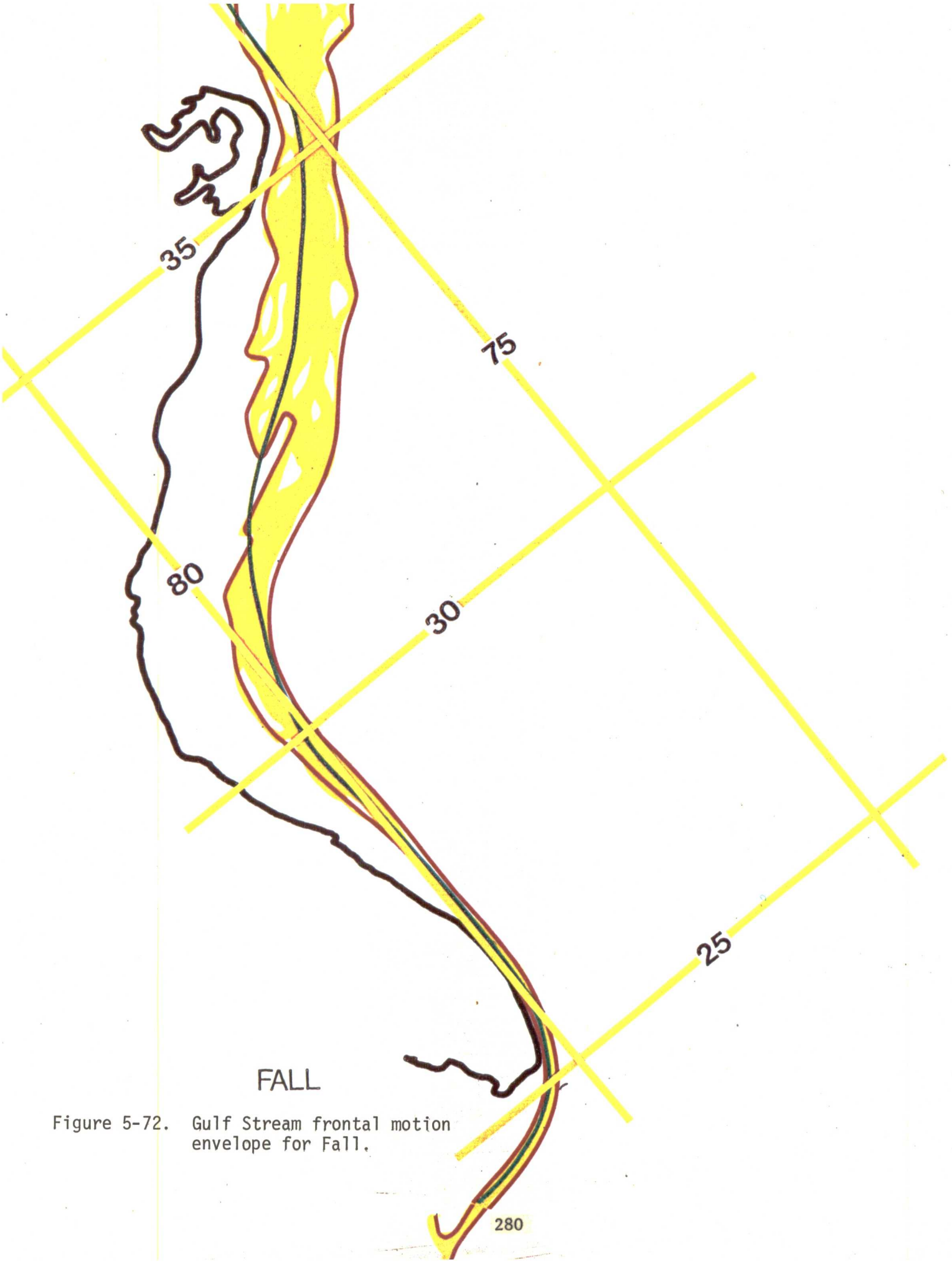

Figure 5-72. Gulf Stream frontal motion envelope for Fall.

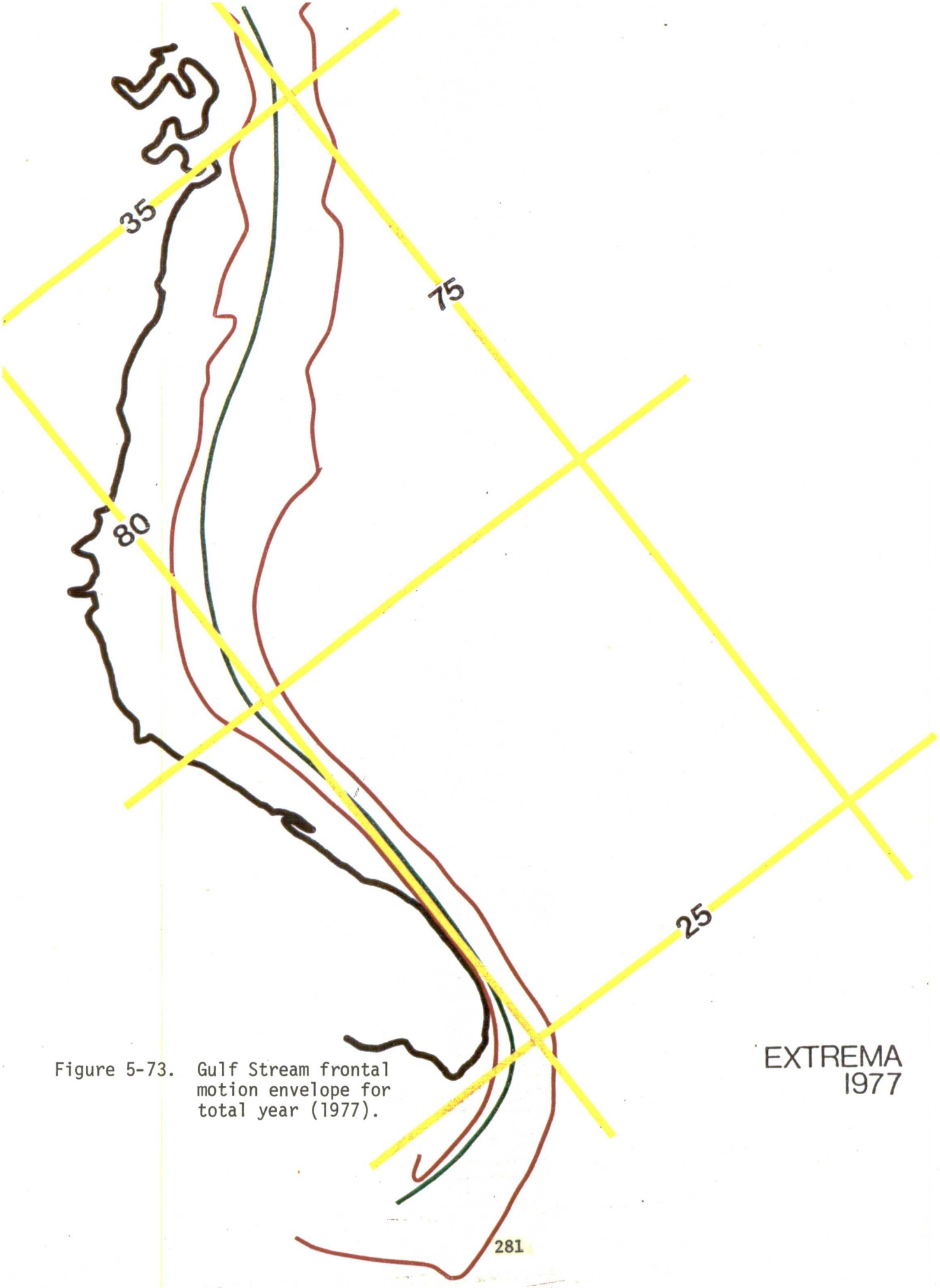

Figure 5-73. Gulf Stream frontal motion envelope for total year (1977).

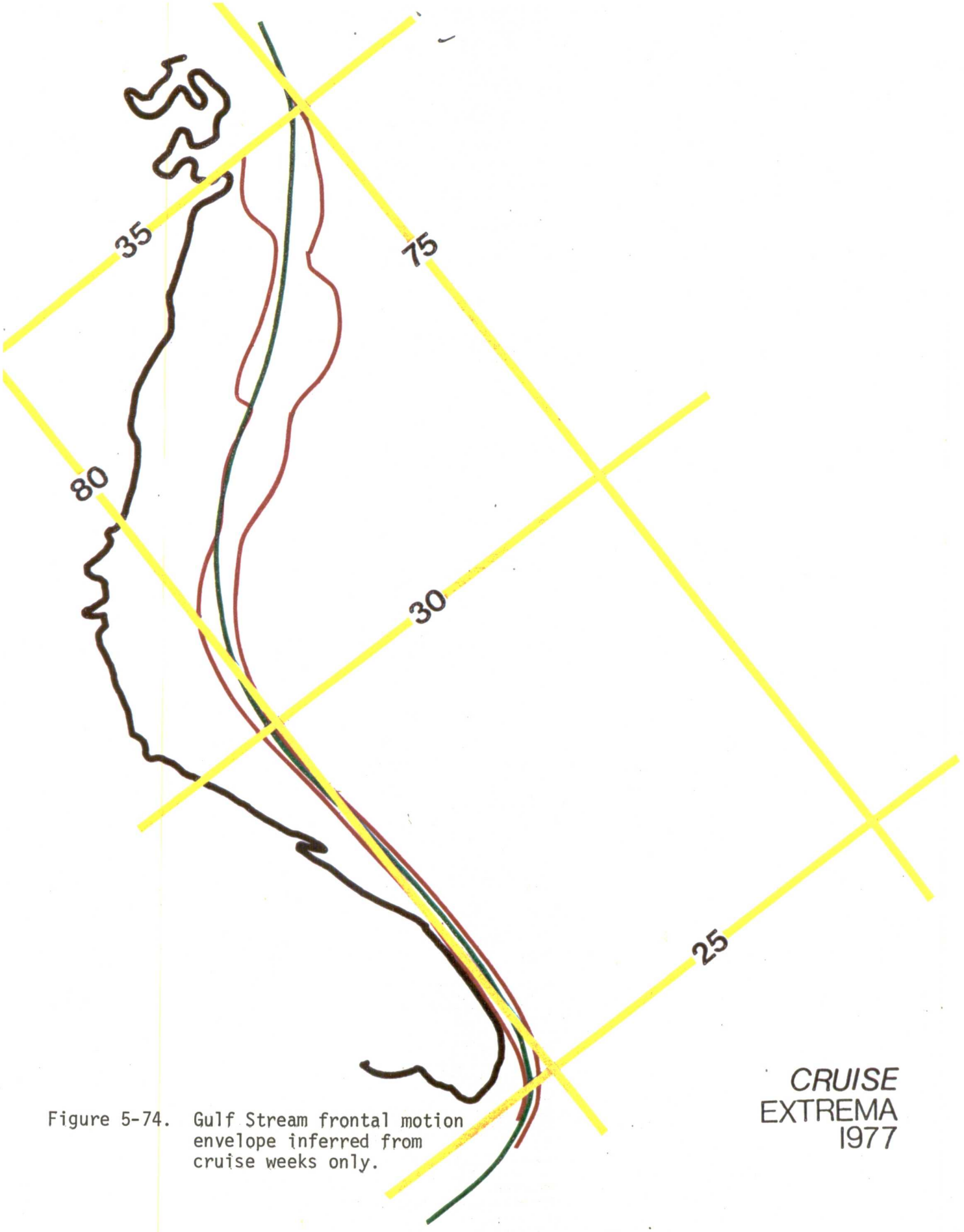

Figure 5-74. Gulf Stream frontal motion envelope inferred from cruise weeks only.

Superimposed about the weak northerly mean flow at mid-shelf are subtidal current fluctuations that were mutually coherent with similar motions near the shelf break and with local winds.

Semi-diurnal tidal currents produced a major part of the total current variability and appear similar (if not slightly stronger) than in the winter period. Semi-diurnal internal tides produced temperature fluctuations with amplitudes of $\pm$ 2 to $\pm$ 5°C. Internal tides were strongest near the shelf break where stratification was greatest.

A frictional equilibrium model that was used to explain a significant portion of the winter subtidal current variability at mid- and inner-shelf appears to also apply during summer conditions. Northward wind stress events produce an offshore mass flux in the surface Ekman layer which causes sea level to fall along the coast, establishing an onshore pressure gradient, which is in approximate balance with the resulting northward geostrophic interior flow over the shelf. The offshore Ekman flux may at times generate an offshore Gulf Stream meander with associated decreasing temperature and northward current speeds at the shelf break. The opposite response would occur for southward wind events.

The model outlined here is a much simplified representation of the shelf water response to a complex mixture of wind and Gulf Stream forcing events, ignoring the effects of density gradients and non-uniform cross-shelf slopes. Current and temperature time series from the shelf break show that, on numerous occasions low-frequency fluctuations, suggestive of offshore (onshore) Gulf Stream meanders, occur following northward (southward) wind events. However, on other occasions current and temperature changes do not appear directly related to wind forcing. The passage of an atmospheric disturbance over the shelf may act as a triggering mechanism for these frontal perturbations which have similar periods as predicted for continental shelf waves (Brooks, 1978). Satellite observations indicate that Gulf Stream meanders propagate to the north, grow rapidly in time, and can eventually evolve into counterclockwise, cold-core spin-off eddies. Thus, an instability process appears to be involved, due to the velocity gradients existing across the Gulf Stream western edge either in the horizontal or vertical plane, inducing horizontal or vertical sheer (barotropic or baroclinic instability). Perhaps wind-induced frontal disturbances provide a triggering mechanism for instabilities which grow to large amplitudes downstream.

Pietrafesa, Atkinson and Blanton (1978) showed observationally and Rooney, Janowitz and Pietrafesa (1978) demonstrated theoretically that the Gulf Stream is regularly deflected 60-110 km offshore of the shelf break at Charleston, due to the topographic influence of the Charleston "bump". These papers are supported in the long-term mooring data by the lack of evidence of major Gulf Stream influence

at that site. The occasional incursion of Gulf Stream eddies across the site was documented on three occasions and it was shown that the eddy signature was an anti-cyclonic rotation of the local velocity vectors and a sudden warming of the entire water column. These findings are contrary to those of previous investigators (Lee, 1975; Duing, Mooers and Lee, 1977; Lee and Mayer, 1977; and Lee and Brooks, 1979) who found that on the Florida and Georgia shelfs, eddies have a cyclonic Eulerian signature and there is evidence of a cooling of the water column as the eddy passes a fixed site. Pietrafesa and Janowitz (1979) demonstrated both observationally and conceptually that as a function of mooring position relative to eddy location, and as a function of hydrographic season, the eddy may in fact have a different character in agreement with present findings for the long-term current meter mooring site.

The subtidal current variability during the months of November, December and January were shown to be highly coherent with the wind, with vertically homogeneous stratification prevailing. The current regime can be modeled using such conventional shelf circulation theories as given by Pietrafesa (1973) and, for downwelling favorable wind cases (northeasterlies), by Scott and Csanady (1976). Thermohaline forcing (i.e. density related) effects are shown to be of minor importance relative to direct wind forcing.

From February through March and into April, a thermohaline transition occurs and density forces become more evident as their importance relative to wind forcing is documented. These data can also be modeled using such theories as those presented by Pietrafesa (1973) and, more recently, by Pietrafesa and Janowitz (1978).

Semi-diurnal tide dominates the tidal period band and the tide is shown to be a stable, regular, deterministic dynamical process, which can be easily modeled as a frictionally modified Poincare wave.

Finally, it is concluded from the analysis of satellite thermal imagery that satellite remote sensing can give highly accurate surface thermal maps in the Georgia Bight, and that seasonal depiction as well as description of short time scale (2-3 day) variability of Gulf Stream/Shelf Water frontal position is practical using those techniques. Determination of seasonal characteristics of the shelf and shelf break waters from hydrographic cruise measurements can be biased by non-representative offshore Gulf Stream positions. In fact, long-term time series of the Gulf Stream western edge are essential to understanding frontal variability in the Georgia Embayment.

5.8 REFERENCES

Atkinson, L. P. 1977. Models of Gulf Stream intrusion into the South Atlantic Bight shelf waters. Geophys. Res. Letters, 583-586.

Beardsley, R.C.. 1974. Circulation on the New England continental shelf: response to strong winter storms. Geophys. Res. Letters, 1, 181-184.

Blanton, J. 1971. Exchange of Gulf Stream Water with North Carolina Shelf Water in Onslow Bay during Stratified Conditions. Deep-Sea Res. 18(2):167-178.

Bradshaw, A. and K. E. Schneider. 1965. The effect of pressure on the electrical conductance of sea water. Deep-Sea Res., 12:151-162.

Broenkow, W. W., W. B. Abrahams, and R. R. McInnis. 1977. A CTD Data Acquisition System for Coastal Applications. Preprint: Proceedings Fourth STD/Ocean Systems Conference, January 12-27, 1977. San Diego, California.

Brooks, D. A. 1978. Subtidal sea level fluctuations and their relation to atmospheric forcing along the North Carolina coast. J. Phys. Oceanogr., 8(3), 481-493.

Brooks, D. A., and C. N. K. Mooers. 1977. Wind forced continental shelf waves in the Florida Current. J. Geophys. Res., 82(18), 2569-2576.

Bumpus, D. F. 1973. A Description of the Circulation on the Continental Shelf of the East Coast of the U.S. In Progress in Oceanography. 6:11-156, Pergamon: NY.

Bumpus, D. F. and E. L. Pierce. 1955. The Hydrography and Distribution of Chaetognaths over the Continental Shelf off North Carolina. Deep-Sea Res. (Suppl.). 3:92-109.

Cox, R. A., F. Culkin, and J. P. Riley. 1967. The electrical conductivity/chlorinity relationship in natural sea water. Deep-Sea Res.. 14:203-220.

Csanady, G. T. 1976. Mean circulation in shallow seas. J. Geophys. Res., 81, 5389-5399.

Curtin, T. B. 1979. Hydrography. In: Summary and Analysis of Physical Oceanographic and Meteorological Data on the Continental Shelf and Blake Plateau from Cape Hatteras to Cape Canaveral. Report to BLM (Contract No. AA550-CTJ-16), ERT, Concord, Ma.

Duing, W. O., C. N. K. Mooers and T. N. Lee. 1977. Low-Frequency variability in the Florida current and relations to atmospheric forcing from 1972-1974. To appear in J. Mar Res. (Richardson Memorial Vol.).

Fofonoff, N. P. 1969. Spectral characteristics of internal waves in the ocean. Deep-Sea Res., Supple. to Vol. 16, 59-71.

Holm-Hansen, O., C. J. Lorenzen, R. W. Holmes and D. H. Strickland. 1965. Fluorometric determination of chlorophyll. J. Conseil Perm. Intern. Exploration Mer. 30(1):3-15.

Huyer, A., B. M. Hickey, J. D. Smith, R. L. Smith, and R. D. Pillsbury. 1975. Alongshore coherence at low frequencies in currents observed over the continental shelf off Oregon and Washington. J. Geophys. Res., 80(24), 3495-3505.

Iselin, C. O'D. 1940. Preliminary report on long period variations in the transport of the Gulf Stream System. Pop. Phys. Oceanogr. and Meteor, 8(1), 40 pp.

Jacobson, S. R. 1974. FESTSA - A system for time series analysis. Computer Services, University of Miami unpublished report.

Lee, T. N. 1975. Florida current spin-off eddies. Deep Sea Res., 22, 753-765.

Lee, T. N. 1978. Measurement of Gulf Stream and wind induced shelf circulation in the South Atlantic Bight. University of Miami unpublished report to DOE.

Lee, T. N., L. P. Atkinson and R. Legeckis. 1979. Initial observations of a Gulf Stream spin-off eddy on the Georgia continental shelf. (To be submitted to Deep-Sea Res.).

Lee, T. N., and D. A. Brooks. 1979. Initial observations of current, temperature and coastal sea level response to atmospheric and Gulf Stream forcing on the Georgia shelf. (Submitted to Geophys. Res. Letters).

Lee, T. N., and D. A. Mayer. 1977. Low-frequency current variability and spin-off eddies off southeast Florida. J. of Mar. Res., 35(1):193-220.

Lee, T. N., and R. Shutts. 1977. Technical program for Aanderaa current meter moorings on continental shelves. University of Miami Technical Report TR 77-5.

Legeckis, R. 1975. Applications of synchronous meteorological satellite data to the study of time-dependent sea surface temperature changes along the boundary of the Gulf Stream. Geophys. Res. Let., 2, 435-438.

Mooers, C. N. K. 1973. A technique for the cross spectrum analysis of pairs of complex-valued time series, with emphasis on properties of polarized components and rotational invariants.

Niiler, P. P., and L. A. Mysak. 1971. Barotropic waves along the eastern continental shelf. Geophys. Fluid Dynamics, 2, 273-288.

Orlanski, I. 1969. The influence of bottom topography on the stability of jets in a baroclinic fluid. J. Atm. Sci., 26, 1216-1232.

Pietrafesa, L. J. 1973. Steady, baroclinic circulation on a continental shelf, Ph.D. dissertation. University of Washington, June.

Pietrafesa, L. J., J. O. Banton and L. P. Atkinson. 1978. Evidence for deflection of the Gulf Stream at the Charleston rise. Gulf Stream, U. S. Dept. of Commerce, NOAA, IV. (9) p 3-7.

Pietrafesa, L. J. and G. S. Janowitz. 1979. A note on the identification of a Gulf Stream Frontal spin-off eddy from eulerian data (Submitted to Geophys. Res. Letters).

Redfield, A. C. 1958. The influence of the continental shelf on the tides of the Atlantic coast of the United States. J. of Mar. Res., 17, 432-438.

Richardson, W. S., W. J. Schmitz, Jr., and P. P. Niiler. 1969. The velocity structure of the Florida Current from the Straits of Florida to Cape Fear. Deep Sea Res., 16 (supplement), 225-231.

Rooney, D. M., G. S. Janowitz and L. J. Pietrafesa. 1978. A simple model of deflection of the Gulf Stream by the Charleston rise. Gulf Stream, U.S. Dept. of Commerce, NOAA, IV (11), p. 3-7.

Scarlett, R. I. 1975. A data processing method for salinity, temperature, depth profiles. Deep-Sea Res., 22:509-515.

Scott, J. T., and G. T. Csanady. 1976. Nearshore currents off Long Island. J. Geophys. Res., 81, 5401-5409.

Stephansson, U., L. P. Atkinson and D. F. Bumpus. 1971. Hydrographic properties and circulation of the North Carolina shelf and slope waters. Deep-Sea Res., 18, 383-420.

Strickland, J. D. H., and T. R. Parson. 1972. A practical handbook of seawater analysis. Fish. Res. Bd. Canada Bull. 167 (2nd edition) 310 pp.

Stumpf, H. G., and P. K. Rao. 1975. Evolution of Gulf Stream eddies as seen in satellite infrared imagery. J. Phys. Oceanogr., 5, 388-393.

von Arx, W. S., D. Bumpus and W. S. Richardson. 1955. On the fine structure of the Gulf Stream front. Deep Sea Res., 3, 46-65.

Webster, F. 1961. A description of Gulf Stream meanders off Onslow Bay. Deep Sea Res., 8, 130-143.

Yentsch, C. S. and D. W. Menzel. 1963. A method for the determination of phytoplantation chlorophyl and phaeophytin by fluorescence. Deep-Sea Research 10, 221-231.

VI. METEOROLOGY/SEA STATE ANALYSIS

6.1 INTRODUCTION - STUDY OBJECTIVES

The availability or generation of sequential maps of surface winds over the region of the current meter moorings is essential for the characterization of the shelf water response to the passage of meteorological fronts, and, therefore, for the interpretation of the subsurface current measurements. To that effect, maps of surface wind streamlines and isotachs were prepared by Dr. J. Fernandez-Partagas for the duration of the mooring deployments, first on a 6-hourly basis, for the first three months, and daily thereafter, in support of the short-term and long-term current meter data analysis, respectively. The study was also intended to address the feasibility of using coastal wind data from shore meteorological stations, satellite-derived winds and the National Weather Service (NWS) predictions to characterize offshore wind conditions.

Finally, correlations of surface wind and wave field data were developed in support of the interpretation of subsurface current measurements, and as a possible tool for the statistical prediction of wave climatology based on offshore wind observations.

6.2 DATA COLLECTION

The spatial and temporal description of the surface wind field was achieved by analyzing wind reports collected operationally by the meteorological services. Observations reported within the area bounded by latitudes 25°N and 35°N, longitude 72°W and the U.S. southeast coast were plotted on maps over a fifteen month period from September 1977 to November 1978 at time intervals of six hours for the first three months of this period and twenty-four hours thereafter. When the time increment was six hours, maps were prepared for 0000, 0600, 1200 and 1800 GMT while daily maps were drawn for 1200 GMT. It should be noted that the area defined above extends much farther east than the Georgia Embayment. This area was chosen to facilitate the wind analysis in the region of interest.

The surface wind observations used in the description of the surface wind field consisted of reports from coastal and island stations, buoys, lighthouses and ships which are operationally received at the National Hurricane Center (NHC), Coral Gables, Florida. These reports are obtained directly from teletype messages or extracted from surface weather maps prepared by NHC. The data base was complemented for the period of September 1977 to November 1977 with wind reports from ships obtained from the National Climatic Center, Asheville, N.C. The latter data are usually variable with a delay of several months. In the mean, the number of non-operational reports is about 27% of the number of operational wind reports for the area of interest.

Wave data used in the present study were also obtained from the National Hurricane Center. For the period from September, 1977, data were reported in the form of tables at variable intervals ranging from two to four hours and, in addition to wind speed and wind direction, provided information of wave height and period. For the period from December, 1977, to August, 1978, data were given in the form of maps on a daily basis and included information of wave height, wave period, and wind direction but not wind speed. Wave data for September, October, and November of 1978 are still unavailable.

Also included in the data basis for surface wind and wave analysis were the meteorological and sea state/wave observations made along the BLM cruises in the Georgia Embayment. Texas Instrument cruise data cover the periods of February, May, August, September, and November 1977. They were reported in the form of logs at variable intervals (approximately every two hours) and contained information of wave height, wave period (except the month of February, 1977) wind speed and wind direction; no wave direction was given. SAI/Skidaway hydrographic cruise data were conducted over the periods of March 10 to March 25, 1978, April 10 to April 24, 1978, July 25 to August 3, 1978, and November, 1978. The November, 1978 data have just been received and are, therefore, not included in the subsequent analyses.

6.3 METHODOLOGY USED IN DATA ANALYSIS

6.3.1 Surface Wind

Surface wind reports operationally received at the National Hurricane Center were plotted on maps bounded by latitudes 25°N and 35°N, longitude 72°W and the U.S. southeast coast in accordance with a standard convention used in meteorology. In addition, some annotation concerning the wind direction and/or speed was written down beside most plotted reports. Once plotted on maps, the wind reports were analyzed by following straightforward streamline-isotach method (see, e.g., Palmer el al., 1955). This wind analysis technique is independent of the dynamic balance of the atmospheric flow; the method just describes the instantaneous wind direction and speed over an area based solely on wind reports. Free-hand streamlines and isotachs were drawn to denote wind direction and speed, respectively. Streamlines were represented by arrowed, solid lines on the map while isotachs at five-knot intervals were shown by dashed lines. Map-to-map space and time continuity for surface wind features were taken into account as streamlines and isotachs were drawn. This data collection and analysis procedure resulted in the production of 729 maps for the period of September 1977 to November 1978, based on more than 18,000 surface wind reports.

Obviously, this surface wind description cannot be presented here and, therefore, it should suffice to display a few maps showing an event of interest in the surface wind field. The event chosen as representative of the methodology followed is a family of cyclones with extratropical characteristics in October 1977. Three cyclones in three days can be identified on the twelve maps (Figure 6-1a through 1) shown for the period October 12 to October 14, 1977. Gale force winds (over 35 kt) are shown to occur in relation to the cyclones. On these maps, winds are plotted according to the standard convention used in meteorology. The direction towards which the wind is blowing is indicated by a shaft while the wind speed is indicated by barbs and flags at the tail end of the shaft. A half-barb represents 5 kt, a full barb represents 10 kt and a flag represents 50 kt. If the wind speed is less than 3 kt, no barb is drawn. Calm winds are indicated by circles. The digits in format XXYY, which are written down beside plotted reports, also refer to wind direction and speed. XX is prescribed to the direction from which the wind is blowing (at 10 degree intervals from 0^{o} to 360^{o}, omitting always the last zero, i.e., 040^{o} - 04); YY is prescribed to be the wind speed (knots).

The description of the surface wind field prepared by J. Fernandez-Partagas was based only on wind reports obtained operationally. However, a test of this description against a similar one obtained from operational as well as non-operational wind reports was also performed. The test was designed to investigate how much different both surface wind descriptions would be. To that effect, a set of 364 maps containing operational and non-operational wind reports, the latter obtained from the National Climatic Center, Asheville, N.C., was analyzed to produce a second description of the surface wind field at 6-h intervals for the period September 1977 to November 1977, and compared with the analysis based on operational reports only over the Georgia Embayment. Differences between both descriptions in wind direction and speed for two locations (31^{o}N, 80 $1/2^{o}$W and 32^{o}N, 79 $1/2^{o}$W) are inferred from corresponding analyzed maps. Description differences in absolute value indicate that the mean difference in wind direction is about 13^{o} and that the mean difference in wind speed is about 1.9 kt. It should be noted that description differences in actual value (original description minus the second description) are nearly zero in the mean and, therefore, do not indicate a systematic bias of one description with respect to the other. These values are within the accuracy that can be normally attached to wind reports at sea and consequently to wind analyses. It can, therefore, be concluded that, for the Georgia Embayment, there is no gain in the description of the surface wind field by analyzing non-operational and operational wind reports instead of analyzing operational reports only. Caution, however, should be taken in generalizing this statement to areas other than the Georgia Embayment. Thus, this statement is not true for an area in the

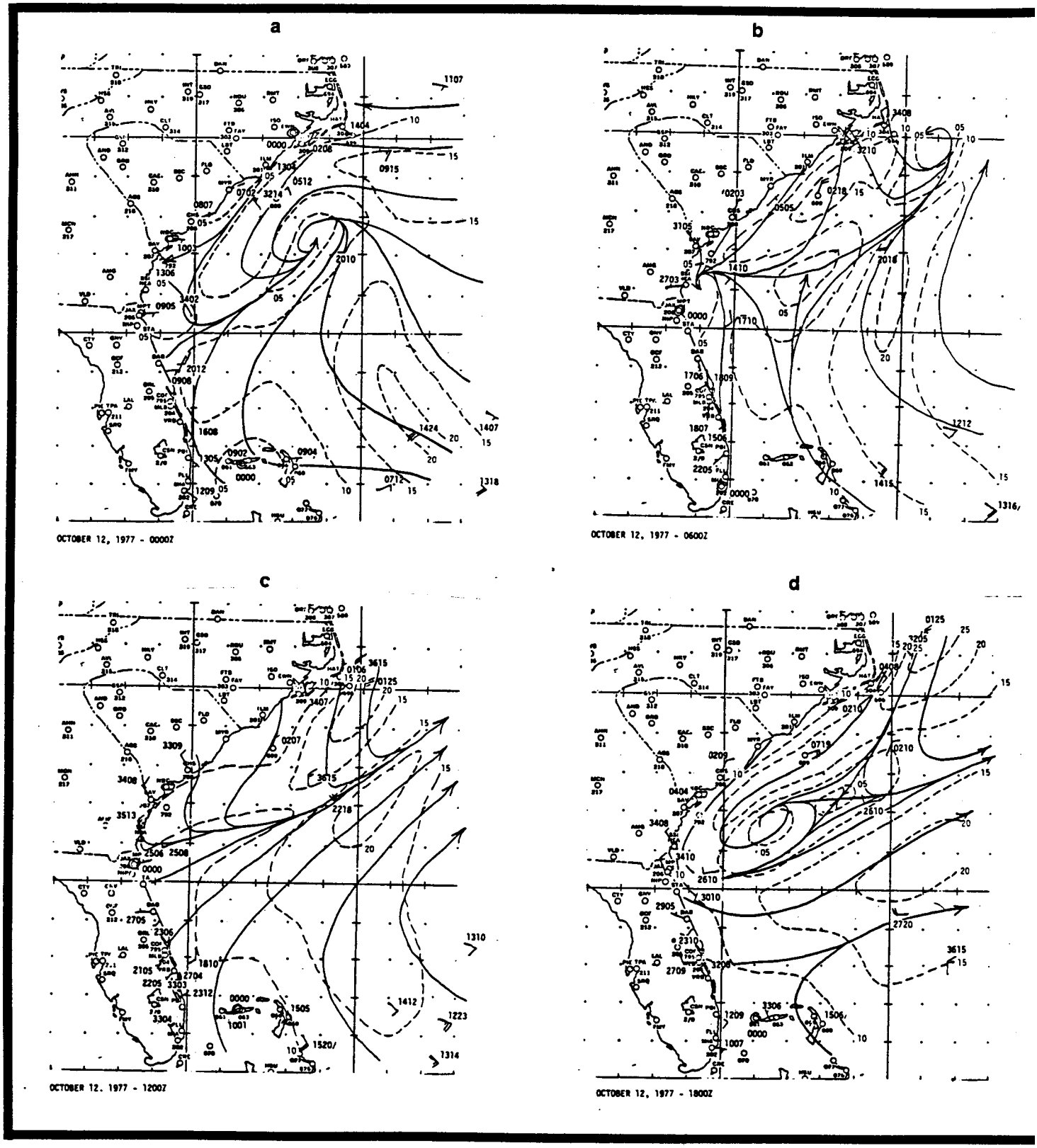

Figure 6-1a, b, c, and d. Example of surface wind maps generated by the streamline-isotach method. Sequence of figures 6-1a to 1 illustrates a family of cyclones with extratropical characteristics in October 1977.

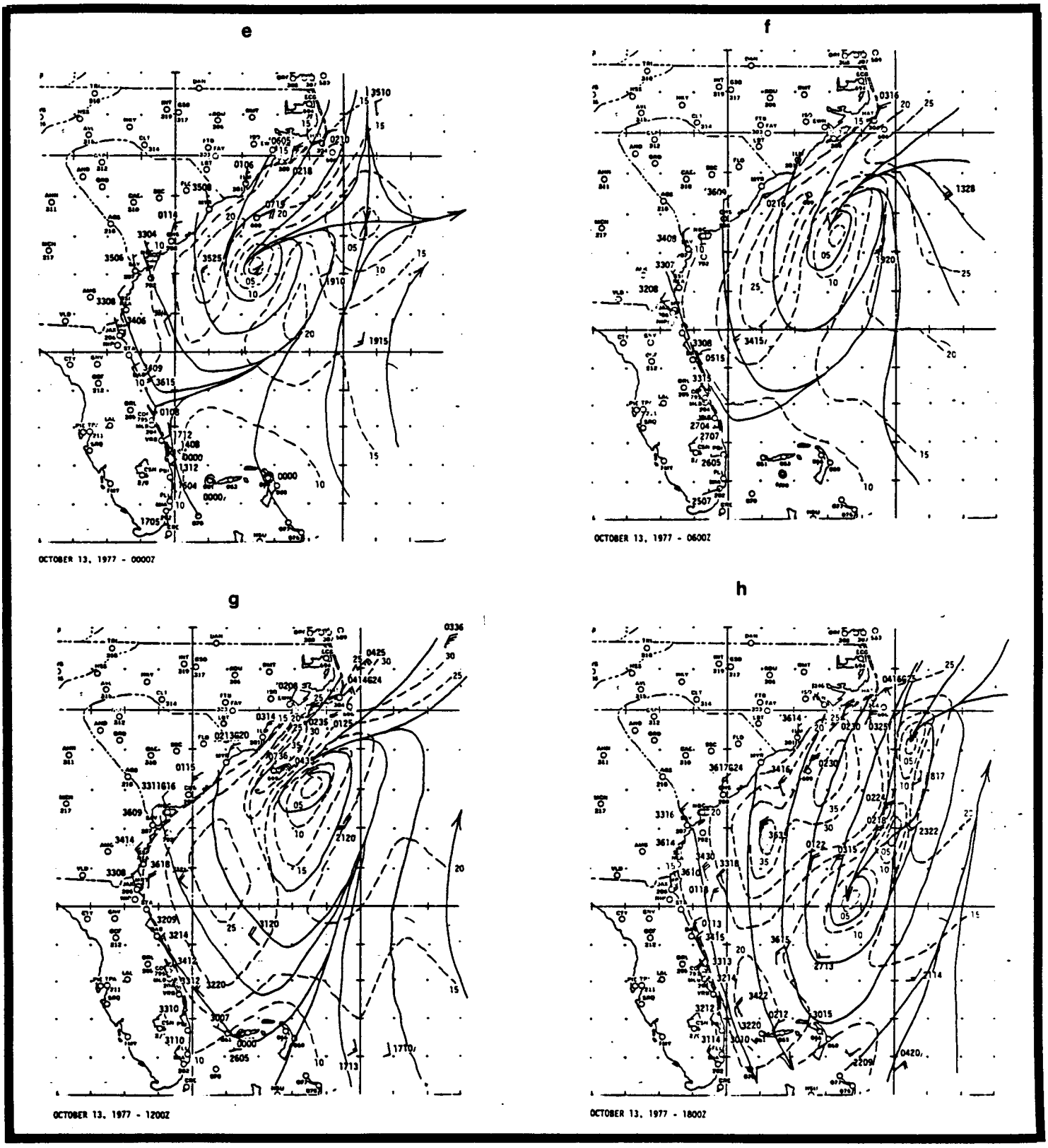

Figure 6-le, f, g, and h. Example of surface wind maps generated by the streamline-isotach method. Sequence of figures 6-la to l illustrates a family of cyclones with extratropical characteristics in October 1977. (Continued).

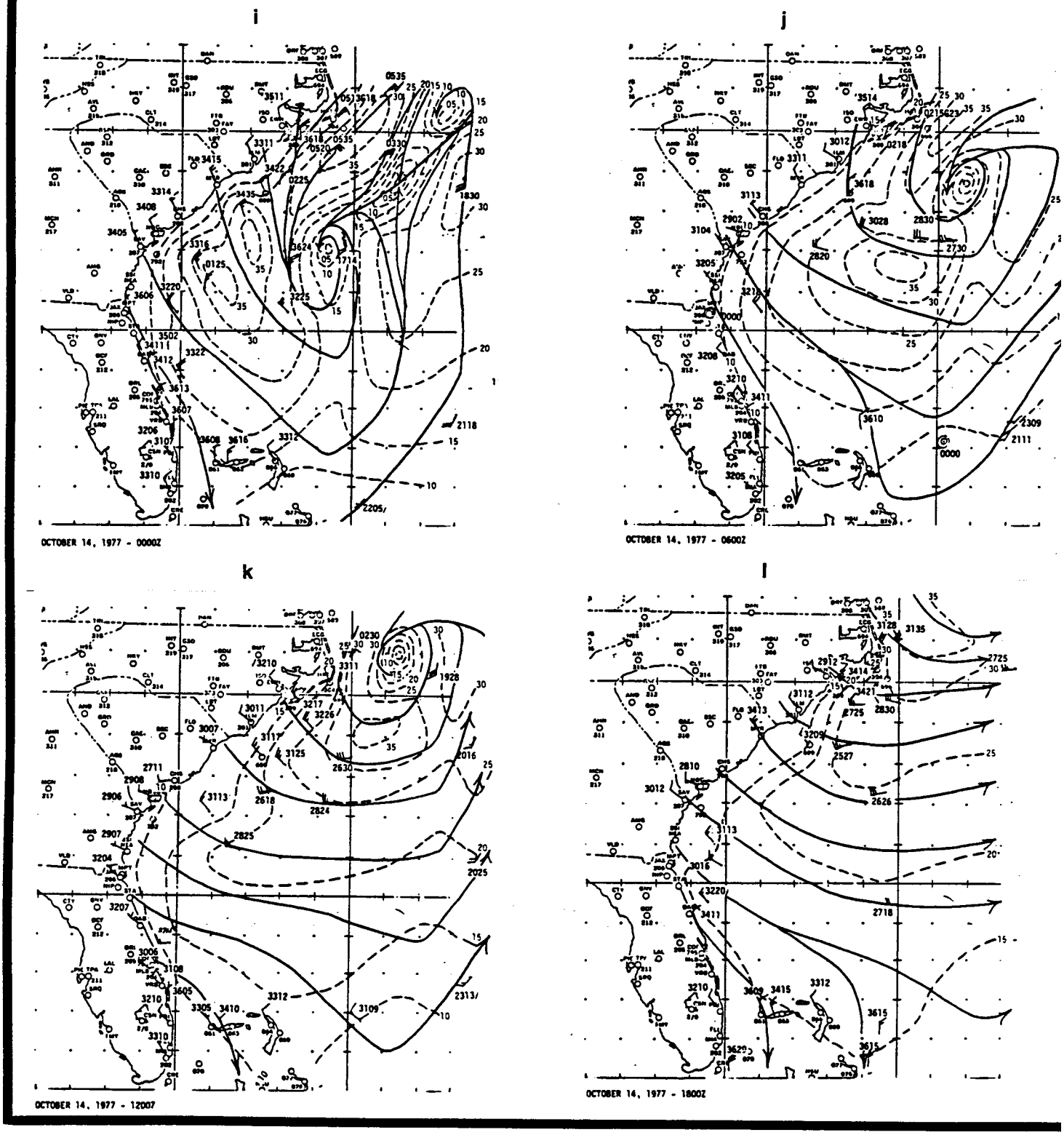

Figure 6-1i, j, k, and l. Example of surface wind maps generated by the streamline-isotach method. Sequence of figures 6-1a to l illustrates a family of cyclones with extratropical characteristics in October 1977. (Continued).

Indian Ocean with very few operational reports and a relatively large number of non-operational reports (Fernandez-Partagas and Duing, 1977).

6.3.2 Wave/Swell Analysis

Figure 6-2 shows the South Atlantic region under study. For purpose of data analysis, the region was divided into five areas. In view of the large amount of data products generated, only representative results are presented in this section, the remaining results being submitted in Volume III, Section 4.

6.3.2.1 Correlation Between Wind and Sea State

In order to establish correlations between wind and sea state, wind information was displayed in the following forms:

(1) plots of wind and wave data, in codes, along cruise tracks

(2) wind-wave roses

(3) frequency distribution of wave heights and wind speeds.

These displays are further described hereafter.

6.3.2.1.1. Plots of Wind and Wave Data, in Codes, Along Cruise Tracks

As indicated previously, meteorological and wave/sea state data were collected routinely on eight hydrographic/current meter rotation cruises. This information has been plotted along the cruise track and an example of such a plot is shown in Figure 6-3. The wind and wave information is given in codes in the form of numbers in three rows. The first and last two digits of the first row are respectively the day of the month and the hour (GMT) of the day. The first and last two digits of the second row denote respectively the wave period in seconds as explained in Table 6-1a and wave height in half-meters as explained in Table 6-1b. In the third row, the first two digits represent wind direction as explained in Table 6-1c and the last two digits are wind speed in knots.

6.3.2.1.2. Wind-wave Roses

Wind-wave roses give indication of wind speed, wind direction, wave height, and wave direction. These are prepared, on monthly basis, for the "short-term" and "long-term" current meter mooring areas covering the entire periods for which data were obtained. In Figure 6-4, wave and wind roses for the "short-term" mooring location are given. The legend H_t/M refers to wave roses indicating that wave height is given in metres. The legend WS/M/SEC refers to wind roses in which WS stands for wind speed and the unit is metre per second.

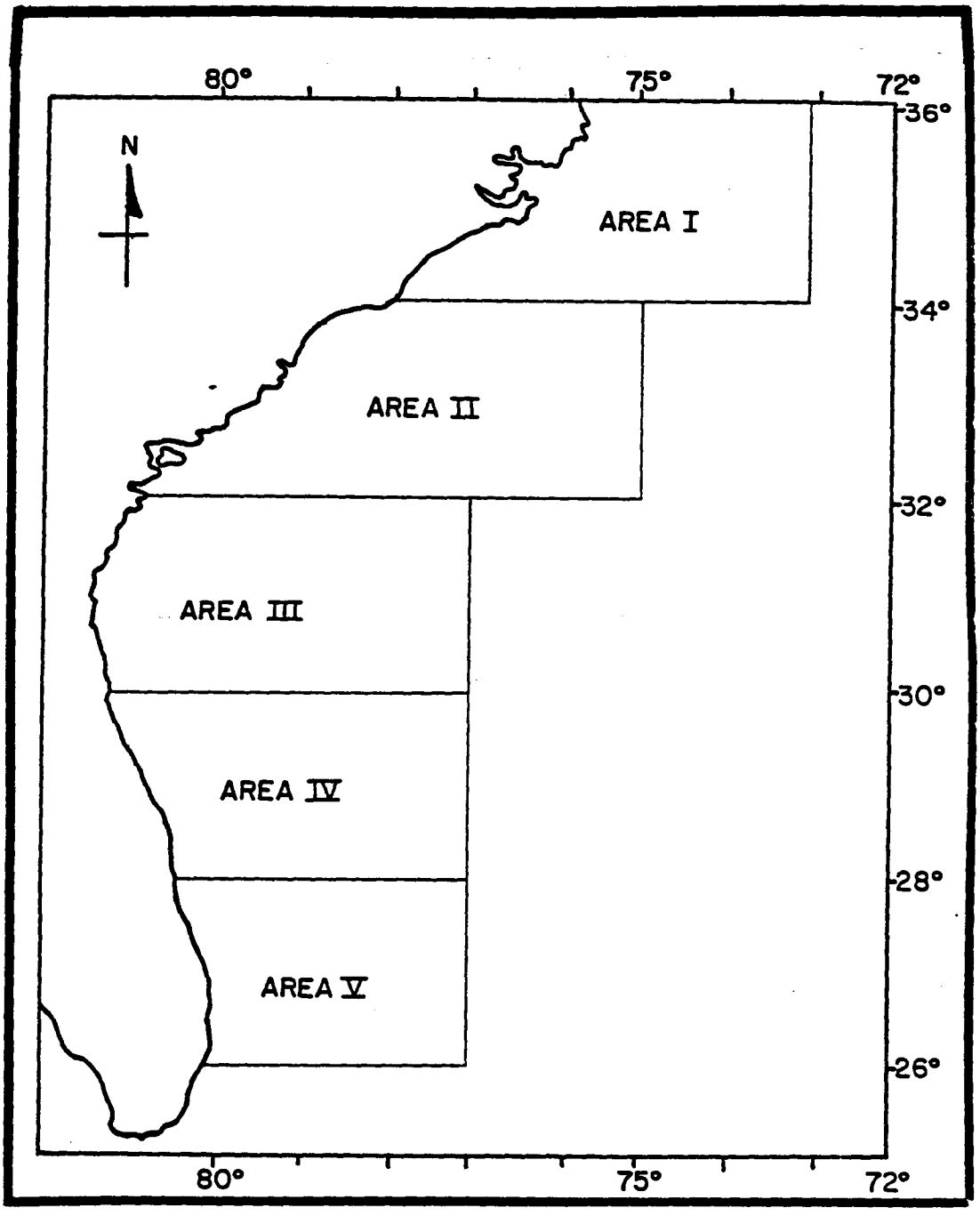

Figure 6-2. Area of data.

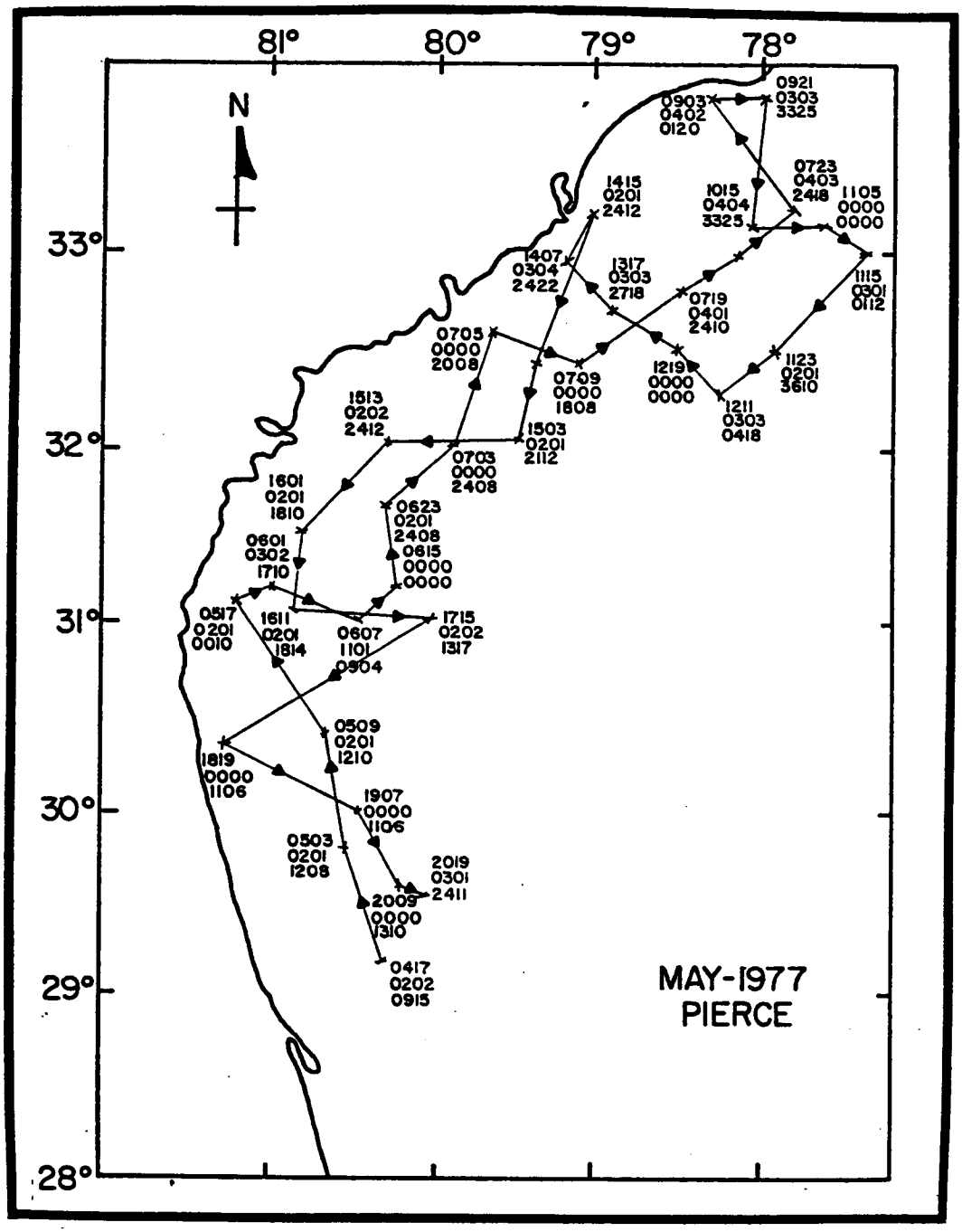

Figure 6-3. Example of plot of wind and wave data, in codes, along cruise tracks.

a

PERIOD OF WIND WAVES IN SECONDS

Report the average period in seconds of the wind waves using two figures:

5 sec. = 05, 10 sec. = 10, etc.

00 = calm; 99 = confused; 11 = not observed

b

HEIGHT OF WIND WAVES

Use "00" for calm. Use two slants "//" when the height was not observed for any reason.

Half Meters Code Figure	Feet	Half-Meters Code Figure	Feet	Half-Meters Code Figure	Feet	Half-Meters Code Figure	Feet
01	2	21	34	41	67	61	100
02	3	22	36	42	69	62	102
03	5	23	38	43	71	63	103
04	7	24	39	44	72	64	105
05	8	25	41	45	74	65	107
06	10	26	43	46	76	66	108
07	12	27	44	47	77	67	110
08	13	28	46	48	79	68	112
09	15	29	48	49	80	69	113
10	16	30	49	50	82	70	115
11	18	31	51	51	84	71	117
12	20	32	52	52	85	72	118
13	21	33	54	53	87	73	120
14	23	34	56	54	89	74	121
15	25	35	57	55	90	75	123
16	26	36	59	56	92	76	125
17	28	37	61	57	94	77	126
18	30	38	62	58	95	78	128
19	31	39	64	59	97	79	130
20	33	40	66	60	98	80	131

c

WIND DIRECTION, TENS OF DEGREES

(From which the wind is coming)

Code Figure	Direction	Code Figure	Direction
00	Calm	19	185° to 194°
01	5° to 14°	20	195° to 204°
02	15° to 24°	21	205° to 214°
03	25° to 34°	22	215° to 224°
04	35° to 44°	23	225° to 234°
05	45° to 54°	24	235° to 244°
06	55° to 64°	25	245° to 254°
07	65° to 74°	26	255° to 264°
08	75° to 84°	27	265° to 274°
09	85° to 94°	28	275° to 284°
10	95° to 104°	29	285° to 294°
11	105° to 114°	30	295° to 304°
12	115° to 124°	31	305° to 314°
13	125° to 134°	32	315° to 324°
14	135° to 144°	33	325° to 334°
15	145° to 154°	34	335° to 344°
16	155° to 164°	35	345° to 354°
17	165° to 174°	36	355° to 4°
18	175° to 184°	99	Direction cannot be determined due to a confused sea

Tables 6-1a, b and c. Codes used in plots of wind and wave data along cruise tracks.

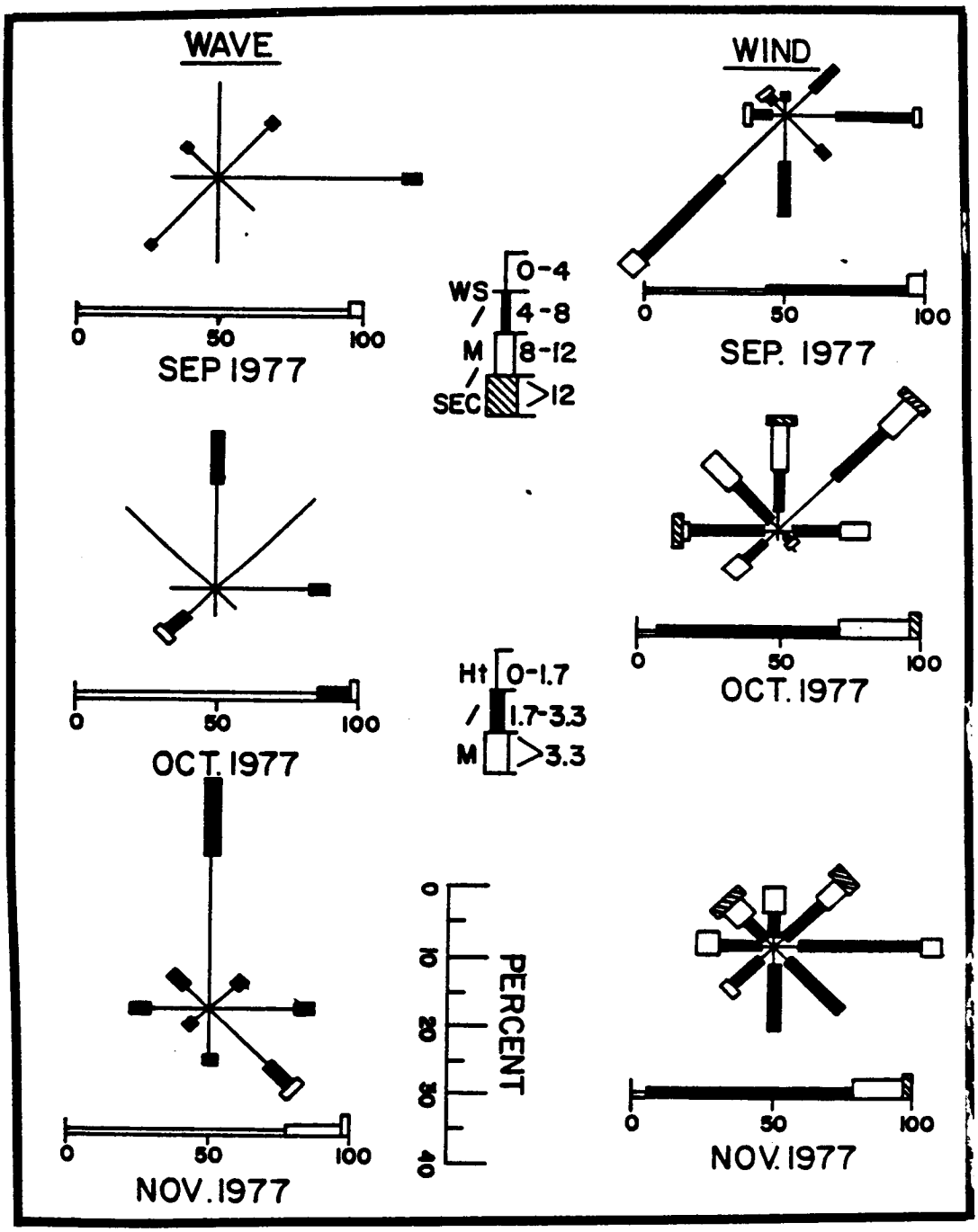

Figure 6-4. Wind-wave roses on monthly basis at the short-term mooring location.

The scale used in the roses for both wind and wave roses is given as PERCENT. Figure 6-5 gives wind and wave roses for the "long-term" mooring location.

6.3.2.1.3. Frequency distribution of wave height and wind speed

Another way of showing the relationship between wind and wave is by means of the joint probability function of wave height and wind speed. Thus, frequency distribution of wave height and wind speed are prepared for all five areas of the South Atlantic region on monthly basis. The data used are those for the cruises and the "short-term" and "long-term" mooring locations covering the months May, August, September, October, and November of 1977 and March, August and November of 1978. It should be noted that these frequency distributions were prepared (and submitted in Volume III) only when sufficient data in a given area were collected during a cruise. Figures 6-6a, b and c are illustrative of the data products prepared. From the frequency distributions, the mean and standard deviation of wave height as functions of wind speed can be obtained; these are also shown in the figures.

6.3.2.2 Waves/Swell Analysis

Important wave parameters are wave height, period, and direction. To correlate wind and wave, wave information was given along with that of wind in Section 6.3.2.1. However, it is certainly meaningful to examine wave information by itself. Such information is given in the forms of

(1) wave roses,
(2) joint distribution of wave height and period, marginal distribution of wave height and marginal distribution of wave period, and
(3) annual wave period distribution.

These are described in the following sections.

6.3.2.2.1. Wave Roses

Wave roses are given for all areas covering the months February, May, August, September, October, November, and December of 1977 and January through November of 1978. The data used include those from cruises and ship observations and extend throughout the entire region. These roses are shown in Volume III, and, for illustrative purposes, in Figure 6-7; the legends in these figures are explained in Section 6.3.2.1 in connection with wind-wave roses.

6.3.2.2.2. Joint Distribution of Wave Height and Period

An example of joint distribution of wave height and period is presented in tabular form (Figure 6-8). Similar distributions for other months and areas are included in Volume III. The data used are

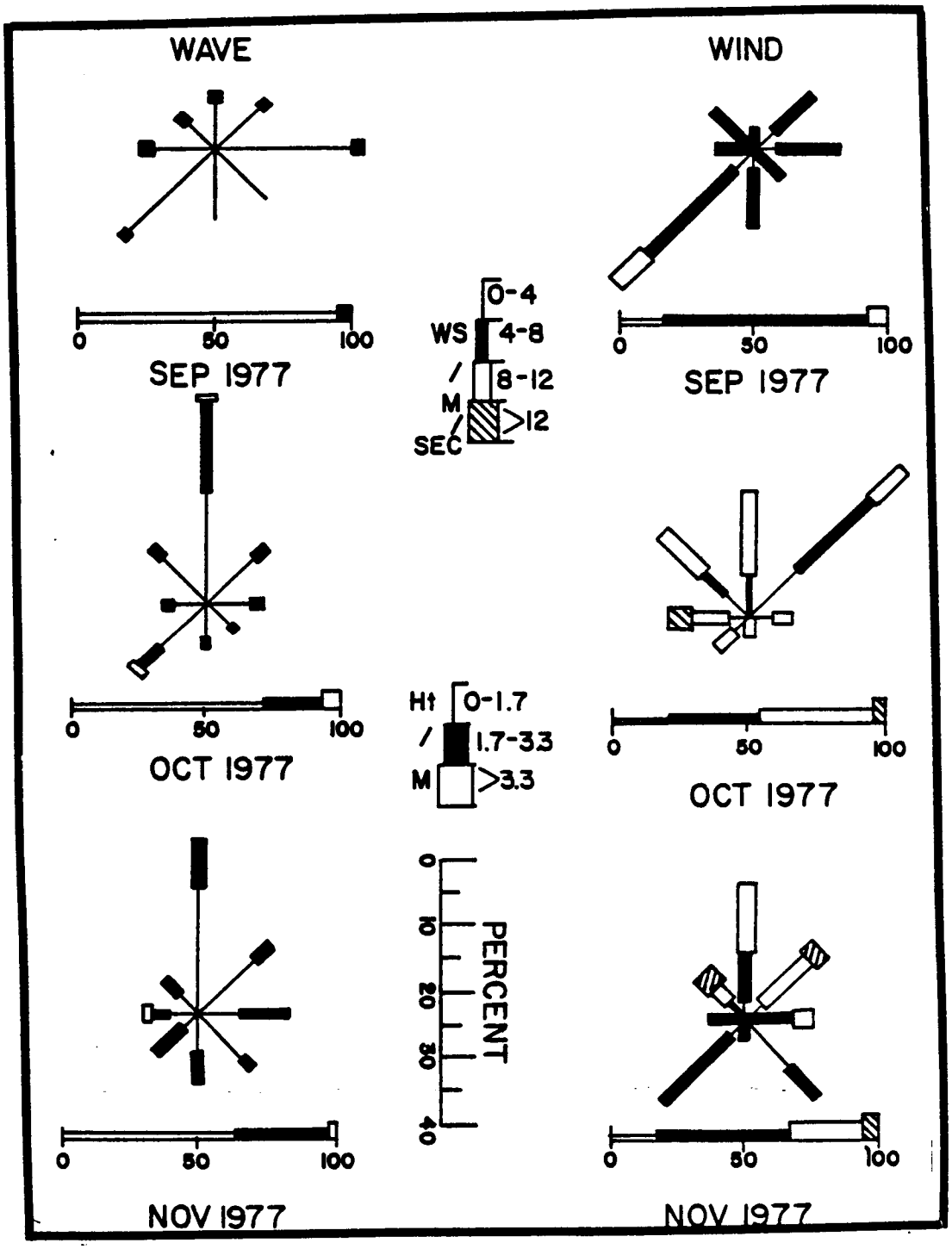

Figure 6-5. Wind-wave roses on monthly basis at the long-term mooring location.

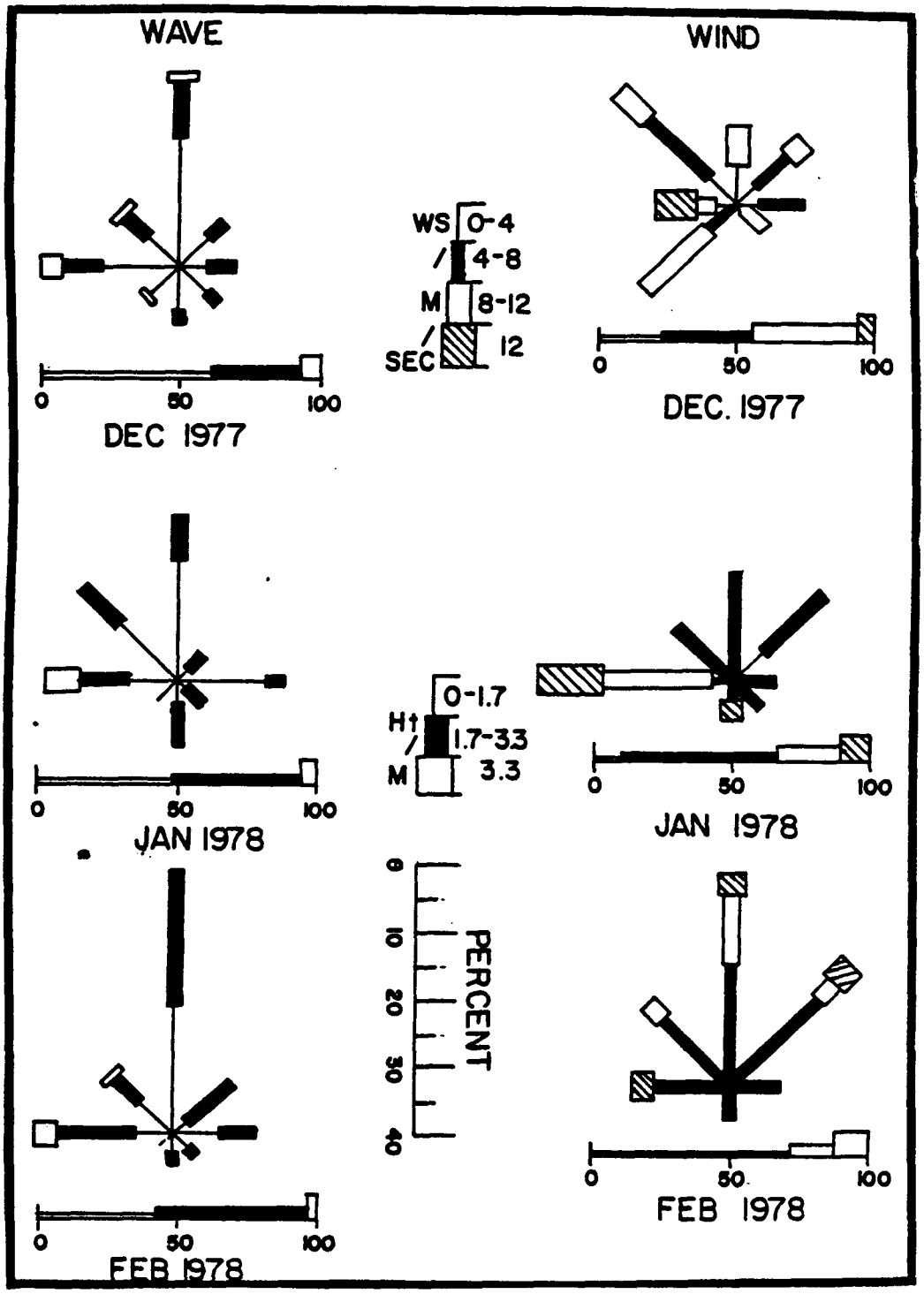

Figure 6-5. Wind-wave roses on monthly basis at the long-term mooring location. (Continued).

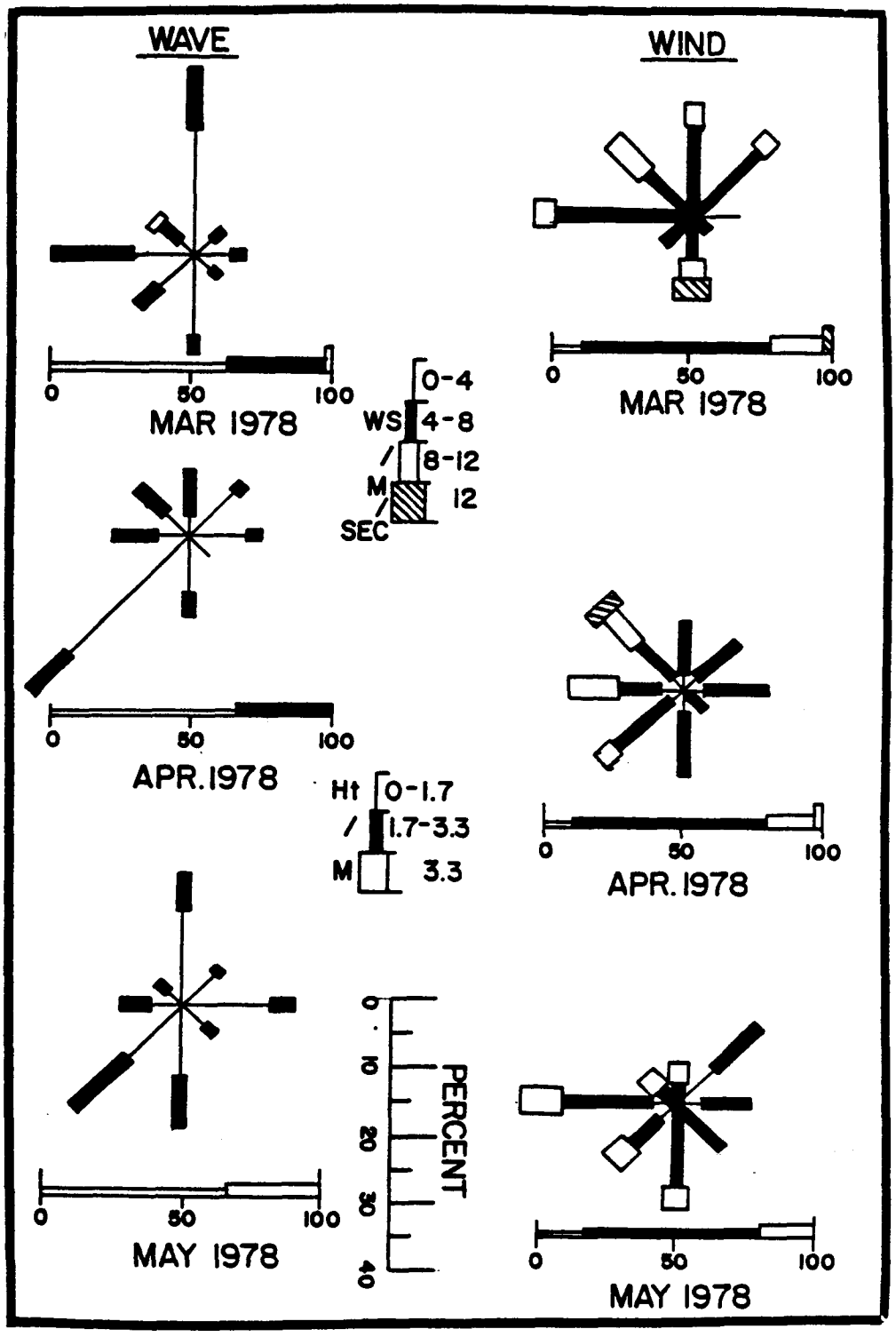

Figure 6-5. Wind-wave roses on monthly basis at the long-term mooring location. (Continued).

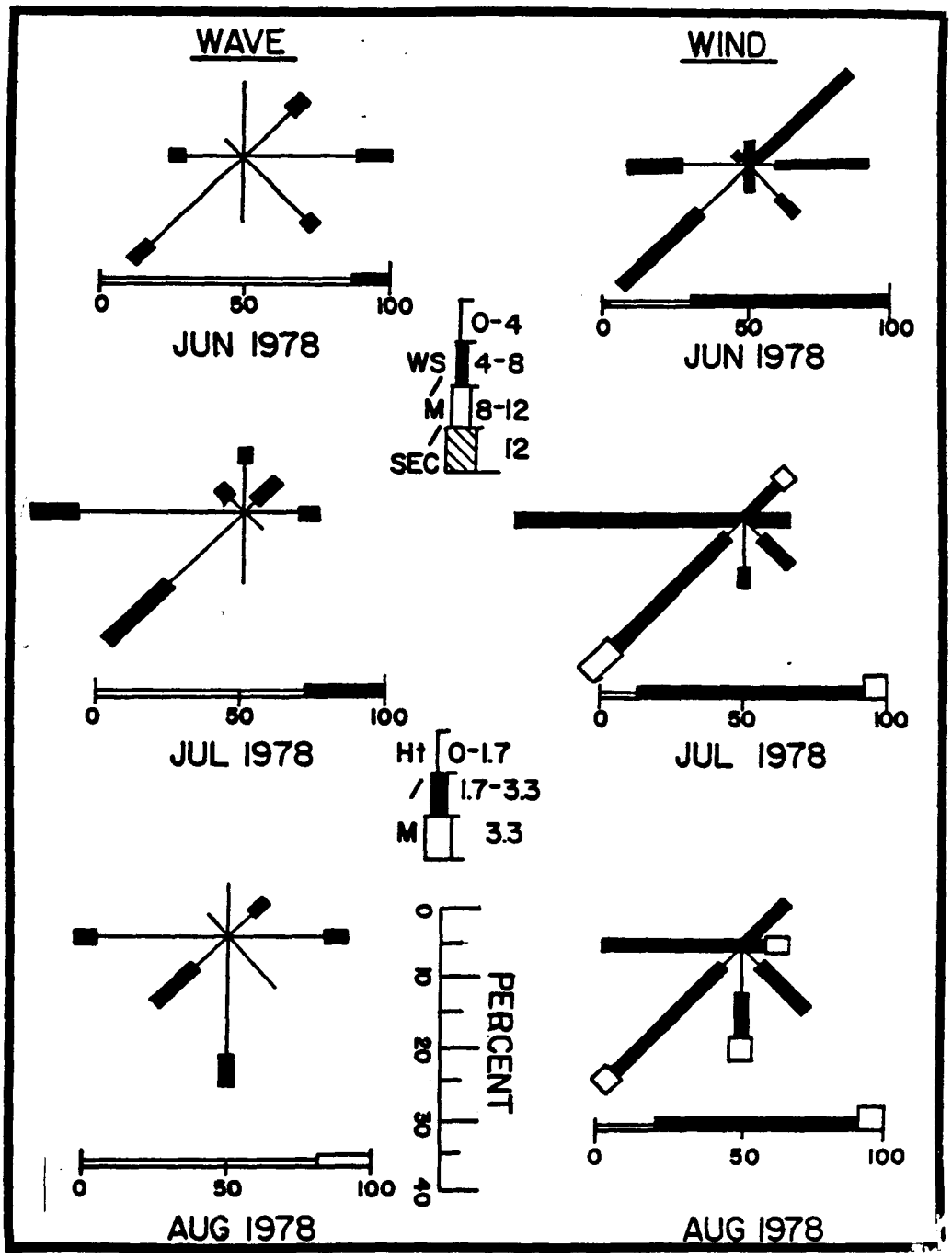

Figure 6-5. Wind-wave roses on monthly basis at the long-term mooring location. (Continued).

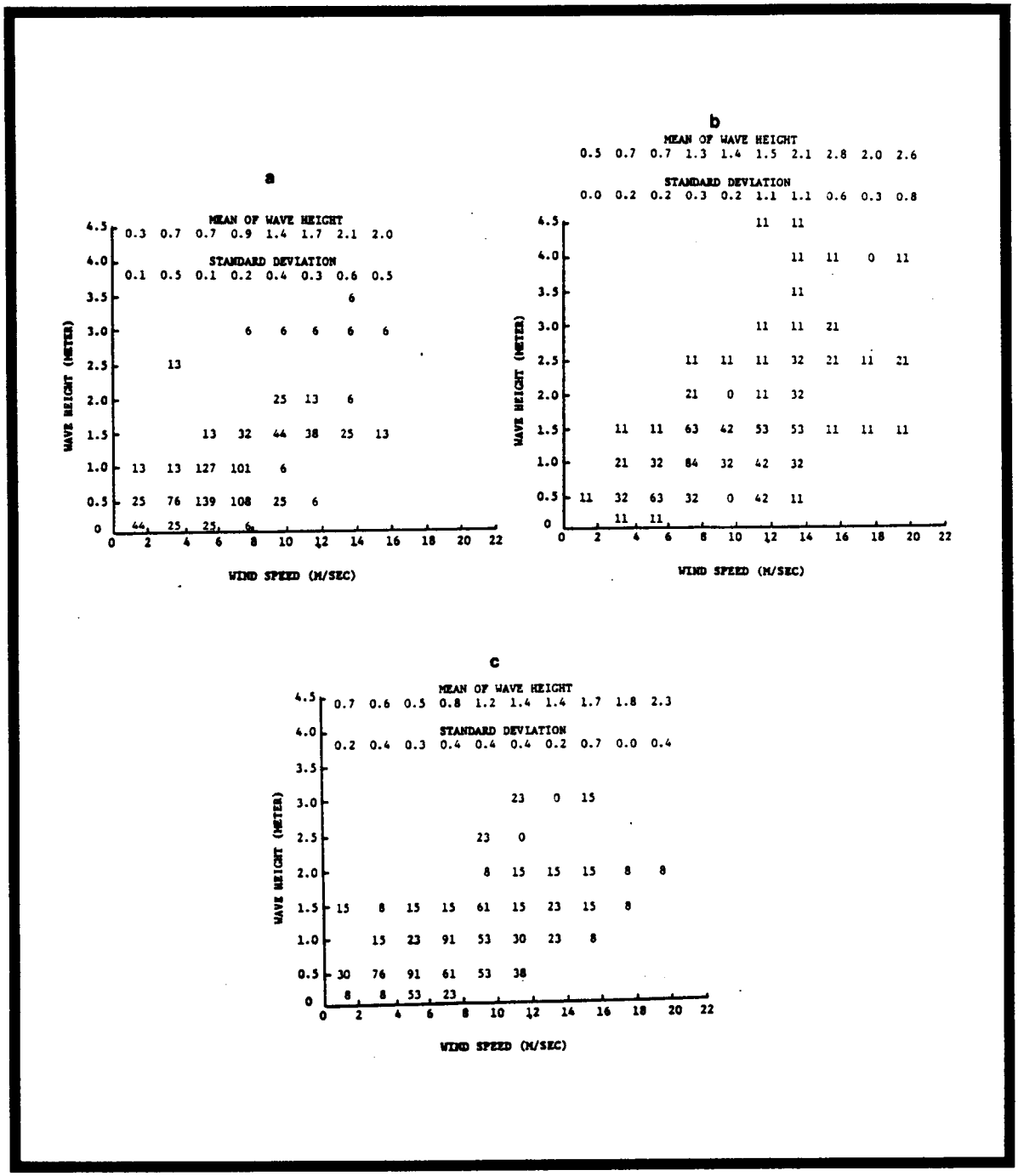

Figure 6-6a, b, and c. Frequency distribution (parts per 1000) of wave heights and wind speeds for Area I in (a) September, (b) October, and (c) November, 1977, respectively.

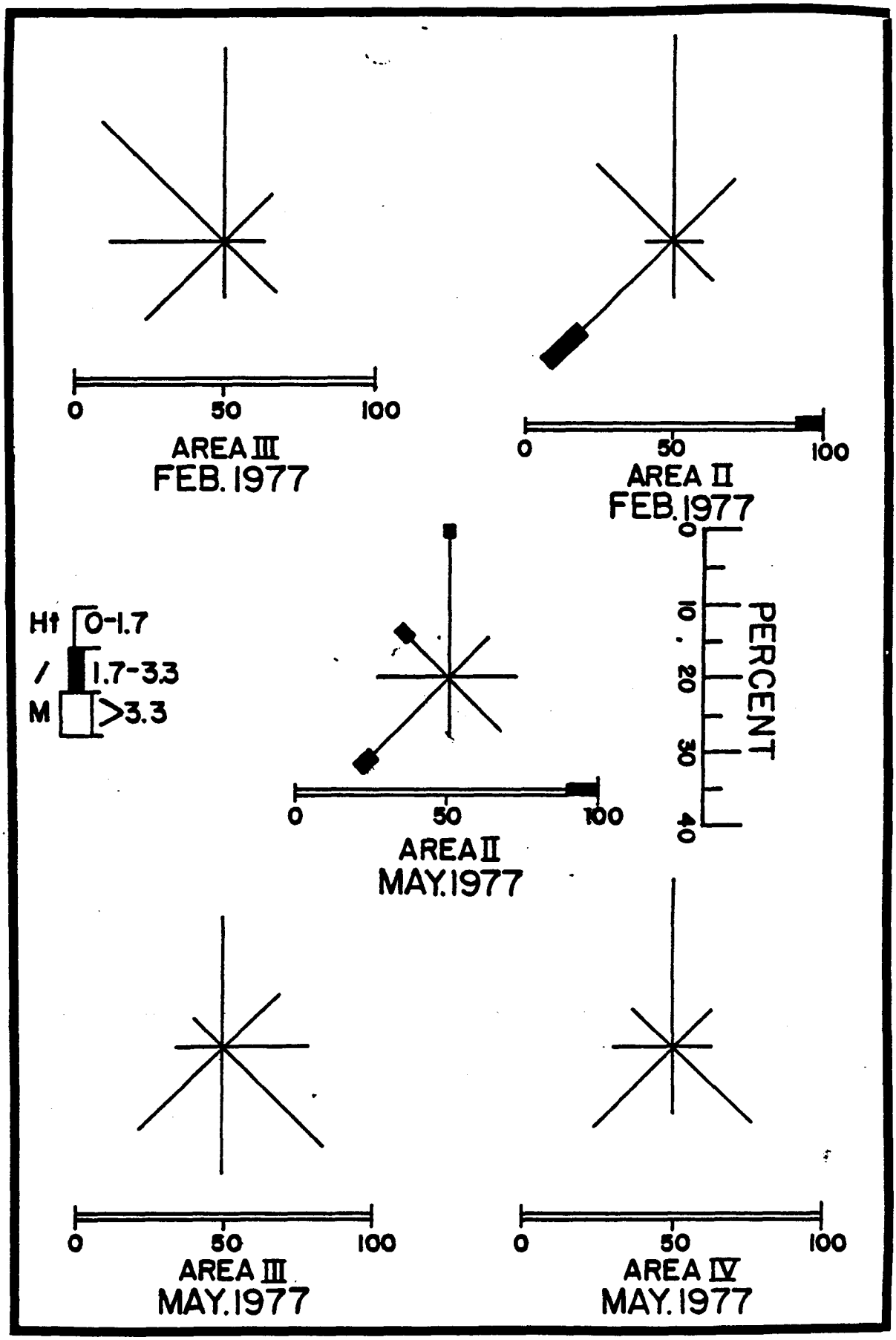

Figure 6-7. Typical wave roses produced on a monthly basis.

PERIOD (SECS)	WAVE HEIGHT (METER)										TOT.	CUM. TOT.	ROW AVG.
	0	0.5	1.0	1.5	2.0	2.5	3.0	3.5	4.0	4.5			
0.0	179										179	1000	0.0
1.0											0	821	0.0
2.0		205	13								218	821	0.53
3.0		90	77	192	51	13					423	603	1.29
4.0		90	38	13	26						167	180	0.93
5.0				13							13	13	1.50
6.0											0	0	0.0
7.0											0	0	0.0
8.0											0	0	0.0
9.0											0	0	0.0
TOTAL	179	385	128	218	77	13	0	0	0	0			
CUM.TOT.	1000	821	436	308	90	13	0	0	0	0			
COL.AVG.	0.0	2.70	3.20	3.18	3.34	3.00	0.0	0.0	0.0	0.0			

AVERAGE WAVE HEIGHT = 0.83 METER

VARIANCE OF HEIGHT = 0.41 METERS SQ.

STANDARD DEVIATION OF HEIGHT = 0.64 METER

AVERAGE WAVE PERIOD = 2.58 SEC.

VARIANCE OF PERIOD = 1.75 SEC. SQ.

STANDARD DEVIATION OF PERIOD = 1.32 SEC.

Figure 6-8. Distribution of wave height vs. period (in observations per 1000 OBS) (May 1977 Area II).

the same as those for the construction of frequency distribution of wave height and wind speed in Section 6.3.2.1. In these figures, the marginal cumulative frequency distribution of wave period and the marginal cumulative frequency distribution of wave height are also computed. Furthermore, for each wave period, the average wave height is shown as row average on the last column. Similarly, for each wave height, the average wave period is recorded as column average on the last row. Finally, the average and standard deviation of wave height, regardless of period, as well as those of wave period, regardless of wave height, are also given. To facilitate visualizing the probabilistic characteristics of wave height and period, the cumulative marginal distribution of wave height and wave period are also plotted, and examples shown in Figures 6-9 and 6-10 respectively.

6.3.2.2.3 Annual Wave Period Distribution

The presentation of wave characteristics, previously given on a monthly basis has also been examined on an annual basis. An illustrative histogram of wave period for area I, from all cruises and ship observations extending between August, 1977, and August, 1978 is shown in Figure 6-11. Similar histograms for the other areas are presented in Volume III.

6.4 DISCUSSION OF RESULTS

6.4.1 Surface Wind Field

Discussed in this section are six applications of the description of the surface wind field prepared as described in Section 6.3.1, hereafter referred to as baseline description.

6.4.1.1 Preparation of Time Series for Surface Winds at Selected Locations

Time series can be easily prepared for a particular location by using wind estimates inferred from the map sequence. An example of these time series is shown in Figure 6-12. Winds are represented in the figure by sticks pointing to the direction from which the wind is blowing; the stick length is proportional to the wind speed. The time series is for a location 32 1/2°N, 79°W and for the period September 1977 to November 1978 chosen to coincide approximately with the location of the long-term mooring. The series is based on maps using a 24-h time interval. Note that strong winds are found more frequently in winter than in summer, and that fluctuations in wind direction are more prominent in winter than in summer.

6.4.1.2 Evaluation of Wind Reports from Ship Cruises

For this evaluation, six-hourly wind reports along the ship cruises were extracted from ship logs and compared with corresponding wind estimates (in space and time) taken from the description of the

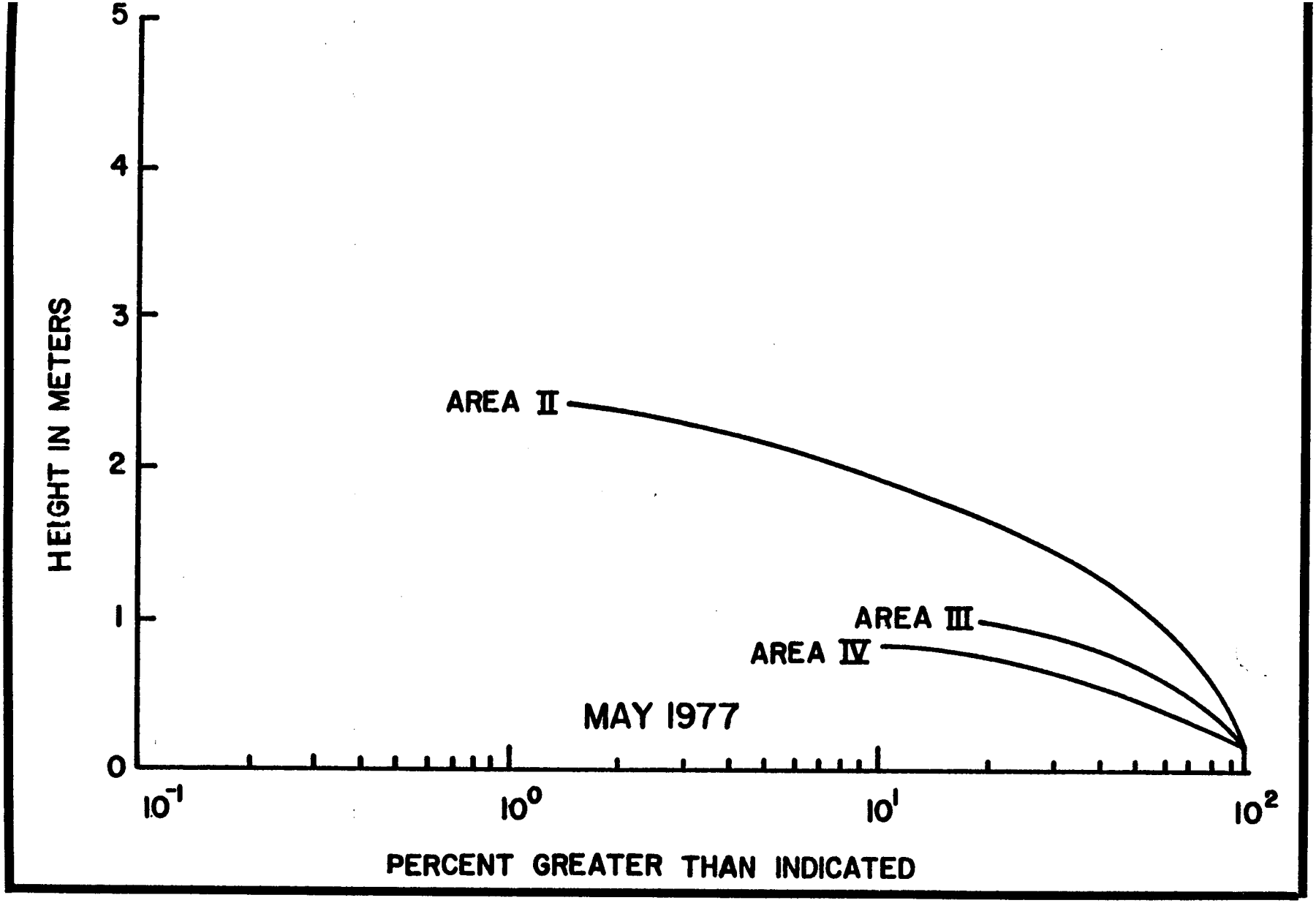

Figure 6-9. Example of wave height cumulative description.

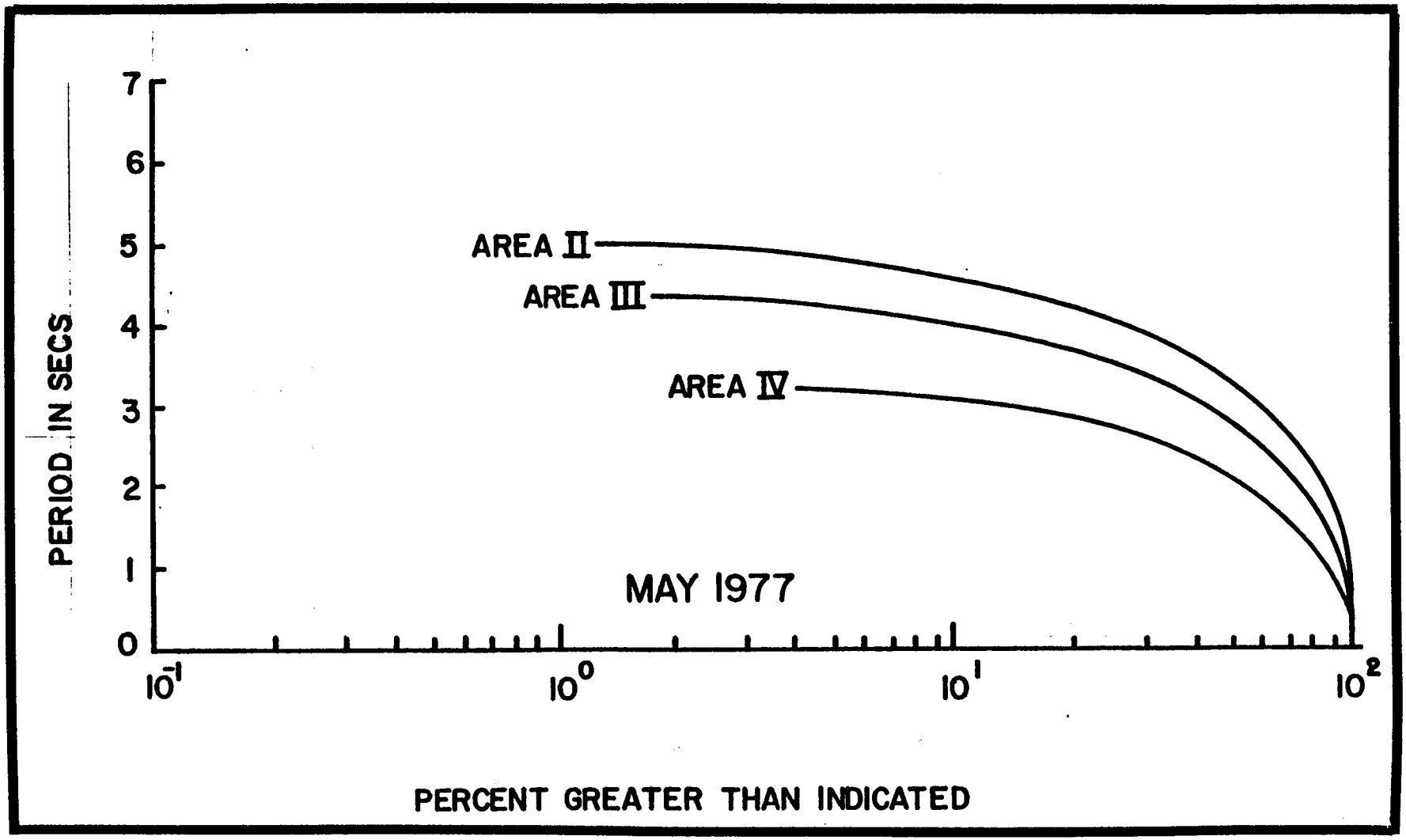

Figure 6-10. Example of wave period cumulative distribution.

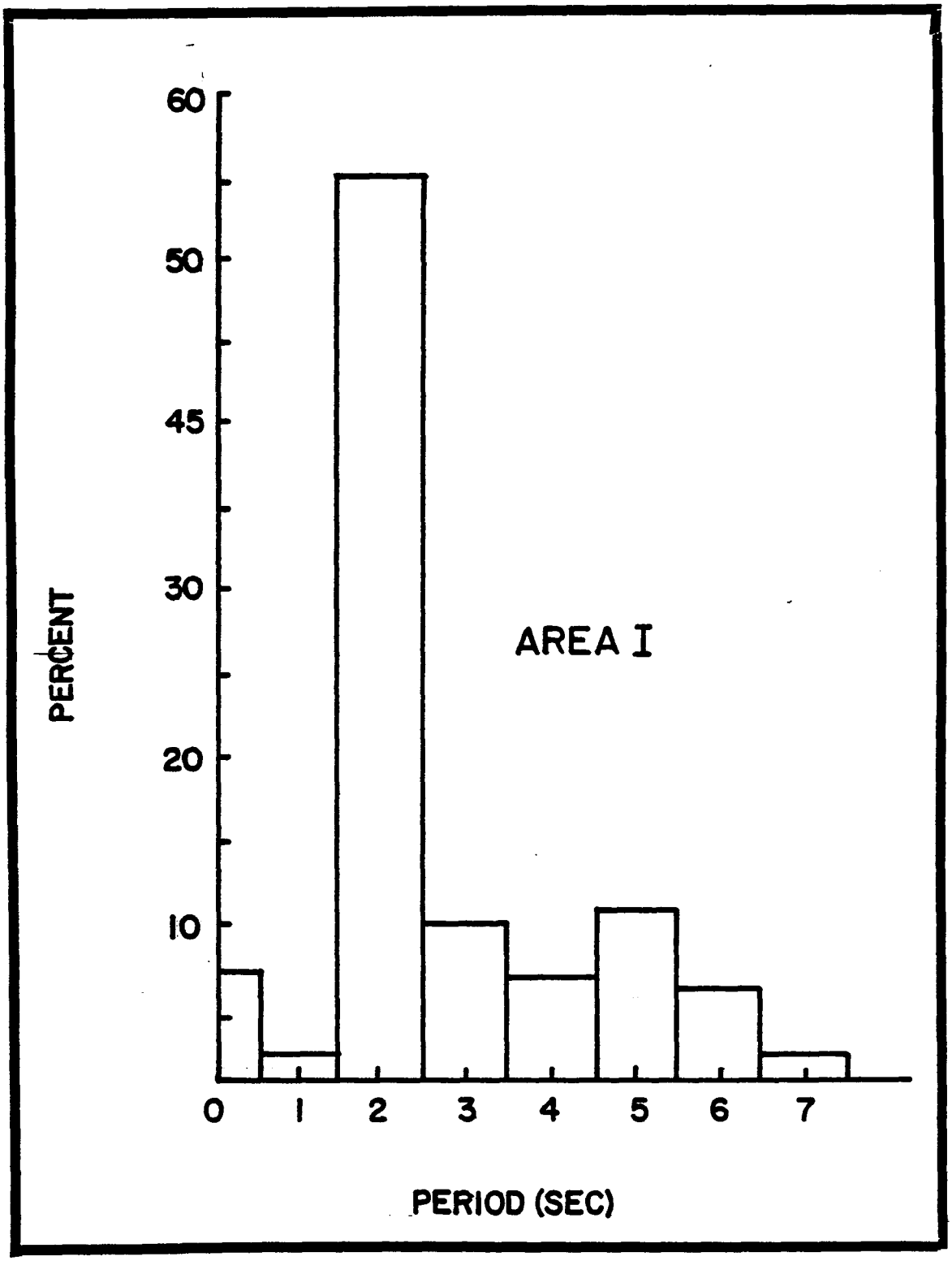

Figure 6-11. Example of annual wave period distribution (Area I).

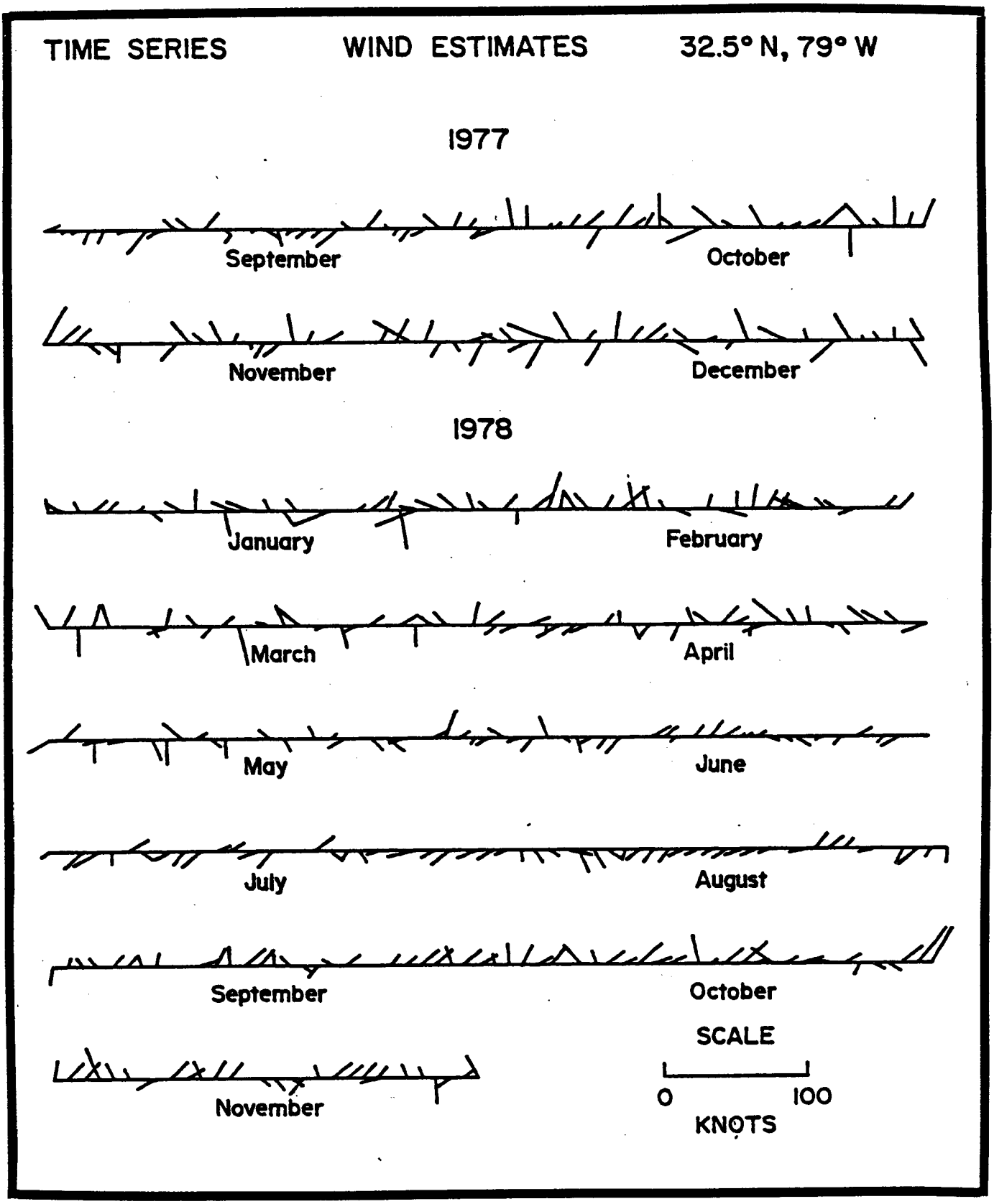

Figure 6-12. Time series of winds at 32 1/2°N, 79°W. Winds are based on 1200 GMT daily maps from September 1977 to November 1978 and are represented by stick diagrams. Sticks point to the direction from which the wind is blowing. For this purpose, north is at the top of the page, east is at the right of the page, south is at the bottom of the page, and west is at the left of the page. The stick length is proportional to the wind speed (kt).

surface wind field or with wind information inferred from NHC surface maps. Results of the comparison of the wind direction (excluding calm winds reported by the ships) and the wind speed during five cruises are summarized in Table 6-2. The table shows the number of ship reports compared for each cruise, and the percentages of $\pm$ 30° wind direction differences and $\pm$ 5 kt wind speed differences between ship reports and our description of the surface wind field. Note from the table that the highest and lowest percentages of $\pm$ 30° wind direction differences are found for the "R/V ISELIN" cruise in July-August 1978 (90%) and for the R/V PIERCE cruise in September 1977 (68%), respectively. The highest and lowest percentages of $\pm$ 5 kt wind speed differences are found for the R/V ISELIN cruise in April 1978 (87%) and the R/V PIERCE cruise in November 1977 (37%), respectively. However, this latter finding for the R/V PIERCE cruise is an exception, and a good agreement between wind reports from the ships and our surface wind description is found in most cases.

6.4.1.3 Evaluation of Satellite-Derived Winds

This evaluation was designed to explore the feasibility of incorporating satellite-derived winds (based on low-level cloud motions) in future descriptions of the surface wind field off the U.S. southeast coast. For this evaluation, 441 satellite-derived winds were obtained from low-level wind charts prepared at NHC for September to November 1977. Wind direction and wind speed differences between the satellite-derived winds and surface winds (inferred from the baseline description) for the corresponding locations and times of the satellite-derived winds were then examined. These differences are presented in histogram form in Figure 6-13. Because expected effects of friction on the sign of these differences fail to show systematically, differences in the figure are given in absolute value. It is found that 70% of the cases show wind direction differences within $\pm$ 30° and that 62% of the cases show wind speed differences within $\pm$ 5 kt. Therefore, in most cases, satellite-derived winds do not differ greatly from surface winds in the baseline description. This implies that the use of satellite-derived winds appears to be acceptable in future descriptions of the surface wind off the U. S. southeast coast.

6.4.1.4 Evaluation of Feasibility of Obtaining Diagnostic Winds Offshore Based on Coastal Reports

This feasibility study involves the comparison of six-hourly wind reports from the Savannah and the Charleston airports for September to November 1977 with simultaneous wind estimates (from our wind description) for two marine locations (31°N, 80 1/2°W and 32°N, 79 1/2°W) which are roughly 60 miles southeast of Savannah and Charleston, respectively. For the Savannah airport vs. 31°N, 80 1/2°W wind comparison, histograms in Figure 6-14a show wind direction differences (Savannah minus 31°N, 80 1/2°W winds) within $\pm$ 30° in 70%

Table 6-2. Evaluation of wind reports from ship cruises vs. winds from the baseline description of the surface wind field.

Ship's Name	Cruise	Number of wind reports	± 30° wind direction differences (% of cases)	± 5 kt wind speed differences (% of cases)
G. W. Pierce	Sep. 1977	44	68	64
Columbus Iselin	Nov. 1977	20	79	70
G. W. Pierce	Nov. 1977	64	78	37
Columbus Iselin	Apr. 1978	37	82	87
Columbus Iselin	July-Aug. 1978	21	90	86

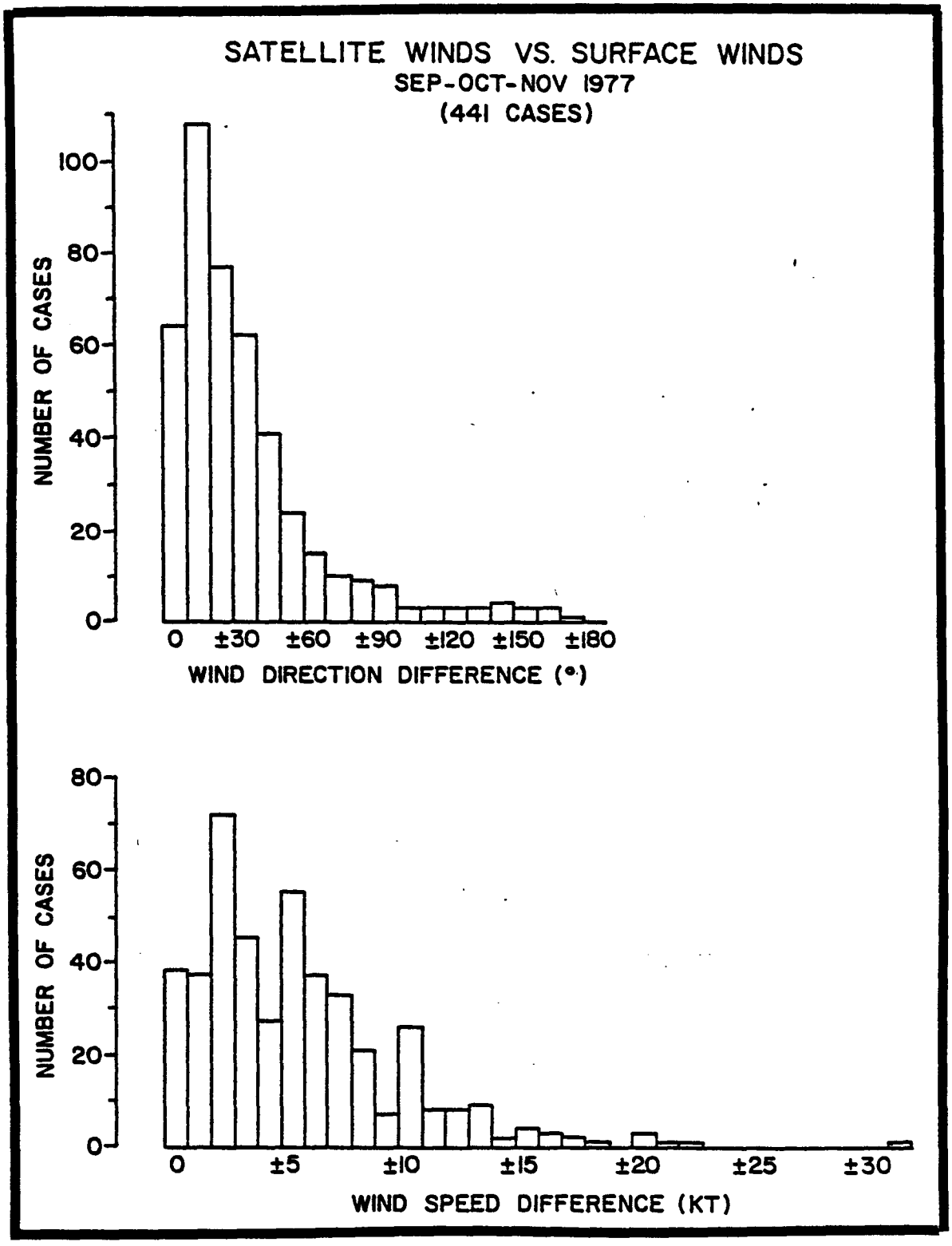

Figure 6-13. Histograms showing wind direction and wind speed differences between satellite-derived winds and winds inferred from the baseline description of the surface wind field.

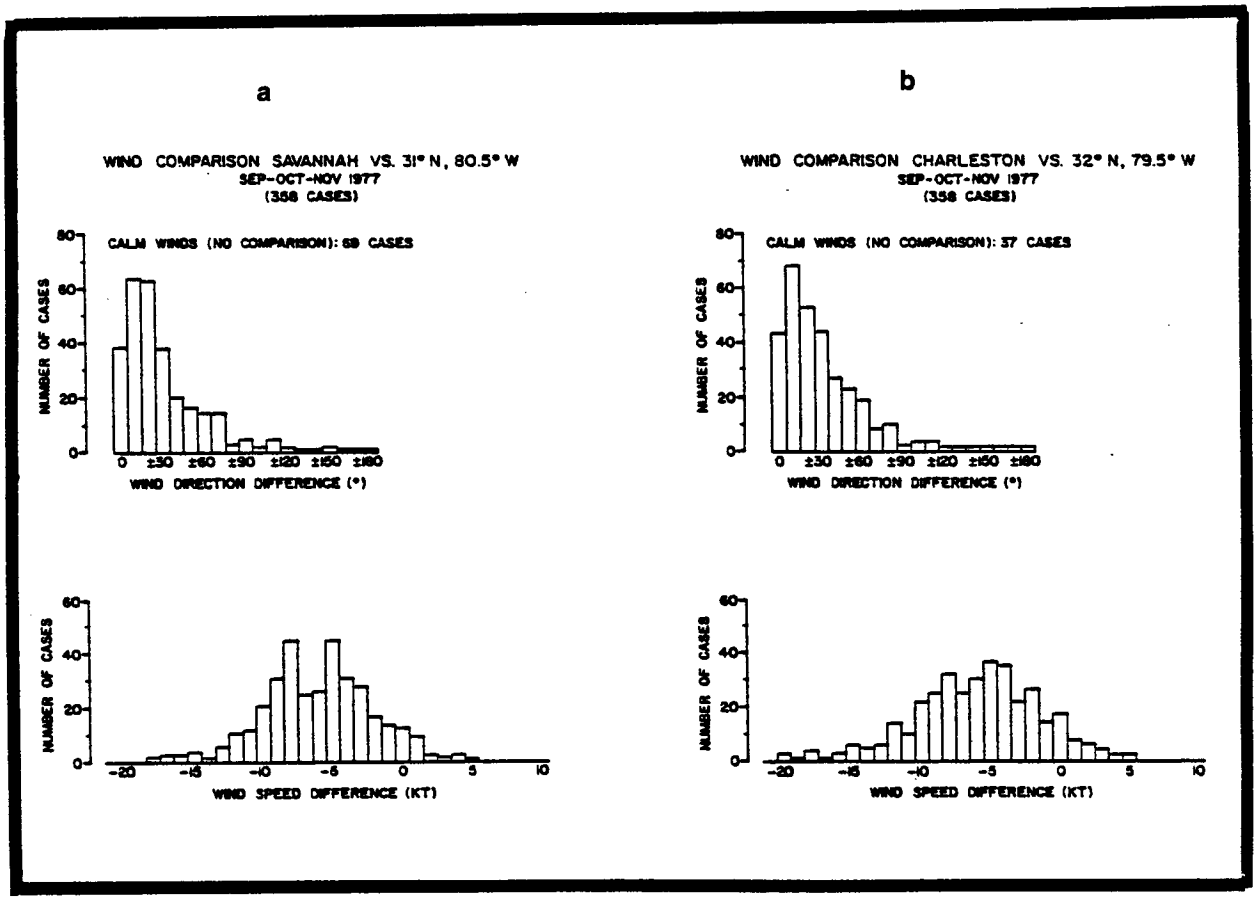

Figure 14a and b. Histograms showing wind direction and wind speed differences between coastal locations and selected offshore locations. No wind direction differences are determined in cases of "calm wind" coastal reports.

of the cases and wind speed differences in the -3 to -9 kt range in the highest percent (64) of the cases. Similar histograms for the Charleston airport vs. 32°N, 79 1/2°W winds (Figure 6-14b) show wind direction differences (Charleston minus 32°N, 79 1/2°W winds) within ± 30° in 65% of the cases, and three wind speed difference ranges: -2 to -8 kt, -3 to -9 kt and -4 to -10 kt with the same highest percent (57) of the cases. These findings suggest that crude estimates of offshore winds are possible in many cases by using the reported wind direction at the coast and by applying a statistical correction (of about + 6 kt) to the reported wind speed at the coast.

6.4.1.5 Evaluation of Anomalies in the Surface Wind Field with Respect to Climatological Conditions

These anomalies can be investigated by obtaining prevailing conditons of the baseline surface wind field over a prescribed time period and comparing these prevailing conditons with the corresponding climatology based on data collected for many years. An anomaly investigation is done on a limited basis for the month of October 1977. The investigation involves both the predominant wind and the frequency of wind speeds over two prescribed speed ranges. These characteristics of the wind field in October 1977 are chosen and processed to conform as close as possible to the climatological wind characteristics for October given by Kirshen (1978). The latter are essentially a rearrangement of results produced by the U.S. Naval Weather Service Detachment (1976). An inspection of this latter publication proved to be extremely helpful in interpreting correctly what is in Kirshen's (1978) displays and, therfore, in designing this anomaly study. Table 6-3 shows the comparison of the predominant wind direction (16 points of the compass) and the averaged speed ($m.s^{-1}$) along this direction in October 1977 with the corresponding climatology (Kirshen, 1978); the comparison is based directly on ship reports obtained operationally and non-operationally for October 1977 and is for predominant winds for four 2° x 2° selected squares off the U. S. southeast coast. Note in the table that the square bounded by the parallels 32 and 34°N and the meridians 76 and 78°W shows the largest anomaly (45°) in the predominant wind direction for October 1977; the largest anomaly (3.1 $m.s^{-1}$) in the averaged speed along the predominant wind direction is found for the square bounded by the parallels 28 and 30°N and the meridians 77 and 79°W. The frequencies (percentage) of wind speeds equal to or over 17.5 $m.s^{-1}$ and equal to or below 5 $m.s^{-1}$ for the 2° x 2° squares in October 1977 (not shown in Table 6-3) are compared with the spatial distribution of these frequencies shown by climatology (Kirshen, 1978; U. S. Naval Weather Service Detachment, 1976). The October 1977 frequencies of wind speeds equal to or over 17.5 $m.s^{-1}$ are not found to differ greatly from climatology. However, the frequencies of wind speeds equal to or below 5 $m.s^{-1}$ are found to be less than expected from climatology, the climatological percent frequency for wind speeds equal to or below 5 $m.s^{-1}$ being approximately, in the 30-40% range; while the

Table 6-3. Comparison of the October 1977 predominant wind direction and averaged speed along this direction with climatology for the month of October (Kirshen, 1978).

2° x 2° square bounded by lat.; long.	Predominant wind direction (16 points of compass)		Averaged wind speed (mps) along the predominant wind direction	
	Oct. 1977	Climatology	Oct. 1977	Climatology
34°N, 36°N; 74°W, 76°W	N	NNE	11.3	8.7
32°N, 34°N; 76°W, 78°W	N	NE	9.3	8.7
30°N, 32°N; 78°W, 80°W	NE	NE	6.7	8.2
28°N, 30°N; 77°W, 79°W	E	ENE	9.8	6.7

corresponding range for October 1977 is about 22-34% This latter finding and those in Table 6-3 suggest more windy than normal conditions off the U. S. southeast coast in October 1977.

6.4.1.6 Evaluation of the Offshore Surface Wind Forecasts

This evaluation is important in that it investigates the possible use of forecast winds as a substitution for unavailable offshore reports. The evaluation is based on 225 wind forecasts for a portion of the Georgia Embayment in September-October-November 1977; the forecasts are for the coastal waters (out to 80 km) between Savannah, Ga., and St. Augustine, Fl. The forecast winds prepared by NHC are verified against winds at the outer limit of the area (31^{o}N, 80 $1/2^{o}$W) about twenty-four hours after forecast time; these winds (observed wind hereafter) are inferred from maps in the baseline surface wind description. In verifying the forecasts, the wind direction and wind speed are verified separately. The wind direction forecast is termed "good" as the observed wind is either within the predicted direction range or shows a deviation of $\pm$ 22 $1/2^{o}$ from the predicted range; a "fair" forecast shows the observed wind to deviate $\pm$ 45^{o} from the predicted direction range and a "poor" forecast shows the observed wind to deviate more than $\pm$ 45^{o} from the predicted direction range. The wind speed forecast is termed "good" if the observed wind shows a difference up to 5 kt from the predicted speed range; the forecast is termed "fair" if the difference is between 6 and 10 kt and "poor" for a difference over 10 kt. The histograms in Figure 6-15 conform to the forecast verification classes discussed above. Based on these histograms, the wind direction forecast is found to be "good" in 69% of the cases and the wind speed forecast is found to be "good" in 84% of the cases. "Fair" forecasts for wind direction are found in 18% of the cases and "fair" forecasts for wind speed are found in 14% of the cases. "Poor" forecasts in 13% and 2% of the cases are found for wind direction and wind speed forecasts, respectively. In summary, forecast winds show to verify to a high degree off the Georgia coast and are, therefore, potentially substitutes for offshore winds based on actual reports.

6.4.2 Meteorological and Sea State Correlations

From plots of wind-wave data along cruise tracks and recalling that the last two-digits of the second and third rows are respectively the wave height and wind speed, the changes taking place in wind and sea state along the cruise tracks are vividly shown in these figures. For example, in Figure 6-3, May, 1977, sudden changes in wind speed and wave height are seen at the upper-right corner of the figure. That is, from May 9, 0300 to 2100 of the same day, wind speed and wave height changed respectively from 20 to 25 knots and 1 to 1.5 m. These quantities remain relatively steady for the next day but suddenly dropped to zero knots and meters two days later. Similar observations can be made of wind-wave condition from other figures.

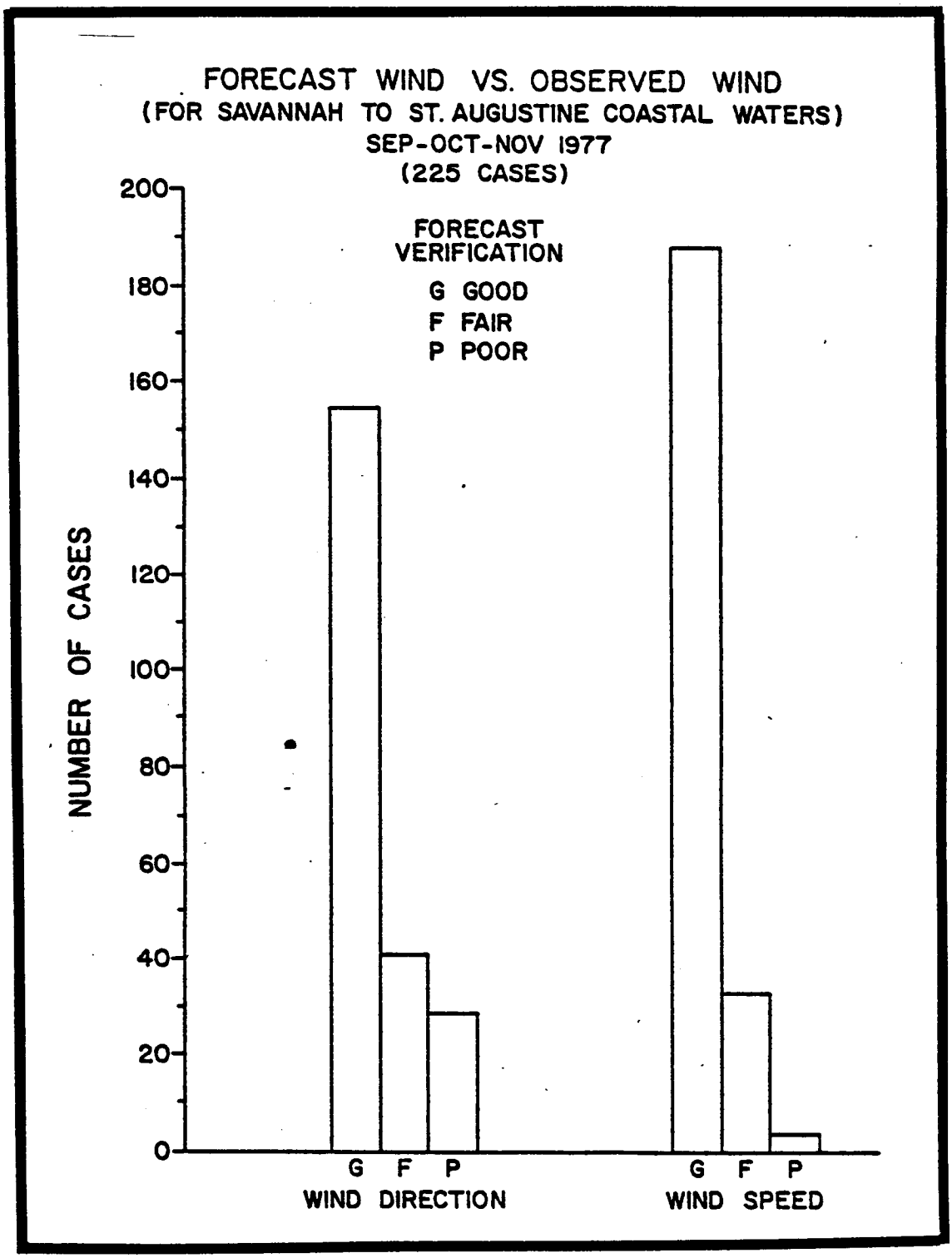

Figure 6-15. Histograms showing the wind forecast verification for Savannah to St. Augustine coastal waters. See text for definition of "good" (G), "fair" (F) and "poor" (P) forecasts.

Examination of the wind-wave roses at the "short-term" and "long-term" mooring locations in Figures 6-4 to 6-5 shows that larger winds and waves occur in "winter months" from October to April than in "summer months." This can be seen from "long-term" mooring records if it noted that the shaded areas denote wind speed in excess of 12 $m.s^{-1}$ and for wave height, the blank areas correspond to wave height larger than 3.3 m. Considering wind and wave directions, it is apparent that during "winter months," the predominant wind and wave are generally in the northerly direction whereas in other months from May to September, they are mostly in the southerly direction. Also, comparison of corresponding wind and wave roses show that predominant wind and wave are in the same general direction.

The correlation between wind speed and wave height is also evident upon examination of frequency distribution of wave height and wind speed. It is noted that "extreme" wave height reaches 3.5 m to 4.5 m in September and October respectively. In fact, regardless of the area under consideration, higher waves and wind speeds occur during the "winter months," the highest being in October, 1977, in area I.

6.5 CONCLUSIONS

Continued collection of wind and wave data is an important area of research which provides the basic environmental information for the design, siting, operation, and risk assessment of and policy decision regarding offshore structures. Similar to any other geophysical phenomenon, the statistics of winds and waves must be continuously analyzed and updated. These data could be effectively utilized in the establishment of probabilistical-statistical models of the wave and wind structures commensurate with the quality of the data.

The surface wind description provided Dr. J. Fernandez-Partagas provides a useful information source (wind direction and speed) for any location and time (within the prescribed area and period of study). The impact of this capability is both meteorological and oceanographical. For oceanographic purposes, the usefulness of this surface wind description is to provide basic information for the assessment of the meteorological forcing of oceanic motions. This information can be readily read off the surface wind maps according to the specific needs of the investigation.

6.6 REFERENCES

Fernandez-Partagas, J. and W. Duing, 1977. Surface wind maps for the western Indian Ocean from August 1975 to October 1976. Technical Report submitted to the Office of Naval Research, Contract No. N00014-75-C-0173. Rosenstiel School of Marine and Atmospheric Sciences, University of Miami, Miami, Florida.

Kirshen, P. H., 1978. Summary and analysis of physical oceanographic and meteorological information on the continental shelf and Blake Plateau from Cape Hatteras to Cape Canaveral. Report to BLM (Contract No. AA550-CT7-16). ERT, Concord, MA.

Palmer, C. E., C. W. Wise, L. J., Stempson, L. J. and G. H. Duncan, 1955. The practical aspect of Tropical Meteorology. Air Force Surveys in Geophysics No. 76. Air Force Cambridge Research Center, Bedford, MA., 195 pp.

U. S. Naval Weather Service Detachment, 1976. Climatic study of the near coastal zone. East coast of the United States. Published by Director, Naval Oceanography and Meteorology, Washington, D. C., 133 pp.

VII. FUTURE WORK

7.1 OUTLINE OF SECOND YEAR'S PROGRAM

The second year of the program has been designed to provide additional information regarding currents, circulation and mixing in the Georgia Embayment region, in order to understand these processes in sufficient detail to predict the transport and distribution of surface or dissolved pollutants throughout the region of study, and to further characterize the interaction between the physical oceanography environment and the biological, geological and chemical systems (the BLM long-term objective).

Techniques used during the first year in data collection and analysis will be refined and procedures updated. Surface transport will be mapped using radio equipped drogues that can be tracked across the study area for extended periods up to two weeks. Subsurface currents will continue to be monitored in the Charleston region by short (winter and summer) and long (1 year) term moorings of VACM current meter strings. The vertical and horizontal distribution of salinity and temperature in the study area will continue to be characterized on a seasonal basis using a CTD, or XBT system and a recording thermosalinograph, and will be supplemented with additional measurements of nutrients, dissolved oxygen, and chlorophyll-a concentrations. The Very High Resolution Radiometry (VHRR), which showed exciting promises during the first year study will be continued for further characterization of the Gulf Stream variability, eddy structure and frontal formation. Furthermore, close liaison and coordination in data collection, storage and reduction will be maintained between other federal agencies and cognizant institutions to insure maximum efficiency in this effort for all concerned programs. In order to realize this objective, a series of meetings/workshops are planned to bring together all PI's, contractors and other responsible for collecting, analyzing and disseminating information in the OCS region. These tasks are further described in the following sections.

7.1.1 Surface Currents

Many oil and gas related pollutants discharged in the marine environment remain for sometime concentrated on the surface and in the near surface layer. As a consequence, knowledge of characteristic movements in these upper layers is crucial to infer the possible paths and rates of pollution migration. The objective of the second year study of surface currents and horizontal mixing processes in the South Atlantic OCS is to provide insight into the expected movement and dispersion of surface pollutants derived from petroleum and gas exploration and production. Results of the proposed study should allow development of a better description of regional circulation and ultimately a parameterization of processes responsible for the local physical environment.

In the second year's study, surface currents will be documented by remote tracking of surface drogues containing radio transmitters deployed on a cross shelf transect passing through the long term subsurface current moorings off Charleston. Two deployments will be conducted (winter and summer) with drogues being tracked for a minimum of 5 days but not more than 14 days. Using wind data, movement of drogues will be corrected for parasitic wind effects. Resulting corrected displacements should provide good estimates of the movement of surface water.

7.1.2 Subsurface Currents

The objective of this study is to determine the temporal and spatial variability in circulation across and along the South Atlantic outer continental shelf with emphasis on the northern region off Charleston, S.C. This includes determination of the multi-level spectral energy distribution of currents in the Northern Georgia Embayment, using two seasonal strings of VACM current meters located on a cross-shelf transect through the position of a third long term mooring deployed for one year near 39° 38'N and 78° 42'W, and the intercomparison of these data with similar records collected in the Carolina Capes Region (DOE-funded study). In addition, this study involves the development of correlations of the observed currents spatial energy distribution with coastal sea level (obtained from NOS), atmospheric variability (collected by NWS and NCC) as well as Gulf Stream fluctuations (determined through hydrographic measurements and by remote sensing techniques).

The long range goal of this effort is to contribute to the understanding of the currents, circulation, and mixing processes in sufficient detail to analytically predict the probable advection and dispersal of pollutants from oil, gas and mineral development activities. The information to be obtained will aid BLM in managerial decisions regarding the conditions that must be placed upon the development of these resources and the possible impacts on the marine environment. The study will also contribute to the understanding of the interaction of the physical dynamics of the OCS region with the biological and chemical systems.

7.1.3 Hydrography

The vertical density structure as well as nutrients, dissolved oxygen and chlorophyll-a concentrations will continue to be monitored on a seasonal basis along six cross-shelf transects spaced approximately equally between New Smyrna, Florida and Cape Fear, North Carolina, according to the methodology developed during the first year's program. This sampling will be augmented by similar data collected under the auspices of DOE, which will attempt to characterize events

such as Gulf Stream eddy formation and decay, bottom intrusions at the shelf break, etc. which all influence circulation over the area of interest.

7.1.4 Gulf Stream Variability

Sea surface temperature will be monitored by satellite thermal imagery techniques to determine the spatial and temporal variability of the Gulf Stream-Shelf water interface over time periods ranging from weeks to months. The knowledge of the variability of the western edge of the Gulf Stream is of critical importance to predict the influence of the Stream in entraining Shelf water.

Presently available VHRR techniques will be applied to the tracking of Gulf Stream-Shelf Water frontal position variability during the Fall, Winter and Spring seasons for the BLM area of interest in the South Atlantic Bight. Monthly and possibly higher frequency variability maps will be generated. The South Atlantic Bight will be divided into two areas (North and South) at approximately Cape Romain. In the southern area, the periodicity and size distribution of the spin-off eddies will be determined and quantitative estimates of the frontal variability derived. To the north, larger amplitude disturbances will be looked at, with the goal of estimating their amplitude and temporal variability characteristics.

7.1.5 Meteorological Forcing

Time series of meteorological data collected by three offshore buoys deployed off Charleston, S.C. at 32^{o} 28'N, 78^{o} 42'W, Savannah and Jacksonville (exact coodinates unknown) as well as wind information provided by the NWS coastal stations will be constructed and analyzed. This analysis will consist of spectra, coherence and phase between any two stations, correlation coefficients and eigenvalue modal analysis if required for a more complete understanding. The analysis will be paralleled by that of subsurface currents and sea level (the latter from NOS) in order to determine shelf forcing mechanisms.

7.2 DATA GAPS LIKELY TO EXIST AFTER COMPLETION OF SECOND YEAR'S STUDY

A major shelf experiment known as GABEX (Georgia Bight Experiment) will be undertaken by DOE in the spring of 1980. Although very comprehensive, this study will fail to address important components of the physical oceanographic characterization of the region of interest, mainly because of funding limitations. The following needs for additional studies not funded by DOE have been identified.

1. Need for deployment of 4 current meter moorings along a cross-shelf transect off Cape Romain, near the 15 (1 current meter), 25 (2 current meters), 40 (2 c m's), and 75 m (3 c m's) isobaths for a period of four months from February to May 1980.

2. Need for continuation of the existing long-term mooring measurements.

3. Need for continuation of analysis of the data provided by the three BLM offshore buoys and correlations with shore station wind data.

4. Need for near-synoptic measurements of temperature structure along a significant portion of the western edge of the Gulf Stream. This would be accomplished on a daily or bi-daily basis for approximately 10 observation days, using an aircraft equipped with a radiometer and air-deployable XBT's

5. Need for a statistical analysis of the amplitude and frequency of occurrence of Gulf Stream western boundary fluctuations, in an attempt to identify Gulf Stream induced current circulation over the shelf, through correlations between Gulf Stream instabilities and current meter signatures. This would be accomplished by remote sensing techniques, using temperature and possibly chlorophyll as tracers. Satellite monitoring of chlorophyll concentrations would aid in the identification of upwellings.

6. Need for a better resolution of the vertical profiles of horizontal current velocities over the shelf. This would be performed using a Cyclosonde profiler for a duration of approximately 20 days, coinciding with the GABEX hydrographic work.

7. Need for simultaneous measurements of vertical velocity and density structures in the vicinity of a coastal front, in order to examine the potential for pollutant exchange between shelf and estuarine waters. This experiment would be performed in conjunction with the DOE Front Flux Experiments.

8. Need for determination of surface current patterns over two tidal cycles in the near shore region adjacent to an estuary, in order to assess the ability of a coastal front to affect surface pollutant migration towards the coastline and within the estuary.